Neurobiological Mechanisms Underlying Episodic Memory Retrieval

by

Dheeraj Roy

B.S., M.S., Drexel University (2010)

Submitted to the Department of Brain and Cognitive Sciences
in Partial Fulfillment of the Requirements for the Degree of

DOCTOR OF PHILOSOPHY IN NEUROSCIENCE

at the

MASSACHUSETTS INSTITUTE OF TECHNOLOGY

June 2017

Signature redacted

Author .....
Department of Brain and Cognitive Sciences
April 28, 2017

Signature redacted

Certified by .....
Susumu Tonegawa
Picower Professor of Neuroscience
Thesis Supervisor

Signature redacted

Accepted by .....
Matthew A. Wilson
Sherman Fairchild Professor of Neuroscience and Picower Scholar
Director of Graduate Education for Brain and Cognitive Sciences

Neurobiological Mechanisms Underlying Episodic Memory Retrieval

by

Dheeraj Roy

Submitted to the Department of Brain and Cognitive Sciences
on April 28, 2017 in Partial Fulfillment of the
Requirements for the Degree of
DOCTOR OF PHILOSOPHY IN NEUROSCIENCE

Abstract

Memory is a central function of the brain and is essential to everyday life. Memory disorders range from those of memory transience, such as Alzheimer's disease, to those of memory persistence, such as post-traumatic stress disorder. To treat memory disorders, a thorough understanding of memory formation and retrieval is critical. To date, most research has focused on memory formation, with the neurobiological basis of memory retrieval largely ignored due to experimental limitations. Here, I present our recent advances in the study of memory retrieval using technologies to engineer the representation of a specific memory, memory engram cells, in the brain. First, using animal models of retrograde amnesia, we demonstrated that direct activation of amnesic engram cells in the hippocampus resulted in robust memory retrieval, indicating the persistence of the original memory. Subsequent experiments identified retained engram cell-specific connectivity in amnesic mice although these engram cells lacked augmented synaptic strength and dendritic spine density. We proposed that a specific pattern of connectivity of engram cells may be the crucial substrate for memory information storage and that augmented synaptic strength and spine density critically contribute to the memory retrieval process. Second, we examined memory engrams in transgenic mouse models of early Alzheimer's disease, which required the development of a novel two-virus approach. We demonstrated that optical induction of long-term potentiation at input synapses on engram cells restored both spine density and long-term memory in early Alzheimer mice, providing causal evidence for the crucial role of augmented spine density in memory retrieval. Third, using activity-dependent labeling, we found that dorsal subiculum had enhanced neuronal activity during memory retrieval as compared memory encoding. Taking advantage of a novel transgenic mouse line that permitted specific genetic access to dorsal subiculum neurons, we demonstrated that the hippocampal output circuits are functionally segregated for memory formation and memory retrieval processes. We suggested that the dorsal subiculum-containing output circuit is dedicated to meet the requirements associated with memory retrieval, such as rapid memory updating and retrieval-driven instinctive emotional responses. Together, these three related thesis projects have important implications for elucidating cellular and circuit mechanisms supporting episodic memory retrieval.

Thesis Supervisor: Susumu Tonegawa

Title: Picower Professor of Neuroscience

This thesis is dedicated to
my parents, Dr. Partha Sarathy Roy and Dr. Sumitra Roy,
my brother, Deepak Roy, and my wife, Shruti Gour Roy;

And to my grandpa, who was not only an amazing scientist,
but also served as Director of All India National Programs,
and worked at the World Health Organization (WHO).

Table of contents

This thesis is written as a composite of Appendices I-VIII.

Chapter 1. Background

Understanding the material basis of memory remains a central goal of modern neuroscience (Dudai and Morris, 2013; Tonegawa et al., 2015a). Historically, philosophers tried to understand the precise location in the human body where information of past experiences is stored. For some time, memory information was attributed to organs such as the heart and kidney. In the Renaissance, Descartes proposed that mental capacities, specifically memory, must be represented in the brain (Descartes, 1649). In the 20th century, Richard Semon was the first to theorize that learning induces physical changes in specific brain cells that retain information and are subsequently reactivated by appropriate stimuli to induce recall. He termed these changes the engram (Schacter, 2001; Semon, 1904, 1909). However, even after Semon's engram theory, some leading scholars wondered whether memory is physically represented in the brain or psychically represented in the mind (Bergson, 1911; McDougall, 1911). It was Shepherd Franz and later Karl Lashley who advocated for the physical theory of information storage in the central nervous system (Franz, 1912; Lashley, 1929, 1950). In particular, Lashley adopted the concept of the engram and was among the first to attempt to localize memory engrams in the brain (Lashley, 1950). Although Lashley's idea of Mass Action was later empirically disproved, researchers after him have tried to identify the location of memory representations in the brain using experimental technologies available at the time (Bruce, 2001; Dudai and Eisenberg, 2004; Hubener and Bonhoeffer, 2010; Josselyn et al., 2015; Thompson, 1976; Tonegawa et al., 2015b). In this section, I will discuss early attempts to identify memory engrams, provide criteria for defining a memory engram and engram cells, and then examine recent studies demonstrating that memory is indeed stored in populations of neurons and their associated circuits.

1.1 Pre-optogenetic studies

At any given moment, animals need to quickly organize their behavior by comparing previous experiences to the currently available sensory cues. This online function is carried out by neural circuits

in the brain, which indicates that memory evolved for two major biological purposes: (1) to replay previous episodes and inform current behavioral outputs, and (2) to integrate past and present experiences (James, 1890). A key question in the study of memory is how new information can be acquired and stored in precisely wired neural circuits (Kandel, 2001). At the cellular and systems level, Ramon y Cajal originally proposed that the strengthening of sites of contact between neurons might be a mechanism of memory storage (Ramon y Cajal, 1893, 1894). These sites of contact were famously termed synapses by Charles Sherrington (Foster and Sherrington, 1897). However, it was Donald Hebb's theoretical integration of neurophysiology and psychology that created the modern paradigm for memory research. Hebb proposed that neuronal assemblies linked by adaptable synaptic connections could encode informational content in the brain and further elaborated that these cell assemblies could provide the basis of a distributed memory system (Hebb, 1949). Since then, many attempts have been made to localize memory engrams in many different species.

1.1.1 Invertebrate studies

In the 1950s, there was little consensus among psychologists that our understanding of the biological basis of learning and memory could be advanced using a reductionist approach, like the use of invertebrate animal models. However, biologists quickly realized that the simplest forms of memory would be conserved across species and therefore should be studied in experimentally tractable animals as a starting point. Probably the best-known example is the giant marine snail Aplysia californica, in which a simple defensive reflex involved less than 100 central nerve cells (Kandel, 1976). This reflex behavior, the withdrawal of the gill upon stimulation of the siphon, exhibited different forms of learning such as habituation, sensitization, and classical conditioning (Pinsker et al., 1973). By examining these simple forms of learning, scientists performed detailed analyses of the cellular and molecular mechanisms underlying non-associative as well as associative learning. Importantly, these studies provided clear evidence that learning correlates with changes in the strength of synaptic connections, thereby supporting

Cajal's and Hebb's ideas on the mechanism of memory storage (Milner et al., 1998). Along with synaptic strength, it was observed that learning paralleled structural changes, such as the elimination or addition of synapses that closely matched the age of the memory (Bailey and Chen, 1989; Glanzman, 1990).

With the goal of pinpointing engrams in intact nervous systems, researchers have extensively studied honeybee and Drosophila melanogaster model systems. In adult honeybees, learning and memory storage occur in mushroom bodies where experience-dependent dendritic branching patterns have been observed (Farris, 2001; Menzel, 2001). Similar to Aplysia, studies in flies identified a biochemical mechanism for memory storage that is based on cAMP-mediated pathways (Dudai, 1988; Tully, 1985). Using cAMP signaling mutants, structural alterations in the sensory neurons of flies have been correlated with learning and short-term memory (Corfas and Dudai, 1991; Gerber et al., 2004). More recently, when a specific odor was paired with shock in flies, defined neuronal populations within the olfactory learning circuit showed modified firing responses. Specifically, pathways in the antennal lobes and the mushroom bodies increased their responses only to the odor used in training, but not to control odors. These experiments support the idea that odor-specific memory traces are formed within these cell populations as a result of Pavlovian conditioning (Liu and Davis, 2009; Yu et al., 2006). However, the precise cellular and/or synaptic localization of engrams in flies requires further investigation.

1.1.2 Bird studies

In the search for neural mechanisms of learning and memory, mammals have been preferred over birds as model systems due to their closer relationship with humans. However, since it was highlighted by the Avian Consortium that birds exhibit cognitive capacities, which had previously been thought to be restricted to primates, memory storage in birds has been extensively studied (Avian Brain Nomenclature Consortium, 2005; Doupe, 1999). Historically, avian studies on memory have used four major paradigms, imprinting, birdsong learning, cache recovery (Clayton and Dickinson, 1998), and gustatory avoidance (Rose, 2000). Imprinting, where a recently hatched chick learns the characteristics of its parents (or an

object), causes dramatic changes in the brains of young birds (Lorenz, 1981). These studies have revealed a localization of the substrate of memory, in particular because the generation of new synapses has been observed during imprinting. To date, it has not been possible to prove causality between the observed changes and the imprinting process itself due to both the distributed nature of the system and a lack of appropriate technologies (Horn, 2004). Regarding birdsongs, juveniles learn the characteristics of the songs of tutors from their own species, in most cases their fathers, which is a process that requires several brain nuclei. This process involves a period of auditory memorization followed by development of the juveniles' own vocalizations, which is analogous to speech acquisition in human infants. It is thought that the neural representation of song memory during memorization is localized to the auditory association cortex, while the neural substrate of vocalization memory is localized to a network of interconnected brain nuclei known as the song system (Bolhuis and Gahr, 2006). More recently, a study examined in vivo dendritic spine dynamics in the crucial birdsong nucleus, HVC, during the juvenile song-learning period of zebra finches. Strikingly, it was shown that even though juveniles exhibit high levels of spine turnover; during the song learning process subsets of spines on sensorimotor neurons undergo stabilization, accumulation, and enlargement. These experiments suggested that successful behavioral learning correlated with rapid stabilization and strengthening of specific synapses (Eales, 1985; Roberts et al., 2010).

The sense of auditory space derives from associations formed between specific auditory cues and locations in the environment where they are produced. Experience has a significant impact on sound localization and therefore the auditory localization pathway became a model system for studying mechanisms of learning (Shinn-Cunningham, 2000). A nocturnal predator, the barn owl (Tyto alba), is the most extensively studied species for this behavior since its capacity for localization is comparable to that of humans. It was first shown in the barn owl that they have the incredible capacity to adapt to environmental changes in a behaviorally relevant manner. In particular, their auditory and visual space maps in the superior colliculus align according to individual visual and auditory cues. Moreover, learning in the barn owl correlates with structural rearrangements of neuronal connections between the internal and

external nucleus of the inferior colliculus (Knudsen, 2002). These observations demonstrate that the birdsong learning process is a powerful paradigm, which holds promise as a future target to identify and visualize the formation of an engram.

1.1.3 Rodent and non-primate mammal studies

The American psychologist Karl Lashley pioneered a systematic hunt for engram regions in the rodent brain by introducing lesions of varying sizes into different sites of the cerebral cortex, and attempting to associate each of these lesions with the animal's ability to solve a maze task (Lashley, 1950). The results showed that behavioral impairments were caused by lesions introduced throughout the brain, and that severity of the impairments was proportional to the size of the lesions. Lashley concluded that the putative memory engram cells are not localized in the cerebral cortex, leading him to formulate the Mass Action Principle. The notion that engram cells for a specific memory are broadly distributed throughout the brain has not been supported by subsequent studies for at least several types of memory, including episodic memory. It is conjectured that Lashley's failure in identifying localized engram cells is because the maze tasks he used were too complex and required multiple regions of the cerebral cortex, and/or the primary sites of storage for this type of memory may reside in subcortical regions.

Richard Thompson and colleagues performed pioneering work in attempting to localize the memory engram for classical eyelid conditioning in rabbits. In this simple paradigm wherein repeated pairings of a neutral conditioned stimulus (e.g., tone, CS) with an unconditioned stimulus (e.g., corneal airpuff, US) produces an adaptive conditioned response (eyeblink, CR) to the CS alone, animals from which the cerebral neocortex or hippocampus had been removed were still able to learn and express the standard delay CR (Thompson and Kim, 1996). Initial work identified the cerebellum as a crucial node for learning, retention, and expression of this simple associative memory (McCormick et al., 1982). It has since been revealed that information about the CS and US arrive in the cerebellum through the pontine nuclei and inferior olive (IO), respectively. Lesions of the pontine nuclei or IO prevents CR acquisition (McCormick et al., 1985; Steinmetz et al., 1987) and precisely timed stimulation of the pontine nuclei and

IO as the CS and US can produce reliable expression of the CR (Mauk et al., 1986; Steinmetz et al., 1986, 1989). This CS and US information arrive within the cerebellum at two sites, the cerebellar cortex and the interpositus nucleus. Through many clever experiments utilizing lesions, pharmacological inactivation, neural stimulation, and single cell recordings, it is understood that through an intricate process of long-term depression (LTD) and long-term potentiation (LTP) at specific synapses, the activity of the interpositus nucleus is responsible for triggering the expression of CR, while the cerebellar cortex shapes the adaptive timing of the CR (Ito and Kano, 1982; McCormick and Thompson, 1984; Lavond and Steinmetz, 1989; Garcia and Mauk, 1998; Bao et al., 2002). Together, these studies suggest that a memory engram for this behavior is found in key sites of the cerebellum, involving interactions between the anterior interpositus and overlying cortex.

A key structure for declarative memory formation in mammals is the hippocampus, where use of rodent models has led to great progress in elucidating the cellular basis of memory. By recording neuronal activity in the hippocampus of awake, behaving rats, a series of elegant experiments observed learning-related changes in receptive field properties of single neurons known as hippocampal place cells. These sparse populations of neurons develop specific place fields as the rat explores and learns about a novel environment (O'Keefe and Dostrovsky, 1971; Wilson and McNaughton, 1993). These place-coding cell populations may represent the spatial engram, which is needed to form a long-term memory of the animal's experience along with valence information. Another well-documented example of experience-dependent neural activity is referred to as replay, which describes the spontaneous reactivation of recent neural activity during periods of high-frequency bursts in the hippocampus. Interestingly, the strength of replay-related reactivation has been correlated with long-term memory expression (Dupret et al., 2010; Louie and Wilson, 2001; Nakashiba et al., 2009).

From hippocampal recording studies, it is clear that the sparse population of place cells persists several days to weeks after learning and remains specific to the environmental cues during learning. Using auditory conditioned stimuli, a variety of response latencies were found in multiple cortical and subcortical areas (Olds et al., 1972). These authors reasoned that learning centers of the brain would

contain cell responses to conditioned stimuli, which were of similar latencies as sensory responses. A subset of the cortical areas analyzed in this study fulfilled this criterion and furthermore these responses were specific to the auditory stimulus used during conditioning. Based on these experiments, it was proposed that these cortical areas comprised learning centers and were thus putative sites involved in memory formation. Several groups have provided correlational evidence between learning-induced plasticity in primary auditory cortex and long-term memory (Gonzalez-Lima and Scheich, 1986; McKernan and Shinnick-Gallagher, 1997; Bao et al., 2001; Kisley and Gerstein, 2001; Weinberger, 2004). Similar results have been reported for neuronal activity changes induced by olfactory associative learning paradigms (Kass et al., 2013).

Many studies have implicated select populations of neurons in specific memories by examining the expression of immediate early genes (IEGs) such as c-Fos, Zif268, and activity-regulated cytoskeleton-associated protein Arc (Flavell and Greenberg, 2008; Guzowski, 2002; Okuno et al., 2012). Several groups found that cell populations active during the acquisition of a fear memory were preferentially reactivated during the recall of that memory in different areas of the mouse brain, such as the amygdala (Reijmers et al., 2007), the hippocampus (Deng et al., 2013; Tayler et al., 2013), layer II cortical areas including sensory cortex (Cowansage et al., 2014; Xie et al., 2014), and the prefrontal cortex (Zelikowsky et al., 2014).

Another approach that has been used to identify probable engram cell populations in the rodent brain employs the random overexpression of the transcription activator cAMP response element-binding protein (CREB) in a small population of neurons in the lateral amygdala, making these cells more likely to be recruited to become a part of putative engram ensembles during subsequent fear conditioning training (Han et al., 2007). By selectively manipulating these high-CREB cells, but not a random population of neurons in the same brain region, via diphtheria toxin-based ablation (Han et al., 2009) or genetic-based inhibition (Hsiang et al., 2014; Zhou et al., 2009) memory recall was disrupted in mice. Similar technology has been used to demonstrate the necessary role of retrosplenial cortex neurons in spatial navigation memory (Czajkowski et al., 2014). Other studies using the Daun02 inactivation method

have shown that contextual memory associated with a positive reinforcer such as cocaine, could be blocked by inactivating a minor portion of nucleus accumbens neurons that were previously active in the drug-associated environment in rats (Koya et al., 2009).

Two-photon microscopy allows in vivo visualization of fine structural morphology down to several hundred micrometers in the cortex of the intact rodent brain (Denk et al., 1990). Such technology has allowed researchers to demonstrate dendritic spine changes that correlate with the acquisition and/or storage of information (Attardo et al., 2015; Moser et al., 1994). An interesting report found that the formation of a contextual fear memory correlated with a transient increase in dendritic spine density in the hippocampus, while similar changes in the anterior cingulate cortex developed over a period of weeks following memory formation; the latter time-dependent process is called systems consolidation of memory (Restivo et al., 2009).

Another well-established model for experience-dependent cortical plasticity is monocular deprivation, where temporary closure of one eye shifts the balance between the strength of the representation of the two eyes in the visual cortex towards the open eye. Inspired by work in the barn owl model system, several researchers combined two-photon microscopy and monocular deprivation to visualize an engram in the neocortex. A series of experiments found that cortical dendritic spines that appeared during monocular deprivation remained in place even after re-establishing normal vision. These spines served as the basis for faster and longer-lasting adaptation responses during a second monocular deprivation, even though this second deprivation did not further increase spine density (Hofer et al., 2009). These results are reminiscent of the concept of savings proposed by Hermann Ebbinghaus more than 100 years ago. Ebbinghaus demonstrated that in every day experiences relearning is easier than first-time learning (Ebbinghaus, 1880). Most studies examining structural correlates of learning and memory focused on dendritic spines, though it is worth noting a few examples that examined presynaptic plasticity. In adult mice, cortical axonal boutons show some degree of structural plasticity under baseline conditions with overall axon branching patterns remaining stable (De Paola et al., 2006). In higher mammals including the cat, a study found that shrinkage and expansion of ocular dominance columns due

to monocular deprivation was reflected in the retraction and growth of thalamic fibers in the visual cortex (Antonini and Stryker, 1993). Similar to presynaptic structural plasticity, relatively less attention has been paid to structural modifications of inhibitory neurons. Branch tips of dendrites of inhibitory neurons in mouse visual cortex undergo constant remodeling, supporting the idea that inhibitory neurons, too, are capable of participating in structural plasticity of memory (Lee et al., 2006). Analogous to excitatory neurons, calcium imaging has revealed that inhibitory neurons exhibit neural activity modifications following sensory deprivation (Kameyama et al., 2010).

1.1.4 Primate studies

In human studies, it was Canadian neurosurgeons Wilder Penfield and Theodore Rasmussen who serendipitously obtained the first tantalizing hint that episodic memories may be localized in brain regions (Penfield and Rasmussen, 1950). As a pre-surgery procedure for human patients, Penfield applied small jolts of electricity to the brain to reveal which regions were responsible for inducing seizures. Remarkably, when stimulating parts of the lateral temporal cortex, approximately 8% of his patients reported vivid recall of random episodic memories: one patient exclaimed "Yes, Doctor, yes, Doctor! Now I hear people laughing - my friends in South Africa ... Yes, they are my two cousins, Bessie and Ann Wheliaw." Another patient reported, "I had a dream. I had a book under my arm. I was talking to a man. The man was trying to reassure me not to worry about the book." This study had the first glance at what geneticists call gain-of-function or sufficiency evidence for the notion that the lateral temporal lobe region harbors the biological locus for episodic memory. Complementing this work, a study conducted several years later by the American neurosurgeon William Scoville and Canadian neuropsychologist Brenda Milner provided loss-of-function or necessity evidence (Scoville and Milner, 1957). To treat the epileptic seizures of a young man, Henry Molaison (H.M.), who suffered seizures caused by a bicycle accident, Scoville resected a large portion of the medial temporal lobes (MTL) from both hemispheres, including the hippocampus and adjacent brain areas. As a consequence of this surgery, H.M. lost his ability to form

new episodic memories (anterograde amnesia), as well as the ability to recall memories of episodes and events that occurred in his life within a year prior to this surgery (graded retrograde amnesia). H.M.'s other types of memory, such as motor memory, were largely unaffected, indicating that episodic memories may be specifically processed in the MTL and in particular in the hippocampus. These pioneering studies led to a notion that at least some types of memory, in this case episodic memory, may be stored in a localized brain region. More recent work using single-unit recordings in humans reported that cells in the hippocampus and surrounding areas were reactivated only during free memory recall of a particular individual, landmark (Quiroga et al., 2005), or episode (Gelbard-Sagiv et al., 2008).

Among early attempts to identify memory engrams in monkeys, one study recorded single-cell activity from the inferotemporal (IT) cortex during a visual delayed matching-to-sample task (Fuster and Jervey, 1981). Many cells responded to the colors of the stimuli, and notably, several cells responded differentially to color depending on whether or not attention circuitry were engaged, thus demonstrating their behaviorally relevant role. Fittingly, the authors demonstrated correlations of these neuronal activities to the encoding, retention, and retrieval of visual information. Later, Yasushi Miyashita revealed a neuronal correlate of visual long-term memory by studying how the anterior ventral temporal cortex represented stimulus-stimulus associations (Miyashita, 1988). By simultaneously recording from over 200 neurons as monkeys performed a visual memory task, single neurons that could respond conjointly to temporally related, but geometrically dissimilar stimuli were observed. That is, certain neurons displayed stimulus selectivity during the learning phase of the task, which then could become associated with unrelated stimuli in a different experience. These elegant studies demonstrated a neuronal correlate of associative visual memory. In a more recent series of experiments, using two-photon imaging in macaques to follow the remodeling of intracortical axons after retinal lesions over extended periods of time, it was found that lesions induced an almost immediate increase in the number of axonal boutons as well as axonal collaterals within the affected cortical region (Yamahachi et al., 2009). Thus, presynaptic elements of cortical circuitry are also modified following experience-dependent changes.

1.2 Memory engram theory and engram cell criteria

During the early part of the 20th century, a German scientist, Richard Semon, advocated for the physical theory of human memory (Semon, 1904, 1909). Until the late 1970s, mainstream psychologists studying human memory processing mostly ignored this theory. It was not until three prominent researchers, Daniel Schacter, James Eich, and Endel Tulving, published an influential article that subsequently led to a revival of Semon's contributions within the academic community (Schacter et al., 1978; Tulving, 2002).

The term engram was coined by Semon, which he defined as "the enduring though primarily latent modification in the irritable substance produced by a stimulus (from an experience)" (Semon, 1904). Another term used by several contemporary neuroscientists is memory trace, which is equivalent to engram. Semon's memory engram theory was built on two fundamental postulates termed the Law of Engraphy and the Law of Ecphory, for memory storage and memory retrieval, respectively (Semon, 1909). The Law of Engraphy posits "all simultaneous excitations (derived from experience)...form a connected simultaneous complex of excitations which, as such acts engraphically, that is to say leaves behind it a connected and to that extent, separate unified engram-complex". The Law of Ecphory posits "the partial return of an energetic situation which has fixed itself engraphically acts in an ecphoric sense upon a simultaneous engram complex". A part of the entire experience (i.e., stimuli) at the time of storage needs to be present at the time of recall in order for successful retrieval of the entire original event to occur (Schacter et al., 1978). This criterion essentially describes the process of pattern completion (Marr, 1970), which was experimentally demonstrated many years later (Leutgeb et al., 2004; Nakazawa et al., 2003).

Although Semon's engram theory was remarkably novel at the time, he did not elaborate on the biological basis of a unified engram-complex. During the decades following the proposal of this theory, several molecular, cellular, imaging, and electrophysiological recording techniques have been developed. Incorporating our current knowledge regarding neurons, synapses, and neuronal circuits into Semon's memory engram theory, we propose usage of engram, engram cells, and other associated terminologies in

the contemporary context. Since recent studies have indicated that the engram of a given memory is not restricted to a single anatomical location, but is distributed in multiple locations with specific patterns of connectivity, we introduced three additional terms: engram cell pathway, engram component, and engram complex.

- Engram refers to the enduring physical and/or chemical changes elicited by experience that underlie the newly formed memory association.
- Engram cells are a population of neurons that are activated by learning, exhibit enduring cellular changes as a consequence of learning, and whose reactivation by a part of the original stimuli delivered during learning results in efficient memory recall. Note that this goes beyond a correlational definition of the term.
- Engram cell pathway is a set of engram cells for a given memory connected by synapses along specific neuronal circuits.
- Engram component is the content of an engram stored in an individual engram cell population within the engram cell pathway. Note that this does not necessarily denote the physiological content of the engram held by a given population, but rather indicates the type of represented mnemonic information.
- Engram complex refers to the whole engram for a given memory that is stored in a set of engram cell populations connected by an engram cell pathway.

1.3 Learning-dependent, persistent modifications

Semon's engram theory of memory described experience-dependent changes as, "the enduring though primarily latent modification in the irritable substance produced by a stimulus" (Semon, 1904). The guiding hypothesis regarding the biological nature of engrams was proposed by Canadian psychologist, Donald Hebb. Hebb proposed that neurons encoding memory undergo enduring strengthening of some of their synapses through co-activation with presynaptic cells; neurons that "fire

together wire together" (Hebb, 1949). Since the discovery of long-term potentiation (LTP) by Bliss and Lomo (1973), which was consistent with Hebb's idea, many studies have been dedicated to the characterization of synaptic plasticity, and their potential role in learning and memory. Activity-dependent increases in the size and density of dendritic spines (widely referred to as structural plasticity) have also been proposed as contributing to memory encoding processes (Bailey and Kandel, 1993; Holtmaat et al., 2006; Matsuo et al., 2008; Teule and Segal, 2016). Further, studies have also suggested that cell-wide alterations, such as augmented intrinsic excitability, play a crucial role in memory formation (Daoudal and Debanne, 2003). We will discuss studies in which observed synaptic and/or cellular changes were correlated with a mnemonic behavior.

1.3.1 Synaptic strength

Until recently, the relationship between synaptic/cellular changes and memory was studied by investigating entire brain subregions rather than specific populations of cells activated by a given learning event that hold the specific memory (i.e., memory engram cells). Synaptic plasticity such as LTP can be induced in the hippocampal CA1 region using high-frequency stimulation protocols in vitro, and because this plasticity is dependent on N-methyl-D-aspartate (NMDA) receptors, efforts have been made to test whether this form of synaptic plasticity has an essential role in episodic memory (Malenka and Bear, 2004). Early pharmacological blockade experiments conducted with an NMDA receptor antagonist, AP5, supported the notion that LTP is essential for spatial learning (Morris et al., 1986; Morris, 2006), and the validity of this notion was confirmed with a genetic ablation of the NMDA receptor from the CA1 region of the hippocampus (Bannerman et al., 2012; Tsien et al., 1996).

In a more recent example, researchers have used contextual fear conditioning paradigms with transgenic mice in which the promoter of an IEG, Arc, drives the expression of dVenus, a destabilized version of the fluorescent protein Venus (Eguchi and Yamaguchi, 2009). They found that fear conditioning induced presynaptic potentiation only in the cortical input to the dVenus-positive basolateral

amygdala (BLA) cells (Nonaka et al., 2014), which supports the notion that synaptic plasticity in a subset of BLA neurons contributes to fear memory encoding. Crucially however, this study did not provide evidence that reactivation of dVenus-positive cells could evoke behavioral recall. From a technical standpoint, it is important to note that the temporal window of Arc labeling in this study was uncontrolled. As a result, BLA neurons were labeled indiscriminately for weeks before the targeted behavioral experience. In another recent study, researchers conditioned a rat to associate a foot shock with optogenetic stimulation of auditory inputs to the lateral amygdala (LA) (Nabavi et al., 2014). Optogenetic delivery of long-term depression (LTD)-inducing stimuli (i.e., low-frequency stimulation) to the auditory inputs inactivated the memory of the shock, while subsequent optogenetic LTP (i.e., high-frequency stimulation) to the same auditory inputs reactivated the memory of the shock. The strength of these experiments was that they provided the first causal link between LTP/LTD mechanisms and memory expression. However, this study did not directly demonstrate that these synaptic processes occurred in the same amygdala cell population that was activated by the initial conditioning (i.e., engram-containing cells).

To claim that an observed increase in synaptic strength reflects a component of the learning-dependent physical/chemical changes occurring in engram cells, three criteria must be met. These criteria are: (1) the increase should be observed in a sub-population of cells activated by the specific learning event, (2) the increase should depend on plasticity associated with the learning episode, and (3) reactivation of the sub-population of cells should result in behavioral recall. These criteria have recently been met experimentally by our study, which is thoroughly discussed in Chapter 2. Another recent study demonstrated that c-fos promoter labeled engram cells in CA1 exhibit specific place fields in an environment, commonly referred to as hippocampal place cells (Trouche et al., 2016). Furthermore, optogenetic silencing of CA1 engram cells for the specific environment unmasked a subset of quiet neurons, revealing the emergence of an alternative map.

1.3.2 Structural plasticity

Utilizing in vivo two-photon laser scanning microscopy, hallmarks of structural plasticity such as the formation and elimination of individual dendritic spines has been examined during sensory stimulation and motor tasks. One study showed that training mice in a forelimb-reaching task resulted in rapid (less than 1 hour) formation of postsynaptic dendritic spines on the output pyramidal neurons of the motor cortex (Xu et al., 2009). These learning-induced spines were preferentially stabilized during subsequent training sessions and maintained long after the completion of behavioral tests. Additionally, the authors found that different motor skills were encoded by a different set of synapses. In another study, training on an accelerated rotarod, but not on a slow rotarod, over two days led to an increase in spine formation in the primary motor cortex (Yang et al., 2009). A novel sensory experience provided by switching animals from standard to enriched housing environments resulted in an increase in spine density 1-2 days later in the barrel cortex. These newly formed spines survived experience-dependent elimination during subsequent imaging sessions in the enriched housing environment, reflecting a long-lasting cellular change. These studies strongly suggested that motor behavior is stored in stably connected synaptic networks, but fell short of demonstrating a causal relationship of the altered structural plasticity with motor performance.

Structural plasticity associated with fast-forming tone fear conditioning memory (Matsuo et al., 2008) and its extinction has also been reported (Lai et al., 2012). Matsuo et al., 2008, used c-fos-tTA mice and quantified newly recruited GluR1-positive AMPA receptors in the CA1 sub-region of the hippocampus. The authors observed a selective increase in mushroom-type spines of engram cells 24 hr after learning. A caveat of this study was that non-engram cells were not directly examined, making it difficult to discern whether or not the changes observed were specific to a defined set of cells active only during learning. In the other study, correlations between fear memory expression and spine elimination, or fear memory extinction and spine formation were reported by imaging postsynaptic dendritic spines of layer V pyramidal neurons in the mouse frontal association cortex. Strikingly, dendritic spine elimination and formation induced by fear conditioning and extinction, respectively, occurred on the same dendritic

branches (within a distance of 2 μm) in a cue- and location-specific manner (Lai et al., 2012). Interestingly, reconditioning following extinction eliminated spines formed during extinction, suggesting that within vastly complex neuronal networks, fear conditioning, extinction, and reconditioning lead to opposing changes at the level of individual synapses. Do these spine dynamics reflect what occurs at the level of cell populations that store engrams for tone-shock association memory? Additional research will help answer such questions, which hold great importance for understanding memory formation and retrieval.

An elegant approach to examine the relationship between dendritic spines and memory would be to selectively remove a large number of spines that were specifically formed during learning (Hubener and Bonhoeffer, 2010) and see whether their removal results in memory loss. In a very recent study, such an experimental manipulation was achieved (Hayashi-Takagi et al., 2015). The authors developed a novel synaptic optoprobe, AS-PaRac1 (activated synapse targeting photoactivatable Rac1), which specifically labels recently potentiated spines and can subsequently induce shrinkage of AS-PaRac1-containing spines in vivo. Using this technology during motor learning, it was found that optical shrinkage of potentiated spines disrupted the acquired learned behavior. Importantly, the original motor learning was unaffected by an identical manipulation of spines evoked by a distinct motor task that requires the same cortical brain region.

1.3.3 Cellular excitability

In addition to synaptic plasticity mechanisms as a candidate for enduring physical/chemical changes evoked by learning in memory engram cells, cell-wide excitability alterations have been extensively studied. Many groups have demonstrated that cells in the lateral amygdala can be genetically engineered to exhibit higher levels of cell-wide excitability even prior to learning, by over-expressing a transcription factor CREB. After tone fear conditioning, ablation of these high-CREB, high-excitability cells impaired fear memory expression, suggesting that the memory engram is preferentially allocated to these cells (Yiu et al., 2014; Zhou et al., 2009). Similar high CREB-induced neuronal allocation has been

reported in the hippocampal DG (Park et al., 2016). A more recent study showed that a shared neuronal ensemble is capable of linking distinct contextual memories, only when these two experiences occur close in time during periods of high excitability in hippocampal CA1 (Cai et al., 2016). Similar memory linking during periods of high excitability has been observed for LA engram cells in a tone fear conditioning paradigm (Rashid et al., 2016). Further, novel context exploration during a narrow time window before or after weak object recognition training results in the formation of a long-term object recognition memory (Nomoto et al., 2016). This phenomenon depends on the degree of overlap between the neuronal ensembles for each experience. These studies suggest that excitability-induced memory allocation may serve as a putative mechanism underlying enduring storage of memory information.

1.4 Engram cells found

The studies discussed so far have linked neuronal populations with particular memory events mostly with correlational evidence and only a few with loss-of-function evidence, but a critical piece of evidence was largely missing. The most direct evidence of engram cells should come from gain-of-function manipulations, where a population of neurons activated by learning is artificially reactivated to mimic behavioral recall elicited by natural cues. Crucially, if artificial reactivation of a cell population induces the recall of that specific memory in the absence of retrieval cues, then this would provide evidence that the population of neurons is sufficient for memory, and thus serves as the neuronal basis for the memory engram (Martin and Morris, 2002). However, this type of gain-of-function experiment is technically challenging, as one has to be able to accurately isolate the neurons involved in a single memory from their seemingly indistinguishable neighbors and activate them with high spatial and temporal precision.

Recent advances in technology such as optogenetics make such manipulations feasible (Boyden et al., 2005; Fenno et al., 2011). By combining the activity-dependent, doxycycline-dependent c-fos-tTA system (Reijmers et al., 2007) and channelrhodopsin-2 (ChR2)-mediated optogenetics, researchers were able to tag a sparse population of dentate gyrus (DG) neurons activated by contextual fear conditioning

(CFC) with ChR2 in mice (Liu et al., 2012; Ramirez et al., 2013). Subsequently, when these cells were reactivated by blue light in a context different from the original one used for conditioning, the mouse subjects displayed freezing behavior as evidence of fear memory recall (Liu et al., 2012). Crucially, this optogenetic reactivation of a fear memory was not due to the activation of pre-wired neural circuits. This was demonstrated by disrupting the activity of the downstream CA1 region only during training, and finding that subsequent optogenetic DG engram activation did not elicit memory retrieval (Ryan et al., 2015), which is discussed in detail in Chapter 2. Similarly, memory recall induced by the artificial reactivation of fear memory cells in retrosplenial cortex has been reported (Cowansage et al., 2014). Using this methodology to manipulate engram cells, studies have reported the creation of a context-specific false memory (Ohkawa et al., 2015; Ramirez et al., 2013), the bidirectional switching of the valence associated with a neutral hippocampal contextual memory (Redondo et al., 2014), countering depression-like behavior by the activation of a positive memory (Ramirez et al., 2015), and the association of positive or negative valence information to a social memory engram in ventral CA1 (Okuyama et al., 2016).

Along with these engram reactivation experiments, loss-of-function studies have also been performed using optogenetics. Genetically labeling c-Fos-positive engram cells with the inhibitory optogenetic channel archaerhodopsin (ArchT) (Chow et al., 2010) allowed researchers to reversibly inhibit CA1 engram cells during natural memory recall, which resulted in impaired memory retrieval (Tanaka et al., 2014). Interestingly, this study found that when a specific CA1 engram population that would otherwise be active during the encoding of an overlapping contextual representation was inhibited, the new representation would simply be stored in other CA1 cells instead. Simply put, inhibiting CA1 engram cells inhibits recall of the labeled memory, but does not inhibit acquisition of new memories of similar contextual content (Matsuo, 2015). In a related study, using an activity-dependent system based on an Arc promoter-driven tamoxifen-inducible Cre recombinase, engram cells were labeled in either the dentate gyrus or CA3 of the hippocampus during acquisition of a contextual fear memory, and

subsequently inactivated using optogenetics. This resulted in impaired fear memory recall (Denny et al., 2014).

Further, the c-fos-tTA system combined with a modified receptor, hM3Dq DREADDs (designer receptors exclusively activated by designer drugs), has been employed to activate a contextual engram and subsequently to generate a hybrid memory representation of two experiences (Garner et al., 2012). Another approach that has been successfully used for gain-of-function experiments included taking advantage of CREB overexpression-based neuronal allocation coupled with exogenous receptors. Two studies used CREB to label small populations of lateral amygdala neurons during fear conditioning with another modified receptor TRPV1 or hM3Dq (Kim et al., 2014; Yiu et al., 2014). When these neurons were reactivated in a novel environment using the TRPV1 ligand (capsaicin) or the DREADDs ligand (clozapine N-oxide, CNO), mice showed fear memory recall.

1.5 Storage vs. retrieval debate on amnesia

The phenomenon whereby a newly formed memory transitions from a fragile, short-term state to a stable, long-term state is termed memory consolidation (Muller and Pilzecker, 1900). A crucial feature of consolidation is a finite time window that begins immediately after the learning event, during which a given memory is susceptible to disruption. The biological importance of this time window has been repeatedly demonstrated by interventions ranging from electroconvulsive shock (Duncan, 1949; McGaugh, 1966) to protein synthesis inhibitors (Davis and Squire, 1984; Flexner et al., 1967), which if delivered specifically during the consolidation window results in retrograde amnesia. Therefore, the prevailing view in neuroscience holds that retrograde amnesia due to disrupting consolidation is a deficit of memory storage (McGaugh, 2000; Nader and Wang, 2006; Squire, 2006). However, an alternative interpretation maintains that the memory engram itself remains intact, but access of retrieval mechanisms to the engram has been distorted (Miller and Matzel, 2006; Riccio et al., 2006; Sara, 2000; Squire, 1982). Since purely behavioral studies rely on memory expression as the sole evidence of memory, it has not

been possible for these approaches to rigorously discriminate between storage and retrieval explanations. Due to the fact that the neurobiology of memory formation is anchored in experimental amnesia, discriminating between these two scenarios holds great scientific value. In addition, similar issues have been debated when amnesia is observed following trauma, stress, drug use, or aging. From a clinical perspective, pathological cases of amnesia that are due to retrieval deficits may in principle be treatable rather than merely preventable. Even though efforts are being made to prevent and treat the various causes of amnesia, there remains no treatment for the symptom of memory loss itself.

Historically, several attempts to demonstrate that amnesia after disrupted memory consolidation is due to a deficit of memory retrievability have yielded inconclusive results and theoretical stalemates (Gold et al., 1973; Hardt et al., 2009; Lewis, 1979; Matzel and Miller, 2009; Miller and Springer, 1974; Sara and Hars, 2006; Spear, 1973). Importantly, the existence of a memory engram in retrograde amnesia has been ostensibly supported by studies showing attenuated amnesia by reminder-induced and spontaneous recovery (Miller and Springer, 1972, 1973; Quartermain et al., 1970; Sara, 1973; Serota, 1971; Springer and Miller, 1972). However, these approaches suffer from significant caveats. Reminder treatments have been shown to result in new learning (Gold et al., 1973; Gold and King, 1974), and spontaneous recovery is partial and may be explained by parallel engrams (Squire and Barondes, 1972). Directly examining memory engrams circumvents the ambiguities of reminder training and spontaneous recovery, because it provides an opportunity to directly evoke memory recall in a neutral context. By doing so, the need to rely on stimuli associated with training to elicit memory recall without the use of confounding experimental parameters such as further training is avoided.

Chapter 2. Retrieval of lost memory from retrograde amnesia

Memory consolidation is the process by which a newly formed and unstable memory transforms into a stable long-term memory. It is unknown whether the process of memory consolidation occurs exclusively by the stabilization of memory engrams. By employing learning-dependent cell labeling, we identified an increase of synaptic strength and dendritic spine density specifically in consolidated memory engram cells. While these properties are lacking in the engram cells under protein synthesis inhibitor-induced amnesia, direct optogenetic activation of these cells results in memory retrieval, and this correlates with the retained engram cell-specific connectivity. We propose that a specific pattern of connectivity of engram cells may be crucial for memory information storage and that strengthened synapses in these cells critically contribute to the memory retrieval process.

2.1 Brief introduction

Memory consolidation is the phenomenon whereby a newly formed memory transitions from a fragile state to a stable, long-term state (Duncan, 1949; McGaugh, 2000; Muller and Pilzecker, 1900). The defining feature of consolidation is a finite time window that begins immediately after learning, during which a memory is susceptible to disruption such as protein synthesis inhibition (Davis and Squire, 1984; Flexner et al., 1963, 1967), resulting in retrograde amnesia. The stabilization of synaptic potentiation is the dominant cellular model of memory consolidation (Govindarajan et al., 2011; Kandel, 2001; Kelleher et al., 2004; Takeuchi et al., 2014) because protein synthesis inhibitors disrupt late-phase long-term potentiation of in vitro slice preparations (Frey et al., 1988; Huang et al., 1996; Krug et al., 1984). Although much is known about the cellular mechanisms of memory consolidation it remains unknown whether these processes occur in memory engram cells. It may be possible to characterize cellular consolidation and empirically separate mnemonic properties in retrograde amnesia by directly probing and manipulating memory engram cells in the brain. The term memory engram originally referred to the hypothetical learned information stored in the brain, which must be reactivated for recall (Josselyn, 2010;

Semon, 1904). Recently, several groups demonstrated that specific hippocampal cells that are activated during memory encoding are both sufficient (Gore et al., 2015; Liu et al., 2012; Ramirez et al., 2013; Redondo et al., 2014; Ye et al., 2016) and necessary (Denny et al., 2014; Tanaka et al., 2014) for driving future recall of a contextual fear memory, and thus represent a component of a distributed memory engram (Cowansage et al., 2014). Here, we applied this engram technology to the issue of cellular consolidation and retrograde amnesia.

2.2 Experimental results

We employed the previously established method for tagging the hippocampal dentate gyrus (DG) component of a contextual memory engram with mCherry (see Experimental methods, Fig. S1, and (Liu et al., 2012; Reijmers et al., 2007)). To disrupt consolidation we systemically injected the protein synthesis inhibitor anisomycin (ANI) or saline (SAL) as a control immediately after contextual fear conditioning (CFC) (Fig. 1A). The presynaptic neurons of the entorhinal cortex (EC) were constitutively labeled with ChR2 expressed from an AAV_8-CaMKIIα-ChR2-EYFP virus (Fig. 1B). Voltage clamp recordings of paired engram ($mCherry^+$) and non-engram ($mCherry^-$) DG cells were conducted simultaneously with optogenetic stimulation of $ChR2^+$ perforant path (PP) axons (Fig. 1C, D). $mCherry^+$ cells of the SAL group showed significantly greater synaptic strength than $mCherry^+$ cells of the ANI engram group, but the $mCherry^-$ cells of the SAL and ANI groups were of comparable synaptic strength (Fig. 1E). Calculation of AMPA/NMDA current ratios (Clem and Huganir, 2010) showed that at 24 hours post-training, $mCherry^+$ engram cells displayed potentiated synapses relative to paired $mCherry^-$ non-engram cells in the SAL group (Fig. 1E). However, no such difference between $mCherry^+$ and $mCherry^-$ was observed in the ANI group. In addition, $mCherry^+$ engram cells of the SAL group showed significantly greater AMPA/NMDA current ratios than $mCherry^+$ engram cells of the ANI group. Analysis of miniature EPSCs of engram and non-engram cells of both SAL and ANI groups showed the same pattern (Fig. S2).

We also quantified dendritic spine density for DG engram cells labeled with an AAV_9-TRE-ChR2-EYFP virus. Spine density of $ChR2^+$ cells was significantly higher than corresponding $ChR2^-$ cells in the SAL group (Fig. 1F, Fig. S3), but spine densities of $ChR2^+$ and $ChR2^-$ cells of the ANI group were similar (see Experimental methods). Spine density of $ChR2^+$ cells of the SAL group was significantly higher than that of ANI $ChR2^+$ cells (Fig.1F), but $ChR2^-$ cells were comparable. This result was confirmed by analysis of the membrane capacitance (Fig. S4G). ChR2 expression did not affect intrinsic properties of DG cells in vitro (Fig. S5A-E). Direct bath application of ANI did not affect intrinsic cellular properties in vitro (Fig. S5F), although it mildly reduced synaptic currents acutely (Fig. S5G-I). Importantly, when anisomycin was injected into c-fos-tTA animals 24 hours post-CFC and engram labeling, engram-cell specific increases in dendritc spine density and synaptic strength were undisturbed (Fig. S6). We also examined engram cells labeled by a context-only experience (Ramirez et al., 2013), and found equivalent engram-cell increases in spine density and synaptic strength (Fig. S7) as those labeled by CFC.

DG cells receive information from EC and relay it to area CA3 via the mossy fibers. We labeled DG engram cells using an AAV_9-TRE-ChR2-EYFP virus and simultaneously labeled CA3 engram cells using an AAV_9-TRE-mCherry virus (Fig. 1G). Connection probability was assessed 24 hours post-CFC by stimulating DG $ChR2^+$ cell terminals optogenetically and recording excitatory postsynaptic potentials in CA3 $mCherry^+$ and $mCherry^-$ cells in ex vivo preparations. CA3 $mCherry^+$ engram cells showed a significantly higher probability of connection than $mCherry^-$ cells with DG $ChR2^+$ engram cells, demonstrating preferential engram cell to engram cell connectivity. Importantly, this form of engram pathway-specific connectivity was unaffected by post-training administration of ANI (Fig. 1G).

We next tested the behavioral effect of optogenetically stimulating engram cells in amnesic mice (Fig 2A). During CFC training in Context B, both SAL and ANI groups responded to the unconditioned stimuli at equivalent levels (Fig. S8). One day post-training, the SAL group displayed robust freezing behavior to the conditioned stimulus of context B, whereas the ANI group showed substantially less freezing behavior (Fig. 2C). Two days post-training, mice were placed into the distinct context A for a 12

min test session consisting of four 3 min epochs of blue light on or off. During this test session, neither group showed freezing behavior during Light-Off epochs, but both froze significantly during Light-On epochs (Fig. 2D). Remarkably, no difference in the levels of light-induced freezing behavior was observed between groups. Three days post-training, the mice were again tested in context B to assay the conditioned response, and retrograde amnesia for the conditioning context was still clearly evident (Fig. 2E). Subjects treated with SAL or ANI following the labeling of a neutral contextual engram (i.e., no shock) did not show freezing behavior in response to light stimulation of engram cells (Fig. 2D). We replicated the DG retrograde amnesia experiment using an alternative widely-used protein synthesis inhibitor, cycloheximide (CHM) (Fig. S9). We examined whether ANI administration immediately after CFC altered the activity dependent synthesis of ChR2-EYFP in DG cells and found that this was not the case (Fig. 2F-H). Nevertheless, the dosage of anisomycin used in this study did inhibit protein synthesis in the DG as shown by Arc^{+} cell counting (Fig. S10). Thus, the dosage of ANI used was sufficient to induce amnesia, but was insufficient to impair c-fos-tTA driven synthesis of virally delivered ChR2-EYFP in DG cells. Extracellular recordings from SAL and ANI-treated mice confirmed the cell counting results (Fig. 2I-K). In line with Fig. S6 and previous reports (Suzuki et al., 2004), anisomycin injection 24 hours post-CFC did not cause retrograde amnesia (Fig. S11). To provide a negative control for light-induced memory retrieval in amnesia, we disrupted memory encoding by activating hM4Di DREADDs receptors (Armbruster et al., 2007) downstream of the DG, in hippocampal CA1, during CFC, and found that subsequent DG engram activation did not elicit memory retrieval (Fig. S12).

The recovery from amnesia by direct light activation of ANI-treated DG engram cells was unexpected because these cells showed neither synaptic potentiation nor increased dendritic spine density. We conducted additional behavioral experiments to confirm and characterize the phenomenon. First, we investigated whether recovery from amnesia can be demonstrated by light-induced optogenetic place avoidance test (OptoPA); this would be a measure of an active fear memory recall (see Experimental methods and (Redondo et al., 2014)), rather than a passive fear response monitored by freezing. SAL and ANI groups displayed equivalent levels of avoidance of the target zone in response to light activation of

the DG engram (Fig. 3A). Second, in our previous study we showed that an application of the standard protocol (i.e., 20 Hz) for activation of the CA1 engram was not effective for memory recall (Ramirez et al., 2013). However, we found that a 4 Hz protocol applied to the CA1 engram of the SAL and ANI groups elicited similar recovery from amnesia (Fig. 3B). Third, we employed tone fear conditioning (TFC) and manipulated the fear engram in lateral amygdala (LA) (Han et al., 2009) and found light-induced recovery of memory from amnesia. Fourth, we asked whether amnesia caused by disruption of reconsolidation of a contextual fear memory (Misanin et al., 1968; Nader et al., 2000a, 2000b) can also be recovered by light-activation of DG engram cells, and indeed it was found to be the case (Fig. 3D). We applied the memory inception method (Experimental methods, (Liu et al., 2014; Ramirez et al., 2013) to DG engram cells and found that both SAL and ANI groups showed freezing behavior that was specific to the original Context A, demonstrating that light-activated Context A engrams formed in the presence of ANI can function as a CS in a context-specific manner (Fig. 3E). Lastly, we tested the longevity of CFC amnesic engrams for memory recovery by light activation, and found that indeed memory recall could be observed 8 days post-training (Fig. S13).

Interactions between the hippocampus and amygdala are crucial for contextual fear memory encoding and retrieval (Redondo et al., 2014). c-Fos expression increases in the hippocampus and amygdala upon exposure of an animal to conditioned stimuli (Besnard et al., 2014; Hall et al., 2001). These previous observations open up the possibility of obtaining cellular level evidence supporting the behavioral level finding that the recovery from amnesia can be accomplished by direct light activation of ANI-treated DG engram cells. Thus, we compared the effects of natural recall and light-induced recall on amygdala c-Fos$^+$ cell counts in amnesic mice (Fig. 4A-C). c-Fos$^+$ cell counts (Fig. 4B) were significantly lower in basolateral amygdala (BLA) and central amygdala (CeA) of ANI-treated mice compared to SAL mice when natural recall cues were delivered, showing that amygdala activity correlates with fear memory expression (Fig. 4C). In contrast, light-induced activation of the contextual engram cells resulted in equivalent amygdala c-Fos$^+$ counts in SAL and ANI groups (Fig. 4C), supporting the optogenetic behavioral data.

Next, we modified this protocol to include labeling of CA3 and BLA engram cells with mCherry and examined the effects of light-induced activation of DG engram cells on the overlap of mCherry$^+$ engram cells and c-Fos$^+$ recall-activated cells in CA3 and BLA (Fig. 4D). The purpose of this experiment was to investigate whether there is preferential connectivity between the upstream engram cells in DG and the downstream engram cells in CA3 or BLA. Natural recall cues resulted in above chance c-Fos$^+$/mCherry$^+$ overlap in both CA3 and BLA, supporting the physiological connectivity data (Fig. 4E-K). c-Fos$^+$/mCherry$^+$ overlap was significantly reduced in the ANI group compared to the SAL group, but was still higher than chance levels, presumably reflecting incomplete amnesic effects of anisomycin (Fig. 4K). Importantly, light-activation of DG engram cells resulted in equivalent c-Fos$^+$/mCherry overlap as natural cue-induced recall, and this was unaffected by post-CFC anisomycin treatment. These data suggest that there is preferential and protein synthesis-independent functional connectivity between DG and CA3 engram cells, supporting the physiological data (Fig. 1G), and that this connectivity also applies between DG and BLA engram cells.

2.3 Discussion

We previously showed that DG cells activated during CFC training and labeled with ChR2 via the promoter of an immediate early gene (IEG) can evoke a freezing response when they are reactivated optogenetically one to two days later (Liu et al., 2012), and this has since been achieved in the cortex (Cowansage et al., 2014). We have also shown that these DG cells, if light-activated while receiving a US, can serve as a surrogate context-specific CS to create a false CS-US association (Ramirez et al., 2013; Redondo et al., 2014), and that activation of DG or amygdala engram cells can induce place preference (Redondo et al., 2014). Furthermore, recent studies showed that optogenetic inhibition of these cells in DG, CA3, or CA1 impairs expression of a CFC memory (Denny et al., 2014; Tanaka et al., 2014). Together, these findings show that engram cells activated by CFC training are both sufficient and necessary to evoke memory recall, satisfying two crucial attributes in defining a component of a

contextual fear memory engram (Josselyn, 2010). What has been left to be demonstrated, however, is that these DG cells undergo enduring physical changes as an experience is encoded and its memory is consolidated. Although synaptic potentiation has long been suspected as a fundamental mechanism for memory and as a crucial component of the enduring physical changes induced by experience, this has not been directly demonstrated, until the current study, as a property of the engram cells. Our data have directly linked the optogenetically and behaviorally defined memory engram cells to synaptic plasticity.

Based on a large volume of previous studies, (Duncan, 1949; Johansen et al., 2011; Kandel, 2001; Kelleher et al., 2004; McGaugh, 1966, 2000; Muller and Pilzecker, 1900), a concept has emerged where retrograde amnesia arises from consolidation failure as a result of disrupting the process that converts a fragile memory engram, formed during the encoding phase, into a stable engram with persistently augmented synaptic strength and spine density. Indeed, our current study has demonstrated that amnesic engram cells in the DG one day after CFC training display low levels of synaptic strength and spine density that are indistinguishable from non-engram cells of the same DG. This correlated with a lack of memory recall elicited by contextual cues. Intriguingly, however, direct activation of DG engram cells of the ANI group elicited as much freezing behavior as the activation of these cells of the SAL group. This unexpected finding is supported by a set of additional cellular and behavioral experiments. While amygdala engram cell reactivation upon exposure to the conditioned context is significantly lower in the ANI group compared to the SAL group, optogenetic activation of DG engram cells results in normal reactivation of downstream CA3 and BLA engram cells (Fig. 4). At the behavioral level, the amnesia rescue was observed under a variety of different conditions in which one or more parameters were altered (Fig. 2-3, Fig. S9, and Fig. S13). Thus, our overall findings indicate that memory engrams survive a post-training administration of protein synthesis inhibitors during the consolidation window and that the memory remains retrievable by ChR2-mediated direct engram activation even after retrograde amnesia is induced. The drive initiated with light-activation of one component of a distributed memory engram (like that in the DG) is sufficient to reactivate engrams in downstream regions (like that in CA3 and BLA) that would also be affected by the systemic injection of a protein synthesis inhibitor (ANI).

Our findings suggest that while a rapid increase of synaptic strength is likely to be crucial during the encoding phase, the augmented synaptic strength is not a crucial component of the stored memory (Chen et al., 2014; Miller and Matzel, 2006; Miller and Sweatt, 2006). This notion is consistent with a recent study showing that an artificial memory could be reversibly disrupted by depression of synaptic strength (Nabavi et al., 2014). On the other hand, persistent and specific connectivity of engram cells which we find between DG engram cells and downstream CA3 or BLA engram cells in both SAL and ANI groups may represent a fundamental mechanism of memory information storage (Hebb, 1949). These findings also suggest that the primary role of augmented synaptic strength during and after the consolidation phase may be to provide natural recall cues with efficient access to the soma of engram cells for their reactivation and, hence, recall.

The integrative memory engram-based approach employed here for parsing memory and amnesia into encoding, consolidation, and retrieval aspects may be of wider use to other experimental and clinical cases of amnesia, such as Alzheimer's disease (Daumas et al., 2008).

2.4 Experimental methods

Subjects

All experiments were conducted in accordance with U.S. National Institutes of Health guidelines and the Massachusetts Institute of Technology Department of Comparative Medicine and Committee of Animal Care. c-fos-tTA transgenic mice were generated as described in (Liu et al., 2012), by breeding TetTag mice (Reijmers et al., 2007) with C57BL/6J mice and selecting offspring carrying only the c-fos-tTA transgene. Mice had access to food and water ad libitum and were socially housed in numbers of two to five littermates until surgery. Following surgery, mice were singly housed. For behavioral experiments, all mice used for the experiments were male and 7–9 weeks old at the time of surgery and had been raised on food containing 40 mg kg^{-1} doxycycline (DOX) for at least one week before surgery, and remained on

DOX food for the remainder of the experiments except for the target engram labeling days. For ex vivo electrophysiology experiments, mice were 24-28 days old at the time of surgery.

Engram labeling strategy

In order to label memory engram cells, we employed adeno-associated viruses that express either mCherry alone or ChR2 fused to an EYFP/mCherry fluorophore under the control of a tetracycline-responsive element (TRE)-containing promoter (AAV_9-TRE-mCherry, AAV_9-TRE-ChR2-EYFP, or AAV_9-TRE-ChR2-mCherry), which are active in cells that contain the tetracycline transactivator (tTA) (Liu et al., 2012). For each engram experiment, we injected one of these viruses into the target brain region of c-fos-tTA transgenic mice, which express tTA under the control of a c-fos promoter (Fig. S1A) (Reijmers et al., 2007). Because c-fos is an activity-dependent gene, the c-fos-tTA transgene selectively expresses tTA in active cells (Fig. S1B). Thus, active cells can express tTA that will then induce the virus to express mCherry or ChR2 in those cells. In order to restrict activity-dependent labeling to targeted training episodes the mice were fed DOX food, which sequesters tTA function and prevents virus expression. Subjects were then taken Off DOX one day prior to training in order to permit the labeling of memory engram cells (Fig. S1C, D, E). Shining 473 nm blue light on a ChR2 positive neuron causes the opening of ChR2 channels, and the rapid influx of cations results in the depolarization of the neuron (Boyden et al., 2005). Therefore, by shining blue light onto ChR2-labeled engram cells, memory recall can be directly evoked (Liu et al., 2012). Patch-clamp recordings in vitro confirmed that light successfully activated ChR2-labeled DG cells following contextual fear conditioning (CFC) (Fig. S1F, G).

Virus-mediated gene expression

The recombinant AAV vectors used for viral production were pAAV-TRE-ChR2-EYFP described in (1), pAAV-TRE-ChR2-mCherry and pAAV-TRE-mCherry described in (Ramirez et al., 2013). The pAAV-hSyn1-HA-hM4Di-IRES-mCitrine plasmid was acquired from Bryan Roth at the University of North Carolina. The pAAV-CaMKIIα-ChR2-EYFP plasmid was acquired from Addgene. Plasmids were

serotyped with AAV_8 or AAV_9 coat proteins and packaged at the University of Massachusetts Medical School Gene Therapy Center and Vector Core. The recombinant AAV vectors were injected with viral titers of 1 X 10^{13} genome copy (GC) ml^{-1} for AAV_9-TRE-ChR2-EYFP, 8.0 × 10^{12} GC ml^{-1} for AAV_9-TRE-ChR2-mCherry, 1.4 X 10^{13} GC ml^{-1} for AAV_9-TRE- mCherry, 3.3 X 10^{12} GC ml^{-1} for AAV_9-hSyn1-HA-hM4Di-IRES-mCitrine, and 8.0 X 10^{12} GC ml^{-1} for AAV_8-CaMKIIα-ChR2-EYFP.

Stereotactic surgery procedure

Mice were anesthetized using 500 mg kg^{-1} avertin, or isoflurane. Bilateral craniotomies were performed using a 0.5 mm diameter drill and the viruses were injected using a glass micropipette attached to a 10 ml Hamilton microsyringe (701LT; Hamilton) through a microelectrode holder (MPH6S; WPI) filled with mineral oil. A microsyringe pump (UMP3; WPI) and its controller (Micro4; WPI) were used to maintain the speed of the injection at 60 nl min^{-1}. The needle was slowly lowered to the target site and remained for 5 min before beginning the injection. After the injection, the needle stayed for 10 minutes before it was slowly withdrawn. After withdrawing of the needle, a custom implant containing two optic fibers (200 mm core diameter; Doric Lenses) was lowered above the injection site. Two jewelry screws were screwed into the skull on either side of bregma. A layer of adhesive cement (C&B Metabond) was applied followed with dental cement (Teets cold cure; A-M Systems) to secure the optic implant. A cap derived from the top part of an Eppendorf tube was inserted to protect the implant. Mice were given 1.5 mg kg^{-1} metacam as analgesic and remained on a heating pad until fully recovered from anesthesia. Mice were allowed to recover for at least 2 weeks before all subsequent behavioral experiments.

Ex vivo patch clamp recording

Stereotactic surgery

For AMPA/NMDA ratio experiments (Fig. 1A-E), entorhinal cortex (EC) injections of AAV_8-CaMKIIα-ChR2-EYFP (500 nl) were targeted unilaterally to (-4.7 mm anteroposterior (AP), +3.35 mm mediolateral (ML), - 3.3 mm dorsoventral (DV)), and dentate gyrus (DG) injections of AAV_9-TRE-mCherry (300 nl)

were targeted unilaterally to (-2.0 mm AP, +1.3 mm ML, –1.9 mm DV). For experiments involving spine counting (Fig. 1F, Fig. S6, and Fig. S7) and intrinsic physiological properties (Fig. S4, Fig. S6, and Fig. S7), injections of AAV_9-TRE-ChR2-EYFP (300 nl) were targeted unilaterally to (-2.0 mm AP, +1.3 mm ML, –1.9 mm DV). For Fig. S4, DG injections of AAV_8-CaMKIIα-ChR2-EYFP (300 nl) were targeted unilaterally to (-2.0 mm AP, +1.3 mm ML, –1.9 mm DV). For DG-CA3 connectivity experiments (Fig. 1G), DG injections of AAV_9-TRE-ChR2-EYFP (100 nl) were targeted unilaterally to (-2.0 mm AP, +1.3 mm ML, –1.9) mm DV, and CA3 injections of AAV_9-TRE-mCherry (150 nl) were targeted unilaterally to (-2.0 mm AP, +2.3 mm ML, –2.2 mm DV).

Animals and slice preparation

All ex vivo experiments were conducted blind to experimental group. Researcher 1 trained the animals and administered drug, while Researcher 2 dispatched the animals and conducted physiological experiments. Mice (P30-P40) were anesthetized with isoflurane, decapitated and brains were quickly removed. Sagittal slices (300 μm thick) were prepared in an oxygenated cutting solution at ~4°C by using a vibratome (VT1000S, Leica). Slices were then incubated at room temperature (~23°C) in oxygenated ACSF until the recordings. The cutting solution contained (in mM): 3 KCl, 0.5 $CaCl_2$, 10 $MgCl_2$, 25 $NaHCO_3$, 1.2 NaH_2PO_4, 10 D-glucose, 230 sucrose, saturated with 95%O_2 - 5%CO_2 (pH 7.3, osmolarity 340 mOsm). The ACSF contained (in mM): 124 NaCl, 3 KCl, 2 $CaCl_2$, 1.3 $MgSO_4$, 25 $NaHCO_3$, 1.2 NaH_2PO_4, 10 D-glucose, saturated with 95%O_2 - 5% CO_2 (pH 7.3, osmolarity 300 mOsm). Individual slices were transferred into a submerged experimental chamber and perfused with oxygenated ACSF warmed at 35°C (±0.5°C) at a rate of 3 ml/min during recordings.

Electrophysiology

Whole cell recordings in current clamp or voltage clamp mode were performed by using an IR-DIC microscope (BX51, Olympus) with a water immersion 40X objective (N.A. 0.8), equipped with four automatic manipulators (Luigs & Neumann) and a CCD camera (Orca R2, Hamamatsu Co). For all the

recordings, borosilicate glass pipettes were fabricated (P97, Sutter Instrument) with resistances of 8 to 10 MΩ. For current clamp recordings, pipettes were filled with the following intracellular solution (in mM): 110 K-gluconate, 10 KCl, 10 HEPES, 4 ATP, 0.3 GTP, 10 phosphocreatine and 0.5% biocytin. The osmolarity of this intracellular solution was 290 mOsm and the pH was 7.25. The AMPA/NMDA ratio measurements were performed by adding 10 μM gabazine (Tocris) in the extracellular solution, and recordings in voltage clamp were performed by using the following intracellular solution (in mM): 117 cesium methansulfonate, 20 HEPES, 0.4 EGTA, 2.8 NaCl, 5 TEA-Cl, 4 Mg-ATP, 0.3 Na-GTP, 10 QX314, 0.1 spermine and 0.5% biocytin. The osmolarity of this intracellular solution was 290 mOsm and the pH was 7.3. Recordings were amplified using up to two dual channel amplifiers (Multiclamp 700B, Molecular Devices), filtered at 2 kHz, digitized (20 kHz), and acquired through an ADC/DAC data acquisition unit (ITC1600, Instrutech) by using custom made software running on Igor Pro (Wavemetrics). Access resistance (RA) was monitored throughout the duration of the experiment and data acquisition was suspended whenever the resting membrane potential was depolarized above -50 mV or the RA was beyond 20 MΩ. All drugs used (Gabazine, NBQX, AP5, ANI) were provided by Tocris.

Optogenetics

Optogenetic stimulation was achieved through a 460 nm LED light source (XLED1, Lumen Dynamics) driven by TTL input with a delay onset of 25 μs (subtracted off-line for the estimation of latencies). Light power on the sample was 33 mW/mm^2. To test ChR2 expression, slices were stimulated with a single light pulse of 1 s, repeated 10 times every 5 s. To test synaptic connections, slices were stimulated with single light pulses of 2 ms, repeated 20 times every 5 s. In voltage clamp mode, cells were held at -70 mV, while in current clamp mode, response to optogenetic stimulation was measured at resting potential. DG-CA3 connectivity (Fig. 1G) was tested in current clamp mode, holding the cell at -70 mV. A train of 15 pulses at 20 Hz was delivered 20 times every 5 s and the average response was computed. The glutamatergic nature of the connection was confirmed by bath application of 10 μM NBQX (N = 4). The effect of ANI treatment on CA3 engram cells was evident from the measurement of the membrane

capacitance (SAL: $mCherry^-$ 89.5 ± 7 pF, $mCherry^+$ 115 ± 9 pF, unpaired t test $P < 0.05$; ANI: $mCherry^-$ 103 ± 14 pF, $mCherry^+$ 95 ± 15 pF, unpaired t test $P = 0.7$).

Analysis

Synaptic connections, in voltage or current clamp mode, were determined by averaging 20 trials. EPSC amplitude was measured from the average maximum peak response by subtracting a baseline obtained 5 ms before light pulse starts (Fig. 1A-E). AMPA/NMDA ratios were measured in voltage clamp mode holding the voltage at -70 mV for AMPA current amplitude and holding the voltage at +40 mV for NMDA current amplitude measurement. The amplitude of the NMDA current was measured 100 ms after the onset of the light to avoid AMPA current overlap. The probability of DG-CA3 connectivity (Fig. 1G) was computed as, P = (successful tests/total test number). Error bars are approximated by binomial distribution. Spontaneous EPSCs (EPSCs) (Fig. S2) were recorded at a holding potential of -70 mV in presence of Gabazine (10 μM). EPSCs were detected using an Igor Pro routine and were defined as inward currents with amplitudes exceeding two times the standard deviation of the baseline noise. Granule cells expressing ChR2-EYFP, which in current clamp mode (at resting potential) responded to optogenetic stimulation with at least one action potential were considered engram cells and were selected for the analysis. The intrinsic electrophysiological properties (Fig. S4) were measured in current clamp mode, holding the cell at –70 mV. Resting membrane potential was measured in current clamp mode without current injection. Action potential threshold was tested with a current ramp injection. Input resistance was measured by injecting a negative -120 pA current lasting 1 s. Membrane time constant was estimated through single exponential fit of the recovery-time from a –10 mV voltage deflection of 1 s duration. Excitability was estimated by linear fit of current (I) vs. firing rate (F) relationship.

Statistics

Statistical analysis was performed using Igor (Wavemetrics), MATLAB (Math works) or Excel (Microsoft). The distribution of the data was tested with the Kolmogorov-Smirnov test. A two sample

Kolmogorov-Smirnov test, a Wilcoxon signed-rank test, a two-tailed paired or unpaired t test was employed for comparisons according to the application. Data are presented as mean ± SEM. To test significance of the connection probability, a Fisher's exact test was employed.

Post hoc immunocytochemistry

Recorded cells were filled with biocytin and subsequently recovered for morphological identification. Slices were first incubated with 4% PFA for 16 hr at 4°C. After washing with 0.5% Triton-X, slices were incubated in 5% normal goat serum (NGS) for 2 hr. Following NGS, slices were incubated in primary antibody (rabbit anti-RFP, 1:1000) overnight at 4°C. After washing with 0.5% Triton-X, slices were visualized by streptavidin CF633 (1:200, Biotium) and anti-rabbit Alexa-555. Before mounting, slices were incubated with DAPI (1:3000) for 30 min.

Spine density analysis

Experiments were conducted blind to experimental group. Researcher 1 imaged dendritic fragments, while Researcher 2 randomized images in advance of manual spine counting. Dentate granule cells were labeled with biocytin during patch clamp recordings. Fluorescence Z-stacks were taken by confocal microscopy (Zeiss LSM700), using 40 X objectives. Z-projected confocal images were generated by Zenblack (Zeiss). A total number of 16 granule cells were analyzed for spine examination (n = 4 cells per group x n = 4 groups). We analyzed 10 dendritic fragments of 10 μm length for each cell. To compute the spine density, the number of spines counted on each fragment was normalized by the cylindrical approximation of the surface of the specific fragment (Fig. 1F). The same applies for Fig. S6, and Fig. S7.

In vivo multi-unit electrophysiological recording

Using an anesthetized setup, multi-unit responses to optogenetic (ChR2) stimulation were recorded from c-fos-tTA mice injected with AAV_9-TRE-ChR2-EYFP virus in the DG. Mice were anesthetized by injection (10 ml kg^{-1}) of a mixture of ketamine (100 mg ml^{-1})/xylazine (20 mg ml^{-1}) and placed in the

stereotactic system. Anesthesia was maintained by a series of booster doses of ketamine (100 mg kg^{-1}). An optrode consisting of a tungsten electrode (0.5 MΩ) attached to an optic fiber (200 μm core diameter), with the tip of the electrode extending beyond the tip of the fiber by 300 μm, was used for simultaneous optical stimulation and extracellular recording. The power intensity of light emitted from the optrode was calibrated to about 10 mW, which was consistent with the power intensity used in behavioral assays. To identify ChR2-positive cells, 15 ms light pulses at 0.2 Hz were delivered to the recording site every 50-70 μm. After light-responsive cells were detected, multi-unit activity in response to trains of 10 light pulses (15 ms) at 20 Hz was recorded. Activity was acquired using an Axon CNS Digidata 1440A system and analyzed using MATLAB, described in (Ramirez et al., 2013).

Behavior

Stereotactic injection and optic fiber implant

DG injections were targeted bilaterally to (-2.0 mm AP, +/- 1.3 mm ML, –1.9 mm DV). DG implants were placed at (-2.0 mm AP, +/- 1.3 mm ML, –1.9 mm DV). CA1 injections were targeted bilaterally to (-2.0 mm AP, +/- 1.5 mm ML, –1.5 mm DV). CA1 implants were placed at (-2.0 mm AP, +/- 1.5 mm ML, –1.4 mm DV). LA injections were targeted bilaterally to (-1.7 mm AP, +/- 3.45 mm ML, –4.2 mm DV). LA implants were placed at (-1.7 mm AP, +/- 3.45 mm ML, –4.0 mm DV). AAV_9-TRE-ChR2-EYFP volumes were 300 nl for DG and 500 nl for CA1. AAV_9-TRE-ChR2-mCherry volumes were 300 nl for DG and 200 nl for LA. AAV_9-hSyn1-HA-hM4Di-IRES-mCitrine volume was 500 nl for CA1. All injection sites were verified histologically. As criteria we only included mice with ChR2-EYFP or ChR2-mCherry expression limited to the targeted regions.

Optogenetics

For all DG and LA behavioral experiments, ChR2 was stimulated using a 473 nm laser delivering blue light at 20 Hz with a 15 ms pulse width, for the designated time period (Liu et al., 2012). For the CA1

experiment, 20 Hz proved ineffective (Ramirez et al., 2013), so here our stimulation protocol was adjusted to 4 Hz with a 15 ms pulse width.

Drug delivery

For consolidation experiments, 150 mg kg^{-1} anisomycin (ANI), or equivalent volume of saline (SAL), was delivered intra-peritoneally immediately after fear conditioning in the anteroom of the training context. For the ANI reconsolidation experiment, a second 150 mg kg^{-1} ANI dose was delivered 2 hours post-reactivation. For the cycloheximide (CHM) consolidation experiment 3 mg kg^{-1} CHM, or equivalent SAL, was delivered subcutaneously immediately after fear conditioning in the anteroom of the training context. For encoding experiments, 5 mg kg^{-1} clozapine-N-oxide (CNO) or SAL was delivered intra-peritoneally one hour before training, in the holding room.

Handling

All the behavioral experiments were conducted using mice that were 10 to 18 weeks of age, during the facility light cycle of the day (6.30 am to 6.30 pm). All behavioral subjects were individually habituated to handling by the investigator by handling for one minute on each of three separate days. Handling took place in the holding room where the mice were housed. Immediately prior to each handling session mice were transported by wheeled cart to and from the vicinity of the experimental context rooms, to habituate them to the journey.

Contextual Fear Conditioning – Consolidation (Figures 2A, 3B, 4A, S9, and S13)

Apparatus

For CFC experiments, two distinct contexts were employed, and used in different rooms. Context A chambers were 30 X 25 X 33 cm chambers with perspex floors, transparent square ceilings, red lighting, and scented with 0.25 % benzaldehyde. The ceilings of the Context A chambers were customized to hold a rotary joint (Doric Lenses) the exterior side of which was connected to a patch cord to a 473 nm laser

that was controlled by a pulse generator. The interior side of the rotary joint was connected to two 0.32 M patch cords. All mice had patch cords fitted to the fiber implant prior to being placed in Context A. Two mice were run simultaneously in two identical Context A chambers. Context B chambers were 29 X 25 X 22 cm chambers with grid floors, opaque triangular ceilings, bright white lighting, and scented with 1 % acetic acid. Four mice were run simultaneously in four identical Context B chambers. All experimental groups were counter-balanced for chamber within contexts. All mice were conditioned in Context B, and tested in Contexts A and B. Experiments showed no generalization of conditioned response between contexts. Floors of chambers were cleaned with Quatricide before and between runs. Mice were transported to and from the experimental room in their home cages using a wheeled cart. The cart and cages remained in an anteroom to the experimental rooms during all behavioral experiments.

Habituation

Four days prior to conditioning, all mice were habituated to Context A. Habituation sessions were 12 min in duration, consisting of four 3 min epochs, with the first and third epochs as the Light-Off epochs, and the second and fourth epochs as the Light-On epochs. During the Light-On epochs, the mouse received light stimulation (20 mW, 20 Hz, 15 ms) for the entire 3 min duration. At the end of 12 min, the mouse was immediately detached from the patch cords, returned to its home cage, and carted back to the holding room.

Training

Mice were trained in Context B using a CFC paradigm. Training sessions were 330 s in duration, and three 0.75 mA shocks of 2 s duration were delivered at 150 s, 210 s, and 270 s. SAL or ANI was delivered immediately after training. After fear conditioning, mice were placed in their home cages, and carted back to the holding room. Mice were kept on regular food without DOX for 24-30 hours prior to training. When training was complete, mice were switched back to food containing 40 mg kg^{-1} DOX.

Testing

All testing sessions in Context B were 180 s in duration. Testing conditions were identical to training conditioning, except that no shocks were presented. At the end of each session mice were placed in their home cages and carted back to the holding room. All testing sessions in Context A were 12 min in duration, and were identical to the habituation sessions, consisting of four 3 min epochs, with the first and third epochs as the Light-Off epochs, and the second and fourth epochs as the Light-On epochs. During the Light-On epochs, the mouse received light stimulation (20 Hz for DG and LA, or 4 Hz for CA1) for the entire 3 min duration. At the end of 12 min, the mouse was immediately detached from the patch cords, returned to its home cage and carted back to the holding room.

Optogenetic Place Avoidance (OptoPA) - (Figure 3A)

Apparatus

Each OptoPA apparatus consisted of two distinct 15 × 15 × 20 cm zones (X and Y) connected to a triangular neutral zone as described in (Redondo et al., 2014). Zone X consisted of black and white striped walls and contained a transparent floor with small irregular indentations. Zone Y consisted of black and white alternating dotted walls and contained a smooth plastic floor. The wall of the neutral zone was customized to hold a rotary joint (Doric Lenses) the exterior side of which was connected to a patch cord to a 473 nm laser that was controlled by a pulse generator. The interior side of the rotary joint was connected to two 0.5 M patch cords. All mice had patch cords fitted to the fiber implant prior to being placed in the apparatus. Two mice were run simultaneously in two identical OptoPA apparatuses. Training contexts were 29 X 25 X 22 cm chambers with grid floors, opaque triangular ceilings, red lighting, and scented with 1 % acetic acid. Four mice were run simultaneously in four identical chambers. All experimental groups were counter-balanced for chamber within contexts.

Habituation

All mice were habituated to the OptoPA apparatus and laser stimulation procedure 4 days prior to training (taken from (Redondo et al., 2014)). Mice were allowed to freely explore both zones X and Y during the 0–3 min baseline epoch, and the naturally preferred zone was determined as the target zone. During the 3–6 min and 9–12 min epochs (Light-On phases), light was administered only when a mouse was within the target zone. At the end of the 12 min, the mouse was immediately detached from the patch cords, returned to its home cage and carted back to the holding room.

Training

Mice were trained using a contextual fear-conditioning paradigm. Training sessions were 500 s in duration, and four 0.75 mA shocks of 2 s duration were delivered at 198 s, 278 s, 358 s and 438 s. SAL or ANI was delivered immediately after training. After fear conditioning, mice were placed in their home cages, and carted back to the holding room. To enable engram labeling, mice were kept on regular food without DOX for 24-30 hours prior to training. When training was complete, mice were switched back to food containing 40 mg kg^{-1} DOX.

Testing

All mice were subjected to 180 s test sessions in the training context, 1 day post training. At the end of each session mice were placed in their home cages and carted back to the holding room. OptoPA tests were conducted 2 days post training. Mice were allowed to freely explore both zones X and Y during the 0–3 min baseline epoch, and the naturally preferred zone was determined as the target zone. During the 3–6 min and 9–12 min epochs (Light-On phases), light was administered only when a mouse was within the target zone. At the end of the 12 min, the mouse was immediately detached from the patch cords, returned to its home cage and carted back to the holding room. As criteria for inclusion in OptoPA experiments, during the baseline phases (0–3 min) of the OptoPA test day, mice that spent more than 90%

of the time in one single zone were excluded. Additionally, mice that spent 100% of the time in one zone in any 3 min phase of the test were also excluded.

Analysis

Automated OptoPA tracking was done using Noldus EthoVision. Raw data was extracted and analyzed using Microsoft Excel. The difference scores (DS) reported in the main figures were obtained by subtracting the time spent in the target zone during the baseline phase from the average time spent in the target zone during the two on phases. Negative difference scores denote that the preference for the target zone during on phases is lower than the preference during the baseline phase.

Tone Fear Conditioning - (Figure 3C)

Apparatus

Three distinct contexts were employed and were used in different rooms. Context A chambers were 30 X 25 X 33 cm with perspex floors, a transparent square ceilings, red lighting, and scented with 0.25 % benzaldehyde. The ceilings of the Context A chambers were customized to hold a rotary joint (Doric Lenses) the exterior side of which was connected to a patch cord to a 473 nm laser that was controlled by a pulse generator. The interior side of the rotary joint was connected to two 0.32 M patch cords. All mice had patch cords fitted to the fiber implant prior to being placed in Context A. Context B chambers were 29 X 25 X 22 cm with grid floors, opaque triangular ceilings, bright white lighting, and scented with 1 % acetic acid. Context C chambers were 29 X 25 X 22 cm with glossy white plastic floors, no ceilings, dim lighting, and scented with 1 ml citral in a tray underneath.

Habituation

Habituation to Context A was identical to Contextual Fear Conditioning.

Training

Mice were trained in Context B using a tone fear conditioning paradigm. Training sessions were 420 s in duration, and three tone presentations (2 kHz and 75 dB) of 20 s duration were delivered at 180 s, 260 s, and 340 s and co-terminated with a 2 s 0.6 mA shock. SAL or ANI was delivered immediately after training. After fear conditioning, mice were placed in their home cages, and carted back to the holding room. To enable engram labeling, mice were kept on regular food without DOX for 24-30 hours prior to training. When training was complete, mice were switched back to food containing 40 mg kg^{-1} DOX.

Testing

All testing sessions in Context C were 420 s in duration and three tone presentations (2 kHz and 75 dB) of 20 s duration were delivered at 180 s, 260 s, and 340 s. Testing sessions in Context A were 12 min in duration, and were identical to the habituation sessions, consisting of four 3 min epochs, with the first and third epochs as the Light-Off epochs, and the second and fourth epochs as the Light-On epochs. During the Light-On epochs, the mouse received light stimulation for the entire 3 min duration. At the end of the 12 min, the mouse was immediately detached from the patch cords, returned to its home cage and carted back to the holding room.

Contextual Fear Conditioning – Reconsolidation Amnesia - (Figure 3D)

Apparatus, Habituation, and Training procedures used for the reconsolidation experiment were identical to those of the consolidation experiment (above). 1 day post training, contextual fear memory was reactivated by a 3 min re-exposure to the training Context B. SAL or ANI was delivered immediately after context re-exposure. 2 days post-training, amnesia due to disrupting reconsolidation was confirmed by 3 min test session in Context B. 3 days post-training, mice were subjected to a Context A test session consisting of four 3 min epochs, with the first and third epochs as the Light-Off epochs, and the second and fourth epochs as the Light-On epochs. During the Light-On epochs, the mouse received light

stimulation (20 Hz) for the entire 3 min duration. At the end of the 12 min, the mouse was immediately detached from the patch cords, returned to its home cage and carted back to the holding room.

Inception of Fear Association - (Figure 3E)

Apparatus

Three distinct contexts were employed and were used in different rooms. Context A chambers were 29 X 25 X 22 cm with black cardboard floors, opaque triangular ceilings, red lighting, and scented with 1 % acetic acid. Context B chambers were 60 X 29 X 30 cm with white Perspex floors, white Perspex walls, no ceilings, bright white lighting, and unscented. The Context C chamber was 30 X 25 X 33 cm were with a metal grid floor, metallic square ceilings, dim white lighting, and scented with 0.25 % benzaldehyde. The ceiling of the Context C chamber was customized to hold a rotary joint (Doric Lenses) the exterior side of which was connected to a patch cord to a 473 nm laser that was controlled by a pulse generator. The interior side of the rotary joint was connected to two 0.32 M patch cords. Four mice were run simultaneously in four identical Context A chambers. Two mice were run simultaneously in two identical Context B chambers. All experimental groups were counter-balanced for chamber within contexts. Mice were run individually in a single Context C chamber.

Context exposure

Mice were exposure to target Context A for 600 s. SAL or ANI was delivered immediately after context exposure. Immediately after context exposure, mice were placed in their home cages, and carted back to the holding room. To enable engram labeling, mice were kept on regular food without DOX for 24-30 hours prior to training. When training was complete, mice were switched back to food containing 40 mg kg^{-1} DOX. 1 day post-exposure to Context A, all mice were exposed to control Context B for 600 s while on DOX.

Fear Inception

2 days post-exposure to Context A, all mice were subjected to a fear inception procedure in Context C as described in (Ramirez et al., 2013). The inception session was 420 s in duration and consisted of 120 s of Light-Off, followed by 300 s of Light-On. Three 0.75 mA shocks of 2 s duration were delivered at 240 s, 300s, and 360 s. At the end of the 420 s, the mouse was immediately detached from the patch cords, returned to its home cage and carted back to the holding room.

Testing

Mice were tested in Context B 4 days post-exposure to Context A, and then tested to Context A 5 days post-exposure to Context A.

Quantification of freezing behavior

All behavioral experiments were analyzed blind to experimental group. Researcher 1 performed behavioral experiments and following the conclusion of each experiment all videos were randomized before manual scoring. Behavioral performance was recorded by digital video camera. For context and tone recall sessions, data were quantified using FreezeFrame software (ActiMetrics) with bout size set at 1.25 ms In the case of fear inception, freezing behavior was manually scored because the dark floor material resulted in inaccurate FreezeFrame data capture. Light stimulation during the habituation and test sessions interfered with the motion detection of the program, and therefore all light-induced freezing behavior was manually quantified by eye. Videos were scored individually, and investigators were blind to experimental condition and test day during all manual scoring.

Behavioral statistics

Data analysis and statistics were conducted using Prism (Graphpad software). Unpaired student's t-tests were used for independent group comparisons, with Welch's correction observed when group variances

were significantly different. Paired student's t-tests were used to assess light-induced freezing behavior within groups.

Immunohistochemistry

Mice were dispatched by overdosing with 750–1000 mg kg^{-1} avertin and perfused transcardially with PBS, followed by 4 % paraformaldehyde (PFA) in PBS. Brains were extracted from the skulls and incubated in 4 % PFA at room temperature overnight. Brains were transferred to PBS and 50 μm coronal slices were taken using a vibratome and collected in PBS. For immunostaining, each slice was placed in PBS + 0.2 % Triton X-100 (PBS-T), with 5 % normal goat serum for 1 h and then incubated with primary antibody at 4°C for 24 h. Slices then underwent three wash steps for 10 min each in PBS-T, followed by 1 h incubation with secondary antibody. Slices underwent three more wash steps of 10 min each in PBS-T, followed by mounting and cover-slipping on microscope slides. All imaging and analyses were performed blind to the experimental conditions. Antibodies used for staining were as follows: to stain for ChR2-EYFP, slices were incubated with primary chicken anti-GFP (Life Technologies) (1:1000) and visualized using anti-chicken Alexa-488 (Life Technologies) (1:200). For ChR2-mCherry, slices were stained using primary rabbit anti-RFP (Rockland) (1:1000) and secondary anti-rabbit Alexa-555 (Life Technologies) (1:200). c-Fos was stained with rabbit anti-c-Fos (1:500, Calbiochem) and anti-rabbit Alexa-568 (Life Technologies) (1:500). Arc was stained with rabbit anti-Arc (1:300, Synaptic Systems) and anti-rabbit Alexa-568 (Life Technologies) (1:500).

Cell counting

All cell counting experiments were conducted blind to experimental group. Researcher 1 trained the animals and administered drug, while Researcher 2 dispatched the animals and conducted cell counting. To quantify the expression pattern of ChR2-EYFP and ChR2-mCherry in SAL and ANI injected c-fos-tTA mice, the number of EYFP/mCherry immunoreactive neurons were counted from 4-5 coronal slices per mouse (n = 3-5 for SAL and ANI groups, respectively). Coronal slices centered on coordinates

covered by the optic fiber implants were taken from dorsal hippocampus (–1.82 mm to –2.30 mm AP). Fluorescence images were acquired using a Zeiss AxioImager.Z1/ApoTome microscope (20 X magnification). Automated cell counting analysis was performed using ImageJ software. The cell body layer of DG granule cells (upper blade), CA3 cells or sub-regions of the amygdala (BLA vs. CeA) were outlined as a region of interest (ROI) according to the DAPI signal in each slice. The number of EYFP-/mCherry-positive cells per section was calculated by thresholding EYFP/mCherry immunoreactivity above background levels. For statistical analysis, we used a one-way ANOVA followed by Tukey's multiple comparisons ($\alpha = 0.05$). Data were analyzed using Microsoft Excel with the Statplus plug-in. All imaging and analyses were performed blind to the experimental conditions. Percentage engram cell reactivation data plotted in Fig. 3E calculated as (($cFos^+$, $ChR2^+$) / (Total $ChR2^+$)) X 100. Total engram cell reactivation was calculated as (($cFos^+$, $ChR2^+$) / (Total $DAPI^+$) X 100. $DAPI^+$ counts were approximation of 5 dorsal DG slices using ImageJ.

Stereotactic injection and optic fiber implant

DG injections of AAV_9-TRE-ChR2-EYFP were targeted bilaterally to (-1.9 mm AP, +/- 1.3 mm ML, –2.0 mm DV). DG implants were placed at (-1.9 mm AP, +/- 1.3 mm ML, –1.85 mm DV). CA3 injections of AAV_9-TRE-mCherry were targeted bilaterally to (-2.0 mm AP, +/- 2.0 mm ML, –1.9 mm DV). BLA injections of AAV_9-TRE-mCherry were targeted bilaterally to (-1.4 mm AP, +/- 3.1 mm ML, –4.6 mm DV). All virus volumes were 300 nl. As criteria we only included mice with ChR2-EYFP expression limited to the targeted region.

Amygdala activation in amnesia - (Figure 4A-C)

Four groups of c-fos-tTA mic e injected with AAV_9-TRE-ChR2-EYFP in the DG along with optic fiber implants were used for this experiment. Memory engram cells for contextual fear conditioning (CFC) were labeled in the DG of all groups. A day after training, two groups of mice (Saline Natural Cues, Anisomycin Natural Cues) were returned to the conditioning context (Context B) for a natural memory

recall test followed by timed perfusions; performed to identify recall-induced $cFos^+$ cells. The remaining groups (Saline ChR2, Anisomycin ChR2) were placed in Context A for DG engram activation followed by timed perfusions. By this protocol, we quantified $cFos^+$ neurons in the amygdala (CeA, BLA) following either natural recall or DG engram activation.

Cellular connectivity in amnesia - (Figure 4D-K)

In support of the physiological connectivity data in Figure 1G, four groups of c-fos-tTA mice injected with AAV_9-TRE-ChR2-EYFP in the DG and AAV_9-TRE-mCherry in CA3 and BLA along with optic fiber implants were prepared for this experiment. Memory engram cells for CFC were labeled in DG, CA3 and BLA of all groups. A day after training, two groups of mice (Saline Natural Cues, Anisomycin Natural Cues) were returned to the conditioning context (Context B) for a natural memory recall test followed by timed perfusions. The remaining groups (Saline ChR2, Anisomycin ChR2) were placed in Context A for DG engram activation followed by timed perfusions. This procedure allowed us to quantify the percentage of engram neurons in CA3 and BLA that were re-activated ($cFos^+$) by either natural recall or DG engram activation.

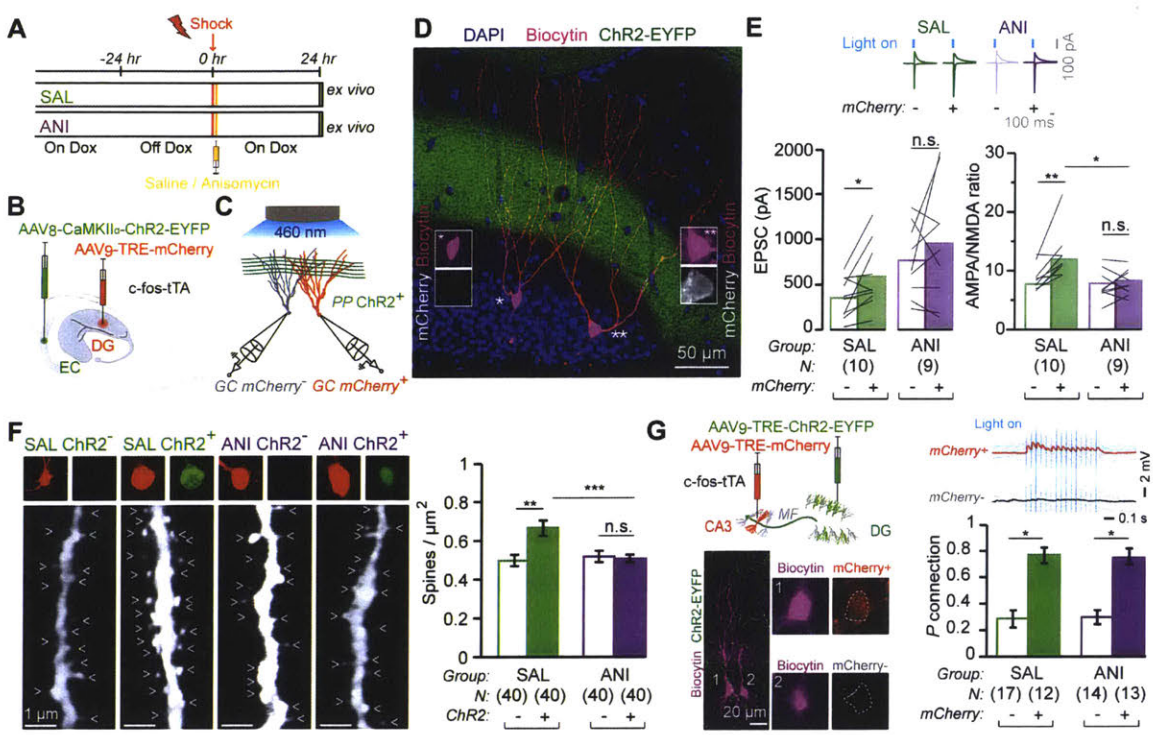

Figure 1: Synaptic Plasticity and Connectivity of Engram Cells.

(A) Mice taken Off DOX 24 hrs before contextual fear conditioning (CFC) and dispatched 24 hrs post training. Saline (SAL) or anisomycin (ANI) administered immediately after training.

(B) AAV_8-CaMKIIα-ChR2-EYFP and AAV_9-TRE-mCherry viruses injected into the entorhinal cortex and dentate gyrus, respectively, of c-fos-tTA mice.

(C) Paired recordings of engram (red) and non-engram (grey) DG cells during optogenetic stimulation of $ChR2^+$ perforant path (PP) axons.

(D) Representative image of a pair of recorded biocytin-labeled engram ($mCherry^+$) and non-engram ($mCherry^-$) DG cells. Note $ChR2^+$ PP axons in green.

(E) (Top) Example traces of AMPA and NMDA receptor-dependent postsynaptic currents in $mCherry^+$ and $mCherry^-$ cells, evoked by light activation of $ChR2^+$ PP axons. (Bottom) EPSC amplitudes and AMPA/NMDA current ratios of $mCherry^+$ and $mCherry^-$ cells of the two groups are displayed as means

(columns) and individual paired data points (grey lines). Paired t-test * $p < 0.05$, ** $p < 0.001$. SAL group compared with the ANI group, unpaired t-test * $p < 0.05$.

(F) (Left) Representative confocal images of biocytin filled dendritic fragments derived from SAL and ANI groups for $ChR2^{+}$ and $ChR2^{-}$ cells (arrow heads: dendritic spines). (Right) Average dendritic spine density showing an increase occurring exclusively in $ChR2^{+}$ fragments. Data are represented as mean ± SEM. Unpaired t tests ** $p < 0.01$, *** $p < 0.001$.

(G) Engram Connectivity. (Top left) AAV_9-TRE-ChR2-EYFP and AAV_9-TRE-mCherry viruses, injected into the DG and CA3, respectively, of c-fos-tTA mice. (Bottom left) Example of $mCherry^{+}$ (1) and $mCherry^{-}$ (2) biocytin-filled CA3 pyramidal cells. Note $ChR2^{+}$ mossy fibers (MF) in green. (Top Right) $mCherry^{+}$ cell but not $mCherry^{-}$ cell displayed EPSPs in response to optogenetic stimulation of MF. (Bottom Right) Probability of connection of DG $ChR2^{+}$ engram axons and CA3 $mCherry^{+}$ and $mCherry^{-}$ cells. Error bars are approximated by binomial distribution. Fisher's exact test: * $p < 0.05$.

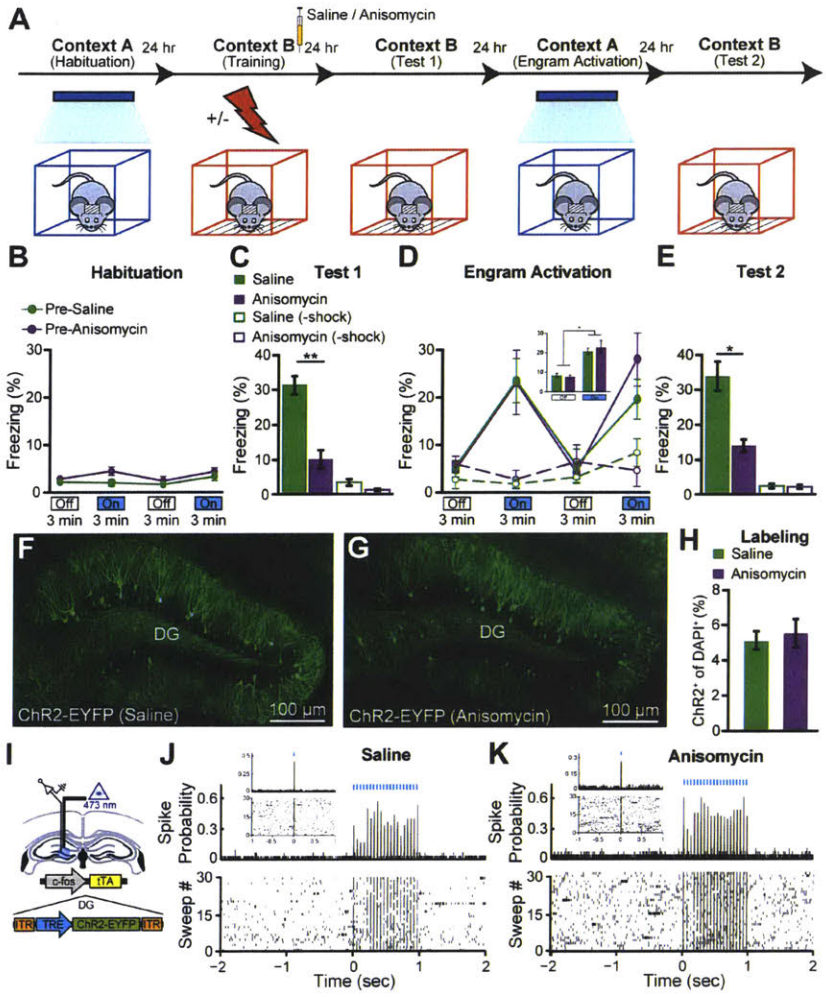

Figure 2: Optogenetic Stimulation of DG Engram Cells Restores Fear Memory in Retrograde Amnesia.

(A) Behavioral schedule. Beige shading signifies that subjects are On DOX, precluding ChR2 expression. Mice taken off DOX 24-30 hrs before CFC in Context B. SAL or ANI was injected into the mice after training.

(B) Habituation to Context A with Light-Off and Light-On epochs. Blue light stimulation of the DG did not cause freezing behavior in naïve, unlabelled mice of the pre-SAL (n = 10) or pre-ANI (n = 8) groups.

(C) Memory recall in Context B 1 day post-training (Test 1). ANI group displayed significantly less freezing than SAL group ($p < 0.005$). No-shock groups with SAL ($n = 4$) or ANI ($n = 4$) did not display freezing upon re-exposure to Context B.

(D) Memory recall in Context A 2 days post-training (Engram Activation) with Light-Off and Light-On epochs. Freezing for the two Light-Off and Light-On epochs are further averaged in the inset. Significant freezing due to light stimulation was observed in both the SAL ($p < 0.01$) and ANI groups ($p < 0.05$). Freezing levels did not differ between groups. SAL and ANI-treated no-shock control groups did not freeze in response to light stimulation of context B engram cells.

(E) Memory recall in Context B 3 days post-training (Test 2). ANI group displayed significantly less freezing than SAL group ($p < 0.05$).

(F, G) Images showing DG sections from c-fos-tTA mice 24 hrs after SAL or ANI treatment.

(H) ChR2-EYFP cell counts from DG sections of SAL ($n = 3$) and ANI ($n = 4$) groups.

(I) In vivo anesthetized recordings (see Materials and Methods).

(J, K) Light pulses induced spikes in DG neurons recorded from head-fixed anesthetized c-fos-tTA mice 24 hrs after treatment with either SAL or ANI.

Data presented as mean ± SEM.

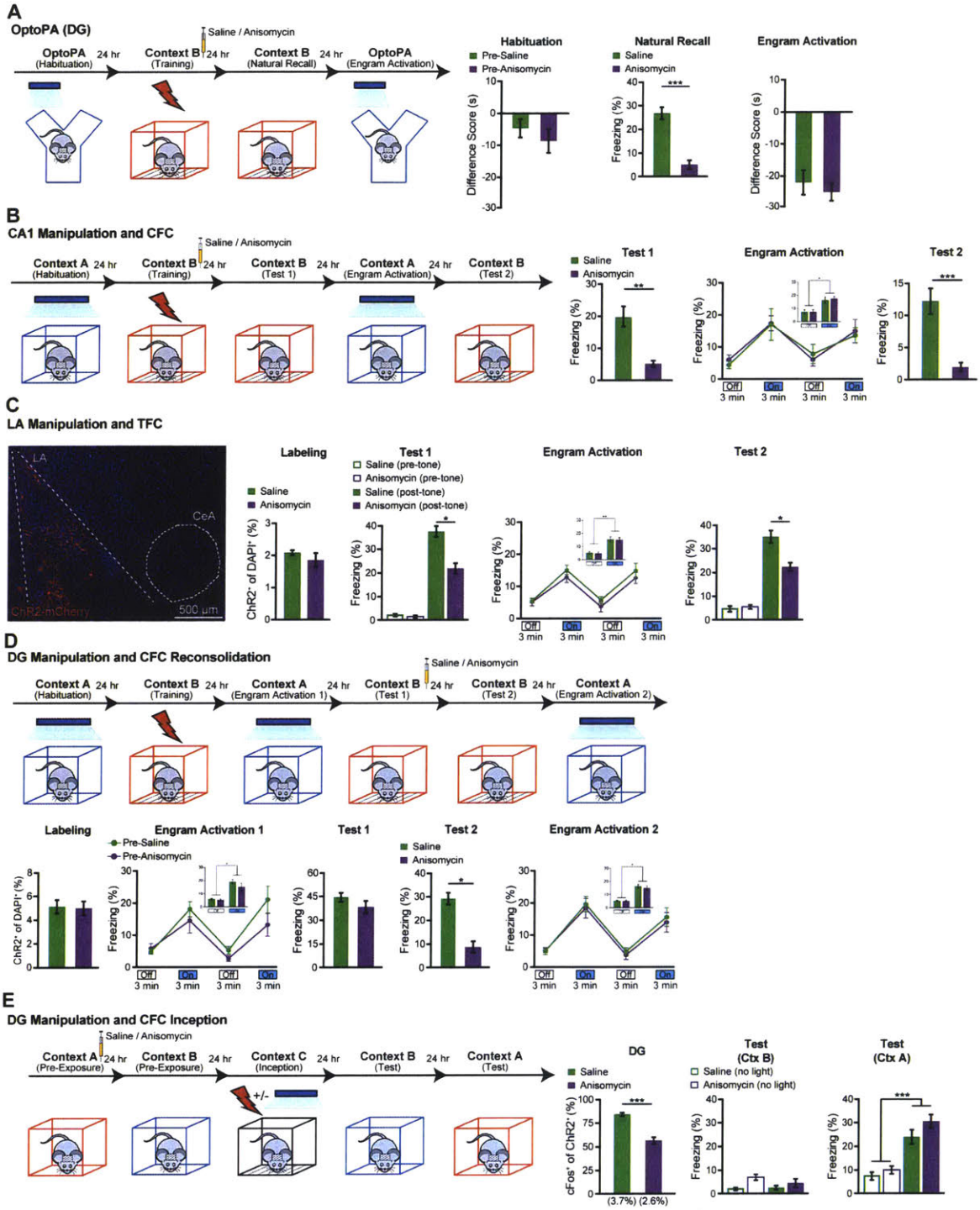
A
OptoPA (DG)
Saline / Anisomycin
OptoPA (Habituation)
24 hr
Context B (Training)
24 hr
Context B (Natural Recall)
24 hr
OptoPA (Engram Activation)
Habituation
Pre-Saline
Pre-Anisomycin
Difference Score (s)
Natural Recall
Saline
Anisomycin
***
Freezing (%)
Engram Activation
Difference Score (s)
B
CA1 Manipulation and CFC
Saline / Anisomycin
Context A (Habituation)
24 hr
Context B (Training)
24 hr
Context B (Test 1)
24 hr
Context A (Engram Activation)
24 hr
Context B (Test 2)
Test 1
Saline
Anisomycin
**
Freezing (%)
Engram Activation
Off
On
3 min
Test 2
***
C
LA Manipulation and TFC
LA
CeA
ChR2-mCherry
500 µm
Labeling
Saline
Anisomycin
ChR2+ of DAPI+ (%)
Test 1
Saline (pre-tone)
Anisomycin (pre-tone)
Saline (post-tone)
Anisomycin (post-tone)
Freezing (%)
Engram Activation
Test 2
D
DG Manipulation and CFC Reconsolidation
Saline / Anisomycin
Context A (Habituation)
24 hr
Context B (Training)
24 hr
Context A (Engram Activation 1)
24 hr
Context B (Test 1)
24 hr
Context B (Test 2)
24 hr
Context A (Engram Activation 2)
Labeling
Engram Activation 1
Pre-Saline
Pre-Anisomycin
Test 1
Test 2
Saline
Anisomycin
Engram Activation 2
E
DG Manipulation and CFC Inception
Saline / Anisomycin
Context A (Pre-Exposure)
24 hr
Context B (Pre-Exposure)
24 hr
Context C (Inception)
24 hr
Context B (Test)
24 hr
Context A (Test)
+/-
DG
Saline
Anisomycin
***
cFos+ of ChR2+ (%)
(3.7%) (2.6%)
Test (Ctx B)
Saline (no light)
Anisomycin (no light)
Freezing (%)
Test (Ctx A)

Figure 3: Recovery of Memory from Amnesia under a Variety of Conditions.

(A) DG engram activation and optogenetic place avoidance (OptoPA). During habituation neither group displayed significant avoidance of target zone. For Natural Recall the ANI group ($n = 10$) displayed significantly less freezing than SAL group ($n = 12$) in Context B ($p < 0.005$). SAL and ANI displayed similar levels of OptoPA.

(B) CA1 engram activation and CFC. 1 day post-CFC (Test 1) ANI group ($n = 9$) displayed significantly less freezing than SAL group ($n = 10$) in Context B ($p < 0.01$). 2 days post-training (Engram Activation), light-activation of CA1 engrams elicited freezing in both SAL ($p < 0.01$) and ANI groups ($p < 0.001$). 3 days post-training (Test 2) ANI group froze less than SAL group in Context B ($p < 0.01$).

(C) Lateral amygdala (LA) engram activation and tone fear conditioning (TFC). The behavioral schedule was identical to that in Fig. 3B, except that context tests were replaced with tone tests in Context C (Experimental methods). (Left) example image of ChR2-mCherry labeling of LA neurons. 2% of DAPI cells were labeled by ChR2. (Right) 1 day post-training (Test 1), ANI group ($n = 9$) displayed significantly less freezing to tone than SAL group ($n = 9$) ($p < 0.05$). 2 days post-training (Engram Activation), significant light-induced freezing was observed for both SAL ($p < 0.005$) and ANI groups ($p < 0.005$). 3 days post-training (Test 2) ANI group froze less to tone than SAL group ($p < 0.05$).

(D) DG engram activation and CFC reconsolidation. ANI ($n = 11$) and SAL ($n = 11$) groups showed similar levels of ChR2 labeling. Both groups showed light-induced freezing behavior 1 day post-training (Engram Activation 1), pre-SAL ($P < 0.001$), pre-ANI ($P < 0.02$). 2 days post training, (Test 1) the fear memory was reactivated by exposure to Context B, and SAL or ANI injected. 3 days post-training, (Test 2) the ANI group froze significantly less than SAL to Context B ($p < 0.01$). 4 days post-training, (Engram Activation 2) significant light-induced freezing was observed for the SAL ($p < 0.001$) and ANI ($p < 0.003$) groups.

(E) DG Inception (Experimental methods) following contextual memory amnesia. Context-only engram was labeled for target Context A, followed by injection of SAL ($n = 11$) or ANI ($n = 11$). Amnesia

demonstrated in ANI group by decreased $ChR2^{+}/c\text{-}Fos^{+}$ co-labeling following Context A re-exposure 1 day post labeling.

Following fear inception, neither SAL nor ANI groups displayed freezing behavior in Context B, while both groups displayed significant freezing in Context A, with no significant difference between groups. No-light inception SAL (n = 7) and ANI (n = 6) controls displayed no freezing to Context A or B. Statistical comparison are performed by using unpaired t tests, *** $p < 0.001$.

Data presented as mean ± SEM.

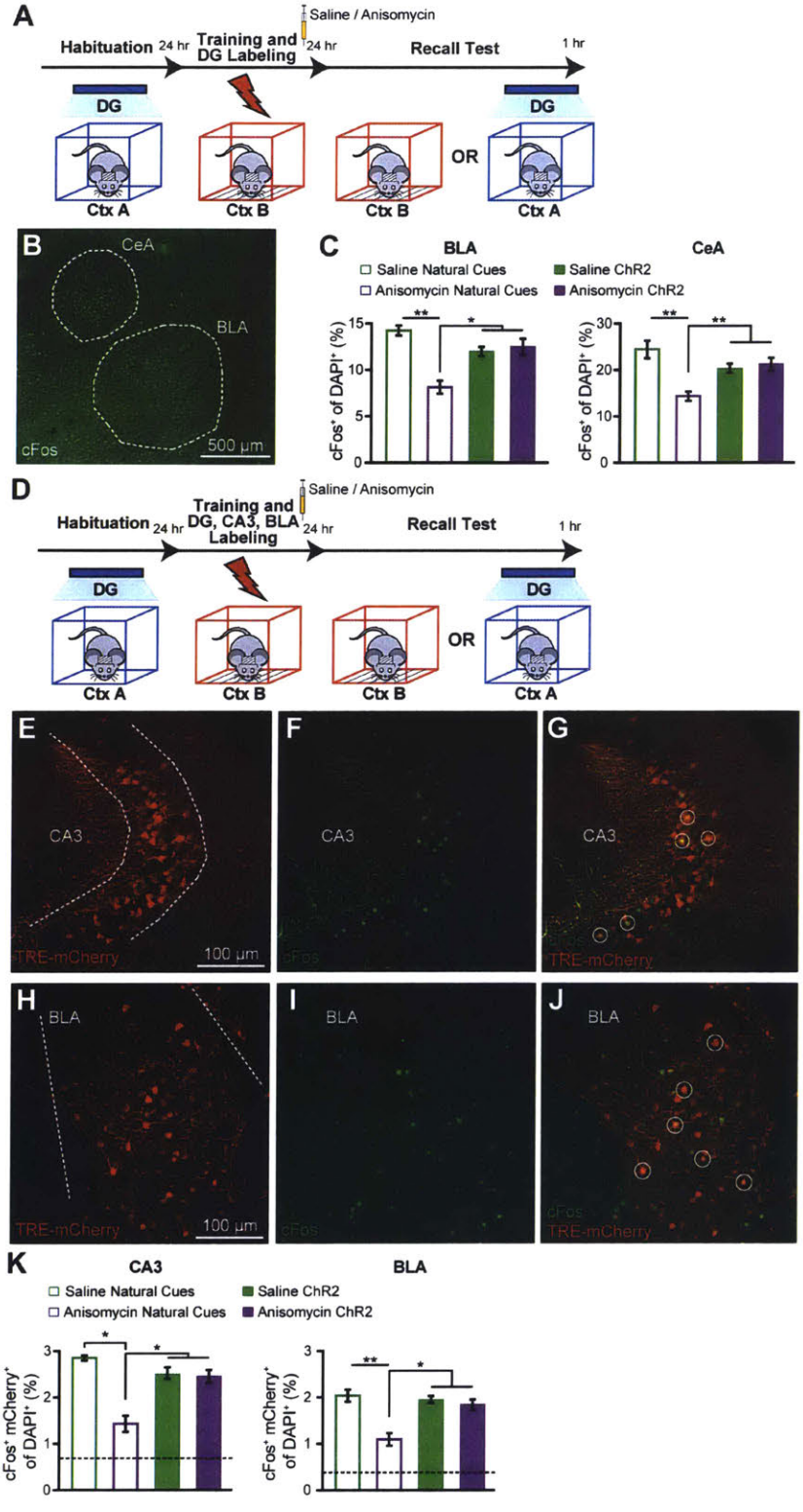
A
Saline / Anisomycin
Habituation 24 hr
Training and DG Labeling
24 hr
Recall Test
1 hr
DG
DG
OR
Ctx A
Ctx B
Ctx B
Ctx A
B
CeA
BLA
cFos
500 µm
C
BLA
CeA
Saline Natural Cues
Anisomycin Natural Cues
Saline ChR2
Anisomycin ChR2
cFos+ of DAPI+ (%)
D
Saline / Anisomycin
Habituation 24 hr
Training and DG, CA3, BLA Labeling
24 hr
Recall Test
1 hr
DG
DG
OR
Ctx A
Ctx B
Ctx B
Ctx A
E
F
G
CA3
CA3
CA3
TRE-mCherry
100 µm
cFos
TRE-mCherry
H
I
J
BLA
BLA
BLA
TRE-mCherry
100 µm
cFos
TRE-mCherry
K
CA3
BLA
Saline Natural Cues
Anisomycin Natural Cues
Saline ChR2
Anisomycin ChR2
cFos+ mCherry+ of DAPI+ (%)

Figure 4: Amygdala Activation and Functional Connectivity in Amnesia by Light Activation of DG Engram

(A) Schedule for cell counting experiments. Mice were either given a natural recall session in Context B, or a light-induced recall session in Context A. Mice were perfused 1 hr post recall.

(B) Representative image showing c-Fos expression in the basolateral amygdala (BLA) and central amygdala (CeA).

(C) c-Fos$^+$ cell counts in the BLA and CeA of mice following natural or light-induced recall (n = 3-4 per group).

(D) Schedule for cell counting experiments. c-fos-tTA mice with AAV$_9$-TRE-ChR2-EYFP injected into the DG and AAV$_9$-TRE-mCherry injected into both CA3 and BLA were fear conditioned off DOX, and 1 day later were given a natural recall session in Context B, or a light-induced recall session in Context A. Mice were perfused 1 hr post recall.

(E – G) Representative images showing mCherry engram cell labeling, c-Fos expression, mCherry$^+$/c-Fos$^+$ overlap in CA3.

(H – J) Representative images showing mCherry engram cell labeling, c-Fos expression, mCherry/c-Fos overlap in BLA.

(K) c-Fos$^+$/mCherry$^+$ overlap cell counts in CA3 and BLA of mice following natural or light-induced recall (n = 3 - 4 per group). Chance levels were estimated at 0.76 (CA3) and 0.42 (BLA). Data are presented as mean ± SEM. Statistical comparison are performed by using unpaired t tests, * $p < 0.05$, ** $p < 0.01$.

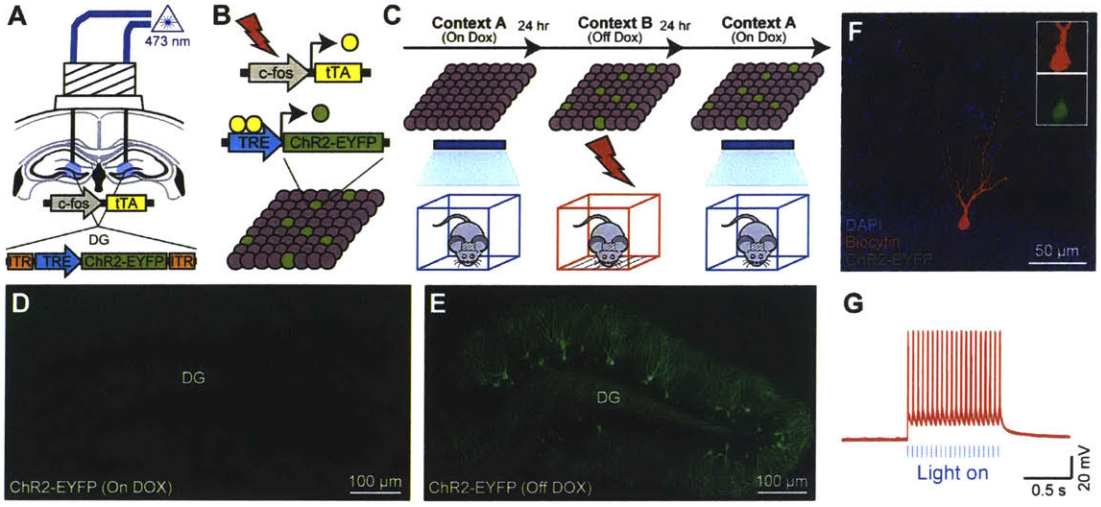

Figure S1: Labeling Dentate Gyrus Engram Cells with ChR2.

(A) Adeno-associated virus carrying ChR2 gene under the control of a TRE promoter (AAV_9-TRE-ChR2-EYFP) was stereotactically injected in the dentate gyrus (DG) of c-fos-tTA transgenic mice. Following virus injections, bilateral optic fibers were implanted into the DG.

(B) When the c-fos promoter is active, tTA is expressed in cells. tTA protein binds to the TRE promoter, resulting in the expression of ChR2-EYFP. DOX prevents binding of tTA to the TRE promoter, restricting expression of ChR2 to defined temporal windows.

(C) Naïve, unlabeled mice were habituated to the patch cord and laser in Context A while On DOX. Mice were taken Off DOX 24-30 hours prior to CFC in Context B. Mice were placed back On DOX immediately after training. DG engrams were evoked by blue laser stimulation of the DG in Context A, at least 24 hours after training.

(D) Representative image showing a DG section from a c-fos-tTA mouse injected with AAV_9-TRE-ChR2-EYFP that was kept On DOX during training. No significant expression of ChR2-EYFP was observed, demonstrating DOX control over the labeling method.

(E) Representative image showing a DG section from a c-fos-tTA mouse injected with AAV_9-TRE-ChR2-EYFP, Off DOX from 24 hours before training. Sparse ChR2-EYFP expression occurs across the DG.

(F) Representative image of a ChR2-EYFP labeled DG neuron injected with biocytin during patch clamp recording.

(G) Blue light stimulation (20 pulses, 20 Hz, 15 ms each) of ChR2-EYFP labeled DG neuron resulted in spikes.

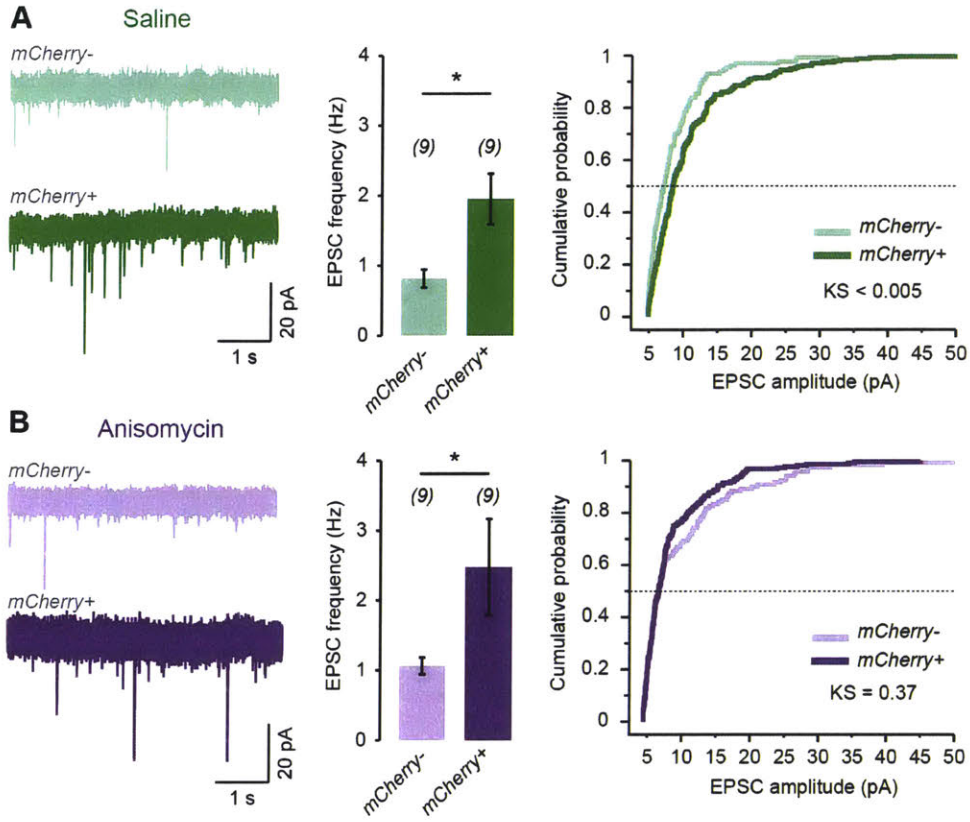

Figure S2: Analysis of Spontaneous EPSCs.

(A) Example of spontaneous EPSC recordings from mCherry$^-$ and mCherry$^+$ DG granule cells collected from cfos-tTA mice injected with AAV$_9$-TRE-mCherry in DG (same cells of Fig. 1A-E). Mice were injected with saline immediately after CFC and sacrificed 24 hr later for ex vivo recording. The mCherry$^+$ group displays higher EPSC frequency (two tailed paired t-test, $P < 0.05$) and higher EPSC amplitude than the mCherry$^-$ group (Kolmogorov-Smirnov test, $P < 0.005$).

(B) Example of spontaneous EPSC recordings from mCherry$^-$ and mCherry$^+$ DG granule cells collected from cFos-tTa mice injected either with AAV$_9$-TRE-mCherry in the DG. Mice were injected with anisomycin immediately after CFC and sacrificed 24 hr later for ex vivo recording. The mCherry$^+$ group displays higher EPSC frequency than the mCherry$^-$ group (two tailed paired t-test, $P < 0.05$) but the distributions of EPSC amplitudes are similar (Kolmogorov-Smirnov test, $P = 0.37$).

The mCherry^{+} cells of the saline group display higher EPSC amplitudes than the mCherry^{+} cells of the anisomycin group (Kolmogorov-Smirnov test, $P < 0.001$), whereas the mCherry^{-} cells of the saline and the anisomycin group display similar EPSC amplitudes (Kolmogorov-Smirnov test, $P = 0.12$).

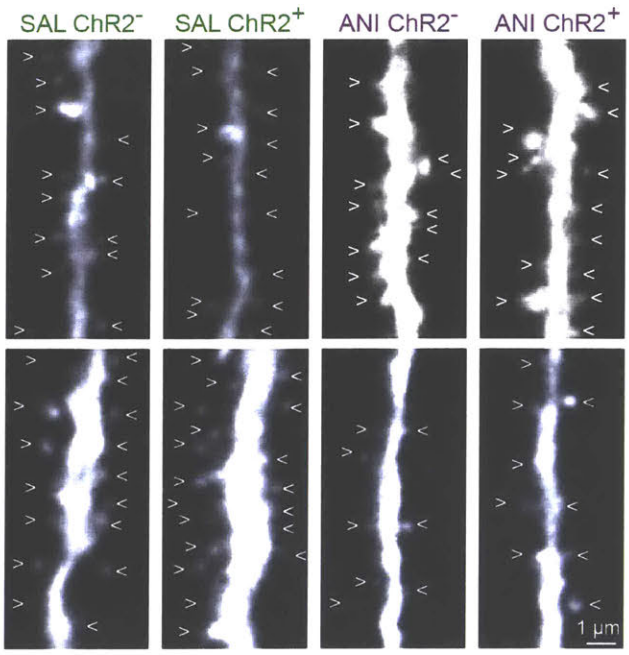

Figure S3: Confocal images of dendritic spines.

Two series (top and bottom) of confocal images of dendritic spines form $ChR2^+$ and $ChR2^-$ DG granule cell dendrites from the Saline (SAL) or the Anisomycin (ANI) group. Scale bar is the same for all the images.

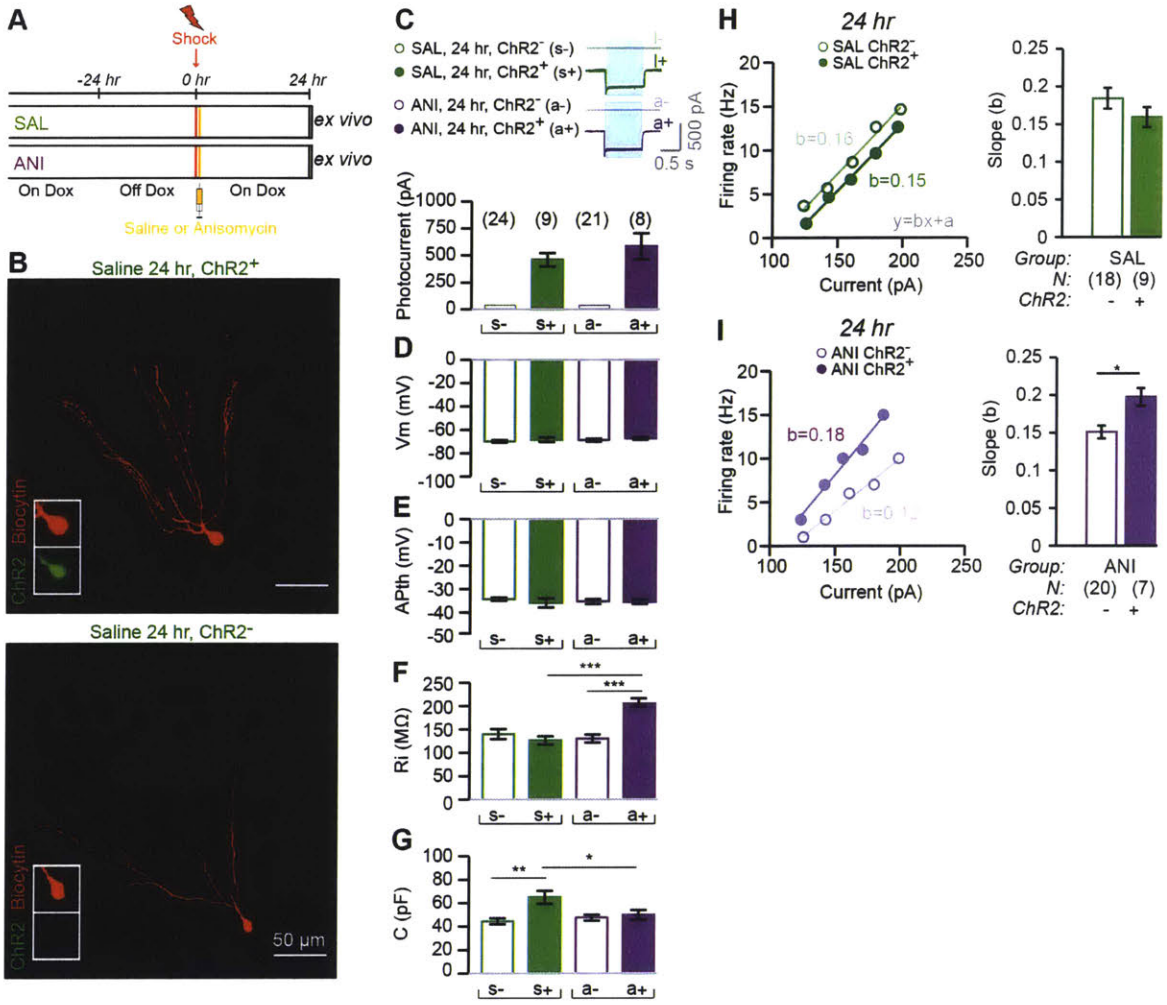

Figure S4: Physiological Profiling of DG Engram Cells.

(A) Schematic of ex vivo physiological experiments. c-fos-tTA mice with AAV_9-TRE-ChR2-EYFP injected into the DG were taken Off DOX 24 hrs before CFC, administered either SAL or ANI, and dispatched 24 hrs post-training,

(B) Representative images of $ChR2^+$ and $ChR2^-$ DG cells taken from the SAL group.

(C-I) Intrinsic physiological properties of engram ($ChR2^+$) and non-engram ($ChR2^-$) cells of the SAL (green), and ANI (purple) groups.

(C) Photocurrent measurements (pA) for $ChR2^+$ and $ChR2^-$ cells. Traces are displayed above bar charts. Blue light evoked comparable current influx in $ChR2^+$ cells but not in $ChR2^-$ cells of all three groups. Cell numbers in parentheses.

(D) Resting membrane potential measurements (Vm) for $ChR2^+$ and $ChR2^-$ cells across groups

(E) Action potential threshold (APth) for $ChR2^+$ and $ChR2^-$ cells across groups.

(F) Input resistance (Ri) for $ChR2^+$ and $ChR2^-$ cells across groups.

(G) Membrane capacitance (C) for $ChR2^+$ and $ChR2^-$ cells across groups.

(H, I) Examples of relationship between current injection and firing rate for the SAL (H) and ANI (I) groups, for engram $ChR2^+$ and non-engram $ChR2^-$ cells. Data are approximated by linear fit (gray formula in H) and the average value of the slope (b) is displayed in the bar charts. The $ChR2^+$ cells from the SAL group (H) display an excitability level similar to $ChR2^-$ cells. The $ChR2^+$ cells from the ANI group (I) display a significant 31% increase in excitability compared to $ChR2^-$ cells.

Data are represented as mean ± SEM. Statistical comparison are performed by using unpaired t tests, * $p < 0.05$, ** $p < 0.05$, and *** $p < 0.001$.

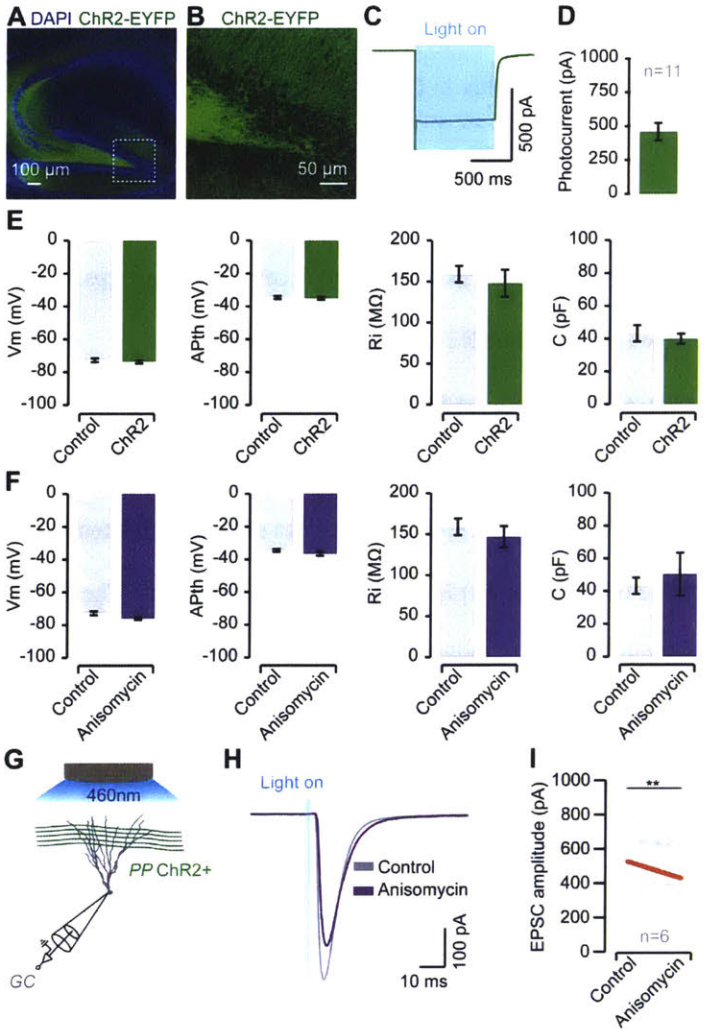

Figure S5: ChR2 and ANI have no Effect on the Intrinsic Properties of DG Granule Cells.

(A-B) The DG of c-fos-tTA transgenic mice were infected using an AAV_8-CaMKIIα-ChR2-EYFP virus. B, from the dotted-line box in A).

(C-D) Optogenetic stimulation of DG cells during voltage clamp recording revealed a robust photocurrent comparable to what was previously shown in Fig. S4C.

(E) ChR2 expression had no effect on the intrinsic properties (resting membrane potential Vm, action potential threshold APth, input resistance Ri and capacitance C) of DG cells ($ChR2^+$ cells n = 11, $ChR2^-$ cells n = 16).

(F) Direct bath application of 40 μM ANI had no effect on the intrinsic properties of DG cells (control n = 11, ANI n = 14).

(G) Voltage clamp recording of a DG cell combined with optogenetic stimulation of $ChR2^+$ axons of the perforant path.

(H) Examples of excitatory postsynaptic currents (EPSCs) recorded in DG cells responding to optogenetic stimulation of the $ChR2^+$ axons of the perforant path in control conditions and following ANI bath application. Note the mild difference.

(I) Average EPSCs of experiments described in panel G-H (n = 6, paired t test ** $p < 0.01$).

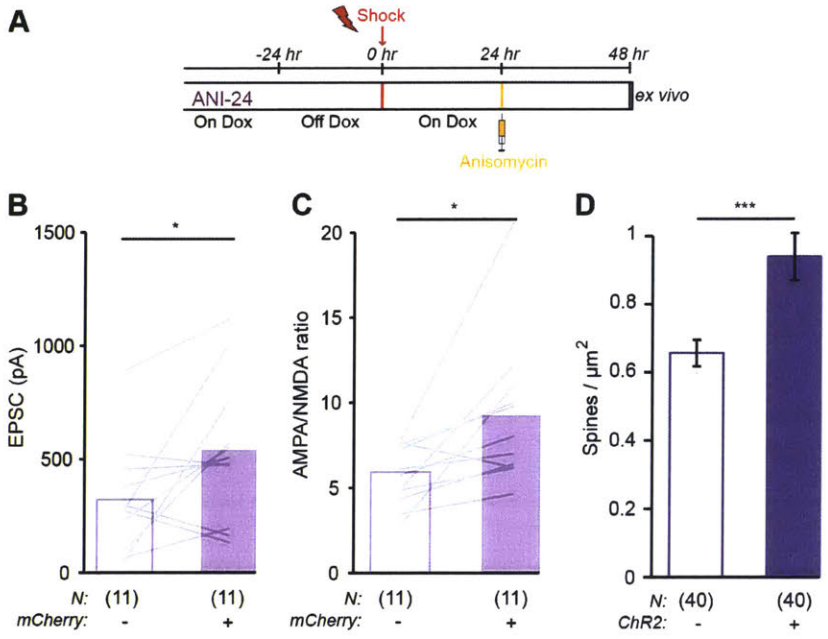

Figure S6: Anisomycin Injection Outside of the Memory Consolidation Window does not Affect Synaptic Strength, AMPA/NMDA Receptor Current Ratio, or Dendritic Spine Density.

(A) cfos-tTA mice injected in the DG either with AAV_9-TRE-mCherry (for synaptic analysis) or AAV_9-TRE-ChR2-EYFP (for spine density analysis) were taken off DOX 24 hr before exposure to contextual fear conditioning, injected with anisomycin 24 hr later and then sacrificed 24 hr after injection for ex vivo recording.

(B) Analysis of synaptic strength. The $mCherry^+$ group displays higher synaptic strength than the $mCherry^-$ group (two tailed paired t-test, $P < 0.05$).

(C) Analysis of AMPA/NMDA receptors ratio. The $mCherry^+$ group displays higher AMPA/NMDA receptors ratio than the $mCherry^-$ group (two tailed paired t-test, $P < 0.05$).

(D) Dendritic spine density analysis of $ChR2^+$ and $ChR2^-$ DG granule cells. The $ChR2^+$ group displays higher spine density than the $ChR2^-$ group (two tailed unpaired t-test, $P < 0.001$).

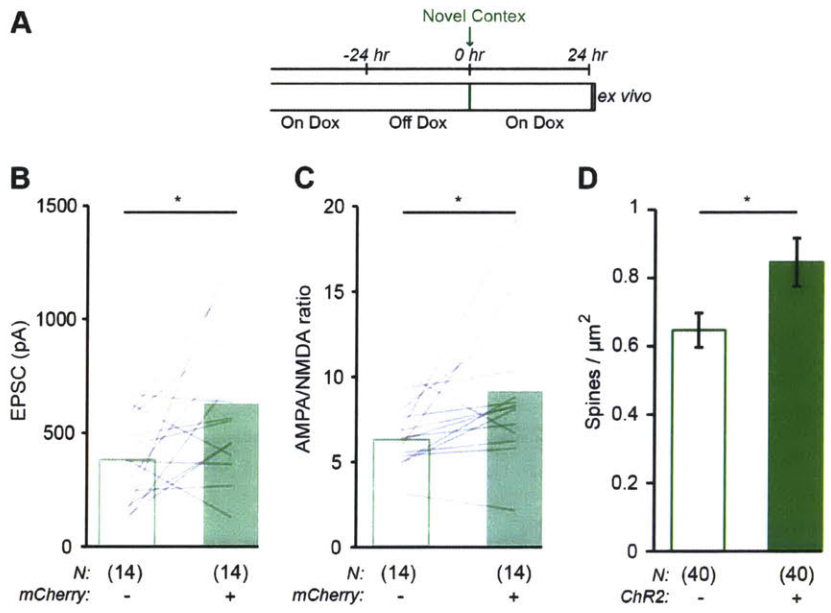

Figure S7: Effect of Exposure to Novel Context on Synaptic Strength, AMPA/NMDA Receptors Current Ratio, and Dendritic Spine Density.

(A) cfos-tTA mice injected in DG either with AAV_9-TRE-mCherry (for synaptic analysis) or AAV_9-TRE-ChR2-EYFP (for spine density analysis) were taken off DOX 24 hr before a 5 min. exposure to a novel context and then sacrificed 24 hr later for ex vivo recording.

(B) Analysis of synaptic strength. The $mCherry^+$ group displays higher synaptic strength than the $mCherry^-$ group (two tailed paired t-test, $P < 0.05$).

(C) Analysis of AMPA/NMDA receptors ratio. The $mCherry^+$ group displays higher AMPA/NMDA receptors ratio than the $mCherry^-$ group (two tailed paired t-test, $P < 0.05$).

(D) Dendritic spine density analysis of $ChR2^+$ and $ChR2^-$ DG granule cells. The $ChR2^+$ group displays higher spine density than the $ChR2^-$ group (two tailed unpaired t-test, $P < 0.05$).

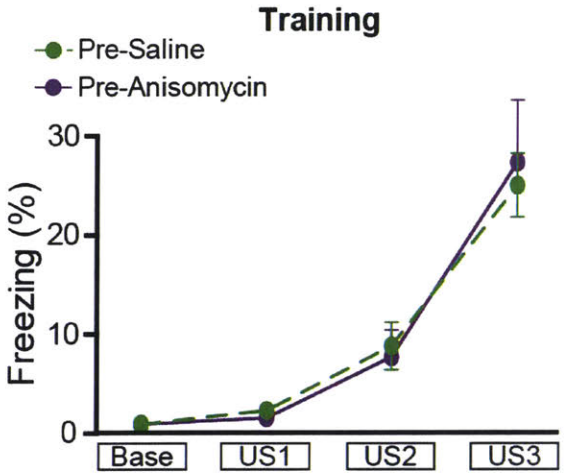

Figure S8: Response to Shock During CFC.

For the DG consolidation experiment (Fig. 2), naïve implanted c-fos-tTA mice were subjected to a CFC protocol while Off DOX, where three 0.75 mA shocks (unconditioned stimulus US1-3) of 2 s duration were delivered at 150 s, 210 s, and 270 s. No difference in unconditioned freezing behavior was observed between the two groups. Data presented as mean ± SEM.

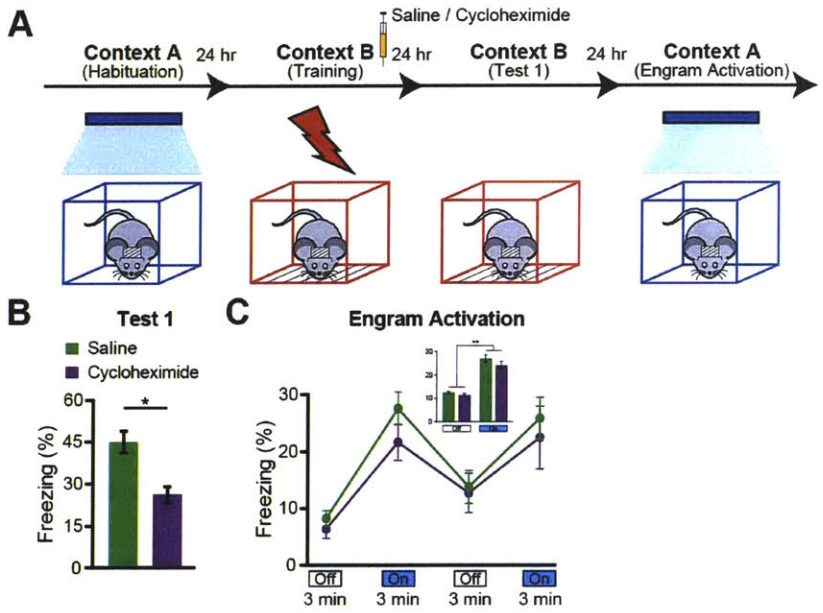

Figure S9: Optogenetic Stimulation of DG Engram Cells Retrieves fear memory in CHM-Induced Retrograde Amnesia.

(A) Schematic of the behavioral schedule used for experiments.

(B) Long-term memory recall in Context B, 1 day post-training. CHM group (N = 9) displayed significantly less freezing behavior to natural contextual cues than the SAL group (N = 9), ($p < 0.04$).

(C) Light-induced memory recall in Context A, 2 days post-training with Light-Off and Light-On epochs. Freezing levels for the two Light-Off and Light-On epochs are further averaged in the inset. Significant freezing due to light stimulation was observed in both the SAL ($p < 0.001$) and CHM groups ($p < 0.01$). Light-induced freezing levels did not differ between groups. Data presented as mean ± SEM.

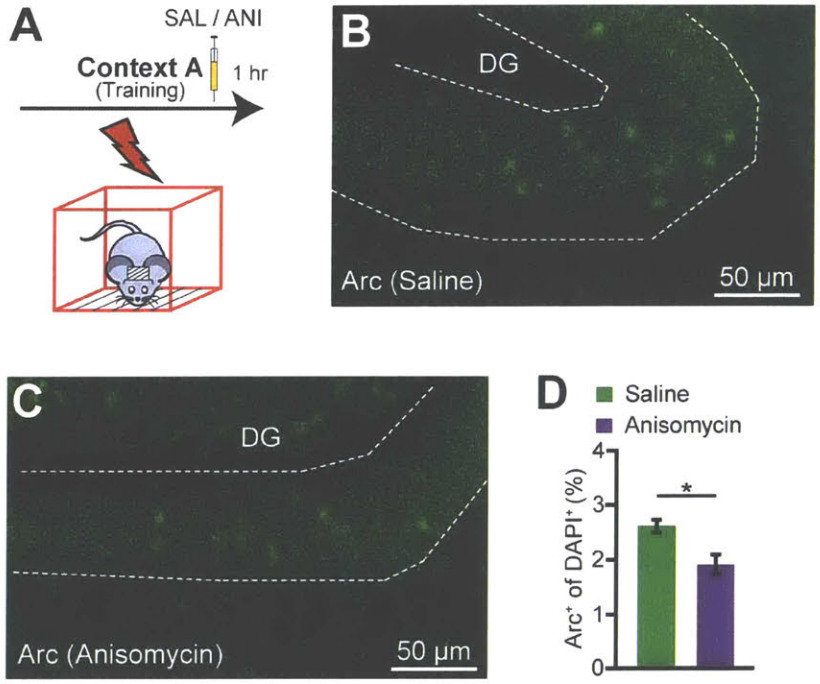

Figure S10: Post-Training Anisomycin Impairs DG Protein Synthesis.

(A) Schematic of the behavioral schedule used for experiments. Mice were pefused 1 hour post-training.

(B) Representative image of Arc staining in the DG of mice treated with saline.

(C) Representative image of Arc staining in the DG of mice treated with anisomycin.

(D) Average percentages of Arc^+ DG cells of SAL and ANI groups.

Data presented as mean ± SEM, * $p < 0.05$.

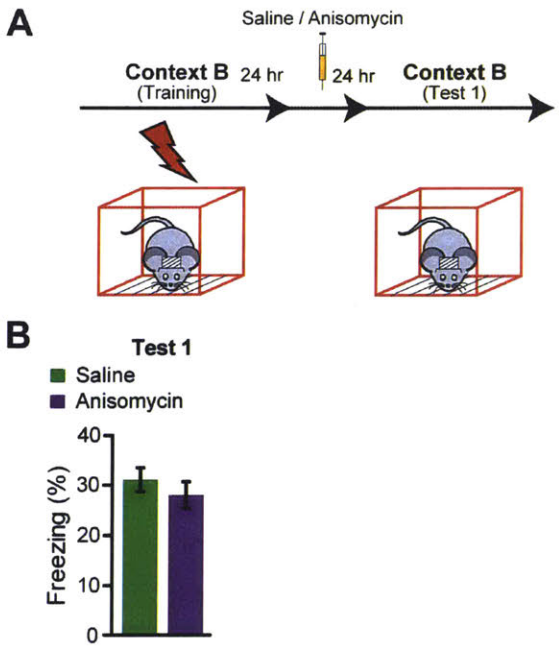

Figure S11: Anisomycin Delivery 24 hours Post-Training did not Induce Retrograde Amnesia.

(A) Schematic of the behavioral schedule used for experiments.

(B) Long-term memory recall in Context B, 1 day post-drug treatment. ANI group (N = 11) displayed equivalent freezing behavior to SAL group (N = 11).

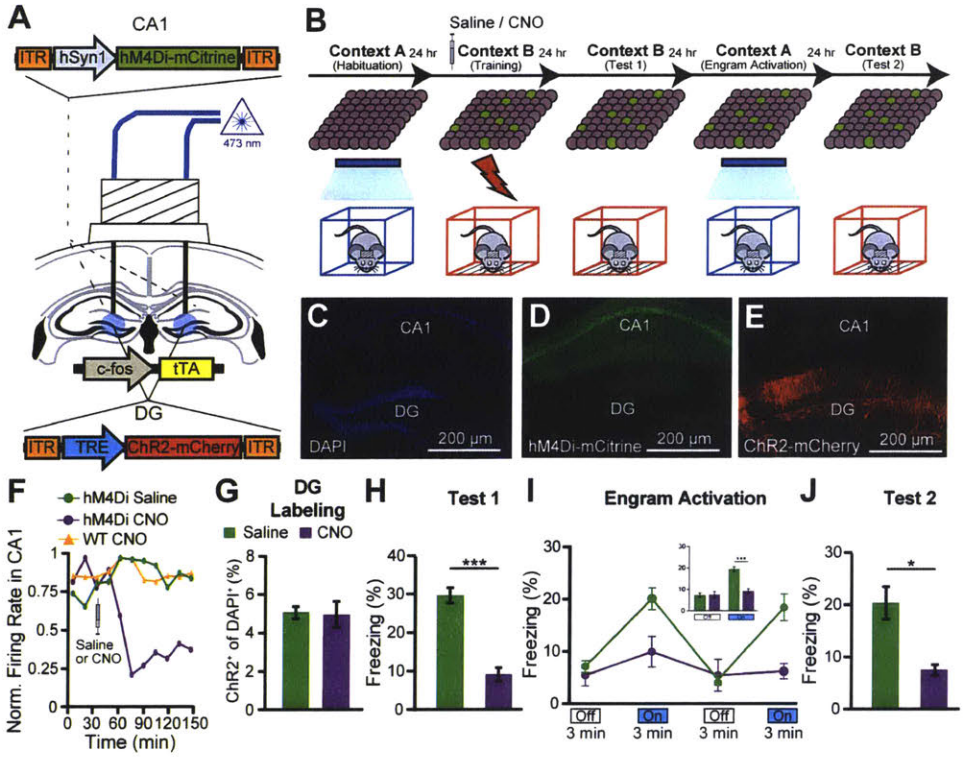

Figure S12: Optogenetic Stimulation of Engram Cells Does Not Retrieve Fear Memory following Anterograde Amnesia due to Impaired Encoding.

(A) An AAV virus carrying the inhibitory DREADDs hM4Di receptor under the control of a hSyn1 promoter (AAV_9-hSyn1-hM4Di-mCitrine) was stereotactically injected in CA1 of c-fos-tTA transgenic mice, with AAV_9-TRE-ChR2-mCherry injected into the DG. Following virus injections, bilateral optic fibers were implanted into DG.

(B) Schematic of the behavioral schedule used for memory encoding experiment. Depictions of DG cell populations. Mice were taken off 24-30 hrs before contextual fear conditioning in Context B and SAL or CNO (5 mg kg^{-1}) 1 hr before training.

(C-E) Representative images showing a hippocampal section from a c-fos-tTA mouse expressing hM4Di-mCitrine in CA1, and ChR2-mCherry in DG.

(F) CNO administration triggered hM4Di receptors to inhibit CA1 neuronal firing.

(G) $ChR2^{+}$ cell counts from DG sections of SAL (n = 4) and CNO (n = 4) treated c-fos-tTA mice. CNO treatment did not impair ChR2 labeling of DG engram cells.

(H) Long-term memory recall in Context B, 1 day post-training. The CNO group (N = 13) showed significantly less freezing behavior than the SAL group (N = 11), ($p < 0.001$).

(I) Light-induced memory recall in Context A, 2 days post-training with Light-Off and Light-On epochs. Freezing levels for the two Light-Off and Light-On epochs are further averaged in the inset. Significant freezing due to light stimulation was observed in both the SAL ($p < 0.0001$) and CNO groups ($p < 0.05$). Light-induced freezing was significantly lower in the CNO group (18.2% ± 1.3% versus 9.3% ± 1.6% freezing; $p < 0.0005$).

(J) Long-term memory recall in Context B, 3 days post-training. The CNO group showed significantly less freezing behavior than the SAL group (20.7% ± 4.7% versus 8.9% ± 1.7% freezing; $p < 0.05$).

Data presented as mean ± SEM.

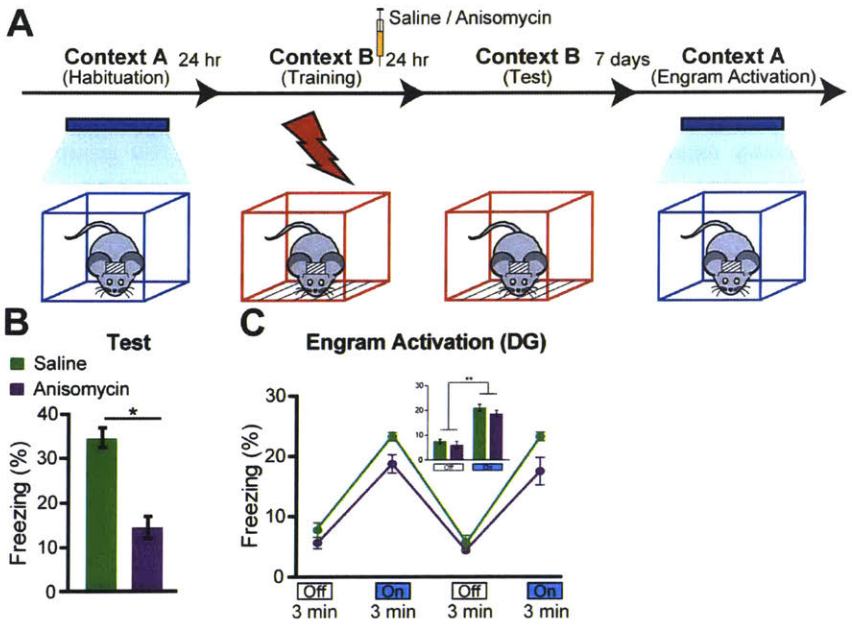

Figure S13: Optogenetic Stimulation of DG Engram Cells Retrieves Fear Memory 8 Days After Impaired Consolidation

(A) Schematic of the behavioral schedule used for experiments.

(B) Long-term memory recall in Context B, 1 day post-training. ANI group (N = 8) displayed less freezing behavior to natural contextual cues than the SAL group (N = 7, $p = 0.015$).

(C) Light-induced memory recall in Context A, 8 days post-training with Light-Off and Light-On epochs. Freezing levels for the two Light-Off and Light-On epochs are further averaged in the inset. Significant freezing due to light stimulation was observed in both the SAL ($p < 0.005$) and ANI groups ($p < 0.005$). Light-induced freezing levels did not differ between groups.

Data presented as mean ± SEM.

Chapter 3. Restoring memory in mouse models of early Alzheimer's disease

Alzheimer's disease (AD) is a neurodegenerative disorder characterized by progressive memory decline and subsequent loss of broader cognitive functions (Selkoe, 2001). Memory decline in early stages of Alzheimer's is mostly limited to episodic memory, for which the hippocampus (HPC) plays a crucial role (Selkoe, 2002). However, it has been uncertain whether the observed amnesia in early stages of Alzheimer's is due to disrupted encoding and consolidation of episodic information, or an impairment in the retrieval of stored memory information. Here we show that in transgenic mouse models of early Alzheimer's, direct optogenetic activation of hippocampal memory engram cells results in memory retrieval despite the fact that these mice are amnesic in long-term memory tests when natural recall cues are utilized, revealing a retrieval, rather than a storage impairment. Prior to amyloid plaque deposition, the amnesia in these mice is age-dependent (Hsia et al., 1999; Jacobsen et al., 2006; Mucke et al., 2000), which correlates with a progressive reduction of spine density of hippocampal dentate gyrus (DG) engram cells. We show that optogenetic induction of long-term potentiation (LTP) at perforant path (PP) synapses of DG engram cells restores both spine density and long-term memory. We also demonstrate that an ablation of DG engram cells containing restored spine density prevents the rescue of long-term memory. Thus, selective rescue of spine density in engram cells may lead to an effective strategy for treating memory loss in early stages of Alzheimer's disease.

3.1 Brief introduction

Alzheimer's disease (AD) is the most common cause of brain degeneration, and typically begins with impairments in cognitive functions (Selkoe, 2001). Most research has focused on understanding the relationship between memory impairments and the formation of two pathological hallmarks seen in late stages of AD: extracellular amyloid plaques and intracellular aggregates of tau protein (Selkoe, 2001, 2002). Early phases of AD have received relatively less attention, although synaptic phenotypes have been identified as major correlates of cognitive impairments in both human patients and mouse models

(Jacobsen et al., 2006; Terry et al., 1991). Several studies have suggested that the episodic memory deficit of AD patients is due to ineffective encoding of new information (Granholm and Butters, 1988; Hodges et al., 1990; Weintraub et al., 2012). However, since cognitive measures used in these studies rely on memory retrieval, it is not possible to rigorously discriminate between impairments in information storage and disrupted retrieval of stored information. This issue has an important clinical implication: if the amnesia is due to retrieval impairments, memory could be restored by technologies involving targeted brain stimulation.

3.2 Experimental results

A mouse model of AD (hereafter referred to as "AD mice") (Jankowsky et al., 2004) overexpresses the delta exon 9 variant of presinilin-1 (PS1), in combination with the Swedish mutation of amyloid precursor protein (APP). Consistent with previous reports (Hsia et al., 1999; Jacobsen et al., 2006; Mucke et al., 2000), 9-month old AD mice showed severe plaque deposition across multiple brains regions (Fig. 1a), specifically in the DG (Fig. 1b) and medial entorhinal cortex (EC) (Fig. 1c); in contrast, 7-month old AD mice lacked amyloid plaques (Fig. 1d and Extended Data Fig. 1a-d). Focusing on these two age groups of AD mice, we quantified short-term (1 hr; STM) and long-term (24 hr; LTM) memory formation using contextual fear conditioning (CFC) (Fig. 1e). Nine-month old AD mice were impaired in both STM and LTM, which suggested a deficit in memory encoding (Fig. 1k-o). In contrast, 7-month old AD mice showed normal levels of training-induced freezing (Fig. 1f) and normal STM (Fig. 1g), but were impaired in LTM (Fig. 1h). Neither control nor 7-month old AD mice displayed freezing behavior in a neutral context (Fig. 1i). In the DG of 7-month old AD mice, the levels of cells which are immediate early gene cFos-positive following CFC training were normal, but were lower compared to control mice following LTM tests (Fig. 1j). The density of DG granule cells and motor behaviors were normal in these mice (Extended Data Fig. 1e-k). Thus, these behavioral- and cellular-level observations confirmed that 7-month old AD mice serve as a mouse model of early AD regarding memory impairments.

Recently, molecular, genetic and optogenetic methods to identify neurons that hold traces, or engrams, of specific memories have been established (Liu et al., 2012; Ramirez et al., 2013). Using this technology, several groups have demonstrated that DG neurons activated during CFC learning are both sufficient (Liu et al., 2012; Ramirez et al., 2013; Redondo et al., 2014; Ryan et al., 2015) and necessary (Denny et al., 2014) for subsequent memory retrieval. In addition, our recent study found that engram cells under protein synthesis inhibitor-induced amnesia were capable of driving acute memory recall if they are directly activated optogenetically (Ryan et al., 2015). In the present study, we have applied this memory engram cell identification and manipulation technology to 7-month old AD mice to determine whether memories could be retrieved in early stages of the disease. Because it is known that the EC/HPC network is among the earliest to show altered synaptic/dendritic properties and these alterations have been suggested as underlying the memory deficits in early AD (Harris et al., 2010; Hyman et al., 1986), we focused on labeling the DG component of CFC memory engram cells of 7-month old AD mice using a double adeno-associated virus system (Fig. 1p-q and see Experimental methods). While on a doxycycline (DOX) diet, DG neurons completely lacked ChR2-EYFP labeling, one day off DOX was sufficient to permit robust ChR2-EYFP expression in control mice (Fig. 1r-s and Extended Data Fig. 2a-c), as well as in 7-month old AD mice (Fig. 1t-u).

As expected, these engram-labeled early AD mice were amnesic a day after CFC training (Fig. 1v). But, remarkably, these mice froze on the next day in a distinct context (Context B) as robustly as equivalently treated control mice in response to blue light stimulation of the engram cells (Fig. 1w). This light-specific freezing was not observed using on DOX mice (Extended Data Fig. 2d-f). A natural recall test conducted on the third day in the conditioning context (Context A) revealed that the observed optogenetic engram reactivation did not restore memory recall by natural cues in early AD mice (Fig. 1x). This was the case even after multiple rounds of light activation of the engram cells (Extended Data Fig. 3). We replicated the successful optogenetic rescue of memory recall in two other models of early AD: a triple transgenic line obtained by mating c-fos-tTA mice with double transgenic APP/PS1 mice (Extended Data Fig. 4a-g) and a widely used triple transgenic AD model (Oddo et al., 2003) (PS1/APP/tau,

Extended Data Fig. 4h-m). These data show that DG engram cells in 7-month old mouse models of early AD are sufficient to induce memory recall upon optogenetic reactivation, which indicates a deficit of memory retrievability during early AD-related memory loss.

Reduced dendritic spines have been implicated in memory impairments of AD (Jacobsen et al., 2006). In addition, our recent study of protein synthesis inhibitor-induced amnesia found reduced engram-cell specific dendritic spine density (Ryan et al., 2015). We detected an age-dependent (Extended Data Fig. 5a) decrease in dendritic spine density of DG engram cells in early AD mice (Fig. 2a-c), showing that long-term memory impairments of early AD correlate with dendritic spine deficits of DG engram cells (Extended Data Fig. 5b). The inability to generate newborn neurons in the DG could play a role in the development of AD-specific cognitive deficits (Rodriguez et al., 2008). However, early AD mice showed similar levels of neurogenesis in DG compared to control mice, which were quantified using doublecortin staining (DCX, Extended Data Fig. 1l-q). We recently proposed that the persistent cellular connectivity between multiple engram cell ensembles is a fundamental mechanism of memory information retention (Ryan et al., 2015). We labeled putative CFC memory engram cells in both medial EC (MEC) and lateral EC (LEC) with oChIEF (Lin et al., 2009) (a variant of ChR2) and simultaneously labeled CFC memory engram cells in the DG with EYFP (Fig. 2d). With this procedure, perforant path terminals are also labeled with oChIEF (Fig. 2e-f). One day after footshocks, we optogenetically activated these terminals and quantified the overlap between putative DG engram cells (i.e. $EYFP^+$, green) and DG cells in which the endogenous cFos (red) had been activated by the optogenetic activation of $oChIEF^+$ perforant paths. Both control and early AD mice showed above-chance and indistinguishable levels of $cFos^+/EYFP^+$ overlap, indicating the preferential functional connectivity between engram cells is maintained in the early AD mice (Fig. 2g-i).

We then hypothesized that the reversal of dendritic spine deficits in DG engram cells of early AD mice may rescue long-term memory. To investigate this possibility, we took advantage of previous findings that spine formation can be induced rapidly by long-term potentiation (LTP) (Engert and Bonhoeffer, 1999; Maletic-Savatic et al., 1999) and that LTP can be induced in vivo using light activation

of oChIEF (Nabavi et al., 2014). We validated learning-dependent labeling, with oChIEF, of neurons in MEC (Fig. 3a-c and Extended Data Fig. 6a-c) and LEC (Fig. 3d) as well as perforant path (PP) terminals in the DG (Fig. 3e-f). In vivo extracellular recording upon light stimulation of oChIEF$^+$ EC axonal terminals in DG showed a reliable spiking response of DG cells in anesthetized control mice (Fig. 3g). Further, in HPC slices from control mice we successfully induced LTP in DG cells using a previously established optical LTP protocol (Nabavi et al., 2014) (Fig. 3h-j). These biocytin-filled DG cells revealed an increase in spine density following in vitro optical LTP (Extended Data Fig. 6d).

In early AD mice, in vivo application of the engram-specific optical LTP protocol restored spine density of DG engram cells to control levels (AD+100 Hz, Fig. 3k-l). Furthermore, this spine restoration in early AD mice correlated with amelioration of long-term memory impairments observed during recall by natural cues (Fig. 3m), an effect which persisted for at least 6 days after training (AD rescue+DTR+saline group, Fig. 3p). The LTP-induced spine restoration and behavioral deficit rescue were protein-synthesis dependent (Extended Data Fig. 7). The rescued memory was context-specific (Extended Data Fig. 8a). In addition, long-term memory recall of age-matched control mice was unaffected by this optical LTP protocol (Extended Data Fig. 8b). In contrast, applying the optical LTP protocol to a large portion of excitatory PP terminals in the DG (i.e., with no restriction to the PP terminals derived from EC engram cells) did not result in long-term memory in early AD mice (Extended Data Fig. 9). To confirm the correlation between restoration of spine density of DG engram cells and amelioration of long-term memory impairments, which were both induced by the optical LTP protocol, we compared the overlap of natural recall cue-induced cFos$^+$ cells and CFC training-labeled DG engram cells after an application of the engram-specific LTP protocol to early AD mice (Fig. 3n). Early AD mice that did not receive the optical LTP protocol showed low levels of cFos$^+$/EYFP$^+$ overlap compared to control mice upon natural recall cue delivery. In contrast, early AD mice that went through the optical LTP protocol showed cFos$^+$/EYFP$^+$ overlap similar to that of control mice (Fig. 3n). Thus, these data suggest that spine density restoration in DG engram cells contributes to the rescue of long-term memory in early AD mice.

Because of the highly redundant connectivity between EC and DG (Tamamaki and Nojyo, 1993), it is possible that the extensive optical LTP protocol also augmented spine density in some non-engram DG cells. To establish a link between the spine rescue in DG engram cells and the behavioral rescue of early AD mice, we developed an engram-specific ablation (Zhan et al., 2013) virus. We confirmed that this diphtheria toxin receptor (DTR)-mediated method efficiently ablated DG engram cells following diphtheria toxin (DT) administration (Fig. 3o), while leaving the nearby DG mossy cells intact (Extended Data Fig. 10). By simultaneously labeling axonal terminals of PP with oChIEF and DG engram cells with DTR, we examined the effect of DG engram cell ablation following optical LTP-induced behavioral rescue (Fig. 3p). Within-animal comparisons (Test 1 vs. Test 2) showed a decrease in freezing behavior of LTP-rescued AD mice in which DG engram cells were ablated. These data strengthen the link between DG engram cells with restored spine density and the long-term behavioral rescue in early AD mice.

To examine if the optical LTP-induced behavioral rescue could be applied to DG engram cells from other learning experiences, we labeled memory engrams for inhibitory avoidance or novel object location in early AD mice (Fig. 4a). Early AD mice showed memory impairments in inhibitory avoidance (IA) memory and novel object location (NOL) spatial memory (Fig. 4b-c). Optical LTP-induced spine rescue at the PP-DG engram synapses was sufficient to reverse long-term memory impairments of early AD mice in both behavioral paradigms, thus demonstrating the versatility of our engram-based intervention.

3.3 Discussion

Prior studies that examined early stages of AD found correlations between memory impairments and synaptic pathology at the EC PP input into the DG (Hsia et al., 1999; Jacobsen et al., 2006; Terry et al., 1991). It has been proposed that these early cognitive deficits are a failure of memory encoding based on behavioral observations in human patients (Hodges et al., 1990; Weintraub et al., 2012). Here, however, we have shown that optogenetic activation of hippocampal cells active during learning elicits

memory recall in mouse models of early AD. To our knowledge, this is the first rigorous demonstration that memory failure in early AD models reflects an impairment in the retrieval of information. Further support for a memory retrieval impairment in early AD comes from the fact that impairments are in long-term memory (at least one day long), but not in short-term memory (~1 hr after training), which is consistent with a retrieval deficit. The retrieval deficit in early AD models is similar to memory deficits observed in amnesia induced by impairing memory consolidation via protein synthesis inhibitors (Ryan et al., 2015). The underlying mechanism of memory failure in early AD patients may not necessarily parallel the molecular and circuit impairments observed in mouse models of early AD. For instance, some early AD patients can exhibit amyloid plaque deposition years before the onset of cognitive decline (Weintraub et al., 2012). However, converging data on the underlying mechanism for genetically- and pharmacologically-induced amnesia in animal models increase the possibility that similar memory retrieval-based failures may also operate in an early stage of AD patients. While we have shown that amnesia in early AD mice is a deficit of memory retrieval, it remains possible that the long-term maintenance of memory storage may also gradually become compromised as the disease proceeds from the early stage to more advanced stages, and eventually lost with neuronal degeneration. Further research will investigate these possibilities.

Our conclusions apply to episodic memory, which involves processing by hippocampal and other medial temporal lobe (MTL) structures. In the literature (Weintraub et al., 2012), it is widely recognized that early AD patients exhibit non-episodic memory deficits as well, which would involve brain structures other than the MTL. Additional work is required to examine mechanisms underlying cognitive impairments in these other types of memories. Nevertheless, our findings already contribute to a better understanding of memory retrieval deficits in several cases of early AD, and may apply to other pathological conditions, such as Huntington's disease (Hodges et al., 1990) in which patients show difficulty in memory recall.

Consistent with several studies highlighting the importance of dendritic spines (Jacobsen et al., 2006; Ryan et al., 2015; Terry et al., 1991; Tonegawa et al., 2015b) in relation to memory processing, we

observed an engram-cell specific decrease in spine density that correlated with memory deficits in early AD. Natural rescue of memory recall in early AD mice required the DG engram cells in which synaptic density deficits have been restored by an application of in vivo optical LTP protocols to the EC cells activated by specific learning. In contrast, the application of optical LTP protocols to a much wider array of excitatory EC cells projecting to the DG, which may be analogous to deep brain stimulation (DBS), did not rescue memory in AD mice. A potential explanation for this observation is that DG granule cells (GCs) may contribute to a variety of memories through their partially overlapping engram cell ensembles in a competitive manner, and that activation of a large number of these ensembles simultaneously may interfere with a selective activation of an individual ensemble. Thus, activation of a more targeted engram cell ensemble may be a key requirement for effective retrieval of the specific memory, which is difficult to achieve with the current DBS strategy.

Genetic manipulations of specific neuronal populations can have profound effects on cognitive impairments of AD (Cisse et al., 2011). We propose that strategies applied to engram circuits can support long-lasting improvements in cognitive functions, which may provide insights and therapeutic value for future approaches that rescue memory in AD patients.

3.4 Experimental methods

Subjects

The APP/PS1 (Jankowsky et al., 2004) double transgenic AD mice, originally described as Line 85, were obtained from Jackson Laboratory (stock number 004462). Under the control of mouse prion promoter elements, these mice express a chimeric mouse/human APP transgene containing Swedish mutations (K595N/M596L) as well as a mutant human PS1 transgene (delta exon 9 variant). To label memory engram cells in APP/PS1 mice, we generated a triple transgenic mouse line by mating c-fos-tTA (Liu et al., 2012; Reijmers et al., 2007) transgenic mice with APP/PS1 double transgenic mice. The PS1/APP/tau (Oddo et al., 2003) triple transgenic AD mice were obtained from Jackson Laboratory (stock number

004807). These 3xTg-AD mice express a mutant human PS1 transgene (M146V), a human APP transgene containing Swedish mutations (KM670/671NL) and a human tau transgene harboring the P301L mutation. All mouse lines were maintained as hemizygotes. Mice had access to food and water ad libitum and were socially housed in numbers of two to five littermates until surgery. Following surgery, mice were singly housed. For behavioral experiments, all mice were male and 7-9 months old. For optogenetic experiments, mice had been raised on food containing 40 mg kg^{-1} DOX for at least one week before surgery, and remained on DOX for the remainder of the experiments except for the target engram labeling days. For in vitro electrophysiology experiments, mice were 24-28 days old at the time of surgery. All experiments were conducted in accordance with U.S. National Institutes of Health (NIH) guidelines and the Massachusetts Institute of Technology Department of Comparative Medicine and Committee of Animal Care.

Viral constructs

Our previously established method (Liu et al., 2012) for labeling memory engram cells combined c-fos-tTA transgenic mice with a doxycycline (DOX)-sensitive adeno-associated virus (AAV). However, in this study, we modified the method using a double-virus system to label memory engram cells in the early AD mice, which already carry two transgenes. The pAAV-c-fos-tTA plasmid was constructed by cloning a 1 kb fragment from the c-fos gene (550 bp upstream of c-fos exon I through 35 bp into exon II) into an AAV backbone using the KpnI restriction site at the 5' terminus and the SpeI restriction site at the 3' terminus. The AAV backbone contained the tTA-Advanced (Urlinger et al., 2000) sequence at the SpeI restriction site. The pAAV-TRE-ChR2-EYFP and pAAV-TRE-EYFP constructs were previously described (Liu et al., 2012; Ramirez et al., 2013). The pAAV-TRE-oChIEF-tdTomato (Lin et al., 2009) plasmid was constructed by replacing the ChR2-EYFP fragment from the pAAV-TRE-ChR2-EYFP plasmid using NheI and MfeI restriction sites. The pAAV-CaMKII-oChIEF-tdTomato plasmid was constructed by replacing the TRE fragment from the pAAV-TRE-oChIEF-tdTomato plasmid using BamHI and EcoRI restriction sites. The pAAV-TRE-DTR-EYFP (Zhou et al., 2013) plasmid was

constructed by replacing the ChR2 fragment from the pAAV-TRE-ChR2-EYFP plasmid using EcoRI and AgeI restriction sites. AAV vectors were serotyped with AAV_9 coat proteins and packaged at the University of Massachusetts Medical School Gene Therapy Center and Vector Core. Viral titers were 1.5 $\times 10^{13}$ genome copy (GC) ml^{-1} for AAV_9-c-fos-tTA, AAV_9-TRE-ChR2-EYFP and AAV_9-TRE-EYFP, 1 $\times 10^{13}$ GC ml^{-1} for AAV_9-TRE-oChIEF-tdTomato, 4 $\times 10^{13}$ GC ml^{-1} for AAV_9-CaMKII-oChIEF-tdTomato and 2 $\times 10^{13}$ GC ml^{-1} for AAV_9-TRE-DTR-EYFP.

Surgery and optic fiber implants

Mice were anesthetized with isoflurane or 500 mg kg^{-1} avertin for stereotaxic injections (Ryan et al., 2015). Injections were targeted bilaterally to the DG (-2.0 mm AP, +/- 1.3 mm ML, -1.9 mm DV), MEC (-4.7 mm AP, +/- 3.35 mm ML, -3.3 mm DV) and LEC (-3.4 mm AP, +/- 4.3 mm ML, -4.0 mm DV). Injection volumes were 300 nl for DG and 400 nl for MEC and LEC. Viruses were injected at 70 nl min^{-1} using a glass micropipette attached to a 10 ml Hamilton microsyringe. The needle was lowered to the target site and remained for 5 min before beginning the injection. After the injection, the needle stayed for 10 min before it was withdrawn. A custom DG implant containing two optic fibers (200 mm core diameter; Doric Lenses) was lowered above the injection site (-2.0 mm AP, +/- 1.3 mm ML, -1.7 mm DV). The implant was secured to the skull with two jewelry screws, adhesive cement (C&B Metabond) and dental cement. An opaque cap derived from the top part of an Eppendorf tube protected the implant. Mice were given 1.5 mg kg^{-1} metacam as analgesic and allowed to recover for 2 weeks before behavioral experiments. All injection sites were verified histologically. As criteria, we only included mice with virus expression limited to the targeted regions.

Systemic injection of kainic acid

For seizure experiments (Liu et al., 2012), mice were taken off DOX for 1 day and injected intraperitoneally with 15 mg kg^{-1} kainic acid (KA). Mice were returned to DOX food 6 hours after KA treatment and perfused the next day for immunohistochemistry procedures.

Immunohistochemistry

Mice were dispatched using 750–1000 mg kg^{-1} avertin and perfused transcardially with PBS, followed by 4% paraformaldehyde (PFA). Brains were extracted and incubated in 4% PFA at room temperature overnight. Brains were transferred to PBS and 50 μm coronal slices were prepared using a vibratome. For immunostaining (Ryan et al., 2015), each slice was placed in PBS + 0.2% Triton X-100 (PBS-T), with 5% normal goat serum for 1 hr and then incubated with primary antibody at 4°C for 24 hr. Slices then underwent three wash steps for 10 min each in PBS-T, followed by 1 hr incubation with secondary antibody. After three more wash steps of 10 min each in PBS-T, slices were mounted on microscope slides. All analyses were performed blind to the experimental conditions. Antibodies used for staining were as follows: to stain for ChR2-EYFP, DTR-EYFP or EYFP alone, slices were incubated with primary chicken anti-GFP (1:1000, Life Technologies) and visualized using anti-chicken Alexa-488 (1:200). For plaques, slices were stained using primary mouse anti-β-amyloid (1:1000, Sigma-Aldrich) and secondary anti-mouse Alexa-488 (1:500). cFos was stained with rabbit anti-cFos (1:500, Calbiochem) and anti-rabbit Alexa-568 (1:300). Adult newborn neurons were stained with guinea pig anti-DCX (1:1000, Millipore) and anti-guinea pig Alexa-555 (1:500). Neuronal nuclei were stained with mouse anti-NeuN (1:200, Millipore) and Alexa-488 (1:200). DG mossy cell axons were stained with mouse anti-CR (1:1000, Swant) and Alexa-555 (1:300).

Cell counting

To characterize the expression pattern of ChR2-EYFP, DTR-EYFP, EYFP alone and oChIEF-tdTomato in control and AD mice, the number of $EYFP^{+}$/$tdTomato^{+}$ neurons were counted from 4-5 coronal slices per mouse (n = 3-5 mice per group). Coronal slices centered on coordinates covered by optic fiber implants were taken for DG quantification and sagittal slices centered on injection coordinates were taken for MEC and LEC. Fluorescence images were acquired using a Zeiss AxioImager.Z1/ApoTome microscope (20X). Automated cell counting analysis was performed using ImageJ software. The cell body layers of DG granule cells (upper blade), MEC or LEC cells were outlined as a region of interest

(ROI) according to the DAPI signal in each slice. The number of $EYFP^+$/$tdTomato^+$ cells per section was calculated by applying a threshold above background fluorescence. Data were analyzed using Microsoft Excel with the Statplus plug-in. A similar approach was applied for quantifying Aβ plaques, $cFos^+$ neurons and adult newborn (DCX^+) neurons. Total engram cell reactivation calculated as (($cFos^+$ $EYFP^+$) / (Total $DAPI^+$)) × 100. Chance overlap calculated as (($cFos^+$ / Total $DAPI^+$) × ($EYFP^+$ / Total $DAPI^+$)) × 100. Percentage of adult newborn neurons expressing neuronal markers was calculated as (($NeuN^+$ DCX^+) / (Total DCX^+) × 100. $DAPI^+$ counts were approximated from 5 coronal/sagittal slices using ImageJ. All counting experiments were conducted blind to experimental group. Researcher 1 trained the animals, prepared slices and randomized images, while Researcher 2 performed semi-automated cell counting. Statistical comparisons were performed using unpaired t tests: $*P < 0.05$, $**P < 0.01$, $***P < 0.001$.

Spine density analysis

Engram cells were labeled using c-fos-tTA-driven synthesis of ChR2-EYFP or EYFP alone. The EYFP signal was amplified using immunohistochemistry procedures after which fluorescence z-stacks were taken by confocal microscopy (Zeiss LSM700) using a 40X objective. Maximum intensity projections were generated using ZEN Black software (Zeiss). Four mice per experimental group were analyzed for dendritic spines. For each mouse, 30-40 dendritic fragments of 10 μm length were quantified (n = 120-160 fragments per group). To measure spine density of DG engram cells with a focus on entorhinal cortical inputs, distal dendritic fragments in the middle-to-outer molecular layer (ML) were selected. For CA3 and CA1 engram cells, apical and basal dendritic fragments were selected. To compute spine density, the number of spines counted on each fragment was normalized by the cylindrical approximation of the surface of the specific fragment. Experiments were conducted blind to experimental group. Researcher 1 imaged dendritic fragments and randomized images, while Researcher 2 performed manual spine counting.

In vitro recordings

Following isoflurane anesthesia, brains were quickly removed and used to prepare sagittal slices (300 μm) in an oxygenated cutting solution at 4°C with a vibratome (Ryan et al., 2015). Slices were incubated at room temperature in oxygenated ACSF until the recordings. The cutting solution contained (in mM): 3 KCl, 0.5 $CaCl_2$, 10 $MgCl_2$, 25 $NaHCO_3$, 1.2 NaH_2PO_4, 10 D-glucose, 230 sucrose, saturated with 95%O_2-5%CO_2 (pH 7.3, osmolarity of 340 mOsm). The ACSF contained (in mM): 124 NaCl, 3 KCl, 2 $CaCl_2$, 1.3 $MgSO_4$, 25 $NaHCO_3$, 1.2 NaH_2PO_4, 10 D-glucose, saturated with 95%O_2-5% CO_2 (pH 7.3, 300 mOsm). Individual slices were transferred to a submerged experimental chamber and perfused with oxygenated ACSF warmed at 35°C (+/- 0.5°C) at a rate of 3 ml min^{-1} during recordings. Current or voltage clamp recordings were performed under an IR-DIC microscope (Olympus) with a 40X water immersion objective (0.8 NA), equipped with four automatic manipulators (Luigs & Neumann) and a CCD camera (Hamamatsu). Borosilicate glass pipettes (Sutter Instruments) were fabricated with resistances of 8-10 MΩ. The intracellular solution (in mM) for current clamp recordings was: 110 K-gluconate, 10 KCl, 10 HEPES, 4 ATP, 0.3 GTP, 10 phosphocreatine, 0.5% biocytin (pH 7.25, 290 mOsm). Recordings used two dual channel amplifiers (Molecular Devices), a 2 kHz filter, 20 kHz digitization and an ADC/DAC data acquisition unit (Instrutech) running on custom software in Igor Pro (Wavemetrics). Data acquisition was suspended whenever the resting membrane potential was depolarized above -50 mV or the access resistance (RA) exceeded 20 MΩ. Optogenetic stimulation was achieved using a 460 nm LED light source (Lumen Dynamics) driven by TTL input with a delay onset of 25 μs (subtracted offline for latency estimation). Light power on the sample was 33 mW/mm^2. To test oChIEF expression, EC cells were stimulated with a single light pulse of 1 s, repeated 10 times every 5 s. DG granule cells were held at -70 mV. Optical LTP protocol: 5 min baseline (10 blue light pulses of 2 ms each, repeated every 30 s) was acquired before the onset of the LTP protocol (100 blue light pulses of 2 ms each at a frequency of 100 Hz, repeated 5 times every 3 min) and the effect on synaptic amplitude was recorded for 30 min (1 pulse of 2 ms every 30 s). Potentiation was observed in 6 out of 30 cells and results were statistically confirmed using a two-tailed paired t test. Experiments were performed in the presence of 10 μM gabazine (Tocris)

and 2 μM CGP55845 (Tocris). Recorded cells were recovered for morphological identification using streptavidin CF633 (Biotium).

In vivo recordings

Multi-unit responses to optical stimulation were recorded in the DG of mice injected with a cocktail of AAV_9-c-fos-tTA and AAV_9-TRE-oChIEF-tdTomato viruses into MEC/LEC. Mice were anesthetized (10 ml kg^{-1}) using a mixture of ketamine (100 mg ml^{-1})/xylazine (20 mg ml^{-1}) and placed in the stereotactic system. Anesthesia was maintained by booster doses of ketamine (100 mg kg^{-1}). An optrode consisting of a tungsten electrode (0.5 MΩ) attached to an optic fiber (200 μm core diameter), with the tip of the electrode extending beyond the tip of the fiber by 300 μm, was used for simultaneous optical stimulation and extracellular recording. The power intensity of light emitted from the optrode was calibrated to about 10 mW, consistent with the power used in behavioral assays. $oChIEF^+$ cells were identified by delivering 20 ms light pulses (1 Hz) to the recording site every 50-100 μm. After light-responsive cells were detected, multi-unit activity in response to trains of light pulses (200 ms) at 100 Hz was recorded. Data acquisition used an Axon CNS Digidata 1440A system. MATLAB analysis was performed, as previously described (Ramirez et al., 2013).

Behavior assays

Experiments were conducted during the light cycle (7 am to 7 pm). Mice were randomly assigned to experimental groups for specific behavioral assays immediately after surgery. Mice were habituated to investigator handling for 1-2 minutes on three consecutive days. Handling took place in the holding room where the mice were housed. Prior to each handling session, mice were transported by wheeled cart to and from the vicinity of the behavior rooms to habituate them to the journey. For natural memory recall sessions, data were quantified using FreezeFrame software. Optogenetic stimulation interfered with the motion detection, and therefore all light-induced freezing behavior was manually quantified. All behavior experiments were analyzed blind to experimental group. Unpaired student's t-tests were used for

independent group comparisons, with Welch's correction when group variances were significantly different. Given behavioral variability, initial assays were performed using a minimum of 10 mice per group to ensure adequate power for any observed differences. Experiments that resulted in significant behavioral effects were replicated three times in the laboratory. Following behavioral protocols, brain sections were prepared to confirm efficient viral labeling in target areas. Animals lacking adequate labeling were excluded prior to behavior quantification.

Contextual fear conditioning

Two distinct contexts were employed (Ryan et al., 2015). Context A were 29 × 25 × 22 cm chambers with grid floors, opaque triangular ceilings, red lighting, and scented with 1% acetic acid. Four mice were run simultaneously in four identical context A chambers. Context B consisted of four 30 × 25 × 33 cm chambers with perspex floors, transparent square ceilings, bright white lighting, and scented with 0.25% benzaldehyde. All mice were conditioned in context A (two 0.60 mA shocks of 2 s duration in 5 min), and tested (3 min) in contexts A and B one day later. Experiments showed no generalization in the neutral context B. All experimental groups were counter-balanced for chamber within contexts. Floors of chambers were cleaned with quatricide before and between runs. Mice were transported to and from the experimental room in their home cages using a wheeled cart. The cart and cages remained in an anteroom to the experimental rooms during all behavioral experiments. For engram labeling, mice were kept on regular food without DOX for 24 hours prior to training. When training was complete, mice were switched back to food containing 40 mg kg^{-1} DOX.

Open field

Spontaneous motor activity was measured in an open field arena (52 × 26 cm) for 10 min. All mice were transferred to the testing room and acclimated for 30 min before the test session. During the testing period, lighting in the room was turned off. The apparatus was cleaned with quatricide before and between runs. Total movements (distance traveled and velocity) in the arena were quantified using an

automated infrared (IR) detection system (EthoVision XT, Noldus). The tracking software plotted heat maps for each mouse, which was averaged to create representative heat maps for each genotype. Raw data was extracted and analyzed using Microsoft Excel.

Engram activation

For light-induced freezing behavior, a context distinct from the CFC training chamber (context A) was used. These were 30 × 25 × 33 cm chambers with perspex floors, square ceilings, white lighting, and scented with 0.25% benzaldehyde. Chamber ceilings were customized to hold a rotary joint (Doric Lenses) connected to two 0.32 m patch cords. All mice had patch cords fitted to the optic fiber implant prior to testing. Two mice were run simultaneously in two identical chambers. ChR2 was stimulated at 20 Hz (15 ms pulse width) using a 473 nm laser (10-15 mW), for the designated epochs. Testing sessions were 12 min in duration, consisting of four 3 min epochs, with the first and third as light-off epochs, and the second and fourth as light-on epochs. At the end of 12 min, the mouse was detached and returned to its home cage. Floors of chambers were cleaned with quatricide before and between runs.

In vivo optical LTP

One day after CFC training and engram labeling (DG+PP terminals) in control and early AD groups, mice were placed in an open field arena (52 × 26 cm) after patch cords were fitted to the fiber implants. Following a 15 min acclimatization period, mice with oChIEF^{+} PP engram terminals in the DG received the optical LTP (Nabavi et al., 2014) protocol (100 blue light pulses of 2 ms each at a frequency of 100 Hz, repeated 5 times every 3 min). This in vivo protocol was repeated 10 times over a 3 hour duration. After induction, mice remained in the arena for an additional 15 min before returning to their home cage. To apply optical LTP to a large portion of excitatory MEC neurons, an AAV virus expressing oChIEF-tdTomato under the CaMKII promoter, rather than a c-fos-tTA/TRE virus (i.e., engram labeling), was used. For protein synthesis inhibition experiments, immediately after the in vivo LTP induction protocol mice received 75 mg kg^{-1} anisomycin (Aniso) or an equivalent volume of saline (Saline) intra-

peritoneally. Mice were then returned to their home cages. An hour later, a second injection of Aniso or Saline was delivered.

Inhibitory avoidance

A 30 × 28 × 34 cm unscented chamber with transparent square ceilings and intermediate lighting was used. The chamber consisted of two sections, one with grid flooring and the other with a white light platform. During the conditioning session (1 min), mice were placed on the light platform, which is the less preferred section of the chamber (relative to the grid section). Once mice entered the grid section of the chamber (all four feet), 0.80 mA shocks of 2 s duration were delivered. On average, each mouse received 2-3 shocks per training session. After 1 min, mice were returned to their home cage. The next day, latency to enter the grid section of the chamber as well as total time on the light platform was measured (3 min test).

Novel object location

Spatial memory was measured in a white plastic chamber (28 × 28 cm) that had patterns (series of parallel lines or circles) on opposite walls. The apparatus was unscented and intermediate lighting was used. All mice were transferred to the behavioral room and acclimated for 30 min before the training session. On day 1, mice were allowed to explore the chamber with patterns for 15 min. On days 2 and 3, mice were introduced into the chamber that had an object (7 cm tall glass flask filled with metal beads) placed adjacent to either patterned wall. The position of the object was counter-balanced within each genotype. On day 4, mice were placed into the chamber with the object either in the same position as the previous exposure (familiar) or at a novel location based on wall patterning. Frequency of visits to the familiar and novel object locations was quantified using an automated detection system (EthoVision XT, Noldus). Total time exploring the object was also measured (nose within 1.5 cm of object). The tracking software plotted heat maps based on exploration time, which was averaged to create representative heat maps for each genotype. Raw data was extracted and analyzed using Microsoft Excel.

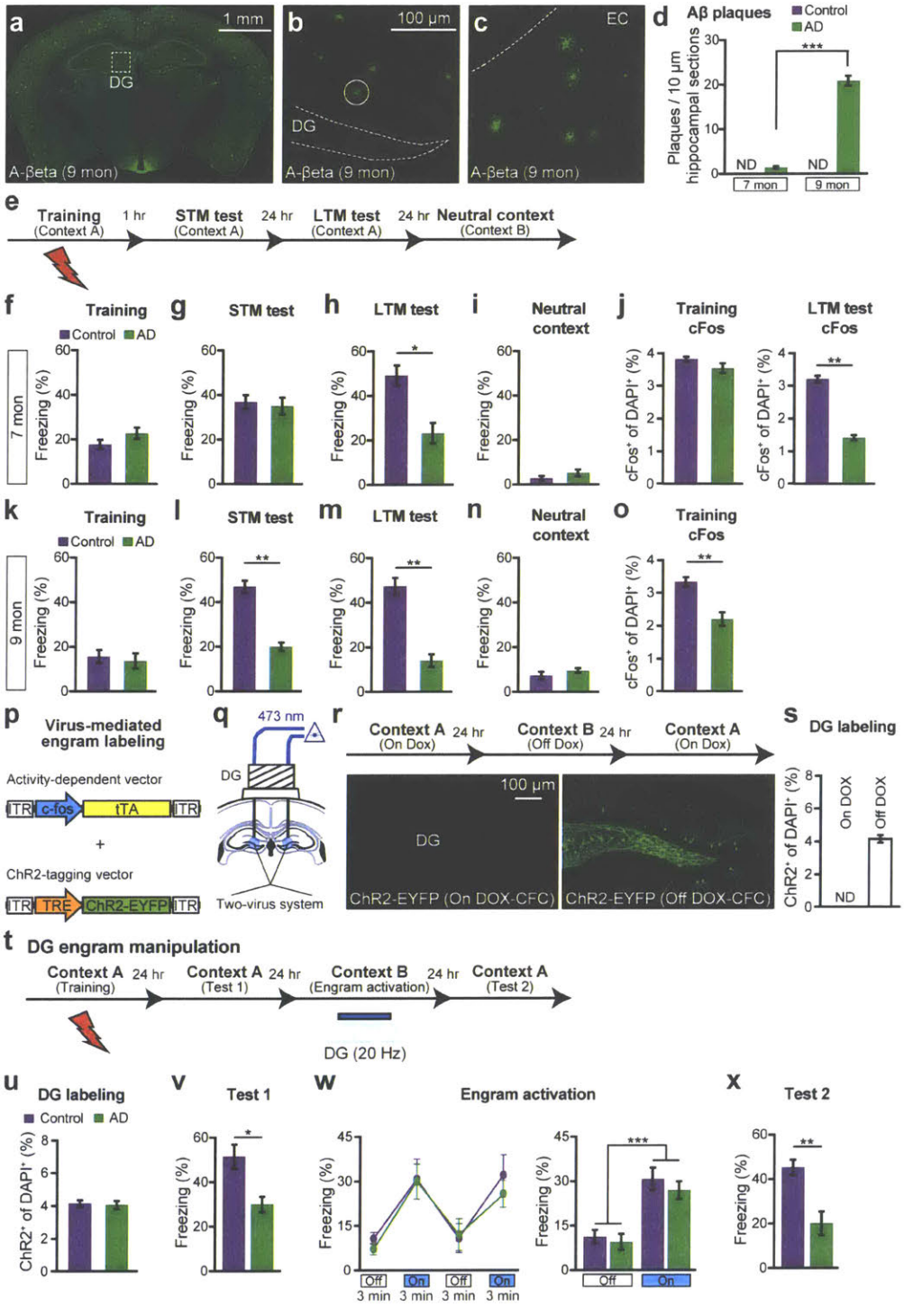
a
1 mm
DG
A-βeta (9 mon)
b
100 μm
DG
A-βeta (9 mon)
c
EC
A-βeta (9 mon)
d
Aβ plaques
Control
AD
Plaques / 10 μm hippocampal sections
***
ND
ND
7 mon
9 mon
e
Training
(Context A)
1 hr
STM test
(Context A)
24 hr
LTM test
(Context A)
24 hr
Neutral context
(Context B)
f
Training
g
STM test
h
LTM test
i
Neutral context
j
Training cFos
LTM test cFos
Control
AD
7 mon
Freezing (%)
cFos+ of DAPI+ (%)
k
Training
l
STM test
m
LTM test
n
Neutral context
o
Training cFos
9 mon
p
Virus-mediated engram labeling
Activity-dependent vector
ITR
c-fos
tTA
ITR
+
ChR2-tagging vector
ITR
TRE
ChR2-EYFP
ITR
q
473 nm
DG
Two-virus system
r
Context A 24 hr
(On Dox)
Context B 24 hr
(Off Dox)
Context A
(On Dox)
100 μm
DG
ChR2-EYFP (On DOX-CFC)
ChR2-EYFP (Off DOX-CFC)
s
DG labeling
ChR2+ of DAPI+ (%)
On DOX
Off DOX
ND
t
DG engram manipulation
Context A 24 hr
(Training)
Context A 24 hr
(Test 1)
Context B 24 hr
(Engram activation)
Context A
(Test 2)
DG (20 Hz)
u
DG labeling
v
Test 1
w
Engram activation
x
Test 2
Off
On
3 min

Figure 1 | Optogenetic activation of memory engrams restores fear memory in early AD mice.

a-c, Aβ plaques in 9-month old AD mice (**a**), in DG (**b**), and in EC (**c**). **d,** Aβ plaque counts in hippocampal sections (n = 4 mice per group). **e,** CFC behavioral schedule (n = 10 mice per group). **f-i,** Freezing levels of 7-month old AD groups during training (**f**), STM test (**g**), LTM test (**h**) or upon exposure to neutral context (**i**). **j,** $cFos^+$ cell counts in the DG of 7-month old mice following CFC training or LTM test, represented in **f, h** (n = 4 mice per group). **k-n,** Freezing levels of 9-month old AD mice during training (**k**), STM test (**l**), LTM test (**m**) or upon exposure to neutral context (**n**). **o,** $cFos^+$ cell counts in the DG of 9-month old mice (n = 3 mice per group) following CFC training represented in **k**. **p,** Virus-mediated engram labeling strategy using a cocktail of AAV_9-c-fos-tTA and AAV_9-TRE-ChR2-EYFP. **q,** AD mice were injected with the two-viruses bilaterally and implanted with an optic fiber bilaterally into the DG. **r,** Behavioral schedule and DG-engram cell labeling (see Experimental methods). **s,** ChR2-$EYFP^+$ cell counts from DG sections shown in **r** (n = 3 mice per group). ND, not detected. **t,** Behavioral schedule for optogenetic activation of DG engram cells. **u,** ChR2-$EYFP^+$ cell counts from DG sections of 7-month old mice (n = 5 mice per group). **v,** Memory recall in Context A 1 day after training (Test 1, n = 9 mice per group). **w,** Freezing by blue light stimulation (left). Average freezing for the two light-off and light-on epochs (right). **x,** Memory recall in Context A 3 days after training (Test 2). Statistical comparisons are performed using unpaired t tests; $*P < 0.05$, $**P < 0.01$, $***P < 0.001$. Data are presented as mean ± SEM.

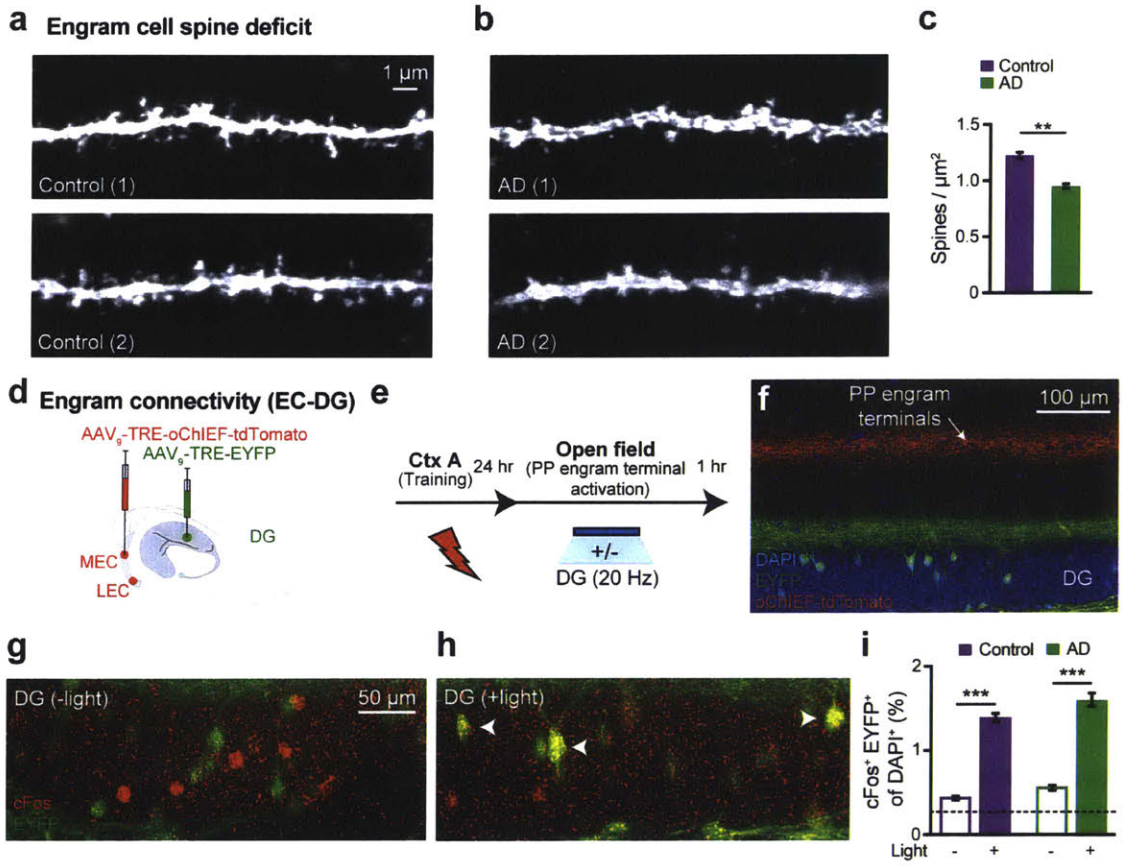

Figure 2 | Neural correlates of amnesia in early AD mice.

a-b, Images showing dendritic spines from DG engram cells of control (**a**) and AD (**b**) groups. **c,** Average spine density showing a decrease in AD mice (n = 7032 spines) compared to controls (n = 9437 spines, n = 4 mice per group). **d,** For engram connectivity, MEC/LEC and DG cells were injected with virus cocktails. **e,** Engram connectivity behavioral schedule. Mice (n = 4 per group) were either given a natural exploration session (Light -) or a PP engram terminal stimulation session (Light +) in an open field. **f,** Image showing simultaneous labeling of engram terminals (red) and engram cells (green). Green terminals reflect mossy cell axons. **g-h,** Images showing $cFos^+/EYFP^+$ overlap in the DG. **i,** $cFos^+/EYFP^+$ counts from control and AD mice. Chance overlap (0.24) calculated (see Experimental methods) and indicated by the dashed line. Statistical comparisons are performed using unpaired t tests; $^{**}P < 0.01$, $^{***}P < 0.001$. Data are presented as mean ± SEM.

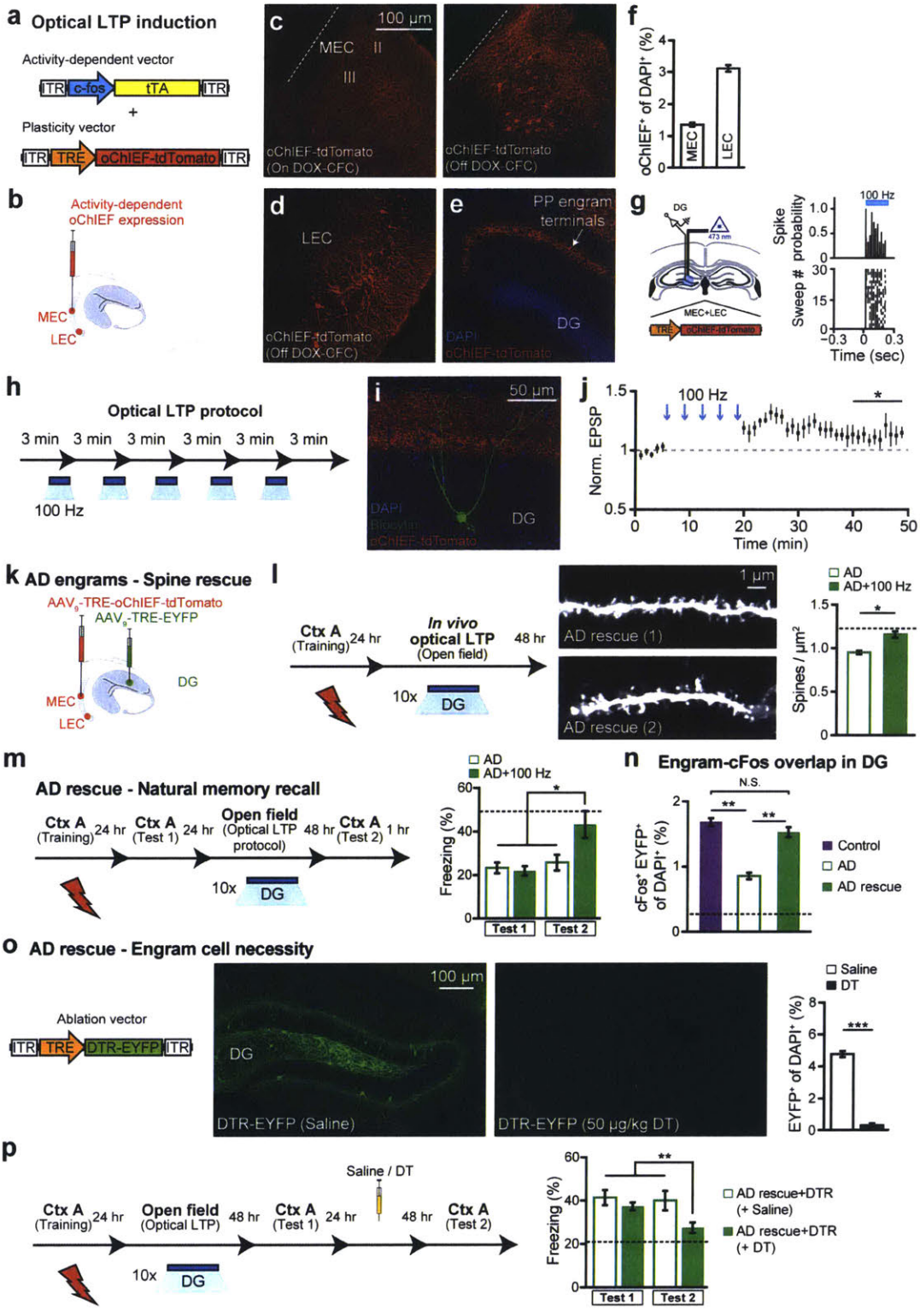
a Optical LTP induction
Activity-dependent vector
ITR c-fos tTA ITR
+
Plasticity vector
ITR TRE oChIEF-tdTomato ITR
b
Activity-dependent oChIEF expression
MEC
LEC
c
100 µm
MEC
II
III
oChIEF-tdTomato (On DOX-CFC)
oChIEF-tdTomato (Off DOX-CFC)
d
LEC
oChIEF-tdTomato (Off DOX-CFC)
e
PP engram terminals
DG
DAPI
oChIEF-tdTomato
f
oChIEF+ of DAPI+ (%)
MEC
LEC
g
DG
473 nm
MEC+LEC
TRE oChIEF-tdTomato
Spike probability
100 Hz
Sweep #
Time (sec)
h
Optical LTP protocol
3 min 3 min 3 min 3 min 3 min 3 min
100 Hz
i
50 µm
DAPI
Bloody
oChIEF-tdTomato
DG
j
100 Hz
Norm. EPSP
Time (min)
k AD engrams - Spine rescue
AAV9-TRE-oChIEF-tdTomato
AAV9-TRE-EYFP
MEC
LEC
DG
l
Ctx A (Training) 24 hr
In vivo optical LTP (Open field)
48 hr
10x DG
1 µm
AD rescue (1)
AD rescue (2)
AD
AD+100 Hz
Spines / µm²
m
AD rescue - Natural memory recall
Ctx A (Training) 24 hr
Ctx A (Test 1) 24 hr
Open field (Optical LTP protocol) 48 hr
Ctx A (Test 2) 1 hr
10x DG
AD
AD+100 Hz
Freezing (%)
Test 1
Test 2
n Engram-cFos overlap in DG
N.S.
cFos+ EYFP+ of DAPI+ (%)
Control
AD
AD rescue
o AD rescue - Engram cell necessity
Ablation vector
ITR TRE DTR-EYFP ITR
100 µm
DG
DTR-EYFP (Saline)
DTR-EYFP (50 µg/kg DT)
Saline
DT
EYFP+ of DAPI+ (%)
p
Saline / DT
Ctx A (Training) 24 hr
Open field (Optical LTP) 48 hr
Ctx A (Test 1) 24 hr
48 hr
Ctx A (Test 2)
10x DG
Freezing (%)
Test 1
Test 2
AD rescue+DTR (+ Saline)
AD rescue+DTR (+ DT)

Figure 3 | Reversal of engram-specific spine deficits rescues memory in early AD mice.

a, Engram-specific optical LTP using two viruses. **b,** Virus cocktail injected into MEC/LEC. **c-e,** Images showing oChIEF labeling 24 hours after CFC: in MEC on DOX (left) and off DOX (right; **c**); in LEC off DOX (**d**); in DG off DOX (sagittal; **e**). Scale bar shown in **c,** applies to **d** and **e**. **f,** oChIEF$^+$ cell counts (n = 3 mice per group). **g,** In vivo spiking of DG neurons in response to 100 Hz light applied to PP terminals. **h,** Optical LTP protocol (Nabavi et al., 2014). **i-j,** In vitro responses of DG cells after optical LTP. Image showing biocytin-filled DG cell receiving oChIEF$^+$ PP terminals (coronal; **i**). Excitatory post-synaptic potentials (EPSPs) showing a 10% increase in amplitude (n = 6 cells; **j**). **k,** For in vivo optical LTP at EC-DG synapses, MEC/LEC and DG cells were injected with virus cocktails. **l,** Protocol for in vivo spine restoration of DG engram cells in AD mice (left). Images showing dendritic spines of DG engram cells following LTP (middle). A two-way ANOVA followed by Bonferroni post-hoc tests revealed a spine density restoration in AD+100 Hz mice ($F_{1,211} = 7.21$, $P < 0.01$, 13025 spines, n = 4 mice per group; right). Dashed line represents control mice spine density (1.21). **m,** Behavioral schedule for memory rescue in AD mice (left). A two-way ANOVA with repeated measures followed by Bonferroni post-hoc tests revealed restored freezing in AD+100 Hz mice ($F_{1,36} = 4.95$, $P < 0.05$, n = 10 mice per group; right). Dashed line represents control mice freezing (48.53). **n,** Following rescue, mice were perfused for cFos$^+$/EYFP$^+$ overlap cell counts. Chance estimated at 0.22. N.S., not significant. **o,** Construct for ablation of engram cells using DTR (left). Images showing DG engram cells after saline/DT administration (middle). DTR-EYFP cell counts (n = 5 mice per group; right). **p,** Behavioral schedule testing the necessity of engram cells following spine restoration (left). Memory recall showed less freezing of AD mice treated with DT (AD rescue + DTR + DT) compared to saline treated mice (n = 9 mice per group; right). Dashed line represents freezing of non-stimulated early AD mice (20.48). Unless specified, statistical comparisons are performed using unpaired t tests; *P < 0.05, **P < 0.01, ***P < 0.001. Data are presented as mean ± SEM.

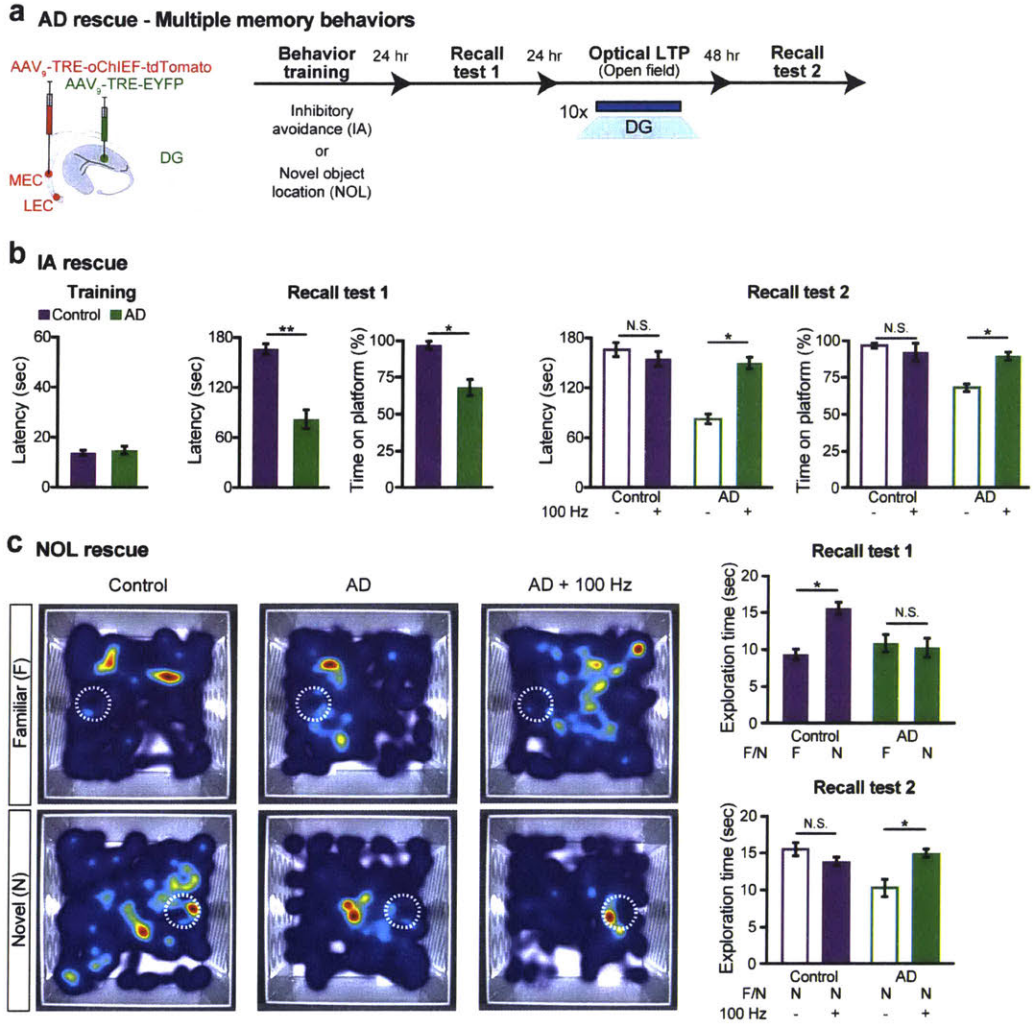

Figure 4 | Recovery of multiple types of hippocampal-dependent memories from amnesia in early AD.

a, MEC/LEC and DG cells were injected with virus cocktails (left). Behavioral schedule for engram labeling (right). **b,** IA long-term rescue (n = 10 mice per group). Latency did not differ between control and AD groups during training. Recall test 1 showed decreased latency and time on platform for AD mice. A two-way ANOVA with repeated measures followed by Bonferroni post-hoc tests revealed a recovery of IA memory in early AD mice (Latency: $F_{1,27} = 25.22$, $P < 0.001$; Time on platform: $F_{1,27} = 6.46$, $P < 0.05$; Recall test 2). **c,** NOL long-term rescue (n = 15 mice per group). Average heat maps showing exploration time for familiar or novel locations (left or right, respectively). White circles

represent object location. Recall test 1 showed comparable exploration of familiar locations by control and AD mice, however AD mice showed decreased exploration of novel locations. A two-way ANOVA with repeated measures followed by Bonferroni post-hoc tests revealed a recovery of NOL memory in early AD mice ($F_{1,56}$ = 5.87, $P < 0.05$; Recall test 2). Unless specified, statistical comparisons are performed using unpaired t tests; *$P < 0.05$, **$P < 0.01$. Data are presented as mean ± SEM.

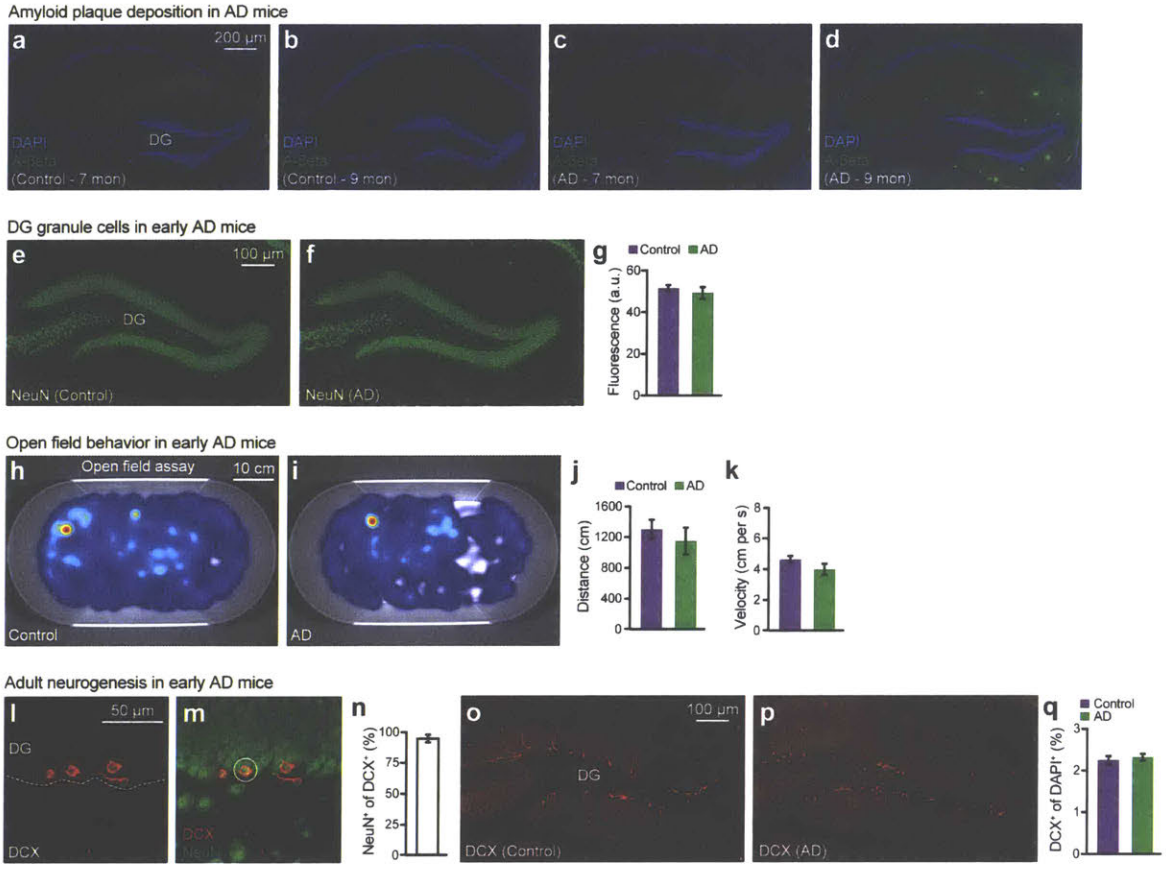

Extended Data Figure 1 | Characterization of 7-month old early AD mice.

a-d, Images showing hippocampal $A\beta^+$ plaques lacking in control mice (**a**, **b**) and 7-month old AD mice (**c**), which showed an age-dependent increase in 9-month old AD mice (**d**). **e-f,** Images showing neuronal nuclei (NeuN) staining of DG granule cells in control (**e**) and 7-month old AD (**f**) mice. **g,** $NeuN^+$ fluorescence intensity of the granule cell layer from control and AD sections shown in **e-f** (n = 8 mice per group). **h-i,** Heat maps showing exploratory behavior in an open field arena from control (**h**) and 7-month old AD (**i**) mice. **j-k,** Distance traveled (**j**) and velocity (**k**) did not differ between control and AD groups (n = 9 mice per group). **l-m,** Images showing adult newborn neurons (DCX^+) in DG sections from control mice (**l**) that are double positive for NeuN (**m**). **n,** Percentage of $NeuN^+$ cells among DCX^+ cells (n = 3 mice). **o-p,** Images showing DCX^+ neurons in DG sections from control (**o**) and AD (**p**) groups (n = 4 mice per group). **q,** DCX^+ cell counts from control and AD mice. Data are presented as mean ± SEM.

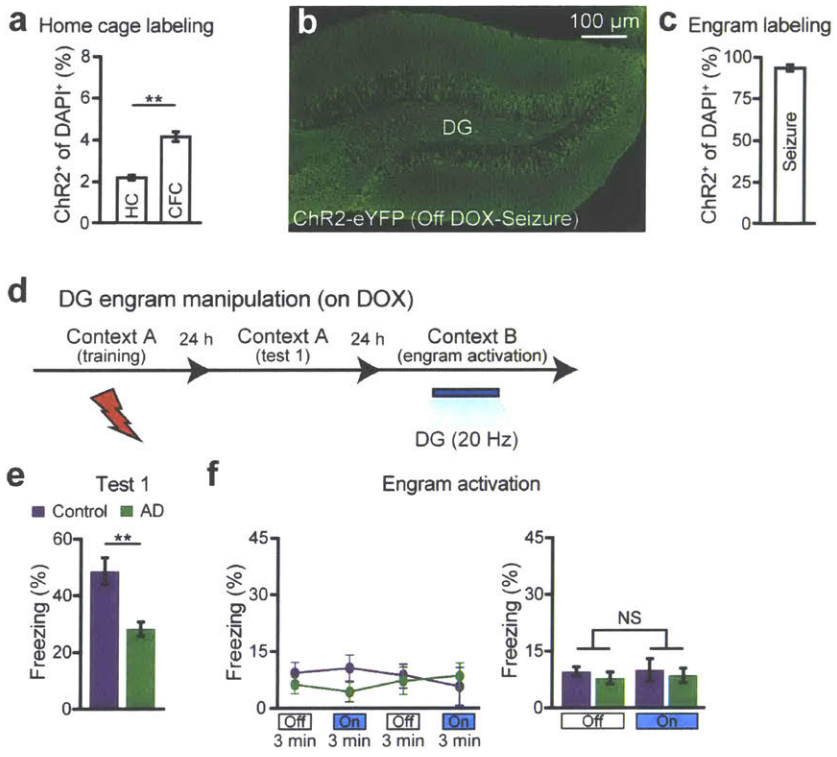

Extended Data Figure 2 | Labeling and engram activation of early AD mice on DOX.

a, Mice are taken off DOX for 24 hours in the home cage (HC) and subsequently trained in CFC. DG sections (n = 3 mice per group) revealed 2.05% ChR2-EYFP labeling in the HC, consistent with the previously established engram tagging strategy (Liu et al., 2012). **b,** Mice were injected with a virus cocktail of AAV_9-c-fos-tTA and AAV_9-TRE-ChR2-EYFP. After one day off DOX, kainic acid was used to induce seizures. Image showing efficient labeling throughout the DG. **c,** ChR2-EYFP cell counts from DG sections shown in **b** (n = 3 mice). **d,** Behavioral schedule for optogenetic activation of DG engram cells. **e,** Memory recall 1 day after training (Test 1) showed less freezing of AD mice compared to control mice (n = 8 mice per group). **f,** Engram activation with blue light stimulation (left). Average freezing for the two light-off and light-on epochs (right). Statistical comparisons are performed using unpaired t tests; $^{**}P < 0.01$. Data are presented as mean ± SEM.

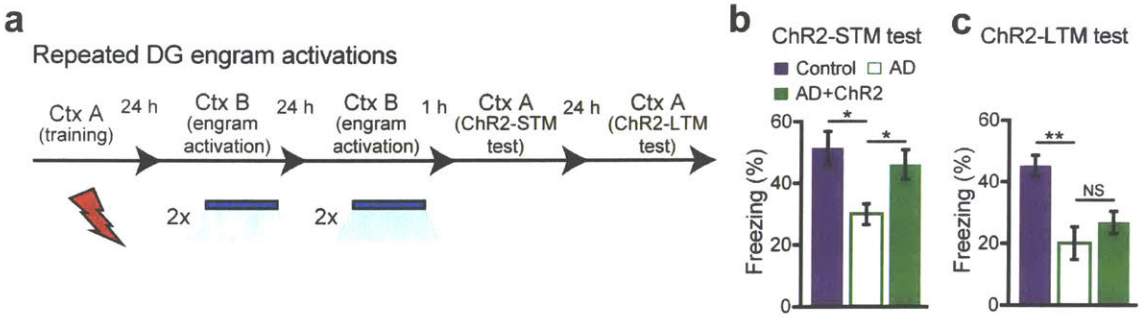

Extended Data Figure 3 | Chronic DG engram activation in early AD mice did not rescue long-term memory.

a, Behavioral schedule for repeated DG engram activation experiment. **b,** AD mice in which a DG memory engram was reactivated twice a day for two days (AD+ChR2) showed increased STM freezing levels compared to memory recall prior to engram reactivation (ChR2-STM test, n = 9 mice per group). **c,** Memory recall 1 day after repeated DG engram activations (ChR2-LTM test). N.S., not significant. Statistical comparisons are performed using unpaired t tests; *P < 0.05, **P < 0.01. Data are presented as mean ± SEM.

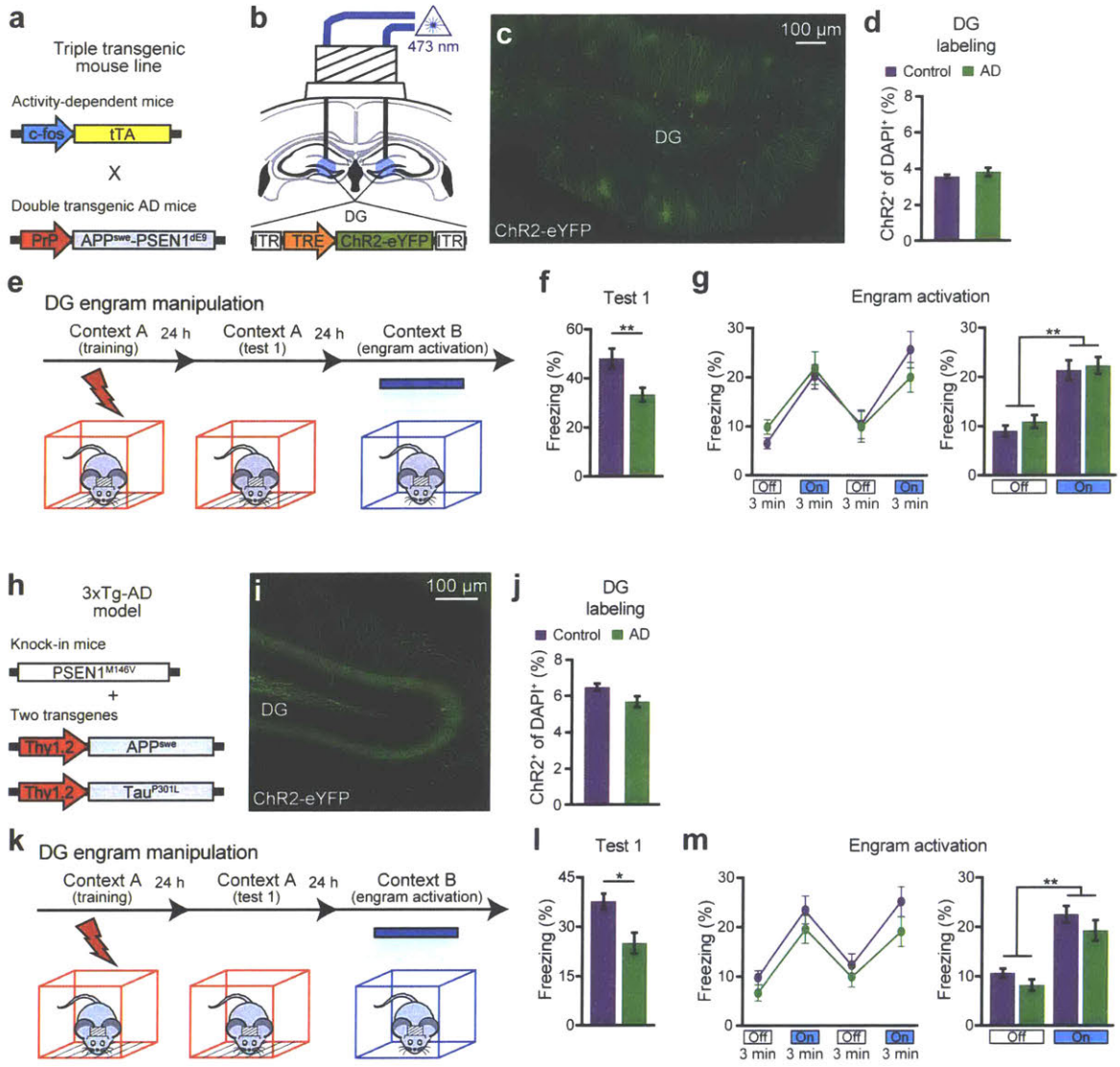

Extended Data Figure 4 | Engram activation restores fear memory in triple transgenic and PS1/APP/tau models of early AD.

a, Triple transgenic mouse line obtained by mating c-fos-tTA transgenic mice (Liu et al., 2012; Reijmers et al., 2007) with double transgenic APP/PS1 AD mice (Jankowsky et al., 2004). These mice combined with a DOX-sensitive AAV virus permits memory engram labeling in early AD. **b,** Triple transgenic mice were injected with AAV_9-TRE-ChR2-EYFP and implanted with an optic fiber targeting the DG. **c,** Image showing DG engram cells of triple transgenic mice 24 hours after CFC. **d,** ChR2-EYFP cell counts from

control and triple transgenic AD mice (n = 5 mice per group). **e,** Behavioral schedule for engram activation. **f,** Memory recall 1 day after training (Test 1) showed less freezing of triple transgenic AD mice compared to control mice (n = 10 mice per group). **g,** Engram activation with blue light stimulation (left). Average freezing for the two light-off and light-on epochs (right). **h,** Triple transgenic AD model (3xTg-AD) as previously reported (Oddo et al., 2003). A cocktail of AAV_9-c-fos-tTA and AAV_9-TRE-ChR2-EYFP viruses were used to label memory engrams in 3xTg-AD mice. **i,** Image showing memory engram cells in the DG of 3xTg-AD mice 24 hours after CFC. **j,** ChR2-EYFP cell counts from DG sections of control and 3xTg-AD mice (n = 4 mice per group). **k,** Behavioral schedule for engram activation. **l,** Memory recall 1 day after training (Test 1) showed less freezing of 3xTg-AD mice compared to control mice (n = 9 mice per group). **m,** Engram activation with blue light stimulation (left). Average freezing for the two light-off and light-on epochs (right). Statistical comparisons are performed using unpaired t tests; $*P < 0.05$, $**P < 0.01$. Data are presented as mean ± SEM.

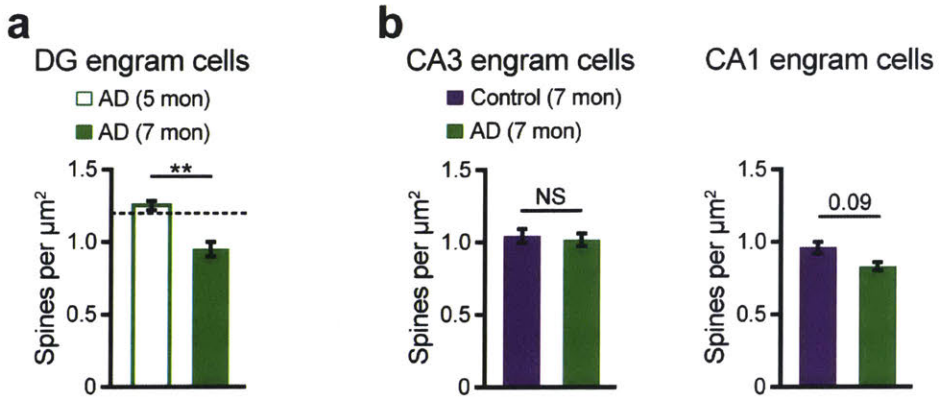

Extended Data Figure 5 | Dendritic spines of engram cells in 7-month old early AD mice.

a, Average dendritic spine density of DG engram cells showed an age-dependent decrease in 7-month old APP/PS1 AD mice (n = 7032 spines) as compared to 5-month old AD mice (n = 4577 spines, n = 4 mice per group). Dashed line represents spine density of control mice (1.21). **b,** (Left) Average dendritic spine density of CA3 engram cells in control (n = 5123 spines) and AD mice (n = 6019 spines, n = 3 mice per group). (Right) Average dendritic spine density of CA1 engram cells in control (n = 9120 spines) and AD mice (n = 7988 spines, n = 5 mice per group). N.S., not significant. Statistical comparisons are performed using unpaired t tests; $^{**}P < 0.01$. Data are presented as mean ± SEM.

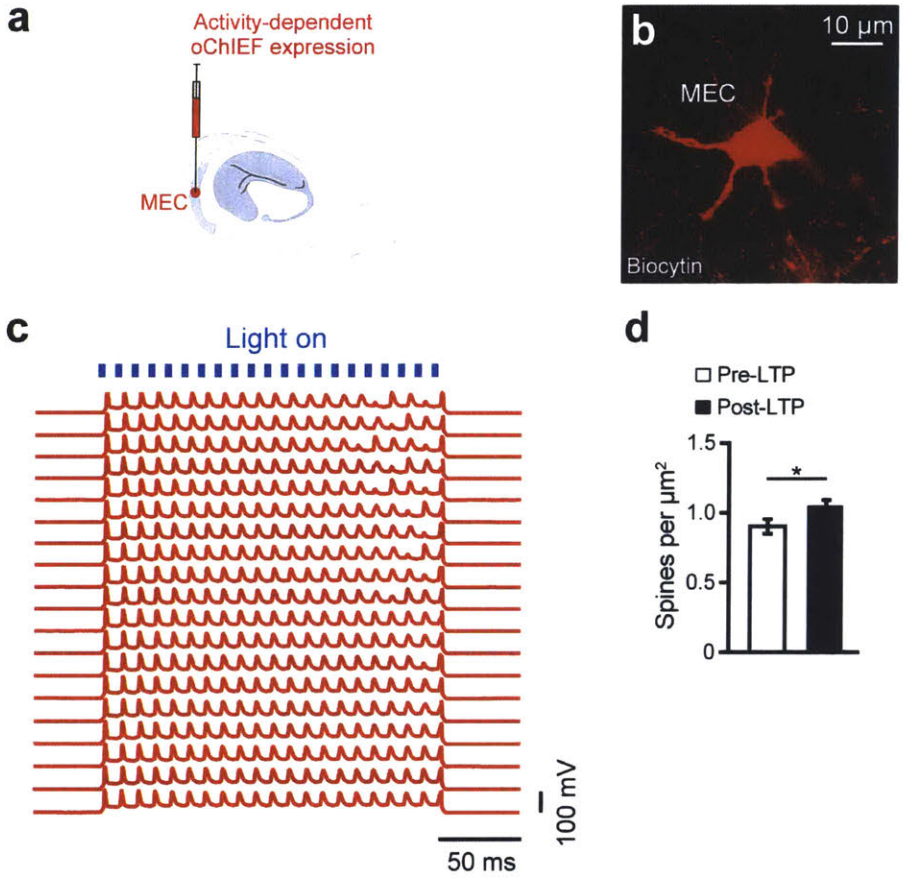

Extended Data Figure 6 | High fidelity responses of oChIEF$^+$ cells and dendritic spines of DG engram cells after in vitro optical LTP.

a, Entorhinal cortex (EC) cells were injected with a virus cocktail containing AAV_9-TRE-oChIEF-tdTomato for activity-dependent labeling. **b,** Image showing a biocytin-filled oChIEF$^+$ stellate cell in EC. **c,** 100 Hz (2 ms pulse width) stimulation of an oChIEF$^+$ cell across 20 consecutive trials. Spiking responses exhibit high fidelity. **d,** Average dendritic spine density of biocytin-filled DG cells showed an increase following optical LTP induction in vitro (n = 1452 spines, n = 6 cells). Statistical comparisons are performed using unpaired t tests; *$P < 0.05$. Data are presented as mean ± SEM.

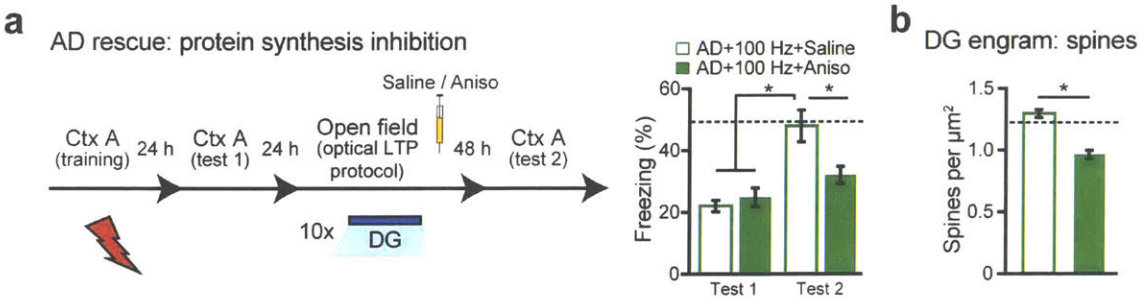

Extended Data Figure 7 | Behavioral rescue and spine restoration by optical LTP is protein-synthesis dependent.

a, Modified behavioral schedule for long-term rescue of memory recall in AD mice in the presence of saline or anisomycin (left). Memory recall 2 days after LTP induction followed by drug administration showed less freezing of AD mice treated with anisomycin (AD + 100 Hz + Aniso) compared to saline treated AD mice (AD + 100 Hz + Saline, n = 9 mice per group; right). Dashed line represents freezing level of control mice (48.53). **b,** Average dendritic spine density in early AD mice treated with anisomycin after LTP induction (n = 4810 spines) was decreased compared to saline treated AD mice (n = 6242 spines, n = 4 mice per group). Dashed line represents spine density of control mice (1.21). Statistical comparisons are performed using unpaired t tests; *P < 0.05. Data are presented as mean ± SEM.

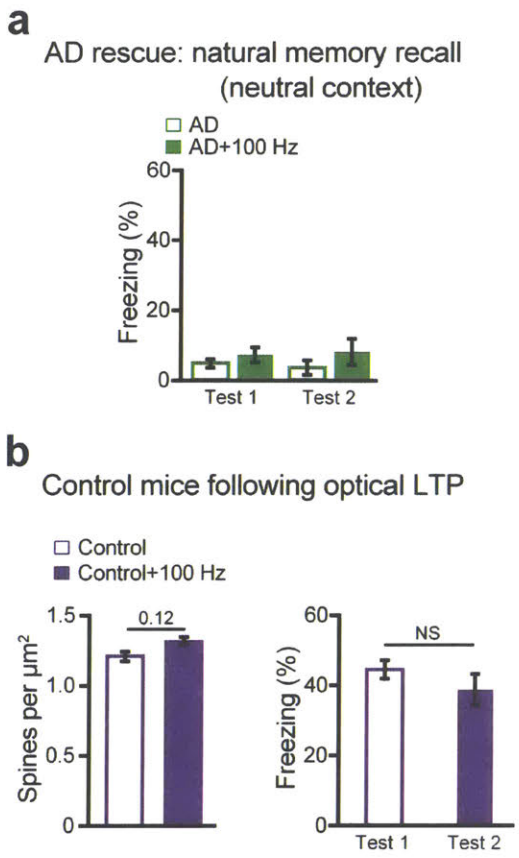

Extended Data Figure 8 | Rescued early AD mice behavior in a neutral context and control mice following in vivo optical LTP.

a, After the long-term rescue of memory recall in AD mice (Test 2, Fig. 3m), animals were placed in an untrained neutral context to measure generalization (n = 10 mice per group). Rescued AD mice (AD+100 Hz) did not display freezing behavior. **b,** (Left) Average dendritic spine density of DG engram cells from control mice remained unchanged following optical LTP induction in vivo (Control + 100 Hz, n = 4211 spines, n = 3 mice; Control data from Figure 2c). (Right) The behavioral rescue protocol applied to early AD mice (Fig. 3m) was tested in age-matched control mice (n = 9 mice per group). Similar freezing levels were observed following optical LTP (Test 2) as compared to memory recall prior to the 100 Hz protocol (Test 1). N.S., not significant. Statistical comparisons are performed using unpaired t tests. Data are presented as mean ± SEM.

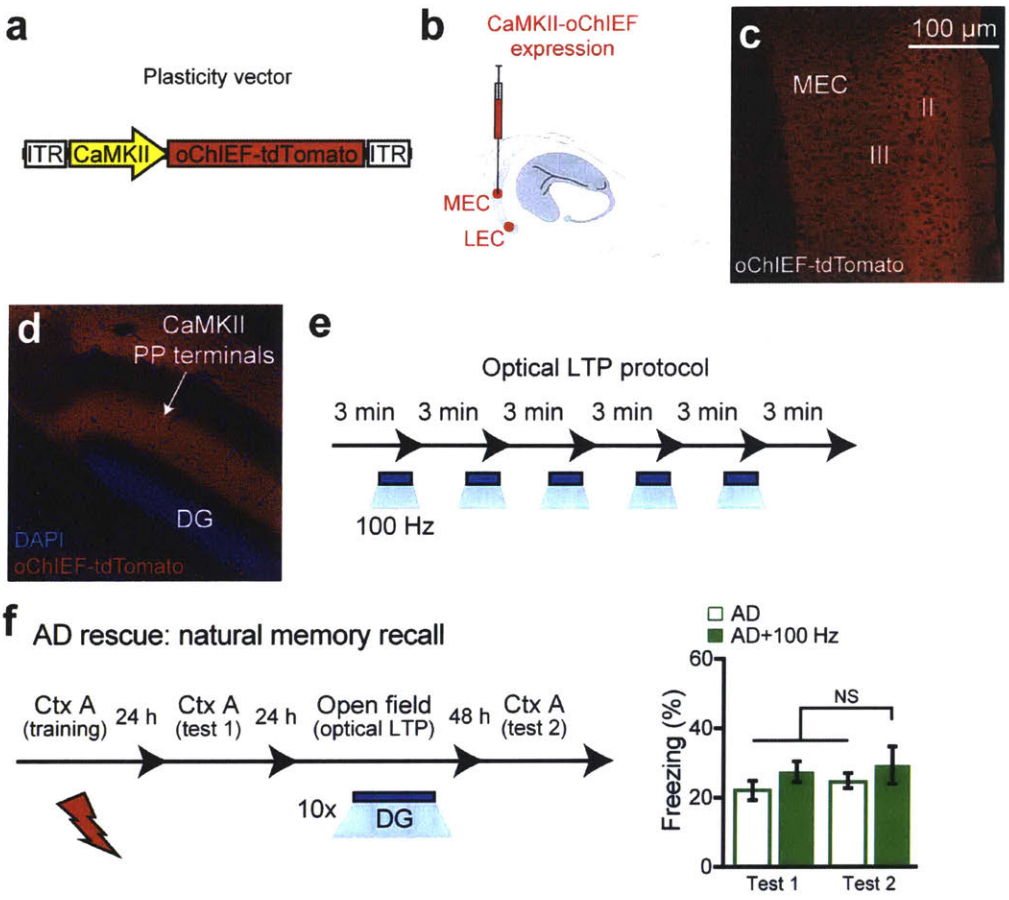

Extended Data Figure 9 | Optical LTP using a CaMKII-oChIEF virus did not rescue memory in early AD mice.

a, AAV virus expressing oChIEF-tdTomato under a CaMKII promoter. **b,** CaMKII-oChIEF virus injected into MEC and LEC. **c-d,** Images showing tdTomato labeling in a large portion of excitatory MEC neurons (**c**) as well as the PP terminals in DG (**d**). **e,** In vivo optical LTP protocol (Nabavi et al., 2014). **f,** Behavioral schedule for long-term rescue of memory recall in AD mice (left). In contrast to the engram-specific strategy, long-term memory could not be rescued by stimulating a large portion of excitatory PP terminals in the DG (right; n = 9 mice per group). N.S. not significant. Statistical comparisons are performed using unpaired t tests. Data are presented as mean ± SEM.

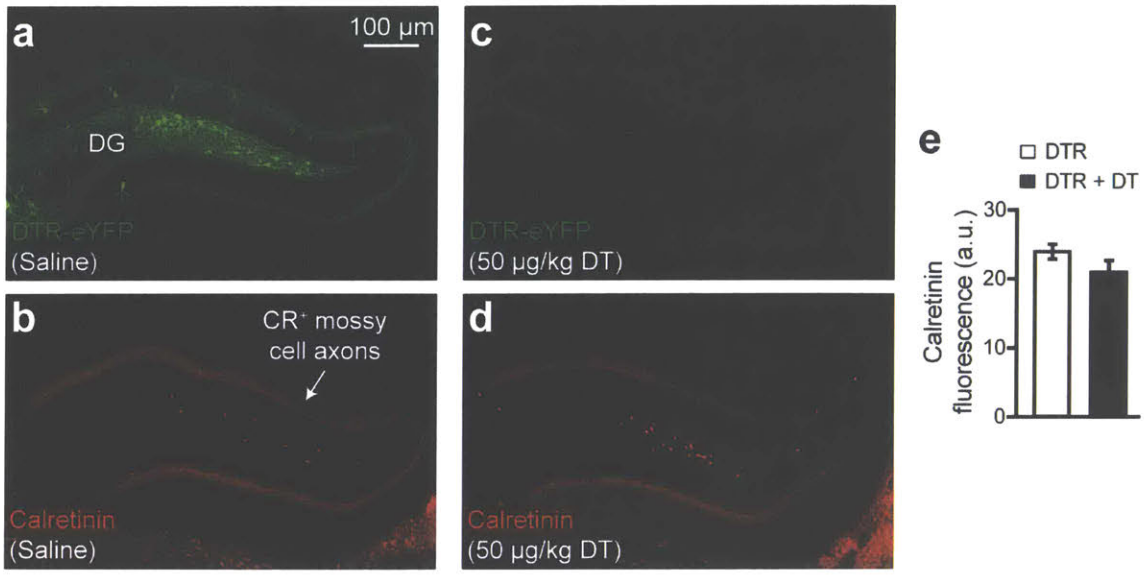

Extended Data Figure 10 | Normal DG mossy cell density after engram cell ablation.

a-d, Images showing DG engram cells after saline treatment (**a**) and the corresponding calretinin positive (CR^+) mossy cell axons (**b**). DTR-EYFP engram cell labeling after DT treatment (**c**) and the respective CR+ mossy cell axons (**d**). **e,** CR^+ fluorescence intensity of mossy cell axons from saline and DT treated DG sections shown in **a-d** (n = 8 mice per group). Data are presented as mean ± SEM.

Chapter 4. Dorsal subiculum is required for episodic memory retrieval

The formation and retrieval of a memory is thought to be accomplished by activation and reactivation, respectively, of the memory-holding cells (engram cells) by a common set of neural circuits, but this hypothesis has not been established. The medial temporal-lobe system is essential for the formation and retrieval of episodic memory for which individual hippocampal subfields and entorhinal cortex layers contribute by carrying out specific functions. One subfield whose function is poorly known is the subiculum. Here, we show that dorsal subiculum and the circuit, CA1 to dorsal subiculum to medial entorhinal cortex layer 5, plays a crucial role selectively in the retrieval of episodic memories. Conversely, the direct CA1 to medial entorhinal cortex layer 5 circuit is essential specifically for memory formation. Our data suggest that the subiculum-containing detour loop is dedicated to meet the requirements associated with recall such as rapid memory updating and retrieval-driven instinctive fear responses.

4.1 Brief introduction

It is generally thought that formation and retrieval of a memory are accomplished by activation and reactivation of memory-holding cells (engram cells), respectively, by a largely common set of neural circuits that convey relevant sensory and/or processed information. However, this hypothesis has not been well studied. One of the best neural systems to prove this issue is the medial temporal lobe (MTL), including the hippocampus (HPC) and entorhinal cortex (EC), which plays crucial roles in episodic memory (Eichenbaum et al., 2007; Squire, 1992). Numerous studies have identified specific and crucial roles of individual HPC subfields and EC layers to the overall mnemonic function (Deng et al., 2010; Hasselmo and McClelland, 1999; Hitti and Siegelbaum, 2014; Moser et al., 2014; Nakazawa et al., 2004). However, the essential function of one HPC subfield, subiculum (Sub), is poorly known. The mammalian HPC formation is organized primarily as a unidirectional circuit, where information transferred from the EC's superficial layers to the dentate gyrus (DG) is processed successively in CA subfields: CA3, CA2,

and CA1. Dorsal CA1 (dCA1) sends its primary projections directly to medial EC layer 5 (EC5) or indirectly via dorsal subiculum (dSub) (a detour circuit). One of the interesting differences between the direct and indirect HPC output pathways is that in the latter, dSub projects not only to EC5, but also to many cortical and subcortical brain regions (Ding, 2013; Kishi et al., 2000).

Using functional magnetic resonance imaging of human subjects, several studies have suggested that the DG and CA subfields are selectively activated during episodic memory formation, whereas subiculum (Sub) is active during the recollection of an episode (Eldridge et al., 2005; Gabrieli et al., 1997). In rodents, ibotenic acid lesions of the CA1 subfield or Sub caused impairments in the acquisition of place navigation (Morris et al., 1990). However, since human imaging studies provide only correlative, rather than causal, evidence and rodent lesions are not well targeted to a specific hippocampal subregion, especially given the close proximity of CA1 and dSub, it has not been possible to identify the essential function of Sub in episodic memory. Furthermore, previous studies did not address the potential purpose of the parallel diverging and converging dCA1 to medial EC5 and dCA1 to dSub to medial EC5 circuits in memory formation versus retrieval.

In this study, we addressed these issues by creating a mouse line expressing Cre recombinase specifically in dSub neurons. Combined with circuit tracing and optogenetic manipulations during behavioral paradigms, we found differential roles of dSub projections in hippocampal memory retrieval and retrieval-induced stress hormone responses. We demonstrate that dSub and the circuit, CA1→dSub→EC5, is selectively required for memory retrieval, while the dSub to mammillary bodies (MB) circuit regulates stress hormones following memory retrieval. In contrast, the direct CA1→EC5 circuit is essential for hippocampal memory formation, but not recall. Our study reveals a functional double-dissociation between parallel hippocampal output circuits that are important for memory formation versus memory retrieval.

4.2 Experimental results

We took advantage of the finding that fibronectin-1 (FN1) gene expression is restricted to dSub neurons (Lein et al., 2004) and created a transgenic mouse line (FN1-Cre) that expresses Cre recombinase under the FN1 promoter (Figure 1A, and see Experimental methods). When infected with a Cre-dependent adeno-associated virus containing an eYFP gene, eYFP expression was highly restricted to dSub neurons and was completely absent in neighboring dCA1 excitatory neurons identified by WFS1 (Figure 1B). The expression of eYFP was restricted to $CaMKII^{+}$ excitatory neurons in both the deep and superficial layers of dSub (Figures 1C-1D, and see Figure S1A). This eYFP expression accounted for over 85% of all excitatory neurons in this brain region, and was dSub-specific along the entire medial-lateral axis (Figures 1E-1K). Further, Cre expression was absent in ventral subiculum (vSub) and medial entorhinal cortex (MEC) in this mouse line (Figures S1B-S1K). Using in situ hybridization, we confirmed that Cre expression in this mouse line is highly restricted to dSub, and the dorsal tegmental nucleus (DTg) in the brain stem (Figure S1L). Thus, FN1-Cre mice allows for the genetic manipulation of dSub excitatory neurons with unprecedented specificity.

We next examined the inputs to dSub excitatory neurons as well as their anterograde brain-wide projection pattern. Consistent with traditional anatomical studies (Ding, 2013; Kishi et al., 2000), monosynaptic retrograde tracing using a Cre-dependent helper virus combined with rabies virus (RV) technology (Wickersham et al., 2007) revealed that dCA1 provides the major input to dSub excitatory neurons (Figures 2A-2C). Other brain areas that provide inputs to dSub include parasubiculum (PaS), retrosplenial agranular cortex (RSA), superficial layers of EC (MEC II/III), nucleus of the diagonal band (NDB), nucleus accumbens shell (Acb Sh), and several thalamic nuclei (Thal Nucl) (Figure 2D, and see Figure S1M).

A Cre-dependent channelrhodopsin-2 (ChR2)-eYFP virus combined with light sheet microscopy of CLARITY (Chung et al., 2013, see Experimental methods)-processed brain samples revealed that major efferents of dSub neurons were directed to RSA, mammillary bodies (MB), medial EC5, and postrhinal cortex (Pos) (Figures 2E-2F). No projections from dSub were observed in the superficial layers

(II/III) of MEC (Figure 2G). These dSub neurons converged on both medial and lateral regions of MB (Figure 2H). Using a Cre-dependent synaptophysin virus to label dSub axonal terminals, we found that these Cre^{+} neurons express vesicular glutamate transporters 1 and 2 (Kaneko et al., 2002), reflecting their excitatory nature (Figures S1N-S1P). Injection of a retrograde tracer, cholera toxin subunit B (CTB), into the MB revealed a gradient of CTB555 with higher intensity labeling in the proximal part of dSub (i.e., closer to CA1), whereas injection into medial EC5 showed a gradient of CTB488 with higher intensity labeling in the distal part of dSub (i.e., away from CA1) (Figures 2I-2M, and see Figure S1Q) (Witter et al., 1990). However, neurons in both proximal and distal parts of dSub were weakly labeled by CTB injected into MB or EC5. Together, these results indicate that dCA1 serves as the main input structure to dSub, and that the majority of dSub neurons send projections to multiple downstream target structures.

To examine the functional role of dSub neurons and their circuits, we performed optogenetic inhibition experiments using a Cre-dependent eArch3.0-eYFP virus. During the contextual fear-conditioning (CFC) paradigm, we confirmed that green light inhibition of dSub decreased behavior-induced immediate early gene cFos-positive neurons (Figures S2A-S2L). Inhibition of dSub neurons during CFC training had no effect on footshock-induced freezing behavior or long-term memory formation (Figure 3A). In contrast, dSub inhibition during CFC recall tests decreased behavioral performance (Figure 3B). Inhibition of dSub neurons had no effect on motor behaviors in an open-field assay (Figure S2M). Inhibition of dSub terminals in medial EC5, but not in MB, also revealed a memory retrieval deficit (Figure 3C). Since the behavioral effect of dSub inhibition in this mouse line is based on eArch expression in approximately 85% of excitatory neurons in this brain region, we examined the effect of a more complete inhibition of dSub neurons. Inhibition of dSub→EC5 terminals in wild type mice using an EF1α-eArch3.0-eYFP virus revealed a greater memory retrieval deficit (Figure S3 vs. Figure 3C). Further, inhibition of vSub→EC5 terminals showed normal levels of memory recall (Figure S3).

Conversely, optogenetic activation of ChR2-eYFP-expressing dSub projections to medial EC5 during CFC recall tests increased recall-induced freezing behavior in the training context, but not in a

neutral context (Figure 3D, and see Figure S4A). This result indicates that dSub is involved in hippocampal memory retrieval in a context-specific manner. Activation of dSub→EC5 in mice that did not receive footshocks during training lacked freezing behavior during the recall test, supporting the specificity of increased memory retrieval in CFC-trained animals. Our interpretation of these optogenetic activation experiments is that in the training context natural recall cues reactivate engram cells in all subfields of the hippocampus, like DG, CA3, and CA1, but also in dSub. When the activity of dSub projections to EC5 is further increased by ChR2 this leads to enhanced freezing due to increased activation of dSub engram cells. On the other hand, in a neutral context lacking the specific natural recall cues to reactivate dSub engram cells, the ChR2 activation without engram labeling is not sufficient to induce memory recall. In another hippocampus-dependent memory paradigm, trace fear-conditioning, dSub→EC5 inhibition impaired memory recall (Figure 3E, and see Figures S4B-S4C). In contrast, inhibition of dSub→EC5 had no effect on the recall of a hippocampus-independent memory formed during delay fear-conditioning (Figures S4D-S4E). Together, these experiments indicate that the dSub→EC5 circuit regulates episodic memory retrieval bidirectionally. We confirmed that the dSub→EC5 projection is also necessary for the retrieval of a positive-valence, hippocampus-dependent (Raybuck and Lattal, 2014) memory formed in a conditioned place preference (CPP) paradigm (Figure 3F, and see Figures S4F-S4G).

During both CFC training and recall, levels of the stress hormone corticosterone (CORT) increases in the blood (Figure 3G), which is believed to be important to prepare the animal for a predicted immediate danger (Kelley et al., 2009). Given our finding that dSub neurons are required for memory retrieval, but not memory formation, we investigated whether the dSub→MB circuit is involved in retrieval-induced stress hormone responses. Optogenetic inhibition of dSub→MB projections following CFC recall, but not following CFC training, prevented the CORT increase (Figure 3G). This deficit was specific to dSub→MB terminal inhibition, since dSub→EC5 terminal inhibition had no effect. In addition, optogenetic activation of ChR2-expressing dSub→MB projections following CFC recall

increased CORT levels, revealing a bidirectional regulation of blood stress hormone levels by the dSub→MB circuit following fear memory retrieval. Interestingly, we did not observe increased CORT levels following CPP memory retrieval (Figure S4H). From our finding that the dSub→EC5 circuit is crucial for CPP memory retrieval (Figure 3F), it is clear that dSub neurons are activated and therefore both downstream EC5 and MB circuits would be activated. The lack of increased CORT levels following CPP memory retrieval suggests that the dSub→MB circuit is necessary but not sufficient to induce CORT. These experiments uncovered a neural circuit originating from dSub that regulates stress hormone responses to conditioned cues.

The dCA1 neurons send primary projections directly to medial EC5, or indirectly via dSub (Ding, 2013). We examined whether the same dCA1 neurons send divergent projections to both dSub and EC5, or whether these two circuits involve distinct subpopulations of dCA1 neurons. To test these possibilities, we conducted monosynaptic retrograde tracing by injecting a Cre-dependent helper virus combined with rabies virus (Wickersham et al., 2007) into dSub of FN1-Cre mice combined with CTB488 injected into medial EC5 (Figures 4A-4C, and see Figure S1Q). We observed three neuronal populations distributed throughout the proximal-distal axis of dCA1, namely RV-mCherry-positive dCA1 cells, CTB488-positive dCA1 cells, and double-positive dCA1 cells (Figures 4D-4F), indicating that dCA1 neurons project collaterally to both dSub and medial EC5 (22%), project to dSub alone (18%), or to medial EC5 alone (23%) (Figure 4G, and see Figures S5A-S5H). A significant proportion of the remaining dCA1 neurons most likely send primary projections to the deep layers of the lateral EC (LEC5) (Knierim et al., 2013), which we confirmed using CTB retrograde tracing (Figure S5I). Further, it has been suggested that proximal and distal dCA1 may play differential roles in memory formation (Nakazawa et al., 2016), however we did not observe differences between dCA1 neurons projecting to dSub and EC5 based on their proximal versus distal location. Thus, these data demonstrate that, although there are distinct dCA1 subpopulations that project to either dSub or EC5, a significant proportion of dCA1 neurons projecting to dSub and EC5 are shared between these two circuits.

Given the selective role of the dSub→EC5 circuit in memory retrieval and our finding that heterogeneous subpopulations of dCA1 neurons project to dSub and medial EC5, respectively, we next investigated the behavioral contributions of the direct dCA1→EC5 circuit. The injection of a Cre-dependent H2B-GFP virus into dCA1 of CA1 pyramidal cell-specific Cre transgenic mice, TRPC4-Cre (Okuyama et al., 2016), resulted in GFP expression restricted to dCA1 pyramidal cells without any expression in dSub (Figure 4H). Terminal inhibition of CA1 axons at medial EC5 during CFC training impaired long-term memory formation (Figure 4I), whereas the same manipulation during CFC recall had no effect on behavioral performance (Figure 4J). Further, consistent with the role of dSub in CFC recall, terminal inhibition of dCA1→dSub during CFC recall, but not during CFC training, decreased behavioral performance (Figures 4K-4L). Therefore, the direct dCA1→EC5 circuit plays a crucial role in the encoding, but not recall, of CFC long-term memory, whereas the indirect dCA1→dSub→EC5 circuit is crucial for memory recall, but not encoding.

A potential purpose of the parallel diverging and converging direct dCA1→EC5 and indirect dCA1→dSub→EC5 circuits could be to support rapid memory updating (Lee, 2010). To test this possibility, we performed the pre-exposure mediated contextual fear-conditioning (PECFC) paradigm with optogenetic terminal inhibition of CA1→EC5 (Figure 4M) or dSub→EC5 (Figure 4N) during the pre-footshock period (context retrieval) only or footshock period (fear association) only, on Day 2. CA1→EC5 inhibition specifically during the footshock period of Day 2 impaired the context-shock association evidenced by decreased freezing on Day 3, whereas inhibition during the pre-footshock period had no effect (Figure 4M). In contrast, dSub→EC5 inhibition during the pre-footshock period of Day 2 impaired the context-shock association on Day 3, while inhibition restricted to the footshock period had no effect (Figure 4N). Together, these data indicate that the dSub→EC5 circuit is crucial for the rapid recall in order to perform memory updating, while the CA1→EC5 circuit is crucial for encoding new information into a long-term memory.

Expression of immediate-early genes (IEGs) has been used to map specific functions onto neuronal activity in a given brain region (Kubik et al., 2007). In order to acquire cellular level evidence supporting the dedicated role of dSub in recall rather than encoding of CFC memory, we monitored IEG cFos activation in dCA1 and dSub during CFC behavior. To measure cFos activation by training or recall, we took advantage of a virus-mediated strategy (Roy et al., 2016) using a cocktail of c-Fos-tTA and TRE-H2B-GFP viruses (Figures 5A-5B). Wild type mice raised on a doxycycline (DOX) diet to prevent activity-dependent labeling by the injected virus cocktail were taken off DOX 24 hr before CFC encoding or recall to visualize H2B-GFP labeling in CA1 and dSub (Figures 5C-5E). There was significant cFos activation in both CA1 and dSub following encoding or recall epochs as compared to the home cage group (Figure 5F). Interestingly, in dSub, memory recall epochs enhanced cFos activation more compared with encoding epochs, whereas there was no difference of cFos activation in CA1 neurons elicited by these epochs (Figure 5G).

Further, we examined the overlap between behavior-induced cFos in CA1 and CA1 cells that were retrogradely labeled by injection of CTB555 into dSub or medial EC5 (Figure S1Q). Consistent with the optogenetic manipulation experiments, CA1 neurons projecting to EC5 showed higher levels of cFos activation during CFC encoding rather than retrieval, whereas CA1 neurons projecting to dSub showed higher levels of cFos activation during retrieval (Figure 5H, and see Figures S5J-S5M). To examine CA1 memory engram cell reactivation following recall, among dSub and EC5 projecting subpopulations, we tagged CA1 engram cells formed during CFC encoding using a virus cocktail of c-Fos-tTA and TRE-ChR2-eYFP (Liu et al., 2012), while simultaneously labeling CA1 cells projecting to dSub or medial EC5 with CTB555. One day after training, we quantified the overlap between recall-induced cFos in CA1 and CA1 engram cells that were retrogradely labeled (Figures 5I-5L). Strikingly, dSub-projecting CA1 engram cells showed higher cFos reactivation following memory retrieval compared to EC5-projecting CA1 engram cells (Figure 5M). Next, following CFC recall, we measured cFos activation levels in the basolateral amygdala (BLA), which plays crucial roles in fear memory encoding and recall (Hall et al., 2001). Terminal inhibition of the dSub→EC5 circuit, but not the dCA1→EC5 circuit, decreased cFos

levels in the BLA (Figure 5N), further indicating that the direct and indirect dCA1 output circuits have differential functional roles in memory retrieval.

We also investigated activation of dSub and dCA1 pyramidal cells in response to training and recall by monitoring in vivo calcium (Ca^{2+}) transients using a miniaturized microendoscope (Kitamura et al., 2015; Sun et al., 2015; Ziv et al., 2013). For this purpose, Cre-dependent GCaMP6f virus was injected into the dSub of FN1-Cre mice to specifically express the Ca^{2+} indicator in dSub cells (Figure 6A, and see Figures S6A-S6B). As expected, expression of GCaMP6f was restricted to dSub, with no expression in CA1 neurons in these mice (Figures 6B, 6D). Similarly for dCA1 neurons, GCaMP6f virus was injected into the dCA1 of dCA1-specific WFS1-Cre mice (Kitamura et al., 2014, and see Experimental methods) (Figures 6C, 6E). With the open field paradigm (Figures S6C-S6G), CA1 neurons showed homogeneous activation profiles, whereas dSub neurons displayed two types of activation profiles (Geva-Sagiv et al., 2016; Sharp and Green, 1994; Staff et al., 2000; Taube, 1993): short-tail cells whose profiles were similar to those of CA1 cells, and long-tail cells in which the post-stimulation activity persisted as long as 15 s (Figures 6F-6G). Consistent with a previous study (Sharp and Green, 1994), dSub neurons exhibited place fields, which were larger in both types of dSub cells compared to CA1 pyramidal cells (Figure 6H, and see Figure S6H).

Next, we investigated Ca^{2+} activity patterns as mice went through the CFC paradigm (Figure 6I, and see Figures S6I-S6K). CA1 showed an increased percentage of active cells during both training and recall periods compared to the pre-footshock period in the context in which a footshock was subsequently delivered. The dSub neurons showed an increased percentage of active cells during recall compared to the pre-footshock or training periods, and no significant difference of active cell percentages was observed between the latter two periods (top row, Figure 6I). We then divided the training and recall periods into two epochs—non-freezing (NF) and freezing (F)—in order to differentiate an effect of the animal's movement state (Ranck, 1973) on the proportion of active cells. During training, the proportion of active CA1 cells was greater during F epochs compared to the NF epochs, whereas these proportions were similar during recall. In contrast, the proportions of active dSub cells were greater during recall compared

to training regardless whether the mice were in F or NF epochs. We then subdivided active dSub cells into short-tail and long-tail cells, and found that the proportion of active short-tail cells were greater during recall compared to training regardless whether mice were in F or NF epochs. In contrast, the proportion of active long-tail dSub cells was greater specifically during recall-induced F epochs, compared to the other three types of epochs (bottom row, Figure 6I). Together, and consistent with the behavior and cFos activation experiments, these data demonstrate distinct contributions of dCA1 and dSub cells to memory encoding and memory recall, respectively.

4.3 Discussion

It has been established that CA1 and Sub serve as the major output structures of the hippocampus (O'Mara, 2006); however, the functional role of Sub in hippocampus-dependent episodic memory has remained elusive. Here, we have shown that optogenetic inhibition of dSub during recall, but not during encoding, impairs behavioral performance in three hippocampal-dependent memory paradigms: CFC, trace fear-conditioning, and conditioned place preference. The activity of dSub neurons is capable of regulating memory recall bidirectionally: its inhibition impairs recall and its activation enhances recall. To our knowledge, this is the first identification of the specific causal role of dSub neurons in episodic memory recall.

Previously, lesions (Morris et al., 1990) as well as optogenetic inhibition (Goshen et al., 2011) showed that in rodents, neuronal activity in the CA1 subfield is necessary for both the encoding and retrieval of long-term memories. In this study, we employed optogenetic inhibition of specific terminals of CA1 cell projections and found that the CA1→dSub circuit is crucial for memory recall but not for encoding, whereas the CA1→EC5 circuit is crucial for memory encoding but not for recall. Supporting this role of the CA1→dSub circuit is the finding that inhibition of the downstream dSub terminals in medial EC5 also impairs memory recall selectively. Together, these data indicate that the hippocampal output pathways are functionally segregated: episodic memory encoding uses primarily the direct

dCA1→EC5 circuit, while episodic memory retrieval uses primarily the indirect dCA1→dSub→EC5 circuit. The functional dissociation between these two dCA1 output circuits is especially striking given that a significant proportion of dCA1 neurons projecting to dSub and EC5 are overlapping, and that the overall difference in cFos activation levels between dCA1 neurons projecting to dSub versus EC5 during either training or recall epochs is approximately 2% of all dCA1 cells. Further, it is intriguing that we found that about 20% of dCA1 engram cells, those projecting to EC5, are not reactivated by memory recall and thus do not contribute to this behavioral epoch. What could be the purpose of these dCA1 engram cells? We speculate that these engram cells are the stable holder of the original memory, which are undisturbed by a retrieval process, and contribute to the generation of engrams in downstream regions, such as remote memory engram cells in the prefrontal cortex.

The dSub neurons displayed two types of activation profiles—short-tail cells and long-tail cells. Interestingly, the proportion of active long-tail dSub neurons is greater specifically during recall-induced freezing epochs compared to training-induced freezing epochs. This may be because activation of long-tail cells requires more powerful drive than short-tail cells, and because such a potent drive may be provided only by reactivation of previously formed CA1 engram cells by recall cues (Tonegawa et al., 2015b), and not by activation of naïve CA1 cells which occurs during training. Further, these cells may correspond to the previously reported non-bursting cells and bursting cells (Geva-Sagiv et al., 2016; Sharp and Green, 1994; Staff et al., 2000; Taube, 1993). One study found that the distribution of bursting neurons in rat ventral subiculum linearly correlated with position along the proximal-distal axis, specifically 24% bursting neurons at the ventral CA1-subiculum border as compared to higher than 50% in distal regions of ventral subiculum (Jarsky et al., 2008). Additional work reported that bursting activity can be regulated by stimulation of afferent projections to the subiculum, bursting plasticity does not require synaptic depolarization or activation of AMPA/NMDA receptors, and that an enhancement in bursting activity required synergistic activation of group I, subtype 1 metabotropic glutamate receptors (mGluRs) and muscarinic acetylcholine receptors (mAChR) (Moore et al., 2009). Another study used *in vivo* injections of retrogradely transported beads into several downstream projection targets and

performed whole-cell current-clamp recordings from the bead-containing subiculum neurons in brain slices. The authors concluded that subicular projections to each downstream target were composed of a mixture of non-bursting and bursting neurons, and that non-bursting cells were preferentially located in proximal subiculum while bursting cells were preferentially located in distal subiculum (Kim and Spruston, 2012). Finally, it has been suggested that the two cell types in subiculum are segregated into parallel pathways that process distinct information (Graves et al., 2012), which is consistent with our findings that the two cell types in dorsal subiculum could support differential roles during memory retrieval.

What advantages would the distinct circuits for memory encoding and recall provide? One possible merit may be related to episodic memories with negative valence. Fear memory retrieval by conditioned cues induces not only an instinctive fear response (anxiety, avoidance, freezing, etc.), but also an increase in blood stress hormones that organizes multiple body systems to prepare the animal for a predicted immediate danger (Kelley et al., 2009). While a recent study showed that an area of the rodent's olfactory cortex plays a key role in the hormonal component of the instinctive fear response to volatile predator odors (Kondoh et al., 2016), neural circuits responsible for triggering both episodic memory retrieval and retrieval-induced stress hormone responses have remained unknown. In this study, we have identified two neural circuits originating from dSub that independently regulate freezing behavior and stress hormone responses to conditioned cues: the dSub→EC5 circuit mediates appropriate freezing behavior during memory retrieval, while the dSub→MB circuit is crucial for memory retrieval-induced stress responses via bed nucleus of the stria terminalis (BNST) and the hypothalamic corticotropin hormone-releasing neurons (Herman et al., 1998). The preferential activation of long-tail dSub neurons by recall cues may contribute to a sustained enhancement of hormonal release from these downstream areas (Bourque et al., 1993). It has been known that glucocorticoid hormone synthesis is enhanced during memory consolidation (Roozendaal, 2002). Similarly, the retrieval-induced enhancement of CORT may promote memory reconsolidation triggered by recall. Therefore, the Sub→MB pathway may regulate

memory retrieval-based emotions and together with the Sub→EC5 pathway that controls the retrieval-based instinctive fear response, would allow for more flexible actions that improve the animal's survival during challenging events in nature.

Another possible merit of distinct circuits for encoding and retrieval of memory may be to perform rapid memory updating. When a new salient stimulus (such as footshock) is delivered while a subject is recalling a previously acquired memory, the original memory is known to be modified (or updated) by incorporating the concurrently delivered salient stimulus. The diverging followed by converging CA1→dSub→EC5 and CA1→EC5 circuits seem to be ideal for this mnemonic processing: the content of the previously formed memory is retrieved by dSub and a stimulus transmitted directly from CA1 will be co-delivered to EC5 to make a new association resulting in memory updating. It has previously been suggested that such memory updating takes place in the PECFC paradigm by converting the previously acquired contextual memory to a context-dependent fear memory (Lee, 2010). Our findings, that in the PECFC paradigm, conversion of a contextual memory to a context-dependent fear memory is impaired by either the inhibition of dSub→EC5 terminals targeted to the short (8 sec) context recall period, or inhibition of CA1→EC5 terminals targeted to the period when an association of the recalled context memory with footshock takes place, supports the crucial role of dSub in memory updating.

Our study is on hippocampus-dependent episodic (or episodic-like) memories, which involves information processing by the hippocampus and other medial temporal lobe structures. Additional work is required to examine whether distinct circuits for encoding and retrieval is a property shared by brain regions responsible for the formation of non-episodic memories, which would involve structures other than the temporal lobe. In this context, it is interesting that a recent study with a worm (Caenorhabditis elegans) showed that aversive long-term memory formation and retrieval are carried out by distinct neural circuits (Jin et al., 2016). Therefore, it is possible that distinct circuits for long-term memory formation versus retrieval may be an evolutionarily conserved feature in many species that are capable of learning.

With regards to cognitive disorders, it is widely believed that subiculum is among the earliest brain regions affected in Alzheimer's disease patients (Hyman et al., 1984). Our findings contribute to a better understanding of neural mechanisms underlying episodic memory formation and may provide insights into pathological conditions affecting memory retrieval.

4.4 Experimental methods

Animals

The C57BL/6J wild type male mice were obtained from Jackson Laboratory. For optogenetic behavioral manipulations of dCA1 neuronal terminals, we used the previously described CA1-specific TRPC4-Cre transgenic mouse line (Okuyama et al., 2016). For in vivo Ca^{2+} imaging of dCA1 neurons, we used the previously described dCA1-specific WFS1-Cre transgenic mouse line (Kitamura et al., 2014). WFS1-Cre mice were used for dCA1-specific Ca^{2+} imaging experiments due to their lower levels of transgene expression compared to TRPC4-Cre mice, which was crucial for stable long-term recordings. All transgenic mouse lines were maintained as hemizygotes. Mice had access to food and water ad libitum and were socially housed in numbers of two to five littermates until surgery. Following surgery, mice were singly housed. For behavioral experiments, all mice were male and 3-5 months old. For virus-mediated activity-dependent labeling experiments (Roy et al., 2016), male mice had been raised on food containing 40 mg kg^{-1} doxycycline (DOX) for at least one week before surgery, and remained on DOX for the remainder of the experiments except for 24 hr preceding the target labeling day. For CLARITY and in vivo Ca^{2+} imaging experiments, male mice were 4-6 months old at the time of surgery. All experiments were conducted in accordance with U.S. National Institutes of Health (NIH) guidelines and the Massachusetts Institute of Technology Department of Comparative Medicine and Committee of Animal Care.

Generation of FN1-Cre mice

Bacterial artificial chromosome (BAC) recombineering was carried out using the EL250 bacterial strain, provided by Dr. Neal Copeland at the Houston Methodist Research Institute. BAC clone RP24-211L16 containing the whole FN1 (NM_001276408.1, Mus musculus fibronectin 1) was obtained from Invitrogen and transferred into EL250. To introduce the Cre sequence in-frame following the first exon of FN1, a BAC modifying cassette was prepared: a 5' homology arm, Cre, the kanamycin resistance gene flanked by FRTs, and a 3' homology arm. The modifying cassette was electroporated into EL250 carrying the BAC clone. Resistant clones were selected and confirmed for appropriate homologous recombination, after which kanamycin was removed using the site-specific recombinase FLP. Purified DNA from the selected clone containing the modified BAC was digested with NotI, which cut both ends of the insert. Insert DNA was purified (1 ng/μl) and microinjected into C57BL/6JCrlj male pronuclei of fertilized eggs. Two-cell stage embryos were transferred to pseudopregnant recipient female mice. The C57BL/6J-Tg(FN1-Cre)41(RBRC03020) transgenic mice were established and maintained in the same background. Cre mRNA expression was visualized by in situ hybridization as previously described (Okuyama et al., 2016).

Viral constructs

The AAV_9-EF1α-DIO-eYFP, AAV_9-EF1α-DIO-ChR2-eYFP, and AAV_9-EF1α-DIO-eArch3.0-eYFP viruses were acquired from the University of North Carolina (UNC) at Chapel Hill Vector Core. The AAV_9-EF1α-DIO-mCherry, AAV_9-EF1α-DIO-eArch3.0-mCherry, and AAV_9-EF1α-eArch3.0-eYFP viruses were acquired from Vector BioLabs. The AAV_2-Syn-DIO-GCaMP6f and AAV_5-Syn-DIO-GCaMP6f viruses were acquired from the University of Pennsylvania Vector Core. The AAV_8-CMV-DIO-Synaptophysin-mCherry construct was provided by Dr. Rachael Neve at the MIT Viral Gene Transfer Core and packaged at the University of Massachusetts Medical School Gene Therapy Center and Vector Core. The pAAV-EF1α-DIO-H2B-GFP plasmid was constructed by cloning the histone H2B gene into a pAAV-EF1α-DIO-GFP backbone, which was serotyped with AAV_9 coat proteins and packaged at

Vigene Biosciences. The c-Fos-tTA (Roy et al., 2016) and TRE-H2B-GFP (Okuyama et al., 2016) vectors were serotyped with AAV_9 and AAV_5 coat proteins respectively, and packaged at the University of Massachusetts Medical School Gene Therapy Center and Vector Core. The TRE-ChR2-eYFP (Liu et al., 2012) vector was serotyped with AAV_9 coat proteins and packaged at Vigene Biosciences. We used our previously established method (Roy et al., 2016) for labeling memory engram cells using a virus cocktail of c-Fos-tTA and TRE-H2B-GFP or c-Fos-tTA and TRE-ChR2-eYFP (Figure 5J). Viral titers were 1.2×10^{13} genome copy (GC) ml^{-1} for AAV_9-EF1α-DIO-eYFP, 4×10^{12} GC ml^{-1} for AAV_9-EF1α-DIO-ChR2-eYFP, 1.6×10^{13} GC ml^{-1} for AAV_9-EF1α-DIO-eArch3.0-eYFP, 3×10^{13} GC ml^{-1} for AAV_9-EF1α-DIO-mCherry and AAV_9-EF1α-DIO-eArch3.0-mCherry, 1×10^{11} GC ml^{-1} for AAV_9-EF1α-eArch3.0-eYFP, 4×10^{12} GC ml^{-1} for AAV_2-Syn-DIO-GCaMP6f and AAV_5-Syn-DIO-GCaMP6f, 1.1×10^{13} GC ml^{-1} for AAV_8-CMV-DIO-Synaptophysin-mCherry, 2×10^{14} GC ml^{-1} for AAV_9-EF1α-DIO-H2B-GFP, 4×10^{13} GC ml^{-1} for AAV_9-c-Fos-tTA, 1.4×10^{13} GC ml^{-1} for AAV_5-TRE-H2B-GFP, and 1.5×10^{13} GC ml^{-1} for AAV_9-TRE-ChR2-eYFP.

Surgery and optic fiber implants

Mice were anesthetized with isoflurane or 500 mg kg^{-1} avertin for stereotaxic injections. Injections were targeted bilaterally to the dCA1 (-2.1 mm AP, +/- 1.5 mm ML, -1.4 mm DV), dSub (-3.08 mm AP, +/- 1.5 mm ML, -1.5 mm DV), vSub (-4.2 mm AP, +/- 3.25 ML, -4.0 mm DV), medial EC5 (-4.63 mm AP, +/- 3.36 mm ML, -2.55 mm DV), MB (-2.8 mm AP, +/- 0.35 mm ML, -4.9 mm DV), and lateral EC5 (-3.40 mm AP, +/- 4.0 mm ML, -4.30 mm DV). Injection volumes were 400 nl for dCA1, 200 nl for dSub and vSub, 300 nl for medial EC5, 300 nl for MB, and 400 nl for lateral EC5. Viruses were injected at 70 nl min^{-1} using a glass micropipette attached to a 10 ml Hamilton microsyringe. The needle was lowered to the target site and remained for 5 min before beginning the injection. After the injection, the needle stayed for 10 min before it was withdrawn. Custom dSub and MB implants containing two optic fibers (200 mm core diameter; Doric Lenses) was lowered above the injection site (dSub: -3.08 mm AP, +/- 1.5 mm ML, -1.2 mm DV; MB: -2.8 mm AP, +/- 0.35 mm ML, -4.8 mm DV). Single optic fiber implants (200 mm

core diameter; Doric Lenses) were lowered above the EC5 injection sites (-4.8 mm AP, +/- 3.36 mm ML, -2.20 mm DV). The implant was secured to the skull with two jewelry screws, adhesive cement (C&B Metabond) and dental cement. An opaque cap derived from the top part of an Eppendorf tube protected the implant. Mice were given 1.5 mg kg^{-1} metacam as analgesic and allowed to recover for 2 weeks before behavioral experiments. All injection sites were verified histologically. As criteria, we only included mice with virus expression limited to the targeted regions.

Retrograde neuronal tracing

Cholera toxin subunit B

To characterize neuronal populations in dSub and dCA1 based on downstream projection targets, we used cholera toxin subunit B (CTB) conjugated to Alexa-488 or Alexa-555 diluted in phosphate buffered saline (PBS) solution at a final concentration of 1% wt vol^{-1}. Diluted CTB was aliquoted and stored at -20°C. For tracing experiments, 50-200 nl CTB was unilaterally injected into target sites. Six days after injections, mice were perfused for histology and imaging.

Rabies virus

To identify major inputs to dSub Cre^{+} neurons, we used a monosynaptic retrograde tracing approach via a Cre-dependent helper virus combined with rabies virus (RV) technology. The first component was an AAV vector that allowed simultaneous expression of three genes: TVA, eGFP, and RV glycoprotein (G). Briefly, this vector was constructed by deleting the sequence between the inverse terminal repeats of pAAV-MCS (Stratagene), and replacing it with a cassette containing the following: human synapsin-1 promoter (Syn, Genbank NG_008437); the Kozak sequence; a FLEX cassette containing the transmembrane isoform of TVA (lacking a start codon), eGFP, and G separated by the highly efficient porcine teschovirus self-cleaving 2A element; the woodchuck post-transcriptional regulatory element (WPRE) and a bovine growth hormone polyadenylation site. This vector was termed pAAV-synP-FLEX-sTpEpB (i.e., the helper virus), serotyped with AAV_{rh8} coat proteins, and packaged at the University of Pennsylvania Vector Core. The second component was a deletion-mutant RV produced by replacing the

eGFP gene in cSPBN-4GFP with the mCherry gene (i.e., the RVΔG-mCherry virus, also known as the rabies virus), which was packaged with the ASLV-A envelope protein. For tracing experiments, 50 nl of the Cre-dependent helper virus was unilaterally injected into dSub of FN1-Cre mice. One week later, 50 nl of RVΔG-mCherry virus was unilaterally injected into the same dSub. Six days after the second viral injection, mice were perfused for histology and imaging.

Immunohistochemistry

Mice were dispatched using 750–1000 mg kg^{-1} avertin and transcardially perfused with PBS, followed by 4% paraformaldehyde (PFA). Brains were extracted and incubated in 4% PFA at room temperature overnight. Brains were transferred to PBS and 50 μm coronal slices were prepared using a vibratome. For immunostaining, each slice was placed in PBS + 0.2% Triton X-100 (PBS-T), with 5% normal goat serum for 1 hr and then incubated with primary antibody at 4°C for 24 hr. Slices then underwent three wash steps for 10 min each in PBS-T, followed by a 2 hr incubation with secondary antibody. After three more wash steps of 10 min each in PBS-T, slices were mounted on microscope slides. All analyses were performed blind to the experimental conditions. Antibodies used for staining were as follows: CA1-specific excitatory neurons were stained with rabbit anti-WFS1 (1:400, Proteintech) and anti-rabbit Alexa-555 (1:500), excitatory neurons were stained with mouse anti-CaMKII (1:200, Abcam) and anti-mouse Alexa-555 (1:300), inhibitory neurons were stained with mouse anti-GAD67 (1:500, Millipore) and anti-mouse Alexa-555 (1:300), nuclei were stained with DAPI (1:3000, Sigma), neuronal nuclei were stained with mouse anti-NeuN (1:200, Millipore) and anti-mouse Alexa-555 (1:300), parvalbumin inhibitory neurons were stained with mouse anti-PV (1:500, Swant) and anti-mouse Alexa-555 (1:300), Wisteria floribunda lectin was stained with biotinylated WFA lectin (1:3000, Vector Labs) and streptavidin Alexa-555 (1:200), calbindin was stained with mouse anti-CALB (1:500, Swant) and anti-mouse Alexa-555 (1:300), vesicular glutamate transporter 1 was stained with rabbit anti-VGLUT1 (1:1000, Synaptic Systems) and anti-rabbit Alexa-488 (1:300), vesicular glutamate transporter 2 was stained with rabbit anti-VGLUT2 (1:500, Synaptic Systems) and anti-rabbit Alexa-488 (1:300), vesicular

glutamate transporter 3 was stained with guinea pig anti-VGLUT3 (1:1000, Millipore) and anti-guinea pig Alexa-488 (1:500), myelin basic protein (MBP) was stained with rabbit anti-MBP (1:1000, Abcam) and anti-rabbit Alexa-546, cFos was stained with rabbit anti-cFos (1:400, Santa Cruz Biotechnology) and anti-rabbit Alexa-488, and TRE-ChR2-eYFP (Figure 5J) was stained with chicken anti-GFP (1:1000, Life Technologies) and anti-chicken Alexa-633.

CLARITY

Mice were anesthetized with 750–1000 mg kg^{-1} avertin and transcardially perfused with a hydrogel monomer solution containing 4% acrylamide, 0.05% bis-acrylamide, 0.25% VA-044 initiator, and 4% PFA in PBS. Brains were incubated in the monomer solution at 4°C for 48-72 hr. For hydrogel tissue embedding, the brains were degassed in a desiccation chamber replacing all the gas with nitrogen, after which polymerization was initiated by raising the solution temperature to 37°C for 1 hr. Brains were extracted from the hydrogel, and washed in clearing solution containing 200 mM boric acid, 4% sodium dodecyl sulfate (SDS), and sodium hydroxide (pH 8.5) at 37°C for 24 hr. Brains were placed in a custom-built electrophoretic tissue-clearing (ETC) chamber, as previously described (Chung et al., 2013). Clearing solution was circulated through the ETC chamber at 37°C for 3 days along with 15V application across the brain sample. After clearing, brains were washed twice for 24 hr each in PBS-T at room temperature. Before imaging, brains were incubated in FocusClear solution for 2 days at room temperature to achieve the optimal refractive index of 1.45. Whole brain fluorescence z-stacks were acquired using a light sheet fluorescence microscope (5x). Stitching and high resolution rendering of z-stacks was performed using an Arivis Vision4D software package at the Harvard Center for Biological Imaging (HCBI).

Cell counting

To quantify the number of neurons in each brain region projecting to dSub Cre^{+} neurons, rabies virus (RV)-$mCherry^{+}$ neurons in each target structure were counted from 4-5 sagittal slices per mouse (n = 4

mice). To quantify the number of dCA1 neurons projecting to lateral EC5, $CTB555^+$ neurons were counted from 5-6 coronal slices per mouse (n = 3 mice). Fluorescence images were acquired using a Zeiss AxioImager.Z1/ApoTome microscope (10, 20, or 40X). Automated cell counting analysis was performed using ImageJ software. $DAPI^+$ counts were approximated from 5 sagittal slices using ImageJ. Percentage of neurons in each brain region projecting to dSub was calculated as $((mCherry^+) / (Total\ DAPI^+)) \times 100$. To characterize dSub Cre^+ eYFP neurons, the overlap between eYFP and several molecular markers (labeled with mCherry-tagged antibodies) were examined. The number of $eYFP^+$, $mCherry^+$, and $eYFP^+$ $mCherry^+$ neurons were counted from 4-5 sagittal slices per mouse (n = 3 mice per group). Percentage of dSub Cre^+ neurons expressing the different molecular markers was calculated as $((eYFP^+\ mCherry^+) / (Total\ eYFP^+)) \times 100$. A similar quantification strategy was used to examine the overlap of cholera toxin subunit B (CTB) 488 and 555 from different downstream brain regions in dSub and dCA1, as well as the overlap of RV-mCherry and CTB488 from different downstream brain regions in dCA1. For these retrograde tracing experiments, the percentage of overlap was calculated as $((eYFP^+\ mCherry^+) / (Total\ DAPI^+)) \times 100$. Chance overlap calculated as $((eYFP^+ / Total\ DAPI^+) \times (mCherry^+ / Total\ DAPI^+)) \times 100$, where $eYFP^+$ and $mCherry^+$ represents the total population of cells labeled by eYFP and mCherry, respectively. For activity-dependent labeling experiments using cFos (as TRE-H2B-GFP signal) or cFos staining, $cFos^+$ neurons were counted from 5-7 sagittal or coronal slices per mouse (n = 5-6 mice). The cell body layers of dCA1, dSub, EC5, MB, or basolateral amygdala (BLA) were outlined as regions of interest (ROIs) and the percentage of $cFos^+$ neurons were calculated as $((cFos^+) / (Total\ DAPI^+)) \times 100$. For $cFos^+$ $CTB555^+$ neurons in dCA1, percentage overlap was calculated as $((cFos^+\ CTB555^+) / (Total\ DAPI^+)) \times 100$. Chance overlap calculated as $((cFos^+ / Total\ DAPI^+) \times (CTB555^+ / Total\ DAPI^+)) \times 100$, where $cFos^+$ and $CTB555^+$ represents the total population of cells labeled by cFos and CTB555, respectively. For $cFos^+$ $ChR2^+$ $CTB555^+$ neurons in dCA1 (Figure 5M), percentage overlap was calculated as $((cFos^+\ ChR2^+\ CTB555^+) / (Total\ DAPI^+)) \times 100$. The numbers of fluorophore-positive cells per section were quantified after applying a threshold above background fluorescence. Data were analyzed using Microsoft Excel with the Statplus plug-in, or Prism 6 software. All counting experiments

were conducted blind to experimental group. Researcher 1 trained the animals, prepared slices and randomized images, while Researcher 2 performed semi-automated cell counting. Statistical comparisons were performed using unpaired t tests, one-sample t tests, and Fisher's exact tests: *$P < 0.05$, **$P < 0.01$, ***$P < 0.001$.

In vivo calcium imaging

Microendoscope surgery

We used our previously established method (Kitamura et al., 2015; Sun et al., 2015) for microendoscope surgeries. Briefly, for Ca^{2+} imaging experiments, unilateral injections were targeted to the right dSub of FN1-Cre mice or the right dCA1 of WFS1-Cre mice. Mice were injected with AAV_2-Syn-DIO-GCaMP6f (FN1-Cre) or AAV_5-Syn-DIO-GCaMP6f (WFS1-Cre). One month after AAV injection, we implanted a microendoscope lens (1 mm diameter) above the dorsal region of CA1 (-2.0 mm AP, +/- 1.5 mm ML, -1.2 mm DV), specifically targeting the medial region along the proximodistal axis, or the dorsal region of Sub (-3.1 mm AP, +/- 1.5 mm ML, -1.0 mm DV). These microendoscope lenses have a working distance of 0.3 mm (Inscopix, Inc.). One month later, the baseplate for a miniaturized microscope camera (Ziv et al., 2013) was attached above the implanted microendoscope. Following baseplate surgeries, mice were habituated to investigator handling and the attachment of a microscope camera for 2 weeks.

Imaging during open field and CFC

Mice were housed in a reverse light cycle room (dark period: 9 am to 9 pm). This is different from the light cycle room for the optogenetic behavior experiments (see below). This was necessary in order to maximize the animal's movement during the open field experiments for best coverage of the arena, which was crucial to examine spatial information and place field properties. All Ca^{2+} imaging experiments were performed during the dark cycle. Open field tests were conducted using a 50 × 50 cm white plastic platform, which lacked walls and was raised by 15 cm above the table. Under dim light conditions, Ca^{2+} activity in the open field arena was collected for 30 min per mouse in order to obtain sufficient numbers

of transients for adequately powered statistical analyses. Contextual fear conditioning (CFC) tests were conducted using a 29 × 25 × 22 cm chamber with grid floors, dim white lighting, and scented with 1% acetic acid. Mice were conditioned (300 s exploration, one 0.75 mA shock of 2 s duration at 300 s, 120 s post-shock period). One day later, mice were returned to the conditioned chamber (7 min) to assess memory recall-induced freezing behavior. Before and between runs in the open field and CFC paradigms, the experimental apparatus was cleaned with quatricide. Mouse behavior, specifically position tracking and freezing epochs, was recorded using an automated infrared (IR) detection system (EthoVision XT, Noldus). As we previously described (Kitamura et al., 2015; Sun et al., 2015), Ca^{2+} events were captured at 20 Hz on an Inscopix miniature microscope.

Image processing and cell identification

We used our previously established method (Sun et al., 2015) for image processing and single cell identification analyses. Briefly, Ca^{2+} imaging movies were motion corrected using Inscopix Mosaic software: translation and rotation; reference region with spatial mean (r = 20 pixels) subtracted, inverted, and spatial mean (r = 5 pixels) applied. Using ImageJ software, each image was divided one pixel at a time by a low pass (r = 20 pixels) filtered version, after which the ΔF/F signal was calculated. Two hundred cell regions of interest (ROIs) were carefully selected from the resulting movie by PCA-ICA method (300 output PCs, 200 ICs, 0.1 weight of temporal information in spatio-temporal ICA, 750 iterations maximum, 1×10^{-5} fractional change to end iterations) in Inscopix Mosaic software, and the independent components (ICs) were binarized using a threshold of 0.5 of the maximum intensity. Non-circular ROIs (i.e., if its length exceeded its width by greater than 2 times) were not included in the analysis. Ca^{2+} events were detected by applying a threshold (greater than 2 standard deviations from the ΔF/F signal) at the local maxima of the ΔF/F signal. Events that occurred within 250 ms of a previous Ca^{2+} event were excluded from the analysis. For ICs that satisfied all criteria, Ca^{2+} traces during behavior were computed. For open field, using this high resolution spatial map, the distribution of Ca^{2+} events were calculated, while event rate heat maps were calculated by binning the behavioral arena into 50 × 50 array

bins, each of which covered a 2 × 2 cm area. Smoothed rate heat maps were constructed with each pixel boxcar averaged over the surrounding 5 × 5 pixel area using a Gaussian smoothing kernel (σ = 2 pixels). For CFC, 8-15 s epochs during pre-footshock periods (Pre), and non-freezing (NF) and freezing (F) periods of training and recall were examined. The total duration examined within each test session was held constant across mice. For the NF and F epoch analysis, the total time was held constant across each of the test sessions, which was necessary in order to make meaningful comparisons between these epochs. On average, 10-20 epochs per mouse were analyzed. Active cells (Figure 6I) were defined as those exhibiting at least 15 significant Ca^{2+} events during a given recording session. We confirmed that these active cell results show robustness to change around this value (15) in the range of 10-18 significant Ca^{2+} events.

Spatial information, place field size, and sparsity

We used our previously established method (Sun et al., 2015) for these analyses. Briefly, the behavior position tracking data was sorted into 5 × 5 cm spatial bins. Ca^{2+} event rate per spatial bin was calculated for all dCA1 and dSub cells. Individual spatial bins were accepted if their event rate exceeded 0.2 Hz. Bins that had mouse occupancy duration less than 100 ms were not included in the analysis. Without smoothing, the spatial information rate in bits per second was calculated for each cell according to (Skaggs et al., 1992):

$$\text{information rate} = \sum_i p_i \lambda_i \log_2 \frac{\lambda_i}{\lambda}$$

where p_i is the probability of the mouse occupying the i-th bin for all i, λ_i is the mean Ca^{2+} event rate in the i-th bin, and λ is the overall Ca^{2+} event rate. Cells with significant spatial information were identified as those above the 95th percentile of all shuffles (all cell event times were shuffled 100 times, for a total of approximately 20,000 shuffles per mouse). To identify a place field, the criterion was at least 4 contiguous spatial bins (16 cm^2). For each place cell, only the largest place field was considered for the place field size analysis. Single cell sparsity is defined as $\langle R \rangle^2 / \langle R \rangle^2$, where R is the calcium activity

rate in a particular spatial bin, and < > denotes the average value over all spatial bins. A sparsity of 0.15 indicates that the cell is active in 15% of the open field arena (Treves and Rolls, 1992).

Classification of short and long tail cells

For each dCA1 and dSub cell, Ca^{2+} events that were greater than 4 standard deviations were included for this analysis. For each cell and each Ca^{2+} event, the total time to decay to 0.33 the maximum value was defined as the event width. Cells that had an average decay time of less than 3.5 s were categorized as short tail cells, while cells that had an average decay time of greater than 3.5 s were categorized as long tail cells. We confirmed that these cell type classification results show robustness to change around this value (3.5 s) in the range of 3.0-4.0 s. The distributions of individual calcium transient durations for the entire population of dCA1 and dSub cells were plotted (the x-axes used a logarithmic scale for optimal visualization of the data). A line fit was included in each population distribution (black lines). The cell type classification results are supported by the fact that dSub calcium transient durations showed a bimodal distribution (Figure S6C).

Corticosterone assay

To measure stress responses following behavior, we used a CORT enzyme-linked immunosorbant assay (ELISA; Enzo Life Sciences). One hour after training or testing sessions, we collected trunk whole blood. For sample collection following optogenetic manipulations (Figure 3G), ChR2 activation (40 min blue light on) and eArch inhibition (10 min green light on, 2 min green light off, repeated for 40 min) was carried out immediately after CFC training or recall. Specifically, once mice were removed from the CFC training context, they were returned to their home cages, optic fibers were attached, and optogenetic manipulations were initiated. Details of the laser light sources and power are provided in the optogenetic manipulations section (see below). Samples remained on ice until centrifugation (2000 × g, for 10 min) to isolate blood plasma. Plasma samples were aliquoted and stored at -80°C. 1-3 days after plasma collection, ELISA assays were performed.

Behavior assays

Experiments were conducted during the light cycle (7 am to 7 pm). Mice were randomly assigned to experimental groups for specific behavioral assays immediately after surgery. Mice were habituated to investigator handling for 1-2 minutes on three consecutive days. Handling took place in the holding room where the mice were housed. Prior to each handling session, mice were transported by wheeled cart to and from the vicinity of the behavior rooms to habituate them to the journey. For natural memory recall sessions, data were quantified using FreezeFrame software. Optogenetic manipulations interfered with motion detection, and therefore freezing behavior in these experiments were manually quantified. All behavior experiments were analyzed blind to experimental group. Unpaired student's t-tests were used for independent group comparisons, with Welch's correction when group variances were significantly different, or two-way ANOVAs followed by Bonferroni post-hoc tests were used. Given behavioral variability, initial assays were performed using a minimum of 10 mice per group to ensure adequate power for any observed differences. Following behavioral protocols, brain sections were prepared to confirm efficient viral labeling in target areas. Animals lacking adequate labeling were excluded prior to behavior quantification.

Contextual fear-conditioning

Two distinct contexts were employed (Roy et al., 2016). The conditioning context were 29 × 25 × 22 cm chambers with grid floors, dim white lighting, and scented with 0.25% benzaldehyde. The neutral context consisted of 30 × 25 × 33 cm chambers with white perspex floors, red lighting, and scented with 1% acetic acid. All mice were conditioned (180 s exploration, one 0.75 mA shock of 2 s duration at 180 s, 120 s post-shock period), and tested (3 min) one day later. Experiments showed no generalization in the neutral context. Floors of chambers were cleaned with quatricide before and between runs. Mice were transported to and from the experimental room in their home cages using a wheeled cart. The cart and cages remained in an anteroom to the experimental rooms during all behavioral experiments. For activity-dependent labeling using cFos (as H2B-GFP signal), mice were kept on regular food without DOX for 24

hours prior to training or recall. When training or recall was complete, mice were switched back to food containing 40 mg kg^{-1} DOX.

Trace and delay fear-conditioning

The conditioning context were 29 × 25 × 22 cm chambers with grid floors, bright white lighting, and scented with 1% acetic acid. The recall test context consisted of 30 × 25 × 33 cm chambers with white perspex floors, red lighting, and scented with 0.25% benzaldehyde. For trace fear-conditioning, mice were conditioned (240 s exploration, 20 s tone, 20 s trace period, a 0.75 mA shock of 2 s duration at 280 s, 60 s post-shock period, repeated 3 more times). For delay fear-conditioning, mice were conditioned (240 s exploration, 20 s tone co-terminating with a 0.75 mA shock of 2 s duration, 60 s post-shock period, repeated 3 more time). For both paradigms, memory recall was tested (14 min; 2 min exploration, 60 s tone, 120 s post-tone period, repeated 3 more times) one day later. The tone was calibrated to 75 dB SPL, with a frequency of 2 kHz. Experiments showed no generalization in the recall test context.

Conditioned place preference

The conditioned place preference (CPP) behavior chamber was a rectangular arena (40 × 15 cm), divided into three quadrants (left, middle, right). The left and right quadrants were 15 cm long, while the middle quadrant was 10 cm long. The left quadrant had grid floors and a pattern (series of parallel lines) on the wall. The right quadrant had smooth polypropylene floors and a pattern (series of circles) on the wall. On day 1 (pre-exposure), mice were allowed to explore the entire arena for 30 min. Experiments showed no preference to any one quadrant. On day 2 (training), mice were confined to the left or right quadrants for 20 min following cocaine (20 mg kg^{-1}) or saline intraperitoneal administration. On days 3-7 (training continued), mice were conditioned in opposite quadrants in an alternating manner (i.e., cocaine left-saline right-cocaine left, etc.) until every mouse received 3 cocaine and 3 saline pairings. For every behavioral cohort, half the mice were conditioned with cocaine in the left quadrant, while the remaining mice received cocaine in the right quadrant. On day 8, memory recall was measured by preference to the left or

right quadrant (10 min). All sessions were performed with dim white lighting. Mouse behavior, specifically position tracking and duration, was recorded using an automated infrared (IR) detection system (EthoVision XT, Noldus). The tracking software plotted heat maps for each mouse, which was averaged to create representative heat maps for each group. Raw data was extracted and analyzed using Microsoft Excel.

Memory updating

We employed the pre-exposure mediated contextual fear-conditioning (PECFC) paradigm to examine memory updating. The behavior context were 29 × 25 × 22 cm chambers with grid floors, dim white lighting, and scented with 0.25% benzaldehyde. On day 1, mice were allowed to explore the context for 6 min. On day 2, mice were conditioned (8 s exploration, one 0.75 mA shock of 2 s duration at 8 s, no post-shock period), and tested for 3 min one day later (day 3).

Open field assay

Spontaneous motor activity was measured in an open field arena (52 × 26 cm) for 10 min. Mice were transferred to the testing room and acclimated for 30 min before the test session. During the testing period, lighting in the room was turned off. The apparatus was cleaned with quatricide before and between runs. Total movement (distance traveled and velocity) in the arena was quantified using an automated infrared (IR) detection system (EthoVision XT, Noldus). The tracking software plotted heat maps for each mouse, which was averaged to create representative heat maps for each group. Raw data were extracted and analyzed using Microsoft Excel.

Optogenetic manipulations

All behavioral paradigms were performed as described above. For experiments that included optogenetic manipulations, the behavior chamber ceilings were customized to hold a rotary joint (Doric Lenses) connected to two 0.32 m optic fibers. All mice had optic fibers attached to their optic fiber implants prior

to training and recall tests. For ChR2 experiments, dSub terminals were stimulated at 20 Hz (15 ms pulse width) using a 473 nm laser (10-15 mW, blue light), for the entire duration (3 min) of CFC recall tests or neutral context tests (Figure 3D). For eArch experiments, dSub cell bodies/terminals, vSub terminals, and dCA1 terminals were inhibited using a 561 nm laser (10 mW, constant green light). For CFC experiments (Figures 3A, 3B, 3C, 4I, 4J, 4K, 4L; Figures S2, S3), green light inhibition was performed during the entire duration (3 min) of training or recall tests. For TFC and DFC training experiments (Figures S4A, S4B), green light inhibition was performed during the entire duration from tone initiation through shock delivery (for all tone-shock pairings). The following day, tone-induced memory recall was tested without green light. For TFC and DFC recall experiments (Figures 3E, S4C), green light inhibition was performed during the first and third tones (each tone is 60 s) in half the mice, while the remaining mice received inhibition during the second and fourth tones. This reflects a counter-balanced experimental design. For CPP training experiments (Figure S4D), green light inhibition was performed during days 2-7, for the entire 20 min session per day (9 min green light on, 1 min green light off, 10 min green light on). For CPP recall experiments (Figure 3F), green light inhibition was performed during the entire duration (10 min) of recall tests on day 8. For memory updating experiments (Figures 4M, 4N), green light inhibition was performed during the entire pre-footshock periods (first 8 s on day 2, left panels) or during the footshock periods alone (last 2 s on day 2, right panels). For open field experiments (Figure S2M), green light inhibition was performed during the entire duration (10 min).

Quantification and statistical analysis

Data are presented as mean values accompanied by SEM. No statistical methods were used to predetermine sample sizes. Data analysis was performed blind to the conditions of the experiments. Data were analyzed using Microsoft Excel with the Statplus plug-in and Prism 6 software. Two-way ANOVA followed by Bonferroni post-hoc test, unpaired t test, Fisher's exact test, one-sample t test, and paired t test were used to test for statistical significance when appropriate. Statistical parameters including the exact value of n, precision measures (mean ± SEM), and statistical significance are reported in the figure

legends. The significance threshold was placed at $\alpha = 0.05$ (NS, $P > 0.05$; *, $P < 0.05$; **, $P < 0.01$; ***, $P < 0.001$).

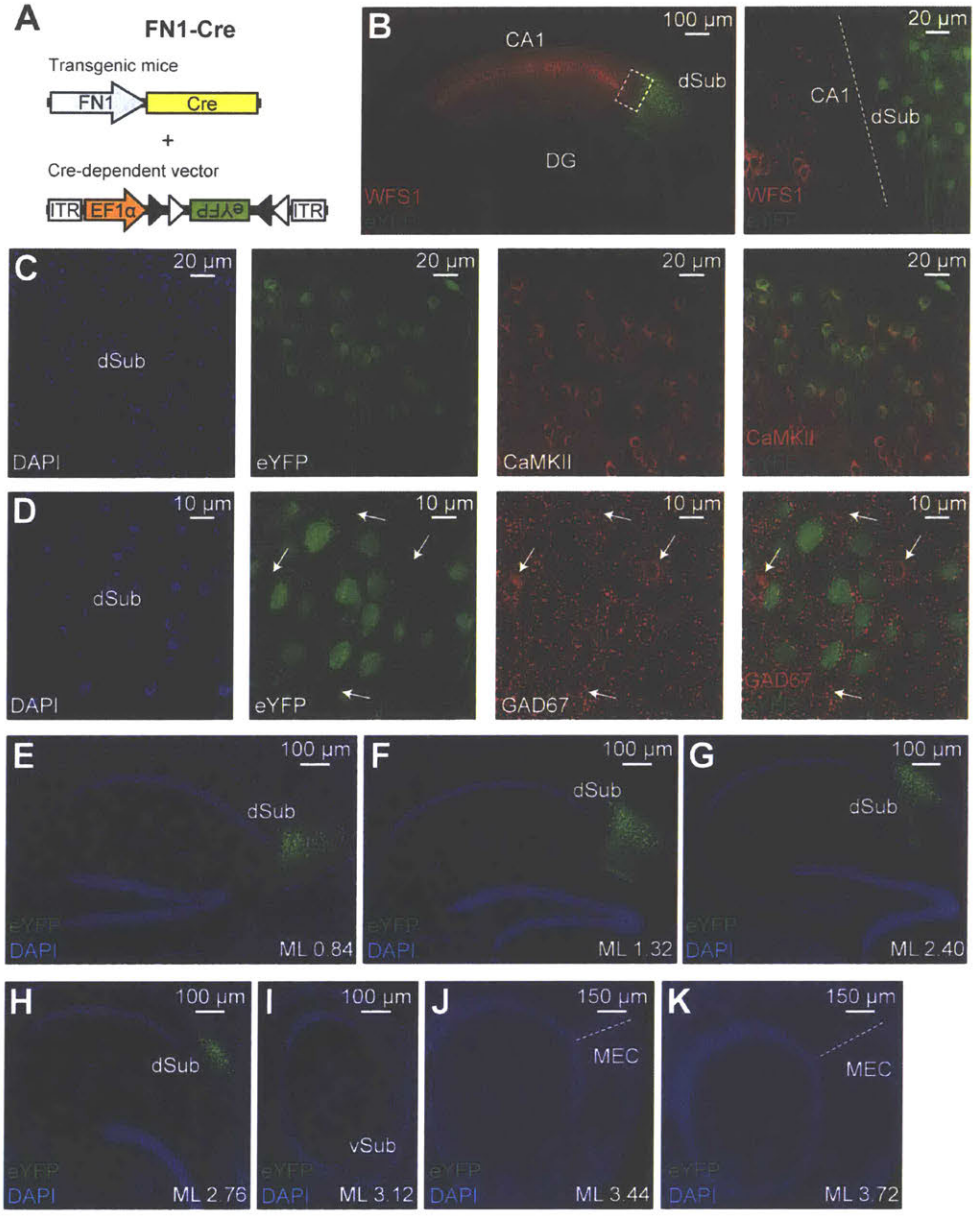
A
FN1-Cre
Transgenic mice
FN1
Cre
+
Cre-dependent vector
ITR
EF1α
eYFP
ITR
B
CA1
dSub
DG
WFS1
100 μm
CA1
dSub
WFS1
20 μm
C
dSub
DAPI
20 μm
eYFP
20 μm
CaMKII
20 μm
CaMKII
20 μm
D
dSub
DAPI
10 μm
eYFP
10 μm
GAD67
10 μm
GAD67
10 μm
E
dSub
DAPI
ML 0.84
100 μm
F
dSub
DAPI
ML 1.32
100 μm
G
dSub
DAPI
ML 2.40
100 μm
H
dSub
DAPI
ML 2.76
100 μm
I
vSub
DAPI
ML 3.12
100 μm
J
MEC
DAPI
ML 3.44
150 μm
K
MEC
DAPI
ML 3.72
150 μm

Figure 1. Genetic targeting of dSub neurons using FN1-Cre mice

(A) FN1-Cre mice were injected with a Cre-dependent virus expressing eYFP into dSub.

(B) Cre^+ dSub neurons (eYFP, green) do not overlap with dCA1 excitatory neurons (labeled with WFS1, red). Sagittal image (left), higher magnification image of boxed region (right). Dashed white line denotes CA1/dSub border (right).

(C, D) Cre^+ dSub neurons (eYFP, green), in sagittal sections, express the excitatory neuronal marker CaMKII (red; C). Over 85% of all $CaMKII^+$ neurons in the dSub region also expressed eYFP (n = 3 mice). Images are taken with a 20x objective. Cre^+ dSub neurons do not express the inhibitory marker GAD67 (red; D). White arrows indicate $GAD67^+$ cell bodies (D). Images are taken with a 40x objective. See also Figure S1A. DAPI staining in blue.

(E-K) Medial to lateral (ML, in millimeters relative to Bregma) sagittal sections show that eYFP signal is restricted to dSub neurons. DAPI staining (blue). No eYFP signal was observed in ventral subiculum (vSub) or medial entorhinal cortex (MEC). Dashed white line denotes perirhinal cortex/MEC border (J, K).

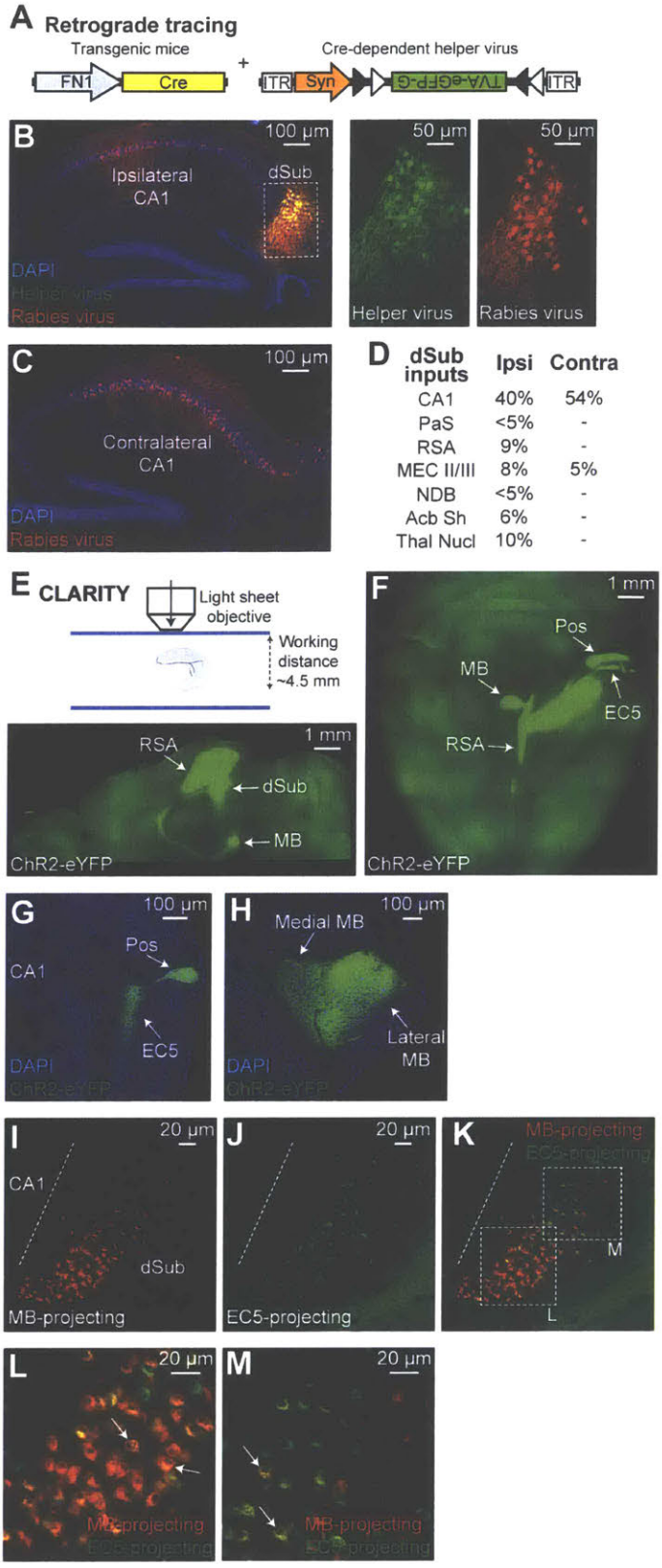
A Retrograde tracing
Transgenic mice
Cre-dependent helper virus
FN1
Cre
ITR
Syn
TVA-eGFP-G
ITR
B
100 µm
Ipsilateral CA1
dSub
DAPI
Helper virus
Rabies virus
50 µm
Helper virus
50 µm
Rabies virus
C
100 µm
Contralateral CA1
DAPI
Rabies virus
D
dSub inputs | Ipsi | Contra
CA1 | 40% | 54%
PaS | <5% | -
RSA | 9% | -
MEC II/III | 8% | 5%
NDB | <5% | -
Acb Sh | 6% | -
Thal Nucl | 10% | -
E CLARITY
Light sheet objective
Working distance ~4.5 mm
RSA
1 mm
dSub
MB
ChR2-eYFP
F
1 mm
Pos
MB
EC5
RSA
ChR2-eYFP
G
100 µm
Pos
CA1
EC5
DAPI
H
100 µm
Medial MB
Lateral MB
DAPI
I
20 µm
CA1
dSub
MB-projecting
J
20 µm
EC5-projecting
K
MB-projecting
EC5-projecting
M
L
L
20 µm
MB-projecting
EC5-projecting
M
20 µm
MB-projecting
EC5-projecting

Figure 2. Input-output organization of dSub excitatory neurons

(A) Monosynaptic retrograde tracing of dSub inputs used a Cre-dependent helper virus (tagged with eGFP) combined with a rabies virus (RV, mCherry) injected into dSub of FN1-Cre mice. Avian leukosis and sarcoma virus subgroup A receptor (TVA) and rabies glycoprotein (G).

(B, C) Representative ipsilateral sections confirmed efficient overlap of helper and RV-infected dSub neurons. Sagittal image (left; B), higher magnification images of boxed region (right; B). Both ipsilateral and contralateral sagittal sections revealed that dorsal CA1 provides the major input to dSub Cre^+ neurons (C).

(D) Inputs to dSub Cre^+ neurons were quantified based on percentage of neurons in the target brain region relative to $DAPI^+$ neurons (n = 4 mice). Ipsilateral (Ipsi) and contralateral (Contra) counts. Parasubiculum (PaS), retrosplenial agranular cortex (RSA), MEC layers II/III (MEC II/III), nucleus of the diagonal band (NDB), nucleus accumbens shell (Acb Sh), and thalamic nuclei (Thal Nucl).

(E) FN1-Cre mice expressing ChR2-eYFP (Cre-dependent virus) in dSub neurons were used for CLARITY followed by light sheet microscopy (top). 2.5 mm optical section in sagittal view shows projections to RSA and mammillary bodies (MB, bottom).

(F) Whole-brain, stitched z-stack (horizontal view) shows all major projections from dSub Cre^+ neurons including RSA, MB, EC5, and postrhinal cortex (Pos).

(G, H) Standard sagittal brain sections of FN1-Cre mice expressing ChR2-eYFP (Cre-dependent virus) in dSub neurons showing dSub projections to EC5 and Pos (G), as well as medial and lateral MB (H).

(I-M) Representative standard sagittal brain sections showing dSub neuronal populations projecting to MB (red, CTB555; I) or EC5 (green, CTB488; J). The respective CTB was injected into MB or EC5. Overlap image (K). Quantification, including weakly labeled CTB^+ neurons, revealed that 81% of dSub

cells were double positive (n = 4 mice). Scale bar in panels I-J applies to panel K. Dashed white line denotes CA1/dSub border. Higher magnification images of boxed regions indicated in Figure 2K (L-M). White arrows indicate dSub neurons that are both $CTB555^{+}$ and $CTB488^{+}$.

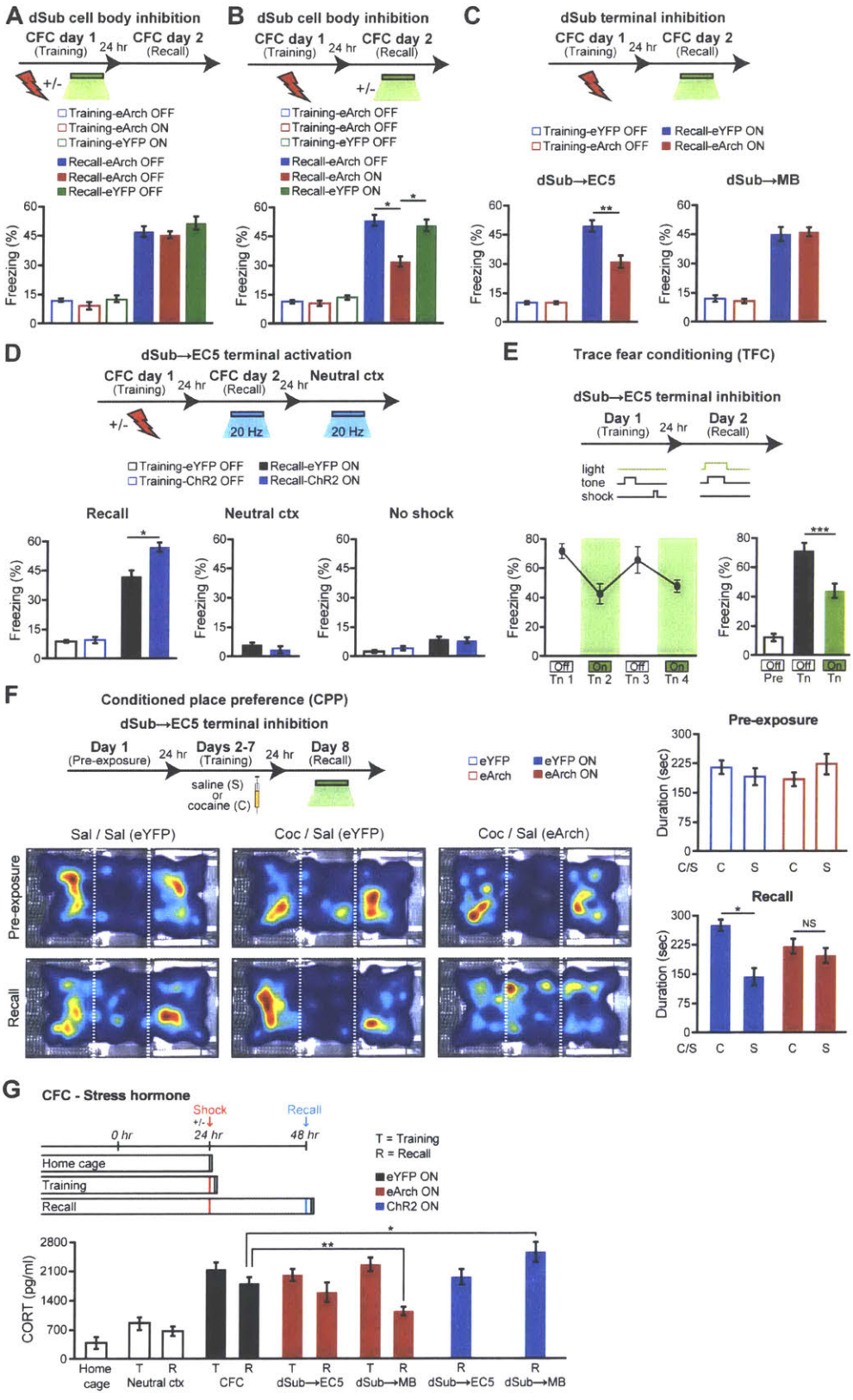
A dSub cell body inhibition
CFC day 1 (Training) 24 hr CFC day 2 (Recall)
+/-
Training-eArch OFF
Training-eArch ON
Training-eYFP ON
Recall-eArch OFF
Recall-eArch OFF
Recall-eYFP OFF
Freezing (%)
B dSub cell body inhibition
CFC day 1 (Training) 24 hr CFC day 2 (Recall)
+/-
Training-eArch OFF
Training-eArch OFF
Training-eYFP OFF
Recall-eArch OFF
Recall-eArch ON
Recall-eYFP ON
Freezing (%)
C dSub terminal inhibition
CFC day 1 (Training) 24 hr CFC day 2 (Recall)
Training-eYFP OFF
Training-eArch OFF
Recall-eYFP ON
Recall-eArch ON
dSub→EC5
dSub→MB
Freezing (%)
D dSub→EC5 terminal activation
CFC day 1 (Training) 24 hr CFC day 2 (Recall) 24 hr Neutral ctx
+/-
20 Hz
20 Hz
Training-eYFP OFF
Training-ChR2 OFF
Recall-eYFP ON
Recall-ChR2 ON
Recall
Neutral ctx
No shock
Freezing (%)
E Trace fear conditioning (TFC)
dSub→EC5 terminal inhibition
Day 1 (Training) 24 hr Day 2 (Recall)
light
tone
shock
Freezing (%)
Off
On
Tn 1
Tn 2
Tn 3
Tn 4
Pre
Tn
F Conditioned place preference (CPP)
dSub→EC5 terminal inhibition
Day 1 (Pre-exposure) 24 hr Days 2-7 (Training) 24 hr Day 8 (Recall)
saline (S) or cocaine (C)
eYFP
eArch
eYFP ON
eArch ON
Sal / Sal (eYFP)
Coc / Sal (eYFP)
Coc / Sal (eArch)
Pre-exposure
Recall
Pre-exposure
Duration (sec)
C/S
C
S
Recall
NS
G CFC - Stress hormone
Shock +/-
Recall
0 hr
24 hr
48 hr
Home cage
Training
Recall
T = Training
R = Recall
eYFP ON
eArch ON
ChR2 ON
CORT (pg/ml)
Home cage
Neutral ctx
CFC
dSub→EC5
dSub→MB
dSub→EC5
dSub→MB

Figure 3. Differential roles of dSub projections in hippocampal memory retrieval and retrieval-induced stress hormone responses

(A, B) FN1-Cre mice were injected with a Cre-dependent virus expressing eArch3.0-eYFP into dSub. Optogenetic inhibition of dSub neurons during contextual fear conditioning (CFC) training had no effect on long-term memory (n = 12 mice per group; A). Inhibition of dSub neurons during CFC recall impaired behavioral performance (n = 12 mice per group; B). A two-way ANOVA followed by Bonferroni post-hoc tests revealed a behavioral epoch-by-eArch interaction and significant eArch-mediated attenuation of freezing (A-B: $F_{1,44} = 5.70$, $P < 0.05$, recall). For dSub optogenetic manipulation experiments, injections were targeted to dSub cell bodies and the extent of virus expression is shown in Figures 1E-1K.

(C) Terminal inhibition of dSub projections to EC5 (bottom left), but not MB (bottom right), disrupted CFC memory recall (n = 11 mice per group). A two-way ANOVA followed by Bonferroni post-hoc tests revealed a dSub terminal-by-eArch interaction and significant eArch-mediated attenuation of freezing ($F_{1,40} = 7.63$, $P < 0.01$, dSub→EC5 terminals).

(D) FN1-Cre mice were injected with a Cre-dependent virus expressing ChR2-eYFP into dSub. Optogenetic activation of dSub→EC5 terminals during CFC memory recall increased freezing levels (left), which was not observed in a neutral context (middle) or using no shock mice (right, n = 10 mice per group).

(E) Inhibition of dSub→EC5 terminals during trace fear conditioning (TFC) recall decreased tone (Tn)-induced freezing levels (n = 12 mice). A two-way ANOVA followed by Bonferroni post-hoc tests revealed a behavioral epoch-by-eArch interaction and significant eArch-mediated attenuation of freezing (E and Figure S4A: $F_{1,44} = 7.11$, $P < 0.05$, recall). Pre-tone baseline freezing (Pre). Recall-induced freezing levels during individual tone presentations (left panel), averaged freezing levels during the two light-off tones and the two light-on tones (right panel).

(F) Inhibition of dSub→EC5 terminals during cocaine-induced conditioned place preference (CPP) recall impaired behavioral performance (n = 14 mice per group). Behavioral schedule (left, top part). Average heat maps showing exploration time during pre-exposure and recall trials (left, bottom part). Dashed white lines demarcate individual zones in the CPP apparatus. Pre-exposure preference duration (right, top graph) and recall preference duration (right, bottom graph). Saline (S or Sal), cocaine (C or Coc). A two-way ANOVA followed by Bonferroni post-hoc tests revealed a drug group-by-eArch interaction and significant eArch-mediated attenuation of preference duration ($F_{1,52} = 5.16$, $P < 0.05$, cocaine). For CPP training inhibition, see Figure S4D. NS, not significant.

(G) Stress hormone: Terminal inhibition of dSub projections to MB, but not EC5, following CFC memory recall tests decreased stress responses as measured by corticosterone (CORT) levels. Optogenetic activation of dSub→MB terminals following CFC memory recall increased CORT levels (n = 10 mice per group). Context (ctx). CORT levels in CPP paradigm are shown in Figure S4E.

Unless specified, statistical comparisons are performed using unpaired t tests; *$P < 0.05$, **$P < 0.01$, ***$P < 0.001$. Data are presented as mean ± SEM.

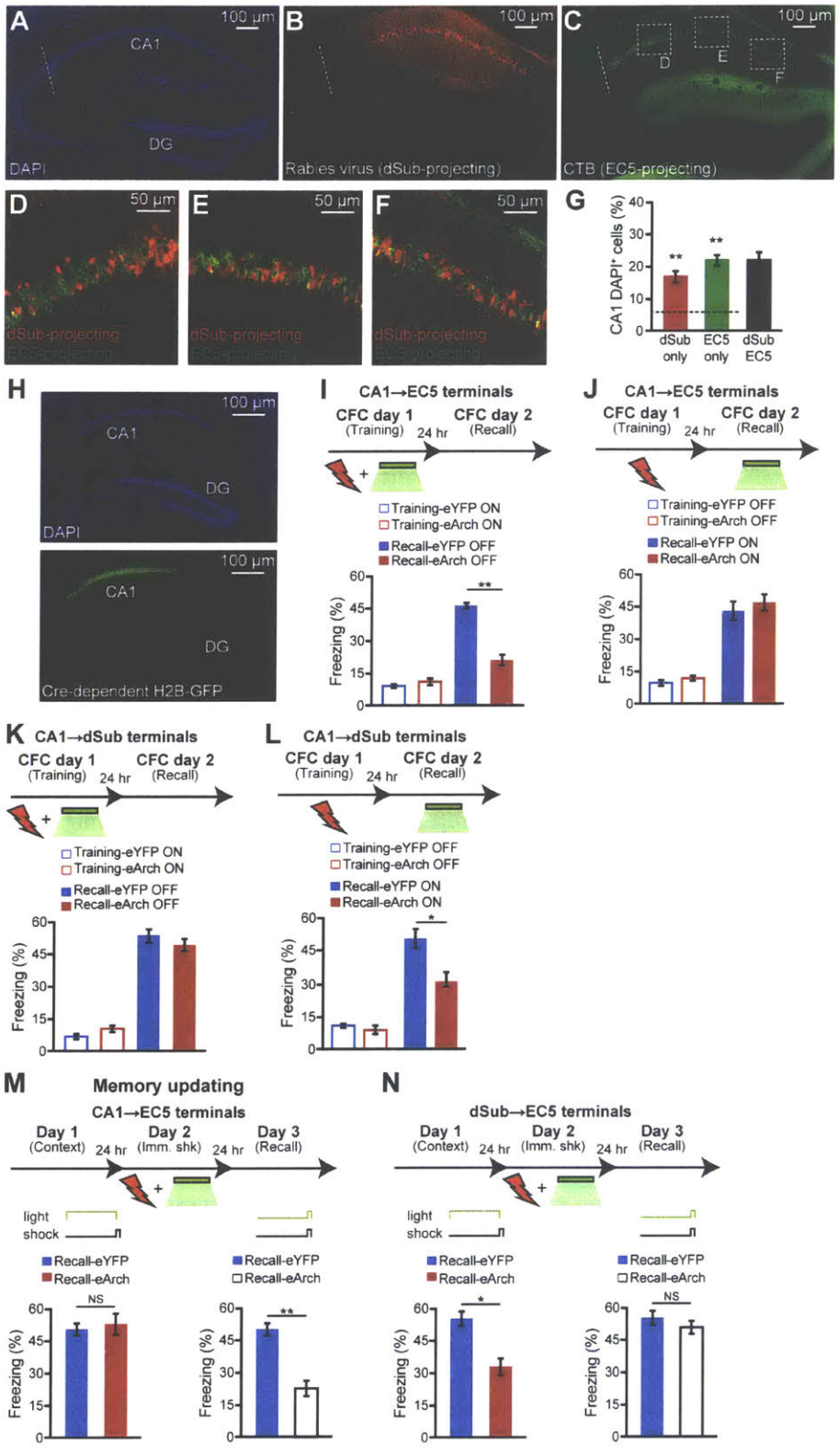
A
100 μm
CA1
DG
DAPI
B
100 μm
Rabies virus (dSub-projecting)
C
100 μm
D
E
F
CTB (EC5-projecting)
D
50 μm
dSub-projecting
E
50 μm
dSub-projecting
F
50 μm
dSub-projecting
G
CA1 DAPI+ cells (%)
40
30
20
10
0
**
**
dSub only
EC5 only
dSub EC5
H
100 μm
CA1
DG
DAPI
100 μm
CA1
DG
Cre-dependent H2B-GFP
I
CA1→EC5 terminals
CFC day 1 (Training)
24 hr
CFC day 2 (Recall)
+
Training-eYFP ON
Training-eArch ON
Recall-eYFP OFF
Recall-eArch OFF
Freezing (%)
60
45
30
15
0
**
J
CA1→EC5 terminals
CFC day 1 (Training)
24 hr
CFC day 2 (Recall)
Training-eYFP OFF
Training-eArch OFF
Recall-eYFP ON
Recall-eArch ON
Freezing (%)
60
45
30
15
0
K
CA1→dSub terminals
CFC day 1 (Training)
24 hr
CFC day 2 (Recall)
+
Training-eYFP ON
Training-eArch ON
Recall-eYFP OFF
Recall-eArch OFF
Freezing (%)
60
45
30
15
0
L
CA1→dSub terminals
CFC day 1 (Training)
24 hr
CFC day 2 (Recall)
Training-eYFP OFF
Training-eArch OFF
Recall-eYFP ON
Recall-eArch ON
*
Freezing (%)
60
45
30
15
0
M
Memory updating
CA1→EC5 terminals
Day 1 (Context)
24 hr
Day 2 (Imm. shk)
24 hr
Day 3 (Recall)
+
light
shock
Recall-eYFP
Recall-eArch
NS
Freezing (%)
60
45
30
15
0
Recall-eYFP
Recall-eArch
**
Freezing (%)
60
45
30
15
0
N
dSub→EC5 terminals
Day 1 (Context)
24 hr
Day 2 (Imm. shk)
24 hr
Day 3 (Recall)
+
light
shock
Recall-eYFP
Recall-eArch
*
Freezing (%)
60
45
30
15
0
Recall-eYFP
Recall-eArch
NS
Freezing (%)
60
45
30
15
0

Figure 4. Projection from CA1 to EC5 is crucial for encoding, but not for retrieval, of hippocampal memories

(A-C) Retrograde monosynaptic identification of dCA1 neurons projecting to dSub (in FN1-Cre mice) using a Cre-dependent helper virus combined with a rabies virus (RV). Simultaneous retrograde monosynaptic identification of dCA1 neurons projecting to EC5 using CTB. DAPI (blue; A), RV-mCherry (red; B), CTB488 (green; C). Representative sagittal sections, dashed white line denotes CA1/CA2 border.

(D-F) Higher magnification images of boxed regions indicated in Figure 4C.

(G) Percentage of dCA1 neurons labeled with mCherry (dSub only), CTB488 (EC5 only), or mCherry and CTB double positive (dSub+EC5, n = 4 mice). Dashed line indicates chance level (6%), calculated from a control experiment (Figures S5A-S5H, and see Methods). One-sample t tests against chance level were performed.

(H) Representative sagittal sections of hippocampus from TRPC4-Cre mice showing dCA1 neurons labeled with a Cre-dependent histone H2B-GFP virus (green, bottom) and stained with DAPI (blue, top).

(I, J) TRPC4-Cre mice were injected with a Cre-dependent virus expressing eArch3.0-eYFP into dCA1. Terminal inhibition of CA1→EC5 during CFC training impaired long-term memory (n = 10 mice per group; I). Inhibition of CA1→EC5 terminals during CFC recall had no effect on behavioral performance (n = 10 mice per group; J). A two-way ANOVA followed by Bonferroni post-hoc tests revealed a behavioral epoch-by-eArch interaction and significant eArch-mediated attenuation of freezing (I-J: $F_{1,36}$ = 9.19, $P < 0.01$, training).

(K, L) Terminal inhibition of CA1→dSub during CFC training had no effect on long-term memory (n = 13 mice per group; K). Inhibition of CA1→dSub terminals during CFC recall disrupted behavioral performance (n = 13 mice per group; L). A two-way ANOVA followed by Bonferroni post-hoc tests

revealed a behavioral epoch-by-eArch interaction and significant eArch-mediated attenuation of freezing (K-L: $F_{1,48} = 5.16$, $P < 0.05$, recall).

(M, N) Memory updating. Experimental schedule (top) for pre-exposure mediated contextual fear conditioning (PECFC) with optogenetic terminal inhibition of CA1→EC5 (using TRPC4-Cre mice; M) and dSub→EC5 (using FN1-Cre mice; N) during the pre-footshock period (left panels) or footshock period alone (right panels) on Day 2. Freezing levels during recall tests (Day 3) to the conditioned context (bottom). eYFP and eArch conditions (n = 12 mice per group). NS, not significant. Immediate shock (Imm. shk). A two-way ANOVA followed by Bonferroni post-hoc tests revealed a behavioral epoch-by-eArch interaction and significant eArch-mediated attenuation of freezing (M: $F_{1,44} = 9.81$, $P < 0.01$, recall in right panel; N: $F_{1,44} = 4.75$, $P < 0.05$, recall in left panel).

Unless specified, statistical comparisons are performed using unpaired t tests; $^{*}P < 0.05$, $^{**}P < 0.01$. Data are presented as mean ± SEM.

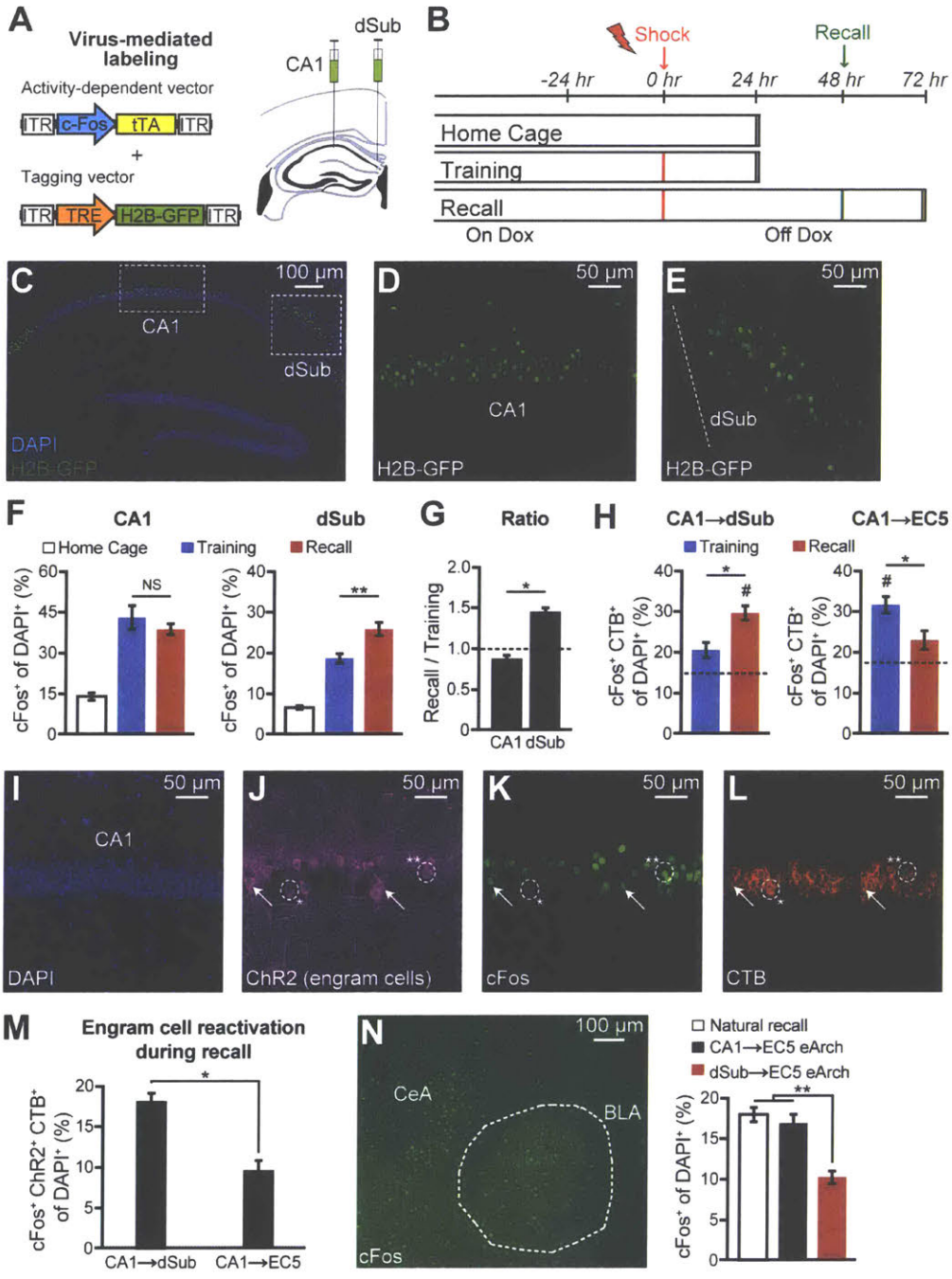
A
Virus-mediated labeling
Activity-dependent vector
ITR c-Fos tTA ITR
+
Tagging vector
ITR TRE H2B-GFP ITR
CA1
dSub
B
Shock
Recall
-24 hr
0 hr
24 hr
48 hr
72 hr
Home Cage
Training
Recall
On Dox
Off Dox
C
100 μm
CA1
dSub
DAPI
H2B-GFP
D
50 μm
CA1
H2B-GFP
E
50 μm
dSub
H2B-GFP
F
CA1
dSub
Home Cage
Training
Recall
cFos+ of DAPI+ (%)
NS
**
G
Ratio
Recall / Training
*
CA1 dSub
H
CA1→dSub
CA1→EC5
Training
Recall
cFos+ CTB+ of DAPI+ (%)
*
#
I
50 μm
CA1
DAPI
J
50 μm
ChR2 (engram cells)
K
50 μm
cFos
L
50 μm
CTB
M
Engram cell reactivation during recall
cFos+ ChR2+ CTB+ of DAPI+ (%)
*
CA1→dSub
CA1→EC5
N
100 μm
CeA
BLA
cFos
Natural recall
CA1→EC5 eArch
dSub→EC5 eArch
cFos+ of DAPI+ (%)
**

Figure 5. Distinct cFos activation patterns in CA1 and dSub neurons

(A) Virus-mediated cFos$^+$ neuronal labeling strategy using a cocktail of c-Fos-tTA and TRE-H2B-GFP (left). Wild-type mice raised on doxycycline (DOX) food were injected with the two viruses bilaterally into CA1 and dSub (right).

(B) Behavioral schedule and H2B-GFP labeling (see Methods). Beige shading indicates animals are maintained on DOX food.

(C-E) Representative sagittal section of hippocampus showing H2B-GFP-labeled cell bodies (green) in CA1 and dSub counterstained with DAPI (blue), following CFC training (C). Boxed regions in C are shown in higher magnification for CA1 (D) and dSub (E). Dashed white line denotes CA1/dSub border (E).

(F) H2B-GFP$^+$ (cFos$^+$) cell counts in CA1 (left) and dSub (right) from home cage, CFC training (encoding), and CFC recall groups (n = 6 mice per group). NS, not significant.

(G) Ratio of recall to training H2B-GFP$^+$ neurons in CA1 and dSub (cell counts from Figure 5F). A ratio of 1.0 indicates comparable H2B-GFP$^+$ counts during training and recall epochs. Statistical comparison used a Fisher's exact test.

(H) Overlap between CFC-induced cFos and CA1 neurons projecting (labeled by CTB555) to dSub (left) or EC5 (right). Representative overlap images are shown in Figures S5I-S5L. Dashed lines indicate chance levels (n = 5 mice per group, see Methods). One-sample t tests against chance level were performed (#$P < 0.05$).

(I-M) Wild-type mice raised on DOX were used for these experiments. Representative coronal section of CA1 showing DAPI staining (I), CFC training-induced cFos-positive engram cells labeled with a cocktail of c-Fos-tTA and TRE-ChR2-eYFP (J), cFos antibody staining following CFC recall tests performed one

day after training and engram labeling (K), and CA1 neurons projecting to either dSub or EC5 visualized by retrograde CTB555 labeling (L). The circled region with a single asterisk (*) shows an engram cell that is $cFos^-$ but $CTB555^+$ and the region with two asterisks (**) shows an engram cell that is $cFos^+$ and $CTB555^+$. White arrows show additional examples of CA1 engram cells that are both $cFos^+$ and $CTB555^+$. Overlap of recall-induced cFos, CA1 engram cells labeled during training, and circuit specific CA1 projection neurons (n = 6 mice per group; M).

(N) Representative coronal section of basolateral amygdala (BLA) showing cFos activation following memory recall (left). $cFos^+$ cell counts (n = 6 mice per group) in BLA following natural recall, and recall with eArch inhibition of the CA1→EC5 or dSub→EC5 circuits (right). TRPC4-Cre mice were used for CA1 circuit manipulations and FN1-Cre mice were used for dSub circuit manipulations.

Unless specified, statistical comparisons are performed using unpaired t tests; $*P < 0.05$, $**P < 0.01$. Data are presented as mean ± SEM.

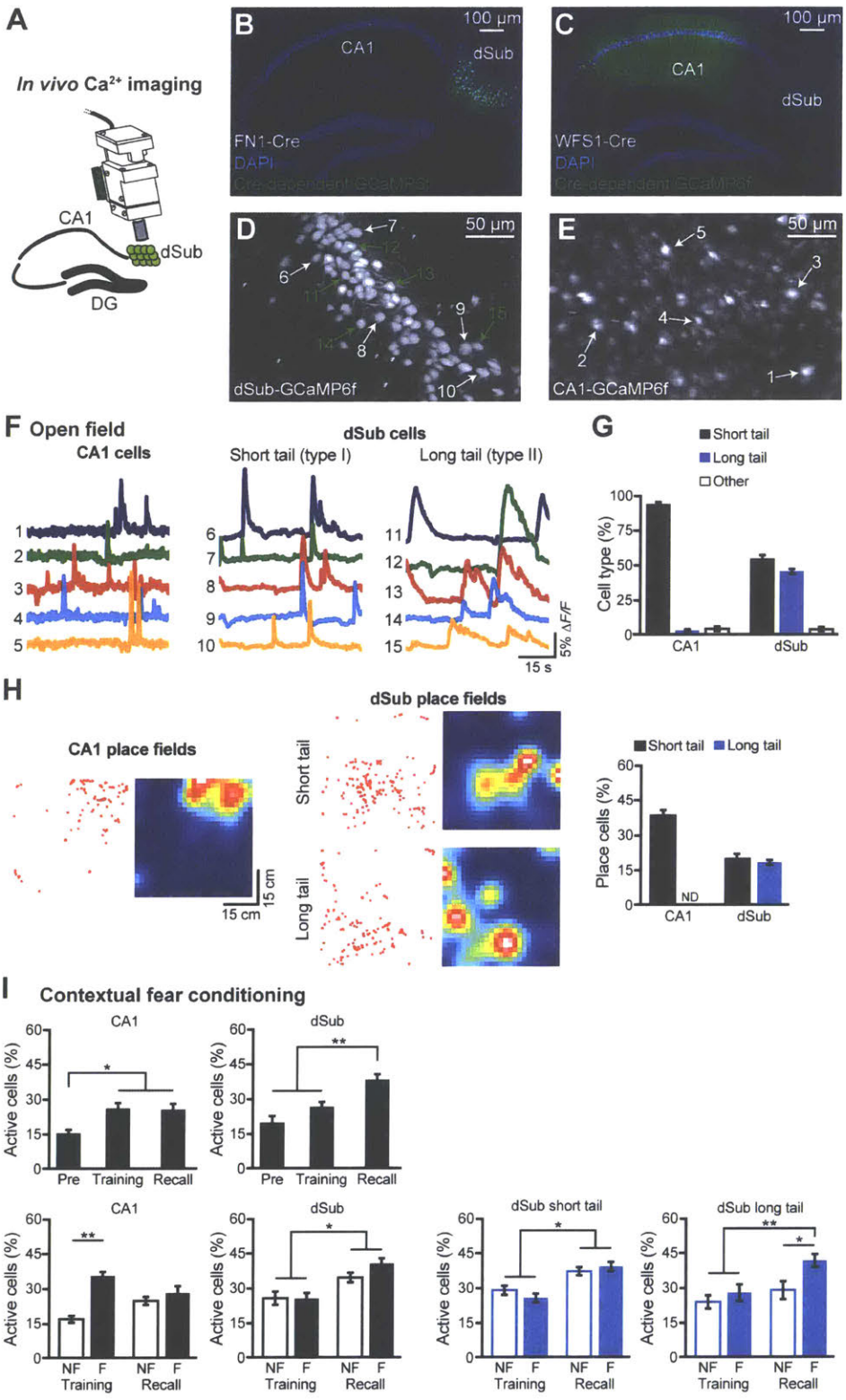
A
In vivo Ca2+ imaging
CA1
dSub
DG
B
100 µm
CA1
dSub
FN1-Cre
DAPI
Cre-dependent GCaMP6f
C
100 µm
CA1
dSub
WFS1-Cre
DAPI
Cre-dependent GCaMP6f
D
50 µm
dSub-GCaMP6f
E
50 µm
CA1-GCaMP6f
F Open field
CA1 cells
dSub cells
Short tail (type I)
Long tail (type II)
5% ΔF/F
15 s
G
Short tail
Long tail
Other
Cell type (%)
CA1
dSub
H
CA1 place fields
dSub place fields
Short tail
Long tail
15 cm
15 cm
Short tail
Long tail
Place cells (%)
ND
CA1
dSub
I
Contextual fear conditioning
CA1
dSub
Active cells (%)
Pre
Training
Recall
CA1
dSub
dSub short tail
dSub long tail
NF
F
Training
Recall

Figure 6. dSub neurons exhibit enhanced neuronal activity during hippocampal memory retrieval

(A-C) Implantation of a microendoscope right above dSub of FN1-Cre mice (A) or dCA1 of WFS1-Cre mice. For dCA1, the medial region along the proximodistal axis was targeted (see also Figures S6A-S6B). Calcium (Ca^{2+}). Representative sagittal sections of hippocampus from FN1-Cre (B) and WFS1-Cre (C) mice showing GCaMP6f-labeled cells (green) and DAPI staining (blue).

(D, E) Representative maximum intensity projection images, as seen through the microendoscope camera, of dSub neurons expressing GCaMP6f (D) or CA1 neurons expressing GCaMP6f (E) acquired during a 30 min recording session in an open field arena (see Experimental methods).

(F, G) Representative Ca^{2+} traces of CA1 cells (left, labeled in E) and two types of dSub cells (middle and right, labeled in D) from the open field paradigm (F), and cell type quantification (n = 759 CA1 cells, n = 428 dSub short tail cells, n = 371 dSub long tail cells, n = 4 mice per group; G). See also Figure S6C.

(H) Representative place field Ca^{2+} events (red dots, left panels) and heat maps (right panels) for CA1 and dSub cells (cell counts in Figure 6G), along with quantification. See also Figure S6D and Experimental methods. ND, not detected.

(I) Ca^{2+} activity during CFC. Pre-footshock levels (Pre). Percentage of active cells (see Experimental methods) during Pre, training, and recall tests (top), including non-freezing (NF) and freezing (F) epochs (bottom), in CA1 and dSub (n = 550 CA1 cells, n = 429 dSub short tail cells, n = 203 dSub long tail cells, n = 3 CA1 mice, n = 4 dSub mice). Within session NF and F comparisons used paired t tests. Comparisons across sessions used a two-way ANOVA with repeated measures followed by Bonferroni post-hoc tests. See also Figures S6E-S6G.

For statistical comparisons, $*P < 0.05$, $**P < 0.01$. Data are presented as mean ± SEM.

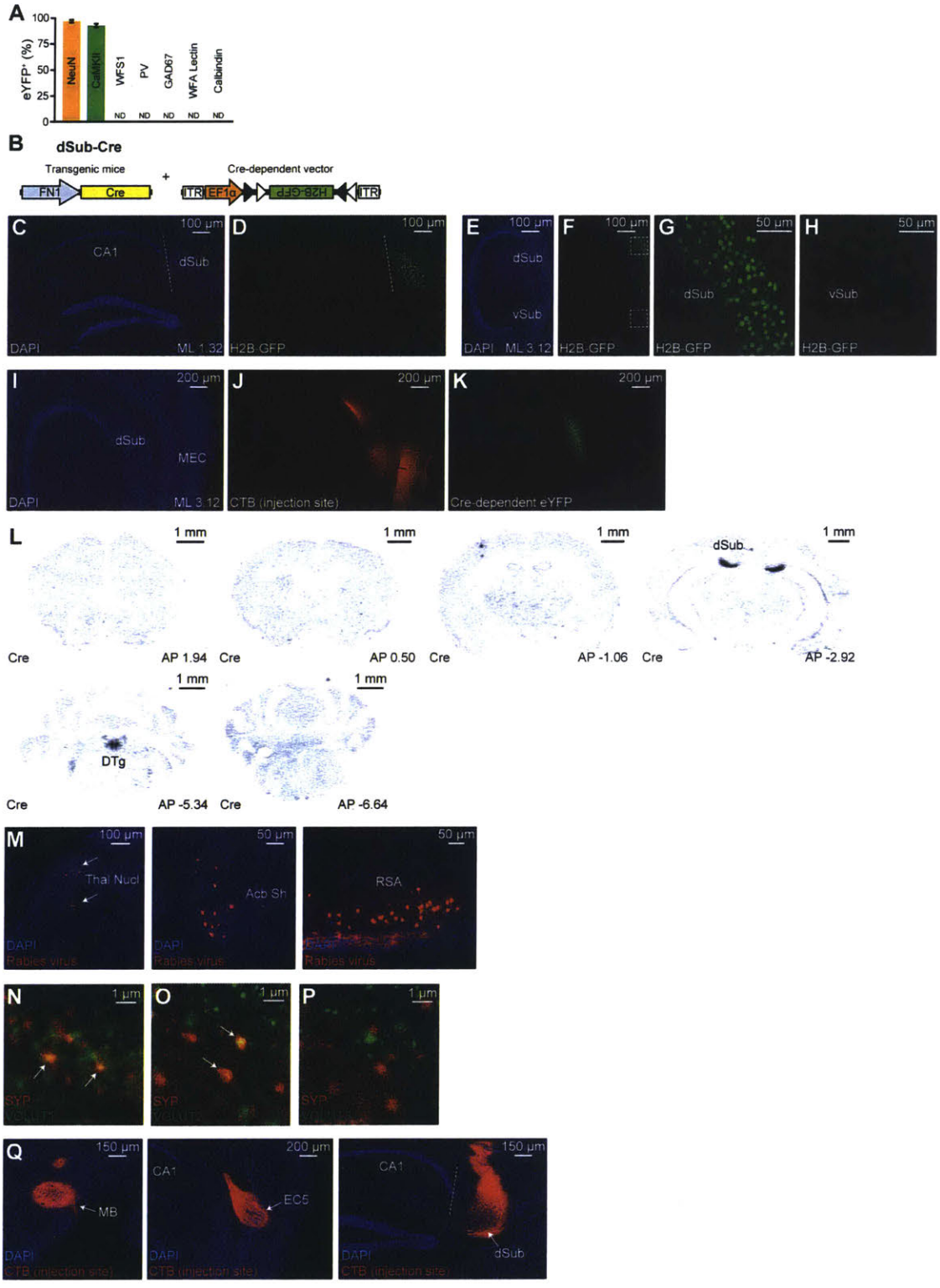
A
eYFP+ (%)
100
75
50
25
0
NeuN
CaMKII
WFS1
PV
GAD67
WFA Lectin
Calbindin
ND
B
dSub-Cre
Transgenic mice
+
Cre-dependent vector
FN1
Cre
ITR
EF1α
ITR
C
CA1
dSub
DAPI
ML 1.32
D
H2B-GFP
E
dSub
vSub
DAPI
ML 3.12
F
H2B-GFP
G
dSub
H2B-GFP
H
vSub
H2B-GFP
I
dSub
MEC
DAPI
ML 3.12
J
CTB (injection site)
K
Cre-dependent eYFP
L
Cre
AP 1.94
AP 0.50
AP -1.06
AP -2.92
DTg
AP -5.34
AP -6.64
M
Thal Nucl
Acb Sh
RSA
DAPI
Rabies virus
N
O
P
SYP
Q
MB
CA1
EC5
dSub
CTB (injection site)

Figure S1. Characterization of FN1-Cre mice

(A) FN1-Cre mice were injected with a Cre-dependent virus expressing eYFP. Percentage of $eYFP^+$ cells in dSub expressing various molecular markers (n = 3 mice per group). Cre^+ dSub neurons expressed the neuronal nuclei (NeuN) protein and the excitatory neuronal marker CaMKII (see Figure 1C). Cre^+ dSub neurons did not overlap with CA1 excitatory neurons labeled with WFS1 (see Figure 1B), parvalbumin (PV) inhibitory neurons, the inhibitory neuronal marker GAD67 (see Figure 1D), Wisteria floribunda (WFA) lectin, or the granule cell marker calbindin. ND, not detected.

(B-D) FN1-Cre mice were injected with a Cre-dependent histone H2B-GFP virus (see Experimental methods viral constructs section; B). Representative medial sagittal sections showing DAPI staining (blue, C) and H2B-GFP labeling in dSub (green, D). Dashed white line (C, D) denotes CA1/dSub border.

(E-H) Representative lateral sagittal sections showing DAPI staining (blue, E) and H2B-GFP labeling (green, F) in dSub, but not vSub. Higher magnification images of boxed regions in F (G-H).

(I-K) FN1-Cre mice were injected with a cocktail of Cre-dependent eYFP virus and CTB into EC5. Representative lateral sagittal sections showing DAPI staining (blue, I), CTB555 (red, J), and eYFP labeling (green, K). CTB555 signal reflects the injection site. Cre-dependent eYFP labeling was observed in dSub, but not MEC.

(L) Cre mRNA expression in FN1-Cre mice by in situ hybridization (ISH) showing clear signals in dSub, and the dorsal tegmental nucleus (DTg) in the brain stem. Anterior to posterior (AP, in millimeters relative to Bregma) coronal sections.

(M) Representative sagittal sections showing brain regions projecting to dSub Cre^+ neurons (see Figure 2D), including thalamic nuclei (Thal Nucl), nucleus accumbens shell (Acb Sh), and retrosplenial agranular cortex (RSA). Rabies virus-positive neurons (red), DAPI staining (blue). White arrows indicate multiple thalamic nuclei containing rabies virus-positive neurons.

(N-P) FN1-Cre mice were injected with a Cre-dependent synaptophysin (SYP) virus to label dSub axonal terminals. Reflecting the excitatory nature of these dSub Cre^+ neurons, SYP labeling (red) overlapped with vesicular glutamate transporters 1 (VGLUT1 in green; N) and 2 (VGLUT2 in green; O). dSub neurons do not express VGLUT3 (green; P), which mainly occurs in non-glutamatergic neurons. White arrows indicate axonal terminals originating from dSub Cre^+ neurons that express VGLUT1 (N) or VGLUT2 (O). Representative 40x sagittal confocal images.

(Q) CTB injection sites. Representative sagittal sections showing DAPI staining (blue) and CTB555 labeling (red). Small volume (50 nl) injections targeting MB (left panel), EC5 (middle panel), or dSub (right panel). Dashed white line (right panel) denotes CA1/dSub border.

Medial to lateral (ML, in millimeters relative to Bregma) coordinates. Data are presented as mean ± SEM.

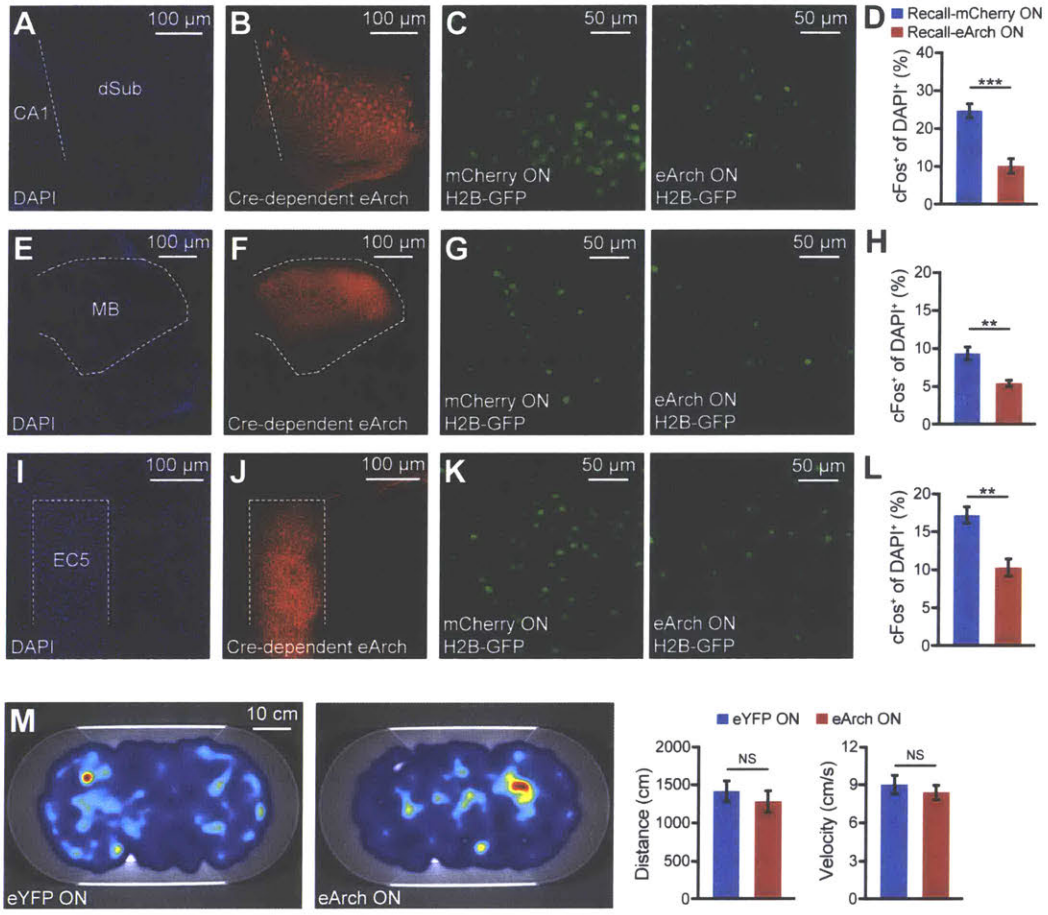

Figure S2. Optogenetic inhibition using eArch decreased memory recall-induced cFos expression in dSub cell bodies as well as terminals

(A-D) FN1-Cre mice were injected in dSub with a Cre-dependent eArch3.0-mCherry or mCherry alone virus (A-B). Dashed white line (A, B) denotes CA1/dSub border. To measure cFos levels, a virus cocktail of c-Fos-tTA and TRE-H2B-GFP viruses were injected into dSub (see Experimental methods; C). Representative cFos expression in dSub cell bodies from mCherry mice (C, left panel) and eArch3.0-mCherry mice (C, right panel). During CFC memory recall, optogenetic inhibition of dSub neurons decreased the percentage of cFos-positive neurons (n = 5 mice per group; D).

(E-H) Axonal terminals originating from dSub Cre^{+} neurons observed in MB (outlined by the white dashed line; E-F). Representative cFos expression in dSub→MB terminals from mCherry mice (G, left

panel) and eArch3.0-mCherry mice (G, right panel). Optogenetic inhibition of dSub terminals in MB during CFC memory recall decreased the percentage of cFos-positive neurons (n = 6 mice per group; H).

(I-L) Axonal terminals originating from dSub Cre^{+} neurons observed in EC5 (outlined by the white dashed line; I-J). Representative cFos expression in dSub→EC5 terminals from mCherry mice (K, left panel) and eArch3.0-mCherry mice (K, right panel). Optogenetic inhibition of dSub terminals in EC5 during CFC memory recall decreased the percentage of cFos-positive neurons (n = 6 mice per group; L).

DAPI staining in representative sagittal sections (A, E, I), eArch3.0-mCherry labeling (B, F, J), and H2B-GFP labeling (C, G, K).

(M) Open field assay. FN1-Cre mice were injected with a Cre-dependent eArch3.0-eYFP or eYFP alone virus into dSub. Optogenetic inhibition of dSub cell bodies during an open field test. Average heat maps (n = 10 mice per group) showing exploration time of eYFP light ON and eArch light ON groups (left). Distance traveled (centimeters, cm) and velocity (cm/second) (right). NS, not significant.

Statistical comparisons are performed using unpaired t tests; $^{**}P < 0.01$, $^{***}P < 0.001$. Data are presented as mean ± SEM.

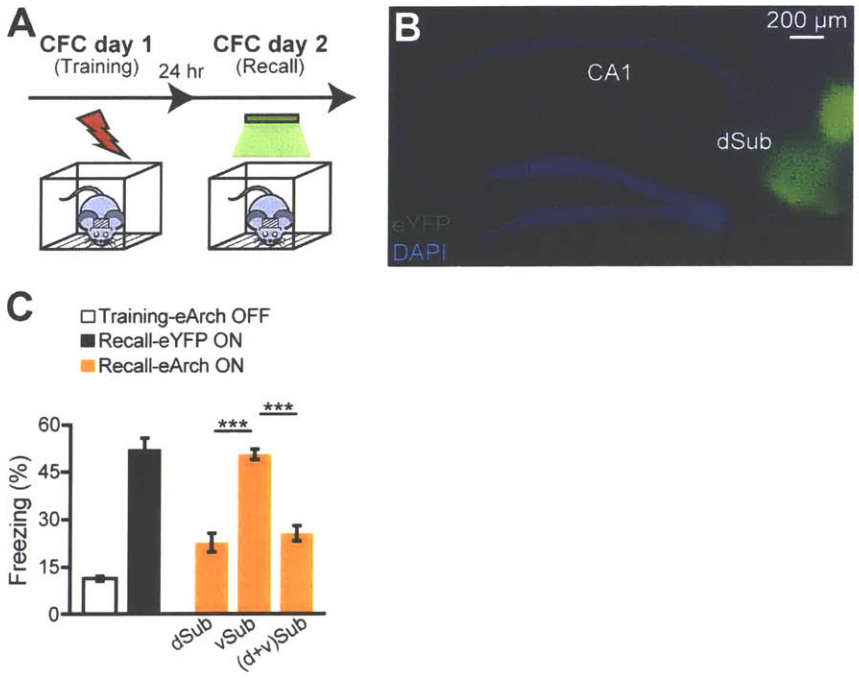

Figure S3. Optogenetic inhibition of dSub and/or vSub terminals in EC5 during CFC memory recall, using wild type mice

(A-C) Wild type C57BL/6J mice were injected with an EF1α-eArch3.0-eYFP virus. Behavioral schedule (A). Representative sagittal section showing eArch3.0-eYFP expression (green, B). DAPI staining (blue). Inhibition of dSub terminals in EC5 by green light during CFC memory recall impaired behavioral performance (n = 12 mice; C), while inhibition of vSub terminals in EC5 by green light showed normal levels of CFC memory recall (n = 14 mice). Consistent with these results, inhibition of both dSub and vSub (d+v) terminals in EC5 revealed a memory retrieval deficit (n = 12 mice).

Statistical comparisons are performed using unpaired t tests; ***$P < 0.001$. Data are presented as mean ± SEM.

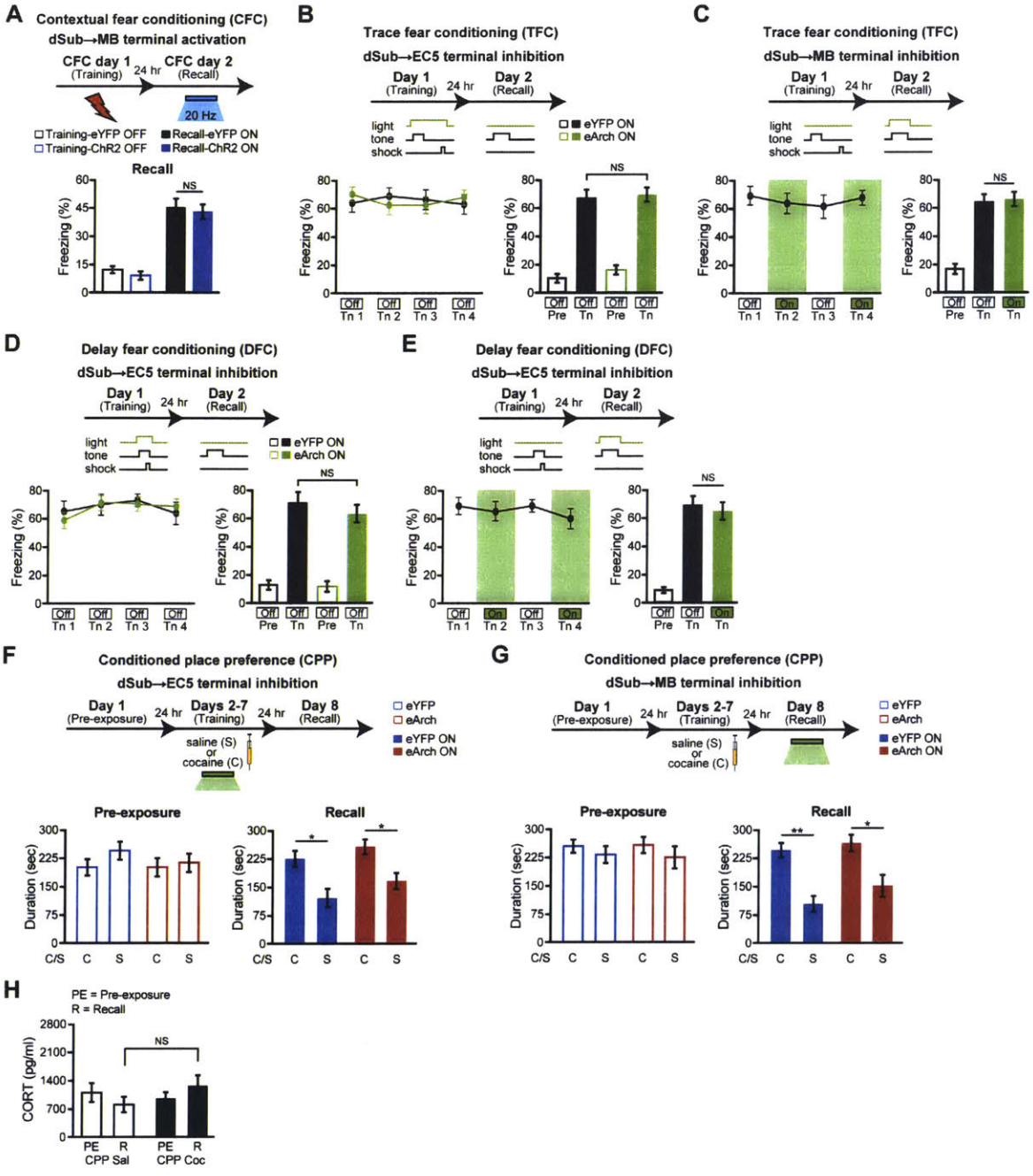
A
Contextual fear conditioning (CFC)
dSub→MB terminal activation
CFC day 1 (Training) 24 hr CFC day 2 (Recall)
20 Hz
Training-eYFP OFF
Training-ChR2 OFF
Recall-eYFP ON
Recall-ChR2 ON
Recall
Freezing (%)
NS
B
Trace fear conditioning (TFC)
dSub→EC5 terminal inhibition
Day 1 (Training) 24 hr Day 2 (Recall)
light
tone
shock
eYFP ON
eArch ON
Freezing (%)
NS
Off Tn 1 Off Tn 2 Off Tn 3 Off Tn 4
Off Pre Off Tn Off Pre Off Tn
C
Trace fear conditioning (TFC)
dSub→MB terminal inhibition
Day 1 (Training) 24 hr Day 2 (Recall)
light
tone
shock
Freezing (%)
NS
Off Tn 1 On Tn 2 Off Tn 3 On Tn 4
Off Pre Off Tn On Tn
D
Delay fear conditioning (DFC)
dSub→EC5 terminal inhibition
Day 1 (Training) 24 hr Day 2 (Recall)
light
tone
shock
eYFP ON
eArch ON
Freezing (%)
NS
Off Tn 1 Off Tn 2 Off Tn 3 Off Tn 4
Off Pre Off Tn Off Pre Off Tn
E
Delay fear conditioning (DFC)
dSub→EC5 terminal inhibition
Day 1 (Training) 24 hr Day 2 (Recall)
light
tone
shock
Freezing (%)
NS
Off Tn 1 On Tn 2 Off Tn 3 On Tn 4
Off Pre Off Tn On Tn
F
Conditioned place preference (CPP)
dSub→EC5 terminal inhibition
Day 1 (Pre-exposure) 24 hr Days 2-7 (Training) 24 hr Day 8 (Recall)
saline (S) or cocaine (C)
eYFP
eArch
eYFP ON
eArch ON
Pre-exposure
Recall
Duration (sec)
C/S C S C S
G
Conditioned place preference (CPP)
dSub→MB terminal inhibition
Day 1 (Pre-exposure) 24 hr Days 2-7 (Training) 24 hr Day 8 (Recall)
saline (S) or cocaine (C)
eYFP
eArch
eYFP ON
eArch ON
Pre-exposure
Recall
Duration (sec)
C/S C S C S
H
PE = Pre-exposure
R = Recall
CORT (pg/ml)
NS
PE R PE R
CPP Sal CPP Coc

Figure S4. Control experiments for optogenetic behavior manipulations

(A) FN1-Cre mice were injected with a Cre-dependent ChR2-eYFP virus into dSub. Optogenetic activation of dSub→MB terminals during contextual fear conditioning (CFC) recall had no effect on freezing levels (n = 8 mice per group). NS, not significant.

(B) FN1-Cre mice were injected with a Cre-dependent eArch3.0-eYFP virus into dSub. Inhibition of dSub→EC5 terminals during trace fear conditioning (TFC) training had no effect on tone (Tn)-induced freezing levels during recall tests (n = 11 mice per group). Pre-tone baseline freezing (Pre). Recall-induced freezing levels during individual tone presentations (left panels), averaged freezing levels (right panels). NS, not significant.

(C) Inhibition of dSub→MB terminals during trace fear conditioning (TFC) recall had no effect on freezing levels (n = 10 mice). Pre-tone baseline freezing (Pre). Recall-induced freezing levels during individual tone presentations (left panel), averaged freezing levels during the two light-off tones and the two light-on tones (right panel). NS, not significant.

(D) Inhibition of dSub→EC5 terminals during delay fear conditioning (DFC) training had no effect on tone (Tn)-induced freezing levels during recall tests (n = 10 mice per group). Pre-tone baseline freezing (Pre). Recall-induced freezing levels during individual tone presentations (left panels), averaged freezing levels (right panels). NS, not significant.

(E) Inhibition of dSub→EC5 terminals during delay fear conditioning (DFC) recall had no effect on tone (Tn)-induced freezing levels (n = 11 mice). Pre-tone baseline freezing (Pre). Recall-induced freezing levels during individual tone presentations (left panels), averaged freezing levels during the two light-off tones and the two light-on tones (right panels). NS, not significant.

(F) Inhibition of dSub→EC5 terminals during cocaine-induced conditioned place preference (CPP) training had no effect on recall tests (n = 13 mice per group). Behavioral schedule (top part). Pre-exposure preference duration (bottom, left graph) and recall preference duration (bottom, right graph). Saline (S or Sal), cocaine (C or Coc).

(G) Inhibition of dSub→MB terminals during CPP recall had no effect (n = 11 mice per group). Behavioral schedule (top part). Pre-exposure preference duration (bottom, left graph) and recall preference duration (bottom, right graph). Saline (S or Sal), cocaine (C or Coc).

(H) CORT levels following CPP memory recall tests were not significantly different between the saline (Sal) and cocaine (Coc) treated animals (n = 7 mice per group). NS, not significant.

Statistical comparisons are performed using unpaired t tests; $*P < 0.05$, $**P < 0.01$. Data are presented as mean ± SEM.

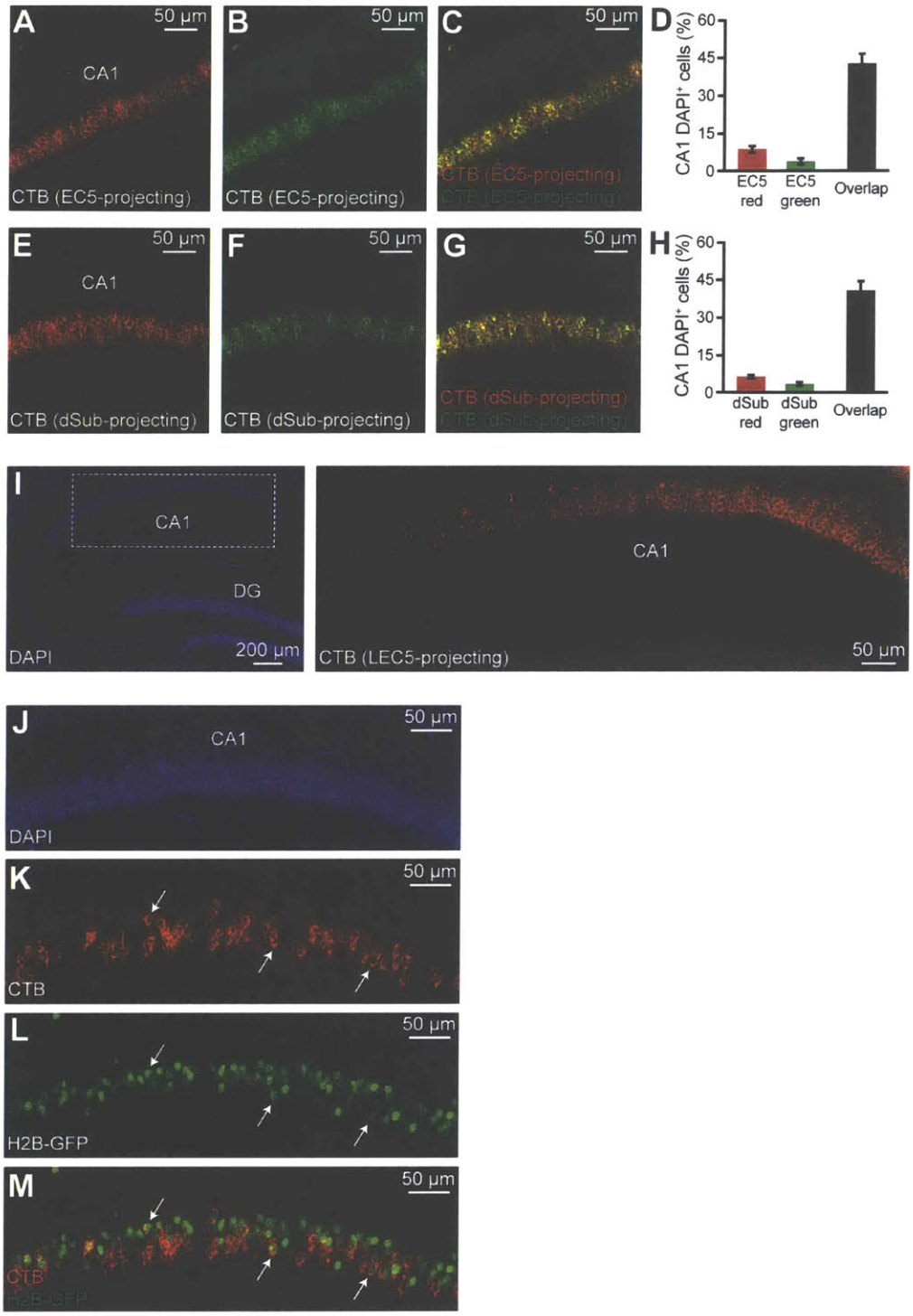
A
50 µm
CA1
CTB (EC5-projecting)
B
50 µm
CTB (EC5-projecting)
C
50 µm
CTB (EC5-projecting)
D
CA1 DAPI+ cells (%)
60
45
30
15
0
EC5 red
EC5 green
Overlap
E
50 µm
CA1
CTB (dSub-projecting)
F
50 µm
CTB (dSub-projecting)
G
50 µm
CTB (dSub-projecting)
H
CA1 DAPI+ cells (%)
60
45
30
15
0
dSub red
dSub green
Overlap
I
CA1
DG
DAPI
200 µm
CA1
CTB (LEC5-projecting)
50 µm
J
50 µm
CA1
DAPI
K
50 µm
CTB
L
50 µm
H2B-GFP
M
50 µm
CTB
H2B-GFP

Figure S5. CTB retrograde tracing and cFos-CTB overlap experiments

(A-H) To quantify the chance level at which retrograde tracing using CTB results in non-overlapping neuronal populations in the upstream target structure, CTB555 and CTB488 were co-injected into either EC5 or dSub. Most EC5-projecting CA1 cells (n = 3 mice; A-D) as well as dSub-projecting CA1 cells (n = 3 mice; E-H) showed high levels of overlap between CTB555 (red) and CTB488 (green). The maximum error between the expected perfect overlap and these experimental data was observed at 6% (CTB555 in CA1 from EC5; D), which is used as the chance level for obtaining non-overlapping neuronal populations in a target upstream structure using CTB dyes (in Figure 4G). Representative coronal sections are shown.

(I) Wild type C57BL/6J mice were injected with CTB555 into deep layers of the lateral entorhinal cortex (LEC5), to retrogradely label CA1 projection neurons. DAPI (blue, left) and CTB (red, right). Representative sagittal section showing hippocampal CA1 (left). Higher magnification image of boxed region showing CTB^+ neurons (right). Quantification revealed that 32% of dCA1 cells were CTB^+ (n = 3 mice).

(J-M) Wild type C57BL/6J mice were injected in dSub or EC5 with CTB555 to retrogradely label dCA1 neurons projecting to either brain region. DAPI (J) and CTB (K). To measure cFos levels, a virus cocktail of c-Fos-tTA and TRE-H2B-GFP viruses were injected into dCA1 (see Experimental methods; L). The overlap of behavior-induced cFos and CTB555 (M) was quantified in Figure 5H. Representative coronal images are taken with a 10x objective. White arrows indicate dCA1 neurons that are both $cFos^+$ and CTB^+.

Data are presented as mean ± SEM.

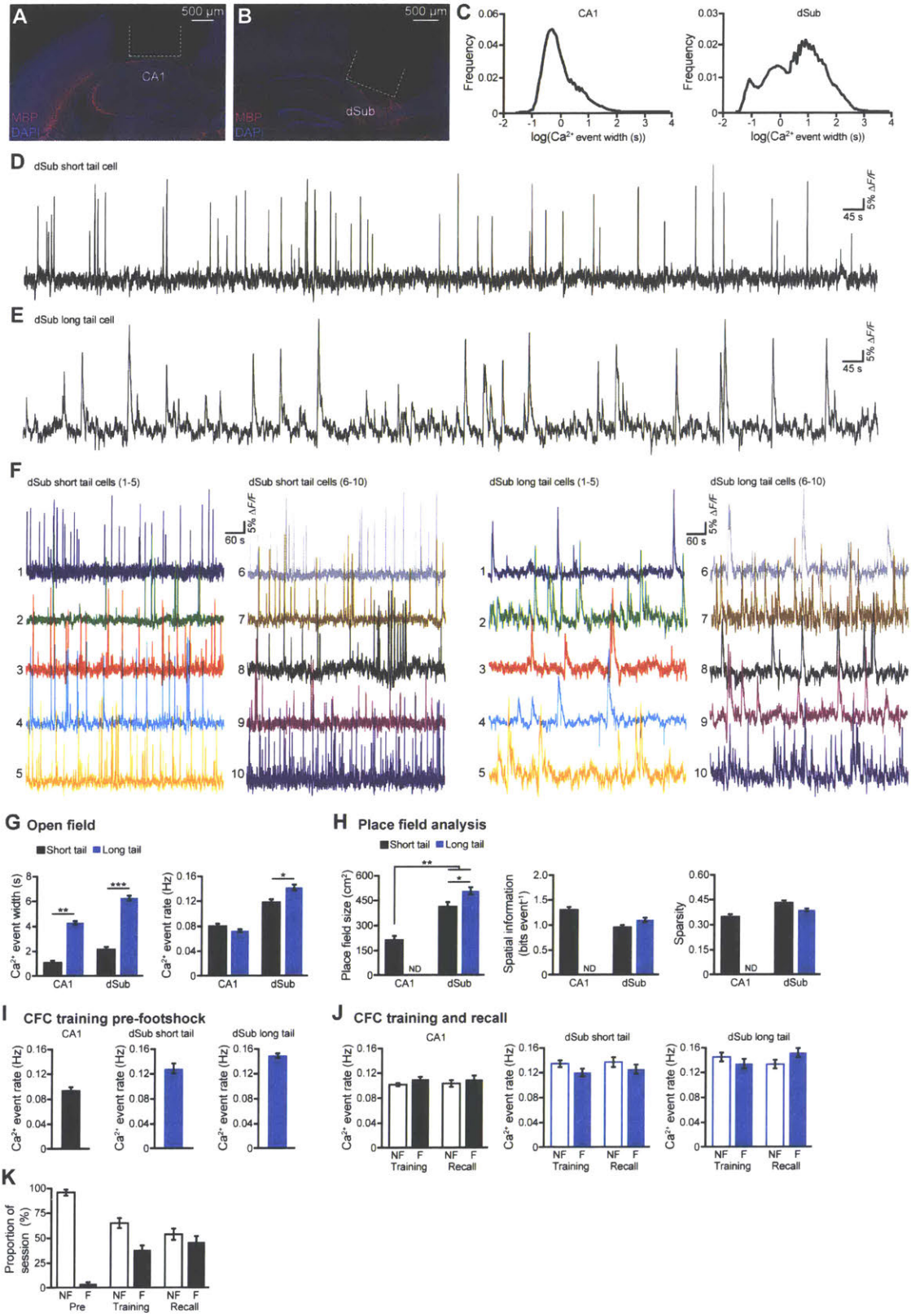
A
500 μm
CA1
MBP
DAPI
B
500 μm
dSub
MBP
DAPI
C
CA1
dSub
Frequency
log(Ca2+ event width (s))
D
dSub short tail cell
5% ΔF/F
45 s
E
dSub long tail cell
5% ΔF/F
45 s
F
dSub short tail cells (1-5)
dSub short tail cells (6-10)
dSub long tail cells (1-5)
dSub long tail cells (6-10)
5% ΔF/F
60 s
G Open field
Short tail
Long tail
Ca2+ event width (s)
Ca2+ event rate (Hz)
CA1
dSub
H Place field analysis
Short tail
Long tail
Place field size (cm2)
Spatial information (bits event-1)
Sparsity
ND
I CFC training pre-footshock
CA1
dSub short tail
dSub long tail
Ca2+ event rate (Hz)
J CFC training and recall
CA1
dSub short tail
dSub long tail
Ca2+ event rate (Hz)
NF F
Training
Recall
K
Proportion of session (%)
NF F
Pre
Training
Recall

Figure S6. Physiological characteristics of CA1 and dSub cells during open field and CFC tests

(A-B) Representative histological sections showing the damage induced by the microendoscope. Coronal image from a CA1-GCaMP6f mouse (A), see also Figure 6C. For CA1, the medial region along the proximodistal axis was targeted. Sagittal image from a dSub-GCaMP6f mouse (B), see also Figure 6B. Approximate microendoscope location outlined by the dashed white lines. DAPI staining (blue) and myelin basic protein (MBP) staining (red).

(C) Distribution of individual Ca^{2+} transient durations for the entire population of dCA1 (left) and dSub (right) cells. Y-axes indicate frequency of events (0.01 corresponds to 1%). X-axes indicate Ca^{2+} event width (s) plotted in logarithmic (log) scale for optimal visualization. Line fit for each distribution (black lines) show that the dSub cell population is bimodal.

(D-E) Representative Ca^{2+} traces from a dSub short tail (D) and a dSub long tail (E) cell during an open field imaging session of 30 minutes.

(F) Ca^{2+} traces from 10 dSub short tail cells during an imaging session of 10 minutes (left two columns). Ca^{2+} traces from 10 dSub long tail cells during an imaging session of 10 minutes (right two columns).

(G) Ca^{2+} activity during the open field paradigm. Ca^{2+} event width (s, left) and rate (Hz, right) are quantified (n = 759 CA1 cells, n = 428 dSub short tail cells, n = 371 dSub long tail cells, n = 4 mice per group).

(H) Place field size (cm^2), spatial information (bits $event^{-1}$), and sparsity quantification (cell counts in Figure S6C). A sparsity value of 0.15 indicates that the cell is active in 15% of the open field arena. ND, not detected.

(I-K) Ca^{2+} event rate during the pre-footshock period of CFC training (I) and non-freezing (NF) and freezing (F) periods of CFC training and recall (n = 550 CA1 cells, n = 429 dSub short tail cells, n = 203

dSub long tail cells, n = 3 CA1 mice, n = 4 dSub mice; J). Proportion of time in each session quantified as NF or F epochs for pre-footshock periods (Pre), training, and recall (K).

Statistical comparisons are performed using unpaired t tests; *P < 0.05, **P < 0.01, ***P < 0.001. Data are presented as mean ± SEM.

Chapter 5. Conclusions and future directions

In the first two projects, we observed dissociation between protein synthesis-dependent synaptic strengthening and memory retention 24 hours after training. This prompts a logical question: how is the memory retained? Undoubtedly, the cellular and molecular processes required for establishing specific connectivity during memory encoding includes synaptic strengthening such as LTP as well as de novo protein synthesis. One possibility is that memory is stored in a specific pattern of connectivity between distributed engram cell ensembles, which is established during encoding and retained during the consolidation time window in a protein synthesis-independent manner. In these studies, we tested this possibility by performing two sets of experiments using ex vivo electrophysiological and in vivo IEG technologies. When both DG and hippocampal CA3 engram cell ensembles were simultaneously labeled and the presynaptic DG engram cells were activated optogenetically, the occurrence of postsynaptic responses in CA3 engram cells was significantly higher (~80%) than CA3 non-engram cells (~25%), and these proportions were not affected by protein synthesis inhibition. In another experiment, engram cells were simultaneously labeled in the DG, CA3, and BLA during contextual fear conditioning. One day after training, re-exposure to the conditioning context preferentially activated engram cells in all three brain regions as measured by c-Fos-positive cell counts, and importantly, this phenomenon was significantly impaired by anisomycin treatment only during the consolidation time window. However, direct optogenetic activation of DG engram cells resulted in a greater than chance level of c-Fos overlap with CA3 or BLA engram cells in both control and anisomycin-treated mice. Together, these results indicated intact functional connectivity among engram cell ensembles distributed in neural circuits encompassing multiple brain regions and supported the hypothesis that consolidated memories are stored by engram cell-specific connectivity formed in a protein synthesis-independent manner. Further work will elucidate the molecular mechanisms underlying this retained connectivity following protein synthesis blockade.

Using the integrative engram-based findings (Roy et al., 2016; Ryan et al., 2015), we suggested that engram cell-specific synaptic strength is necessary for the retrievability of specific memory engrams, while the memory information is encoded in a pattern of engram cell ensemble connectivity. This idea

was supported by the finding that amnesic mice lacked synaptic strength increases after learning, which prevented the effective activation of engram cells by natural recall cues and engram cell spiking that is crucial for successful memory recall. Nevertheless, the information stored in engram cell ensemble connectivity patterns could be retrieved by optogenetic stimulation of various nodes in the engram cell circuit. The notion that synaptic strengthening is crucial for memory retrieval, but not for stable storage of memory per se, is consistent with a number of recent complementary studies. For example, recently it was shown that optogenetically-induced LTD of rat amygdala cells impaired pre-formed conditioned fear memory expression (Nabavi et al., 2014). Importantly, subsequent optogenetically-induced LTP of the same cells restored natural cue-evoked recall of the fear memory. The most parsimonious explanation of these results is that memory information must have persisted in the brain of the rats even after the amygdala synapses were depressed, and moreover that the lack of synaptic potentiation prevented successful memory retrieval. Supporting this perspective is the demonstration that amnesia for a purely contextual memory can be overcome by direct engram activation paired with simultaneous presentation of aversive shock (Ryan et al., 2015). Other research found that contextual fear memories formed during a specific period within adolescent development were not expressed in recall tests until adulthood (Pattwell et al. 2011). Interestingly, this developmental change correlated with delayed learning-specific synaptic potentiation of the BLA fear circuit. Therefore, the fear memory was present during adolescence, but its retrievability was temporarily impaired due to the lack of sufficient synaptic potentiation in BLA ensembles. In Aplysia (Chen et al., 2014), reminder experiments have shown that amnesia for the canonical gill withdrawal sensitization behavior could be restored by additional puffs of serotonin, and that this response persisted despite significantly reduced presynaptic varicosities. Collectively, these studies support a dissociation of synaptic strength and memory persistence, and point to a crucial role for experience-dependent synaptic strengthening in the reactivation/retrievability of a memory engram.

A dissociation between augmented synaptic strengthening and engram cell connectivity as the mechanism for consolidated long-term memory storage has significant implications for the neurobiology of memory consolidation because the conceptual framework described above may be used to attribute

experience-dependent molecular/cellular processes to memory storage or retrieval. Since traditional approaches that demonstrated the formation of a long-term memory relied on memory retrieval itself, it cannot be assumed that the memory consolidation time window is specifically for the storage of information. Within this interpretation, molecular mechanisms that serve to potentiate or strengthen synaptic transmission (Kandel, 2012; Lisman et al., 2012; Sacktor, 2011) are parsimoniously attributable to memory retrievability. Central to this dissociation is the molecular basis for information retention, which is clearly crucial for establishing engram cell connectivity and stably maintaining these complex patterns over time. It is known that NMDA receptor-dependent synaptic plasticity results not just in potentiated synapses, but also in the formation of new functional synaptic connections through synapse unsilencing (Liao et al., 1995). Memory encoding-induced establishment of new functional connectivity could be facilitated by AMPA receptor insertion into pre-existing silent synapses. It is widely accepted that LTP has an early and a late phase, namely E-LTP and L-LTP, with the latter being sensitive to protein synthesis inhibitors (Davis and Squire, 1984). Survival of preferential engram cell connectivity upon protein synthesis inhibitor treatment (Ryan et al., 2015) and in early Alzheimer's disease mice (Roy et al., 2016) suggests that the induction of engram connectivity may share mechanisms common to E-LTP. On the other hand, impairing L-LTP has been shown to prevent synapse unsilencing, which supports the hypothesis that unsilencing silent synapses is unlikely to be a major contributor for the retention of connectivity (Kasten et al., 2007). Another possibility is that a subset of learning-induced dendritic spines is responsible for novel connectivity pattern formation between engram cells. In any of these scenarios, the retention of engram cell connectivity could conceivably be mediated by the homeostatic regulation of steady state AMPA receptor trafficking. Consistent with this idea is a recent study showing that protein synthesis inhibitors, when administered prior to recall tests, transiently impaired AMPA receptor expression and memory retrieval (Lopez et al., 2015). More recently, it has been suggested that microRNAs and/or perineuronal nets (Gallistel and Balsam, 2014; Tsien, 2013) may mediate the long-term maintenance of memory engram.

A major unanswered question regarding engram cell connectivity is the time period during which such complex patterns are maintained in vivo. On a related note, it will be important to determine whether the formation and elimination of connectivity patterns is reversible. Even though it has been shown through engram cell overlap analysis, when the positive or negative emotional valence associated with a contextual memory is reversed, the functional connectivity of DG to BLA engram cells changes (Redondo et al., 2014), a direct analysis of synaptic connections will be necessary to understand the true physiological nature of the plasticity within pre-formed connectivity. Nevertheless, if engram cell connectivity is the substrate of memory information storage, then it will be necessary to fully explore the structure and function of the engram circuit. This would require comprehensive mapping of the entire engram circuit connectome for a given memory. This could be achieved by combining engram labeling technology, whole brain IEG activity measurements (Wheeler et al., 2013), and three-dimensional imaging of intact transparent brains (Chung et al., 2013). Furthermore, by using in vivo calcium imaging of engram cells across multiple brain regions (Lecoq et al., 2014), functional properties of engram circuits can be studied.

Synaptic plasticity is a ubiquitous feature of neurons that seems to have arisen with the first nervous system in a common ancestor of cnidarians and bilaterians over a billion years ago (Tonegawa et al., 2015a). From this evolutionary point of view, synaptic plasticity can be considered a fundamental neuronal property, the disruption of which in brain regions such as the hippocampus or amygdala will impair the encoding and retrieval of memory. In contrast, engram cell connectivity may be a substrate that naturally increases in complexity as brain anatomy evolves. Therefore, for a more complex brain anatomy, there is a greater opportunity for encoding detailed memories through hierarchical engram circuits distributed across brain regions. Consistent with Hebb's original vision (Hebb, 1949), engram cell connectivity patterns are a potential mechanism of information storage. Further research in these directions may provide significant new insights into the storage of memory, and mechanisms underlying efficient memory retrieval.

6. References

Antonini, A., and Stryker, M.P. (1993). Rapid remodeling of axonal arbors in the visual cortex. Science 260, 1819-1821.

Armbruster, B.N., Li, X., Pausch, M.H., Herlitze, S., and Roth, B.L. (2007). Evolving the lock to fit the key to create a family of G protein-coupled receptors potently activated by an inert ligand. Proc. Natl. Acad. Sci. U.S.A. 104, 5163-5168.

Attardo, A., Fitzgerald, J.E., and Schnitzer, M.J. (2015). Impermanence of dendritic spines in live adult CA1 hippocampus. Nature 523, 592-596.

Avian Brain Nomenclature Consortium (2005). Avian brains and a new understanding of vertebrate brain evolution. Nat. Rev. Neurosci. 6, 151-159.

Bailey, C.H., and Chen, M. (1989). Time course of structural changes at identified sensory neuron synapses during long-term sensitization in Aplysia. J. Neurosci. 9, 1774-1780.

Bailey, C.H., and Kandel, E.R. (1993). Structural changes accompanying memory storage. Annu. Rev. Physiol. 55, 397-426.

Bannerman, D.M., Bus, T., Taylor, A., et al. (2012). Dissecting spatial knowledge from spatial choice by hippocampal NMDA receptor deletion. Nat. Neurosci. 15, 1153-1159.

Bao, S., Chan, V.T., and Merzenich, M.M. (2001). Cortical remodeling induced by activity of ventral tegmental dopamine neurons. Nature 412, 79-93.

Bao, S., Chen, L., Kim, J.J., and Thompson, R.F. (2002). Cerebellar cortical inhibition and classical eyeblink conditioning. Proc. Natl. Acad. Sci. USA 99, 1592-1597.

Bergson, H. (1911). Matter and memory. London: Swan Sonnenschein.

Besnard, A., Laroche, S., and Caboche, J. (2014). Comparative dynamics of MAPK/ERK signaling components and immediate early genes in the hippocampus and amygdala following contextual fear conditioning and retrieval. Brain Struct. Funct. 219, 415-430.

Bliss, T.V., and Lomo, T. (1973). Long-lasting potentiation of synaptic transmission in the dentate area of the anesthetized rabbit following stimulation of the perforant path. J. Physiol. 232, 331-356.

Bolhuis, J.J., and Gahr, M. (2006). Neural mechanisms of birdsong memory. Nat. Rev. Neurosci. 7, 347-357.

Bourque, C.W., Oliet, S.H., Kirkpatrick, K., Richard, D., and Fisher, T.E. (1993). Extrinsic and intrinsic modulatory mechanisms involved in regulating the electrical activity of supraoptic neurons. Ann. N. Y. Acad. Sci. 689, 512-519.

Boyden, E.S., Zhang, F., Bamberg, E., Nagel, G., and Deisseroth, K. (2005). Millisecond-timescale, genetically targeted optical control of neural activity. Nat. Neurosci. 8, 1283-1268.

Bruce, D. (2001). Fifty years since Lashley's in search of the engram: refutations and conjectures. J. Hist. Neurosci. 10, 308-318.

Cai, D., Aharoni, D., Shuman, T., et al. (2016). A shared neural ensemble links distinct contextual memories encoded close in time. Nature, doi:10.1038/nature17955.

Chen, S., Cai, D., Pearce, K., et al. (2014). Reinstatement of long-term memory following erasure of its behavioral and synaptic expression. eLife 3, e3896.

Chow, B.Y., Han, X., Dobry, A.S., et al. (2010). High-performance genetically targetable optical neural silencing by light-driven proton pumps. Nature 463, 98-102.

Chung, K., Wallace, J., Kim, S.Y., et al. (2013). Structural and molecular interrogation of intact biological systems. Nature 497, 332-337.

Cisse, M., Halabisky, B., Harris, J., et al. (2011). Reversing EphB2 depletion rescues cognitive functions in Alzheimer model. Nature 469, 47-52.

Clayton, N.S., and Dickinson, A. (1998). Episodic-like memory during cache recovery by scrub jays. Nature 395, 272-274.

Clem, R.L., and Huganir, R.L. (2010). Calcium-permeable AMPA receptor dynamics mediate fear memory erasure. Science 330, 1108-1112.

Corfas, G., and Dudai, Y. (1991). Morphology of a sensory neuron in Drosophila is abnormal in memory mutants and changes during aging. Proc. Natl. Acad. Sci. USA 88, 7252-7256.

Cowansage, K.K., Shuman, T., Dillingham, B.C., et al. (2014). Direct reactivation of a coherent neocortical memory of context. Neuron 84, 432-441.

Czajkowski, R., Jayaprakash, B., Wiltgen, B., et al. (2014). Encoding and storage of spatial information in the retrosplenial cortex. Proc. Natl. Acad. Sci. USA 111, 8661-8666.

Daoudal, G., and Debanne, D. (2003). Long-term plasticity of intrinsic excitability: learning rules and mechanisms. Learn. Mem. 10, 456-465.

Daumas, S., Sandin, J., Chen, K.S., et al. (2008). Faster forgetting contributes to impaired spatial memory in the PDAPP mouse: deficit in memory retrieval associated with increased sensitivity to interference? Learn. Mem. 15, 625-632.

Davis, H.P., and Squire, L.R. (1984). Protein synthesis and memory: a review. Psychol. Bull. 96, 518-559.

De Paola, V., Holtmaat, A., Knott, G., et al. (2006). Cell type-specific structural plasticity of axonal branches and boutons in the adult neocortex. Neuron 49, 861-875.

Deng, W., Aimone, J.B., and Gage, F.H. (2010). New neurons and new memories: how does adult hippocampal neurogenesis affect learning and memory? Nat. Rev. Neurosci. 11, 339-350.

Deng, W., Mayford, M., and Gage, F.H. (2013). Selection of distinct populations of dentate granule cells in response to inputs as a mechanism for pattern separation in mice. eLife 2, e312.

Denk, W., Strickler, J.H., and Webb, W.W. (1990). Two-photon laser scanning fluorescence microscopy. Science 248, 73-76.

Denny, C.A., Kheirbek, M.A., Alba, E.L., et al. (2014). Hippocampal memory traces are differentially modulated by experience, time, and adult neurogenesis. Neuron 83, 189-201.

Descartes, R. (1649). Les Passions de l'âme. The passions of the soul, translated by Stephen H. Voss, 1989. Indianapolis: Hackett Publishing Company.

Ding, S.L. (2013). Comparative anatomy of the prosubiculum, subiculum, presubiculum, postsubiculum, and parasubiculum in human, monkey, and rodent. J. Comp. Neurol. 521, 4145-4162.

Doupe, A.J., and Kuhl, P.K. (1999). Birdsong and human speech: common themes and mechanisms. Annu. Rev. Neurosci. 22, 567-631.

Dudai, Y. (1988). Neurogenetic dissection of learning and short-term memory in Drosophila. Annu. Rev. Neurosci. 11, 537-563.

Dudai, Y., and Eisenberg, M. (2004). Rites of passage of the engram: reconsolidation and the lingering consolidation hypothesis. Neuron 44, 93-100.

Dudai, Y., and Morris, R.G. (2013). Memorable trends. Neuron 80, 742-750.

Duncan, C.P. (1949). The retroactive effect of electroshock on learning. J. Comp. Physiol. Psychol. 42, 32-44.

Dupret, D., O'Neill, J., Pleydell-Bouverie, B., and Csicsvari, J. (2010). The reorganization and reactivation of hippocampal maps predict spatial memory performance. Nat. Neurosci. 13, 995-1002.

Eales, L.A. (1985). Song learning in zebra finches: some effects of song model availability on what is learnt and when. Anim. Behav. 33, 1293-1300.

Ebbinghaus, H. (1880). Ueber das Gedachtniss. Passau: Passavia-Universitatsverlag.

Eguchi, M., and Yamaguchi, S. (2009). In vivo and in vitro visualization of gene expression dynamics over extensive areas of the brain. Neuroimage 44, 1274-1283.

Eichenbaum, E., Yonelinas, A.P., and Ranganath, C. (2007). The medial temporal lobe and recognition memory. Annu. Rev. Neurosci. 30, 123-152.

Eldridge, L.L., Engel, S., Zeineh, M.M., Bookheimer, S.Y., and Knowlton, B.J. (2005). A dissociation of encoding and retrieval processes in the human hippocampus. J. Neurosci. 25, 3280-3286.

Engert, F., and Bonhoeffer, T. (1999). Dendritic spine changes associated with hippocampal long-term synaptic plasticity. Nature 399, 66-70.

Farris, S.M., Robinson, G.E., and Fahrbach, S.E. (2001). Experience- and age-related outgrowth of intrinsic neurons in the mushroom bodies of the adult worker honeybee. J. Neurosci. 21, 6395-6404.

Fenno, L., Yizhar, O., and Deisseroth, K. (2011). The development and application of optogenetics. Annu. Rev. Neurosci. 34, 389-412.

Flavell, S.W., and Greenberg, M.E. (2008). Signaling mechanisms linking neuronal activity to gene expression and plasticity of the nervous system. Annu. Rev. Neurosci. 31, 563-590.

Flexner, J.B., Flexner, L.B., and Stellar, E. (1963). Memory in mice as affected by intracerebral puromycin. Science 141, 57-59.

Flexner, L.B., Flexner, J.B., and Roberts, R.B. (1967). Memory in mice analyzed with antibiotics. Antibiotics are useful to study stages of memory and to indicate molecular events, which sustain memory. Science 155, 1377-1383.

Foster, M., and Sherrington, C.S. (1897). A textbook of physiology, part three: the central nervous system. London: Macmillan and Company Ltd.

Franz, S.I. (1912). New phrenology. Science 35, 321-328.

Frey, U., Krug, M., Reymann, K.G., and Matthies, H. (1988). Anisomycin, an inhibitor of protein synthesis, blocks late phases of LTP phenomena in the hippocampal CA1 region in vitro. Brain Res. 452, 57-65.

Fuster, J.M., and Jervey, J.P. (1981). Inferotemporal neurons distinguish and retain behaviorally relevant features of visual stimuli. Science 212, 952-955.

Gabrieli, J.D., Brewer, J.B., Desmond, J.E., and Glover, G.H. (1997). Separate neural bases of two fundamental memory processes in the human medial temporal lobe. Science 276, 264-266.

Gallistel, C.R., and Balsam, P.D. (2014). Time to rethink the neural mechanisms of learning and memory. Neurobiol. Learn. Mem. 108, 136-144.

Garcia, K.S., and Mauk, M.D. (1998). Pharmacological analysis of cerebellar contributions to the timing and expression of conditioned eyelid responses. Neuropharmacology 37, 471-480.

Garner, A.R., Rowland, D.C., Hwang, S.Y., et al. (2012). Generation of a synthetic memory trace. Science 335, 1513-1516.

Gelbard-Sagiv, H., Mukamel, R., Harel, M., Malach, R., and Fried, I. (2008). Internally generated reactivation of single neurons in human hippocampus during free recall. Science 322, 96-101.

Gerber, B., Tanimoto, H., and Heisenberg, M. (2004). An engram found? Evaluating the evidence from fruit flies. Curr. Opin. Neurobiol. 14, 737-744.

Geva-Sagiv, M., Romani, S., Las, L., and Ulanovsky, N. (2016). Hippocampal global remapping for different sensory modalities in flying bats. Nat. Neurosci. 19, 952-958.

Glanzman, D.L., Kandel, E.R., and Schacher, S. (1990). Target-dependent structural changes accompanying long-term synaptic facilitation in Aplysia neurons. Science 249, 799-802.

Gold, P.E., Haycock, J.W., Marri, J., and McGaugh, J.L. (1973). Retrograde amnesia and the reminder effect: an alternative interpretation. Science 180, 1199-1201.

Gold, P.E., and King, R.A. (1974). Retrograde amnesia: storage failure versus retrieval failure. Psychol. Rev. 81, 465-469.

Gonzalez-Lima, F., and Scheich, H. (1986). Neural substrates for tone-conditioned bradycardia demonstrated with 2-deoxyglucose II. Behav. Brain Res. 20, 281-293.

Gore, F., Schwartz, E.C., Brangers, B.C., et al. (2015). Neural representations of unconditioned stimuli in basolateral amygdala mediate innate and learned responses. Cell 162, 134-145.

Goshen, I., Brodsky, M., Prakash, R., et al. (2011). Dynamics of retrieval strategies for remote memories. Cell 147, 678-689.

Govindarajan, A., Israely, I., Huang S.Y., and Tonegawa, S. (2011). The dendritic branch is the preferred integrative unit for protein synthesis-dependent LTP. Neuron 69, 132-146.

Granholm, E., and Butters, N. (1988). Associative encoding and retrieval in Alzheimer's and Huntington's disease. Brain Cognition 7, 335-347.

Graves, A.R., Moore, S.J., Bloss, E.B., et al. (2012). Hippocampal pyramidal neurons comprise two distinct cell types that are countermodulated by metabotropic receptors. Neuron 76, 776-789.

Guzowski, J.F. (2002). Insights into immediate-early gene function in hippocampal memory consolidation using antisense oligonucleotide and fluorescent imaging approaches. Hippocampus 12, 86-104.

Hall, J., Thomas, K.L., and Everitt, B.J. (2001). Fear memory retrieval induces CREB phosphorylation and Fos expression within the amygdala. Eur. J. Neurosci. 13, 1453-1458.

Han, J.-H., Kushner, S.A., Yiu, A.P., et al. (2007). Neuronal competition and selection during memory formation. Science 316, 457-460.

Han, J.-H., Kushner, S.A., Yiu, A.P., et al. (2009). Selective erasure of a fear memory. Science 323, 1492-1496.

Hardt, O., Wang, S.H., and Nader, K. (2009). Storage or retrieval deficit: the yin and yang of amnesia. Learn. Mem. 16, 224-230.

Harris, J.A., Devidze, N., Verret, L., et al. (2010). Transsynaptic progression of amyloid-β-induced neuronal dysfunction within the entorhinal-hippocampal network. Neuron 68, 428-441.

Hasselmo, M.E., and McClelland, J.L. (1999). Neural models of memory. Curr. Opin. Neurobiol. 9, 184-188.

Hayashi-Takagi, A., Yagishita, S., Nakamura, M., et al. (2015). Labelling and optical erasure of synaptic memory traces in the motor cortex. Nature 525, 333-338.

Hebb, D.O. (1949). The organization of behavior: a neuropsychological theory. New York: Wiley.

Herman, J.P., Dolgas, C.M., and Carlson, S.L. (1998). Ventral subiculum regulates hypothalamo-pituitary-adrenocortical and behavioural responses to cognitive stressors. Neuroscience 86, 449-459.

Hitti, F.L., and Siegelbaum, S.A. (2014). The hippocampal CA2 region is essential for social memory. Nature 508, 88-92.

Hodges, J.R., Salmon, D.P., and Butters, N. (1990). Differential impairment of semantic and episodic memory in Alzheimer's and Huntington's diseases: a controlled prospective study. J. Neurol. Neurosurg. Psychiatry 53, 1089-1095.

Hofer, S.B., Mrsic-Flogel, T.D., Bonhoeffer, T., and Hubener, M. (2009). Experience leaves a lasting structural trace in cortical circuits. Nature 457, 313-317.

Holtmaat, A., Wilbrecht, L., Knott, G.W., Welker, E., and Svoboda, K. (2006). Experience-dependent and cell-type-specific spine growth in the neocortex. Nature 441, 979-983.

Horn, G. (2004). Pathways of the past: the imprint of memory. Nat. Rev. Neurosci. 5, 108-120.

Hsia, A.Y., Masliah, E., McConlogue, L., et al. (1999). Plaque-independent disruption of neural circuits in Alzheimer's disease mouse models. Proc. Natl. Acad. Sci. U.S.A. 96, 3228-3233.

Hsiang, H.-L., Epp, J.R., van der Oever, M.C., et al. (2014). Manipulating a cocaine engram in mice. J. Neurosci. 34, 14115-14127.

Huang, Y.Y., Nguyen, P.V., Abel, T., and Kandel, E.R. (1996). Long-lasting forms of synaptic potentiation in the mammalian hippocampus. Learn. Mem. 3, 74-85.

Hubener, M., and Bonhoeffer, T. (2010). Searching for engrams. Neuron 67, 363-371.

Hyman, B.T., Van Hoesen, G.W., Damasio, A.R., and Barnes, C.L. (1984). Alzheimer's disease: cell-specific pathology isolates the hippocampal formation. Science 225, 1168-1170.

Hyman, B.T., Van Hoesen, G.W., Kromer, L.J., and Damasio, A.R. (1986). Perforant pathway changes and the memory impairment of Alzheimer's disease. Ann. Neurol. 20, 472-481.

Ito, M., and Kano, M. (1982). Long-lasting depression of parallel fiber-Purkinje cell transmission induced by conjunctive stimulation of parallel fibers and climbing fibers in the cerebellar cortex. Neurosci. Lett. 33, 253-258.

James, W. (1890). The principles of psychology. New York: H. Holt and Company.

Jacobsen, J.S., Wu, C.C., Redwine, J.M., et al. (2006). Early-onset behavioral and synaptic deficits in a mouse model of Alzheimer's disease. Proc. Natl. Acad. Sci. USA 103, 5161-5166.

Jankowsky, J.L., Fadale, D.J., Anderson, J., et al. (2004). Mutant presenilins specifically elevate the levels of the 42 residue β-amyloid peptide in vivo: evidence for augmentation of a 42-residue γ secretase. Hum. Mol. Genet. 13, 159-170.

Jarsky, T., Mady, R., Kennedy, B., and Spruston, N. (2008). Distribution of bursting neurons in the CA1 region and the subiculum of the rat hippocampus. J. Comp. Neurol. 506, 535-547.

Jin, X., Pokala, N., and Bargmann, C.I. (2016). Distinct circuits for the formation and retrieval of an imprinted olfactory memory. Cell 164, 632-643.

Johansen, J.P., Cain, C.K., Ostroff, L.E., and LeDoux, J.E. (2001). Molecular mechanisms of fear learning and memory. Cell 147, 509-524.

Josselyn, S. (2010). Continuing the search for the engram: examining the mechanism of fear memories. J. Psychiatry Neurosci. 35, 221-228.

Josselyn, S., Kohler, S., and Frankland, P.W. (2015). Finding the engram. Nat. Rev. Neurosci. 16, 521-534.

Kameyama, K., Sohya, K., Ebina, T., et al. (2010). Difference in binocularity and ocular dominance plasticity between GABAergic and excitatory cortical neurons. J. Neurosci. 30, 1551-1559.

Kaneko, T., Fujiyama, F., and Hioki, H. (2002). Immunohistochemical localization of candidates for vesicular glutamate transporters in the rat brain. J. Comp. Neurol. 444, 39-62.

Kasten, M.R., Fan, Y., and Schulz, P.E. (2007). Activation of silent synapses with sustained but not decremental long-term potentiation. Neurosci. Lett. 417, 84-89.

Kandel, E.R. (1976). Cellular basis of behavior: an introduction to behavioral biology. San Francisco: Freeman.

Kandel, E.R. (2001). The molecular biology of memory storage: a dialogue between genes and synapses. Science 294, 1030-1038.

Kandel, E.R. (2012). The molecular biology of memory: cAMP, PKA, CRE, CREB-1, CREB-2, and CPEB. Mol. Brain 5, 14.

Kass, M.D., Rosenthal, M.C., Pottackal, J., and McGann, J.P. (2013). Fear learning enhances neural responses to threat-predictive sensory stimuli. Science 342, 1389-1392.

Kelleher, R.J., Govindarajan, A., and Tonegawa, S. (2004). Translational regulatory mechanisms in persistent forms of synaptic plasticity. Neuron 44, 59-73.

Kelley, J.B., Balda, M.A., Anderson, K.L., and Itzhak, Y. (2009). Impairments in fear conditioning in mice lacking the nNOS gene. Learn. Mem. 16, 371-378.

Kim, Y., and Spruston, N. (2012). Target-specific output patterns are predicted by the distribution of regular-spiking and bursting pyramidal neurons in the subiculum. Hippocampus 22, 693-706.

Kim, J., Kwon, J.T., Kim, H.S., Josselyn, S.A., and Han, J.H. (2014). Memory recall and modifications by activating neurons with elevated CREB. Nat. Neurosci. 17, 65-72.

Kishi, T., Tsumori, T., Ono, K., et al. (2000). Topographical organization of projections from the subiculum to the hypothalamus in the rat. J. Comp. Neurol. 419, 205-222.

Kisley, M.A., and Gerstein, G.L. (2001). Daily variation and appetitive conditioning-induced plasticity of auditory cortex receptive fields. Eur. J. Neurosci. 13, 1993-2003.

Kitamura, T., Pignatelli, M., Suh, J., et al. (2014). Island cells control temporal association memory. Science 343, 896-901.

Kitamura, T., Sun, C., Martin, J., et al. (2015). Entorhinal cortical ocean cells encode specific contexts and drive context-specific fear memory. Neuron 87, 1317-1331.

Knierim, J.J., Neunuebel, J.P., and Deshmukh, S.S. (2013). Functional correlates of the lateral and medial entorhinal cortex: objects, path integration and local-global reference frames. Philos. Trans. R. Soc. Lond. B. Biol. Sci. 369, 20130369.

Knudsen, E.I. (2002). Instructed learning in the auditory localization pathway of the barn owl. Nature 417, 322-328.

Kondoh, K., Lu, Z., Ye, X., et al. (2016). A specific area of olfactory cortex involved in stress hormone responses to predator odors. Nature 532, 103-106.

Koya, E., Golden, S.A., Harvey, B.K., et al. (2009). Targeted disruption of cocaine-activated nucleus accumbens neurons prevents context-specific sensitization. Nat. Neurosci. 12, 1069-1073.

Krug, M., Lossner, B., and Ott, T. (1984). Anisomycin blocks the late phase of long-term potentiation in the dentate gyrus of freely moving rats. Brain Res. Bull. 13, 39-42.

Kubik, S., Miyashita, T., and Guzowski, J.F. (2007). Using immediate-early genes to map hippocampal subregional functions. Learn. Mem. 14, 758-770.

Lai, C.S.W., Franke, T.F., and Gan, W.-B. (2012). Opposite effects of fear conditioning and extinction on dendritic spine remodeling. Nature 483, 87-91.

Lashley, K.S. (1929). Brain mechanisms and intelligence. Chicago: University of Chicago Press.

Lashley, K.S. (1950). In search of the engram. Symp. Soc. Exp. Biol. 4, 454-482.

Lavond, D.G., and Steinmetz, J.E. (1989). Acquisition of classical conditioning without cerebellar cortex. Behav. Brain Res. 33, 113-164.

Lecoq, J., Savall, J., Vucinic, D., et al. (2014). Visualizing mammalian brain area interactions by dual-axis two-photon calcium imaging. Nat. Neurosci. 17, 1825-1829.

Lee, W.C.A., Huang, H., Feng, G.P., et al. (2006). Dynamic remodeling of dendritic arbors in GABAergic interneurons of adult visual cortex. PLoS Biol. 4, e29.

Lee, J.L. (2010). Memory reconsolidation mediates the updating of hippocampal memory content. Front. Behav. Neurosci. 4, 168.

Lein, E.S., Zhao, X., and Gage, F.H. (2004). Defining a molecular atlas of the hippocampus using DNA microarrays and high-throughput in situ hybridization. J. Neurosci. 24, 3879-3889.

Leutgeb, S., Leutgeb, J.K., Treves, A., Moser, M.-B., and Moser, E.I. (2004). Distinct ensemble codes in hippocampal areas CA3 and CA1. Science 305, 1295-1298.

Lewis, D.J. (1979). Psychobiology of active and inactive memory. Psychol. Bull. 86, 1054-1083.

Liao, D., Hessler, N.A., and Malinow, R. (1995). Activation of postsynaptically silent synapses during pairing-induced LTP in CA1 region of hippocampal slice. Nature 375, 400-404.

Lin, J.Y., Lin, M.Z., Steinbach, P., and Tsien, R.Y. (2009). Characterization of engineered channelrhodopsin variants with improved properties and kinetics. Biophys. J. 96, 1803-1814.

Lisman, J., Yasuda, R., and Raghavachari, S. (2012). Mechanisms of CaMKII action in long-term potentiation. Nat. Rev. Neurosci. 13, 169-182.

Liu, X., and Davis, R.L. (2009). The GABAergic anterior paired lateral neuron suppresses and is suppressed by olfactory learning. Nat. Neurosci. 12, 53-59.

Liu, X., Ramirez, S., Pang, P.T., et al. (2012). Optogenetic stimulation of a hippocampal engram activates fear memory recall. Nature 484, 381-385.

Liu, X., Ramirez, S., Redondo, R.L., and Tonegawa, S. (2014). Identification and manipulation of memory engram cells. Cold Spring Harb. Symp. Quant. Biol. 79, 59-65.

Lopez, J., Gamache, K., Schneider, R., and Nader, K. (2015). Memory retrieval requires ongoing protein synthesis and NMDA receptor activity-mediated AMPA receptor trafficking. J. Neurosci. 35, 2465-2475.

Lorenz, K. (1981). The foundations of ethology. New York: Springer.

Louie, K., and Wilson, M. (2001). Temporally structured replay of awake hippocampal ensemble activity during rapid eye movement sleep. Neuron 29, 145-156.

Malenka, R.C., and Bear, M.F. (2004). LTP and LTD: an embarrassment of riches. Neuron 44, 5-21.

Maletic-Savatic, M., Malinow, R., and Svoboda, K. (1999). Rapid dendritic morphogenesis in CA1 hippocampal dendrites induced by synaptic plasticity. Science 283, 1923-1927.

Marr, D. (1970). A theory for cerebral neocortex. Proc. R. Soc. Lond. B Biol. Sci. 176, 161-234.

Martin, S.J., and Morris, R.G. (2002). New life in an old idea: the synaptic plasticity and memory hypothesis revisited. Hippocampus 12, 609-636.

Matsuo, N., Reijmers, L., and Mayford, M. (2008). Spine-type-specific recruitment of newly synthesized AMPA receptors with learning. Science 319, 1104-1107.

Matsuo, N. (2015). Irreplaceability of neuronal ensembles after memory allocation. Cell Rep. 11, 351-357.

Matzel, L.D., and Miller, R.R. (2009). Parsing storage from retrieval in experimentally induced amnesia. Learn. Mem. 16, 670-671.

Mauk, M.D., Steinmetz, J.E., and Thompson, R.F. (1986). Classical conditioning using stimulation of the inferior olive as the unconditioned stimulus. Proc. Natl. Acad. Sci. USA 83, 5349-5353.

McCormick, D.A., Clark, G.A., Lavond, D.G., and Thompson, R.F. (1982). Initial localization of the memory trace for a basic form of learning. Proc. Natl. Acad. Sci. USA 79, 2731-2735.

McCormick, D.A., and Thompson, R.F. (1984). Cerebellum: essential involvement in the classically conditioned eyelid response. Science 223, 296-299.

McCormick, D.A., Steinmetz, J.E., and Thompson, R.F. (1985). Lesions of the inferior olivary complex cause extinction of the classically conditioned eyeblink response. Brain Res. 359, 120-130.

McDougall, W. (1911). Body and mind: a history and a defense of animism. London: Methuen and Company Ltd.

McGaugh, J.L. (1966). Time-dependent processes in memory storage. Science 153, 1351-1358.

McGaugh, J.L. (2000). Memory - a century of consolidation. Science 287, 248-251.

McKernan, M.G., and Shinnick-Gallagher, P. (1997). Fear conditioning induces a lasting potentiation of synaptic currents in vitro. Nature 390, 607-611.

Menzel, R. (2001). Searching for the memory trace in a mini-brain, the honeybee. Learn. Mem. 8, 53-62.

Miller, R.R., and Springer, A.D. (1972). Induced recovery of memory in rats following electroconvulsive shock. Physiol. Behav. 8, 645-651.

Miller, R.R., and Springer, A.D. (1973). Amnesia, consolidation, and retrieval. Psychol. Rev. 80, 69-79.

Miller, R.R., and Springer, A.D. (1974). Implications of recovery from experimental amnesia. Psychol. Rev. 81, 470-473.

Miller, R.R., and Matzel, L.D. (2006). Retrieval failure versus memory loss in experimental amnesia: definitions and processes. Learn. Mem. 13, 491-497.

Miller, R.R., and Sweatt, J.D. (2006). Amnesia or retrieval deficit? Implications of a molecular approach to the question of reconsolidation. Learn. Mem. 13, 498-505.

Milner, B., Squire, L.R., and Kandel, E.R. (1998). Cognitive neuroscience and the study of memory. Neuron 20, 445-468.

Misanin, J.R., Miller, R.R., and Lewis, D.J. (1968). Retrograde amnesia produced by electroconvulsive shock after reactivation of a consolidated memory trace. Science 160, 554-555.

Miyashita, Y. (1988). Neuronal correlate of visual associative long-term memory in the primate temporal cortex. Nature 335, 817-820.

Moore, S.J., Cooper, D.C., and Spruston, N. (2009). Plasticity of burst firing induced by synergistic activation of metabotropic glutamate and acetylcholine receptors. Neuron 61, 287-300.

Morris, R.G., Anderson, E., Lynch, G.S., and Baudry, M. (1986). Selective impairment of learning and blockade of long-term potentiation by an N-methyl-D-aspartate receptor antagonist, AP5. Nature 319, 774-776.

Morris, R.G., Schenk, F., Tweedie, F., and Jarrard, L.E. (1990). Ibotenate lesions of hippocampus and/or subiculum: dissociating components of allocentric spatial learning. Eur. J. Neurosci. 2, 1016-1028.

Morris, R.G. (2006). Elements of a neurobiological theory of hippocampal function: the role of synaptic plasticity, synaptic tagging and schemas. Eur. J. Neurosci. 23, 2829-2846.

Moser, M.-B., Trommald, M., and Andersen, P. (1994). An increase in dendritic spine density on hippocampal CA1 pyramidal cells following spatial learning in adult rats suggest the formation of new synapses. Proc. Natl. Acad. Sci. USA 91, 12673-12675.

Moser, E.I., Roudi, Y., Witter, M.P., et al. (2014). Grid cells and cortical representation. Nat. Rev. Neurosci. 15, 466-481.

Mucke, L., Masliah, E., Yu, G.Q., et al. (2000). High-level neuronal expression of abeta 1-42 in wild-type human amyloid protein precursor transgenic mice: synaptotoxicity without plaque formation. J. Neurosci. 20, 4050-4058.

Müller, G.E., and Pilzecker, A. (1900). Experimentelle Beiträge zur Lehre vom Gedächtnis. Germany: Leipzig.

Nabavi, S., Fox, R., Proulx, C.D., et al. (2014). Engineering a memory with LTD and LTP. Nature 511, 348-352.

Nader, K., Schafe, G.E., and LeDoux, J.E. (2000a). Fear memories require protein synthesis in the amygdala for reconsolidation after retrieval. Nature 406, 722-726.

Nader, K., Schafe, G.E., and LeDoux, J.E. (2000b). The labile nature of consolidation theory. Nat. Rev. Neurosci. 1, 216-219.

Nader, K., and Wang, S.H. (2006). Fading in. Learn. Mem. 13, 530-535.

Nakashiba, T., Buhl, D., McHugh, T.J., and Tonegawa, S. (2009). Hippocampal CA3 output is crucial for ripple-associated reactivation and consolidation of memory. Neuron 62, 781-787.

Nakazawa, K., Sun, L.D., Quirk, M.C., et al. (2003). Hippocampal CA3 NMDA receptors are crucial for memory acquisition of one-time experience. Neuron 38, 305-315.

Nakazawa, K., McHugh, T.J., Wilson, M.A., and Tonegawa, S. (2004). NMDA receptors, place cells and hippocampal spatial memory. Nat. Rev. Neurosci. 5, 361-372.

Nakazawa, Y., Pevzner, A., Tanaka, K.Z., and Wiltgen, B.J. (2016). Memory retrieval along the proximodistal axis of CA1. Hippocampus 26, 1140-1148.

Nomoto, M., Ohkawa, N., Nishizono, H., et al. (2016). Cellular tagging as a neural network mechanism for behavioural tagging. Nat. Commun. 7, 12319.

Nonaka, A., Toyoda, T., Miura, Y., et al. (2014). Synaptic plasticity associated with a memory engram in the basolateral amygdala. J. Neurosci. 34, 9305-9309.

O'Keefe, J., and Dostrovsky, J. (1971). The hippocampus as a spatial map. Preliminary evidence from unit activity in the freely moving rat. Brain Res. 34, 171-175.

O'Mara, S. (2006). Controlling hippocampal output: the central role of subiculum in hippocampal information processing. Beh. Brain Res. 174, 304-312.

Oddo, S., Caccamo, A., Shepherd, J.D., et al. (2003). Triple-transgenic model of Alzheimer's disease with plaques and tangles : intracellular Abeta and synaptic dysfunction. Neuron 39, 409-421.

Ohkawa, N., Saitoh, Y., Suzuki, A., et al. (2015). Artificial association of pre-stored information to generate a qualitatively new memory. Cell Rep. 11, 261-269.

Okuno, H., Akashi, K., Ishii, Y., et al. (2012). Inverse synaptic tagging of inactive synapses via dynamic interaction of Arc/Arg3.1 with CaMKIIβ. Cell 149, 886-898.

Okuyama, T., Kitamura, T., Roy, D.S., Itohara, S., and Tonegawa, S. (2016). Ventral CA1 neurons store social memory. Science 353, 1536-1541.

Olds, J., Disterhoft, J.F., Segal, M., Kornblith, C.L., and Hirsh, R. (1972). Learning centers of rat brain mapped by measuring latencies of conditioned unit responses. J. Neurophysiol. 35, 202-219.

Park, S., Kramer, E.E., Mercaldo, V., et al. (2016). Neuronal allocation to a hippocampal engram. Neuropsychopharmacology, doi: 10.1038/npp.2016.73.

Pattwell, S.S., Bath, K.G., Casey, B.J., Ninan, I., and Lee, F.S. (2011). Selective early-acquired fear memories undergo temporary suppression during adolescence. Proc. Natl. Acad. Sci. USA 108, 1182-1187.

Penfield, W., and Rasmussen, T. (1950). The cerebral cortex of man: a clinical study of localization of function. New York: Macmillan.

Pinsker, H.M., Hening, W.A., Carew, T.J., and Kandel, E.R. (1973). Long-term sensitization of a defensive withdrawal reflex in Aplysia. Science 182, 1039-1042.

Quartermain, D., McEwen, B.S., and Azmitia, E.C., Jr. (1970). Amnesia produced by electroconvulsive shock or cycloheximide: conditions for recovery. Science 169, 683-686.

Quiroga, R.Q., Reddy, L., Kreiman, G., Koch, C., and Fried, I. (2005). Invariant visual representation by single neurons in the human brain. Nature 435, 1102-1107.

Ramirez, S., Liu, X., Lin, P.-A., et al. (2013). Creating a false memory in the hippocampus. Science 341, 387-391.

Ramirez, S., Liu, X., MacDonald, C.J., et al. (2015). Activating positive memory engrams suppresses depression-like behavior. Nature 522, 335-339.

Ramon y Cajal, S. (1893). Neue Darstellung vom histologischen Bau des Centralnervensystems. Arch. Anat. Physiol. 17, 9-428.

Ramon y Cajal, S. (1894). The Croonian Lecture: la fine structure des centres nerveux. Proc. R. Soc. Lond. 5, 444-468.

Ranck, J.B. (1973). Studies on single neurons in dorsal hippocampal formation and septum in unrestrained rats. I. Behavioral correlates and firing repertoires. Exp. Neurol. 41, 461-531.

Rashid, A.J., Yan, C., Mercaldo, V., et al. (2016). Competition between engrams influences fear memory formation and recall. Science 353, 383-387.

Raybuck, J.D., and Lattal, K.M. (2014). Differential effects of dorsal hippocampal inactivation on expression of recent and remote drug and fear memory. Neurosci. Lett. 569, 1-5.

Redondo, R.L., Kim, J., Arons, A., et al. (2014). Bidirectional switch of the valence associated with a hippocampal contextual memory engram. Nature 513, 426-430.

Reijmers, L.G., Perkins, B.L., Matsuo, N., and Mayford, M. (2007). Localization of a stable neural correlate of associative memory. Science 317, 1230-1233.

Restivo, L., Vetere, G., Bontempi, B., and Ammassari-Teule, M. (2009). The formation of recent and remote memory is associated with time-dependent formation of dendritic spines in the hippocampus and anterior cingulate cortex. J. Neurosci. 29, 8206-8214.

Riccio, D.C., Millin, P.M., and Bogart, A.R. (2006). Reconsolidation: a brief history, a retrieval view, and some recent issues. Learn. Mem. 13, 536-544.

Roberts, T.F., Tschida, K.A., Klein, M.E., and Mooney, R. (2010). Rapid spine stabilization and synaptic enhancement at the onset of behavioral learning. Nature 463, 948-952.

Rodriguez, J.J., Jones, V.C., Tabuchi, M., et al. (2008). Impaired adult neurogenesis in the dentate gyrus of a triple transgenic mouse model of Alzheimer's disease. PLoS One 3, e2935.

Roozendaal, B. (2002). Stress and memory: opposing effects of glucocorticoids on memory consolidation and memory retrieval. Neurobiol. Learn. Mem. 78, 578-595.

Rose, S.P. (2000). God's organism? The chick as a model system for memory studies. Learn. Mem. 7, 1-17.

Roy, D.S., Arons, A., Mitchell, T.I., et al. (2016). Memory retrieval by activating engram cells in mouse models of early Alzheimer's disease. Nature 531, 508-512.

Ryan, T.J., Roy, D.S., Pignatelli, M., Arons, A., and Tonegawa, S. (2015). Engram cells retain memory under retrograde amnesia. Science 348, 1007-1013.

Sacktor, T.C. (2011). How does PKMzeta maintain long-term memory? Nat. Rev. Neurosci. 12, 9-15.

Sara, S.J. (1973). Recovery from hypoxia and ECS-induced amnesia after a single exposure to training environment. Physiol. Behav. 10, 85-89.

Sara, S.J. (2000). Retrieval and reconsolidation: toward a neurobiology of remembering. Learn. Mem. 7, 73-84.

Sara, S.J., and Hars, B. (2006). In memory of consolidation. Learn. Mem. 13, 515-521.

Schacter, D.L., Eich, J.E., and Tulving, E. (1978). Richard Semon's theory of memory. J. Verbal Learn. Verbal Behav. 17, 721-743.

Schacter, D.L. (2001). Forgotten ideas, neglected pioneers: Richard Semon and the story of memory. New York: Routledge.

Scoville, W.B., and Milner, B. (1957). Loss of recent memory after bilateral hippocampal lesions. J. Neurol. Neurosurg. Psychiatry 20, 11-21.

Selkoe, D.J. (2001). Alzheimer's disease: genes, proteins, and therapy. Physiol. Rev. 81, 741-766.

Selkoe, D.J. (2002). Alzheimer's disease is a synaptic failure. Science 298, 789-791.

Semon, R. (1904). Die mneme. The mneme. Leipzig: Wilhelm Engelmann.

Semon, R. (1909). Die nmemischen empfindungen. Mnemic psychology. Leipzig: Wilhelm Engelmann.

Serota, R.G. (1971). Acetoxycycloheximide and transient amnesia in the rat. Proc. Natl. Acad. Sci. USA 68, 1249-1250.

Sharp, P.E., and Green, C. (1994). Spatial correlates of firing patterns of single cells in the subiculum of the freely moving rat. J. Neurosci. 14, 2339-2356.

Shinn-Cunningham, B. (2000). Adapting to remapped auditory localization cues: a decision-theory model. Percept. Psychophys. 62, 33-47.

Spear, N.E. (1973). Retrieval of memory in animals. Psychol. Rev. 80, 163-194.

Springer, A.D., and Miller, R.R. (1972). Retrieval failure induced by electroconvulsive shock: reversal with dissimilar training and recovery agents. Science 177, 628-630.

Squire, L.R., and Barondes, S.H. (1972). Variable decay of memory and its recovery in cycloheximide-treated mice. Proc. Natl. Acad. Sci. USA 69, 1416-1420.

Squire, L.R. (1982). The neuropsychology of human memory. Annu. Rev. Neurosci. 5, 241-273.

Squire, L.R. (1992). Memory and the hippocampus: a synthesis from findings with rats, monkeys, and humans. Psychol. Rev. 99, 195-231.

Squire, L.R. (2006). Lost forever or temporarily misplaced? The long debate about the nature of memory impairment. Learn. Mem. 13, 522-529.

Staff, N.P., Jung, H.Y., Thiagarajan, T., Yao, M., and Spruston, N. (2000). Resting and active properties of pyramidal neurons in subiculum and CA1 of rat hippocampus. J. Neurophysiol. 84, 2398-2408.

Steinmetz, J.E., Rosen, D.J., Chapman, P.F., Lavond, D.G., and Thompson, R.F. (1986). Classical conditioning of the rabbit eyelid response with a mossy-fiber stimulation CS: pontine nuclei and middle cerebellar peduncle stimulation. Behav. Neurosci. 100, 878-887.

Steinmetz, J.E., Logan, C.G., Rosen, D.J., et al. (1987). Initial localization of the acoustic conditioned stimulus projection system to the cerebellum essential for classical eyelid conditioning. Proc. Natl. Acad. Sci. USA 84, 3531-3535.

Steinmetz, J.E., Lavond, D.G., and Thompson, R.F. (1989). Classical conditioning in rabbits using pontine nucleus stimulation as a conditioned stimulus and inferior olive stimulation as an unconditioned stimulus. Synapse 3, 225-233.

Sun, C., Kitamura, T., Yamamoto, J., et al. (2015). Distinct speed dependence of entorhinal island and ocean cells, including respective grid cells. Proc. Natl. Acad. Sci. U. S. A. 112, 9466-9471.

Suzuki, A., Josselyn, S.A., Frankland, P.W., et al. (2004). Memory reconsolidation and extinction have distinct temporal and biochemical signatures. J. Neurosci. 24, 4787-4795.

Takeuchi, T., Duszkiewicz, A.J., and Morris, R.G. (2013). The synaptic plasticity and memory hypothesis : encoding, storage and persistence. Philos. Trans. R. Soc. Lond. B. Biol. Sci. 369, 20130288.

Tamamaki, N., and Nojyo, Y. (1993). Projection of the entorhinal layer II neurons in the rat as revealed by intracellular pressure-injection of neurobiotin. Hippocampus 3, 471-480.

Tanaka, K.Z., Pevzner, A., Hamidi, A.B., et al. (2014). Cortical representations are reinstated by the hippocampus during memory retrieval. Neuron 84, 347-354.

Taube, J.S. (1993). Electrophysiological properties of neurons in the rat subiculum in vitro. Exp. Brain Res. 96, 304-318.

Tayler, K.K., Tanaka, K.Z., Reijmers, L.G., and Wiltgen, B.J. (2013). Reactivation of neural ensembles during the retrieval of recent and remote memory. Curr. Biol. 23, 99-106.

Terry, R.D., Masliah, E., Salmon, D.P., et al. (1991). Physical basis of cognitive alterations in Alzheimer's disease: synapse loss is the major correlate of cognitive impairment. Ann. Neurol. 30, 572-580.

Teule, M., and Segal, M. (2016). Spine dynamics in synaptic plasticity and memory formation. Learn. Mem. 2E, 04024.

Thompson, R.F. (1976). The search for the engram. Am. Psychol. 31, 209-227.

Thompson, R.F., and Kim, J.J. (1996). Memory systems in the brain and localization of a memory. Proc. Natl. Acad. Sci. USA 93, 13438-13444.

Tonegawa, S., Pignatelli, M., Roy, D.S., and Ryan, T.J. (2015a). Memory engram storage and retrieval. Curr. Opin. Neurobiol. 35, 101-109.

Tonegawa, S., Liu, X., Ramirez, S., and Redondo, R. (2015b). Memory engram cells have come of age. Neuron 87, 918-931.

Treves, A., and Rolls, E.T. (1992). Computational constraints suggest the need for two distinct input systems to the hippocampal CA3 network. Hippocampus 2, 189-199.

Trouche, S., Perestenko, P.V., van de Ven, G.M., et al. (2016). Recoding a cocaine-place memory engram to a neutral engram in the hippocampus. Nat. Neurosci. 19, 564-567.

Tsien, J.Z., Huerta, P.T., and Tonegawa, S. (1996). The essential role of hippocampal CA1 NMDA receptor-dependent synaptic plasticity in spatial memory. Cell 87, 1327-1338.

Tsien, R.Y. (2013). Very long-term memories may be stored in the pattern of holes in the perineuronal net. Proc. Natl. Acad. Sci. USA 110, 12456-12461.

Tully, T., and Quinn, W.G. (1985). Classical conditioning and retention in normal and mutant Drosophila melanogaster. J. Comp. Physiol. A 157, 263-277.

Tulving, E. (2002). Episodic memory: from mind to brain. Annu. Rev. Psychol. 53, 1-25.

Urlinger, S., Baron, U., Thellmann, M., et al. (2000). Exploring the sequence space for tetracycline-dependent transcriptional activators : novel mutations yield expanded range and sensitivity. Proc. Natl. Acad. Sci. U.S.A. 97, 7963-7968.

Weinberger, N.M. (2004). Specific long-term memory traces in primary auditory cortex. Nat. Rev. Neurosci. 5, 279-290.

Weintraub, S., Wicklund, A.H., and Salmon, D.P. (2012). The neuropsychological profile of Alzheimer disease. Cold Spring Harb. Perspect. Med. 2, a6171.

Wheeler, A.L., Teixeira, C.M., Wang, A.H., et al. (2013). Identification of a functional connectome for long-term fear memory in mice. PLoS Comput. Biol. 9, e1002853.

Wickersham, I.R., Lyon, D.C., Barnard, R.J., et al. (2007). Monosynaptic restriction of transsynaptic tracing from single, genetically targeted neurons. Neuron 53, 639-647.

Wilson, M.A., and McNaughton, B.L. (1993). Dynamics of the hippocampal ensemble code for space. Science 261, 1055-1058.

Witter, M.P., Ostendorf, R.H., and Groenewegen, H.J. (1990). Heterogeneity in the dorsal subiculum of the rat. Distinct neuronal zones project to different cortical and subcortical targets. Eur. J. Neurosci. 2, 718-725.

Xie, H., Liu, Y., Zhu, Y., et al. (2014). In vivo imaging of immediate early gene expression reveals layer-specific memory traces in the mammalian brain. Proc. Natl. Acad. Sci. USA 111, 2788-2793.

Xu, T., Yu, X., Perlik, A.J., et al. (2009). Rapid formation and selective stabilization of synapses for enduring motor memories. Nature 462, 915-919.

Yamahachi, H., Marik, S.A., McManus, J.N., Denk, W., and Gilbert, C.D. (2009). Rapid axonal sprouting and pruning accompany functional reorganization in primary visual cortex. Neuron 64, 719-729.

Yang, G., Pan, F., and Gan, W.-B. (2009). Stably maintained dendritic spines as associated with lifelong memories. Nature 462, 920-924.

Ye, L., Allen, W.E., Thompson, K.R., et al. (2016). Wiring and molecular features of prefrontal ensembles representing distinct experiences. Cell 165, 1-13.

Yiu, A.P., Mercaldo, V., Yan, C., et al. (2014). Neurons are recruited to a memory trace based on relative neuronal excitability immediately before training. Neuron 83, 722-735.

Yu, D., Akalal, D.B.G., and Davis, R.L. (2006). Drosophila α/β mushroom body neurons form a branch-specific, long-term cellular memory trace after spaced olfactory conditioning. Neuron 52, 845-855.

Zelikowsky, M., Hersman, S., Chawla, M.K., Barnes, C.A., and Fanselow, M.S. (2014). Neuronal ensembles in amygdala, hippocampus, and prefrontal cortex track differential components of contextual fear. J. Neurosci. 34, 8462-8466.

Zhan, C., Zhou, J., Feng, Q., et al. (2013). Acute and long-term suppression of feeding behavior by POMC neurons in the brainstem and hypothalamus, respectively. J. Neurosci. 33, 3624-3632.

Zhou, Y., Won, J., Karlsson, M.G., et al. (2009). CREB regulates excitability and the allocation of memory to subsets of neurons in the amygdala. Nat. Neurosci. 12, 1438-1443.

Ziv, Y., Burns, L.D., Cocker, E.D., et al. (2013). Long-term dynamics of CA1 hippocampal place codes. Nat. Neurosci. 16, 264-266.

7. Acknowledgements

I would like to start by thanking my thesis advisor, Susumu, for accepting me into his prestigious research laboratory at MIT, for teaching me the true meaning of being a scientist, for encouraging me to think of creative solutions to unravel how memories are formed and recalled, and for being my friend. I can never thank you enough for these past 5 years, but I know that working together has made me a better scientist.

All the discussions I had with my thesis committee members, Prof. Mark Bear and Prof. Matthew Wilson, have been an invaluable learning experience for me. In addition, I would like to acknowledge Tomas Ryan and Xu Liu, my official and unofficial lab mentors for helping me start working in the lab.

I owe everything I have achieved in my life to my unconditionally loving parents, who never gave up on me when I was down, and are always right next to me to help me get right back up. Mom and Dad, it is an honor to be your son.

My brother, Deepak, who I can only describe as the 'best older sibling' anyone could ever ask for, always motivates me, gives me much needed advice, and reminds me to be a good human being no matter what we achieve in our professional careers. Without this support, I could have never made it through my PhD program.

I owe a lot to my better half, my wife Shruti, for being patient when my work hours extended well beyond dinnertime, for allowing me to come home and continue working as if I never left the laboratory, and for making me a better person in every way possible. Thank you.

Finally, and very importantly, a major part of my PhD training came from working with super talented undergraduate students, graduate students, post-doctoral fellows, research scientists, technical staff, and administrative staff. Without their constant support, I cannot imagine how much more difficult my PhD years would have been. I am very, very grateful!

and Ti_2Ni incoherently precipitate in the B2 matrix upon cooling from 700°C to 87°C. The B2 matrix transforms completely to B19 upon further cooling to 22°C, aided by the simultaneous Ti_2Cu/B19 epitaxies (Figs. 3 and 4, Table 1, and table S3). The B19/Ti_2Cu epitaxy provides an internal stress pattern, which stabilizes the B19 phase at low temperatures. During stress cycling, the equivalent epitaxy alternatingly stabilizes the B2 phase. At each temperature and stress, the transforming phases attain equilibrium by forming a compatible morphology directed by the internal epitaxy-generated stress distribution. Complete transformation is attained at each cycle because the epitaxial stresses are reversible. Hence, we propose that the epitaxially promoted completion of the B2↔B19 phase transformation creates the low-fatigue state of the $Ti_{54}Ni_{34}Cu_{12}$ films. The Ti_2Cu precipitates act like sentinels, assuring that the B2↔B19 transformation proceeds toward completion at each cycle. The transformation will return the film to a stress state and morphology that are compatible with the pristine state. The decrease of the anisotropic peak broadening of the epitaxy-effected XRD peaks indicates trainability.

This proposal must be revisited in light of the favorable values of the quantitative compatibility criteria calculated from the lattice parameters of both alloys $Ti_{51}Ni_{36}Cu_{13}$ and $Ti_{54}Ni_{34}Cu_{12}$ (Table 2). These values approach the ideal triplet (λ = 1, CCI = CCII = 0) and suggest good reversibility even in polycrystals (*29*), although they are inferior to those for $Zn_{45}Au_{30}Cu_{25}$ (*19*). The values for sample 2 are closer to the ideal than those for sample 1, which is in accord with the vastly better fatigue characteristics of sample 2. The question then arises whether this large difference of the fatigue life results from the observed epitaxy or that of the two triplets listed in Table 2. We observe that despite their reversibility, the phase transformations in SMAs are of first order (nucleation- and growth-controlled). We suggest that the epitaxy leads to reversible nucleation, whereas the low cofactors promote reversible near-equilibrium growth so that the combination of both mechanisms yields the observed ultralow fatigue. In the limit of CCI and CCII→0, no energy will be stored in the product phase in the form of twin boundaries. This creates a strongly reproducible, and therefore repeatably transformable, equilibrium state.

Given the fatigue-controlling importance of the dual epitaxy of Ti_2Cu in TiNiCu-based (SMA) films, it is natural to search for other alloying elements that have the potential to play a similar role. Following this lead, we can assume that structurally related Ti_2Ag precipitates will act very similar to Ti_2Cu. Because TiNiAg SMAs display transformation characteristics comparable with that of TiNiCu (*30*), they could be promising candidates for biocompatible ultralow fatigue SMA films. Elastocaloric cooling requires bulk materials, which is a difficult but, in principle, solvable challenge. More generally, we expect similar behavior in phase-transforming materials that contain dual-epitaxial precipitates.

REFERENCES AND NOTES

1. K. Otsuka, X. Ren, *Prog. Mater. Sci.* **50**, 511–678 (2005).
2. J. Mohd Jani, M. Leary, A. Subic, M. A. Gibson, *Mater. Des.* **56**, 1078–1113 (2014).
3. T. Duerig, A. Pelton, D. Stöckel, *Mater. Sci. Eng. A* **273–275**, 149–160 (1999).
4. D. W. Raboud, M. G. Faulkner, A. W. Lipsett, *Smart Mater. Struct.* **9**, 684–692 (2000).
5. E. Bonnot, R. Romero, L. Mañosa, E. Vives, A. Planes, *Phys. Rev. Lett.* **100**, 125901 (2008).
6. K. Otsuka, C. M. Wayman, Eds., *Shape Memory Materials* (Cambridge Univ. Press, Cambridge, 1999).
7. J. Cui *et al.*, *Nat. Mater.* **5**, 286–290 (2006).
8. K. Bhattacharya, S. Conti, G. Zanzotto, J. Zimmer, *Nature* **428**, 55–59 (2004).
9. X. Moya, S. Kar-Narayan, N. D. Mathur, *Nat. Mater.* **13**, 439–450 (2014).
10. W. J. Buehler, J. V. Gilfrich, R. C. Wiley, *J. Appl. Phys.* **34**, 1475–1477 (1963).
11. S. A. Shabalovskaya, *Biomed. Mater. Eng.* **12**, 69–109 (2002).
12. N. B. Morgan, *Mater. Sci. Eng. A* **378**, 16–23 (2004).
13. A. R. Pelton, *J. Mater. Eng. Perform.* **20**, 613–617 (2011).
14. G. Eggeler, E. Hornbogen, A. Yawny, A. Heckmann, M. Wagner, *Mater. Sci. Eng. A* **378**, 24–33 (2004).
15. S. Miyazaki, K. Mizukoshi, T. Ueki, T. Sakuma, Y. Liu, *Mater. Sci. Eng. A* **273–275**, 658–663 (1999).
16. E. Hornbogen, *J. Mater. Sci.* **39**, 385–399 (2004).
17. K. Gall, H. J. Maier, *Acta Mater.* **50**, 4643–4657 (2002).
18. R. D. James, Z. Zhang, in *Magnetism and Structure in Functional Materials*, A. Planes, L. Manosa, A. Saxena, Eds. (Springer, New York, 2005), vol. 79.
19. Y. Song, X. Chen, V. Dabade, T. W. Shield, R. D. James, *Nature* **502**, 85–88 (2013).
20. S. Miyazaki, Y. Q. Fu, W. M. Huang, Eds., *Thin Film Shape Memory Alloys* (Cambridge Univ. Press, Cambridge, 2009).
21. K. Bhattacharya, R. D. James, *Science* **307**, 53–54 (2005).
22. C. Bechtold, C. Chluba, R. Lima de Miranda, E. Quandt, *Appl. Phys. Lett.* **101**, 091903 (2012).
23. R. Lima de Miranda, C. Zamponi, E. Quandt, *Adv. Eng. Mater.* **15**, 66–69 (2013).
24. G. Siekmeyer, A. Schüßler, R. de Miranda, E. Quandt, *J. Mater. Eng. Perform.* **23**, 2437–2445 (2014).
25. Materials and methods are available as supplementary materials on *Science* Online.
26. K. Bhattacharya, *Microstructure of Martensite: Why It Forms and How It Gives Rise to the Shape-Memory Effect* (Oxford Univ. Press, Oxford, 2003).
27. A. C. Larson, R. B. Von Dreele, "General Structure Analysis System (GSAS)," Los Alamos National Laboratory Report LAUR 86-748 (2004).
28. P. Stephens, *J. Appl. Cryst.* **32**, 281–289 (1999).
29. K. Bhattacharya, R. V. Kohn, *Acta Mater.* **44**, 529–542 (1996).
30. C. Zamponi, M. Wuttig, E. Quandt, *Scripta Mater.* **56**, 1075–1077 (2007).
31. H. Scott, *J. Appl. Cryst.* **16**, 159–163 (1983).

ACKNOWLEDGMENTS

The work at the University of Kiel was supported by the Deutsche Forschungsgemeinschaft (DFG) via the Priority Program 1599. L.K. and J.S. appreciate the assistance of V. Duppel (Max Planck Institute for solid state research) for recording the electron diffraction patterns, B. V. Lotsch for enabling electron microscopy, and C. Szillus for TEM sample preparation. The work at the University of Maryland was supported by grant DOE DESC0005448; use of the Advanced Photon Source - Argonne National Laboratory was supported by the U.S. Department of Energy (DOE) Office of Science, under contract DE-AC02-06CH11357. M.W. and W.G. thank P. Zavalij for his guidance with the Rietveld refinement and J. Steiner for the compatibility calculations. The synchrotron diffraction data are available from the corresponding author. Other data are available in the main text and the supplementary materials.

SUPPLEMENTARY MATERIALS

www.sciencemag.org/content/348/6238/1004/suppl/DC1
Materials and Methods
Figs. S1 to S9
Tables S1 to S4
Reference (*32*)

12 September 2014; accepted 14 April 2015
10.1126/science.1261164

MEMORY

Engram cells retain memory under retrograde amnesia

Tomás J. Ryan,[1,2]* Dheeraj S. Roy,[1]* Michele Pignatelli,[1]* Autumn Arons,[1,2] Susumu Tonegawa[1,2]†

Memory consolidation is the process by which a newly formed and unstable memory transforms into a stable long-term memory. It is unknown whether the process of memory consolidation occurs exclusively through the stabilization of memory engrams. By using learning-dependent cell labeling, we identified an increase of synaptic strength and dendritic spine density specifically in consolidated memory engram cells. Although these properties are lacking in engram cells under protein synthesis inhibitor–induced amnesia, direct optogenetic activation of these cells results in memory retrieval, and this correlates with retained engram cell–specific connectivity. We propose that a specific pattern of connectivity of engram cells may be crucial for memory information storage and that strengthened synapses in these cells critically contribute to the memory retrieval process.

Memory consolidation is the phenomenon by which a newly formed memory transitions from a fragile state to a stable, long-term state (*1–3*). The defining feature of consolidation is a finite time window that begins immediately after learning, during which a memory is susceptible to disruptions, such as protein synthesis inhibition (*4–6*), resulting in retrograde amnesia. The stabilization of synaptic potentiation is the dominant cellular model of memory consolidation (*7–10*) because protein synthesis inhibitors disrupt late-phase

long-term potentiation of in vitro slice preparations (*11*–*13*). Although much is known about the cellular mechanisms of memory consolidation, it remains unknown whether these processes occur in memory engram cells. It may be possible to characterize cellular consolidation and empirically separate mnemonic properties in retrograde amnesia by directly probing and manipulating memory engram cells in the brain. The term memory engram originally referred to the hypothetical learned information stored in the brain, which must be reactivated for recall (*14*, *15*). Recently, several groups demonstrated that specific hippocampal cells that are activated during memory encoding are both sufficient (*16*–*18*) and necessary (*19*, *20*) for driving future recall of a contextual fear memory and thus represent a component of a distributed memory engram (*21*). Here, we applied this engram technology to the issue of cellular consolidation and retrograde amnesia.

We used the previously established method for tagging the hippocampal dentate gyrus (DG) component of a contextual memory engram with mCherry (supplementary materials, materials and methods, and fig. S1) (*16*, *22*). To disrupt consolidation, we systemically injected the protein synthesis inhibitor anisomycin (ANI) or saline (SAL) as a control immediately after contextual fear conditioning (CFC) (Fig. 1A). The presynaptic neurons of the entorhinal cortex (EC) were constitutively labeled with ChR2 expressed from an AAV_8-CaMKIIα-ChR2-EYFP virus (Fig. 1B). Voltage clamp recordings of paired engram ($mCherry^+$) and nonengram ($mCherry^-$) DG cells were conducted simultaneously with optogenetic stimulation of $ChR2^+$ perforant path (PP) axons (Fig. 1, C and D). $mCherry^+$ cells of the SAL group showed significantly greater synaptic strength than did paired $mCherry^-$ cells, whereas in the ANI group, $mCherry^+$ and $mCherry^-$ cells were of comparable synaptic strength (Fig. 1E). Calculation of AMPA/*N*-methyl-D-aspartate (NMDA) receptor current ratios (*23*) showed that at 24 hours after training, $mCherry^+$ engram cells displayed potentiated synapses relative to paired $mCherry^-$ non-engram

[1]RIKEN-MIT Center for Neural Circuit Genetics at the Picower Institute for Learning and Memory, Department of Biology and Department of Brain and Cognitive Sciences, Massachusetts Institute of Technology, Cambridge, MA 02139, USA. [2]Howard Hughes Medical Institute, Massachusetts Institute of Technology, Cambridge, MA 02139, USA.
*These authors contributed equally to this work. †Corresponding author. E-mail: tonegawa@mit.edu

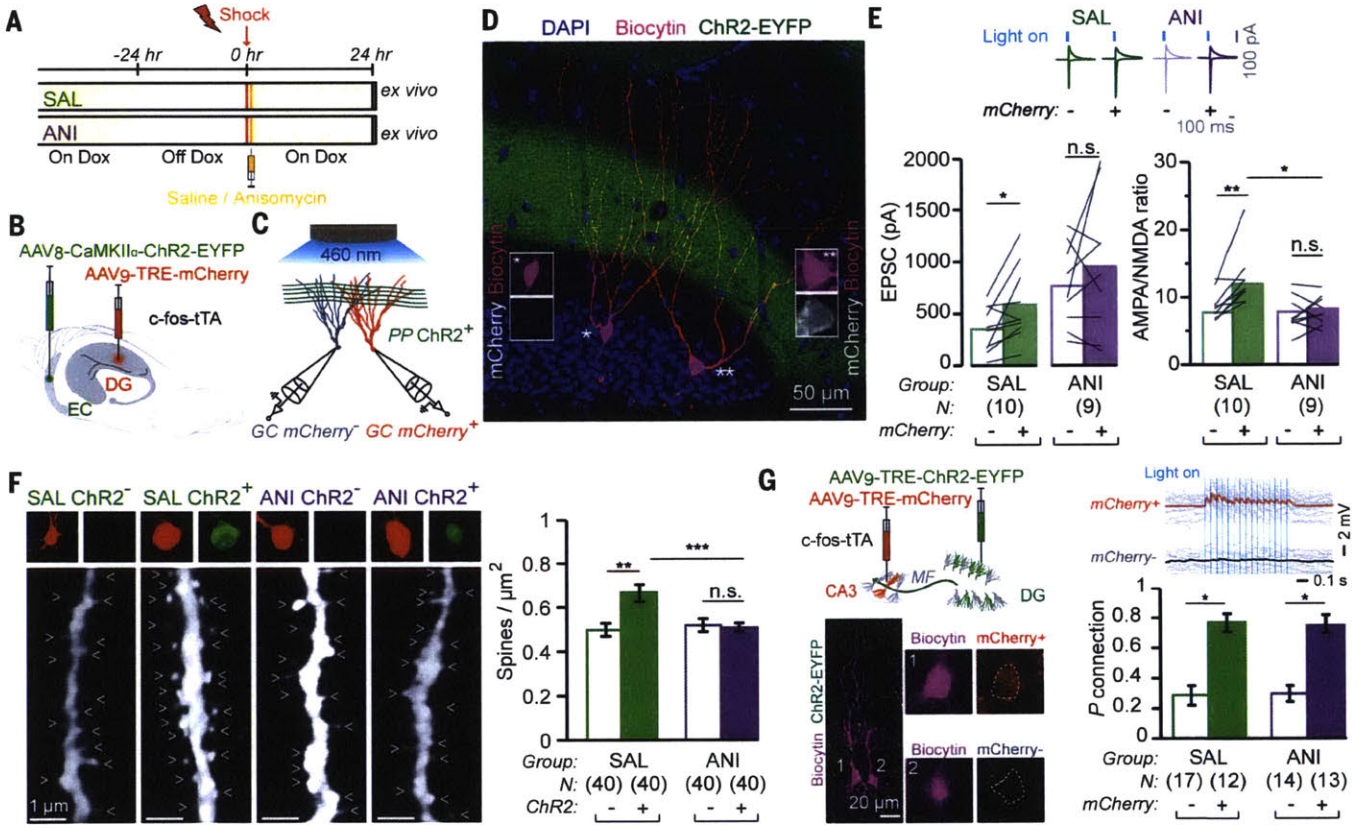

Fig. 1. Synaptic plasticity and connectivity of engram cells. (**A**) Mice taken off doxycycline (DOX) 24 hours before CFC and dispatched 24 hours after training. SAL or ANI was administered immediately after training. (**B**) AAV_8-CaMKIIα-ChR2-EYFP and AAV_9-TRE-mCherry viruses injected into the entorhinal cortex and dentate gyrus, respectively, of c-Fos-tTA mice. (**C**) Paired recordings of engram (red) and nonengram (gray) DG cells during optogenetic stimulation of $ChR2^+$ PP axons. (**D**) Representative image of a pair of recorded biocytin-labeled engram ($mCherry^+$) and nonengram ($mCherry^-$) DG cells. $ChR2^+$ PP axons are in green. (**E**) (Top) Example traces of AMPA and NMDA receptor–dependent postsynaptic currents in $mCherry^+$ and $mCherry^-$ cells, evoked by means of light activation of $ChR2^+$ PP axons. (Bottom) EPSC amplitudes and AMPA/NMDA current ratios of $mCherry^+$ and $mCherry^-$ cells of the two groups are displayed as means (columns) and individual paired data points (gray lines). Paired *t* test; $*P < 0.05$, $**P < 0.001$. SAL group compared with the ANI group, unpaired *t* test; $*P < 0.05$. (**F**) (Left) Representative confocal images of biocytin-filled dendritic fragments derived from SAL and ANI groups for $ChR2^+$ and $ChR2^-$ cells (arrow heads indicate dendritic spines). (Right) Average dendritic spine density showing an increase occurring exclusively in $ChR2^+$ fragments. Data are represented as mean ± SEM. Unpaired *t* tests $**P < 0.01$, $***P < 0.001$. (**G**) Engram connectivity. (Top left) AAV_9-TRE-ChR2-EYFP and AAV_9-TRE-mCherry viruses, injected into the DG and CA3, respectively, of c-Fos-tTA mice. (Bottom left) Example of $mCherry^+$ (1) and $mCherry^-$ (2) biocytin-filled CA3 pyramidal cells. $ChR2^+$ mossy fibers (MF) are in green. (Top right) $mCherry^+$ cell but not $mCherry^-$ cell displayed excitatory postsynaptic potentials in response to optogenetic stimulation of MF. (Bottom right) Probability of connection of DG $ChR2^+$ engram axons and CA3 $mCherry^+$ and $mCherry^-$ cells. Error bars are approximated by using binomial distribution. Fisher's exact test; $*P < 0.05$.

cells in the SAL group (Fig. 1E). However, no such difference between mCherry$^+$ and mCherry$^-$ was observed in the ANI group. In addition, mCherry$^+$ engram cells of the SAL group showed significantly greater AMPA/NMDA current ratios than those of mCherry$^+$ engram cells of the ANI group. Analysis of spontaneous excitatory postsynaptic currents (EPSCs) of engram and non-engram cells of both SAL and ANI groups showed the same pattern (fig. S2).

We also quantified dendritic spine density for DG engram cells labeled with an AAV_9-TRE-ChR2-EYFP virus. Spine density of ChR2$^+$ cells was significantly higher than corresponding ChR2$^-$ cells in the SAL group (Fig. 1F and fig. S3), but spine densities of ChR2$^+$ and ChR2$^-$ cells of the ANI group were similar (supplementary materials, materials and methods). Spine density of ChR2$^+$ cells of the SAL group was significantly higher than that of ANI ChR2$^+$ cells (Fig. 1F), but ChR2$^-$ cell spine density was comparable. This result was confirmed with analysis of the membrane capacitance (fig. S4G). ChR2 expression did not affect intrinsic properties of DG cells in vitro (fig. S5, A to E). Direct bath application of ANI did not affect intrinsic cellular properties in vitro (fig. S5F), although it mildly reduced synaptic currents acutely (fig. S5, G to I). When ANI was injected into c-Fos-tTA animals 24 hours after CFC and engram labeling, engram cell–specific increases in dendritc spine density and synaptic strength were undisturbed (fig. S6). We also examined engram cells labeled by means of a context-only experience (*17*) and found equivalent engram-cell increases in spine density and synaptic strength (fig. S7) as those labeled by means of CFC.

DG cells receive information from EC and relay it to CA3 via the mossy fiber pathway. We labeled DG engram cells using an AAV_9-TRE-ChR2-EYFP virus and simultaneously labeled CA3 engram cells using an AAV_9-TRE-mCherry virus (Fig. 1G). Connection probability was assessed 24 hours after CFC by stimulating DG ChR2$^+$ cell terminals optogenetically and recording excitatory postsynaptic potentials in CA3 mCherry$^+$ and mCherry$^-$ cells in ex vivo preparations. CA3 mCherry$^+$ engram cells showed a significantly higher probability of connection than did mCherry$^-$ cells with DG ChR2$^+$ engram cells, demonstrating preferential engram cell–to–engram cell connectivity. This form of engram pathway–specific connectivity was unaffected by posttraining administration of ANI (Fig. 1G).

We next tested the behavioral effect of optogenetically stimulating engram cells in amnesic mice (Fig. 2A). During CFC training in context B, both SAL and ANI groups responded to the unconditioned stimuli at equivalent levels (fig. S8). One day after training, the SAL group displayed robust freezing behavior to the conditioned stimulus of context B, whereas the ANI group showed substantially less freezing behavior (Fig. 2C). Two days after training, mice were placed into the distinct context A for a 12-min test session consisting of four 3-min epochs of blue light on or off. During this test session, neither group showed freezing behavior during light-off epochs, but both froze significantly during light-on epochs (Fig. 2D). Remarkably, no difference in the levels of light-induced freezing behavior was observed between groups. Three days after training, the mice were again tested in context B in order to assay the conditioned response, and retrograde amnesia for the conditioning context was still clearly evident (Fig. 2E). Subjects treated with SAL or ANI after the labeling of a neutral contextual engram (no shock) did not show freezing behavior in response to light stimulation of engram cells (Fig. 2D). We replicated the DG retrograde amnesia experiment using an alternative widely used protein synthesis inhibitor, cycloheximide (CHM)

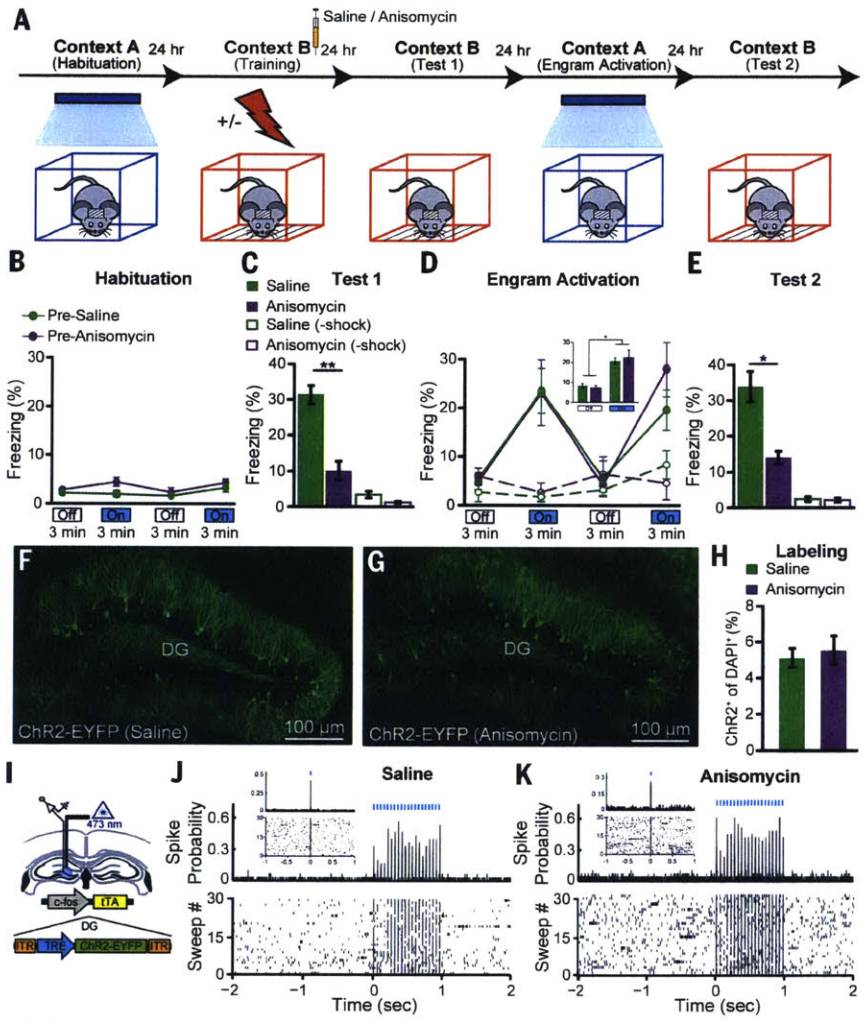

Fig. 2. Optogenetic stimulation of DG engram cells restores fear memory in retrograde amnesia. (**A**) Behavioral schedule. Beige shading signifies that subjects are on DOX, precluding ChR2 expression. Mice are taken off DOX 24 to 30 hours before CFC in context B. SAL or ANI was injected into the mice after training. (**B**) Habituation to context A with light-off and light-on epochs. Blue light stimulation of the DG did not cause freezing behavior in naïve, unlabeled mice of the pre-SAL (n = 10 mice) or pre-ANI (n = 8 mice) groups. (**C**) Memory recall in context B 1 day after training (test 1). ANI group displayed significantly less freezing than SAL group ($P < 0.005$). No-shock groups with SAL (n = 4 mice) or ANI (n = 4 mice) did not display freezing upon reexposure to context B. (**D**) Memory recall in context A 2 days after training (engram activation) with light-off and light-on epochs. Freezing for the two light-off and light-on epochs are further averaged in the inset. Significant freezing due to light stimulation was observed in both the SAL ($P < 0.01$) and ANI groups ($P < 0.05$). Freezing levels did not differ between groups. SAL and ANI-treated no-shock control groups did not freeze in response to light stimulation of context B engram cells. (**E**) Memory recall in context B 3 days after training (test 2). ANI group displayed significantly less freezing than SAL group ($P < 0.05$). (**F** and **G**) Images showing DG sections from c-Fos-tTA mice 24 hours after SAL or ANI treatment. (**H**) ChR2-EYFP cell counts from DG sections of SAL (n = 3 mice) and ANI (n = 4 mice) groups. (**I**) In vivo anesthetized recordings (supplementary materials, materials and methods). (**J** and **K**) Light pulses induced spikes in DG neurons recorded from head-fixed anesthetized c-Fos-tTA mice 24 hours after treatment with either SAL or ANI. Data are presented as mean ± SEM.

(fig. S9). We examined whether ANI administration immediately after CFC altered the activity-dependent synthesis of ChR2-EYFP in DG cells and found that this was not the case (Fig. 2, F to H). Nevertheless, the dosage of ANI used in this study did inhibit protein synthesis in the DG, as shown with Arc^+ cell counting (fig. S10). Thus, the dosage of ANI used was sufficient to induce amnesia but was insufficient to impair c-FostTA–driven synthesis of virally delivered ChR2-EYFP in DG cells. Extracellular recordings from SAL- and ANI-treated mice confirmed the cell counting results (Fig. 2, I to K). In line with fig. S6 and previous reports (*24*), ANI injection 24 hours after CFC did not cause retrograde amnesia (fig. S11). To provide a negative control for light-induced memory retrieval in amnesia, we disrupted memory encoding by activating hM4Di DREADDs receptors (*25*) downstream of the DG, in hippocampal CA1, during CFC, and found that subsequent DG engram activation did not elicit memory retrieval (fig. S12).

The recovery from amnesia through the direct light activation of ANI-treated DG engram cells was unexpected because these cells showed neither synaptic potentiation nor increased dendritic spine density. We conducted additional behavioral experiments in order to confirm and characterize the phenomenon. First, we investigated whether recovery from amnesia can be demonstrated by means of light-induced optogenetic place avoidance test (OptoPA); this would be a measure of an active fear memory recall (supplementary materials, materials and methods) (*18*), rather than a passive fear response monitored with freezing. SAL and ANI groups displayed equivalent levels of avoidance of the target zone in response to light activation of the DG engram (Fig. 3A). Second, in our previous study we showed that an application of the standard protocol (20 Hz) for activation of the CA1 engram was not effective for memory recall (*17*). However, we found that a 4-Hz protocol applied to the CA1 engram of the SAL and ANI groups elicited similar recovery from amnesia (Fig. 3B). Third, we used tone fear conditioning (TFC) and manipulated the fear engram in lateral amygdala (LA) (*26*) and found light-induced recovery of memory from amnesia. Fourth, we asked whether amnesia caused by disruption of reconsolidation of a contextual fear memory (*27*, *28*) can also be recovered through the light-activation of DG engram cells, which was found to be the case (Fig. 4A). We applied the memory inception method (supplementary materials, materials and methods) (*17*, *29*) to DG engram cells and found that both SAL and ANI groups showed freezing behavior that was specific to the original context A, demonstrating that light-activated context A engrams formed in the presence of ANI can function as a conditioned stimulus (CS) in a context-specific manner (Fig. 4B). Last, we tested the longevity of CFC amnesic engrams for memory recovery by means of light activation and found that memory recall could be observed 8 days after training (fig. S13).

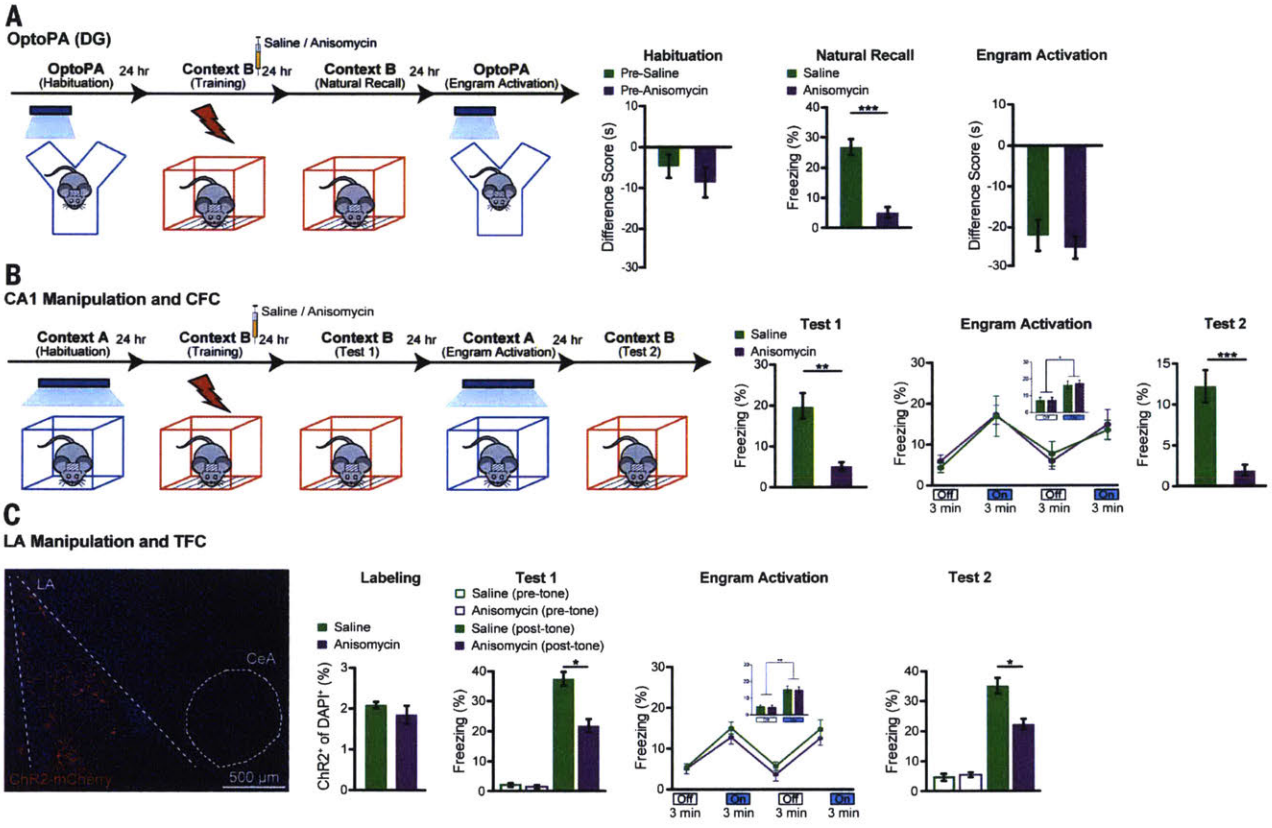

Fig. 3. Recovery of memory from amnesia under a variety of conditions. (**A**) DG engram activation and optogenetic place avoidance (OptoPA). During habituation, neither group displayed significant avoidance of target zone. For natural recall, the ANI group (n = 10 mice) displayed significantly less freezing than SAL group (n = 12 mice) in context B ($P < 0.005$). SAL and ANI groups displayed similar levels of OptoPA. (**B**) CA1 engram activation and CFC. 1 day after CFC (test 1), ANI group (n = 9 mice) displayed significantly less freezing than that of SAL group (n = 10 mice) in context B ($P < 0.01$). Two days after training (engram activation), light-activation of CA1 engrams elicited freezing in both SAL ($P < 0.01$) and ANI groups ($P < 0.001$). Three days after training (test 2), ANI group froze less than did SAL group in context B ($P < 0.01$). (**C**) LA engram activation and TFC. The behavioral schedule was identical to that in Fig. 3B, except that context tests were replaced with tone tests in context C (supplementary materials, materials and methods). (Left) Example image of ChR2-mCherry labeling of LA neurons. Of DAPI cells, 2% were labeled with ChR2. (Right) One day after training (test 1), ANI group (n = 9 mice) displayed significantly less freezing to tone than did SAL group (n = 9 mice) ($P < 0.05$). Two days after training (engram activation), significant light-induced freezing was observed for both SAL ($P < 0.005$) and ANI groups ($P < 0.005$). Three days after training (test 2), ANI group froze less to tone than did SAL group ($P < 0.05$).

Interactions between the hippocampus and amygdala are crucial for contextual fear memory encoding and retrieval (*18*). c-Fos expression increases in the hippocampus and amygdala upon exposure of an animal to conditioned stimuli (*30*, *31*). These previous observations open up the possibility of obtaining cellular-level evidence to support the behavioral-level finding that the recovery from amnesia can be accomplished with direct light activation of ANI-treated DG engram cells. Thus, we compared the effects of natural recall and light-induced recall on amygdala c-Fos$^+$ cell counts in amnesic mice (Fig. 5, A to C). c-Fos$^+$ cell counts (Fig. 5B) were significantly lower in basolateral amygdala (BLA) and central amygdala (CeA) of ANI-treated mice as compared with SAL mice when natural recall cues were delivered, showing that amygdala activity correlates with fear memory expression (Fig. 5C). In contrast, light-induced activation of the contextual engram cells resulted in equivalent amygdala c-Fos$^+$ counts in SAL and ANI groups (Fig. 5C), which supports the optogenetic behavioral data.

Next, we modified this protocol in order to include labeling of CA3 and BLA engram cells with mCherry and examined the effects of light-induced activation of DG engram cells on the overlap of mCherry$^+$ engram cells and c-Fos$^+$ recall-activated cells in CA3 and BLA (Fig. 5D). The purpose of this experiment was to investigate whether there is preferential connectivity between the upstream engram cells in DG and the downstream engram cells in CA3 or BLA. Natural recall cues resulted in above-chance c-Fos$^+$/mCherry$^+$ overlap in both CA3 and BLA, which supports the physiological connectivity data (Fig. 5, E to K). c-Fos$^+$/mCherry$^+$ overlap was significantly reduced in the ANI group as compared with the SAL group but was still higher than chance levels, presumably reflecting incomplete amnesic effects of ANI (Fig. 5K). Light-activation of DG engram cells resulted in equivalent c-Fos$^+$/mCherry$^+$ overlap as natural cue-induced recall, and this was unaffected by post-CFC ANI treatment. These data suggest that there is preferential and protein synthesis–independent functional connectivity between DG and CA3 engram cells, which supports the physiological data (Fig. 1G), and that this connectivity also applies between DG and BLA engram cells.

We previously showed that DG cells activated during CFC training and labeled with ChR2 via the promoter of an immediate early gene (IEG) can evoke a freezing response when they are reactivated optogenetically 1 to 2 days later (*16*), and this has since been achieved in the cortex (*21*). We have also shown that these DG cells, if light-activated while receiving an unconditioned stimulus (US), can serve as a surrogate context-specific CS to create a false CS-US association (*17*, *18*), and that activation of DG or amygdala engram cells can induce place preference (*18*). Furthermore, recent studies showed that optogenetic inhibition of these cells in DG, CA3, or CA1 impairs expression of a CFC memory (*19*, *20*). Together, these findings show that engram cells activated through CFC training are both sufficient and necessary to evoke memory recall, satisfying two crucial attributes in defining a component of a contextual fear memory engram (*15*). What has been left to be demonstrated, however, is that these DG cells undergo enduring physical changes as an experience is encoded and its memory is consolidated. Although synaptic potentiation has long been suspected as a fundamental mechanism for memory and as a crucial component of the enduring physical changes induced by experience, this has not been directly demonstrated,

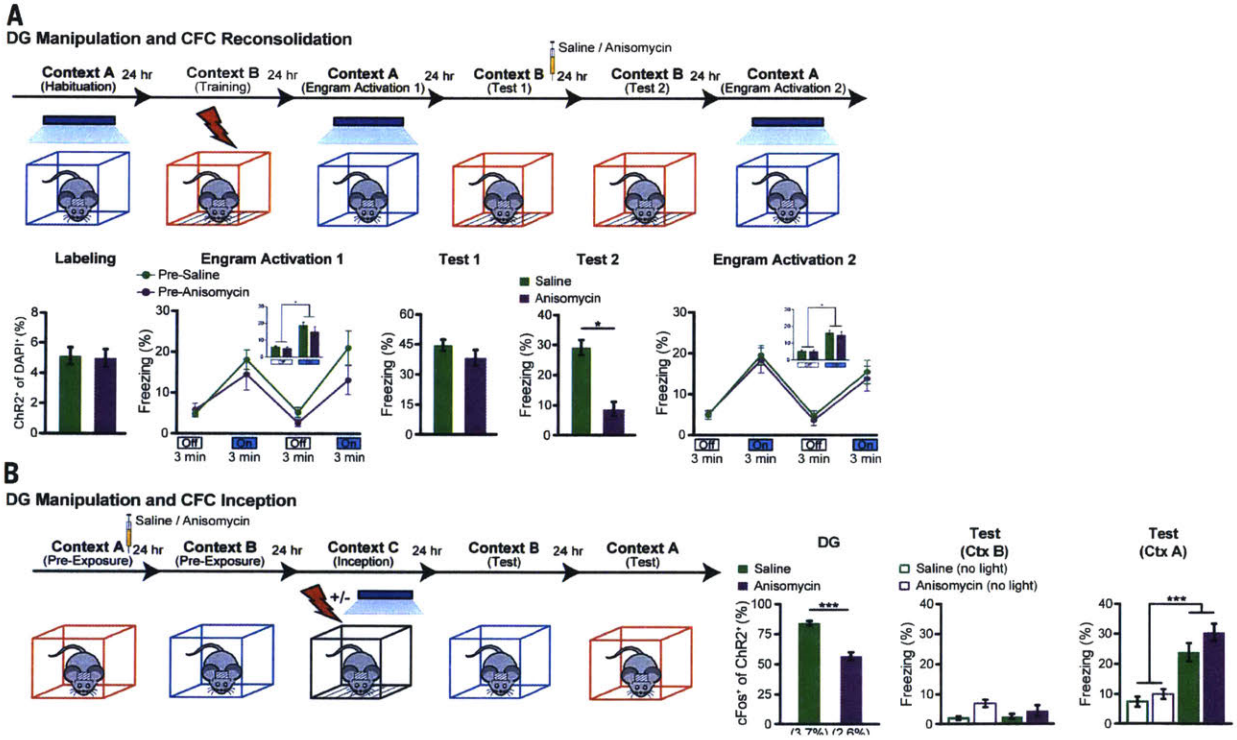

Fig. 4. Reconsolidation and memory updating. (**A**) DG engram activation and CFC reconsolidation. ANI (n = 11 mice) and SAL (n = 11 mice) groups showed similar levels of ChR2 labeling. Both groups showed light-induced freezing behavior 1 day after training (engram activation 1), pre-SAL (P < 0.001), pre-ANI (P < 0.02). Two days after training (test 1), the fear memory was reactivated by exposure to context B, and SAL or ANI was injected. Three days after training (test 2), the ANI group froze significantly less than did the SAL group to context B (P < 0.01). Four days after training (engram activation 2), significant light-induced freezing was observed for the SAL (P < 0.001) and ANI (P < 0.003) groups. (**B**) DG inception (supplementary materials, materials and methods) after contextual memory amnesia. Context-only engram was labeled for target context A, followed by injection of SAL (n = 11 mice) or ANI (n = 11 mice). Amnesia was demonstrated in the ANI group through decreased ChR2$^+$/c-Fos$^+$ colabeling after context A reexposure 1 day after labeling. After fear inception, neither SAL nor ANI groups displayed freezing behavior in context B, whereas both groups displayed significant freezing in context A, with no significant difference between groups. No-light inception SAL (n = 7 mice) and ANI (n = 6 mice) controls displayed no freezing to context A or B. Statistical comparisons are performed by using unpaired t tests; ***P < 0.001. Data are presented as mean ± SEM.

until the current study, as a property of the engram cells. Our data have directly linked the optogenetically and behaviorally defined memory engram cells to synaptic plasticity.

On the basis of a large volume of previous studies, (*1–3, 7, 8, 32–34*), a concept has emerged in which retrograde amnesia arises from consolidation failure as a result of disrupting the process that converts a fragile memory engram, formed during the encoding phase, into a stable engram with persistently augmented synaptic strength and spine density. Indeed, our current study has demonstrated that amnesic engram cells in the DG 1 day after CFC training display low levels of synaptic strength and spine density that are indistinguishable from nonengram cells of the same DG. This correlated with a lack of memory recall elicited by contextual cues.

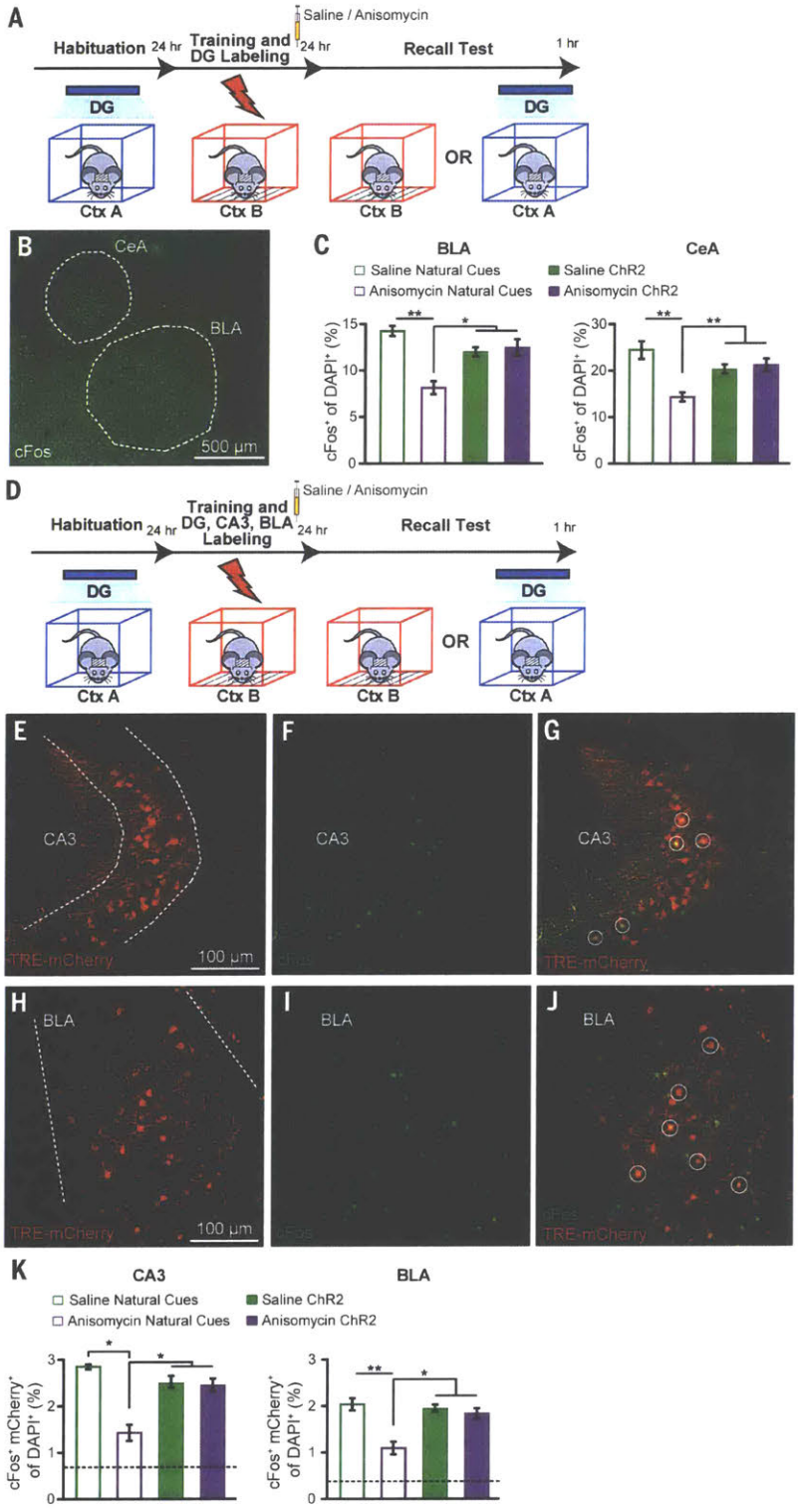

Fig. 5. Amygdala activation and functional connectivity in amnesia through light activation of DG engram. (**A**) Schedule for cell-counting experiments. Mice were either given a natural recall session in context B or a light-induced recall session in context A. Mice were perfused 1 hour after recall. (**B**) Representative image showing c-Fos expression in the BLA and CeA. (**C**) c-Fos$^+$ cell counts in the BLA and CeA of mice after natural or light-induced recall (n = 3 or 4 mice per group). (**D**) Schedule for cell-counting experiments. c-Fos-tTA mice with AAV$_9$-TRE-ChR2-EYFP injected into the DG and AAV$_9$-TRE-mCherry injected into both CA3 and BLA were fear-conditioned off DOX and 1 day later were given a natural recall session in context B or a light-induced recall session in context A. Mice were perfused 1 hour after recall. (**E** to **G**) Representative images showing mCherry engram cell labeling, c-Fos expression, and mCherry$^+$/c-Fos$^+$ overlap in CA3. (**H** to **J**) Representative images showing mCherry engram cell labeling, c-Fos expression, and mCherry/c-Fos overlap in BLA. (**K**) c-Fos$^+$/mCherry$^+$ overlap cell counts in CA3 and BLA of mice after natural or light-induced recall (n = 3 or 4 mice per group). Chance levels were estimated at 0.76 (CA3) and 0.42 (BLA). Data are presented as mean ± SEM. Statistical comparison are performed by using unpaired t tests; *P < 0.05, **P < 0.01.

However, direct activation of DG engram cells of the ANI group elicited as much freezing behavior as did the activation of these cells of the SAL group. This unexpected finding is supported by a set of additional cellular and behavioral experiments. Whereas amygdala engram cell reactivation upon exposure to the conditioned context is significantly lower in the ANI group as compared with the SAL group, optogenetic activation of DG engram cells results in normal reactivation of downstream CA3 and BLA engram cells (Fig. 5). At the behavioral level, the amnesia rescue was observed under a variety of different conditions in which one or more parameters were altered (Figs. 2 and 3 and figs. S9 and S13). Thus, our overall findings indicate that memory engrams survive a posttraining administration of protein synthesis inhibitors during the consolidation window and that the memory remains retrievable by means of ChR2-mediated direct engram activation even after retrograde amnesia is induced. The drive initiated with light-activation of one component of a distributed memory engram (such as that in the DG) is sufficient to reactivate engrams in downstream regions (such as that in CA3 and BLA) that would also be affected by the systemic injection of a protein synthesis inhibitor (ANI).

These findings suggest that although a rapid increase of synaptic strength is likely to be crucial during the encoding phase, the augmented synaptic strength is not a crucial component of the stored memory (*35*–*37*). This perspective is consistent with a recent study showing that an artificial memory could be reversibly disrupted by depression of synaptic strength (*38*). On the other hand, persistent and specific connectivity of engram cells that we find between DG engram cells and downstream CA3 or BLA engram cells in both SAL and ANI groups may represent a fundamental mechanism of memory information storage (*39*). Our findings also suggest that the primary role of augmented synaptic strength during and after the consolidation phase may be to provide natural recall cues with efficient access to the soma of engram cells for their reactivation and, hence, recall.

The integrative memory engram-based approach used here for parsing memory and amnesia into encoding, consolidation, and retrieval aspects may be of wider use to other experimental and clinical cases of amnesia, such as Alzheimer's disease (*40*).

REFERENCES AND NOTES

1. G. E. Müller, A. Pilzecker, *Z. Psychol.* **1**, 1–288 (1900).
2. C. P. Duncan, *J. Comp. Physiol. Psychol.* **42**, 32–44 (1949).
3. J. L. McGaugh, *Science* **287**, 248–251 (2000).
4. J. B. Flexner, L. B. Flexner, E. Stellar, *Science* **141**, 57–59 (1963).
5. L. B. Flexner, J. B. Flexner, R. B. Roberts, *Science* **155**, 1377–1383 (1967).
6. H. P. Davis, L. R. Squire, *Psychol. Bull.* **96**, 518–559 (1984).
7. E. R. Kandel, *Science* **294**, 1030–1038 (2001).
8. R. J. Kelleher 3rd, A. Govindarajan, S. Tonegawa, *Neuron* **44**, 59–73 (2004).
9. T. Takeuchi, A. J. Duszkiewicz, R. G. Morris, *Philos. Trans. R. Soc. Lond. B Biol. Sci.* **369**, 20130288 (2014).
10. A. Govindarajan, I. Israely, S. Y. Huang, S. Tonegawa, *Neuron* **69**, 132–146 (2011).
11. M. Krug, B. Lössner, T. Ott, *Brain Res. Bull.* **13**, 39–42 (1984).
12. U. Frey, M. Krug, K. G. Reymann, H. Matthies, *Brain Res.* **452**, 57–65 (1988).
13. Y. Y. Huang, P. V. Nguyen, T. Abel, E. R. Kandel, *Learn. Mem.* **3**, 74–85 (1996).
14. R. Semon, *Die Mneme als erhaltendes Prinzip im Wechsel des organischen Geschehens* (Wilhelm Engelmann, Leipzig, 1904).
15. S. A. Josselyn, *J. Psychiatry Neurosci.* **35**, 221–228 (2010).
16. X. Liu *et al.*, *Nature* **484**, 381–385 (2012).
17. S. Ramirez *et al.*, *Science* **341**, 387–391 (2013).
18. R. L. Redondo *et al.*, *Nature* **513**, 426–430 (2014).
19. C. A. Denny *et al.*, *Neuron* **83**, 189–201 (2014).
20. K. Z. Tanaka *et al.*, *Neuron* **84**, 347–354 (2014).
21. K. K. Cowansage *et al.*, *Neuron* **84**, 432–441 (2014).
22. L. G. Reijmers, B. L. Perkins, N. Matsuo, M. Mayford, *Science* **317**, 1230–1233 (2007).
23. R. L. Clem, R. L. Huganir, *Science* **330**, 1108–1112 (2010).
24. A. Suzuki *et al.*, *J. Neurosci.* **24**, 4787–4795 (2004).
25. B. N. Armbruster, X. Li, M. H. Pausch, S. Herlitze, B. L. Roth, *Proc. Natl. Acad. Sci. U.S.A.* **104**, 5163–5168 (2007).
26. J. H. Han *et al.*, *Science* **323**, 1492–1496 (2009).
27. J. R. Misanin, R. R. Miller, D. J. Lewis, *Science* **160**, 554–555 (1968).
28. K. Nader, G. E. Schafe, J. E. Le Doux, *Nature* **406**, 722–726 (2000).
29. X. Liu, S. Ramirez, S. Tonegawa, *Philos. Trans. R. Soc. Lond. B Biol. Sci.* **369**, 20130142 (2014).
30. A. Besnard, S. Laroche, J. Caboche, *Brain Struct. Funct.* **219**, 415–430 (2014).
31. J. Hall, K. L. Thomas, B. J. Everitt, *Eur. J. Neurosci.* **13**, 1453–1458 (2001).
32. J. L. McGaugh, *Science* **153**, 1351–1358 (1966).
33. Y. Dudai, *Annu. Rev. Psychol.* **55**, 51–86 (2004).
34. J. P. Johansen, C. K. Cain, L. E. Ostroff, J. E. LeDoux, *Cell* **147**, 509–524 (2011).
35. R. R. Miller, L. D. Matzel, *Learn. Mem.* **13**, 491–497 (2006).
36. C. A. Miller, J. D. Sweatt, *Learn. Mem.* **13**, 498–505 (2006).
37. S. Chen *et al.*, *eLife* **3**, e02844 (2014).
38. S. Nabavi *et al.*, *Nature* **511**, 348–352 (2014).
39. D. O. Hebb, *The Organization of Behavior; A Neuropsychological Theory* (Wiley, New York, 1949).
40. S. Daumas *et al.*, *Learn. Mem.* **15**, 625–632 (2008).

ACKNOWLEDGMENTS

We thank X. Liu and B. Roth for sharing reagents; X. Zhou, Y. Wang, W. Yu, S. Huang, and T. O'Connor for technical assistance; J. Z. Young for proofreading; and other members of the Tonegawa Laboratory for their comments and support. This work was supported by the RIKEN Brain Science Institute, Howard Hughes Medical Institute, and the JPB Foundation (to S.T.). pAAV-TRE-ChR2-EYFP, pAAV-TRE-ChR2-mCherry, and pAAV-TRE-mCherry were developed by X.L., in the group of S.T., at the Massachusetts Institute of Technology; therefore, a materials transfer agreement (MTA) is required to obtain these virus plasmids.

SUPPLEMENTARY MATERIALS

www.sciencemag.org/content/348/6238/1007/suppl/DC1
Materials and Methods
Figs. S1 to S13
Reference (*41*)

22 December 2014; accepted 30 April 2015
10.1126/science.aaa5542

COGNITIVE NEUROSCIENCE

Unlearning implicit social biases during sleep

Xiaoqing Hu,[1,2] James W. Antony,[1,3] Jessica D. Creery,[1] Iliana M. Vargas,[1] Galen V. Bodenhausen,[1] Ken A. Paller[1]*

Although people may endorse egalitarianism and tolerance, social biases can remain operative and drive harmful actions in an unconscious manner. Here, we investigated training to reduce implicit racial and gender bias. Forty participants processed counterstereotype information paired with one sound for each type of bias. Biases were reduced immediately after training. During subsequent slow-wave sleep, one sound was unobtrusively presented to each participant, repeatedly, to reactivate one type of training. Corresponding bias reductions were fortified in comparison with the social bias not externally reactivated during sleep. This advantage remained 1 week later, the magnitude of which was associated with time in slow-wave and rapid-eye-movement sleep after training. We conclude that memory reactivation during sleep enhances counterstereotype training and that maintaining a bias reduction is sleep-dependent.

Social interactions are often fraught with bias. Our preconceptions about other people can influence many types of behavior. For example, documented policing errors have repeatedly shown the potential harm of racial profiling (*1*). In experiments that used a first-person-shooter videogame, both White and Black participants were more likely to shoot Black than White individuals, even when they held a harmless object rather than a gun (*2*). When hiring potential research assistants, both male and female faculty members were more likely to hire male than equally qualified female candidates (*3*).

Although the tendency for people to endorse racist or sexist attitudes explicitly has decreased in recent years (*4*), social biases may nevertheless influence people's behavior in an implicit or unconscious manner, regardless of their intentions or efforts to avoid bias (*5*). Ample evidence indicates that implicit biases can drive discriminatory behaviors and exacerbate intergroup conflict (*5*–*8*). For instance, implicit racial biases decrease investments given to racial out-group members

[1]Department of Psychology, Northwestern University, Evanston, IL 60208, USA. [2]Department of Psychology, University of Texas at Austin, Austin, TX 78712, USA. [3]Princeton Neuroscience Institute, Princeton University, Princeton, NJ 08544, USA.
***Corresponding author. E-mail: kap@northwestern.edu**

Available online at www.sciencedirect.com

ScienceDirect

Current Opinion in Neurobiology

Memory engram storage and retrieval

Susumu Tonegawa[1,2], Michele Pignatelli[1], Dheeraj S Roy[1] and Tomás J Ryan[1,2]

A great deal of experimental investment is directed towards questions regarding the mechanisms of memory storage. Such studies have traditionally been restricted to investigation of the anatomical structures, physiological processes, and molecular pathways necessary for the capacity of memory storage, and have avoided the question of how individual memories are stored in the brain. Memory engram technology allows the labeling and subsequent manipulation of components of specific memory engrams in particular brain regions, and it has been established that cell ensembles labeled by this method are both sufficient and necessary for memory recall. Recent research has employed this technology to probe fundamental questions of memory consolidation, differentiating between mechanisms of memory retrieval from the true neurobiology of memory storage.

Addresses

[1] RIKEN-MIT Center for Neural Circuit Genetics at the Picower Institute for Learning and Memory, Department of Biology and Department of Brain and Cognitive Sciences, Massachusetts Institute of Technology, Cambridge, MA 02139, USA

[2] Howard Hughes Medical Institute, Massachusetts Institute of Technology, Cambridge, MA 02139, USA

Corresponding author: Tonegawa, Susumu (tonegawa@mit.edu)

Current Opinion in Neurobiology 2015, **35**:101–109

This review comes from a themed issue on **Circuit plasticity and memory**

Edited by **Thomas Mrsic-Flogel** and **Alessandro Treves**

http://dx.doi.org/10.1016/j.conb.2015.07.009

Introduction

Memory refers to the storage of learned information in the brain, and is crucial for adaptive behavior in animals [1]. Understanding the material basis of memory remains a central goal of modern neuroscience [2]. The hypothetical material basis of learned information, the memory *engram*, was first conceived by Richard Semon who theorized that learning induces persistent changes in specific brain cells that retain information and are subsequently reactivated upon appropriate retrieval conditions [3•,4,5]. However, experimental searches for specific memory engrams and memory engram-bearing cells using brain lesions proved inconclusive due to methodological limitations and the likely distributed nature of a memory engram throughout the brain [6••]. Here we review recent experimental studies on the identification of memory engram cells, with a focus on the mechanisms of memory storage. A more comprehensive review of recent memory engram studies is available elsewhere [7••].

Memory function and the hippocampus

The medial temporal lobe (MTL), in particular the hippocampus, was implicated in memory of events or episodes by neurological studies of human clinical patients, where its direct electrophysiological stimulation evoked the recall of untargeted episodic memories [8]. Subsequent study of humans lacking large regions of the MTL showed dramatic amnesia for episodic memories [9]. Rodent behavioral studies have since established that the hippocampus is a central brain region for contextual memory storage and retrieval [10,11]. Much is now known about brain structures, neural circuits, and molecules involved in memory encoding and consolidation [12••,13,14], but comparatively few studies have attempted to investigate how individual memory engrams are stored in the brain [15].

Synaptic plasticity as a mechanism of memory

Lasting memories have long been hypothesized to be encoded as structural changes at synaptic junctions of sparse neuronal assemblies [16]. Ramón y Cajal originally proposed that the strengthening of synaptic connections of existing neurons might be a mechanism of memory storage [17], but it was Donald Hebb's theoretical integration of neurophysiology and psychology that created the modern paradigm for memory research [16]. Hebb proposed that neuronal assemblies linked by adaptable synaptic connections could encode informational content in the brain. Empirical research into the physiological nature of memory storage has been dominated by various versions of Hebbian synaptic plasticity [18]. The typical experimental model of synaptic plasticity is long-term potentiation (LTP) [19], most studies of which rely on *in vitro* experimental paradigms where synaptic stimulation patterns are substituted for behavioral training. It is clear that memory and synaptic plasticity have many properties in common [20•]. NMDA receptor function is necessary for the encoding of many types of memory, as well as for the induction of synaptic plasticity [13,21]. Moreover, both memory consolidation and LTP have a late, protein synthesis-dependent phase [20•,22]. Despite these biological commonalities, and many serious theoretical efforts to integrate memory storage and synaptic

plasticity [23–27], it remains a controversial subject without a clear consensus [28–30].

Limitations of standard methodology

Two confounds have hindered progress towards a satisfactory synthesis of synaptic plasticity and memory. First, behavioral studies of memory have relied on the disruption of brain regions, circuits, or molecules [12••,13,14], and have thus addressed the importance of these structures and signaling pathways to the *capacities* of memory storage or retrieval, rather than the storage of individual memory engrams themselves. Second, typical conceptions of memory conflate the properties of memory storage and memory retrieval. But it is a fundamental premise of psychology that successful memory function presupposes not only the retention of learned information, but also its successful retrieval [1]. Therefore a given case of apparent memory loss (amnesia) may in principle be due to a damaged memory engram, or an inability to retrieve that particular engram [31–34]. Both of these confounds have recently been overcome through the development of memory engram technology [35••].

Sea change: memory engram technology

Identification and functional activation of engram cells

In order to progress in memory research it is crucial to identify the engrams and engram cells for specific experiences. The challenge of identifying individual memory engrams and engram cells amidst the complexity of the brain becomes less daunting if we co-opt natural brain activity during learning to point us to the relevant brain cells. This concept has been realized through the development of memory engram technology, which allows the labeling and subsequent manipulation of engram-bearing cells [35••]. Engram technology is based on the experimental fusion of immediate early gene (IEG) labeling and optogenetics. The expression of IEGs, such as *c-fos* or *arc*, is a marker of neuronal activity [36]. Thus the promoters of IEGs can be co-opted to tag neurons that are active during a given learning experience with an exogenous target protein (Figure 1) [37••]. Temporal specificity of labeling is achieved by engineering the labeling mechanism to be inhibited by administering doxycycline (DOX). When engram cells of the hippocampus dentate gyrus (DG) are labeled during contextual fear conditioning with channelrhodopsin-2 (ChR2) [38], their subsequent stimulation with blue light is sufficient to elicit retrieval of a target contextual fear memory, as measured by conditioned freezing behavior [35••]. Crucial control experiments, where engram cells for neutral contexts were stimulated in fear-conditioned mice, demonstrated that the information stored in labeled engram cells is specific to the target experience [35••]. Importantly, memory recall by natural cues reactivates the same engram cells [39••] satisfying another important criteria, the ecphoric nature of an engram [4].

Physiological characterization of engram cells

The storage of lasting memory in the brain must involve persistent plasticity of engram cell structure and/or physiology. Indeed, *ex vivo* characterization of DG engram cells revealed two engram cell-specific properties [40••]. First, engram cells showed significantly increased dendritic spine density relative to non-engram cells. Second, patch clamp recordings of excitatory postsynaptic currents in paired engram and non-engram cells elicited by presynaptic stimulation of perforant path axons showed substantially higher synaptic strength in engram cells.

The above two properties are clear cases of plasticity occurring exclusively in engram cells, and are reminiscent of Hebbian plasticity. If this plasticity is representing mnemonic information then it should be encoded by the specific training experience. Protein synthesis is necessary for late phase synaptic plasticity and memory consolidation, and indeed when the protein synthesis inhibitor anisomycin was administered to animals immediately after fear conditioning, retrograde amnesia was observed one day later. Analysis of engram cells one day after anisomycin treatment showed that the anisomycin abolished engram-cell specific increases in both dendritic spine density and synaptic strength, but did not alter either property in non-engram cells. Importantly, anisomycin treatment one day post-training (outside the consolidation window) impaired neither the dendritic spine density increase nor the synaptic strength augmentation of engram cells [40••]. Therefore engram cell-specific structural and synaptic plasticity is protein synthesis-dependent and consolidated with the target training experience.

Retrieval of lost memory from amnesia: dissociation of engram cell plasticity and memory

Surprisingly, direct optogenetic activation of amnesic engram cells in mice resulted in successful retrieval of the ostensibly lost contextual fear memory. The generality of the memory retrieval finding was tested in a range of experimental conditions [40••]. First, lost memory was retrieved by optogenetic stimulation of ChR2-labeled engram cells in hippocampal CA1. Second, amnesia for tone fear memory was generated with anisomycin, and the memory was retrieved by optogenetic stimulation of lateral amygdala (LA) engram cells. Third, lost memory was retrieved from amnesia due to impaired reconsolidation by activation of DG engram cells. Fourth, an alternative protein synthesis inhibitor, cycloheximide, was used to generate amnesia and subsequent activation of DG engram cells again retrieved the target memory. Finally, a contextual updating protocol [39••] was used to show that amnesic engram cells retained information about context specificity, and could be restored to a condition where they could be retrieved by natural contextual cues [40••].

Figure 1

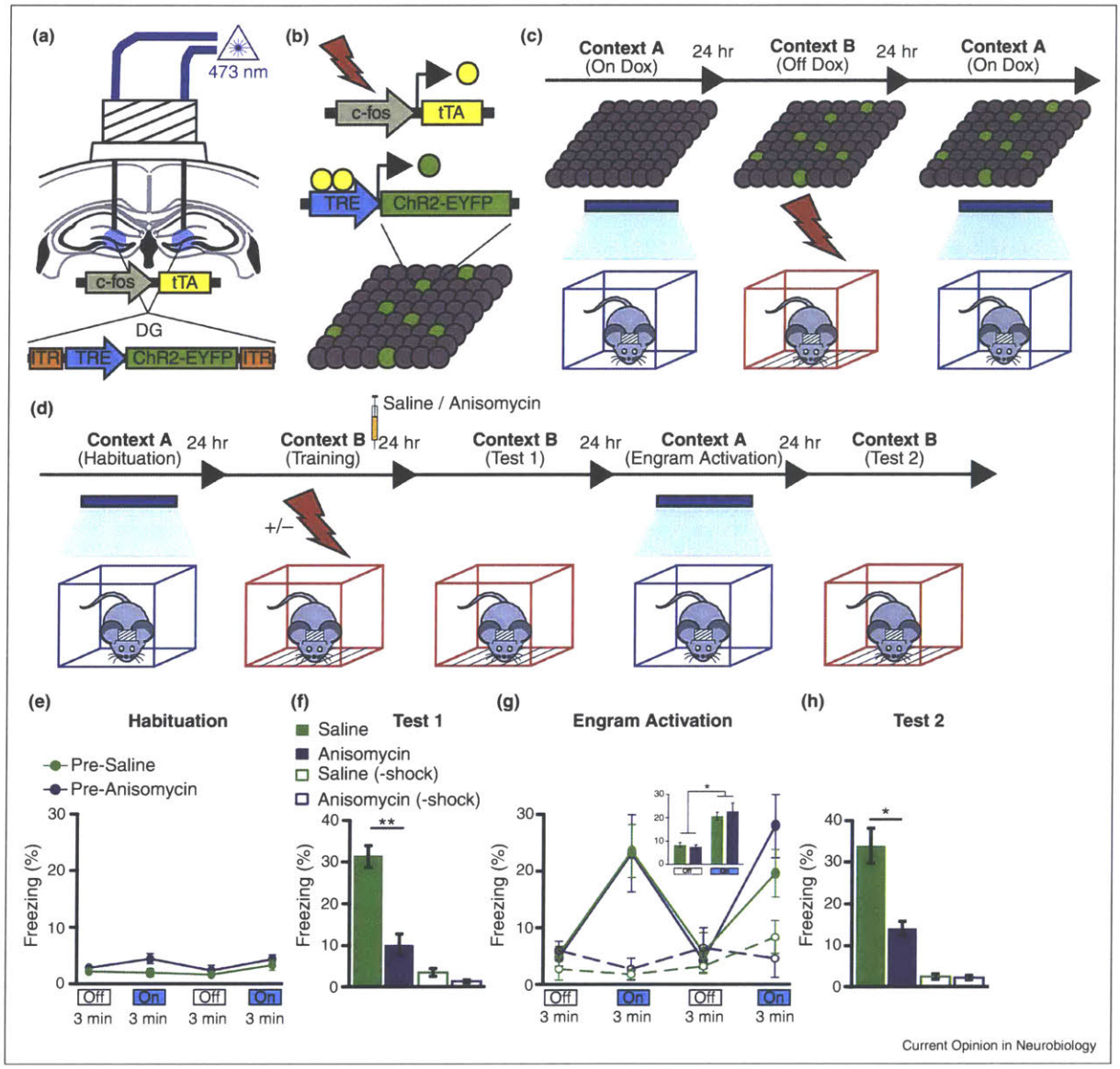

Engram Labeling Technology and Memory Retrieval in Retrograde Amnesia. **(A)** Basic composition of the engram labeling system. Virus expressing TRE-ChR2 and optic fibers are targeted to the dentate gyrus of c-Fos-tTA transgenic mice. **(B)** In the absence of DOX, DG neurons that are active during the formation of a memory are labeled with ChR2. **(C)** Basic behavioral schedule for labeling and activation of engram cells. Animals are habituated to Context A with light stimulation while on DOX, trained by contextual fear conditioning in Context B while off DOX, and tested again in Context A with light stimulation while on DOX. **(D)** Behavioral schedule for generating amnesia by disrupting memory consolidation. Saline or anisomycin was injected into the mice after training. **(E)** Habituation to Context A with Light-Off and Light-On epochs. Blue light stimulation of the DG did not cause freezing behavior in naïve, unlabeled mice. **(F)** Memory recall in Context B 1 day post-training (Test 1). The anisomycin group showed impaired memory recall relative to the saline group as measured by conditioned freezing behavior to Context B. No-shock groups did not display freezing upon re-exposure to Context B. **(G)** Memory recall in Context A 2 days post-training (Engram Activation) with Light-Off and Light-On epochs. Freezing for the two Light-Off and Light-On epochs are further averaged in the inset. Freezing levels did not differ between groups. **(H)** Memory recall in Context B 3 days post-training (Test 2). The anisomycin group displayed significantly less freezing than the saline group.

Taken together, the behavioral and physiological results clearly show that engram cell-specific structural and synaptic plasticity is strongly correlated with normal memory function, since both engram cell plasticity and memory expression are sensitive to protein synthesis inhibition during the consolidation window. Nevertheless, these findings showed a stark dissociation between synaptic plasticity and memory content, since engram cells retained memory information even in the absence of engram cell-specific increases in spine density and synaptic strength.

Connectivity between engram cells as the mechanism for retained memory

The dissociation of engram cell plasticity and memory prompted the question; how can the consolidated memory be stored? One hypothesis would be that memory may be stored in a specific pattern of connectivity between engram cell ensembles distributed in multiple brain regions and this connectivity pattern is established during encoding and retained during consolidation in a protein synthesis-independent manner (Figure 2).

This hypothesis was tested by two different types of experiments using *ex vivo* electrophysiological and *in vivo* IEG technologies [40••]. First, when both DG and hippocampal CA3 engram cell ensembles were simultaneously labeled and the presynaptic DG engram cells were activated optogenetically, the occurrence of the postsynaptic response of CA3 engram cells was significantly higher (~80%) than that of CA3 non-engram cells (~25%) and these proportions were not affected by anisomycin treatment. Second, engram cells were simultaneously labeled in the DG, CA3, and basolateral amygdala (BLA) during contextual fear conditioning. One day after training, re-exposure to the conditioning context preferentially activated engram cells in all three brain regions as measured by endogenous c-Fos$^+$ cell counts, and this phenomenon was significantly impaired by anisomycin treatment in the consolidation window when natural recall cues were used. Nevertheless, direct optogenetic activation of DG engram cells resulted in a greater than chance level of c-Fos$^+$ overlap with CA3 or BLA engram cells in both control and anisomycin-treated mice.

Figure 2

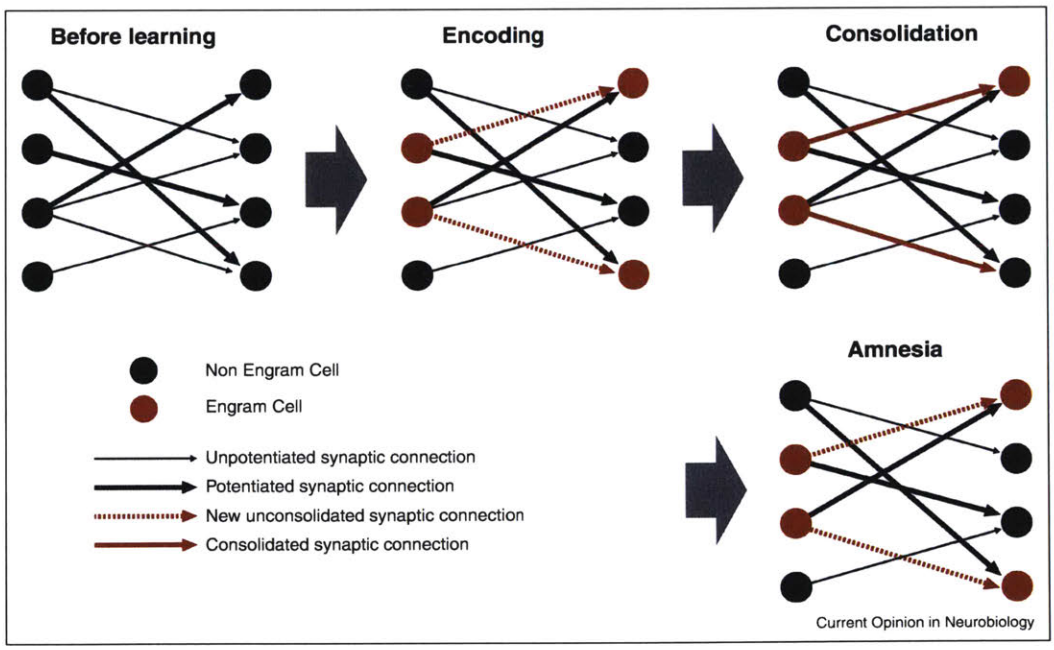

Engram Cell Connectivity. Schematic illustrating the dynamics of synaptic connectivity in a neural ensemble recruited during the formation of a new memory. Before learning the neural network presents a connectivity arrangement characterized by a mix of potentiated (thick black line) and unpotentiated (thin black line) synapses. During memory encoding, a sparse number of cells (engram cells, red) are recruited, giving rise to new connections or activating preexisting ones (dashed red line). Immediately after encoding the process of memory consolidation enables the stabilization of the new connections (thick red line). The stabilization is characterized by an enhancement of synaptic strength and is fundamental for memory retrieval. Disruption of the consolidation process by interventions such as protein synthesis inhibitors impairs the stabilization/potentiation of new synaptic connections (dashed red line) resulting in retrograde amnesia. Synaptic connectivity provides a substrate for memory storage whereas the potentiation of synapses is required for memory retrieval.

These results demonstrate intact functional connectivity among engram cell ensembles distributed in neural circuits encompassing multiple brain regions and reinforces the hypothesis that consolidated memory is stored by engram cell-specific connectivity formed in a protein synthesis-independent manner (Figure 2).

Synaptic strengthening as a mechanism of memory retrievability

Based on these integrative findings, we propose that enhanced engram cell-specific synaptic strength is crucial for the retrievability of particular memory engrams [33•], while the memory information content itself is encoded in a pattern of engram cell ensemble connectivity. Under amnesia, the impaired synaptic strengthening prevents effective activation of engram cells by natural recall cues and subsequent engram cell spiking (Figure 3). However, the information stored in engram cell ensemble connectivity can be retrieved by the optogenetic stimulation of various nodes in the engram cell circuit. The notion that synaptic strengthening is crucial for memory retrieval, but not for stable storage of memory *per se*, is consistent with a number of complementary studies. It was recently shown that optogenetically-induced long-term depression (LTD) of rat amygdala cells impaired existing conditioned fear responses [41•]. However, subsequent optogenetically-induced LTP of the same cells restored natural cue-evoked recall of the fear memory. Therefore, the memory information must have persisted in the brain of the rats even after the amygdala synapses were depressed, but the lack of synaptic potentiation prevented successful memory retrieval. Supporting this perspective is the demonstration that amnesia for a purely contextual memory can be overcome by direct engram activation paired simultaneous presentation of aversive shock [40••]. Other correlative studies have shown that contextual fear memories formed during a certain period of adolescent development were not expressed in recall tests until the transition into adulthood, and this developmental change correlated with a delayed learning-specific synaptic potentiation of the BLA fear circuit [42]. Thus, the fear memory was present during adolescence, but its retrievability was temporarily impaired due to lack of BLA synaptic strength. In addition, reminder experiments in *Aplysia* showed that amnesia for gill withdrawal sensitization can be restored by extra puffs of serotonin, and that this response persisted despite significantly altered presynaptic varicosities [43]. Collectively these studies strongly support a dissociation of synaptic strength and memory persistence, and point to its crucial role in the reactivation of a memory engram and retrievability of a memory.

Engram cell ensemble circuit

If engram cells are truly carrying memory information at the holistic level of an engram circuit, then inhibition of engram cells at various nodes of an engram circuit should inhibit retrieval of the target memory. This prediction has

Figure 3

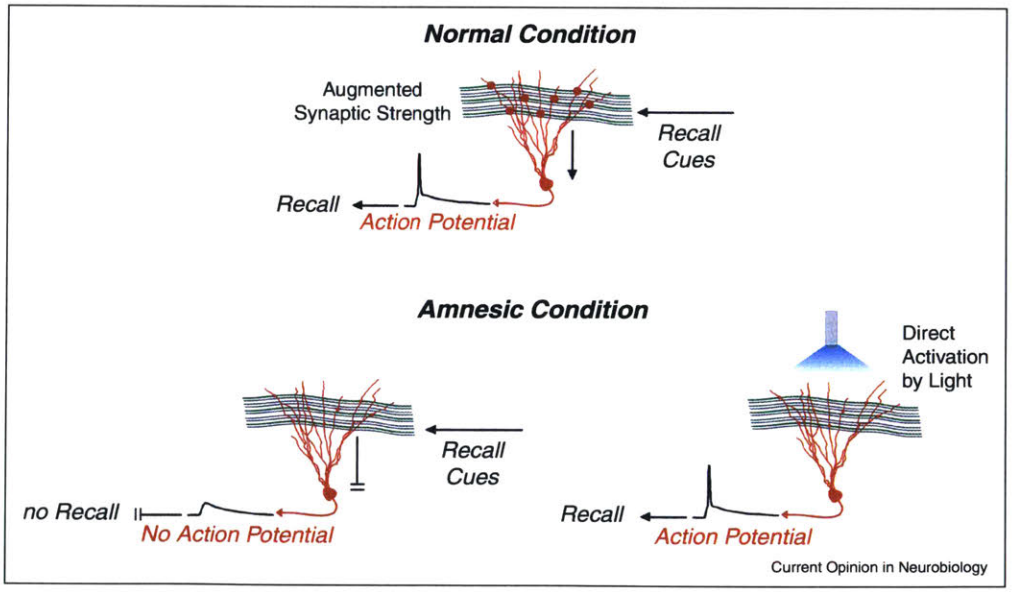

Augmented Synaptic Strength for Recall. Under normal conditions, a consolidated engram cell is efficiently activated by recall cues from the animal's environment through potentiated synaptic inputs. Under amnesic conditions, engram cells are present but lack synaptic potentiation and are thus only weakly evoked by recall cues. Nevertheless, direct activation of engram cells is sufficient to overcome impaired synaptic potentiation and results in memory retrieval.

been satisfied by studies showing that individual fear memories require engram cells from multiple brain regions. Optogenetic inhibition of engram cells labeled with the IEGs *c fos* and *arc* in hippocampal CA1 [44•] and DG [45•] caused impairments both in downstream engram cell reactivation and contextual fear memory recall. Moreover, when CREB is artificially expressed in the LA, it biases certain LA cells to acquire the fear engram during tone fear conditioning [15]. Subsequent interference with these LA engram cells by either ablation or acute chemogenetic inhibition [46••,47•] impaired fear memory recall. In addition, optogenetic inhibition of BLA cells representing valence-specific unconditioned stimuli impaired memory recall elicited by associated tone and odor conditioned stimuli [48]. Taken together, these studies clearly show that a functional memory requires multiple nodes on an engram cell ensemble circuit.

Recently it has been demonstrated that retrieval of a positive memory by optogenetic activation of DG engram cells was impaired by simultaneous inhibition of downstream BLA engram cell projections to the nucleus accumbens [49•]. Thus, the downstream connectivity of engram cells is crucial for the retrieval of memory. The converse scenario has also been investigated, where inhibition of upstream areas was optogenetically bypassed by direct activation of downstream engram cells. In an experiment where contextual memory retrieval was acutely impaired by pharmacological inhibition of AMPA receptors in the hippocampus, simultaneous optogenetic activation of downstream engram cells in the retrosplenial cortex successfully evoked memory retrieval [50•]. These findings provide evidence for the encoding of memory across an engram cell ensemble circuit.

An important prerequisite of any putative memory storage mechanism is activity-dependency during encoding. This criterion has been tested by chemogenetic inhibition of CA1 neurons during encoding [40••]. This procedure generated anterograde amnesia that was irretrievable even by direct stimulation of upstream DG engram cells. Finally, any putative substrate of memory storage should hold the potential for plasticity following further relevant new learning. To this end, it has been shown that when the positive or negative emotional valence associated with a specific contextual memory was reversed in an optogenetic counter-conditioning schedule, the functional connectivity of DG and BLA engram cells was abolished [51].

Conclusions and future directions

Implications for memory research

The differentiation of synaptic plasticity and engram connectivity described here (Table 1) has significant implications for interpreting the neurobiology of memory consolidation and synaptic plasticity, because the conceptual and empirical framework introduced here can be used to attribute cellular signaling pathways to memory storage or retrieval. Molecular mechanisms that serve to potentiate or strengthen AMPA receptor transmission are parsimoniously attributable to memory retrievability [52–54].

What then would be molecular mechanisms for information retention in the substrate of engram cell connectivity?

It is known that NMDA receptor-dependent synaptic plasticity results not just in potentiated synapses, but also in the formation of new functional synaptic connections through synapse unsilencing [55•]. The trafficking of a basal level of AMPA receptors into pre-existing silent synapses may facilitate the encoding of new functional connectivity. Nevertheless, LTP is known to be characterized by an early phase and a late phase, E-LTP and L-LTP, the latter sensitive to protein synthesis inhibitors [56]. The survival of engram connectivity upon protein synthesis inhibitors treatment suggests that the induction of engram connectivity may share mechanisms common to E-LTP. However, by impairing the late phase, it has been shown that the unsilencing can be prevented,

Table 1

Comparison of putative plasticity mechanisms and suitability for memory storage or retrieval

Plasticity Mechanism:	Synaptic Strength	Engram Cell Connectivity
Locus:	Single engram cells or synapses	Engram Circuit
Extent:	Increases depending on active synapse and spine numbers involved, but essentially limited to single engram cells	Increases in complexity and computaional capacity the more brain regions and neurons involved
Mechanism:	Changes in AMPA receptor trafficking and dendritic spine formation on engram cells	Changes in specific connectivity patterns of engram cell assemblies
Requirement for Protein Synthesis:	Yes, protein synthesis inhibitors impair engram cell synaptic plasticity	No, protein synthesis inhibitors have no effect on engram cell connectivity
Necessary for Memory Retrieval:	Yes, when synaptic plasticity is impaired, amnesia results	Yes, impairing engram cell or circuit activity prevents memory retrieval
Necessary for Memory Storage:	No, direct activation of target engram can retrieve memory	Yes, encoding of memory in circuit is necessary for memory formation, and valence reversal alters engram connectivity

suggesting that 'silent synapses' can only partially support the engram connectivity [57]. Alternatively, a subset of learning-induced dendritic spine formation may be responsible for novel connectivity patterns between engram cells. Under any of these scenarios, the retention of engram connectivity could conceivably be mediated by the homeostatic regulation of steady state AMPA receptor trafficking. Consistent with this perspective is a recent study showing that protein synthesis inhibitors, when administered before recall tests, transiently impaired AMPA receptor expression and memory retrieval [58•]. Alternatively, the maintenance of memory engram connectivity might be mediated by specific molecular players that are yet to be fully characterized in the context of memory function, such as perineuronal net components or microRNAs [59•,60].

It is currently unknown for how long engram cell connectivity persists, and whether it is permanent or reversible. Though it has been shown through engram overlap analysis that when the positive or negative emotional valence associated with a contextual memory is reversed, the functional connectivity of DG/BLA engram cells changes [51], a direct analysis of synaptic connections will be necessary to understand the true physiological nature of the plasticity of connectivity.

Regardless of the specific underlying molecular mechanisms, if engram cell connectivity is the substrate of memory information storage, then it will be necessary to fully explore the structure and function of the engram circuit. Such a task would require the comprehensive mapping of the entire engram circuit connectome for a given memory; the memory *engrome*. This could be achieved by combining engram labeling technology, whole brain IEG activity measurements [61], and three dimensional imaging of intact transparent brains [62]. The functional properties of engram circuits could be studied *in vivo* by calcium imaging of engram cell activity in multiple brain regions [63].

Applications

Manipulation of engram circuits presents many opportunities for significant practical applications. The efficacy of this technology for artificially updating existing memories [39••,64], as well as for reversing the emotional valence associated with contextual memories [51], has been established. Such interventions based on engram technology may have utility for the treatments of post-traumatic stress disorder. In addition, positive memory engram activation has recently been shown to alleviate stress-induced models of depression in mice [49•]. Furthermore, tagging and interfering with engram cells for cocaine-related memories has been reported as possible treatment avenues of drug addiction [65]. Cases of pathological amnesia that are due to retrieval failures should be much more amenable to restorative interventions than instances of *bona fide* memory loss. The particular approach to amnesia discussed in this review could be employed for investigating and potentially treating various types of clinical amnesia, such as Alzheimer's disease.

Evolutionary significance

From an evolutionary perspective, synaptic plasticity is a ubiquitous feature of neurons that seems to have arisen with the first nervous system in a common ancestor of cnidarians and bilaterians over a billion years ago [66]. On this basis, synaptic plasticity can be a considered a fundamental neuronal property, the disruption of which in brain regions such as the hippocampus or amygdala will impair the encoding and retrieval of memory. On the other hand, engram cell connectivity is a substrate that naturally increases in complexity as brain anatomy evolves (Table 1). Therefore the more complex the brain, the greater the opportunity for the storage of detailed memories through hierarchical engram circuits distributed throughout brain regions. Connectivity patterns among engram cell assemblies are a potential mechanism of information storage that is in keeping with what Hebb originally envisioned [16]. Further research in this direction may provide significant new insights into the storage of memory.

Conflict of interest statement

Nothing declared.

Acknowledgements

We thank Ralph Miller, Daniel Schacter, and members of the Tonegawa laboratory for useful discussions. This work was supported by the RIKEN Brain Science Institute, Howard Hughes Medical Institute, and the JPB Foundation (to S.T.).

References and recommended reading

Papers of particular interest, published within the period of review, have been highlighted as:

- • of special interest
- •• of outstanding interest

1. James W: *The principles of psychology*. New York: H. Holt and Company; 1890.

2. Dudai Y, Morris RG: **Memorable trends**. *Neuron* 2013, **80**:742-750.

3. • Semon R: *Die mneme*. [The mneme]. Leipzig: Wilhelm Engelmann; 1904.
This book describes a theory of memory where the engram idea was originated.

4. Semon R: *Die nmemischen empfindungen*. [Mnemic psychology]. Leipzig: Wilhelm Engelmann; 1909.

5. Schacter DL: *Forgotten ideas, neglected pioneers: Richard Semon and the story of memory*. New York: Routledge; 2001.

6. •• Lashley K: **In search of the engram**. *Symp Soc Exp Biol* 1950, **4**:454-482.
This is an early experimental investigation of engram location in the brain.

7. •• Tonegawa S, Liu X, Ramirez S, Redondo RL: **Memory engram cells have come of age**. *Neuron* 2015. in press.
This review provides a comprehensive account of recent memory engram studies.

8. Penfield W, Rasmussen T: *The cerebral cortex of man: a clinical study of localization of function*. New York: Macmillan; 1950.

9. Scoville WB, Milner B: **Loss of recent memory after bilateral hippocampal lesions**. *J Neurol Neurosurg Psychiatry* 1957, **20**:11-21.

10. Morris RG, Garrud P, Rawlins JN, O'Keefe J: **Place navigation impaired in rats with hippocampal lesions**. *Nature* 1982, **297**:681-683.

11. Moser MB, Moser EI: **Distributed encoding and retrieval of spatial memory in the hippocampus**. *J Neurosci* 1998, **18**:7535-7542.

12. •• McGaugh JL: **Memory – a century of consolidation**. *Science* 2000, **287**:248-251.
This review summarizes a 50 year perspective of memory consolidation research.

13. Nakazawa K, McHugh TJ, Wilson MA, Tonegawa S: **NMDA receptors, place cells and hippocampal spatial memory**. *Nat Rev Neurosci* 2004, **5**:361-372.

14. Johansen JP, Cain CK, Ostroff LE, LeDoux JE: **Molecular mechanisms of fear learning and memory**. *Cell* 2011, **147**:509-524.

15. Josselyn SA: **Continuing the search for the engram: examining the mechanism of fear memories**. *J Psychiatry Neurosci* 2010, **35**:221-228.

16. Hebb DO: *The organization of behavior; a neuropsychological theory*. New York: Wiley; 1949.

17. Ramón, Cajal S: **The Croonian Lecture: La Fine Structure des Centres Nerveux**. *Proc R Soc Lond* 1894, **5**:444-468.

18. Sejnowski TJ: **The book of Hebb**. *Neuron* 1999, **24**:773-776.

19. Bliss TV, Lomo T: **Long-lasting potentiation of synaptic transmission in the dentate area of the anaesthetized rabbit following stimulation of the perforant path**. *J Physiol* 1973, **232**:331-356.

20. • Kandel ER: **The molecular biology of memory storage: a dialogue between genes and synapses**. *Science* 2001, **294**:1030-1038.
This review summarizes the canonical perspective of the molecular and cellular biology of memory storage.

21. Park P, Volianskis A, Sanderson TM, Bortolotto ZA, Jane DE, Zhuo M, Kaang BK, Collingridge GL: **NMDA receptor-dependent long-term potentiation comprises a family of temporally overlapping forms of synaptic plasticity that are induced by different patterns of stimulation**. *Philos Trans R Soc Lond B Biol Sci* 2014, **369**:20130131.

22. Huang YY, Nguyen PV, Abel T, Kandel ER: **Long-lasting forms of synaptic potentiation in the mammalian hippocampus**. *Learn Mem* 1996, **3**:74-85.

23. Martin SJ, Grimwood PD, Morris RG: **Synaptic plasticity and memory: an evaluation of the hypothesis**. *Annu Rev Neurosci* 2000, **23**:649-711.

24. Paulsen O, Sejnowski TJ: **Natural patterns of activity and long-term synaptic plasticity**. *Curr Opin Neurobiol* 2000, **10**:172-179.

25. Neves G, Cooke SF, Bliss TV: **Synaptic plasticity, memory and the hippocampus: a neural network approach to causality**. *Nat Rev Neurosci* 2008, **9**:65-75.

26. Takeuchi T, Duszkiewicz AJ, Morris RG: **The synaptic plasticity and memory hypothesis: encoding, storage and persistence**. *Philos Trans R Soc Lond B Biol Sci* 2014, **369**:20130288.

27. Abraham WC, Robins A: **Memory retention – the synaptic stability versus plasticity dilemma**. *Trends Neurosci* 2005, **28**:73-78.

28. Shors TJ, Matzel LD: **Long-term potentiation: what's learning got to do with it?** *Behav Brain Sci* 1997, **20**:597-614 discussion 614–555.

29. Gallistel CR, Matzel LD: **The neuroscience of learning: beyond the Hebbian synapse**. *Annu Rev Psychol* 2013, **64**:169-200.

30. Taylor AM, Bus T, Sprengel R, Seeburg PH, Rawlins JN, Bannerman DM: **Hippocampal NMDA receptors are important for behavioural inhibition but not for encoding associative spatial memories**. *Philos Trans R Soc Lond B Biol Sci* 2014, **369**:20130149.

31. Ribot T: *Les maladies de la mémoire*. [Diseases of memory]. Paris: Germer Baillere; 1881.

32. Warrington EK, Weiskrantz L: **Amnesic syndrome: consolidation or retrieval?** *Nature* 1970, **228**:628-630.

33. • Miller RR, Matzel LD: **Retrieval failure versus memory loss in experimental amnesia: definitions and processes**. *Learn Mem* 2006, **13**:491-497.
This review summarizes the retrieval perspective of retrograde amnesia.

34. Squire LR: **Lost forever or temporarily misplaced? The long debate about the nature of memory impairment**. *Learn Mem* 2006, **13**:522-529.

35. •• Liu X, Ramirez S, Pang PT, Puryear CB, Govindarajan A, Deisseroth K, Tonegawa S: **Optogenetic stimulation of a hippocampal engram activates fear memory recall**. *Nature* 2012, **484**:381-385.
This study provided the first demonstration that activation of putative memory engram cells is sufficient for the recall of specific memories.

36. Greenberg ME, Ziff EB: **Stimulation of 3T3 cells induces transcription of the c-fos proto-oncogene**. *Nature* 1984, **311**:433-438.

37. •• Reijmers LG, Perkins BL, Matsuo N, Mayford M: **Localization of a stable neural correlate of associative memory**. *Science* 2007, **317**:1230-1233.
This study details the generation and application of the c-Fos-tTA transgenic mouse for labeling of cell ensembles that are active during a specific experience.

38. Boyden ES, Zhang F, Bamberg E, Nagel G, Deisseroth K: **Millisecond-timescale, genetically targeted optical control of neural activity**. *Nat Neurosci* 2005, **8**:1263-1268.

39. •• Ramirez S, Liu X, Lin PA, Suh J, Pignatelli M, Redondo RL, Ryan TJ, Tonegawa S: **Creating a false memory in the hippocampus**. *Science* 2013, **341**:387-391.
This study was the first to show that a specific ensemble of hippocampal cells carries specific information of contextual memories and can be artificially updated with new targeted information.

40. •• Ryan TJ, Roy DS, Pignatelli M, Arons A, Tonegawa S: **Memory. Engram cells retain memory under retrograde amnesia**. *Science* 2015, **348**:1007-1013.
This paper provides the first physiological and structural charactrerization of memory engram cells and challenges standard conceptions of memory consolidation and storage.

41. • Nabavi S, Fox R, Proulx CD, Lin JY, Tsien RY, Malinow R: **Engineering a memory with LTD and LTP**. *Nature* 2014, **511**:348-352.
This paper showed that behavioral performance for a learned task can be reversibly impaired by optogenetic depression and potentiation of amygdala synapses.

42. Pattwell SS, Bath KG, Casey BJ, Ninan I, Lee FS: **Selective early-acquired fear memories undergo temporary suppression during adolescence**. *Proc Natl Acad Sci U S A* 2011, **108**:1182-1187.

43. Chen S, Cai D, Pearce K, Sun PY, Roberts AC, Glanzman DL: **Reinstatement of long-term memory following erasure of its behavioral and synaptic expression in**. *Elife* 2014:3.

44. • Tanaka KZ, Pevzner A, Hamidi AB, Nakazawa Y, Graham J, Wiltgen BJ: **Cortical representations are reinstated by the hippocampus during memory retrieval**. *Neuron* 2014, **84**:347-354.
This study proved that specific memory engrams can be labeled and manipulated in hippocampal CA1.

45. • Denny CA, Kheirbek MA, Alba EL, Tanaka KF, Brachman RA, Laughman KB, Tomm NK, Turi GF, Losonczy A, Hen R: **Hippocampal memory traces are differentially modulated by experience, time, and adult neurogenesis**. *Neuron* 2014, **83**:189-201.
This study showed that memory engram cells in the dentate gyrus are necessary for normal contextual memory recall.

46. •• Han JH, Kushner SA, Yiu AP, Hsiang HL, Buch T, Waisman A, Bontempi B, Neve RL, Frankland PW, Josselyn SA: **Selective erasure of a fear memory**. *Science* 2009, **323**:1492-1496.

This pioneering study provided the first causal demonstration that memory information can be encoded in a sparse population of cells in the amygdala.

47. Zhou Y, Won J, Karlsson MG, Zhou M, Rogerson T, Balaji J, Neve R, Poirazi P, Silva AJ: **CREB regulates excitability and the allocation of memory to subsets of neurons in the amygdala**. *Nat Neurosci* 2009, **12**:1438-1443.
This study investigated the physiological role of intrinsic cell excitability for memory allocation.

48. Gore F, Schwartz EC, Brangers BC, Aladi S, Stujenske JM, Likhtik E, Russo MJ, Gordon JA, Salzman CD, Axel R: **Neural representations of unconditioned stimuli in basolateral amygdala mediate innate and learned responses**. *Cell* 2015, **162**:134-145.

49. Ramirez S, Liu X, MacDonald CJ, Moffa A, Zhou J, Redondo RL, Tonegawa S: **Activating positive memory engrams suppresses depression-like behaviour**. *Nature* 2015, **522**:335-339.
This study showed that depression-like behavior in mice can be ameliorated by direct activation of positive memory engrams.

50. Cowansage KK, Shuman T, Dillingham BC, Chang A, Golshani P, Mayford M: **Direct reactivation of a coherent neocortical memory of context**. *Neuron* 2014, **84**:432-441.
This study demonstrated that engram cells can be tagged and manipulated in the cortex, and also that engram technology can be used to bypass acute retrieval blockages induced by AMPA receptor antagonism.

51. Redondo RL, Kim J, Arons AL, Ramirez S, Liu X, Tonegawa S: **Bidirectional switch of the valence associated with a hippocampal contextual memory engram**. *Nature* 2014, **513**:426-430.

52. Kandel ER: **The molecular biology of memory: cAMP, PKA, CRE, CREB-1, CREB-2, and CPEB**. *Mol Brain* 2012, **5**:14.

53. Lisman J, Yasuda R, Raghavachari S: **Mechanisms of CaMKII action in long-term potentiation**. *Nat Rev Neurosci* 2012, **13**:169-182.

54. Sacktor TC: **How does PKMzeta maintain long-term memory?** *Nat Rev Neurosci* 2011, **12**:9-15.

55. Liao D, Hessler NA, Malinow R: **Activation of postsynaptically silent synapses during pairing-induced LTP in CA1 region of hippocampal slice**. *Nature* 1995, **375**:400-404.
This study provided the first experimental demonstration of silent synapses, and discriminated between potentiation of existing synapses and potentiation of new synapses.

56. Davis HP, Squire LR: **Protein synthesis and memory: a review**. *Psychol Bull* 1984, **96**:518-559.

57. Kasten MR, Fan Y, Schulz PE: **Activation of silent synapses with sustained but not decremental long-term potentiation**. *Neurosci Lett* 2007, **417**:84-89.

58. Lopez J, Gamache K, Schneider R, Nader K: **Memory retrieval requires ongoing protein synthesis and NMDA receptor activity-mediated AMPA receptor trafficking**. *J Neurosci* 2015, **35**:2465-2475.
This study showed that tonic levels of protein synthesis-dependent AMPA receptor trafficking are necessary for memory recall.

59. Tsien RY: **Very long-term memories may be stored in the pattern of holes in the perineuronal net**. *Proc Natl Acad Sci U S A* 2013, **110**:12456-12461.
This review presents a radical theory on the potential storage of memory in perineuronal nets.

60. Gallistel CR, Balsam PD: **Time to rethink the neural mechanisms of learning and memory**. *Neurobiol Learn Mem* 2014, **108**:136-144.

61. Wheeler AL, Teixeira CM, Wang AH, Xiong X, Kovacevic N, Lerch JP, McIntosh AR, Parkinson J, Frankland PW: **Identification of a functional connectome for long-term fear memory in mice**. *PLoS Comput Biol* 2013, **9**:e1002853.

62. Chung K, Wallace J, Kim SY, Kalyanasundaram S, Andalman AS, Davidson TJ, Mirzabekov JJ, Zalocusky KA, Mattis J, Denisin AK *et al.*: **Structural and molecular interrogation of intact biological systems**. *Nature* 2013, **497**:332-337.

63. Lecoq J, Savall J, Vucinic D, Grewe BF, Kim H, Li JZ, Kitch LJ, Schnitzer MJ: **Visualizing mammalian brain area interactions by dual-axis two-photon calcium imaging**. *Nat Neurosci* 2014, **17**:1825-1829.

64. Ohkawa N, Saitoh Y, Suzuki A, Tsujimura S, Murayama E, Kosugi S, Nishizono H, Matsuo M, Takahashi Y, Nagase M *et al.*: **Artificial association of pre-stored information to generate a qualitatively new memory**. *Cell Rep* 2015.

65. Hsiang HL, Epp JR, van den Oever MC, Yan C, Rashid AJ, Insel N, Ye L, Niibori Y, Deisseroth K, Frankland PW *et al.*: **Manipulating a 'cocaine engram' in mice**. *J Neurosci* 2014, **34**:14115-14127.

66. Ryan TJ, Grant SG: **The origin and evolution of synapses**. *Nat Rev Neurosci* 2009, **10**:701-712.

LETTER

doi:10.1038/nature17172

Memory retrieval by activating engram cells in mouse models of early Alzheimer's disease

Dheeraj S. Roy[1], Autumn Arons[1,2], Teryn I. Mitchell[1], Michele Pignatelli[1], Tomás J. Ryan[1,2] & Susumu Tonegawa[1,2]

Alzheimer's disease (AD) is a neurodegenerative disorder characterized by progressive memory decline and subsequent loss of broader cognitive functions[1]. Memory decline in the early stages of AD is mostly limited to episodic memory, for which the hippocampus has a crucial role[2]. However, it has been uncertain whether the observed amnesia in the early stages of AD is due to disrupted encoding and consolidation of episodic information, or an impairment in the retrieval of stored memory information. Here we show that in transgenic mouse models of early AD, direct optogenetic activation of hippocampal memory engram cells results in memory retrieval despite the fact that these mice are amnesic in long-term memory tests when natural recall cues are used, revealing a retrieval, rather than a storage impairment. Before amyloid plaque deposition, the amnesia in these mice is age-dependent[3–5], which correlates with a progressive reduction in spine density of hippocampal dentate gyrus engram cells. We show that optogenetic induction of long-term potentiation at perforant path synapses of dentate gyrus engram cells restores both spine density and long-term memory. We also demonstrate that an ablation of dentate gyrus engram cells containing restored spine density prevents the rescue of long-term memory. Thus, selective rescue of spine density in engram cells may lead to an effective strategy for treating memory loss in the early stages of AD.

AD is the most common cause of brain degeneration, and typically begins with impairments in cognitive functions[1]. Most research has focused on understanding the relationship between memory impairments and the formation of two pathological hallmarks seen in the late stages of AD: extracellular amyloid plaques and intracellular aggregates of tau protein[1,2]. The early phases of AD have received relatively less attention, although synaptic phenotypes have been identified as major correlates of cognitive impairments in both human patients and mouse models[3,6]. Several studies have suggested that the episodic memory deficit of AD patients is due to ineffective encoding of new information[7–9]. However, since the cognitive measures used in these studies rely on memory retrieval, it is not possible to discriminate rigorously between impairments in information storage and disrupted retrieval of stored information. This issue has an important clinical implication: if the amnesia is due to retrieval impairments, memory could be restored by technologies involving targeted brain stimulation.

A mouse model of AD (hereafter referred to as 'AD mice')[10] overexpresses the delta exon 9 variant of presenilin 1 (PS1; also known as PSEN1), in combination with the Swedish mutation of β-amyloid precursor (APP). Consistent with previous reports[3–5], 9-month-old AD mice showed severe plaque deposition across multiple brain regions (Fig. 1a), specifically in the dentate gyrus (DG) (Fig. 1b) and medial entorhinal cortex (EC) (Fig. 1c); in contrast, 7-month-old AD mice lacked amyloid plaques (Fig. 1d and Extended Data Fig. 1a–d). Focusing on these two age groups of AD mice, we quantified short-term (1 h; STM) and long-term (24 h; LTM) memory formation using contextual fear conditioning (CFC) (Fig. 1e). Nine-month-old AD mice were impaired in both STM and LTM, which suggested a deficit in memory encoding (Fig. 1k–o). By contrast, 7-month-old AD mice showed normal levels of training-induced freezing (Fig. 1f) and normal STM (Fig. 1g), but were impaired in LTM (Fig. 1h). Neither control nor 7-month-old AD mice displayed freezing behaviour in a neutral context (Fig. 1i). In the DG of 7-month-old AD mice, the levels of cells that were immediate early gene c-Fos-positive after CFC training were normal, but were lower compared with control mice after LTM tests (Fig. 1j). Motor behaviours and the density of DG granule cells were normal in these mice (Extended Data Fig. 1e–k). Thus, these behavioural- and cellular-level observations confirmed that 7-month-old AD mice serve as a mouse model of early AD regarding memory impairments.

Recently, molecular, genetic and optogenetic methods to identify neurons that hold traces, or engrams, of specific memories have been established[11,12]. Using this technology, several groups have demonstrated that DG neurons activated during CFC learning are both sufficient[11–14] and necessary[15] for subsequent memory retrieval. In addition, our recent study found that engram cells under protein-synthesis-inhibitor-induced amnesia were capable of driving acute memory recall if they were directly activated optogenetically[14]. Here, we applied this memory engram cell identification and manipulation technology to 7-month-old AD mice to determine whether memories could be retrieved in the early stages of the disease. Because it is known that the EC–hippocampus (HPC) network is among the earliest to show altered synaptic/dendritic properties and these alterations have been suggested to underlie the memory deficits in early AD[16,17], we focused on labelling the DG component of CFC memory engram cells of 7-month-old AD mice using a double adeno-associated virus (AAV) system (Fig. 1p, q and Methods). Although on a doxycycline (DOX) diet DG neurons completely lacked channelrhodopsin 2 (ChR2)–enhanced yellow fluorescent protein (eYFP) labelling, 1 day off DOX was sufficient to permit robust ChR2–eYFP expression in control mice (Fig. 1r, s and Extended Data Fig. 2a–c), as well as in 7-month-old AD mice (Fig. 1t, u).

As expected, these engram-labelled early AD mice were amnesic a day after CFC training (Fig. 1v). But, remarkably, these mice froze on the next day in a distinct context (context B) as robustly as equivalently treated control mice in response to blue light stimulation of the engram cells (Fig. 1w). This light-specific freezing was not observed using on-DOX mice (Extended Data Fig. 2d–f). A natural recall test conducted on the third day in the conditioning context (context A) revealed that the observed optogenetic engram reactivation did not restore memory recall by natural cues in early AD mice (Fig. 1x). This was the case even after multiple rounds of light activation of the engram cells (Extended Data Fig. 3). We replicated the successful optogenetic rescue of memory recall in two other models of early AD: a triple transgenic line obtained by mating *c-Fos-tTA* mice with double-transgenic APP/PS1 mice (Extended Data Fig. 4a–g) and a widely used triple-transgenic AD model[18] (PS1/APP/tau (also known as MAPT); Extended Data Fig. 4h–m). These data show that DG engram cells in 7-month-old mouse models of early AD are sufficient to induce memory recall upon optogenetic reactivation, which indicates a deficit of memory retrievability during early AD-related memory loss.

[1]RIKEN-MIT Center for Neural Circuit Genetics at the Picower Institute for Learning and Memory, Department of Biology and Department of Brain and Cognitive Sciences, Massachusetts Institute of Technology, Cambridge, Massachusetts 02139, USA. [2]Howard Hughes Medical Institute, Massachusetts Institute of Technology, Cambridge, Massachusetts 02139, USA.

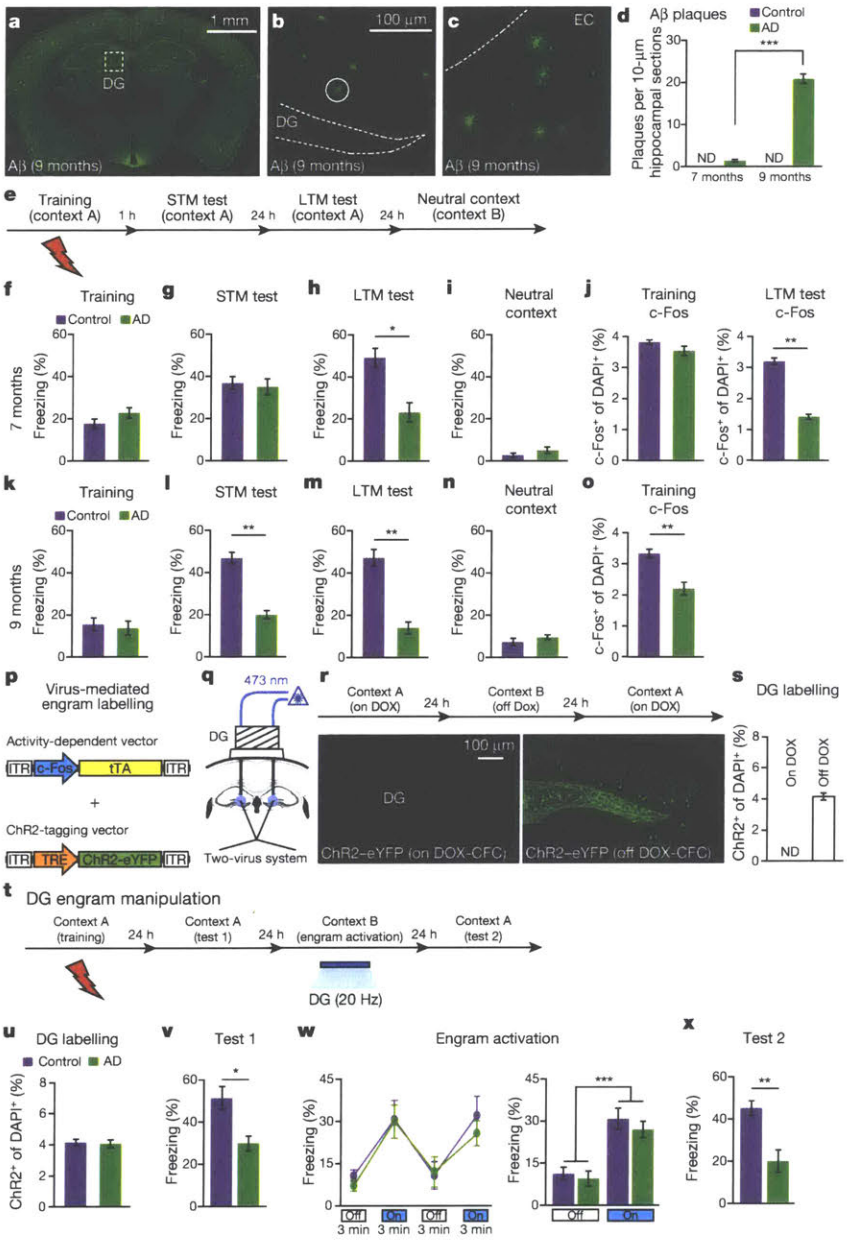

Figure 1 | Optogenetic activation of memory engrams restores fear memory in early AD mice. a–c, Amyloid-β (Aβ) plaques in 9-month-old AD mice (**a**), in the DG (**b**), and in the EC (**c**). **d**, Plaque counts in HPC sections ($n = 4$ mice per group). ND, not detected. **e**, CFC behavioural schedule ($n = 10$ mice per group). **f–i**, Freezing levels of 7-month-old AD groups during training (**f**), STM test (**g**), LTM test (**h**) or exposure to neutral context (**i**). **j**, c-Fos$^+$ cell counts in the DG of 7-month-old mice after CFC training or LTM test, represented in **f**, **h** ($n = 4$ mice per group). DAPI, 4′,6-diamidino-2-phenylindole. **k–n**, Freezing levels of 9-month-old AD mice during training (**k**), STM test (**l**), LTM test (**m**) or exposure to neutral context (**n**). **o**, c-Fos$^+$ cell counts in the DG of 9-month-old mice ($n = 3$ mice per group) after CFC training represented in **k**. **p**, Virus-mediated engram labelling strategy using a cocktail of AAV$_9$-c-Fos-tTA and AAV$_9$-TRE-ChR2-eYFP. **q**, AD mice were injected with the two viruses bilaterally and implanted with an optic fibre bilaterally into the DG. **r**, Behavioural schedule and DG engram cell labelling (see Methods). **s**, ChR2–eYFP$^+$ cell counts from DG sections shown in **r** ($n = 3$ mice per group). **t**, Behavioural schedule for optogenetic activation of DG engram cells. **u**, ChR2–eYFP$^+$ cell counts from 7-month-old mice ($n = 5$ mice per group). **v**, Memory recall in context A 1 day after training (test 1, $n = 9$ mice per group). **w**, Freezing by blue light stimulation (left). Average freezing for two light-off and light-on epochs (right). **x**, Memory recall in context A 3 days after training (test 2). Statistical comparisons are performed using unpaired *t*-tests; $^*P < 0.05$, $^{**}P < 0.01$, $^{***}P < 0.001$. Data are presented as mean ± standard error of the mean (s.e.m.).

Reduced dendritic spines have been implicated in memory impairments of AD[3]. In addition, our recent study of protein-synthesis-inhibitor-induced amnesia found reduced engram-cell-specific dendritic spine density[14]. We detected an age-dependent (Extended Data Fig. 5a) decrease in dendritic spine density of DG engram cells in early AD mice (Fig. 2a–c), showing that the long-term memory impairments of early AD correlate with dendritic spine deficits of DG engram cells (Extended Data Fig. 5b). The inability to generate newborn neurons in the DG could play a part in the development of AD-specific cognitive deficits[19]. However, early AD mice showed similar levels of neurogenesis in the DG compared with control mice, which were quantified using doublecortin (DCX) staining (Extended Data Fig. 1l–q). We recently proposed that the persistent cellular connectivity between multiple engram cell ensembles is a fundamental mechanism of memory information

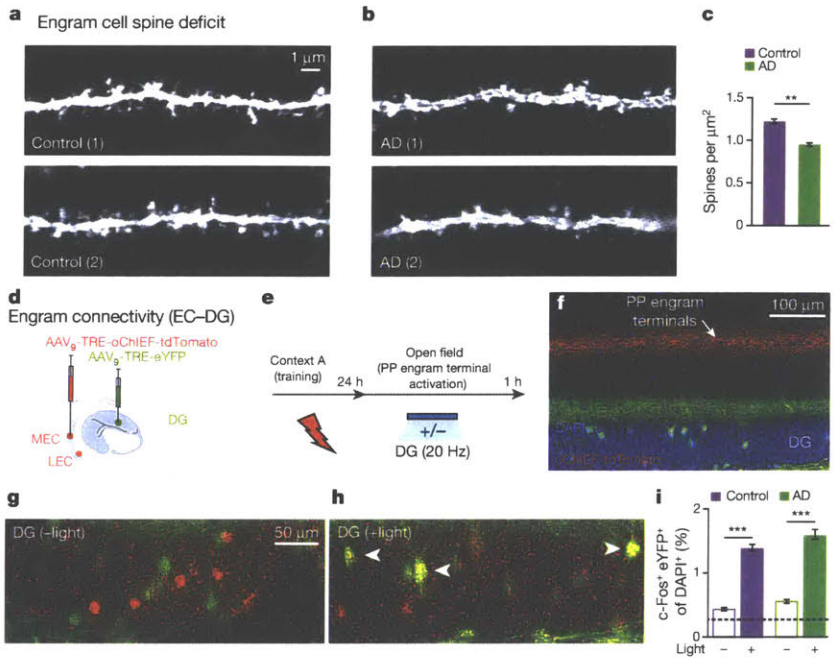

Figure 2 | Neural correlates of amnesia in early AD mice. a, **b**, Images showing dendritic spines from DG engram cells of control (**a**) and AD (**b**) groups. **c**, Average spine density showing a decrease in AD mice ($n = 7{,}032$ spines) compared with controls ($n = 9{,}437$ spines, $n = 4$ mice per group). **d**, For engram connectivity, MEC/LEC and DG cells were injected with virus cocktails. **e**, Engram connectivity behavioural schedule. Mice ($n = 4$ per group) were either given a natural exploration session (−) or a PP engram terminal stimulation session (+) in an open field. **f**, Image showing simultaneous labelling of engram terminals (red) and engram cells (green). Green terminals reflect mossy cell axons. **g**, **h**, Images showing c-Fos$^+$/eYFP$^+$ overlap in the DG. **i**, c-Fos$^+$/eYFP$^+$ counts from control and AD mice. Chance overlap (0.24) was calculated (see Methods) and indicated by the dashed line. Statistical comparisons are performed using unpaired *t*-tests; $^{**}P < 0.01$, $^{***}P < 0.001$. Data are presented as mean ± s.e.m.

retention[14]. We labelled putative CFC memory engram cells in both medial EC (MEC) and lateral EC (LEC) with oChIEF[20] (a variant of ChR2) and simultaneously labelled CFC memory engram cells in the DG with eYFP (Fig. 2d). With this procedure, perforant path (PP) terminals are also labelled with oChIEF (Fig. 2e, f). One day after foot-shocks, we optogenetically activated these terminals and quantified the overlap between putative DG engram cells (that is, eYFP$^+$, green) and DG cells in which the endogenous c-Fos (red) had been activated by the optogenetic activation of oChIEF$^+$ PP terminals. Both control and early AD mice showed above-chance and indistinguishable levels of c-Fos$^+$/eYFP$^+$ overlap, indicating that the preferential functional connectivity between engram cells is maintained in the early AD mice (Fig. 2g–i).

We then hypothesized that the reversal of dendritic spine deficits in DG engram cells of early AD mice may rescue long-term memory. To investigate this possibility, we took advantage of previous findings that spine formation can be induced rapidly by long-term potentiation (LTP)[21,22] and that LTP can be induced *in vivo* using light activation of oChIEF[23]. We validated learning-dependent labelling, with oChIEF, of neurons in the MEC (Fig. 3a–c and Extended Data Fig. 6a–c) and LEC (Fig. 3d) as well as PP terminals in the DG (Fig. 3e, f). *In vivo* extracellular recording upon light stimulation of oChIEF$^+$ EC axonal terminals in the DG showed a reliable spiking response of DG cells in anaesthetized control mice (Fig. 3g). Furthermore, in HPC slices from control mice we successfully induced LTP in DG cells using a previously established optical LTP protocol[23] (Fig. 3h–j). These biocytin-filled DG cells revealed an increase in spine density after *in vitro* optical LTP (Extended Data Fig. 6d).

In early AD mice, *in vivo* application of the engram-specific optical LTP protocol restored spine density of DG engram cells to control levels (AD + 100 Hz group; Fig. 3k, l). Furthermore, this spine restoration in early AD mice correlated with amelioration of long-term memory impairments observed during recall by natural cues (Fig. 3m), an effect that persisted for at least 6 days after training (AD rescue + diphtheria toxin receptor (DTR) + saline group; Fig. 3p). The LTP-induced spine restoration and behavioural deficit rescue were protein-synthesis dependent (Extended Data Fig. 7). The rescued memory was context-specific (Extended Data Fig. 8a). In addition, long-term memory recall of age-matched control mice was unaffected by this optical LTP protocol (Extended Data Fig. 8b). By contrast, applying the optical LTP protocol to a large portion of excitatory PP terminals in the DG (that is, with no restriction to the PP terminals derived from EC engram cells) did not result in long-term memory rescue in early AD mice (Extended Data Fig. 9). To confirm the correlation between restoration of spine density of DG engram cells and amelioration of long-term memory impairments, which were both induced by the optical LTP protocol, we compared the overlap of natural-recall-cue-induced c-Fos$^+$ cells and CFC-training-labelled DG engram cells after an application of the engram-specific LTP protocol to early AD mice (Fig. 3n). Early AD mice that did not receive the optical LTP protocol showed low levels of c-Fos$^+$/eYFP$^+$ overlap compared with control mice upon natural recall cue delivery. By contrast, early AD mice that went through the optical LTP protocol showed c-Fos$^+$/eYFP$^+$ overlap similar to that of control mice (Fig. 3n). Thus, these data suggest that spine density restoration in DG engram cells contributes to the rescue of long-term memory in early AD mice.

Because of the highly redundant connectivity between the EC and DG[24], it is possible that the extensive optical LTP protocol also augmented spine density in some non-engram DG cells. To establish a link between the spine rescue in DG engram cells and the behavioural rescue of early AD mice, we developed an engram-specific ablation[25] virus. We confirmed that this DTR-mediated method efficiently ablated DG engram cells after diphtheria toxin (DT) administration (Fig. 3o), while leaving the nearby DG mossy cells intact (Extended Data Fig. 10). By simultaneously labelling axonal terminals of PP with oChIEF and DG engram cells with DTR, we examined the effect of DG engram cell ablation after optical LTP-induced behavioural rescue (Fig. 3p). Within-animal comparisons (test 1 versus test 2) showed a decrease in freezing behaviour of LTP-rescued AD mice in which DG engram cells were ablated. These data strengthen the link between DG engram cells with restored spine density and long-term behavioural rescue in early AD mice.

To examine whether the optical LTP-induced behavioural rescue could be applied to DG engram cells from other learning experiences, we labelled memory engrams for inhibitory avoidance or novel object location in early AD mice (Fig. 4a). Early AD mice showed memory impairments in inhibitory avoidance memory and novel object location spatial memory (Fig. 4b, c). Optical LTP-induced spine rescue at the PP–DG engram synapses was sufficient to reverse long-term memory impairments of early AD mice in both behavioural paradigms, thus demonstrating the versatility of our engram-based intervention.

Previous studies that examined the early stages of AD found correlations between memory impairments and synaptic pathology at the

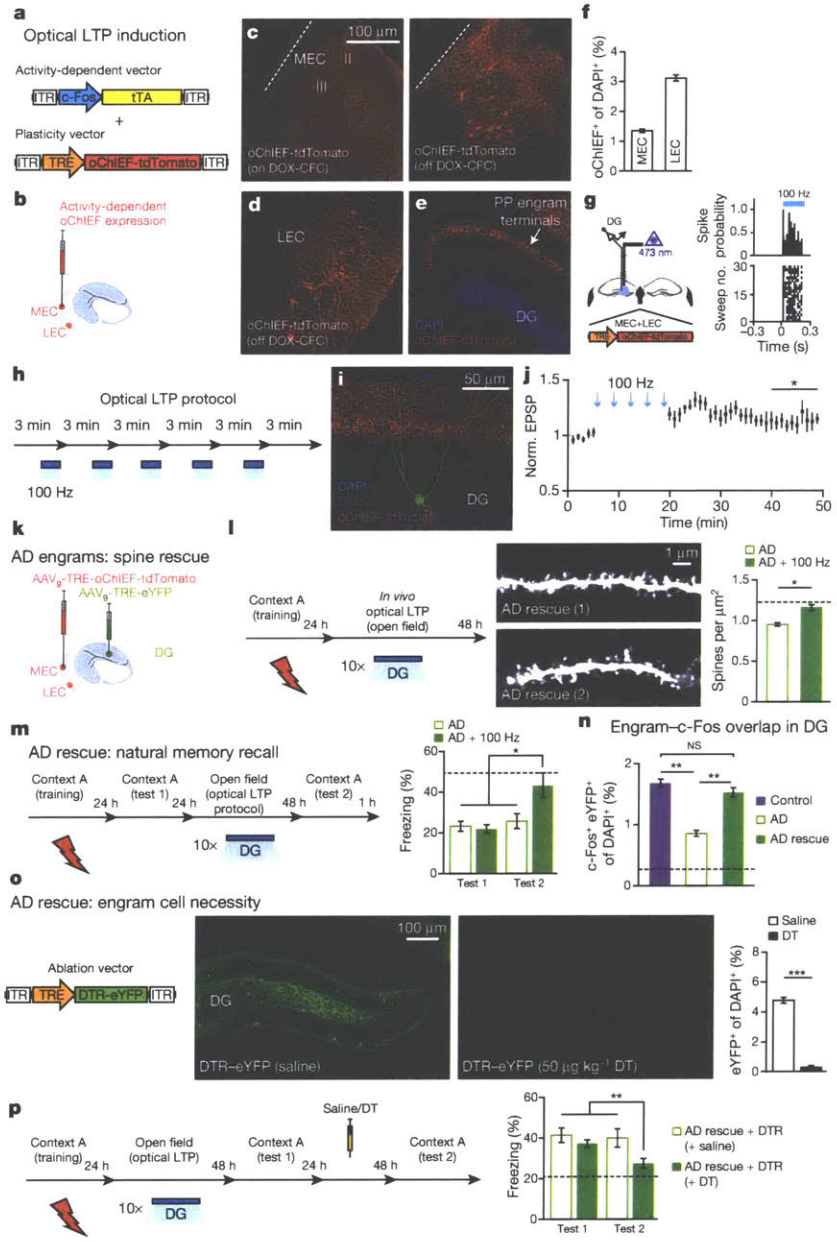

Figure 3 | Reversal of engram-specific spine deficits rescues memory in early AD mice. **a**, Engram-specific optical LTP using two viruses. **b**, Virus cocktail injected into MEC/LEC. **c**–**e**, Images showing oChIEF labelling 24 h after CFC: in MEC on DOX (left; **c**) and off DOX (right; **c**); in LEC off DOX (**d**); in DG off DOX (sagittal; **e**). Scale bar shown in **c** applies to **d** and **e**. **f**, oChIEF$^+$ cell counts ($n = 3$ mice per group). **g**, *In vivo* spiking of DG neurons in response to 100 Hz light applied to PP terminals. **h**, Optical LTP protocol[23]. **i**, **j**, *In vitro* responses of DG cells after optical LTP. Image showing biocytin-filled DG cell receiving oChIEF$^+$ PP terminals (coronal; **i**). Normalized (Norm.) excitatory post-synaptic potentials (EPSPs) showing a 10% increase in amplitude ($n = 6$ cells; **j** and Methods). **k**, For *in vivo* optical LTP at EC–DG synapses, MEC/LEC and DG cells were injected with virus cocktails. **l**, Protocol for *in vivo* spine restoration of DG engram cells in AD mice (left). Images showing dendritic spines of DG engram cells after LTP (middle). A two-way analysis of variance (ANOVA) followed by Bonferroni post-hoc tests revealed a spine density restoration in AD + 100 Hz mice ($F_{1,211} = 7.21$, $P < 0.01$, 13,025 spines, $n = 4$ mice per group; right). Dashed line represents control mice spine density (1.21). **m**, Behavioural schedule for memory rescue in AD mice (left). A two-way ANOVA with repeated measures followed by Bonferroni post-hoc tests revealed restored freezing in AD + 100 Hz mice ($F_{1,36} = 4.95$, $P < 0.05$, $n = 10$ mice per group; right). Dashed line represents control mice freezing (48.53). **n**, After rescue, mice were perfused for c-Fos$^+$/eYFP$^+$ overlap cell counts. Chance was estimated at 0.22. NS, not significant. **o**, Construct for ablation of engram cells using DTR (left). Images showing DG engram cells after saline/DT administration (middle). DTR–eYFP cell counts ($n = 5$ mice per group; right). **p**, Behavioural schedule testing the necessity of engram cells after spine restoration (left). Memory recall showed less freezing of AD mice treated with DT (AD rescue + DTR + DT) compared with saline-treated mice ($n = 9$ mice per group; right). Dashed line represents freezing of non-stimulated early AD mice (20.48). Unless specified, statistical comparisons are performed using unpaired *t*-tests; $^*P < 0.05$, $^{**}P < 0.01$, $^{***}P < 0.001$. Data are presented as mean ± s.e.m.

EC PP input into the DG[3,4,6]. It has been proposed that these early cognitive deficits are a failure of memory encoding on the basis of behavioural observations in human patients[8,9]. However, we have shown that optogenetic activation of HPC cells active during learning elicits memory recall in mouse models of early AD. To our knowledge, this is the first rigorous demonstration that memory failure in early AD models reflects an impairment in the retrieval of information. Further support for a memory retrieval impairment in early AD comes from the fact that impairments are in LTM (at least 1 day long), but not in STM (~1 h after training), which is consistent with a retrieval deficit. The retrieval deficit in early AD models is similar to memory deficits observed in amnesia induced by impairing memory consolidation via protein synthesis inhibitors[14]. The underlying mechanism of memory failure in early AD patients may not necessarily parallel the molecular and circuit impairments observed in mouse models of early AD. For instance, some early AD patients can exhibit amyloid plaque deposition years before the onset of cognitive decline[9]. However, converging data on the underlying mechanism for genetically and pharmacologically induced amnesia in animal models increase the possibility that similar memory-retrieval-based failures may also operate in an early stage of AD patients. While we have shown that amnesia in early AD mice is a deficit of memory retrieval, it remains possible that the long-term maintenance of memory storage may also gradually become compromised as the disease proceeds from the early stage to more advanced stages, and eventually lost with neuronal degeneration. Further research will investigate these possibilities.

Our conclusions apply to episodic memory, which involves processing by HPC and other medial temporal lobe structures. In the literature[9], it is widely recognized that early AD patients exhibit non-episodic memory deficits as well, which would involve brain structures other than the medial temporal lobe. Additional work is required to examine the mechanisms underlying cognitive impairments in these other types of memories. Nevertheless, our findings already contribute to a better understanding of memory retrieval deficits in several cases of early AD, and may apply to other pathological conditions, such as Huntington's disease[8], in which patients show difficulty in memory recall.

Consistent with several studies highlighting the importance of dendritic spines[3,6,14,26] in relation to memory processing, we observed an engram-cell-specific decrease in spine density that correlated with

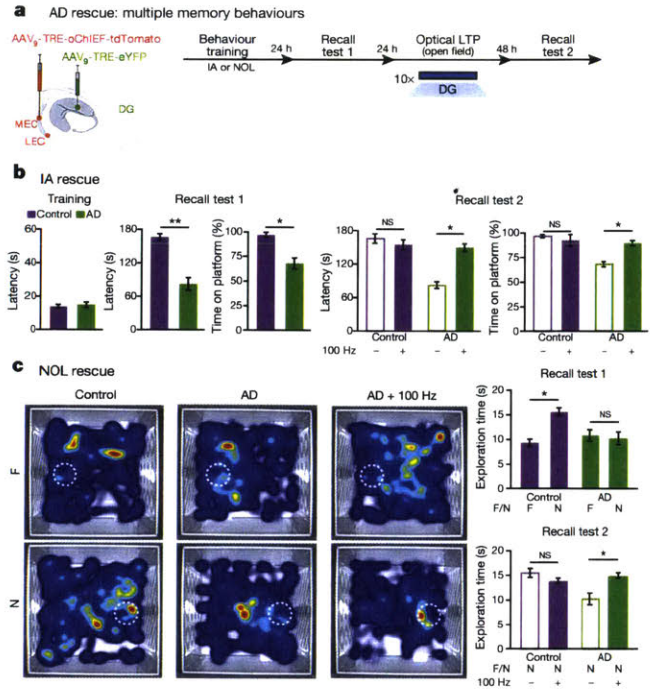

Figure 4 | Recovery of multiple types of HPC-dependent memories from amnesia in early AD. a, MEC/LEC and DG cells were injected with virus cocktails (left). Behavioural schedule for engram labelling (right). **b**, Inhibitory avoidance (IA) long-term rescue ($n = 10$ mice per group). Recall test 1 showed decreased latency and time on platform for AD mice. A two-way ANOVA with repeated measures followed by Bonferroni post-hoc tests revealed a recovery of IA memory in early AD mice (latency: $F_{1,27} = 25.22$, $P < 0.001$; time on platform: $F_{1,27} = 6.46$, $P < 0.05$; recall test 2). **c**, Novel object location (NOL) long-term rescue ($n = 15$ mice per group). Average heat maps showing exploration time for familiar (F) or novel (N) locations (left or right, respectively). White circles represent object location. Recall test 1 showed comparable exploration of familiar locations by control and AD mice; however, AD mice showed decreased exploration of novel locations. A two-way ANOVA with repeated measures followed by Bonferroni post-hoc tests revealed a recovery of NOL memory in early AD mice ($F_{1,56} = 5.87$, $P < 0.05$; recall test 2). Unless specified, statistical comparisons are performed using unpaired t-tests; $^{*}P < 0.05$, $^{**}P < 0.01$. Data are presented as mean ± s.e.m. NS, not significant.

memory deficits in early AD. Natural rescue of memory recall in early AD mice required the DG engram cells in which synaptic density deficits have been restored by *in vivo* optical LTP protocols applied to the EC cells activated during learning. By contrast, the application of optical LTP protocols to a much wider array of excitatory EC cells projecting to the DG, which may be analogous to deep brain stimulation, did not rescue memory in AD mice. A potential explanation for this observation is that DG granule cells may contribute to a variety of memories through their partially overlapping engram cell ensembles in a competitive manner, and that activation of a large number of these ensembles simultaneously may interfere with a selective activation of an individual ensemble. Thus, activation of a more targeted engram cell ensemble may be a key requirement for effective retrieval of the specific memory, which is difficult to achieve with the current deep brain stimulation strategy.

Genetic manipulations of specific neuronal populations can have profound effects on cognitive impairments of AD[27]. We propose that strategies applied to engram circuits can support long-lasting improvements in cognitive functions, which may provide insights and therapeutic value for future approaches that rescue memory in AD patients.

Online Content Methods, along with any additional Extended Data display items and Source Data, are available in the online version of the paper; references unique to these sections appear only in the online paper.

Received 6 August 2015; accepted 28 January 2016.
Published online 16 March 2016.

1. Selkoe, D. J. Alzheimer's disease: genes, proteins, and therapy. *Physiol. Rev.* **81,** 741–766 (2001).
2. Selkoe, D. J. Alzheimer's disease is a synaptic failure. *Science* **298,** 789–791 (2002).
3. Jacobsen, J. S. *et al.* Early-onset behavioral and synaptic deficits in a mouse model of Alzheimer's disease. *Proc. Natl Acad. Sci. USA* **103,** 5161–5166 (2006).
4. Hsia, A. Y. *et al.* Plaque-independent disruption of neural circuits in Alzheimer's disease mouse models. *Proc. Natl Acad. Sci. USA* **96,** 3228–3233 (1999).
5. Mucke, L. *et al.* High-level neuronal expression of $A\beta_{1-42}$ in wild-type human amyloid protein precursor transgenic mice: synaptotoxicity without plaque formation. *J. Neurosci.* **20,** 4050–4058 (2000).
6. Terry, R. D. *et al.* Physical basis of cognitive alterations in Alzheimer's disease: synapse loss is the major correlate of cognitive impairment. *Ann. Neurol.* **30,** 572–580 (1991).
7. Granholm, E. & Butters, N. Associative encoding and retrieval in Alzheimer's and Huntington's disease. *Brain Cogn.* **7,** 335–347 (1988).
8. Hodges, J. R., Salmon, D. P. & Butters, N. Differential impairment of semantic and episodic memory in Alzheimer's and Huntington's diseases: a controlled prospective study. *J. Neurol. Neurosurg. Psychiatry* **53,** 1089–1095 (1990).
9. Weintraub, S., Wicklund, A. H. & Salmon, D. P. The neuropsychological profile of Alzheimer disease. *Cold Spring Harb. Perspect. Med.* **2,** a006171 (2012).
10. Jankowsky, J. L. *et al.* Mutant presenilins specifically elevate the levels of the 42 residue β-amyloid peptide *in vivo*: evidence for augmentation of a 42-specific γ secretase. *Hum. Mol. Genet.* **13,** 159–170 (2004).
11. Liu, X. *et al.* Optogenetic stimulation of a hippocampal engram activates fear memory recall. *Nature* **484,** 381–385 (2012).
12. Ramirez, S. *et al.* Creating a false memory in the hippocampus. *Science* **341,** 387–391 (2013).
13. Redondo, R. L. *et al.* Bidirectional switch of the valence associated with a hippocampal contextual memory engram. *Nature* **513,** 426–430 (2014).
14. Ryan, T. J., Roy, D. S., Pignatelli, M., Arons, A. & Tonegawa, S. Engram cells retain memory under retrograde amnesia. *Science* **348,** 1007–1013 (2015).
15. Denny, C. A. *et al.* Hippocampal memory traces are differentially modulated by experience, time, and adult neurogenesis. *Neuron* **83,** 189–201 (2014).
16. Harris, J. A. *et al.* Transsynaptic progression of amyloid-β-induced neuronal dysfunction within the entorhinal-hippocampal network. *Neuron* **68,** 428–441 (2010).
17. Hyman, B. T., Van Hoesen, G. W., Kromer, L. J. & Damasio, A. R. Perforant pathway changes and the memory impairment of Alzheimer's disease. *Ann. Neurol.* **20,** 472–481 (1986).
18. Oddo, S. *et al.* Triple-transgenic model of Alzheimer's disease with plaques and tangles: intracellular Aβ and synaptic dysfunction. *Neuron* **39,** 409–421 (2003).
19. Rodríguez, J. J. *et al.* Impaired adult neurogenesis in the dentate gyrus of a triple transgenic mouse model of Alzheimer's disease. *PLoS One* **3,** e2935 (2008).
20. Lin, J. Y., Lin, M. Z., Steinbach, P. & Tsien, R. Y. Characterization of engineered channelrhodopsin variants with improved properties and kinetics. *Biophys. J.* **96,** 1803–1814 (2009).
21. Maletic-Savatic, M., Malinow, R. & Svoboda, K. Rapid dendritic morphogenesis in CA1 hippocampal dendrites induced by synaptic activity. *Science* **283,** 1923–1927 (1999).
22. Engert, F. & Bonhoeffer, T. Dendritic spine changes associated with hippocampal long-term synaptic plasticity. *Nature* **399,** 66–70 (1999).
23. Nabavi, S. *et al.* Engineering a memory with LTD and LTP. *Nature* **511,** 348–352 (2014).
24. Tamamaki, N. & Nojyo, Y. Projection of the entorhinal layer II neurons in the rat as revealed by intracellular pressure-injection of neurobiotin. *Hippocampus* **3,** 471–480 (1993).
25. Zhan, C. *et al.* Acute and long-term suppression of feeding behavior by POMC neurons in the brainstem and hypothalamus, respectively. *J. Neurosci.* **33,** 3624–3632 (2013).
26. Tonegawa, S., Liu, X., Ramirez, S. & Redondo, R. Memory engram cells have come of age. *Neuron* **87,** 918–931 (2015).
27. Cissé, M. *et al.* Reversing EphB2 depletion rescues cognitive functions in Alzheimer model. *Nature* **469,** 47–52 (2011).

Acknowledgements We thank X. Liu for the c-Fos-tTA construct; S. Huang, T. Okuyama and T. Kitamura for help with experiments; W. Yu, S. LeBlanc and X. Zhou for technical assistance; L. Brenner for proofreading; and all members of the Tonegawa laboratory for their support. We thank M. Luo for sharing the DTR coding sequence. This work was supported by the RIKEN Brain Science Institute, the Howard Hughes Medical Institute, and the JPB Foundation (to S.T.).

Author Contributions D.S.R. and S.T. contributed to the study design. D.S.R., A.A., T.I.M., M.P. and T.J.R. contributed to the data collection and interpretation. D.S.R. cloned all constructs. D.S.R. and A.A. conducted the surgeries, behaviour experiments and histological analyses. D.S.R. and S.T. wrote the paper. All authors discussed and commented on the manuscript.

Author Information Reprints and permissions information is available at www.nature.com/reprints. The authors declare no competing financial interests. Readers are welcome to comment on the online version of the paper. Correspondence and requests for materials should be addressed to S.T. (tonegawa@mit.edu).

SOCIAL MEMORY

Ventral CA1 neurons store social memory

Teruhiro Okuyama,[1] Takashi Kitamura,[1] Dheeraj S. Roy,[1] Shigeyoshi Itohara,[2] Susumu Tonegawa[1,2,3]*

The medial temporal lobe, including the hippocampus, has been implicated in social memory. However, it remains unknown which parts of these brain regions and their circuits hold social memory. Here, we show that ventral hippocampal CA1 (vCA1) neurons of a mouse and their projections to nucleus accumbens (NAc) shell play a necessary and sufficient role in social memory. Both the proportion of activated vCA1 cells and the strength and stability of the responding cells are greater in response to a familiar mouse than to a previously unencountered mouse. Optogenetic reactivation of vCA1 neurons that respond to the familiar mouse enabled memory retrieval and the association of these neurons with unconditioned stimuli. Thus, vCA1 neurons and their NAc shell projections are a component of the storage site of social memory.

The ability to recognize and memorize familiar conspecifics (social memory) is crucial for animals that exhibit social interactions (*1*, *2*). Lesion and recording studies in humans and monkeys have suggested that the medial temporal lobe or the hippocampus plays an essential role in social memory (*3*–*6*). In mice, most early lesion or recording studies concluded that the hippocampus is dispensable for recognizing a familiar conspecific (*7*–*9*), whereas a few recent studies suggested the contrary (*10*–*12*). Although these human and animal studies identified brain areas important for social memory, the precise cellular populations storing this type of memory and their essential circuits are unknown.

The intrinsic pattern of connectivity in the hippocampus is fairly invariable along the longitudinal axis (*13*) across many species (*14*). However, the afferent and efferent connectivity along this axis changes from one end to the other, suggesting that dorsal and ventral hippocampus of rodents (corresponding to posterior and anterior hippocampus, respectively, of primates) may have distinct functions (*14*, *15*). It is well established that the rodent dorsal hippocampus (dHPC) plays an essential role in episodic memory (*15*). In contrast, the memory function of the ventral hippocampus (vHPC) is poorly known. In this study, we generated a transgenic mouse line, transient receptor potential channel 4–Cre (Trpc4-Cre), to investigate the potential role and physiological characteristics of the pyramidal neurons in the CA1 subfield of the ventral hippocampus (vCA1) in social memory.

Mice naturally spend more time interacting with a previously unencountered ("novel") mouse than a familiar one (*16*); social memory can be quantified by measuring the relative interaction durations with a novel and a familiar mouse under free-choice conditions (social discrimination test or SDT) (Fig. 1, A and B). This ability to socially discriminate between the novel and familiar mice persisted for 30 min after a familiarization session, but disappeared by 24 hours (Fig. 1C). To investigate the potential role of vHPC and dHPC in social memory, we targeted bilateral injections of adeno-associated virus 8 (AAV8)–calcium/calmodulin-dependent protein kinase II (CaMKII):eArchT–enhanced yellow fluorescent protein (EYFP) and optic fiber implants to vCA1 or dorsal CA1 (dCA1) of wild-type mice (Fig. 1D). Expression of eArchT-EYFP was abundant in vCA1 or dCA1, although it was also observed to a lesser extent in CA3 and the dentate gyrus (DG) (Fig. 1, E and F). Optogenetic cell body inhibition of vHPC but not dHPC resulted in a deficit in the SDT (Fig. 1, G, H, O, and P). In the resident-intruder test (Fig. 1I and fig. S1), optogenetic inhibition of vHPC but not dHPC increased the sniffing duration toward a familiar intruder with no effect when a novel intruder was used (Fig. 1, J and K).

To identify downstream brain region(s) involved in social memory, we injected AAV9–tetracycline response element (TRE):channelrhodopsin-2 (ChR2)–EYFP into vCA1 of c-fos:tetracycline transactivator (tTA) mice to label neurons activated by social interaction (*17*, *18*). NAc shell, olfactory bulb (OB), and basolateral amygdala (BLA) were the major targets of the social interaction–specific vCA1 neuronal projections (fig. S2). Moreover, retrograde tracer cholera toxin subunit B (CTB)–Alexa555 injection into NAc, OB, or BLA labeled vCA1 but not dCA1 neurons (fig. S3). We then examined whether any of these projections are necessary for social memory by bilaterally injecting AAV8-CaMKII:eArchT-EYFP into vHPC and then optogenetically inhibiting axonal terminals of the vCA1 neurons in the respective target areas while the mice went through the SDT (Fig. 1, L to N, Q to S, and fig. S4). vHPC-NAc projections, but not vHPC-OB or vHPC-BLA, were essential for social discrimination behavior.

To more rigorously establish the functional role of the vCA1-NAc connection, we generated a CA1 pyramidal cell–specific Cre mouse line, Trpc4-Cre, that covers both vCA1 and dCA1 (fig. S5 and Methods). Using Trpc4-Cre mice, we selectively targeted vCA1 excitatory pyramidal neurons by injecting AAV9–human synapsin (hsyn): double-floxed inverse open reading frame (DIO)–eArchT-EYFP into vCA1 (Fig. 2, A and B, and fig. S6). We confirmed that the vCA1 neurons specifically project to the NAc shell but not to the NAc core, as identified by tyrosine hydroxylase (TH) staining (Fig. 2C). Further, CTB injection into NAc labeled the Trpc4-expressing deep layer (vCA1d), but not the superficial layer (vCA1s), pyramidal cells in vCA1 (Fig. 2B). Bilateral injections of AAV9-hsyn:DIO-eArchT-EYFP into the vCA1 of Trpc4-Cre mice and optogenetic inhibition of vCA1 cell body (Fig. 2, D and H) or its axonal terminals in NAc (Fig. 2, F, G, and J) resulted in a SDT deficit similar to that observed by vHPC-NAc inhibition (compare Fig. 2G with Fig. 1L). Optogenetic inhibition of vCA1 cell body during the familiarization period also led to a similar SDT defect (fig. S8). The possibility that these deficits are due to inhibition of dorsal CA2 (dCA2) activity is excluded because dCA2 is unlabeled with eArchT-EYFP in these mice (fig. S6C). dCA1 cell body inhibition was carried out using Wfs1-Cre mouse line expressing Cre in dCA1 but not in vCA1 or dCA2 (fig. S9) (*19*), which showed no deficit in a SDT (Fig. 2, E and I).

Inhibition of vCA1-NAc shell projections in Trpc4-Cre mice only during the interaction with a novel mouse did not affect the SDT (Fig. 2K, middle, and fig. S7A), whereas inhibition only during interaction with a familiar mouse disrupted social discrimination between the two mice (Fig. 2K, right, and fig. S7A). In contrast, when a pair of novel mice (Fig. 2L and fig. S7B), novel and familiar objects (fig. S10A), or novel and familiar contexts (fig. S10B) were used, there was no effect of vCA1-NAc shell inhibition.

We performed a SDT using Trpc4-Cre mice expressing AAV9–elongation factor 1α (EF1α):DIO-ChR2-EYFP in vCA1 while stimulating vCA1-NAc shell projections (Fig. 2, M and N, and fig. S7). Optogenetic activation of vCA1-NAc shell terminals during social interaction with a novel mouse disrupted the SDT (Fig. 2M, middle, and fig. S7C). With a pair of novel mice as the targets, stimulating vCA1-NAc shell projections during interactions with one of the novel mice greatly reduced the sniffing duration of that mouse compared to the other novel mouse (Fig. 2N and fig. S7D). Optogenetic activation of vCA1-NAc shell terminal during interaction with a familiar mouse had no effect in the SDT (Fig. 2M, right, and fig. S7C). Light activation did not affect the SDT in the EYFP control groups (fig. S11, A and B). With novel objects in place of mice, interactions of the test mouse were not affected by activation of the vCA1-NAc shell projections (fig. S11C).

[1]RIKEN–MIT Center for Neural Circuit Genetics at the Picower Institute for Learning and Memory, Department of Biology and Department of Brain and Cognitive Sciences, Massachusetts Institute of Technology (MIT), Cambridge, MA 02139, USA. [2]Brain Science Institute, RIKEN, Saitama, 351-0198, Japan. [3]Howard Hughes Medical Institute at MIT, Cambridge, MA 02139, USA.
*Corresponding author. Email: tonegawa@mit.edu

These results suggest that increased activation of the vCA1-NAc shell projections while the test mouse was in the novel-mouse domain disrupted the discriminatory social behavior by making the test mouse perceive the novel mouse as familiar.

To monitor the activity of vCA1 cells before and after the familiarization of a conspecific mouse, we injected AAV5-hsyn:DIO-GCaMP6f into the vCA1 of Trpc4-Cre mice and implanted a microprism grin lens targeting the pyramidal cell layer in vCA1 (Fig. 3, A and B; see Methods) (*20*, *21*). Ca^{2+} events in vCA1 neurons (Fig. 3, D and E) were recorded during exposure to two novel mice (A and B) in two consecutive 5-min sessions with mouse A and mouse B in counterbalanced positions, followed by a 5-min control session with no mice (Before group). The test mice were subjected to 3-day-long or 2-hour-long familiarization with mouse A, and the recording sequence was repeated after 30 min or 24 hours' separation (After-1 group) (Fig. 3F). For each neuron, we calculated a "preference score" based on the head position of the test mouse during each recorded Ca^{2+} event and identified vCA1 cells that exhibited selective activation by mouse A or mouse B (Fig. 3G and fig. S12). There was a significant increase in the proportion of mouse-A neurons after 3 days' or 2 hours' familiarization to mouse A (Fig. 3H). In contrast, there was no effect of familiarization on the proportion of cells active around mouse sampling locations in control sessions (No mouse). Similarly, familiarization had no effect on the proportion of mouse-A neurons in dCA1 of Wfs1-Cre transgenic mice (Fig. 3, C and H).

We determined the preference score of mouse-A neurons in Before group and After-1 group, as well as After-2 group that had a second 3-day familiarization. The preference scores of individual mouse-A neurons were not correlated between Before group and After-1 group, whereas these scores were correlated between After-1 group and After-2 group (Fig. 3, I to L). In addition, mouse-A neurons of After-1 group showed an increase in Ca^{2+} event probability around the mouse-A sniffing area, whereas mouse-A neurons did not show such an increase in Ca^{2+} probability in the mouse B sniffing area (Fig. 3M). Although the individual mouse-A neurons were still significantly activated by mouse A (Fig. 3, N

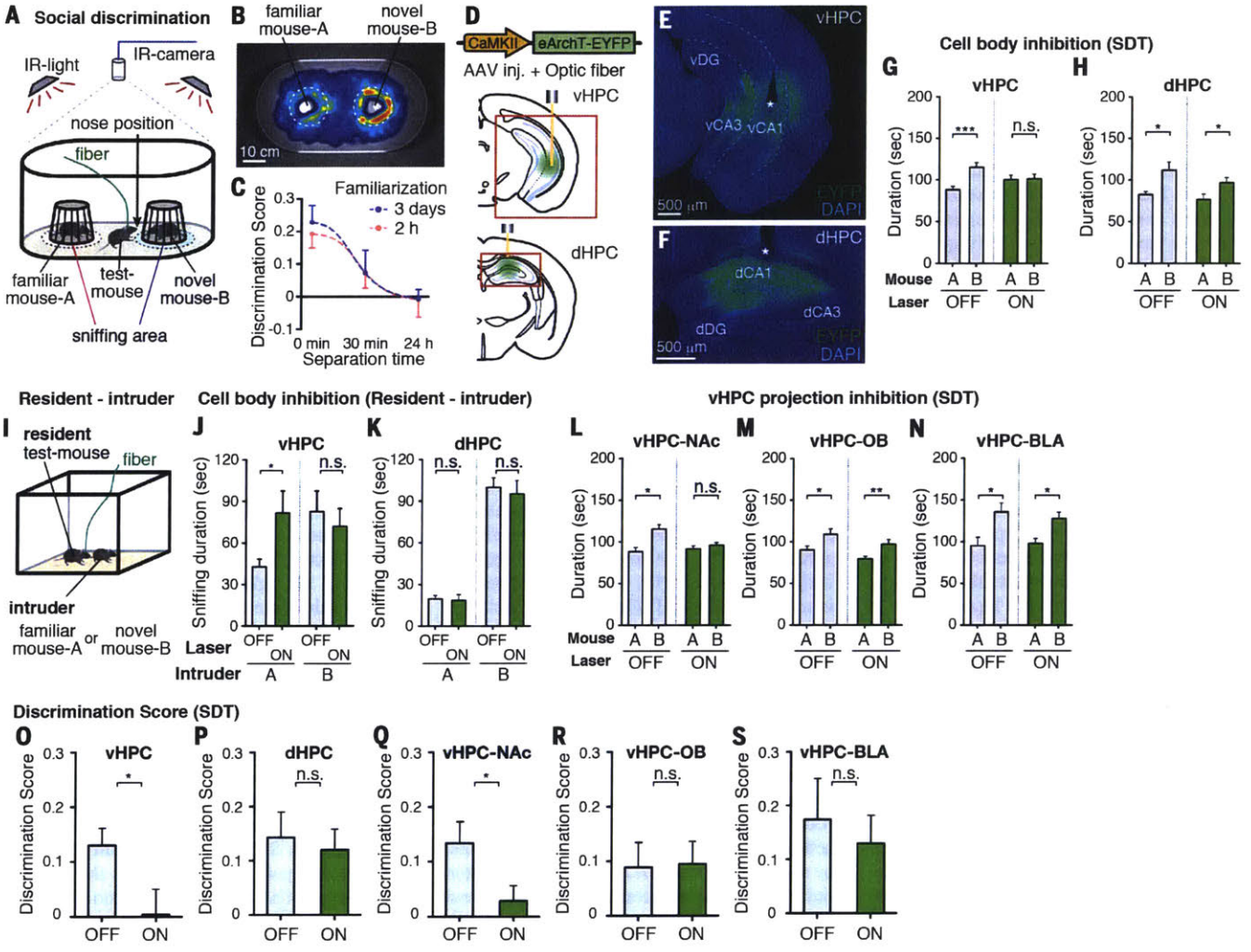

Fig. 1. vHPC in social memory. (**A**) Social discrimination test (SDT). (**B**) Representative heat map of test-mouse position during the SDT. (**C**) Kinetics of the SDT (see Methods). (**D** to **F**) Expression of AAV8-CaMKII:eArchT-EYFP (green) in vHPC or dHPC of wild-type mice. Asterisk indicates optic fiber tip. (**G** and **H**) Total duration in the sniffing area of familiar mouse A or novel mouse B during a SDT with inhibition of vHPC [(G) and (O), $n = 17$ mice] or dHPC [(H) and (P), $n = 14$ mice]. (**I**) Resident-intruder test. (**J** and **K**) Total sniffing duration by the resident to intruder [(J), vHPC inhibition; (K), dHPC inhibition] in familiar-intruder group (left) and novel-intruder group (right) ($n = 7$ mice, each group). (**L** to **N**) Total duration in sniffing area during a SDT observed in wild-type mice bilaterally injected with AAV8-CaMKII:eArchT-EYFP into vHPC and implanted with optical fibers targeting NAc [(L) and (Q), $n = 23$ mice], OB [(M) and (R), $n = 16$ mice], or BLA [(N) and (S), $n = 13$ mice]. (**O** to **S**) Comparison of discrimination scores. Green bars, laser on; gray bars, laser off. Significance for multiple comparisons: paired t test, $^*P < 0.05$; $^{**}P < 0.01$; $^{***}P < 0.001$, n.s., not significant. Data presented as mean ± SEM.

and O), Ca^{2+} event probability of these neurons in mouse-A area was reduced when the recordings were conducted after 24 hours' separation following familiarization (Fig. 3P).

The c-fos:tTA/TRE system permits labeling and manipulations of memory engram cells (*17*, *22*). We used this technology to characterize mouse-A neurons. First, we injected AAV9-TRE:fluorescent timer (FT)–Slow into the vCA1 of c-fos:tTA mice and induced expression of FT-Slow in neurons activated by social interaction (Fig. 4A). The fluorescence of FT-Slow changes naturally over time (*23*), from blue (pseudo-green), 12 hours after induction, to red, 72 hours after induction (Fig. 4, A and B, and fig. S13). Test mice interacted with mouse A twice, or with mouse A and then mouse B, with a 72-hour separation (Fig. 4, C and D). The proportions of reactivated cells with an overlap of red and blue signal was significantly higher in test mice exposed to the same mouse A twice, versus those exposed to mouse A followed by mouse B (Fig. 4E and fig. S13). A similar quantitative analysis of vCA1 reactivation using H2B-EGFP [nuclear localized EGFP (enhanced green fluorescent protein)] and c-Fos expression showed comparable results (fig. S14).

Second, we targeted injection of AAV9-TRE: ChR2-EYFP and optic fibers to vCA1 of c-fos:tTA mice and labeled vCA1 cells that were activated by 2 hours of exposure to a mouse A with ChR2 while the c-fos:tTA mouse was off doxycycline (OFF-Dox) (Fig. 4, F and G, and fig. S2). As expected, social memory was absent in the SDT conducted after 24 hours' separation (Fig. 4H, left), but was present when blue light was shone to the whole test box (Fig. 4H, right). Control experiments conducted with no ChR2 mice (Fig. 4I) or a pair of novel mice during the SDT (fig. S15A) did not show social memory. Restricting blue light to mouse-A area but not mouse-B area also caused the restoration of social memory (Fig. 4J). These results suggest that even after social memory cannot be retrieved by natural cues, the memory engram cells for the familiar mouse are sufficiently retained and can be reactivated optogenetically for memory retrieval (*17*, *24*). Indeed, the proportion of mouse-A neurons reactivated by blue light is much greater than that reactivated by natural cues (i.e., mouse A) after a 3-day separation (compare fig. S16G and Fig. 4E). We further investigated the parameters that affect social memory, including the postfamiliarization separation periods, the proportion of reactivated familiar mouse-A neurons, the nature of recall cues (natural versus optogenetic), and the strength of the reactivation methods (figs. S14 and S16). The data indicate that optogenetic stimulation is more effective than natural stimulation in reactivating memory engram cells and that a certain minimum threshold level of reactivation of mouse-A neurons will have to be reached for social memory to be expressed in the SDT paradigm.

Third, we used the memory inception protocol (Fig. 4K) (*22*). After 24 hours' separation, ChR2-labeled mouse-A neurons were light-activated simultaneously with foot-shock delivery [i.e., negative unconditioned stimulus (US)] or cocaine administration (i.e., positive US). The test mouse exhibited avoidance or approach behavior toward mouse A, respectively, in a SDT conducted the next day (Fig. 4, K to N). Negative control groups with no ChR2 (i.e., AAV9-TRE:EYFP alone) (Fig. 4, O and P) or no US (fig. S15B) did not show any behavioral alterations. No avoidance or approaching behavior was observed when two novel mice (B and B') were used as the target mice during the test (fig. S15, C and D). AAV9-TRE: ChR2-EYFP injection into dCA1 of c-fos:tTA mice did not lead to memory inception (fig. S17).

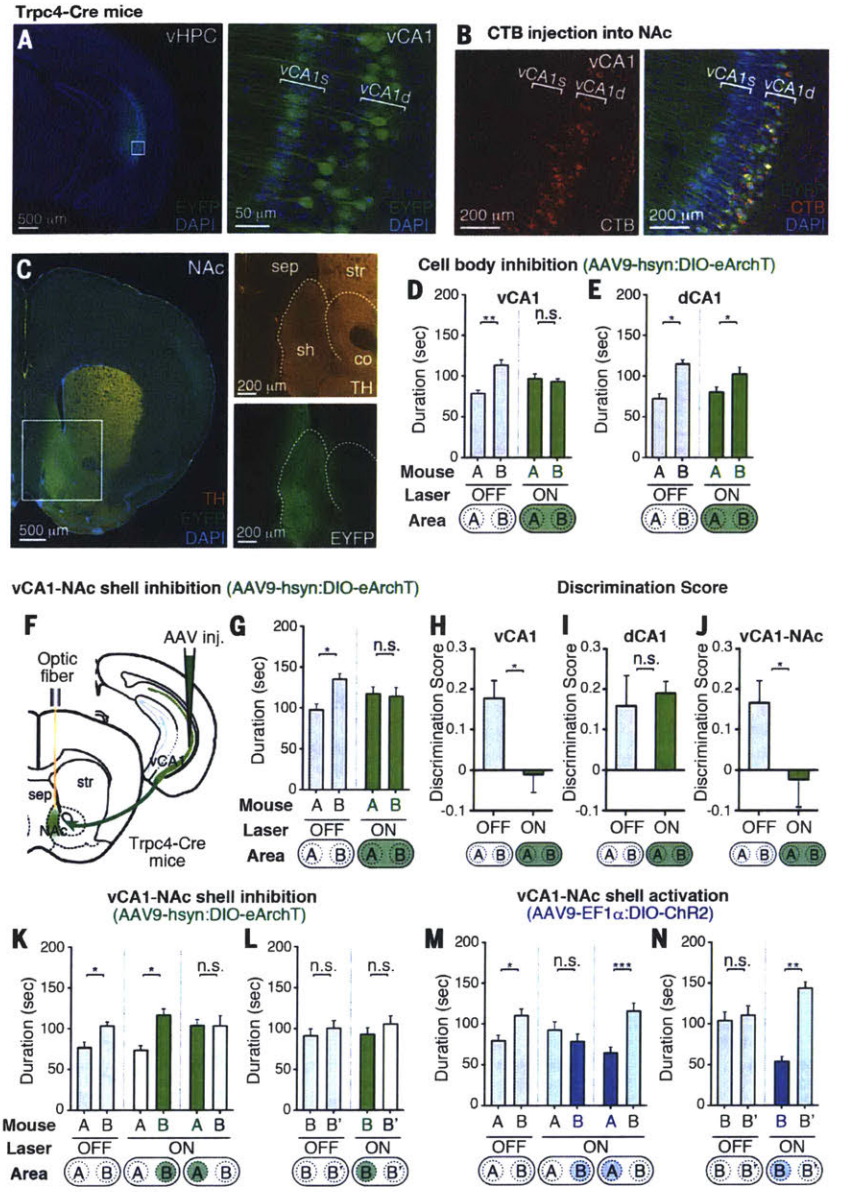

Fig. 2. vCA1-NAc circuit in a SDT. (**A**) Coronal vHPC sections of a Trpc4-Cre mouse injected with AAV9-hsyn:DIO-eArchT-EYFP into vCA1, stained with anti-GFP (green) and DAPI (4′,6-diamidino-2-phenylindole, blue). (**B**) CTB-Alexa555 (red) injection into NAc and stained with anti-GFP (green) and DAPI (blue). (**C**) Coronal NAc sections of a Trpc4-Cre mouse injected with AAV9-hsyn:DIO-eArchT-EYFP into vCA1, stained with anti-GFP (green), anti-TH (orange), and DAPI (blue). NAc shell (sh); NAc core (co); septum (sep); striatum (str). Boxed areas in (A) and (C) are magnified. (**D** and **E**) Cell body inhibition of vCA1 and dCA1 during a SDT in Trpc4-Cre and Wfs1-Cre mice, respectively. (**F**) Manipulation of vCA1-NAc shell projections. (**G** and **K** to **N**) SDT in Trpc4-Cre mice during vCA1-NAc manipulation. vCA1 injections of AAV9-hsyn:DIO-eArchT-EYFP [(G), n =14 mice; (K) and (L), each n = 12 mice] and AAV9-EF1α:DIO-ChR2-EYFP [(M) and (N), each n = 14 mice]. (**H** to **J**) Comparison of discrimination scores. Bottom, targeting area for the laser stimulation. Mouse A, familiar mouse; mouse B and -B', novel mouse. Green bars, green laser on; blue bars, blue laser on; gray bars, laser off. Significance for multiple comparisons: paired t test, $^{*}P < 0.05$; $^{**}P < 0.01$; n.s., not significant. Data presented as mean ± SEM.

The possibility that the observed optogenetic recall or memory inception is due to memory held in adjacent dCA2 is excluded because no labeling of dCA2 cells with ChR2 could be observed under our experimental conditions (fig. S17, D to F).

We have established that vCA1 and its projections to NAc shell play a necessary and sufficient role in social memory in the mouse. Furthermore, we have provided evidence that vCA1 pyramidal cells hold the memory of a familiar mouse; a population of vCA1 pyramidal cells are activated by exposure to a familiar mouse, a large fraction of these cells are reactivated by reexposure to the same mouse, and optogenetic reactivation of the vCA1 cells previously activated by exposure to a familiar mouse elicited recall of the specific social memory as

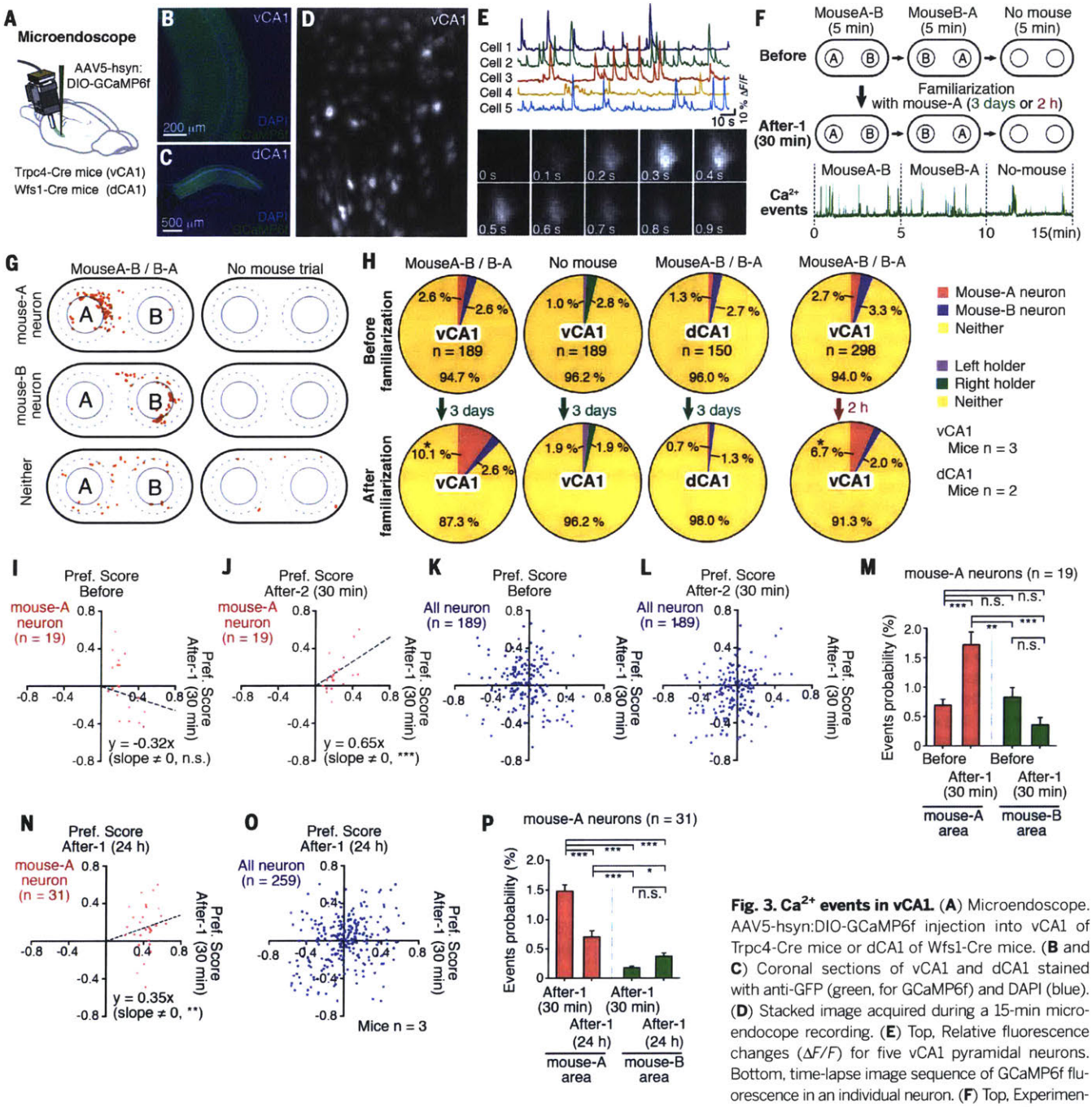

Fig. 3. Ca^{2+} events in vCA1. (**A**) Microendoscope. AAV5-hsyn:DIO-GCaMP6f injection into vCA1 of Trpc4-Cre mice or dCA1 of Wfs1-Cre mice. (**B** and **C**) Coronal sections of vCA1 and dCA1 stained with anti-GFP (green, for GCaMP6f) and DAPI (blue). (**D**) Stacked image acquired during a 15-min microendocope recording. (**E**) Top, Relative fluorescence changes ($\Delta F/F$) for five vCA1 pyramidal neurons. Bottom, time-lapse image sequence of GCaMP6f fluorescence in an individual neuron. (**F**) Top, Experimental protocol for microendoscope recording. Bottom, relative fluorescence changes during 15-min recording. (**G**) Representative mouse-A neuron, mouse-B neuron, and neither neuron. Head position at each Ca^{2+} event (red dots). (**H**) Proportion of mouse-A, mouse-B, or neither neurons in vCA1 and dCA1, before and after familiarization (3 days or 2 hours) (chi-square test, $^{*}P < 0.05$). (**I** to **L** and **N** to **O**) Comparison of the preference scores of mouse-A neurons [(I), (J), and (N), red dots] and all recorded neurons [(K), (L), and (O), blue dots] between After-1 (30 min) and Before sessions [(I) and (K); linear regression, $P = 0.208$], between After-1 (30 min) and After-2 (30 min) [(J) and (L), linear regression, $P = 0.0002$; Spearman rank correlation test, $r = 0.65$), and between After-1 (30 min) and After-1 (24 hours) [(N) and (O), linear regression, $P = 0.0019$; Spearman rank correlation test, $r = 0.23$). (**M** and **P**) Comparison of Ca^{2+} event probabilities of mouse-A neurons [analysis of variance (ANOVA); post-hoc, Scheffe, $^{***}P < 0.001$, $^{**}P < 0.01$). Data presented as mean ± SEM.

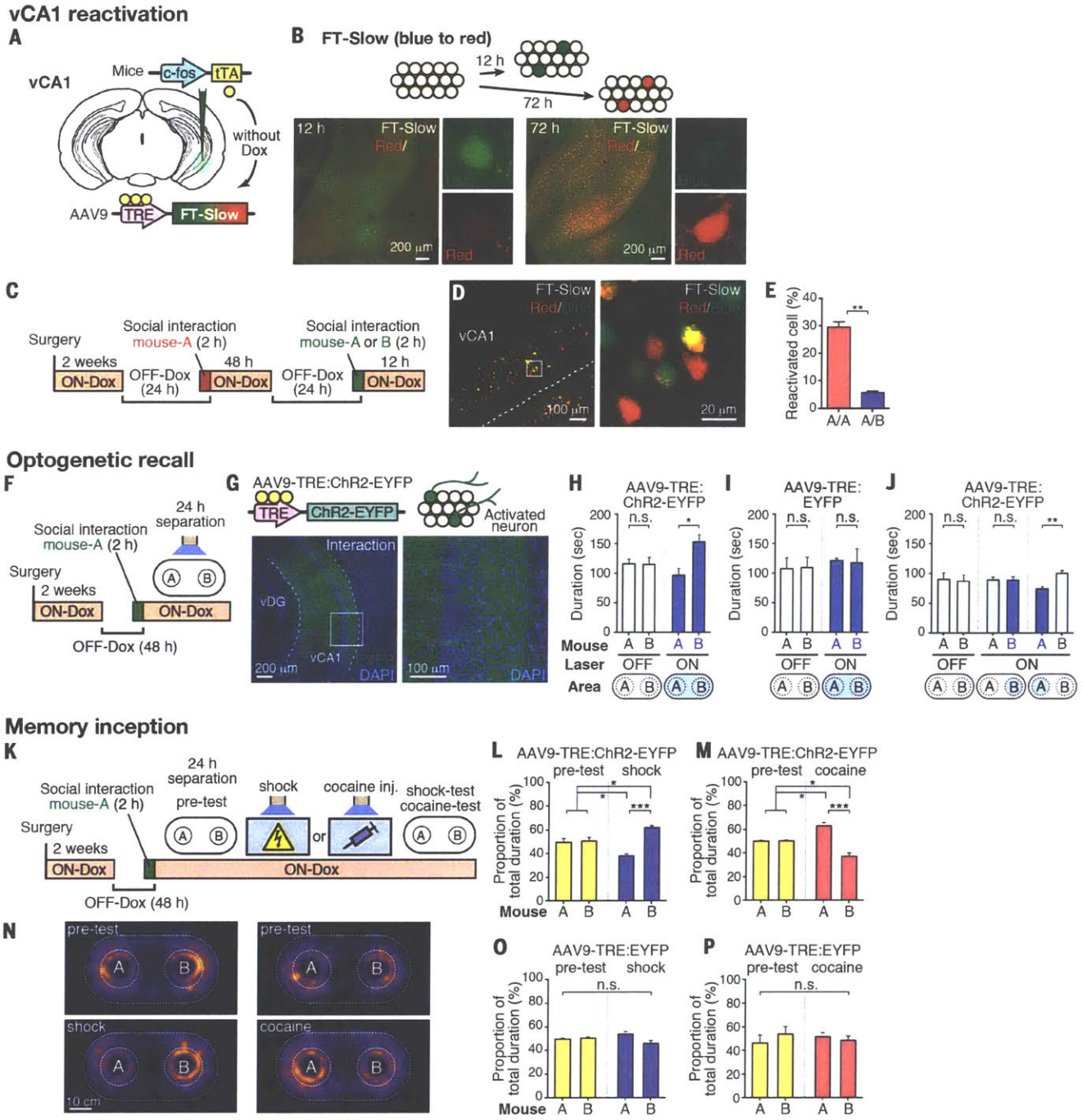

Fig. 4. Social-memory engrams. (**A**) Activity-dependent labeling method. (**B**) Injection of AAV9-TRE:FT-Slow into vCA1 of c-fos:tTA mice. Top, fluorescent color alteration of FT-Slow. Bottom, coronal vCA1 sections 12 hours (left) and 72 hours (right) after induction. Representative images of a blue-form (pseudo-green color)– or red-form (red)–expressing cell. (**C**) Protocol for visualizing two activated neuronal populations. (**D**) FT-Slow blue form–, red form–, and double (yellow)–positive cells in vCA1 (left) with magnified image (right). (**E**) Percentage of reactivated cells when the test mouse was exposed to the same mouse A twice (A/A) or mouse A and then mouse B (A/B) (n = 3 mice, each group). (**F**) Protocol for optogenetic recall of social-memory engram. (**G**) vCA1 section of c-fos:tTA mice injected with AAV9-TRE:ChR2-EYFP showing ChR2-labeling by social interaction. (**H** to **J**) SDT with or without activation of engram cells. Blue bars, blue laser on; gray bars, laser off. Bottom, targeting area for the laser stimulation. (**K**) Protocol for memory inception. (**L**, **M**, **O**, and **P**) Proportion of total duration in the sniffing area of mouse A or mouse B (yellow bars, pretest; blue bars, shock test; red bars, cocaine test). c-fos:tTA mice injected with AAV9-TRE:ChR2-EYFP [(H), (J), (L), and (M)] or AAV9-TRE:EYFP [(I), (O), and (P)]. (**N**) Heat map representing nose position of test mice. (H), n = 10 mice; (I), n = 6 mice; (J), n = 10 mice, (L), n = 10 mice; (M), n = 14 mice; (O), n = 7 mice; (P), n = 7 mice; significance for multiple comparisons: paired t test [(H) to (I)] and ANOVA, post-hoc, Scheffe [(L), M), (O), and (P)], $^*P < 0.05$; $^{**}P < 0.01$; n.s., not significant. Data presented as mean ± SEM.

monitored by a social discrimination test. Thus, the vCA1 cells activated by the exposure to a familiar mouse satisfy the criteria to be met by engram cells for a specific memory (*25*). It is interesting that this recall of the social memory by light can occur even after the mice have fallen into an amnesic state. This indicates that the specific social memory information is retained in the specific vCA1 cell population during at least 1 day after encoding but that natural recall cues are not strong enough to reactivate these cells for memory recall; in contrast, the 20-Hz blue light is stronger and reactivates the engram cells above the threshold necessary for recall. This interpretation of light-mediated recall of the social memory is supported by the inception experiment; the social memory is retained in the amnesic mice, and the light-reactivated engram serves as a CS and becomes associated with a high-valence US (footshocks or cocaine) to evoke avoidance or preference behavior.

The present study helps to resolve the controversy (*7*–*9*) regarding the necessity of mouse hippocampus for social memory and corroborates previous observations made in primates (*4*–*6*). In macaques, a large population of neurons in the anterior hippocampus responded to socially relevant cues such as faces and voices of individuals (*6*). In human medial temporal lobe, including the anterior hippocampus, there are cells that respond more to famous or personally relevant people than to unfamiliar people (*4*, *5*). The overall results suggest evolutionary conservation of the role of the hippocampal areas as the sites of social memory.

Recent studies have shown that dCA2 is critical for sociocognitive memory processing (*10*, *11*, *26*). dCA2 neurons have longitudinal rostro-caudal projections to vCA1 (fig. S18) (*27*, *28*) and connect with the deep layer of CA1 more strongly than with the superficial layer (*28*). It is thus possible that the dCA2-vCA1d-NAc circuit composes the engram cell ensemble pathway for social memory (*25*). However, it is also possible that the role of dCA2 in social memory is to convey to vCA1d appropriately processed and socially relevant cues, rather than holding memory information per se.

Compared to other forms of episodic memory, social memory lasts no more than a few hours (Fig. 1C) under laboratory conditions (*29*, *30*), although it can be prolonged to a week by vasopressin release, or to 24 hours by group housing (*12*, *29*, *31*). We have demonstrated by optogenetics that the engram cells for social memory formed in a laboratory environment can be retained in vCA1 for at least 2 days. Thus, the relatively short duration of social memory is apparently due to inefficient retrieval rather than failed retention of the memory. It would be interesting to test the hypothesis that increased vasopressin and/or group housing prolongs social memory duration by promoting the retrieval process.

Overall, our study establishes vCA1 and its NAc projections as a site of social memory and provides insights and clues to the neuronal mechanisms underlying this important form of memory (fig. S19).

REFERENCES AND NOTES

1. L. A. McGraw, L. J. Young, *Trends Neurosci.* **33**, 103–109 (2010).
2. T. Okuyama *et al.*, *Science* **343**, 91–94 (2014).
3. C. N. Smith *et al.*, *Proc. Natl. Acad. Sci. U.S.A.* **111**, 9935–9940 (2014).
4. R. Q. Quiroga, L. Reddy, G. Kreiman, C. Koch, I. Fried, *Nature* **435**, 1102–1107 (2005).
5. I. V. Viskontas, R. Q. Quiroga, I. Fried, *Proc. Natl. Acad. Sci. U.S. A.* **106**, 21329–21334 (2009).
6. J. Sliwa, A. Planté, J. R. Duhamel, S. Wirth, *Cereb. Cortex* **26**, 950–966 (2016).
7. M. von Heimendahl, R. P. Rao, M. Brecht, *J. Neurosci.* **32**, 2129–2141 (2012).
8. A. S. Squires, R. Peddle, S. J. Milway, C. W. Harley, *Neurobiol. Learn. Mem.* **85**, 95–101 (2006).
9. D. M. Bannerman, M. Lemaire, S. Beggs, J. N. Rawlins, S. D. Iversen, *Exp. Brain Res.* **138**, 100–109 (2001).
10. F. L. Hitti, S. A. Siegelbaum, *Nature* **508**, 88–92 (2014).
11. E. L. Stevenson, H. K. Caldwell, *Eur. J. Neurosci.* **40**, 3294–3301 (2014).
12. J. H. Kogan, P. W. Frankland, A. J. Silva, *Hippocampus* **10**, 47–56 (2000).
13. P. Andersen, T. V. Bliss, K. K. Skrede, *Exp. Brain Res.* **13**, 222–238 (1971).
14. B. A. Strange, M. P. Witter, E. S. Lein, E. I. Moser, *Nat. Rev. Neurosci.* **15**, 655–669 (2014).
15. M. S. Fanselow, H. W. Dong, *Neuron* **65**, 7–19 (2010).
16. J. Camats Perna, M. Engelmann, in *Current Opinion in Behavioral Neurosciences*, M. Geyer, B. Ellenbrook, C. Marsden, Eds. (Springer, 2015), pp. 1–21.
17. X. Liu *et al.*, *Nature* **484**, 381–385 (2012).
18. L. G. Reijmers, B. L. Perkins, N. Matsuo, M. Mayford, *Science* **317**, 1230–1233 (2007).
19. T. Kitamura *et al.*, *Science* **343**, 896–901 (2014).
20. Y. Ziv *et al.*, *Nat. Neurosci.* **16**, 264–266 (2013).
21. T. W. Chen *et al.*, *Nature* **499**, 295–300 (2013).
22. S. Ramirez *et al.*, *Science* **341**, 387–391 (2013).
23. F. V. Subach *et al.*, *Nat. Chem. Biol.* **5**, 118–126 (2009).
24. T. J. Ryan, D. S. Roy, M. Pignatelli, A. Arons, S. Tonegawa, *Science* **348**, 1007–1013 (2015).
25. S. Tonegawa, X. Liu, S. Ramirez, R. Redondo, *Neuron* **87**, 918–931 (2015).
26. D. A. Caruana, G. M. Alexander, S. M. Dudek, *Learn. Mem.* **19**, 391–400 (2012).
27. N. Tamamaki, K. Abe, Y. Nojyo, *Brain Res.* **452**, 255–272 (1988).
28. K. Kohara *et al.*, *Nat. Neurosci.* **17**, 269–279 (2014).
29. R. M. Bluthé, G. Gheusi, R. Dantzer, *Psychoneuroendocrinology* **18**, 323–335 (1993).
30. D. H. Thor, W. R. Holloway, *J. Comp. Physiol. Psychol.* **96**, 1000–1006 (1982).
31. A. S. Smith, S. K. Williams Avram, A. Cymerblit-Sabba, J. Song, W. S. Young, *Mol. Psychiatry* **21**, 1137–1144 (2016).

ACKNOWLEDGMENTS

We thank C. Sun, X. Liu, S. LeBlanc, J. Derwin, W. Yu, F. Bushard, S. Huang, G. Das, T. O'Connor, J. Young, and L. Brenner for their help. Supported by the RIKEN Brain Science Institute, Howard Hughes Medical Institute, the JPB Foundation (to S.T.), and Japan Society for the Promotion of Science Grant-in-Aid (to T.O.). All data and computer codes necessary to understand and assess the conclusions of this research are available in the supplementary materials. AAV9-hSyn:DIO-eArchT3.0-EYFP, AAV9-TRE:FT-Slow, AAV9-TRE:ChR2-EYFP, and AAV9-TRE:EYFP were developed at MIT by the group of S.T.; virus plasmids are available through a material transfer agreement. The Trpc4-Cre transgenic mouse line was developed at RIKEN BSI by the group of S.I. and is available through a material transfer agreement.

SUPPLEMENTARY MATERIALS

www.sciencemag.org/content/353/6307/1536/suppl/DC1
Materials and Methods
Figs. S1 to S19
References (*32*–*35*)

16 March 2016; accepted 29 July 2016
10.1126/science.aaf7003

VIROLOGY

MAVS-dependent host species range and pathogenicity of human hepatitis A virus

Asuka Hirai-Yuki,[1,2] Lucinda Hensley,[1,2] David R. McGivern,[1,3] Olga González-López,[1,2] Anshuman Das,[1,2] Hui Feng,[1,2] Lu Sun,[1,2] Justin E. Wilson,[1,2,4] Fengyu Hu,[1,2] Zongdi Feng,[1,2]* William Lovell,[1] Ichiro Misumi,[1,2,4] Jenny P.-Y. Ting,[1,2,4] Stephanie Montgomery,[1,5] John Cullen,[6] Jason K. Whitmire,[1,2,4] Stanley M. Lemon[1,2,3]†

Hepatotropic viruses are important causes of human disease, but the intrahepatic immune response to hepatitis viruses is poorly understood because of a lack of tractable small-animal models. We describe a murine model of hepatitis A virus (HAV) infection that recapitulates critical features of type A hepatitis in humans. We demonstrate that the capacity of HAV to evade MAVS-mediated type I interferon responses defines its host species range. HAV-induced liver injury was associated with interferon-independent intrinsic hepatocellular apoptosis and hepatic inflammation that unexpectedly resulted from MAVS and IRF3/7 signaling. This murine model thus reveals a previously undefined link between innate immune responses to virus infection and acute liver injury, providing a new paradigm for viral pathogenesis in the liver.

Although viral hepatitis is an important cause of human morbidity worldwide, there are no small-animal models that accurately recapitulate liver disease caused by any of the five responsible viruses (*1*, *2*). Previous studies have relied heavily on nonhuman primates, especially chimpanzees (*3*, *4*), to investigate pathogenesis and immune responses to hepatitis viruses. This has handicapped efforts to understand host responses within the unique immunologic environment of the liver (*5*, *6*). Recent NIH policies effectively eliminate the use of chimpanzees

LEM2 04036

a0005

In Search of Engram Cells

AUT

Dheeraj S Roy and Susumu Tonegawa, Massachusetts Institute of Technology, Cambridge, MA, United States

s0010 Introduction

p0015 Understanding the material basis of memory remains a central goal of modern neuroscience (Dudai and Morris, 2013; Tonegawa et al., 2015a). Historically, philosophers tried to understand the precise location in the human body where information of past experiences is stored. For some time, memory information was attributed to organs such as the heart and kidney. In the Renaissance, Descartes (1649) proposed that mental capacities, specifically memory, must be represented in the brain. In the 20th century, Richard Semon was the first to theorize that learning induces physical changes in specific brain cells that retain information and are subsequently reactivated by appropriate stimuli to induce recall. He termed these changes the engram (Schacter, 2001; Semon, 1904, 1909). However, even after Semon's engram theory, some leading scholars wondered whether memory is physically represented in the brain or the mind (Bergson, 1911; McDougall, 1911). It was Shepherd Franz and later Karl Lashley who advocated for the physical theory of information storage in the central nervous system (Franz, 1912; Lashley, 1929, 1950). In particular, Lashley (1950) adopted the concept of the engram and was among the first to attempt to localize memory engrams in the brain. Although Lashley's idea of mass action was later empirically disproved, researchers after him have tried to identify the location of memory representations in the brain using experimental technologies available at the time (Bruce, 2001; Dudai and Eisenberg, 2004; Hubener and Bonhoeffer, 2010; Josselyn et al., 2015; Thompson, 1976; Tonegawa et al., 2015b). In this chapter, we will first discuss early attempts to identify memory engrams, provide updated criteria for defining an engram and engram cells, and then examine recent studies demonstrating that memory is indeed stored in populations of neurons and their associated circuits.

s0015 Preoptogenetic Studies

p0020 At any given moment, animals need to quickly organize their behavior by comparing previous experiences to the currently available sensory cues. This online function is carried out by neural circuits in the brain, which indicates that memory evolved for two major biological purposes: (1) to replay previous episodes and inform current behavioral outputs, and (2) to integrate past and present

experiences (James, 1890). A key question in the study of memory is how new information can be acquired and stored in precisely wired neural circuits (Kandel, 2001). At the cellular and systems level, Ramon y Cajal (1893, 1894) originally proposed that the strengthening of sites of contact between neurons might be a mechanism of memory storage. These sites of contact were famously termed synapses by Charles Sherrington (Foster and Sherrington, 1897). However, it was Donald Hebb's theoretical integration of neurophysiology and psychology that created the modern paradigm for memory research. Hebb (1949) proposed that neuronal assemblies linked by adaptable synaptic connections could encode informational content in the brain and further elaborated that these cell assemblies could provide the basis of a distributed memory system. Since then, many attempts have been made to localize memory engrams in many different species. Among early studies, notable and pioneering examples are summarized in the following sections.

s0020 Invertebrate Studies

p0025 In the 1950s, there was little consensus among psychologists that our understanding of the biological basis of learning and memory could be advanced using a reductionist approach, like the use of invertebrate animal models. However, biologists quickly realized that the simplest forms of memory would be conserved across species and therefore should be studied in experimentally tractable animals as a starting point. Probably the best known example is the giant marine snail *Aplysia californica*, in which a simple defensive reflex involved less than 100 central nerve cells (Kandel, 1976). This reflex behavior, the withdrawal of the gill upon stimulation of the siphon, exhibited different forms of learning such as habituation, sensitization, and classical conditioning (Pinsker et al., 1973). By examining these simple forms of learning, scientists performed detailed analyses of the cellular and molecular mechanisms underlying nonassociative as well as associative learning. Importantly, these studies provided clear evidence that learning correlates with changes in the strength of synaptic connections, thereby supporting Cajal's and Hebb's ideas on the mechanism of memory storage (Milner et al., 1998). Along with synaptic strength, it was observed that learning paralleled structural changes, such as the elimination or addition of synapses that closely matched the age of the memory (Bailey and Chen, 1989; Glanzman et al., 1990).

p0030 With the goal of pinpointing engrams in intact nervous systems, researchers have extensively studied honeybee and *Drosophila melanogaster* model systems. In adult honeybees, learning and memory storage occur in mushroom bodies where experience-dependent dendritic branching patterns have been observed (Farris et al., 2001; Menzel, 2001). Similar to *Aplysia*, studies in flies identified a biochemical mechanism for memory storage that is based on cAMP-mediated pathways (Dudai, 1988; Tully and Quinn, 1985). Using cAMP-signaling mutants, structural alterations in the sensory neurons of flies have been correlated with learning and short-term memory (Corfas and Dudai, 1991; Gerber et al., 2004). More recently, when a specific odor was paired with shock in flies, defined neuronal populations within the olfactory learning circuit showed modified firing responses. Specifically, pathways in the antennal lobes and the mushroom bodies increased their responses only to the odor used in training but not to control odors. These experiments support the idea that odor-specific memory traces are formed within these cell populations as a result of Pavlovian conditioning (Liu and Davis, 2009; Yu et al., 2006). However, the precise cellular and/or synaptic localization of engrams in flies requires further investigation.

s0025 Bird Studies

p0035 In the search for neural mechanisms of learning and memory, mammals have been preferred over birds as model systems due to their closer relationship with humans. However, since it was highlighted by the Avian Consortium that birds exhibit cognitive capacities which had previously been thought to be restricted to primates, memory storage in birds has been extensively studied (Avian Brain Nomenclature Consortium, 2005; Doupe and Kuhl, 1999). Historically, avian studies on memory have used four major paradigms: imprinting, birdsong learning, cache recovery (Clayton and Dickinson, 1998), and gustatory avoidance (Rose, 2000). Imprinting, where a recently hatched chick learns the characteristics of its parents (or an object), causes dramatic changes in the brains of young birds (Lorenz, 1981). These studies have revealed a localization of the substrate of memory, in particular because the generation of new synapses has been observed during imprinting. To date, it has not been possible to prove causality between the observed changes and the imprinting process itself due to both the distributed nature of the system and a lack of appropriate technologies (Horn, 2004). Regarding birdsongs, juveniles learn the characteristics of the songs of tutors from their own species, in most cases their fathers, which is a process that requires several brain nuclei. This process involves a period of auditory memorization followed by development of the juveniles' own vocalizations, which is analogous to speech acquisition in human infants. It is thought that the neural representation of song memory during memorization is localized to the auditory association cortex, while the neural substrate of vocalization memory is localized to a network of interconnected brain nuclei known as the song system (Bolhuis and Gahr, 2006). More recently, a study examined in vivo dendritic spine dynamics in the crucial birdsong nucleus, high vocal center (HVC), during the juvenile song-learning period of zebra finches. Strikingly, it was shown that even though juveniles exhibit high levels of spine turnover; during the song-learning process, subsets of spines on sensorimotor neurons undergo stabilization, accumulation, and enlargement. These experiments suggested that successful behavioral learning correlated with rapid stabilization and strengthening of specific synapses (Eales, 1985; Roberts et al., 2010).

p0040 The sense of auditory space derives from associations formed between specific auditory cues and locations in the environment where they are produced. Experience has a significant impact on sound localization and therefore the auditory localization pathway became a model system for studying mechanisms of learning (Shinn-Cunningham, 2000). A nocturnal predator, the barn owl (*Tyto alba*), is the most extensively studied species for this behavior since its capacity for localization is comparable

to that of humans. It was first shown in the barn owl that they have the incredible capacity to adapt to environmental changes in a behaviorally relevant manner. In particular, their auditory and visual space maps in the superior colliculus align according to individual visual and auditory cues. Moreover, learning in the barn owl correlates with structural rearrangements of neuronal connections between the internal and external nucleus of the inferior colliculus (Knudsen, 2002). These observations demonstrate that the birdsong learning process is a powerful paradigm, which holds promise as a future target to identify and visualize the formation of an engram.

s0030 Rodent and Nonprimate Mammal Studies

p0045 The American psychologist Karl Lashley (1950) pioneered a systematic hunt for engram regions in the rodent brain by introducing lesions of varying sizes into different sites of the cerebral cortex and attempting to associate each of these lesions with the animal's ability to solve a maze task. The results showed that behavioral impairments were caused by lesions introduced throughout the brain, and that severity of the impairments was proportional to the size of the lesions. Lashley concluded that the putative memory engram cells are not localized in the cerebral cortex, leading him to formulate the mass action principle. The notion that engram cells for a specific memory are broadly distributed throughout the brain has not been supported by subsequent studies for at least several types of memory, including episodic memory. It is conjectured that Lashley's failure in identifying localized engram cells is because the maze tasks he used were too complex and required multiple regions of the cerebral cortex, and/or the primary sites of storage for this type of memory may reside in subcortical regions.

p0050 Richard Thompson et al. performed pioneering work in attempting to localize the memory engram for classical eyelid conditioning in rabbits. In this simple paradigm wherein repeated pairings of a neutral conditioned stimulus (e.g., tone, CS) with an unconditioned stimulus (e.g., corneal airpuff, US) produces an adaptive conditioned response (eyeblink, CR) to the CS alone, animals from which the cerebral neocortex or hippocampus had been removed were still able to learn and express the standard delay CR (Thompson and Kim, 1996). Initial work identified the cerebellum as a crucial node for learning, retention, and expression of this simple associative memory (McCormick et al., 1982). It has since been revealed that information about the CS and US arrives in the cerebellum through the pontine nuclei and inferior olive (IO), respectively. Lesions of the pontine nuclei or IO prevents CR acquisition (McCormick et al., 1985; Steinmetz et al., 1987) and precisely timed stimulation of the pontine nuclei and IO as the CS and US can produce reliable expression of the CR (Mauk et al., 1986; Steinmetz et al., 1986, 1989). This CS and US information arrive within the cerebellum at two sites, the cerebellar cortex and the interpositus nucleus. Through many clever experiments utilizing lesions, pharmacological inactivation, neural stimulation, and single cell recordings, it is understood that through an intricate process of long-term depression (LTD) and long-term potentiation (LTP) at specific synapses, the activity of the interpositus nucleus is responsible for triggering the expression of CR, while the cerebellar cortex shapes the adaptive timing of the CR (Ito and Kano, 1982; McCormick and Thompson, 1984; Lavond and Steinmetz, 1989; Garcia and Mauk, 1998; Bao et al., 2002). Together, these studies suggest that a memory engram for this behavior is found in key sites of the cerebellum, involving interactions between the anterior interpositus and overlying cortex.

p0055 A key structure for declarative memory formation in mammals is the hippocampus, where use of rodent models has led to great progress in elucidating the cellular basis of memory. By recording neuronal activity in the hippocampus of awake, behaving rats, a series of elegant experiments observed learning-related changes in receptive field properties of single neurons known as hippocampal place cells. These sparse populations of neurons develop specific place fields as the rat explores and learns about a novel environment (O'Keefe and Dostrovsky, 1971; Wilson and McNaughton, 1993). These place-coding cell populations may represent the spatial engram, which is needed to form a long-term memory of the animal's experience along with valence information. Another well-documented example of experience-dependent neural activity is referred to as replay, which describes the spontaneous reactivation of recent neural activity during periods of high-frequency bursts in the hippocampus. Interestingly, the strength of replay-related reactivation has been correlated with long-term memory expression (Dupret et al., 2010; Louie and Wilson, 2001; Nakashiba et al., 2009).

p0060 From hippocampal recording studies, it is clear that the sparse population of place cells persists several days to weeks after learning and remains specific to the environmental cues during learning. Using auditory CS, a variety of response latencies were found in multiple cortical and subcortical areas (Olds et al., 1972). These authors reasoned that learning centers of the brain would contain cell responses to CS, which were of similar latencies as sensory responses. A subset of the cortical areas analyzed in this study fulfilled this criterion and furthermore these responses were specific to the auditory stimulus used during conditioning. Based on these experiments, it was proposed that these cortical areas comprised learning centers and were thus putative sites involved in memory formation. Several groups have provided correlational evidence between learning-induced plasticity in primary auditory cortex and long-term memory (Gonzalez-Lima and Scheich, 1986; McKernan and Shinnick-Gallagher, 1997; Bao et al., 2001; Kisley and Gerstein, 2001; Weinberger, 2004). Similar results have been reported for neuronal activity changes induced by olfactory associative learning paradigms (Kass et al., 2013).

p0065 Many studies have implicated select populations of neurons in specific memories by examining the expression of immediate early genes (IEGs) such as cFos, Zif268, and activity-regulated cytoskeleton-associated protein Arc (Flavell and Greenberg, 2008; Guzowski, 2002; Okuno et al., 2012). Several groups found that cell populations active during the acquisition of a fear memory were preferentially reactivated during the recall of that memory in different areas of the mouse brain, such as the amygdala (Reijmers et al., 2007), the hippocampus (Deng et al., 2013; Tayler et al., 2013), layer II cortical areas including sensory cortex (Cowansage et al., 2014; Xie et al., 2014), and the prefrontal cortex (Zelikowsky et al., 2014).

p0070 Another approach that has been used to identify probable engram cell populations in the rodent brain employs the random overexpression of the transcription activator cAMP response element binding protein (CREB) in a small population of neurons in the lateral amygdala (LA), making these cells more likely to be recruited to become a part of putative engram ensembles during subsequent fear conditioning training (Han et al., 2007). By selectively manipulating these high-CREB cells, but not a random population of neurons in the same brain region, via diphtheria toxin-based ablation (Han et al., 2009) or genetic-based inhibition (Hsiang et al., 2014; Zhou et al., 2009) memory recall was disrupted in mice. Similar technology has been used to demonstrate the necessary role of retrosplenial cortex neurons in spatial navigation memory (Czajkowski et al., 2014). Other studies using the Daun02 inactivation method have shown that contextual memory associated with a positive reinforcer such as cocaine could be blocked by inactivating a minor portion of nucleus accumbens (NAcc) neurons that were previously active in the drug-associated environment in rats (Koya et al., 2009).

p0075 Two-photon microscopy allows in vivo visualization of fine structural morphology down to several hundred micrometers in the cortex of the intact rodent brain (Denk et al., 1990). Such technology has allowed researchers to demonstrate dendritic spine changes that correlate with the acquisition and/or storage of information (Attardo et al., 2015; Moser et al., 1994). An interesting report found that the formation of a contextual fear memory correlated with a transient increase in dendritic spine density in the hippocampus, while similar changes in the anterior cingulate cortex (ACC) developed over a period of weeks following memory formation; the latter time-dependent process is called systems consolidation of memory (Restivo et al., 2009).

p0080 Another well-established model for experience-dependent cortical plasticity is monocular deprivation, where temporary closure of one eye shifts the balance between the strength of the representation of the two eyes in the visual cortex toward the open eye. Inspired by work in the barn owl model system, several researchers combined two-photon microscopy and monocular deprivation to visualize an engram in the neocortex. A series of experiments found that cortical dendritic spines that appeared during monocular deprivation remained in place even after reestablishing normal vision. These spines served as the basis for faster and longer-lasting adaptation responses during a second monocular deprivation, even though this second deprivation did not further increase spine density (Hofer et al., 2009). These results are reminiscent of the concept of savings proposed by Hermann Ebbinghaus more than 100 years ago. Ebbinghaus (1880) demonstrated that in every day experiences relearning is easier than first-time learning. Most studies examining structural correlates of learning and memory focused on dendritic spines, though it is worth noting a few examples that examined presynaptic plasticity. In adult mice, cortical axonal boutons show some degree of structural plasticity under baseline conditions with overall axon branching patterns remaining stable (De Paola et al., 2006). In higher mammals including the cat, a study found that shrinkage and expansion of ocular dominance columns due to monocular deprivation was reflected in the retraction and growth of thalamic fibers in the visual cortex (Antonini and Stryker, 1993). Similar to presynaptic structural plasticity, relatively less attention has been paid to structural modifications of inhibitory neurons. Branch tips of dendrites of inhibitory neurons in mouse visual cortex undergo constant remodeling, supporting the idea that inhibitory neurons, too, are capable of participating in structural plasticity of memory (Lee et al., 2006). Analogous to excitatory neurons, calcium imaging has revealed that inhibitory neurons exhibit neural activity modifications following sensory deprivation (Kameyama et al., 2010).

s0035 Primate Studies

p0085 In human studies, it was Canadian neurosurgeons Wilder Penfield and Theodore Rasmussen (1950) who serendipitously obtained the first tantalizing hint that episodic memories may be localized in brain regions. As a presurgery procedure for human patients, Penfield applied small jolts of electricity to the brain to reveal which regions were responsible for inducing seizures. Remarkably, when stimulating parts of the lateral temporal cortex, approximately 8% of his patients reported vivid recall of random episodic memories: one patient exclaimed, "Yes, Doctor, yes, Doctor! Now I hear people laughing—my friends in South Africa … Yes, they are my two cousins, Bessie and Ann Wheliaw." Another patient reported, "I had a dream. I had a book under my arm. I was talking to a man. The man was trying to reassure me not to worry about the book." This study had the first glance at what geneticists call gain-of-function or sufficiency evidence for the notion that the lateral temporal lobe region harbors the biological locus for episodic memory. Complementing this work, a study conducted several years later by the American neurosurgeon William Scoville and Canadian neuropsychologist Brenda Milner provided loss-of-function or necessity evidence (Scoville and Milner, 1957). To treat the epileptic seizures of a young man, Henry Molaison (H.M.), who suffered seizures caused by a bicycle accident, Scoville resected a large portion of the medial temporal lobes (MTLs) from both hemispheres, including the hippocampus and adjacent brain areas. As a consequence of this surgery, H.M. lost his ability to form new episodic memories (anterograde amnesia), as well as the ability to recall memories of episodes and events that occurred in his life within a year prior to this surgery (graded retrograde amnesia). H.M.'s other types of memory, such as motor memory, were largely unaffected, indicating that episodic memories may be specifically processed in the MTL and in particular in the hippocampus. These pioneering studies led to a notion that at least some types of memory, in this case episodic memory, may be stored in a localized brain region. More recent work using single-unit recordings in humans reported that cells in the hippocampus and surrounding areas were reactivated only during free memory recall of a particular individual, landmark (Quiroga et al., 2005), or episode (Gelbard-Sagiv et al., 2008).

p0090 Among early attempts to identify memory engrams in monkeys, one study recorded single-cell activity from the inferotemporal (IT) cortex during a visual delayed matching-to-sample task (Fuster and Jervey, 1981). Many cells responded to the colors of the stimuli, and notably, several cells responded differentially to color depending on whether or not attention circuitry was engaged, thus demonstrating their behaviorally relevant role. Fittingly, the authors demonstrated correlations of these neuronal activities to the encoding, retention, and retrieval of visual information. Later, Yasushi Miyashita (1988) revealed a neuronal correlate of visual

long-term memory by studying how the anterior ventral temporal cortex represented stimulus–stimulus associations. By simultaneously recording from over 200 neurons as monkeys performed a visual memory task, single neurons that could respond conjointly to temporally related, but geometrically dissimilar stimuli were observed. That is, certain neurons displayed stimulus selectivity during the learning phase of the task, which then could become associated with unrelated stimuli in a different experience. These elegant studies demonstrated a neuronal correlate of associative visual memory. In a more recent series of experiments, using two-photon imaging in macaques to follow the remodeling of intracortical axons after retinal lesions over extended periods of time, it was found that lesions induced an almost immediate increase in the number of axonal boutons as well as axonal collaterals within the affected cortical region (Yamahachi et al., 2009). Thus, presynaptic elements of cortical circuitry are also modified following experience-dependent changes.

s0040 Semon's Engram Theory

p0095 During the early part of the 20th century, a German scientist, Richard Semon (1904, 1909), advocated for the physical theory of human memory. Until the late 1970s, mainstream psychologists studying human memory processing mostly ignored this theory. It was not until three prominent researchers, Daniel Schacter et al. (1978), published an influential article that subsequently led to a revival of Semon's contributions within the academic community.

p0100 The term engram was coined by Semon (1904), which he defined as "the enduring though primarily latent modification in the irritable substance produced by a stimulus (from an experience)." Another term used by several contemporary neuroscientists is memory trace, which is equivalent to engram. Semon's memory engram theory was built on two fundamental postulates termed the Law of Engraphy and the Law of Ecphory, for memory storage and memory retrieval, respectively (Semon, 1909). The Law of Engraphy posits "all simultaneous excitations (derived from experience)…form a connected simultaneous complex of excitations which, as such acts engraphically, that is to say leaves behind it a connected and to that extent, separate unified engram-complex." The Law of Ecphory posits "the partial return of an energetic situation which has fixed itself engraphically acts in an ecphoric sense upon a simultaneous engram complex." A part of the entire experience (i.e., stimuli) at the time of storage needs to be present at the time of recall for successful retrieval of the entire original event to occur (Schacter et al., 1978). This criterion essentially describes the process of pattern completion (Marr, 1970), which was experimentally demonstrated many years later (Leutgeb et al., 2004; Nakazawa et al., 2003).

s0045 Engram Cell Criteria

p0105 Although Semon's engram theory was remarkably novel at the time, he did not elaborate on the biological basis of a unified engram complex. During the decades following the proposal of this theory, several molecular, cellular, imaging, and electrophysiological recording techniques have been developed. Incorporating our current knowledge regarding neurons, synapses, and neuronal circuits into Semon's memory engram theory, we propose usage of engram, engram cells, and other associated terminologies in the contemporary context. Since recent studies have indicated that the engram of a given memory is not restricted to a single anatomical location, but is distributed in multiple locations with specific patterns of connectivity, we introduced three additional terms: engram cell pathway, engram component, and engram complex.

u0010 • Engram refers to the enduring physical and/or chemical changes elicited by experience that underlie the newly formed memory association.

u0015 • Engram cells are a population of neurons that are activated by learning, exhibit enduring cellular changes as a consequence of learning, and whose reactivation by a part of the original stimuli delivered during learning results in efficient memory recall. Note that this goes beyond a correlational definition of the term.

u0020 • Engram cell pathway is a set of engram cells for a given memory connected by synapses along specific neuronal circuits.

u0025 • Engram component is the content of an engram stored in an individual engram cell population within the engram cell pathway. Note that this does not necessarily denote the physiological content of the engram held by a given population but rather indicates the type of represented mnemonic information.

u0030 • Engram complex refers to the whole engram for a given memory that is stored in a set of engram cell populations connected by an engram cell pathway.

s0050 Engram Cells Found

p0135 The studies discussed so far have linked neuronal populations with particular memory events mostly with correlational evidence and only a few with loss-of-function evidence, but a critical piece of evidence was largely missing. The most direct evidence of engram cells should come from gain-of-function manipulations, where a population of neurons activated by learning are artificially reactivated to mimic behavioral recall elicited by natural cues. Crucially, if artificial reactivation of a cell population induces the recall of that specific memory in the absence of retrieval cues, then this would provide evidence that the population of neurons is sufficient for memory, and thus serves as the neuronal basis for the memory engram (Martin and Morris, 2002). However,

this type of gain-of-function experiment is technically challenging, as one has to be able to accurately isolate the neurons involved in a single memory from their seemingly indistinguishable neighbors and activate them with high spatial and temporal precision.

s0055 Gain-of-Function and Loss-of-Function Evidence by Optogenetics

p0140 Recent advances in technology such as optogenetics make such manipulations feasible (Boyden et al., 2005; Fenno et al., 2011). By combining the activity-dependent, doxycycline-dependent *c-fos–tTA* (tetracycline transactivator) system (Reijmers et al., 2007) and channelrhodopsin-2 (ChR2)-mediated optogenetics, researchers were able to tag a sparse population of dentate gyrus (DG) neurons activated by contextual fear conditioning (CFC) with ChR2 in mice (Liu et al., 2012; Ramirez et al., 2013). Subsequently, when these cells were reactivated by blue light in a context different from the original one used for conditioning, the mouse subjects displayed freezing behavior as evidence of fear memory recall (Liu et al., 2012). Crucially, this optogenetic reactivation of a fear memory was not due to the activation of prewired neural circuits. This was demonstrated by disrupting the activity of the downstream CA1 region only during training, and finding that subsequent optogenetic DG engram activation did not elicit memory retrieval (Ryan et al., 2015). Similarly, memory recall induced by the artificial reactivation of fear memory cells in retrosplenial cortex has been reported (Cowansage et al., 2014). Using this methodology to manipulate engram cells, studies have reported the creation of a context-specific false memory (Ohkawa et al., 2015; Ramirez et al., 2013), the bidirectional switching of the valence associated with a neutral hippocampal contextual memory (Redondo et al., 2014), countering depression-like behavior by the activation of a positive memory (Ramirez et al., 2015), retrieving memory in retrograde amnesia due to disrupted consolidation/reconsolidation (Ryan et al., 2015), and restoring memory in mouse models of early Alzheimer's disease (AD) (Roy et al., 2016).

p0145 Along with these engram reactivation experiments, loss-of-function studies have also been performed using optogenetics. Genetically labeling cFos-positive engram cells with the inhibitory optogenetic channel archaerhodopsin (ArchT) (Chow et al., 2010) allowed researchers to reversibly inhibit CA1 engram cells during natural memory recall, which resulted in impaired memory retrieval (Tanaka et al., 2014). Interestingly, this study found that when a specific CA1 engram population that would otherwise be active during the encoding of an overlapping contextual representation was inhibited, the new representation would simply be stored in other CA1 cells instead. Simply put, inhibiting CA1 engram cells inhibits recall of the labeled memory but does not inhibit acquisition of new memories of similar contextual content (Matsuo, 2015). In a related study, using an activity-dependent system based on an *Arc* promoter-driven tamoxifen-inducible Cre recombinase, engram cells were labeled in either the DG or CA3 of the hippocampus during acquisition of a contextual fear memory and subsequently inactivated using optogenetics. This resulted in impaired fear memory recall (Denny et al., 2014).

p0150 Further, the *c-fos–tTA* system combined with a modified receptor, hM3Dq DREADDs (designer receptors exclusively activated by designer drugs), has been employed to activate a contextual engram and subsequently to generate a hybrid memory representation of two experiences (Garner et al., 2012). Another approach that has been successfully used for gain-of-function experiments included taking advantage of CREB overexpression-based neuronal allocation coupled with exogenous receptors. Two studies used CREB to label small populations of LA neurons during fear conditioning with another modified receptor TRPV1 or hM3Dq (Kim et al., 2014; Yiu et al., 2014). When these neurons were reactivated in a novel environment using the TRPV1 ligand (capsaicin) or the DREADDs ligand (clozapine N-oxide), mice showed fear memory recall.

s0060 Learning-Dependent, Persistent Modifications of Engram Cells

p0155 Semon's engram theory of memory described experience-dependent changes as, "the enduring though primarily latent modification in the irritable substance produced by a stimulus" (Semon, 1904). The guiding hypothesis regarding the biological nature of engrams was proposed by Canadian psychologist, Donald Hebb. Hebb (1949) proposed that neurons encoding memory undergo enduring strengthening of some of their synapses through coactivation with presynaptic cells; neurons that "fire together wire together." Since the discovery of LTP by Bliss and Lomo (1973), which was consistent with Hebb's idea, many studies have been dedicated to the characterization of synaptic plasticity, and their potential role in learning and memory. Activity-dependent increases in the size and density of dendritic spines (widely referred to as structural plasticity) have also been proposed as contributing to memory encoding processes (Bailey and Kandel, 1993; Holtmaat et al., 2006; Matsuo et al., 2008; Teule and Segal, 2016). Further, studies have also suggested that cell-wide alterations, such as augmented intrinsic excitability, play a crucial role in memory formation (Daoudal and Debanne, 2003). However, until recently none of these studies could link activity-dependent alterations of synapses and neurons directly to engram cells.

p0160 We will discuss studies in which observed synaptic and/or cellular changes were correlated with a mnemonic behavior. Then, we will refer to a recent study in which an enduring change has been demonstrated in a population of DG granule cells that satisfy all criteria for engram cells—namely, activation by learning and memory recall by reactivation.

s0065 *Synaptic Strength*

p0165 Until recently, the relationship between synaptic/cellular changes and memory was studied by investigating entire brain subregions rather than specific populations of cells activated by a given learning event that hold the specific memory (i.e., memory engram cells). Synaptic plasticity such as LTP can be induced in the hippocampal CA1 region using high-frequency stimulation protocols in vitro, and because this plasticity is dependent on *N*-methyl-D-aspartate (NMDA) receptors, efforts have been made to test whether this form of synaptic plasticity has an essential role in episodic memory (Malenka and Bear, 2004). Early pharmacological blockade

experiments conducted with an NMDA receptor antagonist, AP5, supported the notion that LTP is essential for spatial learning (Morris et al., 1986; Morris, 2006), and the validity of this notion was confirmed with a genetic ablation of the NMDA receptor from the CA1 region of the hippocampus (Bannerman et al., 2012; Tsien et al., 1996).

p0170 In a more recent example, researchers have used CFC paradigms with transgenic mice in which the promoter of an IEG, *Arc*, drives the expression of dVenus, a destabilized version of the fluorescent protein Venus (Eguchi and Yamaguchi, 2009). They found that fear conditioning induced presynaptic potentiation only in the cortical input to the dVenus-positive basolateral amygdala (BLA) cells (Nonaka et al., 2014), which supports the notion that synaptic plasticity in a subset of BLA neurons contributes to fear memory encoding. Crucially however, this study did not provide evidence that reactivation of dVenus-positive cells could evoke behavioral recall. From a technical standpoint, it is important to note that the temporal window of *Arc* labeling in this study was uncontrolled. As a result, BLA neurons were labeled indiscriminately for weeks before the targeted behavioral experience. In another recent study, researchers conditioned a rat to associate a foot shock with optogenetic stimulation of auditory inputs to the LA (Nabavi et al., 2014). Optogenetic delivery of LTD-inducing stimuli (i.e., low-frequency stimulation) to the auditory inputs inactivated the memory of the shock, while subsequent optogenetic LTP (i.e., high-frequency stimulation) to the same auditory inputs reactivated the memory of the shock. The strength of these experiments was that they provided the first causal link between LTP/LTD mechanisms and memory expression. However, this study did not directly demonstrate that these synaptic processes occurred in the same amygdala cell population that was activated by the initial conditioning (i.e., engram-containing cells).

p0175 To claim that an observed increase in synaptic strength reflects a component of the learning-dependent physical/chemical changes occurring in engram cells, three criteria must be met. These criteria are (1) the increase should be observed in a subpopulation of cells activated by the specific learning event, (2) the increase should depend on plasticity associated with the learning episode, and (3) reactivation of the subpopulation of cells should result in behavioral recall. These criteria have recently been met experimentally. In the study (Ryan et al., 2015), hippocampal DG granule cells that were activated by CFC were labeled with a *c-fos* promoter-driven fluorophore mCherry. Simultaneously, presynaptic entorhinal cortex cells were labeled with ChR2 driven by a constitutive CaMKII promoter so that perforant path axons that synapse onto DG engram and nonengram cells could be simultaneously stimulated with light while performing ex vivo patch-clamp recordings. Similar to long-term memory tests, 24 h after training, the α-amino-3-hydroxy-5-methyl-4-isoxazolepropionic acid receptor (AMPA)/NMDA excitatory postsynaptic current ratio was reported to be significantly higher in engram cells compared to neighboring nonengram cells in the same hippocampal slices. Behaviorally, mice that were treated with the protein synthesis inhibitor anisomycin immediately after training showed retrograde amnesia and importantly, engram cell-specific increases in synaptic strength were lacking. However, when anisomycin was administered 24 h after training (outside the consolidation time window), no effect on engram cell synaptic strength was observed and no amnesia occurred. Similar physiological findings were made in the same study using measurements of spontaneous excitatory postsynaptic currents. The engram cell-specific increase in synaptic strength is a form of plasticity that is directly attributable to the training experience. In the future, the generality of these findings should be demonstrated by analyzing engram cells in other subregions of the hippocampus as well as other brain regions. Building on these findings, a recent study demonstrated that *c-fos* promoter labeled engram cells in CA1 exhibit specific place fields in an environment, commonly referred to as hippocampal place cells (Trouche et al., 2016). Furthermore, optogenetic silencing of CA1 engram cells for the specific environment unmasked a subset of quiet neurons, revealing the emergence of an alternative map.

s0070 ***Structural Plasticity***

p0180 Utilizing in vivo two-photon laser scanning microscopy, hallmarks of structural plasticity such as the formation and elimination of individual dendritic spines has been examined during sensory stimulation and motor tasks. One study showed that training mice in a forelimb-reaching task resulted in rapid (less than 1 h) formation of postsynaptic dendritic spines on the output pyramidal neurons of the motor cortex (Xu et al., 2009). These learning-induced spines were preferentially stabilized during subsequent training sessions and maintained long after the completion of behavioral tests. Additionally, the authors found that different motor skills were encoded by a different set of synapses. In another study, training on an accelerated rotarod, but not on a slow rotarod, over 2 days led to an increase in spine formation in the primary motor cortex (Yang et al., 2009). A novel sensory experience provided by switching animals from standard to enriched housing environments resulted in an increase in spine density 1–2 days later in the barrel cortex. These newly formed spines survived experience-dependent elimination during subsequent imaging sessions in the enriched housing environment, reflecting a long-lasting cellular change. These studies strongly suggested that motor behavior is stored in stably connected synaptic networks, but fell short of demonstrating a causal relationship of the altered structural plasticity with motor performance.

p0185 Structural plasticity associated with fast-forming tone fear conditioning memory (Matsuo et al., 2008) and its extinction has also been reported (Lai et al., 2012). Matsuo et al. (2008), used *c-fos–tTA* mice and quantified newly recruited GluR1-positive AMPA receptors in the CA1 subregion of the hippocampus. The authors observed a selective increase in mushroom-type spines of engram cells 24 h after learning. A caveat of this study was that nonengram cells were not directly examined, making it difficult to discern whether or not the changes observed were specific to a defined set of cells active only during learning. In the other study, correlations between fear memory expression and spine elimination, or fear memory extinction and spine formation were reported by imaging postsynaptic dendritic spines of layer V pyramidal neurons in the mouse frontal association cortex. Strikingly, dendritic spine elimination and formation induced by fear conditioning and extinction, respectively, occurred on the same dendritic branches (within a distance of 2 μm) in a cue- and location-specific manner (Lai et al., 2012). Interestingly, reconditioning following extinction eliminated spines formed during extinction, suggesting that within vastly complex neuronal networks, fear conditioning, extinction, and

reconditioning lead to opposing changes at the level of individual synapses. Do these spine dynamics reflect what occurs at the level of cell populations that store engrams for tone-shock association memory? Additional research will help answer such questions, which hold great importance for understanding memory formation and retrieval.

p0190 Two studies investigated synaptic structural plasticity in the DG cell population holding an engram component for the contextual information of a CFC experience (Roy et al., 2016; Ryan et al., 2015). These DG cells had been activated by CFC and labeled by ChR2. Their optogenetic reactivation evoked the context-specific fear memory recall, satisfying a key criterion for engram-bearing cells. Furthermore, ex vivo patch-clamp recordings and high-resolution confocal imaging revealed that these ChR2-positive DG cells possessed an increased spine density in the distal dendrites compared to the neighboring ChR2-negative DG cells 24 h after CFC training (Ryan et al., 2015). The engram cell-specific increase in dendritic spine density was abolished by anisomycin treatment immediately after training but not 24 h later. These data serve as direct evidence for increased structural plasticity in memory engram cells that parallel the engram cell-specific synaptic plasticity discussed earlier. In the future, researchers must improve the temporal control of engram labeling to precisely observe changes occurring during and immediately after training episodes, which will also make it possible to examine engram cells for working memory and decision-making tasks.

p0195 Thus far, the research has demonstrated that memory engram cells in the hippocampus exhibit increased dendritic spine density that parallels the learning event. An even more elegant approach to examine the relationship between dendritic spines of engram cells and memory would be to selectively remove a large number of spines that were specifically formed during learning (Hubener and Bonhoeffer, 2010) and see whether their removal results in memory loss. In a very recent study, such an experimental manipulation was achieved (Hayashi-Takagi et al., 2015). The authors developed a novel synaptic optoprobe, AS-PaRac1 (activated synapse targeting photoactivatable Rac1), which specifically labels recently potentiated spines and can subsequently induce shrinkage of AS-PaRac1-containing spines in vivo. Using this technology during motor learning, it was found that optical shrinkage of potentiated spines disrupted the acquired learned behavior. Importantly, the original motor learning was unaffected by an identical manipulation of spines evoked by a distinct motor task that requires the same cortical brain region. These experiments indicated that synaptic optogenetic methods could be utilized to visualize and manipulate single memory engrams at the level of synapses.

s0075 *Cellular Excitability*

p0200 In addition to synaptic plasticity mechanisms as a candidate for enduring physical/chemical changes evoked by learning in memory engram cells, cell-wide excitability alterations have been extensively studied. Many groups have demonstrated that cells in the LA can be genetically engineered to exhibit higher levels of cell-wide excitability even prior to learning, by overexpressing a transcription factor CREB. After tone fear conditioning, ablation of these high-CREB, high-excitability cells impaired fear memory expression, suggesting that the memory engram is preferentially allocated to these cells (Yiu et al., 2014; Zhou et al., 2009). Similar high CREB-induced neuronal allocation has been reported in the hippocampal DG (Park et al., 2016). A more recent study showed that a shared neuronal ensemble is capable of linking distinct contextual memories, only when these two experiences occur close in time during periods of high excitability in hippocampal CA1 (Cai et al., 2016). Similar memory linking during periods of high excitability has been observed for LA engram cells in a tone fear conditioning paradigm (Rashid et al., 2016). Further, novel context exploration during a narrow time window before or after weak object recognition training results in the formation of a long-term object recognition memory (Nomoto et al., 2016). This phenomenon depends on the degree of overlap between the neuronal ensembles for each experience. These studies suggest that excitability-induced memory allocation may serve as a putative mechanism underlying enduring storage of memory information.

s0080 *Connectivity Between Engram Cells as the Mechanism for Retained Memory*

p0205 In the study by Ryan et al. (2015), the authors observed dissociation between protein synthesis-dependent synaptic strengthening and memory retention 24 h after training. This prompts a logical question: how is the memory retained? Undoubtedly, the cellular and molecular processes required for establishing specific connectivity during memory encoding includes synaptic strengthening such as LTP as well as de novo protein synthesis. One possibility is that memory is stored in a specific pattern of connectivity between distributed engram cell ensembles, which is established during encoding and retained during the consolidation time window in a protein synthesis-independent manner. In the same study, the authors tested this possibility by performing two sets of experiments using ex vivo electrophysiological and in vivo IEG technologies. When both DG and hippocampal CA3 engram cell ensembles were simultaneously labeled and the presynaptic DG engram cells were activated optogenetically, the occurrence of postsynaptic responses in CA3 engram cells was significantly higher (~80%) than CA3 nonengram cells (~25%), and these proportions were not affected by protein synthesis inhibition. In another experiment, engram cells were simultaneously labeled in the DG, CA3, and BLA during CFC. One day after training, reexposure to the conditioning context preferentially activated engram cells in all three brain regions as measured by cFos-positive cell counts, and importantly, this phenomenon was significantly impaired by anisomycin treatment only during the consolidation time window. However, direct optogenetic activation of DG engram cells resulted in a greater than chance level of cFos overlap with CA3 or BLA engram cells in both control and anisomycin-treated mice. Together, these results indicated intact functional connectivity among engram cell ensembles distributed in neural circuits encompassing multiple brain regions and supported the hypothesis that consolidated memories are stored by engram cell-specific connectivity formed in a protein synthesis-independent manner. Further work will elucidate the molecular mechanisms underlying this retained connectivity following protein synthesis blockade.

s0085 ***Synaptic Strengthening as a Mechanism for Memory Retrieval***

p0210 Using the integrative engram-based findings, the authors suggested that engram cell-specific synaptic strength is necessary for the retrievability of specific memory engrams (Ryan et al., 2015), while the memory information is encoded in a pattern of engram cell ensemble connectivity. This idea was supported by the finding that amnesic mice lacked synaptic strength increases after learning, which prevented the effective activation of engram cells by natural recall cues and engram cell spiking that is crucial for successful memory recall. Nevertheless, the information stored in engram cell ensemble connectivity patterns could be retrieved by optogenetic stimulation of various nodes in the engram cell circuit. The notion that synaptic strengthening is crucial for memory retrieval, but not for stable storage of memory per se, is consistent with a number of recent complementary studies. For example, recently it was shown that optogenetically induced LTD of rat amygdala cells impaired preformed conditioned fear memory expression (Nabavi et al., 2014). Importantly, subsequent optogenetically induced LTP of the same cells restored natural cue-evoked recall of the fear memory. The most parsimonious explanation of these results is that memory information must have persisted in the brain of the rats even after the amygdala synapses were depressed, and moreover that the lack of synaptic potentiation prevented successful memory retrieval. Supporting this perspective is the demonstration that amnesia for a purely contextual memory can be overcome by direct engram activation paired with simultaneous presentation of aversive shock (Ryan et al., 2015). Other research found that contextual fear memories formed during a specific period within adolescent development were not expressed in recall tests until adulthood (Pattwell et al., 2011). Interestingly, this developmental change correlated with delayed learning-specific synaptic potentiation of the BLA fear circuit. Therefore, the fear memory was present during adolescence but its retrievability was temporarily impaired due to the lack of sufficient synaptic potentiation in BLA ensembles. In *Aplysia* (Chen et al., 2014), reminder experiments have shown that amnesia for the canonical gill withdrawal sensitization behavior could be restored by additional puffs of serotonin, and that this response persisted despite significantly reduced presynaptic varicosities. Collectively, these studies support a dissociation of synaptic strength and memory persistence, and point to a crucial role for experience-dependent synaptic strengthening in the reactivation/retrievability of a memory engram.

s0090 ***Implications for Memory Engram Research***

p0215 A dissociation between augmented synaptic strengthening and engram cell connectivity as the mechanism for consolidated memory storage has significant implications for the neurobiology of memory consolidation because the conceptual framework described earlier may be used to attribute experience-dependent molecular/cellular processes to memory storage or retrieval. Since traditional approaches that demonstrated the formation of a long-term memory relied on memory retrieval itself, it cannot be assumed that the memory consolidation time window is specifically for the storage of information. Within this interpretation, molecular mechanisms that serve to potentiate or strengthen synaptic transmission (Kandel, 2012; Lisman et al., 2012; Sacktor, 2011) are parsimoniously attributable to memory retrievability. Central to this dissociation is the molecular basis for information retention, which is clearly crucial for establishing engram cell connectivity and stably maintaining these complex patterns over time. It is known that NMDA receptor-dependent synaptic plasticity results not just in potentiated synapses but also in the formation of new functional synaptic connections through synapse unsilencing (Liao et al., 1995). Memory encoding-induced establishment of new functional connectivity could be facilitated by AMPA receptor insertion into preexisting silent synapses. It is widely accepted that LTP has an early and a late phase, namely E-LTP and L-LTP, with the latter being sensitive to protein synthesis inhibitors (Davis and Squire, 1984). Survival of preferential engram cell connectivity upon protein synthesis inhibitor treatment (Ryan et al., 2015) suggests that the induction of engram connectivity may share mechanisms common to E-LTP. On the other hand, impairing L-LTP has been shown to prevent synapse unsilencing, which supports the hypothesis that unsilencing silent synapses is unlikely to be a major contributor for the retention of connectivity (Kasten et al., 2007). Another possibility is that a subset of learning-induced dendritic spines is responsible for novel connectivity pattern formation between engram cells. In any of these scenarios, the retention of engram cell connectivity could conceivably be mediated by the homeostatic regulation of steady-state AMPA receptor trafficking. Consistent with this idea is a recent study showing that protein synthesis inhibitors, when administered prior to recall tests, transiently impaired AMPA receptor expression and memory retrieval (Lopez et al., 2015). More recently, it has been suggested that microRNAs and/or perineuronal nets (Gallistel and Balsam, 2014; Tsien, 2013) may mediate the long-term maintenance of memory engram.

p0220 A major unanswered question regarding engram cell connectivity is the time period during which such complex patterns are maintained in vivo. On a related note, it will be important to determine whether the formation and elimination of connectivity patterns is reversible. Even though it has been shown through engram cell overlap analysis, when the positive or negative emotional valence associated with a contextual memory is reversed, the functional connectivity of DG to BLA engram cells changes (Redondo et al., 2014), a direct analysis of synaptic connections will be necessary to understand the true physiological nature of the plasticity within preformed connectivity. Nevertheless, if engram cell connectivity is the substrate of memory information storage, then it will be necessary to fully explore the structure and function of the engram circuit. This would require comprehensive mapping of the entire engram circuit connectome for a given memory. This could be achieved by combining engram labeling technology, whole-brain IEG activity measurements (Wheeler et al., 2013), and three-dimensional imaging of intact transparent brains (Chung et al., 2013). Furthermore, by using in vivo calcium imaging of engram cells across multiple brain regions (Lecoq et al., 2014), functional properties of engram circuits can be studied.

p0225 Synaptic plasticity is a ubiquitous feature of neurons that seems to have arisen with the first nervous system in a common ancestor of cnidarians and bilaterians over a billion years ago (Tonegawa et al., 2015a). From this evolutionary point of view, synaptic plasticity can be considered a fundamental neuronal property, the disruption of which in brain regions such as the

hippocampus or amygdala will impair the encoding and retrieval of memory. In contrast, engram cell connectivity may be a substrate that naturally increases in complexity as brain anatomy evolves. Therefore, for a more complex brain anatomy, there is a greater opportunity for encoding detailed memories through hierarchical engram circuits distributed across brain regions. Consistent with Hebb's original vision (Hebb, 1949), engram cell connectivity patterns are a potential mechanism of information storage. Further research in this direction may provide significant new insights into the storage of memory.

s0095 Storage Versus Retrieval Debate on Amnesia

p0230 The phenomenon whereby a newly formed memory transitions from a fragile, short-term state to a stable, long-term state is termed memory consolidation (Müller and Pilzecker, 1900). A crucial feature of consolidation is a finite time window that begins immediately after the learning event, during which a given memory is susceptible to disruption. The biological importance of this time window has been repeatedly demonstrated by interventions ranging from electroconvulsive shock (Duncan, 1949; McGaugh, 1966) to protein synthesis inhibitors (Davis and Squire, 1984; Flexner et al., 1967), which if delivered specifically during the consolidation window results in retrograde amnesia. Therefore, the prevailing view in neuroscience holds that retrograde amnesia due to disrupting consolidation is a deficit of memory storage (McGaugh, 2000; Nader and Wang, 2006; Squire, 2006). However, an alternative interpretation maintains that the memory engram itself remains intact, but access of retrieval mechanisms to the engram has been distorted (Miller and Matzel, 2006; Riccio et al., 2006; Sara, 2000; Squire, 1982). Since purely behavioral studies rely on memory expression as the sole evidence of memory, it has not been possible for these approaches to rigorously discriminate between storage and retrieval explanations. Due to the fact that the neurobiology of memory formation is anchored in experimental amnesia, discriminating between these two scenarios holds great scientific value. In addition, similar issues have been debated when amnesia is observed following trauma, stress, drug use, or aging. From a clinical perspective, pathological cases of amnesia that are due to retrieval deficits may in principle be treatable rather than merely preventable. Even though efforts are being made to prevent and treat the various causes of amnesia, there remains no treatment for the symptom of memory loss itself.

p0235 Historically, several attempts to demonstrate that amnesia after disrupted memory consolidation is due to a deficit of memory retrievability have yielded inconclusive results and theoretical stalemates (Gold et al., 1973; Hardt et al., 2009; Lewis, 1979; Matzel and Miller, 2009; Miller and Springer, 1974; Sara and Hars, 2006; Spear, 1973). Importantly, the existence of a memory engram in retrograde amnesia has been ostensibly supported by studies showing attenuated amnesia by reminder-induced and spontaneous recovery (Miller and Springer, 1972, 1973; Quartermain et al., 1970; Sara, 1973; Serota, 1971; Springer and Miller, 1972). However, these approaches suffer from significant caveats. Reminder treatments have been shown to result in new learning (Gold et al., 1973; Gold and King, 1974), and spontaneous recovery is partial and may be explained by parallel engrams (Squire and Barondes, 1972). Directly examining memory engrams circumvents the ambiguities of reminder training and spontaneous recovery, because it provides an opportunity to directly evoke memory recall in a neutral context. By doing so, the need to rely on stimuli associated with training to elicit memory recall without the use of confounding experimental parameters such as further training is avoided.

s0100 Retrieval of Lost Memory From Retrograde Amnesia

p0240 One study investigated retrograde amnesia due to disrupted memory consolidation using memory engram technologies (Ryan et al., 2015; Tonegawa et al., 2015a). Notably, direct optogenetic activation of amnesic DG engram cells in mice resulted in full retrieval of the ostensibly lost contextual fear memory. This optogenetic-based retrieval of memory persisted for at least 8 days after training, reflecting the longevity of engram cells and their corresponding circuits in amnesic mice. To substantiate this striking behavioral result, generality of the optogenetic memory retrieval was examined across a range of experimental conditions. Lost memory was retrieved by optogenetic stimulation of ChR2-labeled engram cells in hippocampal CA1. Amnesia for tone fear memory was generated with anisomycin, but the memory was retrieved by optogenetic stimulation of LA engram cells. Similar to the consolidation experiment, lost memory was also retrieved from retrograde amnesia due to disrupted memory reconsolidation by direct activation of DG engram cells. An alternative protein synthesis inhibitor, cycloheximide, was used to generate amnesia and subsequent activation of DG engram cells again retrieved the target memory. Finally, using a contextual updating protocol (Ramirez et al., 2013), the authors showed that amnesic engram cells retained information about context specificity and could be restored to a condition where they could be retrieved by natural contextual cues. In addition to behavioral measurements, ex vivo characterization of DG engram cells revealed two engram cell-specific properties. First, engram cells formed under normal conditions (i.e., no posttraining addition of protein synthesis inhibitors) showed significantly increased dendritic spine density relative to nonengram cells. Second, patch-clamp recordings of excitatory postsynaptic currents in paired engram and nonengram cells elicited by presynaptic stimulation of perforant path axons showed substantially higher synaptic strength in engram cells.

p0245 Clearly, hallmarks of synaptic plasticity occurred exclusively in engram cells for a given learning episode. One day after anisomycin treatment, analysis of engram cells showed that protein synthesis inhibition had abolished engram-cell-specific increases in both dendritic spine density and synaptic strength, but did not alter either property in nonengram cells (Ryan et al., 2015). Importantly, anisomycin treatment 24 h after training (i.e., outside the consolidation time window) had no effect on engram cell-specific structural and synaptic plasticity. Together, these behavioral, physiological, and cell biological results clearly showed that engram cell-specific structural and synaptic plasticity is strongly correlated with normal memory function. In addition, these findings showed a stark dissociation between protein synthesis-dependent synaptic plasticity (L-LTP) and memory, since engram cells

retained memory information 24 h after training even when protein synthesis-dependent engram cell-specific increases in spine density and synaptic strength was lacking.

s0105 **Restoring Memory in Mouse Models of Early Alzheimer's Disease**

p0250 AD is the most common cause of brain degeneration and typically begins with impairments in cognitive functions (Selkoe, 2001, 2002). Most research has focused on understanding the relationship between memory impairments and the formation of two pathological hallmarks seen in late stages of AD: extracellular amyloid plaques and intracellular aggregates of tau protein. Early phases of AD have received relatively less attention, although synaptic phenotypes have been identified as major correlates of cognitive impairments in both human patients and mouse models (Jacobsen et al., 2006; Terry et al., 1991). Several studies have suggested that the episodic memory deficit of AD patients is due to ineffective encoding of new information (Granholm and Butters, 1988; Hodges et al., 1990; Weintraub et al., 2012). However, since cognitive measures used in these studies rely on memory retrieval, it has not been possible to rigorously discriminate between impairments in information storage and disrupted retrieval of stored information. This issue has an important clinical implication: if the amnesia is due to retrieval impairments, memory could be restored by technologies involving targeted brain stimulation.

p0255 Focusing on memory engrams, a very recent study examined long-term memory impairments in mouse models of early AD (Roy et al., 2016). Using APP/PS1 AD mice (Jankowsky et al., 2004), the authors observed that amyloid plaque deposition started in 9-month old mice, however memory deficits were clearly visible several months before plaque deposition. In a contextual fear conditioning paradigm, 7-month old AD mice exhibited normal short-term memory but performed poorly 24 h later in long-term memory tests. This behavioral impairment correlated with a decreased number of cFos-positive cells in the DG as well as decreased engram cell-specific dendritic spine density in AD mice. However, preferential functional connectivity between engram cells was maintained in the early AD mice. Next, to examine whether functional DG engram cells persisted in early AD mice, despite these animals being amnesic at the behavioral level, the authors developed a novel strategy using a double adenoassociated virus system to label engrams (Roy et al., 2016). As expected, engram-labeled early AD mice were amnesic a day after fear conditioning; but remarkably, these mice exhibited memory recall as robustly as equivalently treated control mice in response to blue light stimulation of engram cells. These experiments indicated a deficit of memory retrievability during early AD-related memory loss. Following early findings (Engert and Bonhoeffer, 1999; Hyman et al., 1986; Maletic-Savatic et al., 1999) that LTP induction results in a spine density increase, Roy et al. (2016) applied repeated optogenetic LTP induction specifically to entorhinal cortex engram cell inputs into DG engrams. This procedure reversed the spine density deficit in early AD mice. Crucially, this spine restoration led to the rescue of a long-term fear memory in AD mice, an effect that persisted for at least 6 days after training. In contrast, applying the optogenetic LTP protocol to a large portion of excitatory entorhinal cortex terminals in the DG (i.e., with no restriction to the terminals derived from entorhinal cortex engram cells) did not restore long-term memory. The authors also demonstrated that an ablation of DG engram cells containing restored spine density prevents the rescue of long-term memory in early AD mice. The versatility of this engram-based intervention was supported by showing long-term memory restoration in AD mice using other memory paradigms: inhibitory avoidance and novel object location paradigms. Together, it is clear that genetic manipulations of specific neuronal populations can have profound effects on cognitive impairments of AD (Cisse et al., 2011). These strategies applied to engram circuits are capable of supporting long-lasting improvements in cognitive functions, which may provide insights and therapeutic value for future approaches that would rescue memory in AD patients.

s0110 **Engram Cell Pathways**

p0260 When describing neuronal ensembles participating in a given memory, Semon often used the phrase engram complex to suggest that the entire engram would be composed of multiple components. Prior to optogenetics, studies suggested that each of the different hippocampal subregions might play a different role in the formation of a contextual memory (Ji and Maren, 2008; Lee and Kesner, 2004; Leutgeb et al., 2004). Also, for contextual fear or reward memory representations, distinct subpopulations of BLA cells are recruited to provide engrams for negative or positive valence (Redondo et al., 2014). Therefore, a notion of distinct engram cell pathways emerges for each memory. How each engram component in the pathway contributes to the overall engram complex is a matter of great interest. Only recently have studies on this topic begun, but engram pathways for a few additional memories can already be conceived. For example, for episodic memories, the hippocampus is known to play a crucial role in associating "what," "where," and "when" information (Squire and Wixted, 2011; Tulving, 2002). DG and CA3 engrams provide context information along with ocean cells in layer II of medial entorhinal cortex (Kitamura et al., 2015), while CA1 engrams may provide both spatial and temporal sequence information via time cells (MacDonald et al., 2011). Similarly, an engram pathway would likely be crucial for tone fear conditioning memories. Auditory information may be stored in an engram in the auditory cortex (Weinberger, 2004); the context in which the tone occurred may be stored in hippocampal engrams; and the association of tone, context, and foot shocks may be stored in amygdala engram cells (Ehrlich et al., 2009). Together, these three populations of engram cells, each harboring a distinct engram component may constitute an engram cell pathway for the tone conditioning memory engram complex. With regard to plasticity, it is possible that potentiated synapses in engram cells may be just a contributing element of a memory engram complex and that a specific pattern of connectivity between different types of engram cell populations along the engram cell pathway maintains the content of a memory engram complex (Hebb, 1949). Consistent with this idea, a study

suggested that for a contextual fear memory, preferential connectivity of DG engram cells with engram cells in downstream CA3 and BLA is the crucial substrate for the consolidated memory (Ryan et al., 2015). It has been shown that optogenetic stimulation of upstream DG engram cells cannot retrieve memory if the activity of the downstream CA1 subfield receives chemogenetic inhibition specifically during training (Ryan et al., 2015).

p0265 Memory engram pathways may be linear, but parallel pathways could also contribute to an engram complex. In one study, the authors showed that blocking CA1 neuronal activity by prolonged optogenetic inhibition during the recall of remote memory resulted in elevated activity in the ACC (Goshen et al., 2011). This compensation mechanism bypassed the requirement of CA1 and resulted in normal remote memory recall. Another recent study found that inhibiting dorsal hippocampus activity by local infusions of glutamate receptor antagonists interrupted natural contextual fear memory recall when the animal was returned to the original fear-conditioned context, but light activation of memory engram cells in the retrosplenial cortex was sufficient to overcome this impairment and rescued the behavior phenotype (Cowansage et al., 2014). Taken together, these results support the existence of multiple functional engram pathways for a given memory. Animals may preferentially use one default pathway for normal memory recall, but under certain conditions other latent pathways could be brought online to compensate for the default one, which allows greater flexibility to the process of encoding and retrieving memories.

p0270 When engram pathways of greater complexity are being studied, it is important that appropriate test conditions are applied to demonstrate necessity and sufficiency for engram cell populations along these pathways. Temporally and spatially restricted perturbations are required to reveal the role of a given engram cell population. Traditional lesion and pharmacological blockade experiments have suggested that hippocampal CA1 is not necessary for the recall of remote memory, yet acute inhibition of CA1 with optogenetics caused defects in remote memory recall. Further investigation showed that with extended optogenetic inhibition protocols, which mimicked the effects of lesion and drug treatments, additional structures such as the ACC compensated for inactivation of CA1 (Goshen et al., 2011). Thus, necessity of CA1 for remote memory recall can only be revealed with acute interventions. Similar temporal dynamics may also apply to engram cells in other brain areas, including thalamic nuclei (Do-Monte et al., 2015).

p0275 Spatially nonselective inhibition of all dorsal DG neurons had no effect on memory recall, making them seem unnecessary for this process (Kheirbek et al., 2013). However, memory was impaired if a selected subset of DG neurons previously active during training was inhibited during recall, indicating that DG engram cells are indeed necessary for memory recall (Denny et al., 2014). Similarly, selective activation of an engram cell population in the DG induced the recall of a previously formed fear memory (Liu et al., 2012; Roy et al., 2016), demonstrating the sufficiency of engram cells for memory recall in DG, while nonselective activation of dorsal DG neurons not only failed to induce artificial memory recall but actually abolished natural memory recall in the original context (Kheirbek et al., 2013). The latter result may be due to neuronal competition and lateral inhibition among different subpopulations of cells within the subregion as reported by other studies (Han et al., 2007; Tanaka et al., 2014), and illustrates that precise spatial resolution is needed to properly characterize the contribution of engram cells.

p0280 Rigorous experimental strategies must be applied to the study of engram cell pathways to identify specific functional contributions to animal behavior. One possibility is to follow what geneticists termed epistasis analyses. In these experiments, scientists identified functional roles of specific genes as well as their downstream target genes in a variety of intracellular processes. Using an analogous approach for neural circuits, a recent study demonstrated that retrieval of a positive memory by optogenetic activation of DG engram cells was prevented by simultaneous inhibition of downstream BLA engram cell projections to the NAcc (Ramirez et al., 2015). This finding identified specific downstream connectivity of engram cells that is crucial for the optogenetic retrieval of positive memory. Even so, in trying to map these functional engram pathways, it is critical to keep in mind that flexible and dynamic systems are involved; as such, nonrigid models are required, with changing necessity and sufficiency functions for different components.

s0115 Engram Cell Engineering

p0285 The great virtue of gain-of-function engram technology is not only that it allows researchers to identify populations of engram cells and thereby directly characterize their properties but also that it allows scientists to engineer engram cells—activate and inactivate them—using optogenetic or pharmacogenetic techniques and thereby manipulate the mnemonic status of the animals in vivo both in health and disease. These studies have just begun and here we discuss three examples in mice. These are creating a false memory, switching memory valence, and attenuating depression-related behavior by activating a positive memory. These studies help expand our knowledge about how memory is stored and retrieved but are also revealing neural circuits underlying interactions of memory with other cognitive functions, such as emotion.

s0120 Creating a False Memory

p0290 Even though memory is constructive in nature, the act of recalling a memory renders it labile and highly susceptible to modification (Bartlett, 1932; Lewis, 1979; Nader et al., 2000; Przybyslawski and Sara, 1997). In humans, memory distortions and illusions occur frequently, which often results from incorporation of misinformation from external sources (Loftus, 2003; Roediger and McDermott, 1995; Schacter and Loftus, 2013). Several cognitive studies in humans have reported robust activity in the hippocampus during the recall of both false and genuine memories (Cabeza et al., 2001). However, human studies performed using

behavioral and functional magnetic resonance imaging techniques have not been able to delineate the brain regions and circuits that are responsible for generation of false memories. In rodents, two lesion studies investigated object recognition memory in rats with perirhinal cortex lesions and found that the subjects tended to treat novel experiences as familiar, thus leading to the false recognition of objects (McTighe et al., 2010; Romberg et al., 2012). Interestingly, studies on false memories in animal models are rare, and this may be a contributing factor to the slow progress in the elucidation of potential neuronal mechanisms underlying human false memories.

p0295 In light of the fact that humans have a rich repertoire of mental representations generated internally by processes such as conscious or unconscious recall, dreaming, and imagination (Schacter et al., 2007), one possible reason for the formation of an episodic false memory is that the memory of a past experience becomes associated with a current external event of high valence. Using a method that permits optogenetic labeling and manipulation of memory engram cells (Liu et al., 2012), a study tested this possibility in mice (Ramirez et al., 2013). The authors labeled contextual engram cells in the DG with ChR2 by exposing mice to context A, thereby activating cFos in the engram. On the next day, as the labeling window was shut down by switching mice from regular to doxycycline food, mice received foot shocks in a distinct context B as their context A engram cells were artificially reactivated with pulses of blue light (Fig. 1). On the third day, when the animals were reintroduced to context A to test the context A shock association memory, animals displayed freezing behavior despite never having received foot shocks in context A. The freezing behavior was not due to generalization because the mice did not freeze above background levels in another distinct context C. Of course, these mice also froze when tested in context B, indicating that they also formed a genuine context B shock association memory. Importantly, freezing levels in context B were significantly lower than in a group of mice that did not receive blue light delivery on day 2 while foot shocks were delivered. This observation suggests that formation of the false and genuine memory representations on day 2 were in competition. An additional observation made in this study was that, although the mice with the false fear memory for context B did not freeze in a distinct third context C, they did freeze significantly when blue

AU2

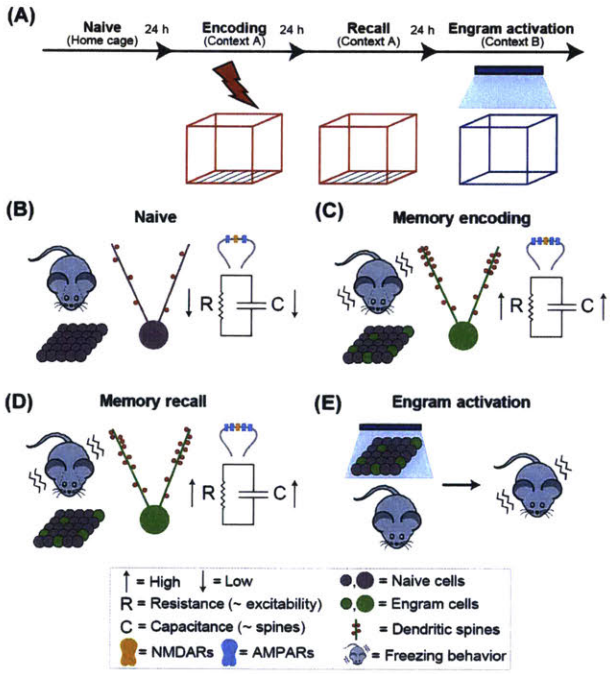

f0010 **Figure 1** Tagging and manipulating memory engrams. Using the activity-dependent labeling technology developed by Liu et al. (2012), memory engram cells for a contextual fear memory can be tagged with ChR2 and subsequently reactivated with blue light to induce memory recall (A). Prior to memory encoding, neurons in naïve animals exhibit baseline physiological properties such as dendritic spine density and AMPA/NMDA ratio (B). During memory encoding, tagged engram cells (green) develop augmented spine density as well as AMPA/NMDA ratio, which correlates with freezing behavior (C). During natural memory recall, engram cell properties are similar to those following encoding (D). Importantly, in a neutral context, engram cell reactivation with blue light induces freezing behavior (E). *AMPAR*, alpha-amino-3-hydroxy-5-methyl-4-isoxazole propionic acid receptor; *NMDAR*, *N*-methyl-D-aspartate receptor.

light was delivered in context C. This indicates that the engram for the false memory is as light reactivatable as the engram for the genuine memory, as previously reported (Liu et al., 2012). Moreover, using the same cFos-driven ChR2-labeling strategy, a recent study demonstrated that, in addition to optogenetically driving a hippocampal contextual engram, BLA cells responding to a stimulus of high valence can be simultaneously activated to form an association with the hippocampal-driven contextual memory (Ohkawa et al., 2015). The synchronous activation of hippocampus cells representing a CS (e.g., context) and the amygdala cells representing an US (e.g., foot shocks) led to the creation of a new associative fear memory and shared similar molecular mechanisms as the formation of a genuine fear memory (i.e., protein synthesis dependence and NMDA dependence).

p0300 Such findings indicate that at least some form of false memory is generated by an association of internal brain activity representing recall of a past experience with the current external or internal experience of high valence (Ohkawa et al., 2015; Ramirez et al., 2013). Since the underlying neurophysiological mechanisms for such an association are similar to the ones that occurred when a genuine memory was formed, it is not surprising that the subjects behaved as if the false memory was formed by a perceived real experience.

p0305 Although, further studies are necessary to assess the relationship between the artificially induced false memory in these animal models and human false memories, the optogenetically induced false memory is consistent with the temporal context model in humans, which posits that contextual memory reactivation can be linked to novel information that is presented at the time of reactivation (Gershman et al., 2013; St Jacques and Schacter, 2013). A crucial point here is that the formation of false memories in humans often occurs as a result of recombining mnemonic elements of discrete past experiences into a new, reconstructed memory that is not a veridical representation of the past. These memories in humans are not formed de novo and require pre-existing memories as a scaffold onto which distinct experiences can be incorporated to update the memory itself (Garner et al., 2012; Gershman et al., 2013; Tse et al., 2007). The optogenetically induced mouse false memory shares this feature of human false memories.

s0125 Switching Memory Valence

p0310 Although most studies on engram cells have focused on their properties in one anatomical region, diverse engram components within an engram cell pathway range across multiple brain regions. For example, the hippocampus and associated cortex are known to play a crucial role in episodic memories by associating the emotionally neutral components of the episode: information like what, where, and when (Anderson and Phelps, 2001; Zola-Morgan et al., 1991). On the other hand, the amygdala is known to be the main hub for the storage of emotional valences associated with experiences. The amygdala receives inputs from all sensory modalities, including processed inputs from the hippocampus, perirhinal, and entorhinal cortices, and the prefrontal cortex (Sah et al., 2003; Senn et al., 2014; Trouche et al., 2013). Neurons in the amygdala respond to positive as well as negative values (Paton et al., 2006) and inactivating the amygdala prevents the association between neutral stimuli and emotion both in an anterograde (Miserendino et al., 1990) and retrograde manner (Han et al., 2009).

p0315 Considering the distinct properties of the hippocampus and the amygdala, do engram neurons in these two brain regions link up to form and drive a specific memory (i.e., contextual fear representation)? If so, does the contextual component of a hippocampal engram have the flexibility to associate with different engram components (i.e., fear or pleasure) in the amygdala? These issues were addressed by applying memory engram technology to fear (foot shocks) or reward (male mice interacting with female mice) conditioned mice (Gore et al., 2015; Redondo et al., 2014). The contextual component (context A) of the context-specific fear or reward conditioning engram complex in the hippocampal DG was labeled with ChR2 following the previously established protocol (Liu et al., 2012), and the resulting fear or reward memory was confirmed with an optogenetic place avoidance or place preference test. These animals were then subjected, in a distinct context (context B), to a second conditioning session with US of the opposite valence (from foot shocks to female exposure or vice versa) as their context A engram cells were reactivated by blue light pulses (Ramirez et al., 2013). These mice switched the overall valence of the memory from negative to positive or positive to negative, corresponding to the order of two successive conditionings. Further, it was shown that the negative to positive switch is achieved not only by the prevalence of the reward memory but also by the diminishing of the fear memory. The reversal of the dominant valence associated with the DG memory engram was also demonstrated at the cellular level by comparing the level of engram reactivation in the amygdala after DG optogenetic engram stimulation in experimental and control mice. Only mice that underwent the memory reversal protocol showed a reduction in DG engram to amygdala engram functional connectivity. Intriguingly, this switch of valence was not observed when the amygdala engram was labeled and its light activation was used during the protocol. These results indicated that in the DG, neurons carrying the memory engram for a given neutral context exhibit sufficient plasticity such that it is possible for the valence of a conditioned response evoked by their reactivation to be reversed by reassociating this contextual memory engram with new US of the opposite valence (Tonegawa et al., 2015b).

s0130 Countering Depression by Positive Valence Engram Activation

p0320 The conceptual framework of the interaction between the neural circuits governing memory valence and those encoding neutral components of episodic memory is that the engrams for the latter, like the one in the DG, are free to associate with either positive or negative valence engrams in the amygdala. The development of new technologies that permit engineering of these engrams opens up the possibility of adding a novel approach to the classical approaches for the treatment of psychopathologies (Wolpe, 1958). For

example, depression is characterized by a pervasive and persistent blunted mood that is accompanied by motivational impairments and a loss of interest or pleasure in normally enjoyable activities. However, how positive episodes interact with psychiatric disease-related impairments at the neural circuit and systems levels has remained largely unknown (Keller et al., 2000).

p0325 In a recent study, the researchers demonstrated that optogenetic reactivation of engram cells formed in the DG by a naturally rewarding experience was sufficient to acutely suppress depression-related behavior (Ramirez et al., 2015). This study further demonstrated that glutamatergic transmission from the amygdala's axonal terminals to the NAcc shell is necessary for the real-time antidepressant-like effects of the reactivated DG engram cells. Notably, the NAcc has recently been identified as a potential therapeutic node for deep brain stimulation to alleviate anhedonia (Schlaepfer et al., 2008) in humans, and previous reports also identified amygdala axonal terminals onto NAcc as being sufficient to support self-stimulation and reward-seeking behavior in a dopamine D1 receptor-mediated manner (Britt et al., 2012; Stuber et al., 2011). It is important to note here that directly reactivating cells associated with a positive memory is qualitatively different from exposing depressed subjects to naturally rewarding experiences, which would normally activate these corresponding brain areas in the healthy brain. In the psychiatric diseased-related state, acute administration of naturally rewarding external cues may not have access to, or sufficiently activate, the positive valence engram cells' representations associated with the positive experience. Direct optogenetic stimulation of these cells may be able to overcome this obstacle.

p0330 It is possible that the acute behavioral changes observed during optogenetic stimulation (Ramirez et al., 2015) may reflect the degree to which directly stimulating neurons might bypass the plasticity that normally requires antidepressants weeks or months to achieve, thereby temporarily suppressing the depression-like state. However, the neural underpinnings inducing and correlating with long-lasting rescues have remained poorly understood. Two studies (Friedman et al., 2014; Ramirez et al., 2015) found that chronic activation of the ventral tegmental area (VTA) dopaminergic reward system, or chronic reactivation of DG engram cells previously active during a positive experience, respectively, had antidepressant-like behavioral consequences that outlasted acute optical stimulation. The former study identified an optogenetically induced increase in K^+ channels and subsequent normalization of VTA firing rates as crucial contributors to the antidepressant-like effects. In the latter study, while the causal link between chronically reactivated positive memory engrams and the corresponding rescue of behaviors remains elusive, many tantalizing hypotheses surface. These include a normalization of VTA firing rates, epigenetic and differential modification of effector proteins (e.g., CREB, BDNF) in areas upstream and downstream of the hippocampus, a reversal of neural atrophy in areas such as CA3 and prefrontal cortex, or hypertrophy in the BLA. Together, these studies provide causal evidence that sparse populations of cells can be directly manipulated in a terminal-specific and activity-dependent manner to modulate a specific behavioral program associated with psychiatric disease-related states.

s0135 Conclusions and Perspectives

p0335 Many lines of evidence for the long-sought memory engram and engram-containing cells have recently been reported. Such evidence has been obtained by combining multiple technologies, each addressing a specific level of complexity: molecular and cellular neurobiology, physiological recordings, multiphoton imaging, transgenics, viral vector-mediated gene insertions, and optogenetic and pharmacogenetic manipulations of neurons and their circuits as animals undergo mnemonic behaviors. The evidence falls into three major categories (Table 1). A large number of earlier studies accumulated correlations between physiological and structural properties of neurons in a given area of the brain, and one or more aspects of mnemonic behavior. The second type of evidence has been based on a loss-of-function strategy; numerous studies demonstrated that animals or humans suffering from physical or chemical lesions of restricted brain areas, or animals with pharmacological manipulations, are impaired in certain aspects of mnemonic behaviors. However, the traditional loss-of-function studies mostly failed in pinpointing the specific cellular subpopulations that are essential for a specific mnemonic behavior. More recent studies of this type have overcome this shortcoming by taking advantage of transgenic, optogenetic, and/or pharmacogenetic technologies (Denny et al., 2014; Han et al., 2009; Zhou et al., 2009).

AU3

p0340 A technically challenging type of evidence has been gain-of-function. To perform such experiments, a specific population of neurons that is activated by learning first had to be identified, and then a method had to be developed by which subsequent reactivation of these cells would elicit behavioral recall of the specific memory without relying on natural recall cues. This was accomplished by combining the activity-dependent, doxycycline-regulated *c-fos–tTA* system (Reijmers et al., 2007) and ChR2-mediated optogenetics to elicit a hippocampal-dependent contextual fear memory (Liu et al., 2012). This finding was extended to neurons in the retrosplenial cortex for the same memory task (Cowansage et al., 2014). Further, the data obtained by applying pharmacogenetic methods to CREB-overexpressing LA cells, known to be required for tone fear conditioning, reinforced the gain-of-function evidence, although these studies did not demonstrate that the cells manipulated were initially activated by learning (Kim et al., 2014; Yiu et al., 2014).

p0345 Despite the fact that the memory engram has clearly come of age, a number of issues remain to be investigated. A central issue is the nature of the enduring changes that occur in the engram cells and their connections. A first study addressing this issue (Ryan et al., 2015) demonstrated the long-held hypothesis that synaptic strengthening, manifested by increased AMPA/NMDA current ratio as well as a change in structural plasticity as indicated by increased density of dendritic spines, did occur specifically in engram-positive cells as opposed to engram-negative cells in the same hippocampal subregion (i.e., the DG). The demonstration of learning-induced changes strongly argues that they are indeed cells that carry an engram component, rather than cells necessary just for performance. However, this study did not determine the in vivo firing patterns of the engram cells (e.g., are they place cells?

t0010 **Table 1** Three lines of evidence for memory engram cells

Evidence	*Technology*	*Brain area(s)*	*References*
Gain of function	*c-fos-tTA* with tetO-ChR2, tetO-DREADDs (hM3Dq)	HPC, BLA, cortex	Liu et al. (2012), Garner et al. (2012), Ramirez et al. (2013, 2015), Redondo et al. (2014), Ryan et al. (2015), and Ohkawa et al. (2015)
	c-fos-tTA with tetO-oChIEF	EC, HPC	Roy et al. (2016)
	c-fos-tTA with tetO-ChEF	RSC	Cowansage et al. (2014)
	Enhanced neural excitability via TRPV1/ capsaicin	LA	Kim et al. (2014)
	Enhanced neural excitability via CREB overexpression, DREADDs, ChR2	LA, CA1	Yiu et al. (2014), Cai et al. (2016), and Rashid et al. (2016)
	c-fos–ChR2	BLA, PFC	Gore et al. (2015) and Ye et al. (2016)
Loss of function	CREB overexpression, inducible diphtheria toxin system	LA	Han et al. (2007, 2009)
	CREB overexpression, allatostatin (AlstR) receptor system	LA, RSC	Zhou et al. (2009) and Czajkowski et al. (2014)
	Enhanced neural excitability via CREB overexpression, DREADDs (hM4Di)	LA, DG	Hsiang et al. (2014) and Park et al. (2016)
	c-fos-LacZ with Daun02 system	NAcc	Koya et al. (2009)
	c-fos-tTA with tetO-Cre/DIO-ArchT, tetO-TeNT, tetO-ArchT	HPC	Tanaka et al. (2014), Matsuo (2015), and Nomoto et al. (2016)
	Arc-CreER^{T2} with DIO-Arch	HPC	Denny et al. (2014)
	Arc-AS-PaRac1	Motor cortex	Hayashi-Takagi et al. (2015)
	c-fos-tTA with tetO-ArchT, in vivo electrophysiology	HPC	Trouche et al. (2016)
Observational (new studies)	catFISH	PFC, HPC, BLA	Zelikowsky et al. (2014)
	In vivo optical imaging	OB	Kass et al. (2013)
	Two-photon microscopy	Visual cortex	Yamahachi et al. (2009)
	c-fos-tTA with tetO-H2B	Cortex, HPC, BLA	Tayler et al. (2013) and Trouche et al. (2013)
	In vivo optical imaging	Cortex	Xie et al. (2013) AC4
	c-fos-tTA with tetO-tauLacZ	LA, BLA	Reijmers et al. (2007)
	c-fos-tTA with tetO-tauLacZ	HPC	Deng et al. (2014) AC5
	c-fos-tTA with tetO-GFP-GluR1	HPC	Matsuo et al. (2008)
	Arc-dVenus	BLA	Nonaka et al. (2014)
Observational (examples from older studies)	In vivo electrophysiology	Various	Olds et al. (1972)
	In vivo electrophysiology	IT cortex	Fuster and Jervey (1981)
	In vivo electrophysiology	IT cortex	Miyashita (1988)
	In vivo electrophysiology, lesions	Cerebellum	McCormick et al. (1982)

Representative studies on memory engram cells categorized by types of supporting evidence (observation, loss of function, and gain of function), with methods used, brain areas involved, and publications listed.

BLA, basolateral amygdala; *CREB*, cAMP response element binding protein; *DG*, dentate gyrus; *DREADDs*, designer receptors exclusively activated by designer drugs; *EC*, entorhinal cortex; *HPC*, hippocampus; *IT*, inferotemporal; *LA*, lateral amygdala; *NAcc*, nucleus accumbens; *PFC*, prefrontal cortex; *tTA*, tetracycline transactivator.

What firing pattern would be observed before and after recall cues are delivered, etc.?). A recent study (Trouche et al., 2016) using similar technology as Ryan et al. (2015) reported that CA1 engram cells exhibit place-specific firing in an environment, thereby adding to the understanding of cFos-positive engram cells. Nevertheless, the integrative evidence linking the enduring changes to a specific memory has been obtained to date in only one study and only for contextual fear memory engram cells in the DG (Ryan et al., 2015). Memory, however, appears in many different types (e.g., emotional, procedural, working, semantic, perceptual), each supported by one or more distinct brain regions and systems. The basic technology used to identify a memory engram and engram cells for classical conditioning may, in principle, be applicable to other types of memories. In the future, significant modifications of the technology may be needed to identify engram cells for each type of memory. For instance, procedural or habit memories develop slowly with multiple rounds of training. Can one identify the putative habit engram cells and their circuits, and elucidate how they may change as training is repeated and learning advances? Can one identify early habit memory engram cells and accelerate the process of learning by optogenetic activation of these cells? Or can one perform the converse experiment and inhibit the process of motor learning? An additional example includes the memory for a temporal sequence of events—a crucial component of episodic memory. Are there engram cell ensemble(s) that hold the sequence information identifiable by the current engram cell technology? Or is the technology effective only for the memories of individual events, and will other methods have to be invented to identify the mechanism that orchestrates the sequence of expression of the individual event engrams? These studies are expected to reveal both common and memory type-specific features of engram cells.

p0350 The universality, causality, and detailed kinetics of enduring changes in engram cells, as well as their connections, during the encoding versus subsequent cellular consolidation phase will have to be determined. This line of thought takes us to other highly interesting questions that can be explored by the engram manipulation technology. For instance, what is the role of protein and mRNA synthesis in engram cells? It is generally thought that learning elicits new rounds of transcription and translation in the soma and dendrites of neurons that have encoded stimuli selected from experience. These molecular events have been thought to stabilize the storage of the memory information encoded initially by a rapid macromolecule synthesis-independent process. However, this view has been challenged by the finding that posttraining protein synthesis is dispensable for the retention of 1-day-old memory (Ryan et al., 2015; Gold, 2016). Further studies seeking to resolve these issues will be greatly aided by also performing within subjects' analyses (i.e., light off vs. light on epochs during a single session) while subsequently measuring physiological and structural changes in engram-positive and engram-negative cells.

p0355 An exciting prospect for memory research triggered by engram identification and manipulation technologies is to elucidate the pathways comprising the engram complex for various types of memories and to identify the unique role of each contributing engram cell population. To date, this notion of an engram pathway has been investigated for CFC, for which contextual engram cells in the DG and fear/reward engram cells in the BLA were identified (Gore et al., 2015; Redondo et al., 2014). But, it is likely that several other hippocampal and entorhinal cortical sites located between the DG and amygdala for signal transfer are likely to hold unique engrams as well. It would be extremely interesting to identify their nature and the dynamic interactions between component engrams in multiple brain regions. The demonstration that valence-regulated behavior of animals can be controlled by manipulating memory engram cells along the hippocampus–amygdala–NAcc function circuit is another example of an exciting advance made by the engram pathway notion (Fig. 2; Ramirez et al., 2015). Finally, a very recent and exciting advance supporting the engram pathway idea is the restoration of episodic memories in mouse models of early AD by optically strengthening engram cell–engram cell synapses between the medial entorhinal cortex and DG connection (Roy et al., 2016).

p0360 When considering several crucial cognitive behavioral processes such as emotion, decision making, attention, and consciousness, memory is known to play an important role. Efforts to discern how neural circuits underlying these cognitive functions intersect with memory engram circuits, in health and in neurological disorders will be greatly aided by memory engram identification and manipulation technologies. One day, probably in a not so distant future, we may even be able to combine the knowledge obtained by these studies with minimally invasive technologies (Kim et al., 2013; Chen et al., 2015) to develop novel therapeutic methods for a variety of brain disorders.

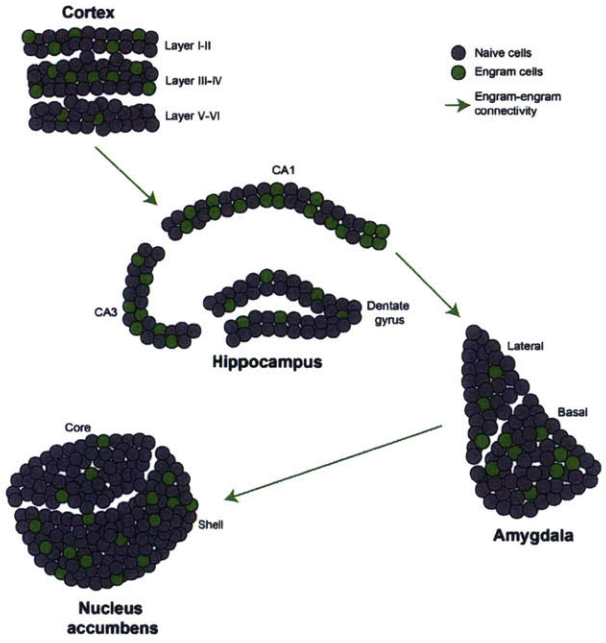

f0015 **Figure 2** Engram cell ensemble pathways. During the formation of an episodic memory, engram cells can be visualized in several participating brain structures including cortical regions, hippocampus, amygdala, and nucleus accumbens. A striking feature of these memory engram cells is that they exhibit preferential engram–engram connectivity between brain regions, which results in the formation of engram cell ensemble pathways.

ack0010 **Acknowledgments**

We thank M. Morrissey, T. Ryan, and L. Brenner for comments on the manuscript. This work was supported by the RIKEN Brain Science Institute, Howard Hughes Medical Institute, and the JPB Foundation (to S.T.).

References

Anderson, A.K., Phelps, E.A., 2001. Lesions of the human amygdala impair enhanced perception of emotionally salient events. Nature 411, 305–309.
Antonini, A., Stryker, M.P., 1993. Rapid remodeling of axonal arbors in the visual cortex. Science 260, 1819–1821.
Attardo, A., Fitzgerald, J.E., Schnitzer, M.J., 2015. Impermanence of dendritic spines in live adult CA1 hippocampus. Nature 523, 592–596.
Avian Brain Nomenclature Consortium, 2005. Avian brains and a new understanding of vertebrate brain evolution. Nat. Rev. Neurosci. 6, 151–159.
Bailey, C.H., Chen, M., 1989. Time course of structural changes at identified sensory neuron synapses during long-term sensitization in *Aplysia*. J. Neurosci. 9, 1774–1780.
Bailey, C.H., Kandel, E.R., 1993. Structural changes accompanying memory storage. Annu. Rev. Physiol. 55, 397–426.
Bannerman, D.M., Bus, T., Taylor, A., et al., 2012. Dissecting spatial knowledge from spatial choice by hippocampal NMDA receptor deletion. Nat. Neurosci. 15, 1153–1159.
Bao, S., Chan, V.T., Merzenich, M.M., 2001. Cortical remodeling induced by activity of ventral tegmental dopamine neurons. Nature 412, 79–93.
Bao, S., Chen, L., Kim, J.J., Thompson, R.F., 2002. Cerebellar cortical inhibition and classical eyeblink conditioning. Proc. Natl. Acad. Sci. U.S.A. 99, 1592–1597.
Bartlett, F.C., 1932. Remembering: A Study in Experimental and Social Psychology. Cambridge University Press.
Bergson, H., 1911. Matter and Memory. Swan Sonnenschein, London.
Bliss, T.V., Lomo, T., 1973. Long-lasting potentiation of synaptic transmission in the dentate area of the anesthetized rabbit following stimulation of the perforant path. J. Physiol. 232, 331–356.
Bolhuis, J.J., Gahr, M., 2006. Neural mechanisms of birdsong memory. Nat. Rev. Neurosci. 7, 347–357.
Boyden, E.S., Zhang, F., Bamberg, E., Nagel, G., Deisseroth, K., 2005. Millisecond-timescale, genetically targeted optical control of neural activity. Nat. Neurosci. 8, 1263–1268.
Britt, J.P., Benaliouad, F., McDevitt, R.A., et al., 2012. Synaptic and behavioral profile of multiple glutamatergic inputs to the nucleus accumbens. Neuron 76, 790–803.
Bruce, D., 2001. Fifty years since Lashley's in search of the engram: refutations and conjectures. J. Hist. Neurosci. 10, 308–318.
Cabeza, R., Rao, S.M., Wagner, A.D., Mayer, A.R., Schacter, D.L., 2001. Can medial temporal lobe regions distinguish true from false? An event-related functional MRI study of veridical and illusory recognition memory. Proc. Natl. Acad. Sci. U.S.A. 98, 4805–4810.
Cai, D., Aharoni, D., Shuman, T., et al., 2016. A shared neural ensemble links distinct contextual memories encoded close in time. Nature. http://dx.doi.org/10.1038/nature17955.
Chen, S., Cai, D., Pearce, K., et al., 2014. Reinstatement of long-term memory following erasure of its behavioral and synaptic expression. eLife 3, e3896.
Chen, R., Romero, G., Christiansen, M.G., Mohr, A., Anikeeva, P., 2015. Wireless magnetothermal deep brain stimulation. Science 347, 1477–1480.
Chow, B.Y., Han, X., Dobry, A.S., et al., 2010. High-performance genetically targetable optical neural silencing by light-driven proton pumps. Nature 463, 98–102.
Chung, K., Wallace, J., Kim, S.Y., et al., 2013. Structural and molecular interrogation of intact biological systems. Nature 497, 332–337.
Cisse, M., Halabisky, B., Harris, J., et al., 2011. Reversing EphB2 depletion rescues cognitive functions in Alzheimer model. Nature 469, 47–52.
Clayton, N.S., Dickinson, A., 1998. Episodic-like memory during cache recovery by scrub jays. Nature 395, 272–274.
Corfas, G., Dudai, Y., 1991. Morphology of a sensory neuron in *Drosophila* is abnormal in memory mutants and changes during aging. Proc. Natl. Acad. Sci. U.S.A. 88, 7252–7256.
Cowansage, K.K., Shuman, T., Dillingham, B.C., et al., 2014. Direct reactivation of a coherent neocortical memory of context. Neuron 84, 432–441.
Czajkowski, R., Jayaprakash, B., Wiltgen, B., et al., 2014. Encoding and storage of spatial information in the retrosplenial cortex. Proc. Natl. Acad. Sci. U.S.A. 111, 8661–8666.
Daoudal, G., Debanne, D., 2003. Long-term plasticity of intrinsic excitability: learning rules and mechanisms. Learn. Mem. 10, 456–465.
Davis, H.P., Squire, L.R., 1984. Protein synthesis and memory: a review. Psychol. Bull. 96, 518–559.
De Paola, V., Holtmaat, A., Knott, G., et al., 2006. Cell type-specific structural plasticity of axonal branches and boutons in the adult neocortex. Neuron 49, 861–875.
Deng, W., Mayford, M., Gage, F.H., 2013. Selection of distinct populations of dentate granule cells in response to inputs as a mechanism for pattern separation in mice. eLife 2, e312.
Denk, W., Strickler, J.H., Webb, W.W., 1990. Two-photon laser scanning fluorescence microscopy. Science 248, 73–76.
Denny, C.A., Kheirbek, M.A., Alba, E.L., et al., 2014. Hippocampal memory traces are differentially modulated by experience, time, and adult neurogenesis. Neuron 83, 189–201.
Descartes, R., 1649. Les Passions de l'âme (The Passions of the Soul, Stephen H. Voss, 1989, Trans.). Hackett Publishing Company, Indianapolis.
Do-Monte, F.H., Quinones-Laracuente, K., Quirk, G.J., 2015. A temporal shift in the circuits mediating retrieval of fear memory. Nature 519, 460–463.
Doupe, A.J., Kuhl, P.K., 1999. Birdsong and human speech: common themes and mechanisms. Annu. Rev. Neurosci. 22, 567–631.
Dudai, Y., 1988. Neurogenetic dissection of learning and short-term memory in *Drosophila*. Annu. Rev. Neurosci. 11, 537–563.
Dudai, Y., Eisenberg, M., 2004. Rites of passage of the engram: reconsolidation and the lingering consolidation hypothesis. Neuron 44, 93–100.
Dudai, Y., Morris, R.G., 2013. Memorable trends. Neuron 80, 742–750.
Duncan, C.P., 1949. The retroactive effect of electroshock on learning. J. Comp. Physiol. Psychol. 42, 32–44.
Dupret, D., O'Neill, J., Pleydell-Bouverie, B., Csicsvari, J., 2010. The reorganization and reactivation of hippocampal maps predict spatial memory performance. Nat. Neurosci. 13, 995–1002.
Eales, L.A., 1985. Song learning in zebra finches: some effects of song model availability on what is learnt and when. Anim. Behav. 33, 1293–1300.
Ebbinghaus, H., 1880. Ueber das Gedachtniss. Passavia-Universitatsverlag, Passau.
Eguchi, M., Yamaguchi, S., 2009. In vivo and in vitro visualization of gene expression dynamics over extensive areas of the brain. Neuroimage 44, 1274–1283.
Ehrlich, I., Humeau, Y., Grenier, F., et al., 2009. Amygdala inhibitory circuits and the control of fear memory. Neuron 62, 757–771.
Engert, F., Bonhoeffer, T., 1999. Dendritic spine changes associated with hippocampal long-term synaptic plasticity. Nature 399, 66–70.
Farris, S.M., Robinson, G.E., Fahrbach, S.E., 2001. Experience- and age-related outgrowth of intrinsic neurons in the mushroom bodies of the adult worker honeybee. J. Neurosci. 21, 6395–6404.
Fenno, L., Yizhar, O., Deisseroth, K., 2011. The development and application of optogenetics. Annu. Rev. Neurosci. 34, 389–412.
Flavell, S.W., Greenberg, M.E., 2008. Signaling mechanisms linking neuronal activity to gene expression and plasticity of the nervous system. Annu. Rev. Neurosci. 31, 563–590.
Flexner, L.B., Flexner, J.B., Roberts, R.B., 1967. Memory in mice analyzed with antibiotics. Antibiotics are useful to study stages of memory and to indicate molecular events, which sustain memory. Science 155, 1377–1383.
Foster, M., Sherrington, C.S., 1897. A Textbook of Physiology, Part Three: The Central Nervous System. Macmillan and Company Ltd, London.
Franz, S.I., 1912. New phrenology. Science 35, 321–328.
Friedman, A., Walsh, J., Juarez, B., 2014. Enhancing depression mechanisms in midbrain dopamine neurons achieves homeostatic resilience. Science 344, 313–319.
Fuster, J.M., Jervey, J.P., 1981. Inferotemporal neurons distinguish and retain behaviorally relevant features of visual stimuli. Science 212, 952–955.
Gallistel, C.R., Balsam, P.D., 2014. Time to rethink the neural mechanisms of learning and memory. Neurobiol. Learn. Mem. 108, 136–144.
Garcia, K.S., Mauk, M.D., 1998. Pharmacological analysis of cerebellar contributions to the timing and expression of conditioned eyelid responses. Neuropharmacology 37, 471–480.

Garner, A.R., Rowland, D.C., Hwang, S.Y., et al., 2012. Generation of a synthetic memory trace. Science 335, 1513–1516.
Gelbard-Sagiv, H., Mukamel, R., Harel, M., Malach, R., Fried, I., 2008. Internally generated reactivation of single neurons in human hippocampus during free recall. Science 322, 96–101.
Gerber, B., Tanimoto, H., Heisenberg, M., 2004. An engram found? Evaluating the evidence from fruit flies. Curr. Opin. Neurobiol. 14, 737–744.
Gershman, S.J., Schapiro, A.C., Hupbach, A., Norman, K.A., 2013. Neural context reinstatement predicts memory misattribution. J. Neurosci. 33, 8590–8595.
Glanzman, D.L., Kandel, E.R., Schacher, S., 1990. Target-dependent structural changes accompanying long-term synaptic facilitation in *Aplysia* neurons. Science 249, 799–802.
Gold, P.E., Haycock, J.W., Marri, J., McGaugh, J.L., 1973. Retrograde amnesia and the reminder effect: an alternative interpretation. Science 180, 1199–1201.
Gold, P.E., King, R.A., 1974. Retrograde amnesia: storage failure versus retrieval failure. Psychol. Rev. 81, 465–469.
Gold, P.E., 2016. Protein synthesis and memory. Learn. Mem. 2E, 04031.
Gonzalez-Lima, F., Scheich, H., 1986. Neural substrates for tone-conditioned bradycardia demonstrated with 2-deoxyglucose II. Behav. Brain Res. 20, 281–293.
Gore, F., Schwartz, E.C., Brangers, B.C., et al., 2015. Neural representations of unconditioned stimuli in basolateral amygdala mediate innate and learned responses. Cell 162, 134–145.
Goshen, I., Brodsky, M., Prakash, R., et al., 2011. Dynamics of retrieval strategies for remote memories. Cell 147, 678–689.
Granholm, E., Butters, N., 1988. Associative encoding and retrieval in Alzheimer's and Huntington's disease. Brain Cogn. 7, 335–347.
Guzowski, J.F., 2002. Insights into immediate-early gene function in hippocampal memory consolidation using antisense oligonucleotide and fluorescent imaging approaches. Hippocampus 12, 86–104.
Han, J.-H., Kushner, S.A., Yiu, A.P., et al., 2007. Neuronal competition and selection during memory formation. Science 316, 457–460.
Han, J.-H., Kushner, S.A., Yiu, A.P., et al., 2009. Selective erasure of a fear memory. Science 323, 1492–1496.
Hardt, O., Wang, S.H., Nader, K., 2009. Storage or retrieval deficit: the yin and yang of amnesia. Learn. Mem. 16, 224–230.
Hayashi-Takagi, A., Yagishita, S., Nakamura, M., et al., 2015. Labelling and optical erasure of synaptic memory traces in the motor cortex. Nature 525, 333–338.
Hebb, D.O., 1949. The Organization of Behavior: A Neuropsychological Theory. Wiley, New York.
Hodges, J.R., Salmon, D.P., Butters, N., 1990. Differential impairment of semantic and episodic memory in Alzheimer's and Huntington's diseases: a controlled prospective study. J. Neurol. Neurosurg. Psychiatry 53, 1089–1095.
Hofer, S.B., Mrsic-Flogel, T.D., Bonhoeffer, T., Hubener, M., 2009. Experience leaves a lasting structural trace in cortical circuits. Nature 457, 313–317.
Holtmaat, A., Wilbrecht, L., Knott, G.W., Welker, E., Svoboda, K., 2006. Experience-dependent and cell-type-specific spine growth in the neocortex. Nature 441, 979–983.
Horn, G., 2004. Pathways of the past: the imprint of memory. Nat. Rev. Neurosci. 5, 108–120.
Hsiang, H.-L., Epp, J.R., van der Oever, M.C., et al., 2014. Manipulating a cocaine engram in mice. J. Neurosci. 34, 14115–14127.
Hubener, M., Bonhoeffer, T., 2010. Searching for engrams. Neuron 67, 363–371.
Hyman, B.T., Van Hoesen, G.W., Kromer, L.J., Damasio, A.R., 1986. Perforant pathway changes and the memory impairment of Alzheimer's disease. Ann. Neurol. 20, 472–481.
Ito, M., Kano, M., 1982. Long-lasting depression of parallel fiber-Purkinje cell transmission induced by conjunctive stimulation of parallel fibers and climbing fibers in the cerebellar cortex. Neurosci. Lett. 33, 253–258.
James, W., 1890. The Principles of Psychology. H. Holt and Company, New York.
Jacobsen, J.S., Wu, C.C., Redwine, J.M., et al., 2006. Early-onset behavioral and synaptic deficits in a mouse model of Alzheimer's disease. Proc. Natl. Acad. Sci. U.S.A. 103, 5161–5166.
Jankowsky, J.L., Fadale, D.J., Anderson, J., et al., 2004. Mutant presenilins specifically elevate the levels of the 42 residue β-amyloid peptide *in vivo*: evidence for augmentation of a 42-residue γ secretase. Hum. Mol. Genet. 13, 159–170.
Ji, S., Maren, S., 2008. Differential roles for hippocampal areas CA1 and CA3 in the contextual encoding and retrieval of extinguished fear. Learn. Mem. 15, 244–251.
Josselyn, S., Kohler, S., Frankland, P.W., 2015. Finding the engram. Nat. Rev. Neurosci. 16, 521–534.
Kameyama, K., Sohya, K., Ebina, T., et al., 2010. Difference in binocularity and ocular dominance plasticity between GABAergic and excitatory cortical neurons. J. Neurosci. 30, 1551–1559.
Kasten, M.R., Fan, Y., Schulz, P.E., 2007. Activation of silent synapses with sustained but not decremental long-term potentiation. Neurosci. Lett. 417, 84–89.
Kandel, E.R., 1976. Cellular Basis of Behavior: An Introduction to Behavioral Biology. Freeman, San Francisco.
Kandel, E.R., 2001. The molecular biology of memory storage: a dialogue between genes and synapses. Science 294, 1030–1038.
Kandel, E.R., 2012. The molecular biology of memory: cAMP, PKA, CRE, CREB-1, CREB-2, and CPEB. Mol. Brain 5, 14.
Kass, M.D., Rosenthal, M.C., Pottackal, J., McGann, J.P., 2013. Fear learning enhances neural responses to threat-predictive sensory stimuli. Science 342, 1389–1392.
Keller, M.B., McCullough, J.P., Klein, D.N., et al., 2000. A comparison of nefazodone, the cognitive behavioral-analysis system of psychotherapy, and their combination for the treatment of chronic depression. N. Engl. J. Med. 342, 1462–1470.
Kheirbek, M.A., Drew, L.J., Burghardt, N.S., et al., 2013. Differential control of learning and anxiety along the dorsoventral axis of the dentate gyrus. Neuron 77, 955–968.
Kim, T.I., McCall, J.G., Jung, Y.H., et al., 2013. Injectable, cellular-scale optoelectronics with applications for wireless optogenetics. Science 340, 211–216.
Kim, J., Kwon, J.T., Kim, H.S., Josselyn, S.A., Han, J.H., 2014. Memory recall and modifications by activating neurons with elevated CREB. Nat. Neurosci. 17, 65–72.
Kisley, M.A., Gerstein, G.L., 2001. Daily variation and appetitive conditioning-induced plasticity of auditory cortex receptive fields. Eur. J. Neurosci. 13, 1993–2003.
Kitamura, T., Sun, C., Martin, J., et al., 2015. Entorhinal cortical ocean cells encode specific contexts and drive context-specific fear memory. Neuron 87, 1317–1331.
Knudsen, E.I., 2002. Instructed learning in the auditory localization pathway of the barn owl. Nature 417, 322–328.
Koya, E., Golden, S.A., Harvey, B.K., et al., 2009. Targeted disruption of cocaine-activated nucleus accumbens neurons prevents context-specific sensitization. Nat. Neurosci. 12, 1069–1073.
Lai, C.S.W., Franke, T.F., Gan, W.-B., 2012. Opposite effects of fear conditioning and extinction on dendritic spine remodeling. Nature 483, 87–91.
Lashley, K.S., 1929. Brain Mechanisms and Intelligence. University of Chicago Press, Chicago.
Lashley, K.S., 1950. In search of the engram. Symp. Soc. Exp. Biol. 4, 454–482.
Lavond, D.G., Steinmetz, J.E., 1989. Acquisition of classical conditioning without cerebellar cortex. Behav. Brain Res. 33, 113–164.
Lecoq, J., Savall, J., Vucinic, D., et al., 2014. Visualizing mammalian brain area interactions by dual-axis two-photon calcium imaging. Nat. Neurosci. 17, 1825–1829.
Lee, I., Kesner, R.P., 2004. Differential contributions of dorsal hippocampal subregions to memory acquisition and retrieval in contextual fear conditioning. Hippocampus 14, 301–310.
Lee, W.C.A., Huang, H., Feng, G.P., et al., 2006. Dynamic remodeling of dendritic arbors in GABAergic interneurons of adult visual cortex. PLoS Biol. 4, e29.
Leutgeb, S., Leutgeb, J.K., Treves, A., Moser, M.-B., Moser, E.I., 2004. Distinct ensemble codes in hippocampal areas CA3 and CA1. Science 305, 1295–1298.
Lewis, D.J., 1979. Psychobiology of active and inactive memory. Psychol. Bull. 86, 1054–1083.
Liao, D., Hessler, N.A., Malinow, R., 1995. Activation of postsynaptically silent synapses during pairing-induced LTP in CA1 region of hippocampal slice. Nature 375, 400–404.
Lisman, J., Yasuda, R., Raghavachari, S., 2012. Mechanisms of CaMKII action in long-term potentiation. Nat. Rev. Neurosci. 13, 169–182.
Liu, X., Davis, R.L., 2009. The GABAergic anterior paired lateral neuron suppresses and is suppressed by olfactory learning. Nat. Neurosci. 12, 53–59.
Liu, X., Ramirez, S., Pang, P.T., et al., 2012. Optogenetic stimulation of a hippocampal engram activates fear memory recall. Nature 484, 381–385.
Loftus, E., 2003. Our changeable memories: legal and practical implications. Nat. Rev. Neurosci. 4, 2–5.
Lopez, J., Gamache, K., Schneider, R., Nader, K., 2015. Memory retrieval requires ongoing protein synthesis and NMDA receptor activity-mediated AMPA receptor trafficking. J. Neurosci. 35, 2465–2475.
Lorenz, K., 1981. The Foundations of Ethology. Springer, New York.

Louie, K., Wilson, M., 2001. Temporally structured replay of awake hippocampal ensemble activity during rapid eye movement sleep. Neuron 29, 145–156.
MacDonald, C.J., Lepage, K.Q., Eden, U.T., Eichenbaum, H., 2011. Hippocampal time cells bridge the gap in memory for discontiguous events. Neuron 44, 5–21.
Malenka, R.C., Bear, M.F., 2004. LTP and LTD: an embarrassment of riches. Neuron 44, 5–21.
Maletic-Savatic, M., Malinow, R., Svoboda, K., 1999. Rapid dendritic morphogenesis in CA1 hippocampal dendrites induced by synaptic plasticity. Science 283, 1923–1927.
Marr, D., 1970. A theory for cerebral neocortex. Proc. R. Soc. Lond. B Biol. Sci. 176, 161–234.
Martin, S.J., Morris, R.G., 2002. New life in an old idea: the synaptic plasticity and memory hypothesis revisited. Hippocampus 12, 609–636.
Matsuo, N., Reijmers, L., Mayford, M., 2008. Spine-type-specific recruitment of newly synthesized AMPA receptors with learning. Science 319, 1104–1107.
Matsuo, N., 2015. Irreplaceability of neuronal ensembles after memory allocation. Cell Rep. 11, 351–357.
Matzel, L.D., Miller, R.R., 2009. Parsing storage from retrieval in experimentally induced amnesia. Learn. Mem. 16, 670–671.
Mauk, M.D., Steinmetz, J.E., Thompson, R.F., 1986. Classical conditioning using stimulation of the inferior olive as the unconditioned stimulus. Proc. Natl. Acad. Sci. U.S.A. 83, 5349–5353.
McCormick, D.A., Clark, G.A., Lavond, D.G., Thompson, R.F., 1982. Initial localization of the memory trace for a basic form of learning. Proc. Natl. Acad. Sci. U.S.A. 79, 2731–2735.
McCormick, D.A., Thompson, R.F., 1984. Cerebellum: essential involvement in the classically conditioned eyelid response. Science 223, 296–299.
McCormick, D.A., Steinmetz, J.E., Thompson, R.F., 1985. Lesions of the inferior olivary complex cause extinction of the classically conditioned eyeblink response. Brain Res. 359, 120–130.
McDougall, W., 1911. Body and Mind: A History and a Defense of Animism. Methuen and Company Ltd, London.
McGaugh, J.L., 1966. Time-dependent processes in memory storage. Science 153, 1351–1358.
McGaugh, J.L., 2000. Memory – a century of consolidation. Science 287, 248–251.
McKernan, M.G., Shinnick-Gallagher, P., 1997. Fear conditioning induces a lasting potentiation of synaptic currents in vitro. Nature 390, 607–611.
McTighe, S.M., Cowell, R.A., Winters, B.D., Bussey, T.J., Saksida, L.M., 2010. Paradoxical false memory for objects after brain damage. Science 330, 1408–1410.
Menzel, R., 2001. Searching for the memory trace in a mini-brain, the honeybee. Learn. Mem. 8, 53–62.
Miller, R.R., Matzel, L.D., 2006. Retrieval failure versus memory loss in experimental amnesia: definitions and processes. Learn. Mem. 13, 491–497.
Miller, R.R., Springer, A.D., 1972. Induced recovery of memory in rats following electroconvulsive shock. Physiol. Behav. 8, 645–651.
Miller, R.R., Springer, A.D., 1973. Amnesia, consolidation, and retrieval. Psychol. Rev. 80, 69–79.
Miller, R.R., Springer, A.D., 1974. Implications of recovery from experimental amnesia. Psychol. Rev. 81, 470–473.
Milner, B., Squire, L.R., Kandel, E.R., 1998. Cognitive neuroscience and the study of memory. Neuron 20, 445–468.
Miserendino, M.J., Sananes, C.B., Melia, K.R., Davis, M., 1990. Blocking of acquisition but not expression of conditioned fear-potentiated startle by NMDA antagonists in the amygdala. Nature 345, 716–718.
Miyashita, Y., 1988. Neuronal correlate of visual associative long-term memory in the primate temporal cortex. Nature 335, 817–820.
Morris, R.G., Anderson, E., Lynch, G.S., Baudry, M., 1986. Selective impairment of learning and blockade of long-term potentiation by an *N*-methyl-D-aspartate receptor antagonist, AP5. Nature 319, 774–776.
Morris, R.G., 2006. Elements of a neurobiological theory of hippocampal function: the role of synaptic plasticity, synaptic tagging and schemas. Eur. J. Neurosci. 23, 2829–2846.
Moser, M.-B., Trommald, M., Andersen, P., 1994. An increase in dendritic spine density on hippocampal CA1 pyramidal cells following spatial learning in adult rats suggest the formation of new synapses. Proc. Natl. Acad. Sci. U.S.A. 91, 12673–12675.
Müller, G.E., Pilzecker, A., 1900. Experimentelle Beiträge zur Lehre vom Gedächtnis. Leipzig, Germany.
Nabavi, S., Fox, R., Proulx, C.D., et al., 2014. Engineering a memory with LTD and LTP. Nature 511, 348–352.
Nader, K., Schafe, G.E., LeDoux, J.E., 2000. The labile nature of consolidation theory. Nat. Rev. Neurosci. 1, 216–219.
Nader, K., Wang, S.H., 2006. Fading in. Learn. Mem. 13, 530–535.
Nakashiba, T., Buhl, D., McHugh, T.J., Tonegawa, S., 2009. Hippocampal CA3 output is crucial for ripple-associated reactivation and consolidation of memory. Neuron 62, 781–787.
Nakazawa, K., Sun, L.D., Quirk, M.C., et al., 2003. Hippocampal CA3 NMDA receptors are crucial for memory acquisition of one-time experience. Neuron 38, 305–315.
Nomoto, M., Ohkawa, N., Nishizono, H., et al., 2016. Cellular tagging as a neural network mechanism for behavioural tagging. Nat. Commun. 7, 12319.
Nonaka, A., Toyoda, T., Miura, Y., et al., 2014. Synaptic plasticity associated with a memory engram in the basolateral amygdala. J. Neurosci. 34, 9305–9309.
O'Keefe, J., Dostrovsky, J., 1971. The hippocampus as a spatial map. Preliminary evidence from unit activity in the freely moving rat. Brain Res. 34, 171–175.
Ohkawa, N., Saitoh, Y., Suzuki, A., et al., 2015. Artificial association of pre-stored information to generate a qualitatively new memory. Cell Rep. 11, 261–269.
Okuno, H., Akashi, K., Ishii, Y., et al., 2012. Inverse synaptic tagging of inactive synapses via dynamic interaction of Arc/Arg3.1 with CaMKIIβ. Cell 149, 886–898.
Olds, J., Disterhoft, J.F., Segal, M., Kornblith, C.L., Hirsh, R., 1972. Learning centers of rat brain mapped by measuring latencies of conditioned unit responses. J. Neurophysiol. 35, 202–219.
Paton, J.J., Belova, M.A., Morrison, S.E., Salzman, C.D., 2006. The primate amygdala represents the positive and negative value of visual stimuli during learning. Nature 439, 865–870.
Park, S., Kramer, E.E., Mercaldo, V., et al., 2016. Neuronal allocation to a hippocampal engram. Neuropsychopharmacology. http://dx.doi.org/10.1038/npp.2016.73.
Pattwell, S.S., Bath, K.G., Casey, B.J., Ninan, I., Lee, F.S., 2011. Selective early-acquired fear memories undergo temporary suppression during adolescence. Proc. Natl. Acad. Sci. U.S.A. 108, 1182–1187.
Penfield, W., Rasmussen, T., 1950. The Cerebral Cortex of Man: A Clinical Study of Localization of Function. Macmillan, New York.
Pinsker, H.M., Hening, W.A., Carew, T.J., Kandel, E.R., 1973. Long-term sensitization of a defensive withdrawal reflex in *Aplysia*. Science 182, 1039–1042.
Przybyslawski, J., Sara, S.J., 1997. Reconsolidation of memory after its reactivation. Behav. Brain Res. 84, 241–246.
Quartermain, D., McEwen, B.S., Azmitia Jr., E.C., 1970. Amnesia produced by electroconvulsive shock or cycloheximide: conditions for recovery. Science 169, 683–686.
Quiroga, R.Q., Reddy, L., Kreiman, G., Koch, C., Fried, I., 2005. Invariant visual representation by single neurons in the human brain. Nature 435, 1102–1107.
Ramirez, S., Liu, X., Lin, P.-A., et al., 2013. Creating a false memory in the hippocampus. Science 341, 387–391.
Ramirez, S., Liu, X., MacDonald, C.J., et al., 2015. Activating positive memory engrams suppresses depression-like behavior. Nature 522, 335–339.
Ramon y Cajal, S., 1893. Neue Darstellung vom histologischen Bau des Centralnervensystems. Arch. Anat. Physiol. 17, 9–428.
Ramon y Cajal, S., 1894. The Croonian Lecture: la fine structure des centres nerveux. Proc. R. Soc. Lond. 5, 444–468.
Rashid, A.J., Yan, C., Mercaldo, V., et al., 2016. Competition between engrams influences fear memory formation and recall. Science 353, 383–387.
Redondo, R.L., Kim, J., Arons, A., et al., 2014. Bidirectional switch of the valence associated with a hippocampal contextual memory engram. Nature 513, 426–430.
Reijmers, L.G., Perkins, B.L., Matsuo, N., Mayford, M., 2007. Localization of a stable neural correlate of associative memory. Science 317, 1230–1233.
Restivo, L., Vetere, G., Bontempi, B., Ammassari-Teule, M., 2009. The formation of recent and remote memory is associated with time-dependent formation of dendritic spines in the hippocampus and anterior cingulate cortex. J. Neurosci. 29, 8206–8214.
Riccio, D.C., Millin, P.M., Bogart, A.R., 2006. Reconsolidation: a brief history, a retrieval view, and some recent issues. Learn. Mem. 13, 536–544.
Roberts, T.F., Tschida, K.A., Klein, M.E., Mooney, R., 2010. Rapid spine stabilization and synaptic enhancement at the onset of behavioral learning. Nature 463, 948–952.
Roediger, H.L., McDermott, K.B., 1995. Creating false memories: remembering words not presented in lists. J. Exp. Psychol. Learn. Mem. Cogn. 21, 803–814.
Romberg, C., McTighe, S.M., Heath, C.J., et al., 2012. False recognition in a mouse model of Alzheimer's disease: rescue with sensory restriction and memantine. Brain 135, 2103–2114.

Rose, S.P., 2000. God's organism? The chick as a model system for memory studies. Learn. Mem. 7, 1–17.
Roy, D.S., Arons, A., Mitchell, T.I., et al., 2016. Memory retrieval by activating engram cells in mouse models of early Alzheimer's disease. Nature 531, 508–512.
Ryan, T.J., Roy, D.S., Pignatelli, M., Arons, A., Tonegawa, S., 2015. Engram cells retain memory under retrograde amnesia. Science 348, 1007–1013.
Sacktor, T.C., 2011. How does PKMzeta maintain long-term memory? Nat. Rev. Neurosci. 12, 9–15.
Sah, P., Faber, E.S.L., Lopez De Armentia, M., Power, J., 2003. The amygdaloid complex: anatomy and physiology. Physiol. Rev. 83, 803–834.
Sara, S.J., 1973. Recovery from hypoxia and ECS-induced amnesia after a single exposure to training environment. Physiol. Behav. 10, 85–89.
Sara, S.J., 2000. Retrieval and reconsolidation: toward a neurobiology of remembering. Learn. Mem. 7, 73–84.
Sara, S.J., Hars, B., 2006. In memory of consolidation. Learn. Mem. 13, 515–521.
Schacter, D.L., Eich, J.E., Tulving, E., 1978. Richard Semon's theory of memory. J. Verbal Learn. Verbal Behav. 17, 721–743.
Schacter, D.L., 2001. Forgotten Ideas, Neglected Pioneers: Richard Semon and the Story of Memory. Routledge, New York.
Schacter, D.L., Addis, D.R., Buckner, R.L., 2007. Remembering the past to imagine the future: the prospective brain. Nat. Rev. Neurosci. 8, 657–661.
Schacter, D.L., Loftus, E.F., 2013. Memory and law: what can cognitive neuroscience contribute? Nat. Neurosci. 16, 119–123.
Schlaepfer, T.E., Cohen, M.X., Frick, C., et al., 2008. Deep brain stimulation to reward circuitry alleviates anhedonia in refractory major depression. Neuropsychopharmacology 33, 368–377.
Scoville, W.B., Milner, B., 1957. Loss of recent memory after bilateral hippocampal lesions. J. Neurol. Neurosurg. Psychiatry 20, 11–21.
Selkoe, D.J., 2001. Alzheimer's disease: genes, proteins, and therapy. Physiol. Rev. 81, 741–766.
Selkoe, D.J., 2002. Alzheimer's disease is a synaptic failure. Science 298, 789–791.
Semon, R., 1904. Die Mneme (The Mneme). Wilhelm Engelmann, Leipzig.
Semon, R., 1909. Die Mnemischen Empfindungen (Mnemic Psychology). Wilhelm Engelmann, Leipzig.
Senn, V., Wolff, S.B.E., Herry, C., et al., 2014. Long-range connectivity defines behavioral specificity of amygdala neurons. Neuron 81, 428–437.
Serota, R.G., 1971. Acetoxycycloheximide and transient amnesia in the rat. Proc. Natl. Acad. Sci. U.S.A. 68, 1249–1250.
Shinn-Cunningham, B., 2000. Adapting to remapped auditory localization cues: a decision-theory model. Percept. Psychophys. 62, 33–47.
Spear, N.E., 1973. Retrieval of memory in animals. Psychol. Rev. 80, 163–194.
Springer, A.D., Miller, R.R., 1972. Retrieval failure induced by electroconvulsive shock: reversal with dissimilar training and recovery agents. Science 177, 628–630.
Squire, L.R., Barondes, S.H., 1972. Variable decay of memory and its recovery in cycloheximide-treated mice. Proc. Natl. Acad. Sci. U.S.A. 69, 1416–1420.
Squire, L.R., 1982. The neuropsychology of human memory. Annu. Rev. Neurosci. 5, 241–273.
Squire, L.R., 2006. Lost forever or temporarily misplaced? The long debate about the nature of memory impairment. Learn. Mem. 13, 522–529.
Squire, L.R., Wixted, J.T., 2011. The cognitive neuroscience of human memory since H.M. Annu. Rev. Neurosci. 34, 259–288.
St Jacques, P.L., Schacter, D.L., 2013. Modifying memory: selectively enhancing and updating personal memories for a museum tour by reactivating them. Psychol. Sci. 24, 537–543.
Steinmetz, J.E., Rosen, D.J., Chapman, P.F., Lavond, D.G., Thompson, R.F., 1986. Classical conditioning of the rabbit eyelid response with a mossy-fiber stimulation CS: pontine nuclei and middle cerebellar peduncle stimulation. Behav. Neurosci. 100, 878–887.
Steinmetz, J.E., Logan, C.G., Rosen, D.J., et al., 1987. Initial localization of the acoustic conditioned stimulus projection system to the cerebellum essential for classical eyelid conditioning. Proc. Natl. Acad. Sci. U.S.A. 84, 3531–3535.
Steinmetz, J.E., Lavond, D.G., Thompson, R.F., 1989. Classical conditioning in rabbits using pontine nucleus stimulation as a conditioned stimulus and inferior olive stimulation as an unconditioned stimulus. Synapse 3, 225–233.
Stuber, G.D., Sparta, D.R., Stamatakis, A.M., et al., 2011. Excitatory transmission from the amygdala to nucleus accumbens facilitates reward seeking. Nature 475, 377–380.
Tanaka, K.Z., Pevzner, A., Hamidi, A.B., et al., 2014. Cortical representations are reinstated by the hippocampus during memory retrieval. Neuron 84, 347–354.
Tayler, K.K., Tanaka, K.Z., Reijmers, L.G., Wiltgen, B.J., 2013. Reactivation of neural ensembles during the retrieval of recent and remote memory. Curr. Biol. 23, 99–106.
Terry, R.D., Masliah, E., Salmon, D.P., et al., 1991. Physical basis of cognitive alterations in Alzheimer's disease: synapse loss is the major correlate of cognitive impairment. Ann. Neurol. 30, 572–580.
Teule, M., Segal, M., 2016. Spine dynamics in synaptic plasticity and memory formation. Learn. Mem. 2E, 04024.
Thompson, R.F., 1976. The search for the engram. Am. Psychol. 31, 209–227.
Thompson, R.F., Kim, J.J., 1996. Memory systems in the brain and localization of a memory. Proc. Natl. Acad. Sci. U.S.A. 93, 13438–13444.
Tonegawa, S., Pignatelli, M., Roy, D.S., Ryan, T.J., 2015a. Memory engram storage and retrieval. Curr. Opin. Neurobiol. 35, 101–109.
Tonegawa, S., Liu, X., Ramirez, S., Redondo, R., 2015b. Memory engram cells have come of age. Neuron 87, 918–931.
Trouche, S., Sasaki, J.M., Tu, T., Reijmers, L.G., 2013. Fear extinction causes target-specific remodeling of perisomatic inhibitory synapses. Neuron 80, 1054–1065.
Trouche, S., Perestenko, P.V., van de Ven, G.M., et al., 2016. Recoding a cocaine-place memory engram to a neutral engram in the hippocampus. Nat. Neurosci. 19, 564–567.
Tse, D., Langston, R.F., Kakeyama, M., et al., 2007. Schemas and memory consolidation. Science 316, 76–82.
Tsien, J.Z., Huerta, P.T., Tonegawa, S., 1996. The essential role of hippocampal CA1 NMDA receptor-dependent synaptic plasticity in spatial memory. Cell 87, 1327–1338.
Tsien, R.Y., 2013. Very long-term memories may be stored in the pattern of holes in the perineuronal net. Proc. Natl. Acad. Sci. U.S.A. 110, 12456–12461.
Tully, T., Quinn, W.G., 1985. Classical conditioning and retention in normal and mutant *Drosophila melanogaster*. J. Comp. Physiol. A 157, 263–277.
Tulving, E., 2002. Episodic memory: from mind to brain. Annu. Rev. Psychol. 53, 1–25.
Weinberger, N.M., 2004. Specific long-term memory traces in primary auditory cortex. Nat. Rev. Neurosci. 5, 279–290.
Weintraub, S., Wicklund, A.H., Salmon, D.P., 2012. The neuropsychological profile of Alzheimer disease. Cold Spring Harb. Perspect. Med. 2, a6171.
Wheeler, A.L., Teixeira, C.M., Wang, A.H., et al., 2013. Identification of a functional connectome for long-term fear memory in mice. PLoS Comput. Biol. 9, e1002853.
Wilson, M.A., McNaughton, B.L., 1993. Dynamics of the hippocampal ensemble code for space. Science 261, 1055–1058.
Wolpe, J., 1958. Psychotherapy by Reciprocal Inhibition. Stanford University Press.
Xie, H., Liu, Y., Zhu, Y., et al., 2014. In vivo imaging of immediate early gene expression reveals layer-specific memory traces in the mammalian brain. Proc. Natl. Acad. Sci. U.S.A. 111, 2788–2793.
Xu, T., Yu, X., Perlik, A.J., et al., 2009. Rapid formation and selective stabilization of synapses for enduring motor memories. Nature 462, 915–919.
Yamahachi, H., Marik, S.A., McManus, J.N., Denk, W., Gilbert, C.D., 2009. Rapid axonal sprouting and pruning accompany functional reorganization in primary visual cortex. Neuron 64, 719–729.
Yang, G., Pan, F., Gan, W.-B., 2009. Stably maintained dendritic spines as associated with lifelong memories. Nature 462, 920–924.
Ye, L., Allen, W.E., Thompson, K.R., et al., 2016. Wiring and molecular features of prefrontal ensembles representing distinct experiences. Cell 165, 1–13.
Yiu, A.P., Mercaldo, V., Yan, C., et al., 2014. Neurons are recruited to a memory trace based on relative neuronal excitability immediately before training. Neuron 83, 722–735.
Yu, D., Akalal, D.B.G., Davis, R.L., 2006. Drosophila α/β mushroom body neurons form a branch-specific, long-term cellular memory trace after spaced olfactory conditioning. Neuron 52, 845–855.
Zelikowsky, M., Hersman, S., Chawla, M.K., Barnes, C.A., Fanselow, M.S., 2014. Neuronal ensembles in amygdala, hippocampus, and prefrontal cortex track differential components of contextual fear. J. Neurosci. 34, 8462–8466.
Zhou, Y., Won, J., Karlsson, M.G., et al., 2009. CREB regulates excitability and the allocation of memory to subsets of neurons in the amygdala. Nat. Neurosci. 12, 1438–1443.
Zola-Morgan, S., Squire, L.R., Alvarez-Royo, P., Clower, R.P., 1991. Independence of memory functions and emotional behavior: separate contributions of the hippocampal formation and the amygdala. Hippocampus 1, 207–220.

Manipulating memory in space and time

Dheeraj S Roy[1] and Susumu Tonegawa[1,2]

[1] RIKEN-MIT Center for Neural Circuit Genetics at the Picower Institute for Learning and Memory, Department of Biology and Department of Brain and Cognitive Sciences, Massachusetts Institute of Technology, Cambridge, MA 02139, USA
[2] Howard Hughes Medical Institute, Massachusetts Institute of Technology, Cambridge, MA 02139, USA

Corresponding author: Tonegawa, Susumu (tonegawa@mit.edu)

Highlights:

- Identification and manipulations of memory engrams and engram cells
- Creating false memory by manipulating engram cells
- Countering depression-like behaviors by stimulating positive valence engram cells
- Restoring memory in early Alzheimer's mouse models by engineering engram cells

Word count: 2,315 (max approx. 2,000)

Abstract

One of the most fascinating aspects of an animal's brain is its ability to acquire new information from experience and retain this information over time as memory. The search for physical correlates of memory, the memory engram, has been a longstanding endeavor in modern neurobiology. Recent advances in transgenic and optogenetic tools have enabled the identification, visualization, and manipulations of natural, sensory-evoked, engram cells for a specific memory residing in specific brain regions. These studies are paving the way not only to understand memory mechanisms in unprecedented detail, but also to repair the abnormal state of mind associated with memory by engineering.

Introduction

Understanding the material basis of memory remains a central goal of modern neuroscience [1,2]. Descartes proposed that mental capacities, specifically memory, must be represented in the brain [3]. At the onset of the 20th century, Richard Semon theorized that learning induces enduring physical changes in specific brain cells that retain information of the experience and are subsequently reactivated by appropriate stimuli to induce recall. He termed these physical changes the engram [4,5]. Another term that is used by some contemporary neuroscientists is memory trace, which can be considered to be equivalent to Semon's engram. Even after Semon's engram theory, some leading scholars wondered whether memory is physically represented in the brain or psychically represented in the mind. It was Karl Lashley who advocated the physical theory of information storage in the central nervous system. In particular, Lashley adopted the concept of the engram and was among the first to attempt to localize memory engrams in the brain [6]. While Lashley's idea of Mass Action was later empirically disproved, some researchers after him continued to identify the location of memory representations in the brain [7]. In this review, we will discuss recent experimental studies demonstrating that memory is indeed stored in specific populations of brain cells and their associated circuits, with a focus on memory manipulation studies. More comprehensive reviews of recent memory engram studies, including early attempts, is available elsewhere [8••,9•,10].

Engram cell identification

Several groups found that cell populations active during the acquisition of a fear memory were preferentially reactivated during the recall of that memory in different areas of the mouse brain, such as the amygdala [11•], the hippocampus [12,13], layer II cortical areas including sensory cortex [14,15], and the prefrontal cortex [16]. Another approach that has been used to identify possible engram cell populations in the rodent brain employed the random overexpression of the transcription activator cAMP response element-binding protein (CREB) in a small population of neurons, making these cells more likely to be recruited to become a part of putative engram cell populations during subsequent learning [17]. By selectively manipulating these high-CREB cells via diphtheria toxin-based ablation [18•] or genetic-based inhibition [19•,20-23] memory recall was disrupted in mice. More recent studies showed that a shared neuronal ensemble is capable of linking distinct memories, only when two experiences occur close in time during periods of high excitability in hippocampal CA1 [24] and lateral amygdala [25]. Further, novel context exploration

during a narrow time window before or after weak object recognition training results in the formation of a long-term object recognition memory [26].

The most direct evidence of engram cells should come from gain-of-function manipulations, where a population of neurons activated by learning is artificially reactivated to mimic behavioral recall elicited by natural cues [27]. By combining the activity-dependent, doxycycline-dependent *c-fos-tTA* system and channelrhodopsin-2 (ChR2)-mediated optogenetics, researchers were able to tag a sparse population of dentate gyrus (DG) neurons activated by contextual fear conditioning with ChR2 in mice [28••]. Subsequently, when these cells were reactivated by blue light in a context different from the original one used for conditioning, the mouse subjects displayed freezing behavior as evidence of fear memory recall (Figure 1). Crucially, this optogenetic reactivation of a fear memory was not due to the activation of pre-wired neural circuits. This was demonstrated by disrupting the activity of the downstream CA1 region only during training, and finding that subsequent optogenetic DG engram activation did not elicit memory retrieval [29••]. Similarly, memory recall induced by the artificial reactivation of fear memory cells has been reported for multiple brain regions [14,30-32]. Along with these engram reactivation experiments, loss-of-function studies have also been performed [33-35].

Creating a false memory by manipulating engram cells

Memory recall is constructive in nature and the act of recalling a memory renders it labile and highly susceptible to modification [36]. In humans, memory distortions and illusions occur frequently, which often results from incorporation of misinformation from external sources [37]. In light of the fact that humans have a rich repertoire of mental representations generated internally [38], one possible reason for the formation of an episodic false memory is that the memory of a past experience becomes associated with a current external event of high valence.

Using a method that permits optogenetic labeling and manipulation of memory engram cells [28••], a study tested this possibility in mice [39••]. The authors labeled contextual engram cells in the DG with ChR2 by exposing mice to context A (Figure 2), thereby activating c-Fos in the engram. On the next day, as the labeling window was shut down by switching mice from regular to doxycycline-containing food, mice received foot shocks in a distinct context B as their context A engram cells were artificially reactivated with pulses of blue light. On the third day, when the animals were reintroduced to context A to test the context A-shock association memory, animals displayed freezing behavior despite never having received foot shocks in context A. The freezing behavior was not due to generalization because the mice did not freeze above background levels in another distinct context C. Of course, these mice also froze when tested in context B, indicating that they also formed a genuine context B-shock association memory. Importantly, freezing levels in context B were significantly lower than in a group of mice that did not receive blue light delivery on day 2 while foot shocks were delivered. This observation suggests that formation of the false and genuine memory representations on day 2 were in competition. Moreover, using the same cFos-driven ChR2 labeling strategy, a recent study demonstrated that, in addition to optogenetically driving a hippocampal contextual engram, basolateral amygdala cells responding to a stimulus of high valence can be simultaneously activated to form an association with the hippocampal-driven contextual memory [40•]. Such findings indicate that at least some form of false memory is

generated by an association of internal brain activity representing recall of a past experience with the current external or internal experience of high valence [39••,40•,41].

Countering depression by positive valence engram activation

The conceptual framework of the interaction between the neural circuits governing memory valence and those encoding neutral components of an episode is that the engrams for the latter, like the one in the hippocampus, are free to associate with either positive or negative valence engrams in the amygdala [42••]. The development of new technologies that permit engineering of these engrams opens up the possibility of adding a novel approach to the classical approaches for the treatment of psychopathologies. For example, depression is characterized by a pervasive and persistent blunted mood that is accompanied by motivational impairments and a loss of interest or pleasure in normally enjoyable activities. How positive episodes interact with psychiatric disease-related impairments at the neural circuit level has remained unknown.

In a recent study, the researchers demonstrated that optogenetic reactivation of engram cells formed in the DG by a naturally rewarding experience was sufficient to acutely suppress depression-related behavior [43••]. This study further demonstrated that glutamatergic transmission from the amygdala's axonal terminals to the nucleus accumbens (NAcc) shell is necessary for the real-time antidepressant-like effects of the reactivated DG engram cells. Notably, the NAcc has recently been identified as a potential therapeutic node for deep brain stimulation to alleviate anhedonia in humans [44], and previous reports also identified amygdala axonal terminals onto NAcc as being sufficient to support self-stimulation and reward-seeking behavior in a dopamine D1 receptor-mediated manner [45]. It is important to note here that directly reactivating cells associated with a positive memory is qualitatively different from exposing depressed subjects to naturally rewarding experiences, which would normally activate these corresponding brain areas in the healthy brain. In the psychiatric diseased-related state, acute administration of naturally rewarding external cues may not have access to, or sufficiently activate, the positive valence engram cells' representations associated with the positive experience. Direct optogenetic stimulation of these cells may be able to overcome this obstacle. These studies provide causal evidence that engram cells can be directly manipulated to modulate a specific behavioral program associated with psychiatric disease-related states.

Restoring memory engrams in mouse models of early Alzheimer's disease

Alzheimer's disease (AD) is the most common cause of brain degeneration, and typically begins with impairments in cognitive functions [46]. Most research has focused on understanding the relationship between memory impairments and the formation of pathological hallmarks seen in late stages of AD. Early phases of AD have received relatively less attention, although synaptic phenotypes have been identified as major correlates of cognitive impairments in both human patients and mouse models [47]. Several studies have suggested that the episodic memory deficit of AD patients is due to ineffective encoding of new information [48]. However, since cognitive measures used in these studies rely on memory retrieval, it has not been possible to rigorously discriminate between impairments in information storage and disrupted retrieval of stored

information. This issue has an important clinical implication: if the amnesia is due to retrieval impairments, memory could be restored by technologies involving targeted brain stimulation.

Focusing on memory engrams, a recent study examined long-term memory impairments in mouse models of early AD [49••]. Using APP/PS1 AD mice, the authors observed that amyloid plaque deposition started in 9-month old mice, however memory deficits were clearly visible several months before plaque deposition. In a contextual fear-conditioning paradigm, 7-month old AD mice exhibited normal short-term memory but performed poorly 24 hr later in long-term memory tests. This behavioral impairment correlated with a decreased number of c-Fos-positive cells in the DG as well as decreased engram cell-specific dendritic spine density in AD mice. However, preferential functional connectivity between engram cells was maintained in the early AD mice. Next, in order to examine whether functional DG engram cells persisted in early AD mice, despite these animals being amnesic at the behavioral level, the authors developed a novel strategy using a double adeno-associated virus system to label engrams [49••]. As expected, engram-labeled early AD mice were amnesic a day after fear conditioning; but remarkably, these mice exhibited memory recall as robustly as equivalently treated control mice in response to blue light stimulation of engram cells. Following early findings [50] that long-term potentiation (LTP) induction results in a spine density increase, Roy et al. [49••] applied repeated optogenetic LTP induction specifically to entorhinal cortex engram cell inputs into DG engrams. This procedure reversed the spine density deficit in early AD mice. Crucially, this spine restoration led to the rescue of a long-term fear memory recall in AD mice. The authors also demonstrated that an ablation of DG engram cells containing restored spine density prevents the rescue of long-term memory recall in early AD mice [49••,51,52•]. Together, it is clear that genetic manipulations of specific neuronal populations can have profound effects on cognitive impairments of AD.

Conclusions and perspectives

Many lines of evidence for the long-sought memory engram and engram-containing cells have recently been reported. Such evidence has been obtained by combining multiple technologies, each addressing a specific level of complexity [8••,9•,10]. Despite the fact that the memory engram has clearly come of age, a number of issues remain to be investigated. A central issue is the nature of the enduring changes that occur in the engram cells and their connections. A first study addressing this issue [29••] demonstrated the validity of the long-held hypothesis that synaptic strengthening and structural plasticity occurred specifically in engram-positive cells as opposed to engram-negative cells in the same brain region. The demonstration of learning-induced changes strongly argues that they are indeed cells that carry an engram component, rather than cells necessary just for performance. However, this study did not determine the *in vivo* firing patterns of the engram cells (e.g., are they place cells? What firing pattern would be observed before and after recall cues are delivered, etc.?). A recent study [53•] using similar technology as [29••] reported that CA1 engram cells exhibit place-specific firing in an environment, thereby adding to the understanding of cFos-positive engram cells.

Memory, however, appears in many different types (e.g., emotional, procedural, working, semantic, perceptual), each supported by one or more distinct brain regions. The basic technology used to identify memory engram cells for classical conditioning may, in principle, be applicable to other types of memories. For instance, procedural or habit memories develop slowly with multiple rounds

of training. Can one identify the putative habit engram cells and their circuits, and elucidate how they may change as training is repeated and learning advances? An additional example includes the memory for a temporal sequence of events – a crucial component of episodic memory. Are there engram cell ensemble(s) that hold the sequence information identifiable by the current engram cell technology? These studies are expected to reveal both common and memory type-specific features of engram cells.

One of the great advantages of the gain-of-function demonstration of memory engrams compared to the loss-of-function demonstration is the availability of specific engram cells not only for basic research but also for their engineering by optogenetic and other technologies. This permitted manipulations of memory-associated cognitions and behaviors both in health (e.g., false memory inception) and neurological (e.g., early AD) or psychiatric (e.g., depression) diseases. These studies conducted with animal models are providing proof of concept evidence for the potential future development of therapies based on direct manipulation of patients.

Conflict of interest statement

Nothing declared.

Acknowledgements

This work was supported by the RIKEN Brain Science Institute, Howard Hughes Medical Institute, and the JPB Foundation to ST.

References and recommended reading

Papers of particular interest, published within the period of review, have been highlighted as:

• of special interest
•• of outstanding interest

1. Dudai Y, Morris RG: **Memorable trends**. *Neuron* 2013, **80**:742-750.

2. Tonegawa S, Pignatelli M, Roy DS, Ryan TJ: **Memory engram storage and retrieval**. *Curr Opin Neurobiol* 2015, **35**:101-109.

3. Descartes R: *Les passions de l'âme*. The passions of the soul, translated by Stephen H. Voss. Indianapolis: Hackett Publishing Company; 1989.

4. Schacter DL: *Forgotten ideas, neglected pioneers: Richard Semon and the story of memory*. New York: Routledge; 2001.

5. Semon R: *Die mneme*. The mneme. Leipzig: Wilhelm Engelmann; 1904.

6. Lashley KS: **In search of the engram**. *Symp Soc Exp Biol* 1950, **4**:454-482.

7. Hubener M, Bonhoeffer T: **Searching for engrams**. *Neuron* 2010, **67**:363-371.

•• 8. Tonegawa S, Liu X, Ramirez S, Redondo R: **Memory engram cells have come of age**. *Neuron* 2015, **87**:918-931.
An extensive review of the studies on the identification and manipulations of memory engrams.

• 9. Roy DS, Tonegawa S: *In search of engram cells*. Learn Mem 2E: 04036, in press; 2017.
A book chapter that expands the review [8••] with a full account of the pre-optogenetic period of the engram search.

10. Josselyn S, Kohler S, Frankland PW: **Finding the engram**. *Nat Rev Neurosci* 2015, **16**:521-534.

• 11. Reijmers LG, Perkins BL, Matsuo N, Mayford M: **Localization of a stable neural correlate of associative memory**. *Science* 2007, **317**:1230-1233.
This study detailed the generation of *c-fos-tTA* transgenic mice for labeling cell ensembles that are active during a specific experience.

12. Deng W, Mayford M, Gage FH: **Selection of distinct populations of dentate granule cells in response to inputs as a mechanism for pattern separation in mice**. *eLife* 2013, **2**:e312.

13. Tayler KK, Tanaka KZ, Reijmers LG, Wiltgen BJ: **Reactivation of neural ensembles during the retrieval of recent and remote memory**. *Curr Biol* 2013, **23**:99-106.

14. Cowansage KK, Shuman T, Dillingham BC, Chang A, Golshani P, Mayford M: **Direct reactivation of a coherent neocortical memory of context**. *Neuron* 2014, **84**:432-441.

15. Xie H, Liu Y, Zhu Y, Ding X, Yang Y, Guan JS: **In vivo imaging of immediate early gene expression reveals layer-specific memory traces in the mammalian brain**. *Proc Natl Acad Sci USA* 2014, **111**:2788-2793.

16. Zelikowsky M, Hersman S, Chawla MK, Barnes CA, Fanselow MS: **Neuronal ensembles in amygdala, hippocampus, and prefrontal cortex track differential components of contextual fear**. *J Neurosci* 2014, **34**:8462-8466.

17. Han J-H, Kushner SA, Yiu AP, Cole CJ, Matynia A, Brown RA, Neve RL, Guzowski JF, Silva AJ, Josselyn SA: **Neuronal competition and selection during memory formation**. *Science* 2007, **316**:457-460.

• 18. Han J-H, Kushner SA, Yiu AP, Hsiang H-L, Buch T, Waisman A, Bontempi B, Neve RL, Frankland PW, Josselyn SA: **Selective erasure of a fear memory**. *Science* 2009, **323**:1492-1496.
This study provided causal evidence that memory information can be encoded in sparse populations of cells in the amygdala.

• 19. Zhou Y, Won J, Karlsson MG, Zhou M, Rogerson T, Balaji J, Neve R, Poirazi P, Silva AJ: **CREB regulates excitability and the allocation of memory to subsets of neurons in the amygdala**. *Nat Neurosci* 2009, **12**:1438-1443.
This study investigated the physiological role of intrinsic cell excitability for memory allocation.

20. Hsiang H-L, Epp JR, van der Oever MC, Yan C, Rashid AJ, Insel N, Ye L, Niibori Y, Deisseroth K, Frankland PW *et al.*: **Manipulating a cocaine engram in mice**. *J Neurosci* 2014, **34**:14115-14127.

21. Yiu AP, Mercaldo V, Yan C, Richards B, Rashid AJ, Hsiang H-L, Pressey J, Mahadevan V, Tran MM, Kushner SA *et al.*: **Neurons are recruited to a memory trace based on relative neuronal excitability immediately before training**. *Neuron* 2014, **83**:722-735.

22. Czajkowski R, Jayaprakash B, Wiltgen B, Rogerson T, Guzman-Karlsson MC, Barth AL, Trachtenberg JT, Silva AJ: **Encoding and storage of spatial information in the retrosplenial cortex**. *Proc Natl Acad Sci USA* 2014, **111**:8661-8666.

23. Park S, Kramer EE, Mercaldo V, Rashid AJ, Insel N, Frankland PW, Josselyn SA: **Neuronal allocation to a hippocampal engram**. *Neuropsychopharmacology* 2016, **41**:2987-2993.

24. Cai D, Aharoni D, Shuman T, Shobe J, Biane J, Song W, Wei B, Veshkini M, La-Vu M, Lou J *et al.*: **A shared neural ensemble links distinct contextual memories encoded close in time**. *Nature* 2016, **534**:115-118.

25. Rashid AJ, Yan C, Mercaldo V, Hsiang H-L, Park S, Cole CJ, De Cristofaro A, Yu J, Ramakrishnan C, Lee SY *et al.*: **Competition between engrams influences fear memory formation and recall**. *Science* 2016, **353**:383-387.

26. Nomoto M, Ohkawa N, Nishizono H, Yokose J, Suzuki A, Matsuo M, Tsujimura S, Takahashi Y, Nagase M, Watabe AM *et al.*: **Cellular tagging as a neural network mechanism for behavioural tagging**. *Nat Commun* 2016, **7**:12319.

27. Martin SJ, Morris RG: **New life in an old idea: the synaptic plasticity and memory hypothesis revisited**. *Hippocampus* 2002, **12**:609-636.

•• 28. Liu X, Ramirez S, Pang PT, Puryear CB, Govindarajan A, Deisseroth K, Tonegawa S: **Optogenetic stimulation of a hippocampal engram activates fear memory recall**. *Nature* 2012, **484**:381-385.
This study provided the first demonstration that activation of putative memory engram cells is sufficient for the recall of specific memories.

•• 29. Ryan TJ, Roy DS, Pignatelli M, Arons A, Tonegawa S: **Engram cells retain memory under retrograde amnesia**. *Science* 2015, **348**:1007-1013.
This paper detailed the physiological characterization of memory engram cells and challenges standard conceptions of memory consolidation.

30. Kim J, Kwon JT, Kim HS, Josselyn SA, Han J-H: **Memory recall and modifications by activating neurons with elevated CREB**. *Nat Neurosci* 2014, **17**:65-72.

31. Gore F, Schwartz EC, Brangers BC, Aladi S, Stujenske JM, Likhtik E, Russo MJ, Gordon JA, Salzman CD, Axel R: **Neural representations of unconditioned stimuli in basolateral amygdala mediate innate and learned responses**. *Cell* 2015, **162**:134-145.

32. Ye L, Allen WE, Thompson KR, Tian Q, Hsueh B, Ramakrishnan C, Wang AC, Jennings JH, Adhikari A, Halpern CH *et al.*: **Wiring and molecular features of prefrontal ensembles representing distinct experiences**. *Cell* 2016, **165**:1-13.

33. Tanaka KZ, Pevzner A, Hamidi AB, Nakazawa Y, Graham J, Wiltgen B: **Cortical representations are reinstated by the hippocampus during memory retrieval**. *Neuron* 2014, **84**:347-354.

34. Denny CA, Kheirbek MA, Alba EL, Tanaka KF, Brachman RA, Laughman KB, Tomm NK, Turi GF, Losonczy A, Hen R: **Hippocampal memory traces are differentially modulated by experience, time, and adult neurogenesis**. *Neuron* 2014, **83**:189-201.

35. Matsuo N: **Irreplaceability of neuronal ensembles after memory allocation**. *Cell Rep* 2015, **11**:351-357.

36. Nader K, Schafe GE, LeDoux JE: **The labile nature of consolidation theory**. *Nat Rev Neurosci* 2000, **1**:216-219.

37. Schacter DL, Loftus EF: **Memory and law: what can cognitive neuroscience contribute?** *Nat Neurosci* 2013, **16**:119-123.

38. Schacter DL, Addis DR, Buckner RL: **Remembering the past to imagine the future: the prospective brain**. *Nat Rev Neurosci* 2007, **8**:657-661.

•• 39. Ramirez S, Liu X, Lin P-A, Suh J, Pignatelli M, Redondo RL, Ryan TJ, Tonegawa S: **Creating a false memory in the hippocampus**. *Science* 2013, **341**:387-391.
This study showed that a specific hippocampal ensemble could be artificially updated with new information.

• 40. Ohkawa N, Saitoh Y, Suzuki A, Tsujimura S, Murayama E, Kosugi S, Nishizono H, Matsuo M, Takahashi Y, Nagase M *et al.*: **Artificial association of pre-stored information to generate a qualitatively new memory**. *Cell Rep* 2015, **11**:261-269.
This study showed that hippocampal and amygdala ensembles could be simultaneously activated to form an associative memory.

41. Garner AR, Rowland DC, Hwang SY, Baumgaertel K, Roth BL, Kentros C, Mayford M: **Generation of a synthetic memory trace**. *Science* 2012, **335**:1513-1516.

•• 42. Redondo RL, Kim J, Arons AL, Ramirez S, Liu X, Tonegawa S: **Bidirectional switch of the valence associated with a hippocampal contextual memory engram**. *Nature* 2014, **513**:426-430.

•• 43. Ramirez S, Liu X, MacDonald CJ, Moffa A, Zhou J, Redondo RL, Tonegawa S: **Activating positive memory engrams suppresses depression-like behavior**. *Nature* 2015, **522**:335-339.

This study showed that depression-like behavior in mice could be ameliorated by activation of positive memory engrams.

44. Schlaepfer TE, Cohen MX, Frick C, Kosel M, Brodesser D, Axmacher N, Joe AY, Kreft M, Lenartz D, Sturm V: **Deep brain stimulation to reward circuitry alleviates anhedonia in refractory major depression**. *Neuropsychopharmacology* 2008, **33**:368-377.

45. Stuber GD, Sparta DR, Stamatakis AM, van Leeuwen WA, Hardjoprajitno JE, Cho S, Tye KM, Kempadoo KA, Zhang F, Deisseroth K *et al.*: **Excitatory transmission from the amygdala to nucleus accumbens facilitates reward seeking**. *Nature* 2011, **475**:377-380.

46. Selkoe DJ: **Alzheimer's disease is a synaptic failure**. *Science* 2002, **298**:789-791.

47. Jacobsen JS, Wu CC, Redwine JM, Comery TA, Arias R, Bowlby M, Martone R, Morrison JH, Pangalos MN, Reinhart PH *et al.*: **Early-onset behavioral and synaptic deficits in a mouse model of Alzheimer's disease**. *Proc Natl Acad Sci USA* 2006, **103**:5161-5166.

48. Weintraub S, Wicklund AH, Salmon DP: **The neuropsychological profile of Alzheimer disease**. *Cold Spring Harb Perspect Med* 2012, **2**:a6171.

•• 49. Roy DS, Arons A, Mitchell TI, Pignatelli M, Ryan TJ, Tonegawa S: **Memory retrieval by activating engram cells in mouse models of early Alzheimer's disease**. *Nature* 2016, **531**:508-512.
This study provided the first demonstration that optogenetic-induced potentiation in memory engram circuits could rescue dendritic spine deficits and restore long-term fear memories in early Alzheimer mice.

50. Engert F, Bonhoeffer T: **Dendritic spine changes associated with hippocampal long-term synaptic plasticity**. *Nature* 1999, **399**:66-70.

51. Matsuo N, Reijmers L, Mayford M: **Spine-type-specific recruitment of newly synthesized AMPA receptors with learning**. *Science* 2008, **319**:1104-1107.

• 52. Hayashi-Takagi A, Yagishita S, Nakamura M, Shirai F, Wu YI, Loshbaugh AL, Kuhlman B, Hahn KM, Kasai H: **Labelling and optical erasure of synaptic memory traces in the motor cortex**. *Nature* 2015, **525**:333-338.
This study detailed the generation of a synaptic optoprobe for labeling and manipulating recently potentiated dendritic spines.

• 53. Trouche S, Perestenko PV, van de Ven GM, Bratley CT, McNamara CG, Campo-Urriza N, Black SL, Reijmers LG, Dupret D: **Recoding a cocaine-place memory engram to a neutral engram in the hippocampus**. *Nat Neurosci* 2016, **19**:564-567.
This paper reported the place-specific firing patterns of hippocampal CA1 memory engram cells.

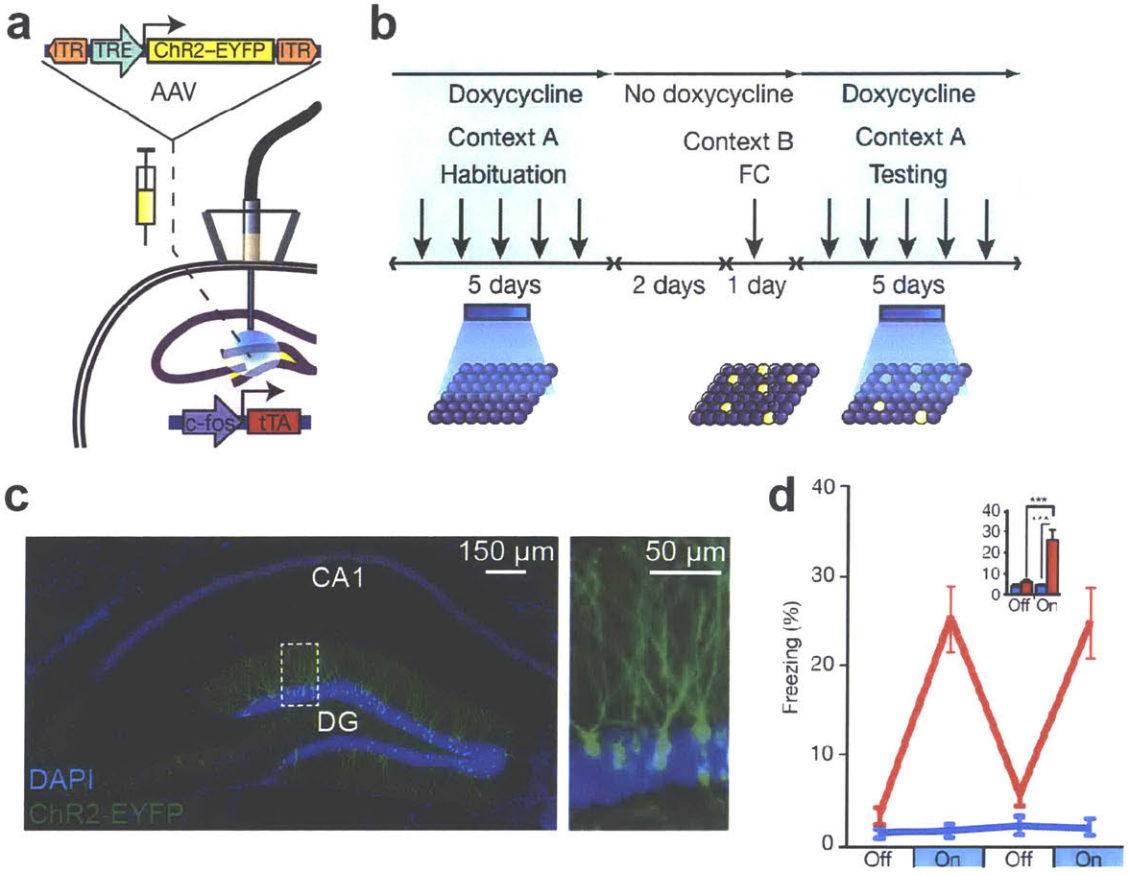

Figure 1. Tagging and manipulating memory engram cells

(a) Using the activity-dependent labeling technology developed by [28••], c-fos-tTA mice were injected with the AAV_9-TRE-ChR2-EYFP virus and implanted with an optic fiber targeting the hippocampal dentate gyrus (DG). (b) Behavioral schedule. Mice were habituated to context A with light stimulation, then taken off doxycycline-containing food for 2 days and fear conditioned (FC) I context B. Mice were put back on doxycycline-containing food and tested in context A with light stimulation. (c) Representative image showing the expression of ChR2-EYFP in memory engram cells of the DG for a contextual fear memory (left). Boxed DG region is magnified (right). (d) Following fear conditioning, blue light stimulation of DG engram cells induces memory recall (freezing behavior) in neutral context A.

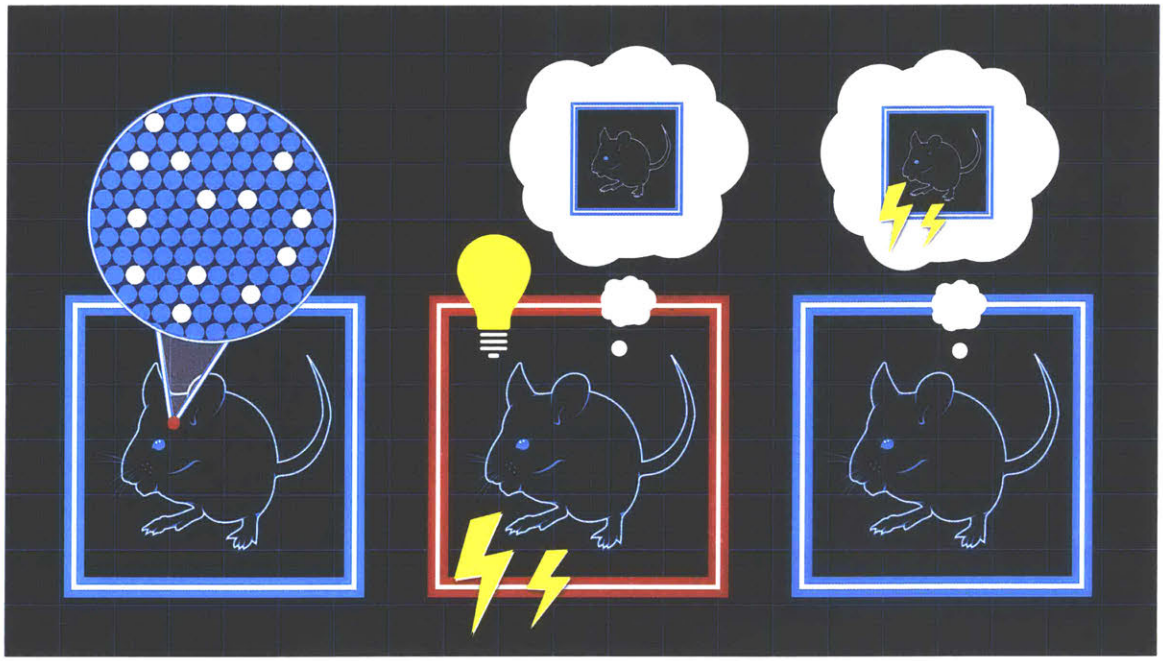

Figure 2. Creating a false memory by manipulating engram cells
Tagging memory engram cells in the hippocampus encoding the blue, neutral context information with ChR2 (left). The next day, mice received mild electric footshocks in the red context with simultaneous light activation of the blue context memory engram cells (middle). On day 3, mice were returned to the blue context and displayed fear memory recall (right).

Distinct neural circuits for the formation and retrieval of episodic memories

Dheeraj S. Roy[1,5], Takashi Kitamura[1,5], Teruhiro Okuyama[1], Sachie K. Ogawa[1], Chen Sun[1], Yuichi Obata[2], Atsushi Yoshiki[2] and Susumu Tonegawa[1,3,4,6,*]

[1] RIKEN-MIT Center for Neural Circuit Genetics at the Picower Institute for Learning and Memory, Department of Biology and Department of Brain and Cognitive Sciences, Massachusetts Institute of Technology, Cambridge, MA 02139, U.S.A.

[2] RIKEN BioResource Center, 3-1-1 Koyadai, Ibaraki 305-0074, Japan

[3] Howard Hughes Medical Institute, Massachusetts Institute of Technology, Cambridge, MA 02139, U.S.A.

[4] RIKEN Brain Science Institute, 2-1 Hirosawa, Wako-shi, Saitama 351-0198, Japan

[5] Co-first author

[6] Lead contact

* Correspondence: tonegawa@mit.edu

SUMMARY

The formation and retrieval of a memory is thought to be accomplished by activation and reactivation, respectively, of the memory-holding cells (engram cells) by a common set of neural circuits, but this hypothesis has not been established. The medial temporal-lobe system is essential for the formation and retrieval of episodic memory for which individual hippocampal subfields and entorhinal cortex layers contribute by carrying out specific functions. One subfield whose function is poorly known is the subiculum. Here, we show that dorsal subiculum and the circuit, CA1 to dorsal subiculum to medial entorhinal cortex layer 5, plays a crucial role selectively in the retrieval of episodic memories. Conversely, the direct CA1 to medial entorhinal cortex layer 5 circuit is essential specifically for memory formation. Our data suggest that the subiculum-containing detour loop is dedicated to meet the requirements associated with recall such as rapid memory updating and retrieval-driven instinctive fear responses.

KEYWORDS

Subiculum, episodic memory, hippocampus, entorhinal cortex, memory formation, memory retrieval, mammillary bodies, stress hormone, neural circuits, memory updating.

HIGHLIGHTS

- dSub and the circuit, CA1→dSub→EC5, is required for hippocampal memory retrieval, but not for formation
- The direct CA1→EC5 circuit is essential for hippocampal memory formation, but not for retrieval
- The dSub→MB circuit regulates memory retrieval-induced stress hormone responses
- The dSub→EC5 circuit contributes to context-dependent memory updating

INTRODUCTION

It is generally thought that formation and retrieval of a memory are accomplished by activation and reactivation of memory-holding cells (engram cells), respectively, by a largely common set of neural circuits that convey relevant sensory and/or processed information. However, this hypothesis has not been well studied. One of the best neural systems to prove this issue is the medial temporal lobe (MTL), including the hippocampus (HPC) and entorhinal cortex (EC), which plays crucial roles in episodic memory (Eichenbaum et al., 2007; Squire, 1992). Numerous studies have identified specific and crucial roles of individual HPC subfields and EC layers to the overall mnemonic function (Deng et al., 2010; Hasselmo and McClelland, 1999; Hitti and Siegelbaum, 2014; Moser et al., 2014; Nakazawa et al., 2004). However, the essential function of one HPC subfield, subiculum (Sub), is poorly known. The mammalian HPC formation is organized primarily as a unidirectional circuit, where information transferred from the EC's superficial layers to the dentate gyrus (DG) is processed successively in CA subfields: CA3, CA2, and CA1. Dorsal CA1 (dCA1) sends its primary projections directly to medial EC layer 5 (EC5) or indirectly via dorsal subiculum (dSub) (a detour circuit). One of the interesting differences between the direct and indirect HPC output pathways is that in the latter, dSub projects not only to EC5, but also to many cortical and subcortical brain regions (Ding, 2013; Kishi et al., 2000).

Using functional magnetic resonance imaging of human subjects, several studies have suggested that the DG and CA subfields are selectively activated during episodic memory formation, whereas subiculum (Sub) is active during the recollection of an episode (Eldridge et al., 2005; Gabrieli et al., 1997). In rodents, ibotenic acid lesions of the CA1 subfield or Sub caused impairments in the acquisition of place navigation (Morris et al., 1990). However, since human imaging studies provide only correlative, rather than causal, evidence and rodent lesions

are not well targeted to a specific hippocampal subregion, especially given the close proximity of CA1 and dSub, it has not been possible to identify the essential function of Sub in episodic memory. Furthermore, previous studies did not address the potential purpose of the parallel diverging and converging dCA1 to medial EC5 and dCA1 to dSub to medial EC5 circuits in memory formation versus retrieval.

In the present study, we addressed these issues by creating a mouse line expressing Cre recombinase specifically in dSub neurons. Combined with circuit tracing and optogenetic manipulations during behavioral paradigms, we found differential roles of dSub projections in hippocampal memory retrieval and retrieval-induced stress hormone responses. We demonstrate that dSub and the circuit, CA1→dSub→EC5, is selectively required for memory retrieval, while the dSub to mammillary bodies (MB) circuit regulates stress hormones following memory retrieval. In contrast, the direct CA1→EC5 circuit is essential for hippocampal memory formation, but not recall. Our study reveals a functional double-dissociation between parallel hippocampal output circuits that are important for memory formation versus memory retrieval.

RESULTS

Generation of FN1-Cre Mice

We took advantage of the finding that fibronectin-1 (FN1) gene expression is restricted to dSub neurons (Lein et al., 2004) and created a transgenic mouse line (FN1-Cre) that expresses Cre recombinase under the FN1 promoter (Figure 1A, and see Methods). When infected with a Cre-dependent adeno-associated virus containing an eYFP gene, eYFP expression was highly restricted to dSub neurons and was completely absent in neighboring dCA1 excitatory neurons identified by WFS1 (Figure 1B). The expression of eYFP was restricted to $CaMKII^{+}$ excitatory neurons in both the deep and superficial layers of dSub (Figures 1C-1D, and see Figure S1A).

This eYFP expression accounted for over 85% of all excitatory neurons in this brain region, and was dSub-specific along the entire medial-lateral axis (Figures 1E-1K). Further, Cre expression was absent in ventral subiculum (vSub) and medial entorhinal cortex (MEC) in this mouse line (Figures S1B-S1K). Using *in situ* hybridization, we confirmed that Cre expression in this mouse line is highly restricted to dSub, and the dorsal tegmental nucleus (DTg) in the brain stem (Figure S1L). Thus, FN1-Cre mice allows for the genetic manipulation of dSub excitatory neurons with unprecedented specificity.

Input-Output Organization of dSub Neurons

We next examined the inputs to dSub excitatory neurons as well as their anterograde brain-wide projection pattern. Monosynaptic retrograde tracing experiments using a Cre-dependent helper virus combined with rabies virus (RV) (Wickersham et al., 2007), labeled 78% of dSub cells relative to all cells (i.e., $DAPI^+$ cells). The results confirmed that dCA1 provides the major input to dSub excitatory neurons (Figures 2A-2C) (Ding, 2013; Kishi et al., 2000). Other brain areas that provide inputs to dSub include parasubiculum (PaS), retrosplenial agranular cortex (RSA), superficial layers of EC (MEC II/III), nucleus of the diagonal band (NDB), nucleus accumbens shell (Acb Sh), and several thalamic nuclei (Thal Nucl) (Figure 2D, and see Figure S1M).

A Cre-dependent channelrhodopsin-2 (ChR2)-eYFP virus combined with light sheet microscopy of CLARITY (Chung et al., 2013, see Methods)-processed brain samples revealed that major efferents of dSub neurons were directed to RSA, mammillary bodies (MB), medial EC5, and postrhinal cortex (Pos) (Figures 2E-2F). No projections from dSub were observed in the superficial layers (II/III) of MEC (Figure 2G). These dSub neurons converged on both medial and lateral regions of MB (Figure 2H). Using a Cre-dependent synaptophysin virus to label dSub axonal terminals, we found that these Cre^+ neurons express vesicular glutamate transporters 1

and 2 (Kaneko et al., 2002), reflecting their excitatory nature (Figures S1N-S1P). Injection of a retrograde tracer, cholera toxin subunit B (CTB), into the MB revealed a gradient of CTB555 with higher intensity labeling in the proximal part of dSub (i.e., closer to CA1), whereas injection into medial EC5 showed a gradient of CTB488 with higher intensity labeling in the distal part of dSub (i.e., away from CA1) (Figures 2I-2M, and see Figure S1Q) (Witter et al., 1990). However, neurons in both proximal and distal parts of dSub were weakly labeled by CTB injected into MB or EC5. Together, these results indicate that dCA1 serves as the main input structure to dSub, and that the majority of dSub neurons send projections to multiple downstream target structures.

The dSub→EC5 Circuit Bidirectionally Regulates Episodic Memory Retrieval

To examine the functional role of dSub neurons and their circuits, we performed optogenetic inhibition experiments using a Cre-dependent eArch3.0-eYFP virus. During the contextual fear-conditioning (CFC) paradigm, we confirmed that green light inhibition of dSub decreased behavior-induced immediate early gene cFos-positive neurons (Figures S2A-S2L). Inhibition of dSub neurons during CFC training had no effect on footshock-induced freezing behavior or long-term memory formation (Figure 3A). In contrast, dSub inhibition during CFC recall tests decreased behavioral performance (Figure 3B). Inhibition of dSub neurons had no effect on motor behaviors in an open-field assay (Figure S2M). Inhibition of dSub terminals in medial EC5, but not in MB, also revealed a memory retrieval deficit (Figure 3C). Since the behavioral effect of dSub inhibition in this mouse line is based on eArch expression in approximately 85% of excitatory neurons in this brain region, we examined the effect of a more complete inhibition of dSub neurons. Inhibition of dSub→EC5 terminals in wild type mice using an EF1α-eArch3.0-

eYFP virus revealed a greater memory retrieval deficit (Figure S3 vs. Figure 3C). Further, inhibition of vSub→EC5 terminals showed normal levels of memory recall (Figure S3).

Conversely, optogenetic activation of ChR2-eYFP-expressing dSub projections to medial EC5 during CFC recall tests increased recall-induced freezing behavior in the training context, but not in a neutral context (Figure 3D, and see Figure S4A). This result indicates that dSub is involved in hippocampal memory retrieval in a context-specific manner. Activation of dSub→EC5 in mice that did not receive footshocks during training lacked freezing behavior during the recall test, supporting the specificity of increased memory retrieval in CFC-trained animals. Our interpretation of these optogenetic activation experiments is that in the training context natural recall cues reactivate engram cells in all subfields of the hippocampus, like DG, CA3, and CA1, but also in dSub. When the activity of dSub projections to EC5 is further increased by ChR2 this leads to enhanced freezing due to increased activation of dSub engram cells. On the other hand, in a neutral context lacking the specific natural recall cues to reactivate dSub engram cells, the ChR2 activation without engram labeling is not sufficient to induce memory recall. In another hippocampus-dependent memory paradigm, trace fear-conditioning, dSub→EC5 inhibition impaired memory recall (Figure 3E, and see Figures S4B-S4C). In contrast, inhibition of dSub→EC5 had no effect on the recall of a hippocampus-independent memory formed during delay fear-conditioning (Figures S4D-S4E). Together, these experiments indicate that the dSub→EC5 circuit regulates episodic memory retrieval bidirectionally. We confirmed that the dSub→EC5 projection is also necessary for the retrieval of a positive-valence, hippocampus-dependent (Raybuck and Lattal, 2014) memory formed in a conditioned place preference (CPP) paradigm (Figure 3F, and see Figures S2N, S4F-S4G).

The dSub→MB Circuit Regulates Retrieval-Induced Stress Hormone Responses

During both CFC training and recall, levels of the stress hormone corticosterone (CORT) increases in the blood (Figure 3G), which is believed to be important to prepare the animal for a predicted immediate danger (Kelley et al., 2009). Given our finding that dSub neurons are required for memory retrieval, but not memory formation, we investigated whether the dSub→MB circuit is involved in retrieval-induced stress hormone responses. Optogenetic inhibition of dSub→MB projections following CFC recall, but not following CFC training, prevented the CORT increase (Figure 3G, and see Figure S2N). This deficit was specific to dSub→MB terminal inhibition, since dSub→EC5 terminal inhibition had no effect. In addition, optogenetic activation of ChR2-expressing dSub→MB projections following CFC recall increased CORT levels, revealing a bidirectional regulation of blood stress hormone levels by the dSub→MB circuit following fear memory retrieval. Interestingly, we did not observe increased CORT levels following CPP memory retrieval (Figure S4H). From our finding that the dSub→EC5 circuit is crucial for CPP memory retrieval (Figure 3F), it is clear that dSub neurons are activated and therefore both downstream EC5 and MB circuits would be activated. The lack of increased CORT levels following CPP memory retrieval suggests that the dSub→MB circuit is necessary but not sufficient to induce CORT. These experiments uncovered a neural circuit originating from dSub that regulates stress hormone responses to conditioned cues.

Heterogeneity of dCA1 Neurons that Project to dSub and EC5

The dCA1 neurons send primary projections directly to medial EC5, or indirectly via dSub (Ding, 2013). We examined whether the same dCA1 neurons send divergent projections to both dSub and EC5, or whether these two circuits involve distinct subpopulations of dCA1 neurons. To test these possibilities, we conducted monosynaptic retrograde tracing by injecting a Cre-

dependent helper virus combined with rabies virus (Wickersham et al., 2007) into dSub of FN1-Cre mice combined with CTB488 injected into medial EC5 (Figures 4A-4C, and see Figure S1Q). We observed three neuronal populations distributed throughout the proximal-distal axis of dCA1, namely RV-mCherry-positive dCA1 cells, CTB488-positive dCA1 cells, and double-positive dCA1 cells (Figures 4D-4F), indicating that dCA1 neurons project collaterally to both dSub and medial EC5 (22%), project to dSub alone (18%), or to medial EC5 alone (23%) (Figure 4G, and see Figures S5A-S5H). A significant proportion of the remaining dCA1 neurons most likely send primary projections to the deep layers of the lateral EC (LEC5) (Knierim et al., 2013), which we confirmed using CTB retrograde tracing (Figure S5I). Further, it has been suggested that proximal and distal dCA1 may play differential roles in memory formation (Nakazawa et al., 2016), however we did not observe differences between dCA1 neurons projecting to dSub and EC5 based on their proximal versus distal location (Figure S5J). Thus, these data demonstrate that, although there are distinct dCA1 subpopulations that project to either dSub or EC5, a significant proportion of dCA1 neurons projecting to dSub and EC5 are shared between these two circuits.

The dCA1→EC5 Circuit is Crucial for Episodic Memory Encoding

Given the selective role of the dSub→EC5 circuit in memory retrieval and our finding that heterogeneous subpopulations of dCA1 neurons project to dSub and medial EC5, respectively, we next investigated the behavioral contributions of the direct dCA1→EC5 circuit. The injection of a Cre-dependent H2B-GFP virus into dCA1 of CA1 pyramidal cell-specific Cre transgenic mice, TRPC4-Cre (Okuyama et al., 2016), resulted in GFP expression restricted to dCA1 pyramidal cells without any expression in dSub (Figure 4H). Terminal inhibition of CA1 axons at medial EC5 during CFC training impaired long-term memory formation (Figure 4I), whereas

the same manipulation during CFC recall had no effect on behavioral performance (Figure 4J). Further, consistent with the role of dSub in CFC recall, terminal inhibition of dCA1→dSub during CFC recall, but not during CFC training, decreased behavioral performance (Figures 4K-4L). Therefore, the direct dCA1→EC5 circuit plays a crucial role in the encoding, but not recall, of CFC long-term memory, whereas the indirect dCA1→dSub→EC5 circuit is crucial for memory recall, but not encoding.

Distinct Roles for the Direct and Indirect Circuits in Memory Updating

A potential purpose of the parallel diverging and converging direct dCA1→EC5 and indirect dCA1→dSub→EC5 circuits could be to support rapid memory updating (Lee, 2010). To test this possibility, we performed the pre-exposure mediated contextual fear-conditioning (PECFC) paradigm with optogenetic terminal inhibition of CA1→EC5 (Figure 4M) or dSub→EC5 (Figure 4N) during the pre-footshock period (context retrieval) only or footshock period (fear association) only, on Day 2. CA1→EC5 inhibition specifically during the footshock period of Day 2 impaired the context-shock association evidenced by decreased freezing on Day 3, whereas inhibition during the pre-footshock period had no effect (Figure 4M). In contrast, dSub→EC5 inhibition during the pre-footshock period of Day 2 impaired the context-shock association on Day 3, while inhibition restricted to the footshock period had no effect (Figure 4N). Together, these data indicate that the dSub→EC5 circuit is crucial for the rapid recall in order to perform memory updating, while the CA1→EC5 circuit is crucial for encoding new information into a long-term memory.

cFos Activation in dCA1 and dSub during Memory Encoding and Retrieval

Expression of immediate-early genes (IEGs) has been used to map specific functions onto neuronal activity in a given brain region (Kubik et al., 2007). In order to acquire cellular level evidence supporting the dedicated role of dSub in recall rather than encoding of CFC memory, we monitored IEG cFos activation in dCA1 and dSub during CFC behavior. To measure cFos activation by training or recall, we took advantage of a virus-mediated strategy (Roy et al., 2016) using a cocktail of c-Fos-tTA and TRE-H2B-GFP viruses (Figures 5A-5B). Wild type mice raised on a doxycycline (DOX) diet to prevent activity-dependent labeling by the injected virus cocktail were taken off DOX 24 hr before CFC encoding or recall to visualize H2B-GFP labeling in CA1 and dSub (Figures 5C-5E). There was significant cFos activation in both CA1 and dSub following encoding or recall epochs as compared to the home cage group (Figure 5F). Interestingly, in dSub, memory recall epochs enhanced cFos activation more compared with encoding epochs, whereas there was no difference of cFos activation in CA1 neurons elicited by these epochs (Figure 5G).

Further, we examined the overlap between behavior-induced cFos in CA1 and CA1 cells that were retrogradely labeled by injection of CTB555 into dSub or medial EC5 (Figure S1Q). Consistent with the optogenetic manipulation experiments, CA1 neurons projecting to EC5 showed higher levels of cFos activation during CFC encoding rather than retrieval, whereas CA1 neurons projecting to dSub showed higher levels of cFos activation during retrieval (Figure 5H, and see Figures S5K-S5N). To examine CA1 memory engram cell reactivation following recall, among dSub and EC5 projecting subpopulations, we tagged CA1 engram cells formed during CFC encoding using a virus cocktail of c-Fos-tTA and TRE-ChR2-eYFP (Liu et al., 2012), while simultaneously labeling CA1 cells projecting to dSub or medial EC5 with CTB555. One day after training, we quantified the overlap between recall-induced cFos in CA1 and CA1 engram

cells that were retrogradely labeled (Figures 5I-5L). Strikingly, dSub-projecting CA1 engram cells showed higher cFos reactivation following memory retrieval compared to EC5-projecting CA1 engram cells (Figure 5M). Next, following CFC recall, we measured cFos activation levels in the basolateral amygdala (BLA), which plays crucial roles in fear memory encoding and recall (Hall et al., 2001). Terminal inhibition of the dSub→EC5 circuit, but not the dCA1→EC5 circuit, decreased cFos levels in the BLA (Figure 5N), further indicating that the direct and indirect dCA1 output circuits have differential functional roles in memory retrieval.

In Vivo Calcium Imaging of dCA1 and dSub Neurons

We also investigated activation of dSub and dCA1 pyramidal cells in response to training and recall by monitoring *in vivo* calcium (Ca^{2+}) transients using a miniaturized microendoscope (Kitamura et al., 2015; Sun et al., 2015; Ziv et al., 2013). For this purpose, Cre-dependent GCaMP6f virus was injected into the dSub of FN1-Cre mice to specifically express the Ca^{2+} indicator in dSub cells (Figure 6A, and see Figures S6A-S6B). As expected, expression of GCaMP6f was restricted to dSub, with no expression in CA1 neurons in these mice (Figures 6B, 6D). Similarly for dCA1 neurons, GCaMP6f virus was injected into the dCA1 of dCA1-specific WFS1-Cre mice (Kitamura et al., 2014, and see Methods) (Figures 6C, 6E). With the open field paradigm (Figures S6C-S6G, and see Movies S1-S2), CA1 neurons showed homogeneous activation profiles, whereas dSub neurons displayed two types of activation profiles (Geva-Sagiv et al., 2016; Sharp and Green, 1994; Staff et al., 2000; Taube, 1993): short-tail cells whose profiles were similar to those of CA1 cells, and long-tail cells in which the post-stimulation activity persisted as long as 15 s (Figures 6F-6G). Consistent with a previous study (Sharp and Green, 1994), dSub neurons exhibited place fields, which were larger in both types of dSub cells compared to CA1 pyramidal cells (Figure 6H, and see Figure S6H).

Next, we investigated Ca^{2+} activity patterns as mice went through the CFC paradigm (Figure 6I, and see Figures S6I-S6K). CA1 showed an increased percentage of active cells during both training and recall periods compared to the pre-footshock period in the context in which a footshock was subsequently delivered. The dSub neurons showed an increased percentage of active cells during recall compared to the pre-footshock or training periods, and no significant difference of active cell percentages was observed between the latter two periods (top row, Figure 6I). We then divided the training and recall periods into two epochs—non-freezing (NF) and freezing (F)—in order to differentiate an effect of the animal's movement state (Ranck, 1973) on the proportion of active cells. During training, the proportion of active CA1 cells was greater during F epochs compared to the NF epochs, whereas these proportions were similar during recall. In contrast, the proportions of active dSub cells were greater during recall compared to training regardless whether the mice were in F or NF epochs. We then subdivided active dSub cells into short-tail and long-tail cells, and found that the proportion of active short-tail cells were greater during recall compared to training regardless whether mice were in F or NF epochs. In contrast, the proportion of active long-tail dSub cells was greater specifically during recall-induced F epochs, compared to the other three types of epochs (bottom row, Figure 6I). Together, and consistent with the behavior and cFos activation experiments, these data demonstrate distinct contributions of dCA1 and dSub cells to memory encoding and memory recall, respectively.

DISCUSSION

It has been established that CA1 and Sub serve as the major output structures of the hippocampus (O'Mara, 2006); however, the functional role of Sub in hippocampus-dependent episodic memory has remained elusive. Here, we have shown that optogenetic inhibition of dSub during

recall, but not during encoding, impairs behavioral performance in three hippocampal-dependent memory paradigms: CFC, trace fear-conditioning, and conditioned place preference. The activity of dSub neurons is capable of regulating memory recall bidirectionally: its inhibition impairs recall and its activation enhances recall. To our knowledge, this is the first identification of the specific causal role of dSub neurons in episodic memory recall.

Previously, lesions (Morris et al., 1990) as well as optogenetic inhibition (Goshen et al., 2011) showed that in rodents, neuronal activity in the CA1 subfield is necessary for both the encoding and retrieval of long-term memories. In this study, we employed optogenetic inhibition of specific terminals of CA1 cell projections and found that the CA1→dSub circuit is crucial for memory recall but not for encoding, whereas the CA1→EC5 circuit is crucial for memory encoding but not for recall. Supporting this role of the CA1→dSub circuit is the finding that inhibition of the downstream dSub terminals in medial EC5 also impairs memory recall selectively. Together, these data indicate that the hippocampal output pathways are functionally segregated: episodic memory encoding uses primarily the direct dCA1→EC5 circuit, while episodic memory retrieval uses primarily the indirect dCA1→dSub→EC5 circuit. The functional dissociation between these two dCA1 output circuits is especially striking given that a significant proportion of dCA1 neurons projecting to dSub and EC5 are overlapping, and that the overall difference in cFos activation levels between dCA1 neurons projecting to dSub versus EC5 during either training or recall epochs is approximately 2% of all dCA1 cells. Further, it is intriguing that we found that about 20% of dCA1 engram cells, those projecting to EC5, are not reactivated by memory recall and thus do not contribute to this behavioral epoch. What could be the purpose of these dCA1 engram cells? We speculate that these engram cells are the stable holder of the

original memory, which are undisturbed by a retrieval process, and contribute to the generation of engrams in downstream regions, such as remote memory engram cells in the prefrontal cortex.

The dSub neurons displayed two types of activation profiles—short-tail cells and long-tail cells. These cells may correspond to the previously reported non-bursting cells and bursting cells (Geva-Sagiv et al., 2016; Sharp and Green, 1994; Staff et al., 2000; Taube, 1993). Interestingly, the proportion of active long-tail dSub neurons is greater specifically during recall-induced freezing epochs compared to training-induced freezing epochs. This may be because activation of long-tail cells requires more powerful drive than short-tail cells, and because such a potent drive may be provided only by reactivation of previously formed CA1 engram cells by recall cues (Tonegawa et al., 2015), and not by activation of naïve CA1 cells which occurs during training.

What advantages would the distinct circuits for memory encoding and recall provide? One possible merit may be related to episodic memories with negative valence. Fear memory retrieval by conditioned cues induces not only an instinctive fear response (anxiety, avoidance, freezing, etc.), but also an increase in blood stress hormones that organizes multiple body systems to prepare the animal for a predicted immediate danger (Kelley et al., 2009). While a recent study showed that an area of the rodent's olfactory cortex plays a key role in the hormonal component of the instinctive fear response to volatile predator odors (Kondoh et al., 2016), neural circuits responsible for triggering both episodic memory retrieval and retrieval-induced stress hormone responses have remained unknown. In this study, we have identified two neural circuits originating from dSub that independently regulate freezing behavior and stress hormone responses to conditioned cues: the dSub→EC5 circuit mediates appropriate freezing behavior during memory retrieval, while the dSub→MB circuit is crucial for memory retrieval-induced

stress responses via bed nucleus of the stria terminalis (BNST) and the hypothalamic corticotropin hormone-releasing neurons (Herman et al., 1998). The preferential activation of long-tail dSub neurons by recall cues may contribute to a sustained enhancement of hormonal release from these downstream areas (Bourque et al., 1993). It has been known that glucocorticoid hormone synthesis is enhanced during memory consolidation (Roozendaal, 2002). Similarly, the retrieval-induced enhancement of CORT may promote memory reconsolidation triggered by recall. Therefore, the Sub→MB pathway may regulate memory retrieval-based emotions and together with the Sub→EC5 pathway that controls the retrieval-based instinctive fear response, would allow for more flexible actions that improve the animal's survival during challenging events in nature.

Another possible merit of distinct circuits for encoding and retrieval of memory may be to perform rapid memory updating. When a new salient stimulus (such as footshock) is delivered while a subject is recalling a previously acquired memory, the original memory is known to be modified (or updated) by incorporating the concurrently delivered salient stimulus. The diverging followed by converging CA1→dSub→EC5 and CA1→EC5 circuits seem to be ideal for this mnemonic processing: the content of the previously formed memory is retrieved by dSub and a stimulus transmitted directly from CA1 will be co-delivered to EC5 to make a new association resulting in memory updating. It has previously been suggested that such memory updating takes place in the PECFC paradigm by converting the previously acquired contextual memory to a context-dependent fear memory (Lee, 2010). Our findings, that in the PECFC paradigm, conversion of a contextual memory to a context-dependent fear memory is impaired by either the inhibition of dSub→EC5 terminals targeted to the short (8 sec) context recall period, or inhibition of CA1→EC5 terminals targeted to the period when an association of the recalled

context memory with footshock takes place, supports the crucial role of dSub in memory updating.

Our study is on hippocampus-dependent episodic (or episodic-like) memories, which involves information processing by the hippocampus and other medial temporal lobe structures. Additional work is required to examine whether distinct circuits for encoding and retrieval is a property shared by brain regions responsible for the formation of non-episodic memories, which would involve structures other than the temporal lobe. In this context, it is interesting that a recent study with a worm (*Caenorhabditis elegans*) showed that aversive long-term memory formation and retrieval are carried out by distinct neural circuits (Jin et al., 2016). Therefore, it is possible that distinct circuits for long-term memory formation versus retrieval may be an evolutionarily conserved feature in many species that are capable of learning. With regards to cognitive disorders, it is widely believed that subiculum is among the earliest brain regions affected in Alzheimer's disease patients (Hyman et al., 1984). Our findings contribute to a better understanding of neural mechanisms underlying episodic memory formation and may provide insights into pathological conditions affecting memory retrieval.

REFERENCES

Bourque, C.W., Oliet, S.H., Kirkpatrick, K., Richard, D., and Fisher, T.E. (1993). Extrinsic and intrinsic modulatory mechanisms involved in regulating the electrical activity of supraoptic neurons. Ann. N. Y. Acad. Sci. *689*, 512-519.

Chung, K., Wallace, J., Kim, S.Y., Kalyanasundaram, S., Andalman, A.S., Davidson, T.J., Mirzabekov, J.J., Zalocusky, K.A., Mattis, J., Denisin, A.K., et al. (2013). Structural and molecular interrogation of intact biological systems. Nature *497*, 332-337.

Deng, W., Aimone, J.B., and Gage, F.H. (2010). New neurons and new memories: how does adult hippocampal neurogenesis affect learning and memory? Nat. Rev. Neurosci. *11*, 339-350.

Ding, S.L. (2013). Comparative anatomy of the prosubiculum, subiculum, presubiculum, postsubiculum, and parasubiculum in human, monkey, and rodent. J. Comp. Neurol. *521*, 4145-4162.

Eichenbaum, E., Yonelinas, A.P., and Ranganath, C. (2007). The medial temporal lobe and recognition memory. Annu. Rev. Neurosci. *30*, 123-152.

Eldridge, L.L., Engel, S., Zeineh, M.M., Bookheimer, S.Y., and Knowlton, B.J. (2005). A dissociation of encoding and retrieval processes in the human hippocampus. J. Neurosci. *25*, 3280-3286.

Gabrieli, J.D., Brewer, J.B., Desmond, J.E., and Glover, G.H. (1997). Separate neural bases of two fundamental memory processes in the human medial temporal lobe. Science *276*, 264-266.

Geva-Sagiv, M., Romani, S., Las, L., and Ulanovsky, N. (2016). Hippocampal global remapping for different sensory modalities in flying bats. Nat. Neurosci. *19*, 952-958.

Goshen, I., Brodsky, M., Prakash, R., Wallace, J., Gradinaru, V., Ramakrishnan, C., and Deisseroth, K. (2011). Dynamics of retrieval strategies for remote memories. Cell *147*, 678-689.

Hall, J., Thomas, K.L., and Everitt, B.J. (2001). Fear memory retrieval induces CREB phosphorylation and Fos expression within the amygdala. Eur. J. Neurosci. *13*, 1453-1458.

Hasselmo, M.E., and McClelland, J.L. (1999). Neural models of memory. Curr. Opin. Neurobiol. *9*, 184-188.

Herman, J.P., Dolgas, C.M., and Carlson, S.L. (1998). Ventral subiculum regulates hypothalamo-pituitary-adrenocortical and behavioural responses to cognitive stressors. Neuroscience *86*, 449-459.

Hitti, F.L., and Siegelbaum, S.A. (2014). The hippocampal CA2 region is essential for social memory. Nature *508*, 88-92.

Hyman, B.T., Van Hoesen, G.W., Damasio, A.R., and Barnes, C.L. (1984). Alzheimer's disease: cell-specific pathology isolates the hippocampal formation. Science *225*, 1168-1170.

Jin, X., Pokala, N., and Bargmann, C.I. (2016). Distinct circuits for the formation and retrieval of an imprinted olfactory memory. Cell *164*, 632-643.

Kaneko, T., Fujiyama, F., and Hioki, H. (2002). Immunohistochemical localization of candidates for vesicular glutamate transporters in the rat brain. J. Comp. Neurol. *444*, 39-62.

Kelley, J.B., Balda, M.A., Anderson, K.L., and Itzhak, Y. (2009). Impairments in fear conditioning in mice lacking the nNOS gene. Learn. Mem. *16*, 371-378.

Kishi, T., Tsumori, T., Ono, K., Yokota, S., Ishino, H., and Yasui, Y. (2000). Topographical organization of projections from the subiculum to the hypothalamus in the rat. J. Comp. Neurol. *419*, 205-222.

Kitamura, T., Pignatelli, M., Suh, J., Kohara, K., Yoshiki, A., Abe, K., and Tonegawa, S. (2014). Island cells control temporal association memory. Science *343*, 896-901.

Kitamura, T., Sun, C., Martin, J., Kitch, L.J., Schnitzer, M.J., and Tonegawa, S. (2015). Entorhinal cortical ocean cells encode specific contexts and drive context-specific fear memory. Neuron *87*, 1317-1331.

Knierim, J.J., Neunuebel, J.P., and Deshmukh, S.S. (2013). Functional correlates of the lateral and medial entorhinal cortex: objects, path integration and local-global reference frames. Philos. Trans. R. Soc. Lond. B. Biol. Sci. *369*, 20130369.

Kondoh, K., Lu, Z., Ye, X., Olson, D.P., Lowell, B.B., and Buck, L.B. (2016). A specific area of olfactory cortex involved in stress hormone responses to predator odors. Nature *532*, 103-106.

Kubik, S., Miyashita, T., and Guzowski, J.F. (2007). Using immediate-early genes to map hippocampal subregional functions. Learn. Mem. *14*, 758-770.

Lee, J.L. (2010). Memory reconsolidation mediates the updating of hippocampal memory content. Front. Behav. Neurosci. *4*, 168.

Lein, E.S., Zhao, X., and Gage, F.H. (2004). Defining a molecular atlas of the hippocampus using DNA microarrays and high-throughput in situ hybridization. J. Neurosci. *24*, 3879-3889.

Liu, X., Ramirez, S., Pang, P.T., Puryear, C.B., Govindarajan, A., Deisseroth, K., and Tonegawa, S. (2012). Optogenetic stimulation of a hippocampal engram activates fear memory recall. Nature *484*, 381-385.

Morris, R.G., Schenk, F., Tweedie, F., and Jarrard, L.E. (1990). Ibotenate lesions of hippocampus and/or subiculum: dissociating components of allocentric spatial learning. Eur. J. Neurosci. *2*, 1016-1028.

Moser, E.I., Roudi, Y., Witter, M.P., Kentros, C., Bonhoeffer, T., and Moser, M.B. (2014). Grid cells and cortical representation. Nat. Rev. Neurosci. *15*, 466-481.

Nakazawa, K., McHugh, T.J., Wilson, M.A., and Tonegawa, S. (2004). NMDA receptors, place cells and hippocampal spatial memory. Nat. Rev. Neurosci. *5*, 361-372.

Nakazawa, Y., Pevzner, A., Tanaka, K.Z., and Wiltgen, B.J. (2016). Memory retrieval along the proximodistal axis of CA1. Hippocampus *26*, 1140-1148.

O'Mara, S. (2006). Controlling hippocampal output: the central role of subiculum in hippocampal information processing. Beh. Brain Res. *174*, 304-312.

Okuyama, T., Kitamura, T., Roy, D.S., Itohara, S., and Tonegawa, S. (2016). Ventral CA1 neurons store social memory. Science *353*, 1536-1541.

Ranck, J.B. (1973). Studies on single neurons in dorsal hippocampal formation and septum in unrestrained rats. I. Behavioral correlates and firing repertoires. Exp. Neurol. *41*, 461-531.

Raybuck, J.D., and Lattal, K.M. (2014). Differential effects of dorsal hippocampal inactivation on expression of recent and remote drug and fear memory. Neurosci. Lett. *569*, 1-5.

Roozendaal, B. (2002). Stress and memory: opposing effects of glucocorticoids on memory consolidation and memory retrieval. Neurobiol. Learn. Mem. *78*, 578-595.

Roy, D.S., Arons, A., Mitchell, T.I., Pignatelli, M., Ryan, T.J., and Tonegawa, S. (2016). Memory retrieval by activating engram cells in mouse models of early Alzheimer's disease. Nature *531*, 508-512.

Sharp, P.E., and Green, C. (1994). Spatial correlates of firing patterns of single cells in the subiculum of the freely moving rat. J. Neurosci. *14*, 2339-2356.

Skaggs, W.E., McNaughton, B.L., and Gothard, K.M. (1992). An information-theoretic approach to deciphering the hippocampal code. Neural Inf. Process. Syst. *5*, 1030-1037.

Squire, L.R. (1992). Memory and the hippocampus: a synthesis from findings with rats, monkeys, and humans. Psychol. Rev. *99*, 195-231.

Staff, N.P., Jung, H.Y., Thiagarajan, T., Yao, M., and Spruston, N. (2000). Resting and active properties of pyramidal neurons in subiculum and CA1 of rat hippocampus. J. Neurophysiol. *84*, 2398-2408.

Sun, C., Kitamura, T., Yamamoto, J., Martin, J., Pignatelli, M., Kitch, L.J., Schnitzer, M.J., and Tonegawa, S. (2015). Distinct speed dependence of entorhinal island and ocean cells, including respective grid cells. Proc. Natl. Acad. Sci. U. S. A. *112*, 9466-9471.

Taube, J.S. (1993). Electrophysiological properties of neurons in the rat subiculum in vitro. Exp. Brain Res. *96*, 304-318.

Tonegawa, S., Liu, X., Ramirez, S., and Redondo, R. (2015). Memory engram cells have come of age. Neuron *87*, 918-931.

Treves, A., and Rolls, E.T. (1992). Computational constraints suggest the need for two distinct input systems to the hippocampal CA3 network. Hippocampus *2*, 189-199.

Wickersham, I.R., Lyon, D.C., Barnard, R.J., Mori, T., Finke, S., Conzelmann, K.K., Young, J.A., and Callaway, E.M. (2007). Monosynaptic restriction of transsynaptic tracing from single, genetically targeted neurons. Neuron *53*, 639-647.

Witter, M.P., Ostendorf, R.H., and Groenewegen, H.J. (1990). Heterogeneity in the dorsal subiculum of the rat. Distinct neuronal zones project to different cortical and subcortical targets. Eur. J. Neurosci. *2*, 718-725.

Ziv, Y., Burns, L.D., Cocker, E.D., Hamel, E.O., Ghosh, K.K., Kitch, L.J., El Gamal, A., and Schnitzer, M.J. (2013). Long-term dynamics of CA1 hippocampal place codes. Nat. Neurosci. *16*, 264-266.

AUTHOR CONTRIBUTIONS

D.S.R., T.K., and S.T. contributed to the study design. D.S.R., T.K., T.O., S.K.O., and C.S. contributed to the data collection and interpretation. D.S.R. and T.K. conducted the surgeries, behavior experiments, and histological analyses. Y.O. and A.Y. generated the dorsal subiculum mouse line. D.S.R. and S.T. wrote the paper. All authors discussed and commented on the manuscript.

ACKNOWLEDGEMENTS

We thank S. LeBlanc, S. Huang, A. Arons, J. Martin, L. Smith, F. Bushard, A. Hamalian, W. Yu, and C. Lovett for help with experiments; N. Mise and Y. Koga for help with generating the dorsal subiculum mouse line; M. Morrissey for comments; L. Brenner for proofreading; and all members of the Tonegawa laboratory for their support. We thank Ian Wickersham for providing rabies virus, Ki Goosens for sharing a microplate reader, and the Harvard Center for Biological Imaging for access to a light sheet fluorescence microscope. This work was supported by the RIKEN Brain Science Institute, the Howard Hughes Medical Institute, and the JPB Foundation (to S.T.).

Main Figures

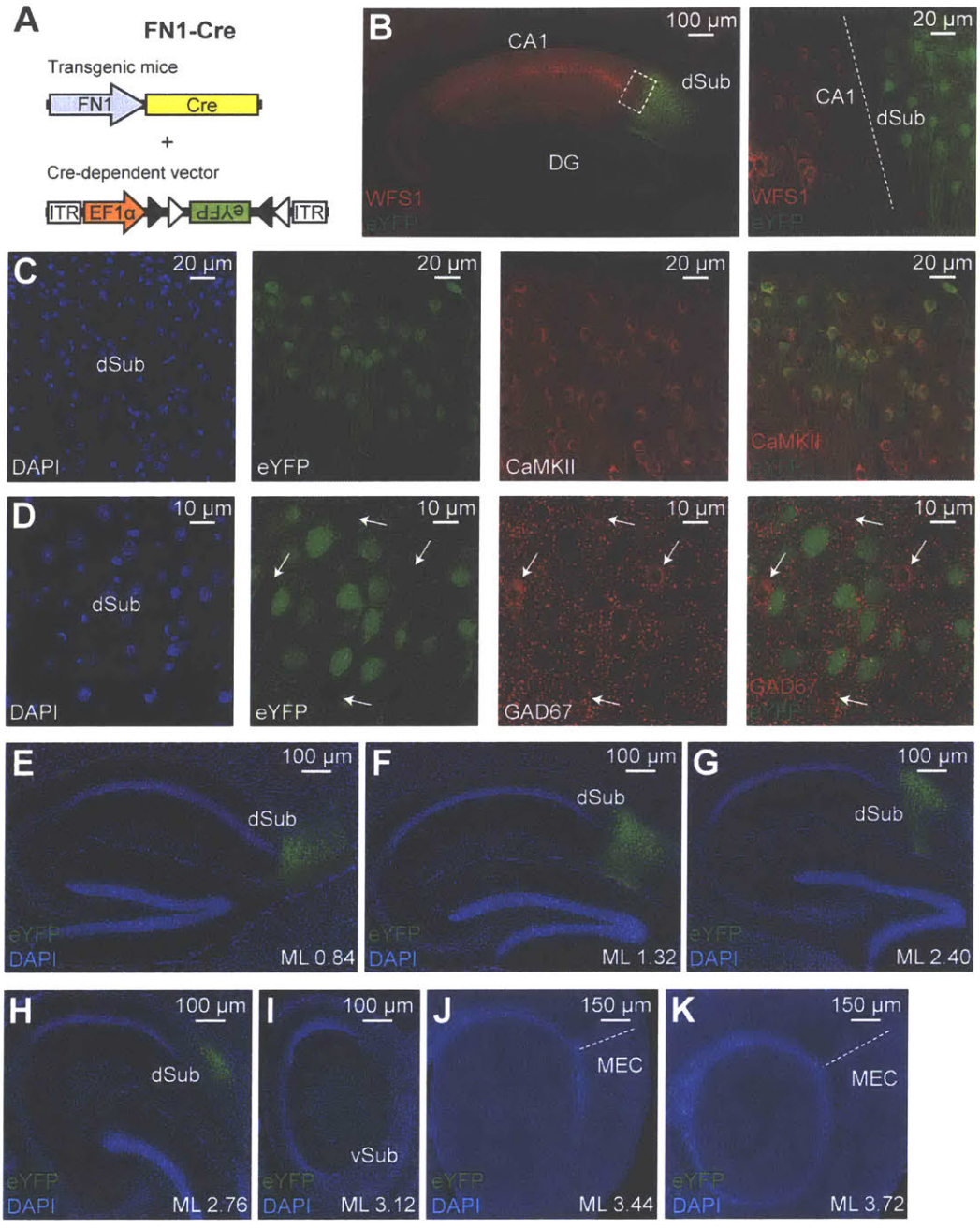

Figure 1. Genetic targeting of dSub neurons using FN1-Cre mice

(A) FN1-Cre mice were injected with a Cre-dependent virus expressing eYFP into dSub.

(B) Cre^+ dSub neurons (eYFP, green) do not overlap with dCA1 excitatory neurons (labeled with WFS1, red). Sagittal image (left), higher magnification image of boxed region (right). Dashed white line denotes CA1/dSub border (right).

(C, D) Cre^+ dSub neurons (eYFP, green), in sagittal sections, express the excitatory neuronal marker CaMKII (red; C). Over 85% of all $CaMKII^+$ neurons in the dSub region also expressed eYFP (n = 3 mice). Images are taken with a 20x objective. Cre^+ dSub neurons do not express the inhibitory marker GAD67 (red; D). White arrows indicate $GAD67^+$ cell bodies (D). Images are taken with a 40x objective. See also Figure S1A. DAPI staining in blue.

(E-K) Medial to lateral (ML, in millimeters relative to Bregma) sagittal sections show that eYFP signal is restricted to dSub neurons. DAPI staining (blue). No eYFP signal was observed in ventral subiculum (vSub) or medial entorhinal cortex (MEC). Dashed white line denotes perirhinal cortex/MEC border (J, K).

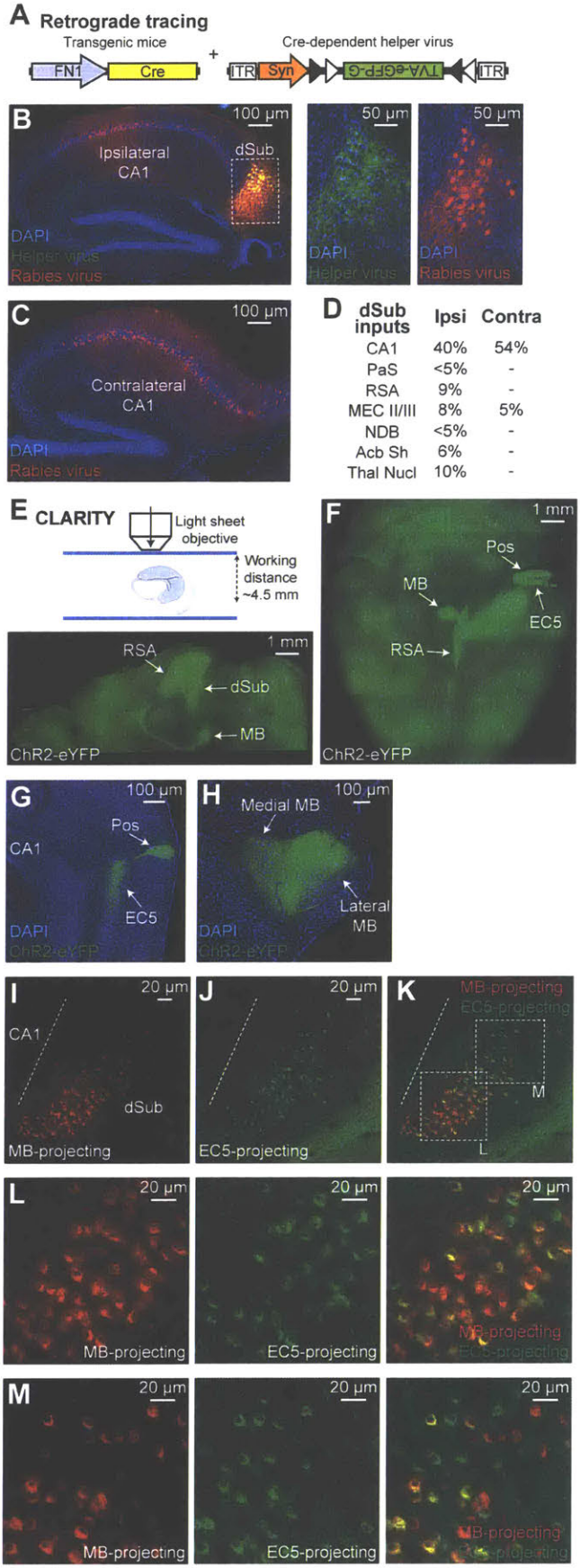
A Retrograde tracing
Transgenic mice
Cre-dependent helper virus
FN1
Cre
ITR
Syn
TVA-eGFP-G
ITR
B
100 µm
Ipsilateral CA1
dSub
DAPI
Helper virus
Rabies virus
50 µm
50 µm
C
100 µm
Contralateral CA1
DAPI
Rabies virus
D
dSub inputs | Ipsi | Contra
CA1 | 40% | 54%
PaS | <5% | -
RSA | 9% | -
MEC II/III | 8% | 5%
NDB | <5% | -
Acb Sh | 6% | -
Thal Nucl | 10% | -
E CLARITY
Light sheet objective
Working distance ~4.5 mm
RSA
1 mm
dSub
MB
ChR2-eYFP
F
1 mm
Pos
MB
EC5
RSA
ChR2-eYFP
G
100 µm
Pos
CA1
EC5
DAPI
ChR2-eYFP
H
Medial MB
100 µm
Lateral MB
DAPI
ChR2-eYFP
I
20 µm
CA1
dSub
MB-projecting
J
20 µm
EC5-projecting
K
MB-projecting
EC5-projecting
M
L
L
20 µm
MB-projecting
20 µm
EC5-projecting
20 µm
MB-projecting
EC5-projecting
M
20 µm
MB-projecting
20 µm
EC5-projecting
20 µm
MB-projecting
EC5-projecting

Figure 2. Input-output organization of dSub excitatory neurons

(A) Monosynaptic retrograde tracing of dSub inputs used a Cre-dependent helper virus (tagged with eGFP) combined with a rabies virus (RV, mCherry) injected into dSub of FN1-Cre mice. Avian leukosis and sarcoma virus subgroup A receptor (TVA) and rabies glycoprotein (G).

(B, C) Representative ipsilateral sections confirmed efficient overlap of helper and RV-infected dSub neurons. Sagittal image (left; B), higher magnification images of boxed region (right; B). Quantification revealed that 78% of dSub cells, relative to $DAPI^+$ neurons, were RV-positive (n = 4 mice), which is the starting population for retrograde tracing. Both ipsilateral and contralateral sagittal sections revealed that dorsal CA1 provides the major input to dSub Cre^+ neurons (C).

(D) Inputs to dSub Cre^+ neurons were quantified based on percentage of neurons in the target brain region relative to $DAPI^+$ neurons (n = 4 mice). Ipsilateral (Ipsi) and contralateral (Contra) counts. Parasubiculum (PaS), retrosplenial agranular cortex (RSA), MEC layers II/III (MEC II/III), nucleus of the diagonal band (NDB), nucleus accumbens shell (Acb Sh), and thalamic nuclei (Thal Nucl).

(E) FN1-Cre mice expressing ChR2-eYFP (Cre-dependent virus) in dSub neurons were used for CLARITY followed by light sheet microscopy (top). 2.5 mm optical section in sagittal view shows projections to RSA and mammillary bodies (MB, bottom).

(F) Whole-brain, stitched z-stack (horizontal view) shows all major projections from dSub Cre^+ neurons including RSA, MB, EC5, and postrhinal cortex (Pos).

(G, H) Standard sagittal brain sections of FN1-Cre mice expressing ChR2-eYFP (Cre-dependent virus) in dSub neurons showing dSub projections to EC5 and Pos (G), as well as medial and lateral MB (H).

(I-M) Representative standard sagittal brain sections showing dSub neuronal populations projecting to MB (red, CTB555; I) or EC5 (green, CTB488; J). The respective CTB was injected into MB or EC5. Overlap image (K). Quantification, including weakly labeled CTB^+ neurons, revealed that 81% of dSub cells were double positive (n = 4 mice). Scale bar in panels I-J applies

to panel K. Dashed white line denotes CA1/dSub border. Higher magnification images of boxed regions indicated in Figure 2K (L-M).

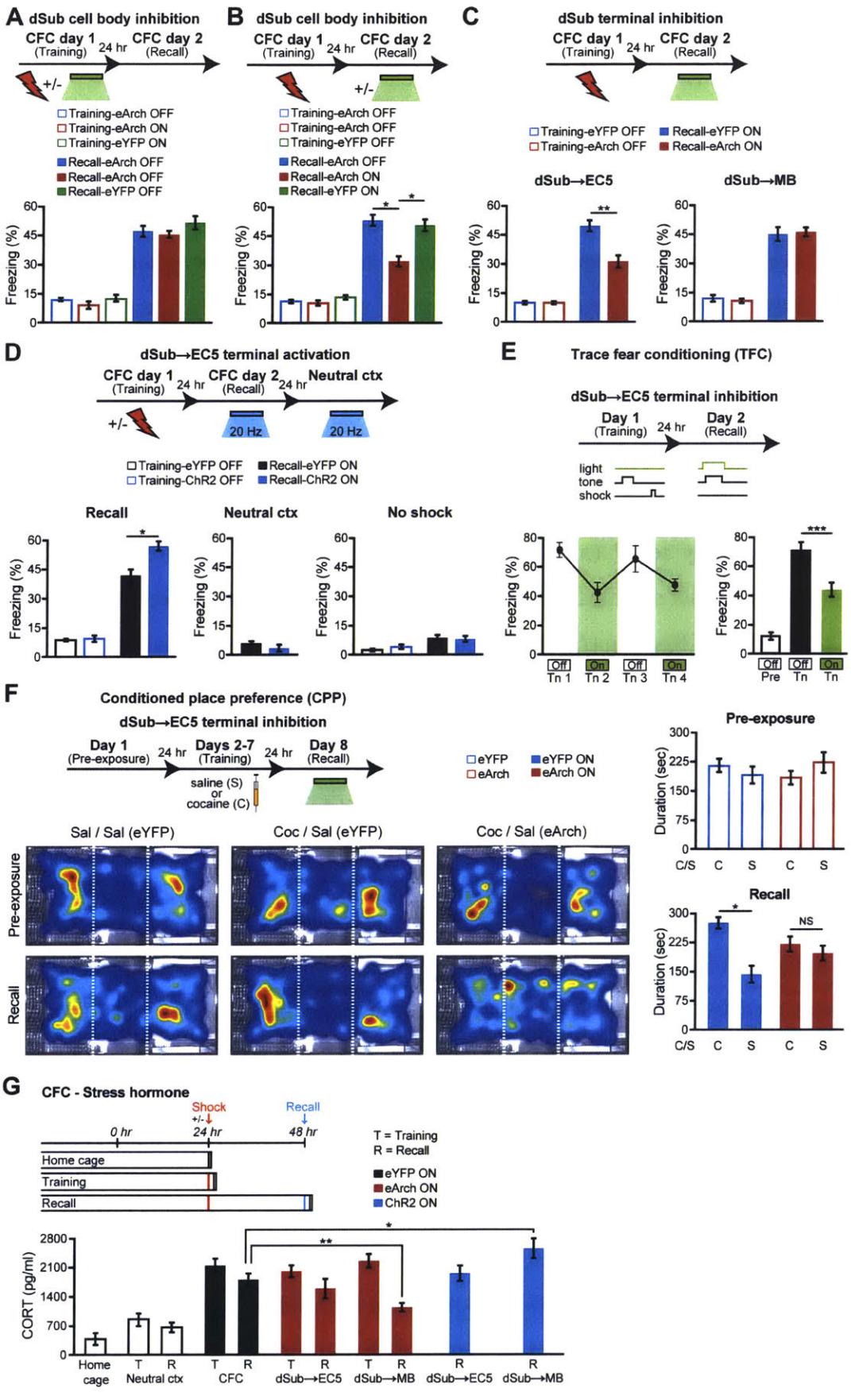
A dSub cell body inhibition
CFC day 1 (Training) 24 hr CFC day 2 (Recall)
+/-
Training-eArch OFF
Training-eArch ON
Training-eYFP ON
Recall-eArch OFF
Recall-eArch OFF
Recall-eYFP OFF
Freezing (%)
B dSub cell body inhibition
CFC day 1 (Training) 24 hr CFC day 2 (Recall)
+/-
Training-eArch OFF
Training-eArch OFF
Training-eYFP OFF
Recall-eArch OFF
Recall-eArch ON
Recall-eYFP ON
Freezing (%)
C dSub terminal inhibition
CFC day 1 (Training) 24 hr CFC day 2 (Recall)
Training-eYFP OFF
Training-eArch OFF
Recall-eYFP ON
Recall-eArch ON
dSub→EC5
dSub→MB
Freezing (%)
D dSub→EC5 terminal activation
CFC day 1 (Training) 24 hr CFC day 2 (Recall) 24 hr Neutral ctx
+/-
20 Hz
20 Hz
Training-eYFP OFF
Training-ChR2 OFF
Recall-eYFP ON
Recall-ChR2 ON
Recall
Neutral ctx
No shock
Freezing (%)
E Trace fear conditioning (TFC)
dSub→EC5 terminal inhibition
Day 1 (Training) 24 hr Day 2 (Recall)
light
tone
shock
Freezing (%)
Off On Off On
Tn 1 Tn 2 Tn 3 Tn 4
Off Off On
Pre Tn Tn
F Conditioned place preference (CPP)
dSub→EC5 terminal inhibition
Day 1 (Pre-exposure) 24 hr Days 2-7 (Training) 24 hr Day 8 (Recall)
saline (S) or cocaine (C)
eYFP
eArch
eYFP ON
eArch ON
Sal / Sal (eYFP)
Coc / Sal (eYFP)
Coc / Sal (eArch)
Pre-exposure
Recall
Pre-exposure
Duration (sec)
C/S C S C S
Recall
NS
Duration (sec)
C/S C S C S
G CFC - Stress hormone
Shock +/-
Recall
0 hr
24 hr
48 hr
Home cage
Training
Recall
T = Training
R = Recall
eYFP ON
eArch ON
ChR2 ON
CORT (pg/ml)
Home cage
T R Neutral ctx
T R CFC
T R dSub→EC5
T R dSub→MB
R dSub→EC5
R dSub→MB

Figure 3. Differential roles of dSub projections in hippocampal memory retrieval and retrieval-induced stress hormone responses

(A, B) FN1-Cre mice were injected with a Cre-dependent virus expressing eArch3.0-eYFP into dSub. Optogenetic inhibition of dSub neurons during contextual fear conditioning (CFC) training had no effect on long-term memory (n = 12 mice per group; A). Inhibition of dSub neurons during CFC recall impaired behavioral performance (n = 12 mice per group; B). A two-way ANOVA followed by Bonferroni post-hoc tests revealed a behavioral epoch-by-eArch interaction and significant eArch-mediated attenuation of freezing (A-B: $F_{1,44} = 5.70$, $P < 0.05$, recall). For dSub optogenetic manipulation experiments, injections were targeted to dSub cell bodies and the extent of virus expression is shown in Figures 1E-1K.

(C) Terminal inhibition of dSub projections to EC5 (bottom left), but not MB (bottom right), disrupted CFC memory recall (n = 11 mice per group). A two-way ANOVA followed by Bonferroni post-hoc tests revealed a dSub terminal-by-eArch interaction and significant eArch-mediated attenuation of freezing ($F_{1,40} = 7.63$, $P < 0.01$, dSub→EC5 terminals).

(D) FN1-Cre mice were injected with a Cre-dependent virus expressing ChR2-eYFP into dSub. Optogenetic activation of dSub→EC5 terminals during CFC memory recall increased freezing levels (left), which was not observed in a neutral context (middle) or using no shock mice (right, n = 10 mice per group).

(E) Inhibition of dSub→EC5 terminals during trace fear conditioning (TFC) recall decreased tone (Tn)-induced freezing levels (n = 12 mice). A two-way ANOVA followed by Bonferroni post-hoc tests revealed a behavioral epoch-by-eArch interaction and significant eArch-mediated attenuation of freezing (E and Figure S4A: $F_{1,44} = 7.11$, $P < 0.05$, recall). Pre-tone baseline freezing (Pre). Recall-induced freezing levels during individual tone presentations (left panel), averaged freezing levels during the two light-off tones and the two light-on tones (right panel).

(F) Inhibition of dSub→EC5 terminals during cocaine-induced conditioned place preference (CPP) recall impaired behavioral performance (n = 14 mice per group). Behavioral schedule (left, top part). Average heat maps showing exploration time during pre-exposure and recall trials (left, bottom part). Dashed white lines demarcate individual zones in the CPP apparatus. Pre-

exposure preference duration (right, top graph) and recall preference duration (right, bottom graph). Saline (S or Sal), cocaine (C or Coc). A two-way ANOVA followed by Bonferroni post-hoc tests revealed a drug group-by-eArch interaction and significant eArch-mediated attenuation of preference duration ($F_{1,52} = 5.16$, $P < 0.05$, cocaine). For CPP training inhibition, see Figure S4D. NS, not significant.

(G) Stress hormone: Terminal inhibition of dSub projections to MB, but not EC5, following CFC memory recall tests decreased stress responses as measured by corticosterone (CORT) levels. Optogenetic activation of dSub→MB terminals following CFC memory recall increased CORT levels (n = 10 mice per group). Context (ctx). CORT levels in CPP paradigm are shown in Figure S4E.

Unless specified, statistical comparisons are performed using unpaired *t* tests; *P < 0.05, **P < 0.01, ***P < 0.001. Data are presented as mean ± SEM.

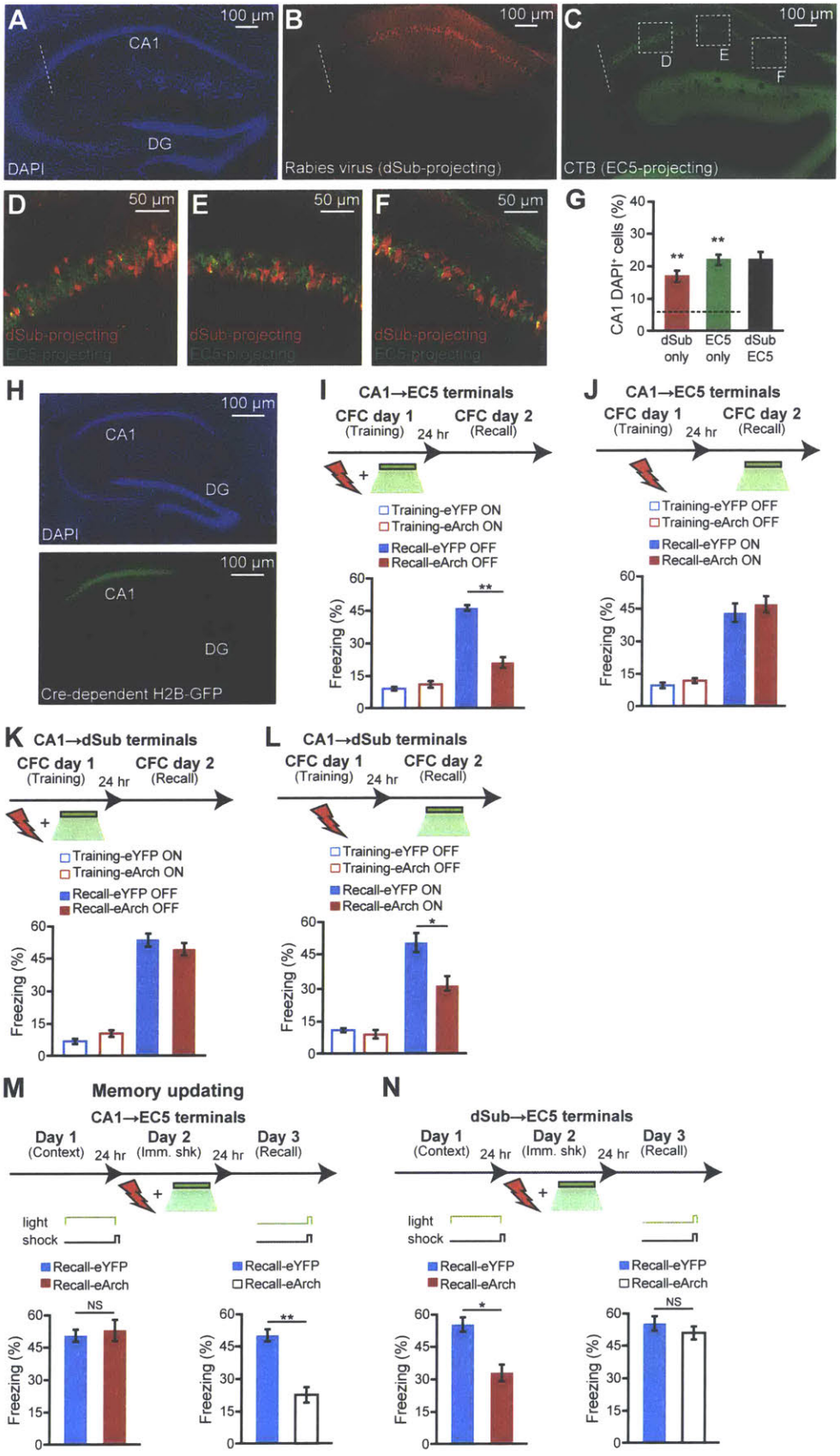
A
100 μm
CA1
DG
DAPI
B
100 μm
Rabies virus (dSub-projecting)
C
100 μm
D
E
F
CTB (EC5-projecting)
D
50 μm
dSub-projecting
EC5-projecting
E
50 μm
dSub-projecting
EC5-projecting
F
50 μm
dSub-projecting
EC5-projecting
G
CA1 DAPI+ cells (%)
40
30
20
10
0
**
**
dSub only
EC5 only
dSub EC5
H
100 μm
CA1
DG
DAPI
100 μm
CA1
DG
Cre-dependent H2B-GFP
I
CA1→EC5 terminals
CFC day 1 (Training)
24 hr
CFC day 2 (Recall)
+
Training-eYFP ON
Training-eArch ON
Recall-eYFP OFF
Recall-eArch OFF
Freezing (%)
60
45
30
15
0
**
J
CA1→EC5 terminals
CFC day 1 (Training)
24 hr
CFC day 2 (Recall)
Training-eYFP OFF
Training-eArch OFF
Recall-eYFP ON
Recall-eArch ON
Freezing (%)
60
45
30
15
0
K
CA1→dSub terminals
CFC day 1 (Training)
24 hr
CFC day 2 (Recall)
+
Training-eYFP ON
Training-eArch ON
Recall-eYFP OFF
Recall-eArch OFF
Freezing (%)
60
45
30
15
0
L
CA1→dSub terminals
CFC day 1 (Training)
24 hr
CFC day 2 (Recall)
Training-eYFP OFF
Training-eArch OFF
Recall-eYFP ON
Recall-eArch ON
*
Freezing (%)
60
45
30
15
0
M
Memory updating
CA1→EC5 terminals
Day 1 (Context)
24 hr
Day 2 (Imm. shk)
24 hr
Day 3 (Recall)
+
light
shock
Recall-eYFP
Recall-eArch
NS
**
Freezing (%)
60
45
30
15
0
N
dSub→EC5 terminals
Day 1 (Context)
24 hr
Day 2 (Imm. shk)
24 hr
Day 3 (Recall)
+
light
shock
Recall-eYFP
Recall-eArch
*
NS
Freezing (%)
60
45
30
15
0

Figure 4. Projection from CA1 to EC5 is crucial for encoding, but not for retrieval, of hippocampal memories

(A-C) Retrograde monosynaptic identification of dCA1 neurons projecting to dSub (in FN1-Cre mice) using a Cre-dependent helper virus combined with a rabies virus (RV). The extent of RV-positive dSub cells, which is the starting population for retrograde tracing, is shown in Figure 2B. Simultaneous retrograde monosynaptic identification of dCA1 neurons projecting to EC5 using CTB. DAPI (blue; A), RV-mCherry (red; B), CTB488 (green; C). Representative sagittal sections, dashed white line denotes CA1/CA2 border.

(D-F) Higher magnification images of boxed regions indicated in Figure 4C.

(G) Percentage of dCA1 neurons labeled with mCherry (dSub only), CTB488 (EC5 only), or mCherry and CTB double positive (dSub+EC5, n = 4 mice). Dashed line indicates chance level (6%), calculated from a control experiment (Figures S5A-S5H, and see Methods). One-sample *t* tests against chance level were performed.

(H) Representative sagittal sections of hippocampus from TRPC4-Cre mice showing dCA1 neurons labeled with a Cre-dependent histone H2B-GFP virus (green, bottom) and stained with DAPI (blue, top).

(I, J) TRPC4-Cre mice were injected with a Cre-dependent virus expressing eArch3.0-eYFP into dCA1. Terminal inhibition of CA1→EC5 during CFC training impaired long-term memory (n = 10 mice per group; I). Inhibition of CA1→EC5 terminals during CFC recall had no effect on behavioral performance (n = 10 mice per group; J). A two-way ANOVA followed by Bonferroni post-hoc tests revealed a behavioral epoch-by-eArch interaction and significant eArch-mediated attenuation of freezing (I-J: $F_{1,36} = 9.19$, $P < 0.01$, training).

(K, L) Terminal inhibition of CA1→dSub during CFC training had no effect on long-term memory (n = 13 mice per group; K). Inhibition of CA1→dSub terminals during CFC recall disrupted behavioral performance (n = 13 mice per group; L). A two-way ANOVA followed by Bonferroni post-hoc tests revealed a behavioral epoch-by-eArch interaction and significant eArch-mediated attenuation of freezing (K-L: $F_{1,48} = 5.16$, $P < 0.05$, recall).

(M, N) Memory updating. Experimental schedule (top) for pre-exposure mediated contextual fear conditioning (PECFC) with optogenetic terminal inhibition of CA1→EC5 (using TRPC4-Cre mice; M) and dSub→EC5 (using FN1-Cre mice; N) during the pre-footshock period (left panels) or footshock period alone (right panels) on Day 2. Freezing levels during recall tests (Day 3) to the conditioned context (bottom). eYFP and eArch conditions (n = 12 mice per group). NS, not significant. Immediate shock (Imm. shk). A two-way ANOVA followed by Bonferroni post-hoc tests revealed a behavioral epoch-by-eArch interaction and significant eArch-mediated attenuation of freezing (M: $F_{1,44} = 9.81$, $P < 0.01$, recall in right panel; N: $F_{1,44} = 4.75$, $P < 0.05$, recall in left panel).

Unless specified, statistical comparisons are performed using unpaired *t* tests; *P < 0.05, **P < 0.01. Data are presented as mean ± SEM.

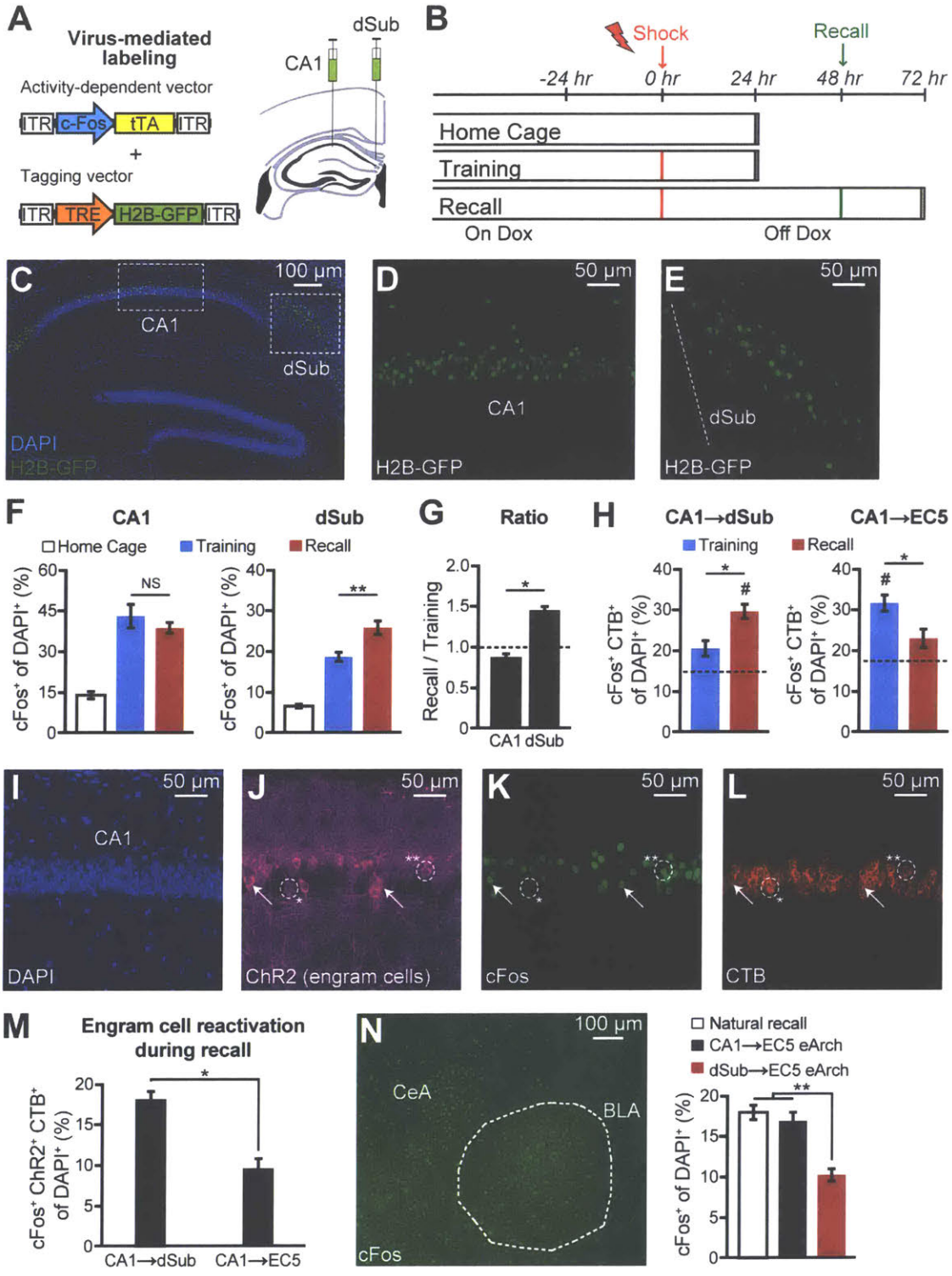
A
Virus-mediated labeling
Activity-dependent vector
ITR c-Fos tTA ITR
+
Tagging vector
ITR TRE H2B-GFP ITR
CA1
dSub
B
Shock
Recall
-24 hr
0 hr
24 hr
48 hr
72 hr
Home Cage
Training
Recall
On Dox
Off Dox
C
100 μm
CA1
dSub
DAPI
H2B-GFP
D
50 μm
CA1
H2B-GFP
E
50 μm
dSub
H2B-GFP
F
CA1
dSub
Home Cage
Training
Recall
cFos+ of DAPI+ (%)
NS
**
G
Ratio
Recall / Training
*
CA1 dSub
H
CA1→dSub
CA1→EC5
Training
Recall
cFos+ CTB+ of DAPI+ (%)
*
#
I
50 μm
CA1
DAPI
J
50 μm
ChR2 (engram cells)
K
50 μm
cFos
L
50 μm
CTB
M
Engram cell reactivation during recall
cFos+ ChR2+ CTB+ of DAPI+ (%)
*
CA1→dSub
CA1→EC5
N
100 μm
CeA
BLA
cFos
Natural recall
CA1→EC5 eArch
dSub→EC5 eArch
cFos+ of DAPI+ (%)
**

Figure 5. Distinct cFos activation patterns in CA1 and dSub neurons

(A) Virus-mediated $cFos^+$ neuronal labeling strategy using a cocktail of c-Fos-tTA and TRE-H2B-GFP (left). Wild-type mice raised on doxycycline (DOX) food were injected with the two viruses bilaterally into CA1 and dSub (right).

(B) Behavioral schedule and H2B-GFP labeling (see Methods). Beige shading indicates animals are maintained on DOX food.

(C-E) Representative sagittal section of hippocampus showing H2B-GFP-labeled cell bodies (green) in CA1 and dSub counterstained with DAPI (blue), following CFC training (C). Boxed regions in C are shown in higher magnification for CA1 (D) and dSub (E). Dashed white line denotes CA1/dSub border (E).

(F) $H2B\text{-}GFP^+$ ($cFos^+$) cell counts in CA1 (left) and dSub (right) from home cage, CFC training (encoding), and CFC recall groups (n = 6 mice per group). NS, not significant.

(G) Ratio of recall to training $H2B\text{-}GFP^+$ neurons in CA1 and dSub (cell counts from Figure 5F). A ratio of 1.0 indicates comparable $H2B\text{-}GFP^+$ counts during training and recall epochs. Statistical comparison used a Fisher's exact test.

(H) Overlap between CFC-induced cFos and CA1 neurons projecting (labeled by CTB555) to dSub (left) or EC5 (right). Representative overlap images are shown in Figures S5K-S5N. Dashed lines indicate chance levels (n = 5 mice per group, see Methods). One-sample *t* tests against chance level were performed (#$P < 0.05$).

(I-M) Wild-type mice raised on DOX were used for these experiments. Representative coronal section of CA1 showing DAPI staining (I), CFC training-induced cFos-positive engram cells labeled with a cocktail of c-Fos-tTA and TRE-ChR2-eYFP (J), cFos antibody staining following CFC recall tests performed one day after training and engram labeling (K), and CA1 neurons projecting to either dSub or EC5 visualized by retrograde CTB555 labeling (L). The circled region with a single asterisk (*) shows an engram cell that is $cFos^-$ but $CTB555^+$ and the region with two asterisks (**) shows an engram cell that is $cFos^+$ and $CTB555^+$. White arrows show additional examples of CA1 engram cells that are both $cFos^+$ and $CTB555^+$. Overlap of recall-

induced cFos, CA1 engram cells labeled during training, and circuit specific CA1 projection neurons (n = 6 mice per group; M).

(N) Representative coronal section of basolateral amygdala (BLA) showing cFos activation following memory recall (left). $cFos^+$ cell counts (n = 6 mice per group) in BLA following natural recall, and recall with eArch inhibition of the CA1→EC5 or dSub→EC5 circuits (right). TRPC4-Cre mice were used for CA1 circuit manipulations and FN1-Cre mice were used for dSub circuit manipulations.

Unless specified, statistical comparisons are performed using unpaired *t* tests; *P < 0.05, **P < 0.01. Data are presented as mean ± SEM.

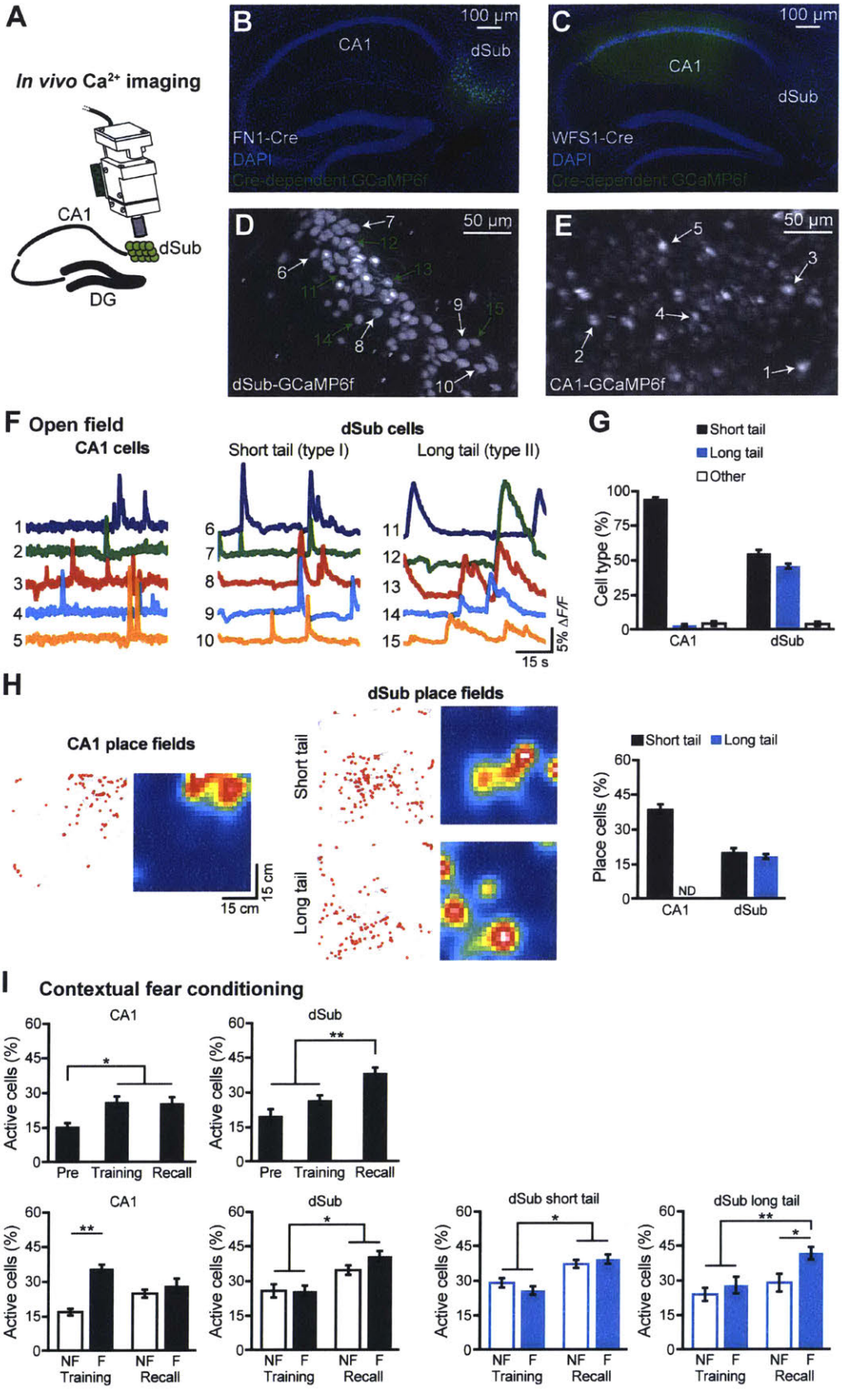
A
In vivo Ca2+ imaging
CA1
dSub
DG
B
100 µm
CA1
dSub
FN1-Cre
DAPI
Cre-dependent GCaMP6f
C
100 µm
CA1
dSub
WFS1-Cre
DAPI
Cre-dependent GCaMP6f
D
50 µm
dSub-GCaMP6f
E
50 µm
CA1-GCaMP6f
F Open field
CA1 cells
dSub cells
Short tail (type I)
Long tail (type II)
5% ΔF/F
15 s
G
Short tail
Long tail
Other
Cell type (%)
CA1
dSub
H
CA1 place fields
dSub place fields
Short tail
Long tail
15 cm
15 cm
Place cells (%)
ND
I
Contextual fear conditioning
CA1
dSub
Active cells (%)
Pre
Training
Recall
dSub short tail
dSub long tail
NF
F
Training
Recall

Figure 6. dSub neurons exhibit enhanced neuronal activity during hippocampal memory retrieval

(A-C) Implantation of a microendoscope right above dSub of FN1-Cre mice (A) or dCA1 of WFS1-Cre mice. For dCA1, the medial region along the proximodistal axis was targeted (see also Figures S6A-S6B). Calcium (Ca^{2+}). Representative sagittal sections of hippocampus from FN1-Cre (B) and WFS1-Cre (C) mice showing GCaMP6f-labeled cells (green) and DAPI staining (blue).

(D, E) Representative maximum intensity projection images, as seen through the microendoscope camera, of dSub neurons expressing GCaMP6f (D) or CA1 neurons expressing GCaMP6f (E) acquired during a 30 min recording session in an open field arena (see Methods).

(F, G) Representative Ca^{2+} traces of CA1 cells (left, labeled in E) and two types of dSub cells (middle and right, labeled in D) from the open field paradigm (F), and cell type quantification (n = 759 CA1 cells, n = 428 dSub short tail cells, n = 371 dSub long tail cells, n = 4 mice per group; G). See also Figure S6C.

(H) Representative place field Ca^{2+} events (red dots, left panels) and heat maps (right panels) for CA1 and dSub cells (cell counts in Figure 6G), along with quantification. See also Figure S6D and Methods. ND, not detected.

(I) Ca^{2+} activity during CFC. Pre-footshock levels (Pre). Percentage of active cells (see Methods) during Pre, training, and recall tests (top), including non-freezing (NF) and freezing (F) epochs (bottom), in CA1 and dSub (n = 550 CA1 cells, n = 429 dSub short tail cells, n = 203 dSub long tail cells, n = 3 CA1 mice, n = 4 dSub mice). Within session NF and F comparisons used paired *t* tests. Comparisons across sessions used a two-way ANOVA with repeated measures followed by Bonferroni post-hoc tests. See also Figures S6E-S6G.

For statistical comparisons, *P < 0.05, **P < 0.01. Data are presented as mean ± SEM.

REPORT

MEMORY RESEARCH

Engrams and circuits crucial for systems consolidation of a memory

Takashi Kitamura,[1]* Sachie K. Ogawa,[1]* Dheeraj S. Roy,[1]* Teruhiro Okuyama,[1] Mark D. Morrissey,[1] Lillian M. Smith,[1] Roger L. Redondo,[1,2]† Susumu Tonegawa[1,2]‡

Episodic memories initially require rapid synaptic plasticity within the hippocampus for their formation and are gradually consolidated in neocortical networks for permanent storage. However, the engrams and circuits that support neocortical memory consolidation have thus far been unknown. We found that neocortical prefrontal memory engram cells, which are critical for remote contextual fear memory, were rapidly generated during initial learning through inputs from both the hippocampal–entorhinal cortex network and the basolateral amygdala. After their generation, the prefrontal engram cells, with support from hippocampal memory engram cells, became functionally mature with time. Whereas hippocampal engram cells gradually became silent with time, engram cells in the basolateral amygdala, which were necessary for fear memory, were maintained. Our data provide new insights into the functional reorganization of engrams and circuits underlying systems consolidation of memory.

Memories are thought to be initially stored within the hippocampal–entorhinal cortex (HPC-EC) network (recent memory) and, over time, slowly consolidated within the neocortex for permanent storage (remote memory) (*1–7*). Systems memory consolidation models suggest that the interaction between the HPC-EC network and the neocortex during and after an experience is crucial (*8–12*). Experimentally, prolonged inhibition of hippocampal or neocortical networks during the consolidation period produces deficits in remote memory formation (*13–15*). However, little is known regarding specific neural circuit mechanisms underlying the formation and maturation of neocortical memories through interactions with the HPC-EC network. Using activity-dependent cell-labeling technology (*16–18*), combined with viral vector–based transgenic, anatomical (*19*, *20*), and optogenetic strategies (*19*, *21*) for circuit-specific manipulations and in vivo calcium imaging (*22*), we investigated the nature and dynamics of neocortical and subcortical memory engram cells [a population of neurons that are activated by learning, have enduring cellular changes, and are reactivated by a part of the original stimuli for recall (*18*)] and their circuits for systems consolidation of memory.

We first traced entorhinal projections to frontal cortical structures [the medial prefrontal cortex (PFC), caudal anterior cingulate cortex (cACC), and retrosplenial cortex (RSC)] involved in contextual fear memory, as well as to the basolateral amygdala (BLA), with injections of the retrograde tracer cholera toxin subunit B–Alexa*555* (hereafter, CTB injections) into these regions (fig. S1). CTB injections resulted in labeling in the medial entorhinal cortex (MEC), specifically in cells in layer Va (Fig. 1, A to D and H, and fig. S2, A to D), indicating that MEC-Va cells have extensive projections to the neocortex and BLA (*23*). We then sought to inhibit these specific projections by bilaterally injecting adeno-associated virus 8 (AAV_8)–calcium/calmodulin-dependent protein kinase II (CaMKII):eArchT-enhanced yellow fluorescent protein (eYFP) in the deep layers of the MEC in wild-type (WT) mice with bilaterally implanted optic fibers above the PFC, cACC, or RSC (Fig. 1, E and J, and fig. S2G). Expression of eArchT-eYFP was abundant in MEC-Va terminals located in each of these regions (Fig. 1, B and I, and fig. S2D). These mice were then subjected to contextual fear conditioning (CFC) while we delivered green light bilaterally to the different cortical areas that have MEC-Va projections during either the conditioning period (day 1) (fig. S2E) or the recall test period (days 2, 8, 15, and 22) (fig. S2F). Axon terminal inhibition with optogenetics of MEC-Va cells within the PFC during day 1 of CFC disrupted memory at days 15 and 22, but not at days 2 or 8 (Fig. 1F). Terminal inhibition during memory recall tests did not affect memory retrieval (Fig. 1G). Last, terminal inhibition in the cACC or RSC during CFC or recall had no effect on memory throughout these periods (Fig. 1, J to L, and fig. S2, G to I).

The above results suggest that MEC-Va input into the PFC during CFC is crucial for the eventual formation of remote memory. This hypothesis was supported by several findings. First, CFC increased the number of c-Fos$^+$ cells in the PFC compared with that in the PFC of home-cage mice (Fig. 1, M to O), whereas context-only exposure did not increase c-Fos activity in the PFC (Fig. 1O). Second, optogenetic terminal inhibition of MEC-Va projections within the PFC during CFC inhibited the observed increase of c-Fos$^+$ cells in the PFC (Fig. 1O). Last, we identified CFC engram cells in the PFC. We targeted injections of AAV_9-c-fos:tetracycline-controlled transactivator (tTA) and AAV_9-tetracycline response element (TRE):channelrhodopsin-2 (ChR2)–mCherry (Fig. 1, P and Q) and optic fibers to the PFC of WT mice and labeled the PFC cells activated by CFC with ChR2 while the mice were off doxycycline (Fig. 1R). Blue light stimulation at 4 Hz, but not at the conventional 20 Hz, of ChR2-mCherry–expressing cells in the PFC induced increased freezing behavior on days 2 and 12 in an unconditioned context (Fig. 1S and fig. S3), compared with freezing under the blue light–off condition. This blue light–induced freezing was prevented when MEC-Va fibers in the PFC were inhibited during CFC on day 1 (Fig. 1, T and U, and fig. S4). Using transsynaptic retrograde tracing combined with the activity-dependent cell labeling, we confirmed that the PFC engram cells generated by CFC received monosynaptic input from MEC-Va cells (Fig. 1, V to X, and fig. S5).

To examine whether PFC engram cells are also reactivated by the conditioned context (rather than by blue light) at recent and remote time points, we targeted injections of AAV_9-TRE:human histone H2B–green fluorescent protein (H2B-GFP) to the PFC of c-fos:tTA transgenic mice (Fig. 2A). The mice underwent CFC on day 1 and then were reexposed to the conditioned (context A) or an unconditioned (context B) context on days 2 or 13 (Fig. 2B). Cells activated by CFC were labeled with H2B-GFP, and the cells activated by the context test were labeled with a c-Fos antibody; we calculated the proportion of double-labeled cells (Fig. 2, A to B, and fig. S6B). Compared with H2B-GFP$^-$ cells, H2B-GFP$^+$ cells (PFC engram cells) were preferentially reactivated in context A on day 13, but not on day 2 (Fig. 2C). There was no difference in c-Fos expression between H2B-GFP$^+$ and H2B-GFP$^-$ cells when mice were tested in context B (Fig. 2C). We also found that the spine density of the PFC engram cells on day 12 was significantly higher than on day 2 (Fig. 2, D and E, and fig. S7), in line with previous findings of a positive correlation between the dendritic spine density of memory engram cells and memory expression triggered by natural recall cues (*24–26*).

To test whether PFC engram cells are necessary for memory recall by natural cues, we bilaterally targeted injections of AAV_9-c-fos:tTA and AAV_9-TRE:ArchT-eGFP (Fig. 2, D and F) and optic fibers to the PFC of WT mice and labeled the PFC engram cells that were activated by CFC with ArchT while the mice were off doxycycline (Fig. 2F). Cell body inhibition of the

[1]RIKEN-MIT Center for Neural Circuit Genetics at the Picower Institute for Learning and Memory, Departments of Biology and Brain and Cognitive Sciences, Massachusetts Institute of Technology, Cambridge, MA 02139, USA. [2]Howard Hughes Medical Institute, Massachusetts Institute of Technology, Cambridge, MA 02139, USA.
*These authors contributed equally to this work. †Present address: Roche Pharmaceutical Research and Early Development, Roche Innovation Center, F. Hoffmann-La Roche, Basel, Switzerland.
‡Corresponding author. Email: tonegawa@mit.edu

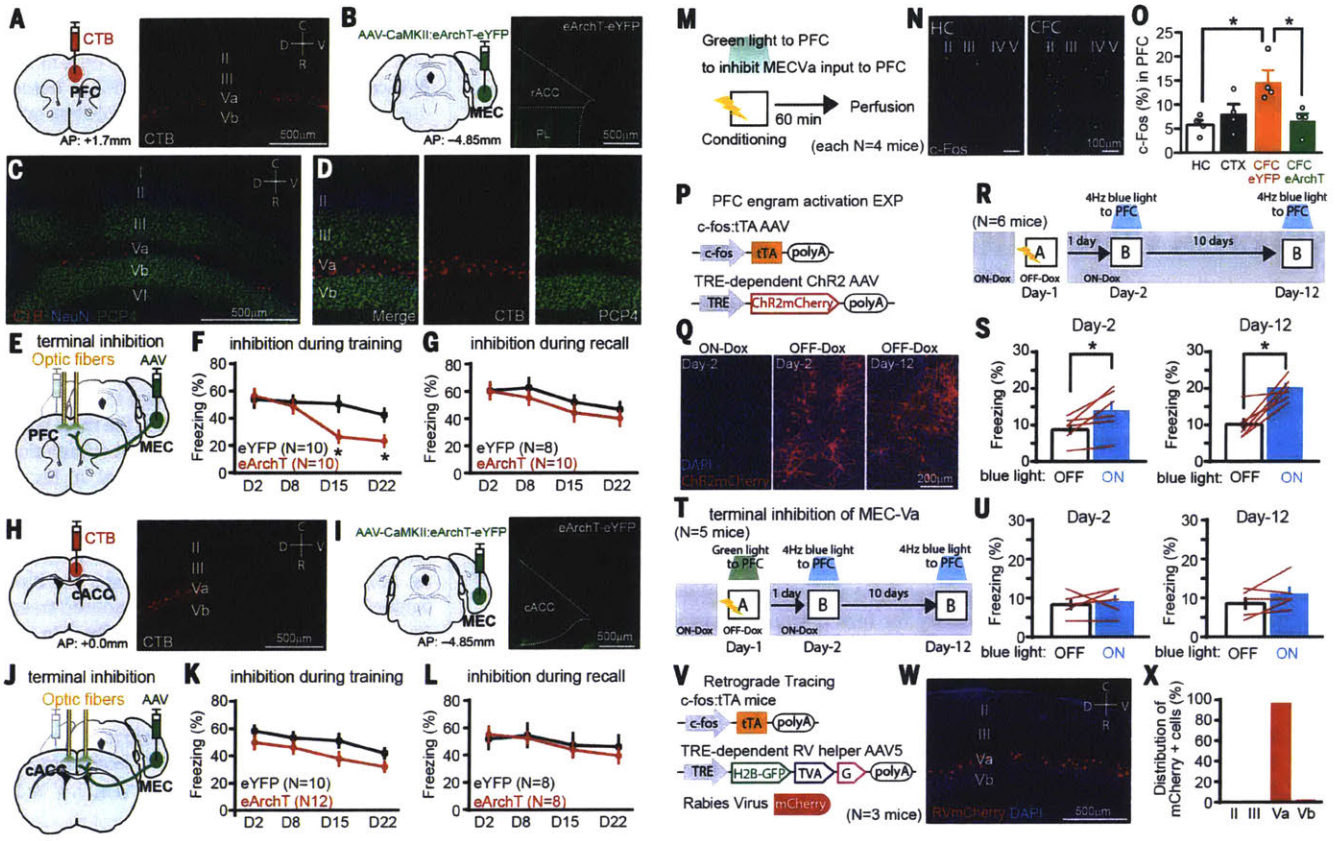

Fig. 1. MEC-Va input to the PFC during conditioning is crucial for generation of PFC engram cells. (**A**) CTB injection into the PFC (left) and sagittal section of the MEC with CTB-labeled cells (red) (right). AP, anterior posterior; C, caudal; R, rostral; D, dorsal; V, ventral. (**B**) AAV_8-CaMKII:eArchT-eYFP injection into the MEC (left) and coronal sections of PFC with MEC-Va axons expressing eYFP (green) (right). rACC, rostral ACC; PL, prelimbic cortex. (**C** and **D**) Sagittal section of MEC with CTB-labeled cells (red), immunostained with anti-PCP4 (green) and anti-NeuN (blue). PCP4 is a marker for layer III and Vb cells in MEC. The images were produced following CTB injection into the BLA. (**E** and **J**) Viral injections and optic fiber implantations. (**F** and **G**) Time courses (D, day) of freezing during recall tests. Green light was shone into the PFC during conditioning (F) or testing (G). (**H**) CTB injection into caudal ACC (cACC) (left) and sagittal section of the MEC with CTB-labeled cells (red) (right). (**I**) AAV_8-CaMKII:eArchT-eYFP injection into the MEC (left) and coronal sections of cACC with MEC-Va axons (green) (right). (**K** and **L**) Time courses of freezing during recall tests. Green light was shone into the cACC during conditioning (K) or testing (L). (**M**) Experimental schedule. (**N**) Coronal section of PFC with anti–c-Fos (green). HC, home cage; CFC, contextual fear conditioning. (**O**) Percentages of c-Fos^+ cells in the PFC of the HC, context exposure (CTX), CFC with eYFP, and CFC with eArchT groups. (**P**) Virus-mediated engram cell labeling with ChR2. (**Q**) Coronal section of PFC with ChR2-mCherry (red). (**R** and **T**) Experimental schedules. (**S** and **U**) Averaged freezing for blue light–off and blue light–on epochs. (**V**) Retrograde transsynaptic labeling with activity-dependent cell labeling. (**W**) Sagittal section of MEC with rabies virus–specific mCherry (red). (**X**) Distribution of 212 $mCherry^+$ cells in the MEC. $^*P < 0.05$; unpaired *t* test compared with eYFP [(F), (G), (K), and (L)], one-way analysis of variance (ANOVA) with Tukey-Kramer test (O), or paired *t* test [(S) and (U)]. Graphs show means ± SEM (in the bar graphs, circles and red lines represent individual animals). Lightning bolt, footshock; polyA, polyadenylation signal; DAPI, 4′,6-diamidino-2-phenylindole; "A", context A (conditioned context); "B", context B (unconditioned context); OFF-Dox, off doxycycline; ON-Dox, on doxycycline.

PFC engram cells by green light during retrieval did not affect recent memory (day 2); however, at the remote time point (day 12), memory retrieval was disrupted compared with the green light–off condition (Fig. 2F).

To further investigate the characteristics of PFC engram cells, we monitored transient calcium (Ca^{2+}) events in PFC cells in vivo. WT mice were injected with AAV_5-human synapsin1 (Syn): GCaMP6f in the PFC and implanted with a micro-gradient-index (GRIN) lens targeting the PFC (Fig. 2, G to I, and fig. S8) (*22*, *27*). On day 1, mice were first exposed to context B, followed by CFC in context A. Mice were then reexposed to both contexts in the same order on days 2 and 15 (Fig. 2J). The averaged frequency of Ca^{2+} events in PFC cells did not significantly change in either a time- or context-dependent manner (fig. S9B). However, a small but significant difference was revealed in the cumulative distribution curves of a rate difference index (assessing context selectivity; see the methods) between day 1 conditioning and day 15 recall and between day 2 recall and day 15 recall (fig. S9C). PFC cells did not appear to discriminate between the two contexts on day 1 before footshock presentation (Fig. 2, K and L). However, after footshock presentation, about 11% of cells showed a significant increase in Ca^{2+} transients [shock-responding (SR) cells] (Fig. 2, K and L). The remaining ~89% of PFC cells did not respond to the shocks [shock-nonresponding (SNR) cells]. The SR cells were less active than the SNR cells during exposure to contexts B and A on day 1 before footshock presentation (Fig. 2, L to N, and fig. S9D). During recall, the transient Ca^{2+} activity of SR cells in context A was significantly higher compared with that in context B on day 15, but not on days 1 or 2, whereas the frequency of Ca^{2+} transient events in SNR cells remained constant, irrespective of context (Fig. 2, M and N). This produced a significant rate difference index of Ca^{2+} activity for context A between the SR and SNR cells on day 15 but not on day 1 (excluding the shock delivery period) or day 2 (Fig. 2O). These results,

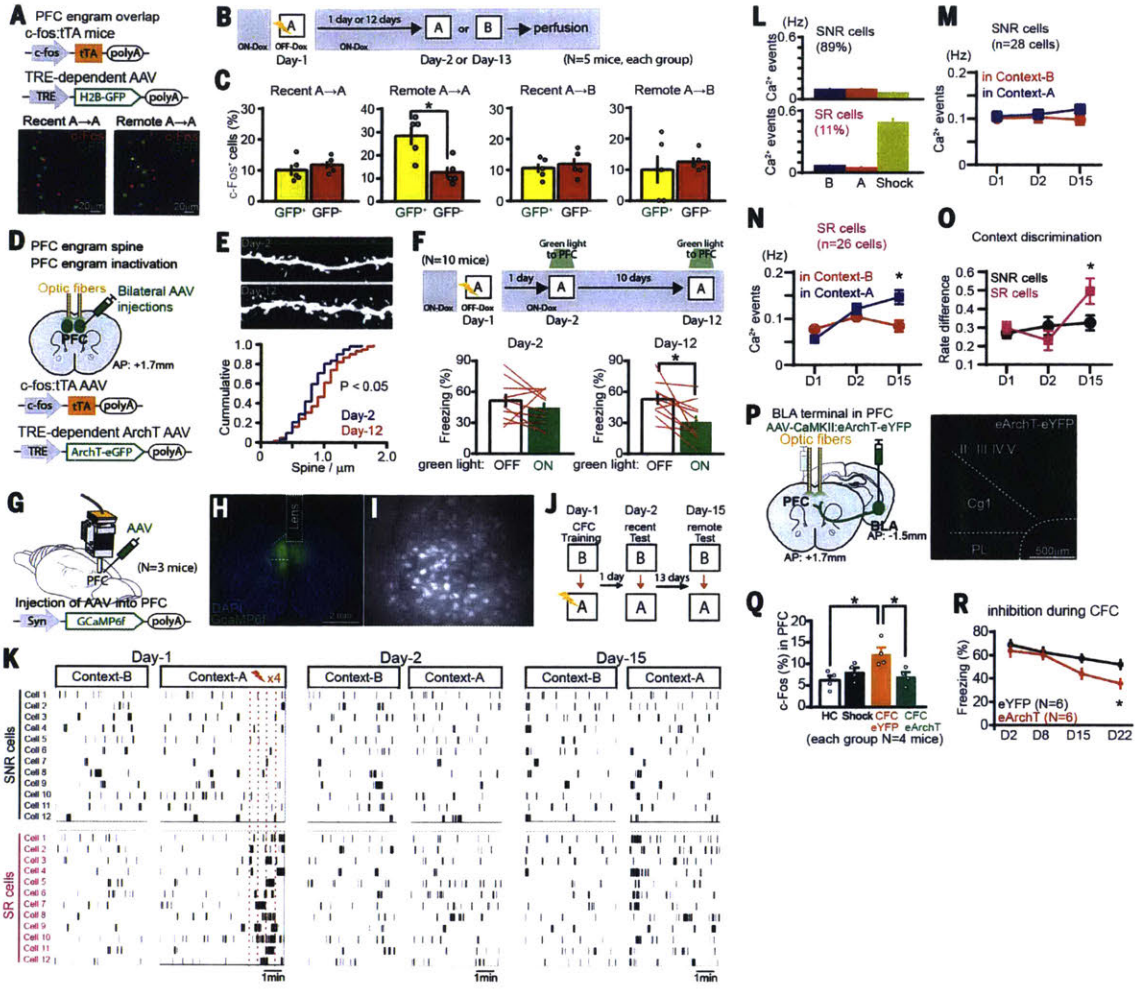

Fig. 2. PFC engram cells mature with time. (**A**) PFC engram cell labeling with H2B-GFP (top) and coronal sections of PFC with H2B-GFP (green) and anti–c-Fos (red) (bottom). Circled cells are double-positive. (**B**) Experimental schedule. (**C**) Percentages of c-Fos$^+$ cells in H2B-GFP$^+$ and H2B-GFP$^-$ cells in PFC. (**D**) PFC engram cell labeling with ArchT. (**E**) Dendritic spines from PFC engram cells (top) and cumulative probability of the spine density of PFC engrams (bottom). (**F**) Experimental schedule (top) and averaged freezing for green light–off and green light–on epochs during recall testing (bottom). (**G** and **H**) Viral injections and GRIN lens implantation. (**I**) Stacked image acquired through the microendoscope over 10 min of imaging in the PFC. (**J**) Experimental schedule. (**K**) Raster plots of Ca^{2+} events (black bars) in shock-nonresponding (SNR) and shock-responding (SR) cells in the PFC (showing 12 example cells). (**L** to **N**) Averaged Ca^{2+} event frequency for SNR and SR cells on days 1, 2, and day 15. (**O**) Averaged rate difference index of Ca^{2+} activity. (**P**) Viral injections and optic fiber implantations (left) and coronal sections of PFC visualizing BLA axons (green) (right). Cg1, cingulate cortex 1 (rACC). (**Q**) Percentages of c-Fos$^+$ cells in the PFC of the HC, shock only, CFC with eYFP, and CFC with eArchT groups. (**R**) Time courses of freezing during recall tests. *$P < 0.05$; unpaired t test [(C), (O), and (R)], Kolmogorov-Smirnov (KS) test (E), paired t test [(F), (M), and (N)], or one-way ANOVA with Tukey-Kramer test (Q). Graphs show means ± SEM.

combined with c-Fos activation data (Fig. 1, M to O), suggest that the SR cells may be the PFC memory engram cells, given that the generation of the PFC engram cells requires both context exposure and footshocks.

Our calcium imaging data suggest that footshock stimulus input into the PFC is crucial for the generation of PFC engram cells. Because the BLA integrates footshock information arriving from the thalamus (*28*) and projects to the PFC (figs. S5I and S10), we optogenetically inhibited the pathway from the BLA to the PFC during CFC (Fig. 2P). Optogenetic inhibition of BLA terminals in the PFC during CFC disrupted the generation of PFC engram cells (Fig. 2Q). The terminal inhibition during CFC also inhibited remote memory formation (Fig. 2R).

To test whether the HPC engram cells play a crucial role in the functional maturation of PFC engram cells during the systems consolidation process, we bilaterally targeted injection of AAV_9-TRE:tetanus toxin light chain (TeTX) or AAV_9-TRE:eYFP (as a control) to the hippocampal dentate gyrus (DG) of c-fos:tTA transgenic mice (Fig. 3A). When the mice were subjected to CFC, DG engram cells were labeled with TeTX. DG engram cell labeling with TeTX caused a robust inhibition of DG engram cell output, as revealed by greatly reduced immunoreactivity of vesicle-associated membrane protein 2 (VAMP2)—which is essential for activity-dependent neurotransmitter release from presynaptic terminals (*13*)—within the stratum lucidum in hippocampal CA3 in mice that were off doxycycline, compared with that in mice that were on doxycycline (Fig. 3, B and C). In TeTX-expressing mice, optogenetic activation of DG engram cells with ChR2 failed to produce the increase in CA3 c-Fos$^+$ cells that was observed in eYFP control mice relative to home-cage controls (Fig. 3D). TeTX expression in HPC engram cells inhibited the reactivation of PFC engram cells, compared with that in the eYFP control group, during exposure to context A 12 days after CFC (Fig. 3, E and F). TeTX expression also blocked the increase in the dendritic spine density of PFC engram cells that was observed in the eYFP group (Fig. 3G). In vivo calcium imaging revealed that TeTX expression in HPC engram cells after CFC blocked the increase in the context discrimination index in SR cells in the PFC (Fig. 3H and fig. S11).

To investigate the postconsolidation fate of HPC engram cells, we crossed c-fos:tTA transgenic mice with TRE:H2B–GFP transgenic mice (*29*), subjected them to CFC, then reexposed them to context A (the conditioned context) or context B (an unconditioned context) on day 2

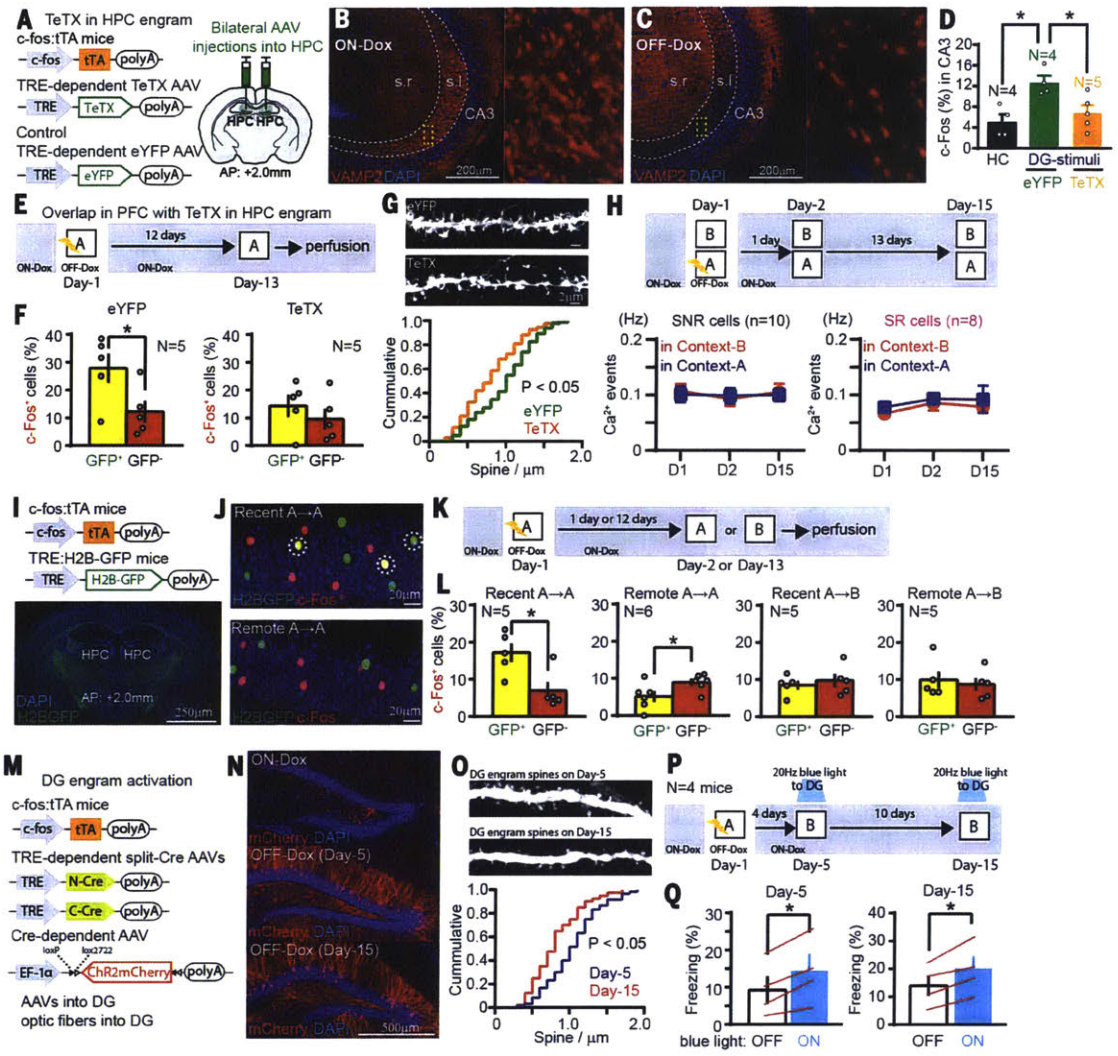

Fig. 3. HPC engram cells support the maturation of PFC engram cells and become silent with time. (**A**) DG engram cell labeling with TeTX. (**B** and **C**) Sagittal sections of HPC with anti-VAMP2 (red). The yellow box indicates the area of magnification (right). s.r., stratum radiatum; s.l., stratum lucidum. (**D**) Percentages of c-Fos$^+$ cells in hippocampal CA3 of the HC, blue light–on mice with eYFP, and blue light–on mice with TeTX. (**E**) Experimental schedule. (**F**) Percentages of c-Fos$^+$ cells in H2B-GFP$^+$ and H2B-GFP$^-$ cells in the PFC of eYFP- and TeTX-expressing mice. (**G**) Dendritic spines from PFC engrams (top) and cumulative probability of the spine density of PFC engrams in eYFP- and TeTX-expressing mice (bottom). (**H**) Experimental schedule (top) and averaged Ca^{2+} event frequency of SNR and SR cells under the TeTX-expressing condition (bottom). (**I**) Transgenic strategy of DG engram cell labeling with H2B-GFP (top) and coronal section of the brain (bottom). (**J**) Coronal sections of DG with H2B-GFP (green) and anti–c-Fos (red). Circled cells are double-positive. (**K** and **P**) Experimental schedules. (**L**) Percentages of c-Fos$^+$ cells in H2B-GFP$^+$ and H2B-GFP$^-$ cells in the DG. (**M**) Long-term DG engram cell labeling with ChR2. (**N**) Coronal sections of DG with ChR2-mCherry (red). (**O**) Dendritic spines from DG engrams (top) and cumulative probability of the spine density of DG engrams (bottom). (**Q**) Averaged freezing for blue light–off and blue light–on epochs. *$P < 0.05$; one-way ANOVA with Tukey-Kramer test (D), unpaired t test [(F) and (L)], KS test [(G) and (O)], or paired t test [(H) and (Q)]. Graphs show means ± SEM.

or 13 (Fig. 3, I to K). Compared with the non-engram cells, DG engram cells were preferentially reactivated in context A on day 2, but not on day 13 (Fig. 3L). No difference was observed in the activation of DG engram and non-engram cells by context B (Fig. 3L). We were unable to maintain labeled DG engram cells with ChR2 beyond 12 days with injection of AAV_9-TRE:ChR2-mCherry. To extend this technical limit, we targeted injections of $AAV_{1,5,8,9}$-TRE:CCre, $AAV_{1,5,8,9}$-TRE:NCre, and AAV_5-elongation factor 1a (EF1a):ChR2-mCherry to the DG of c-fos:tTA transgenic mice (Fig. 3M). We could thus extend viable labeling by a few days (Fig. 3N). The spine density of DG engram cells on day 15 was significantly reduced compared with that on day 5 (Fig. 3O and fig. S12). On both days 5 and 15, optogenetic activation of DG engram cells induced freezing behavior (Fig. 3, P and Q).

Last, we investigated the role of MEC-Va projections into the BLA in recent and remote memory (Fig. 4A and fig. S2A). Inhibition of MEC-Va terminals in the BLA during CFC disrupted contextual fear memory formation. Retrieval was impaired at all time points tested (Fig. 4B). When terminal inhibition was restricted to retrieval, recent memory tested on days 2 and 8 was impaired, but remote memory retrieval on days 15 and 22 was unaffected (Fig. 3C). In contrast, inhibition of PFC engram cell terminals in the BLA did not impair memory retrieval on day 2 but did impair memory retrieval on day 12 (Fig. 4, D and E). To investigate whether the BLA fear memory engram cells formed on day 1 are maintained and used for PFC engram-dependent remote memory recall, we subjected the double transgenic mice (Fig. 4, F and I) to CFC and reexposed them to context A at recent or remote time points (Fig. 4G). BLA engram cells were reactivated equally well by context A at recent and remote time points (Fig. 4H). Similarly, BLA cells activated by recent recall were reactivated equally well by reexposure to context A at recent and remote time points (Fig. 4, J and K).

In this study, we found that PFC memory engram cells for CFC were rapidly formed during day 1 training through inputs from both the MEC-Va and the BLA, but they were not retrievable with natural recall cues. The immature PFC engram cells functionally, structurally,

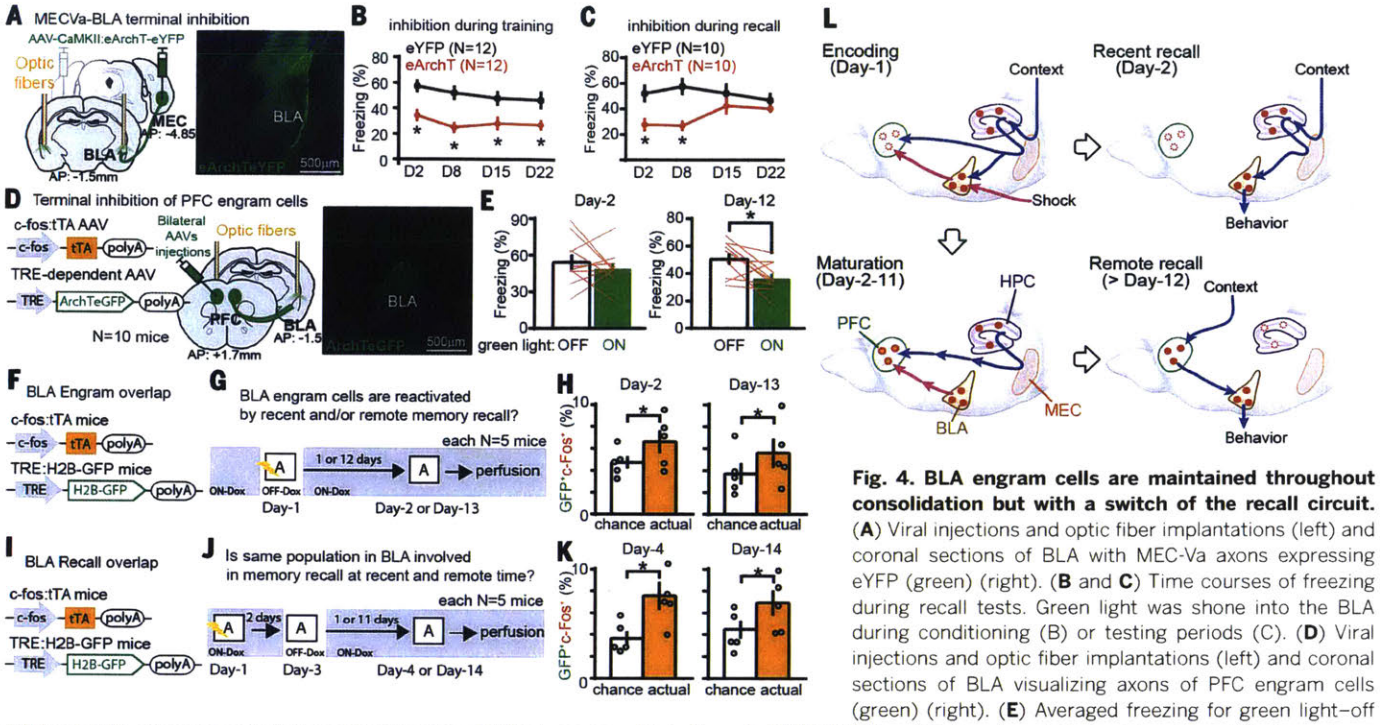

Fig. 4. BLA engram cells are maintained throughout consolidation but with a switch of the recall circuit. (**A**) Viral injections and optic fiber implantations (left) and coronal sections of BLA with MEC-Va axons expressing eYFP (green) (right). (**B** and **C**) Time courses of freezing during recall tests. Green light was shone into the BLA during conditioning (B) or testing periods (C). (**D**) Viral injections and optic fiber implantations (left) and coronal sections of BLA visualizing axons of PFC engram cells (green) (right). (**E**) Averaged freezing for green light–off and green light–on epochs during recall testing. (**F** and **I**) BLA engram cell labeling with H2B-GFP. (**G** and **J**) Experimental schedules. (**H** and **K**) Percentages of double-labeling with c-Fos and H2B-GFP in the BLA compared with the calculated chance percentages. (**L**) A new model for systems consolidation of memory. $^*P < 0.05$; unpaired *t* test [(B), (C), (H), and (K)] or paired *t* test (E). Graphs show means ± SEM.

and physiologically matured during the subsequent few weeks, and this process required inputs from HPC engram cells, presumably through the MEC-Va. In contrast to their formation on day 1, retrieval of the PFC engram at a remote time did not require MEC-Va input. HPC engram cells that formed during training became silent with time; they were not retrieved on day 14 by natural recall cues but were still reactivatable optogenetically for recall. However, fear memory BLA engrams that formed during training were functionally maintained, even after the consolidation-mediated switch in recall circuits (Fig. 4L).

Our model (Fig. 4L) introduces the concept that the prefrontal memory engram is already generated, albeit in an immature form, on day 1 of training through inputs from both the HPC-EC network and the BLA (Fig. 1). The standard model (*1*, *2*, *4*, *6*, *7*, *11*) hypothesizes that remote memory is formed in the cortex by a slow transfer of hippocampal memory. In contrast, in our study, the role of the hippocampus in cortical memory is in the rapid generation of immature engram cells in the PFC during training and in the subsequent functional maturation of these preexisting engram cells (Fig. 2). The immature PFC engram may correspond to the cortical "tagging" suggested in an earlier study (*14*). In a previous study, the BLA was found to be crucial for both recent and remote fear memory expression (*30*). Our results demonstrate an overlapping set of BLA engram cells for both recent and remote fear memory retrieval, which were quickly formed during training (Fig. 4). However, the source of input into the BLA engrams for retrieval shifts from the MEC-Va at recent time points to the PFC engram at remote time points (Fig. 4L). The route through which contextual stimuli activate the mature PFC engram is unknown. Most likely, the information processed in a variety of sensory cortices reaches the PFC via the thalamus (*31*). Supporting this idea, PFC engram cells receive monosynaptic input from both the medial-dorsal and anteromedial thalamus (fig. S5).

Our finding of the lasting hippocampal engrams (Fig. 3Q) is consistent with multiple trace theory (*5*, *11*). However, at the postconsolidation stage, the hippocampal engrams were not activatable by natural recall cues, but rather by optogenetic stimulation. A similar state of hippocampal engrams has previously been observed in anisomycin-induced amnesia (*24*) and mouse models of early Alzheimer's disease (*26*), and the early (day 2) PFC engram cells showed a similar property (Figs. 1S and 2C). Although we did not determine how long after encoding this "silent state" of the hippocampal engram lasts, we speculate that the hippocampal engram eventually loses the original memory information (*29*, *32*, *33*). Alternatively, the silent engram cells may still participate in the successful remote recall of discrete episodic details (*5*, *11*).

As in previous studies (*18*, *20*, *29*), we observed that training resulted in widespread neuronal activation in the neocortex, including the ACC and RSC. However, whereas the activation of PFC neurons is crucial for formation of remote memory, MEC-Va input into the cACC or RSC is dispensable for this process. For remote memory, the PFC may thus have a distinctive role in integrating multiple sensory information stored in various cortical areas (*11*). Last, our data show that the remote memory expressed by the PFC engram is conditioned-context specific, suggesting that it is episodic-like.

REFERENCES AND NOTES

1. D. Marr, *Philos. Trans. R. Soc. London B Biol. Sci.* **262**, 23–81 (1971).
2. L. R. Squire, *Science* **232**, 1612–1619 (1986).
3. J. J. Kim, M. S. Fanselow, *Science* **256**, 675–677 (1992).
4. J. L. McClelland, B. L. McNaughton, R. C. O'Reilly, *Psychol. Rev.* **102**, 419–457 (1995).
5. L. Nadel, M. Moscovitch, *Curr. Opin. Neurobiol.* **7**, 217–227 (1997).
6. D. Tse *et al.*, *Science* **316**, 76–82 (2007).
7. J. L. McClelland, *J. Exp. Psychol. Gen.* **142**, 1190–1210 (2013).
8. G. Buzsáki, *Cereb. Cortex* **6**, 81–92 (1996).
9. A. G. Siapas, M. A. Wilson, *Neuron* **21**, 1123–1128 (1998).
10. B. J. Wiltgen, R. A. Brown, L. E. Talton, A. J. Silva, *Neuron* **44**, 101–108 (2004).
11. P. W. Frankland, B. Bontempi, *Nat. Rev. Neurosci.* **6**, 119–130 (2005).
12. A. R. Preston, H. Eichenbaum, *Curr. Biol.* **23**, R764–R773 (2013).
13. T. Nakashiba, D. L. Buhl, T. J. McHugh, S. Tonegawa, *Neuron* **62**, 781–787 (2009).
14. E. Lesburguères *et al.*, *Science* **331**, 924–928 (2011).
15. M. Zelikowsky, S. Bissiere, M. S. Fanselow, *J. Neurosci.* **32**, 3393–3397 (2012).
16. L. G. Reijmers, B. L. Perkins, N. Matsuo, M. Mayford, *Science* **317**, 1230–1233 (2007).
17. X. Liu *et al.*, *Nature* **484**, 381–385 (2012).

18. S. Tonegawa, X. Liu, S. Ramirez, R. Redondo, *Neuron* **87**, 918–931 (2015).
19. T. Kitamura *et al.*, *Science* **343**, 896–901 (2014).
20. L. Ye *et al.*, *Cell* **165**, 1776–1788 (2016).
21. K. Deisseroth, *Nat. Neurosci.* **18**, 1213–1225 (2015).
22. Y. Ziv *et al.*, *Nat. Neurosci.* **16**, 264–266 (2013).
23. G. Sürmeli *et al.*, *Neuron* **88**, 1040–1053 (2015).
24. T. J. Ryan, D. S. Roy, M. Pignatelli, A. Arons, S. Tonegawa, *Science* **348**, 1007–1013 (2015).
25. A. Hayashi-Takagi *et al.*, *Nature* **525**, 333–338 (2015).
26. D. S. Roy *et al.*, *Nature* **531**, 508–512 (2016).
27. T. Kitamura *et al.*, *Neuron* **87**, 1317–1331 (2015).
28. B. A. Pellman, J. J. Kim, *Trends Neurosci.* **39**, 420–431 (2016).
29. K. K. Tayler, K. Z. Tanaka, L. G. Reijmers, B. J. Wiltgen, *Curr. Biol.* **23**, 99–106 (2013).
30. S. Maren, G. Aharonov, M. S. Fanselow, *Behav. Neurosci.* **110**, 718–726 (1996).
31. F. H. Do-Monte, K. Quiñones-Laracuente, G. J. Quirk, *Nature* **519**, 460–463 (2015).
32. C. A. Denny *et al.*, *Neuron* **83**, 189–201 (2014).
33. T. Kitamura *et al.*, *Cell* **139**, 814–827 (2009).

ACKNOWLEDGMENTS

We thank F. Bushard, J. Martin, T. Ryan, J. Yamamoto, C. Sun, W. Yu, S. Huang, M. Ragion, A. Arons, X. Zhou, C. Ragion, A. Moffa, L. Brenner, A. Hamalian, and D. King for help with experiments and preparing the manuscript; all members of the Tonegawa laboratory for their support; I. Wickersham for providing rabies virus; and Y. Shima and S. B. Nelson for providing TRE3G split Cre AAV. All data necessary to understand and assess the conclusions of this research are available in the supplementary materials. This work was supported by the RIKEN Brain Science Institute, the Howard Hughes Medical Institute, and the JPB Foundation (to S.T.). AAV_9-c-fos:tTA, AAV_9-TRE:ChR2mCherry, AAV_9-TRE:ArchTeGFP, AAV_9-TRE:TeTX, and AAV_9-TRE:eYFP were developed at the Massachusetts Institute of Technology by the group of S.T.; virus plasmids are available through a material transfer agreement.

SUPPLEMENTARY MATERIALS

www.sciencemag.org/content/356/6333/73/suppl/DC1
Materials and Methods
Supplementary Text
Figs. S1 to S12
References (*34–51*)

28 December 2016; accepted 14 March 2017
10.1126/science.aam6808